



Editors: C.A. Brebbia, M. Eglite,
I. Knets, R. Miftahof & V. Popov

Environmental Health and Biomedicine



WITPRESS

Environmental Health & Biomedicine

WIT*PRESS*

WIT Press publishes leading books in Science and Technology.

Visit our website for the current list of titles.

www.witpress.com

WIT*eLibrary*

Home of the Transactions of the Wessex Institute.

Papers presented at Environmental Health & Biomedicine are archived in the WIT eLibrary in volume 15 of WIT Transactions on Biomedicine and Health (ISSN 1743-3525). The WIT eLibrary provides the international scientific community with immediate and permanent access to individual papers presented at WIT conferences.

Visit the WIT eLibrary at www.witpress.com.

SIXTH INTERNATIONAL CONFERENCE ON THE IMPACT OF
ENVIRONMENTAL FACTORS ON HEALTH

&

NINTH INTERNATIONAL CONFERENCE ON MODELLING IN MEDICINE
AND BIOLOGY

Environmental Health & Biomedicine

CONFERENCE CHAIRMEN

C. A. Brebbia

Wessex Institute of Technology, UK

M. Eglite

Riga Stradins University, Latvia

I. Knets

Riga Technical University, Latvia

R. Miftahof

Arabian Gulf University, Bahrain

V. Popov

Wessex Institute of Technology, UK

INTERNATIONAL SCIENTIFIC ADVISORY COMMITTEE

S. Bernad	S. Mekaoui
C. Bignardi	T. Oyabu
D.M. Bonotto	D. Poljak
F. Carvalho	H. Rubio
A. Doi	K. Rumchev
L. Gastaldi	K. Shimano
C. Guiot	R. Shoucri
M. Hyre	P.B. Tchounwou
A. Macpherson	

Organised by

Wessex Institute of Technology, UK

Riga Technical University, Latvia

Riga Stradins University, Latvia

Sponsored by

WIT Transactions on Biomedicine and Health

WIT Transactions

Transactions Editor

Carlos Brebbia

Wessex Institute of Technology
Ashurst Lodge, Ashurst
Southampton SO40 7AA, UK
Email: carlos@wessex.ac.uk

Editorial Board

- B Abersek** University of Maribor, Slovenia
Y N Abousleiman University of Oklahoma, USA
P L Aguilar University of Extremadura, Spain
K S Al Jabri Sultan Qaboos University, Oman
E Alarcon Universidad Politecnica de Madrid, Spain
A Aldama IMTA, Mexico
C Alessandri Universita di Ferrara, Italy
D Almorza Gomar University of Cadiz, Spain
B Alzahabi Kettering University, USA
J A C Ambrosio IDMEC, Portugal
A M Amer Cairo University, Egypt
S A Anagnostopoulos University of Patras, Greece
M Andretta Montecatini, Italy
E Angelino A.R.P.A. Lombardia, Italy
H Antes Technische Universitat Braunschweig, Germany
M A Atherton South Bank University, UK
A G Atkins University of Reading, UK
D Aubry Ecole Centrale de Paris, France
H Azegami Toyohashi University of Technology, Japan
A F M Azevedo University of Porto, Portugal
J Baish Bucknell University, USA
J M Baldasano Universitat Politecnica de Catalunya, Spain
J G Bartzis Institute of Nuclear Technology, Greece
A Bejan Duke University, USA
M P Bekakos Democritus University of Thrace, Greece
G Belingardi Politecnico di Torino, Italy
R Belmans Katholieke Universiteit Leuven, Belgium
C D Bertram The University of New South Wales, Australia
D E Beskos University of Patras, Greece
S K Bhattacharyya Indian Institute of Technology, India
E Blums Latvian Academy of Sciences, Latvia
J Boarder Cartref Consulting Systems, UK
B Bobee Institut National de la Recherche Scientifique, Canada
H Boileau ESIGEC, France
J J Bommer Imperial College London, UK
M Bonnet Ecole Polytechnique, France
C A Borrego University of Aveiro, Portugal
A R Bretones University of Granada, Spain
J A Bryant University of Exeter, UK
F-G Buchholz Universitat Gesanthochschule Paderborn, Germany
M B Bush The University of Western Australia, Australia
F Butera Politecnico di Milano, Italy
J Byrne University of Portsmouth, UK
W Cantwell Liverpool University, UK
D J Cartwright Bucknell University, USA
P G Carydis National Technical University of Athens, Greece
J J Casares Long Universidad de Santiago de Compostela, Spain
M A Celia Princeton University, USA
A Chakrabarti Indian Institute of Science, India
A H-D Cheng University of Mississippi, USA

J Chilton University of Lincoln, UK
C-L Chiu University of Pittsburgh, USA
H Choi Kangnung National University, Korea
A Cieslak Technical University of Lodz, Poland
S Clement Transport System Centre, Australia
M W Collins Brunel University, UK
J J Connor Massachusetts Institute of Technology, USA
M C Constantinou State University of New York at Buffalo, USA
D E Cormack University of Toronto, Canada
M Costantino Royal Bank of Scotland, UK
D F Cutler Royal Botanic Gardens, UK
W Czyczula Krakow University of Technology, Poland
M da Conceicao Cunha University of Coimbra, Portugal
L Dávid Károly Róbert College, Hungary
A Davies University of Hertfordshire, UK
M Davis Temple University, USA
A B de Almeida Instituto Superior Tecnico, Portugal
E R de Arantes e Oliveira Instituto Superior Tecnico, Portugal
L De Biase University of Milan, Italy
R de Borst Delft University of Technology, Netherlands
G De Mey University of Ghent, Belgium
A De Montis Università di Cagliari, Italy
A De Naeyer Universiteit Ghent, Belgium
W P De Wilde Vrije Universiteit Brussel, Belgium
L Debnath University of Texas-Pan American, USA
N J Dedios Mimbela Universidad de Cordoba, Spain
G Degrande Katholieke Universiteit Leuven, Belgium
S del Giudice University of Udine, Italy
G Deplano Università di Cagliari, Italy
I Doltsinis University of Stuttgart, Germany
M Domaszewski Université de Technologie de Belfort-Montbéliard, France
J Dominguez University of Seville, Spain
K Dorow Pacific Northwest National Laboratory, USA
W Dover University College London, UK
C Dowlen South Bank University, UK
J P du Plessis University of Stellenbosch, South Africa
R Duffell University of Hertfordshire, UK
A Ebel University of Cologne, Germany
E E Edoutos Democritus University of Thrace, Greece
G K Egan Monash University, Australia
K M Elawadly Alexandria University, Egypt
K-H Elmer Universität Hannover, Germany
D Elms University of Canterbury, New Zealand
M E M El-Sayed Kettering University, USA
D M Elsom Oxford Brookes University, UK
F Erdogan Lehigh University, USA
F P Escrig University of Seville, Spain
D J Evans Nottingham Trent University, UK
J W Everett Rowan University, USA
M Faghri University of Rhode Island, USA
R A Falconer Cardiff University, UK
M N Fardis University of Patras, Greece
P Fedelinski Silesian Technical University, Poland
H J S Fernando Arizona State University, USA
S Finger Carnegie Mellon University, USA
J I Frankel University of Tennessee, USA
D M Fraser University of Cape Town, South Africa
M J Fritzler University of Calgary, Canada
U Gabbert Otto-von-Guericke Universität Magdeburg, Germany
G Gambolati Università di Padova, Italy
C J Gantes National Technical University of Athens, Greece
L Gaul Universität Stuttgart, Germany
A Genco University of Palermo, Italy
N Georgantzis Universität Jaume I, Spain
P Giudici Università di Pavia, Italy
F Gomez Universidad Politecnica de Valencia, Spain
R Gomez Martin University of Granada, Spain
D Goulias University of Maryland, USA
K G Goulias Pennsylvania State University, USA
F Grandori Politecnico di Milano, Italy
W E Grant Texas A & M University, USA
S Grilli University of Rhode Island, USA

- R H J Grimshaw** Loughborough University, UK
- D Gross** Technische Hochschule Darmstadt, Germany
- R Grundmann** Technische Universitat Dresden, Germany
- A Gualtierotti** IDHEAP, Switzerland
- R C Gupta** National University of Singapore, Singapore
- J M Hale** University of Newcastle, UK
- K Hameyer** Katholieke Universiteit Leuven, Belgium
- C Hanke** Danish Technical University, Denmark
- K Hayami** University of Toyko, Japan
- Y Hayashi** Nagoya University, Japan
- L Haydock** Newage International Limited, UK
- A H Hendrickx** Free University of Brussels, Belgium
- C Herman** John Hopkins University, USA
- I Hideaki** Nagoya University, Japan
- D A Hills** University of Oxford, UK
- W F Huebner** Southwest Research Institute, USA
- J A C Humphrey** Bucknell University, USA
- M Y Hussaini** Florida State University, USA
- W Hutchinson** Edith Cowan University, Australia
- T H Hyde** University of Nottingham, UK
- M Iguchi** Science University of Tokyo, Japan
- D B Ingham** University of Leeds, UK
- L Int Panis** VITO Expertisecentrum IMS, Belgium
- N Ishikawa** National Defence Academy, Japan
- J Jaafar** UiTm, Malaysia
- W Jager** Technical University of Dresden, Germany
- Y Jaluria** Rutgers University, USA
- C M Jefferson** University of the West of England, UK
- P R Johnston** Griffith University, Australia
- D R H Jones** University of Cambridge, UK
- N Jones** University of Liverpool, UK
- D Kaliampakos** National Technical University of Athens, Greece
- N Kamiya** Nagoya University, Japan
- D L Karabalis** University of Patras, Greece
- M Karlsson** Linkoping University, Sweden
- T Katayama** Doshisha University, Japan
- K L Katsifarakis** Aristotle University of Thessaloniki, Greece
- J T Katsikadelis** National Technical University of Athens, Greece
- E Kausel** Massachusetts Institute of Technology, USA
- H Kawashima** The University of Tokyo, Japan
- B A Kazimee** Washington State University, USA
- S Kim** University of Wisconsin-Madison, USA
- D Kirkland** Nicholas Grimshaw & Partners Ltd, UK
- E Kita** Nagoya University, Japan
- A S Kobayashi** University of Washington, USA
- T Kobayashi** University of Tokyo, Japan
- D Koga** Saga University, Japan
- S Kotake** University of Tokyo, Japan
- A N Kounadis** National Technical University of Athens, Greece
- W B Kratzig** Ruhr Universitat Bochum, Germany
- T Krauthammer** Penn State University, USA
- C-H Lai** University of Greenwich, UK
- M Langseth** Norwegian University of Science and Technology, Norway
- B S Larsen** Technical University of Denmark, Denmark
- F Lattarulo** Politecnico di Bari, Italy
- A Lebedev** Moscow State University, Russia
- L J Leon** University of Montreal, Canada
- D Lewis** Mississippi State University, USA
- S Ighobashi** University of California Irvine, USA
- K-C Lin** University of New Brunswick, Canada
- A A Liolios** Democritus University of Thrace, Greece
- S Lomov** Katholieke Universiteit Leuven, Belgium
- J W S Longhurst** University of the West of England, UK
- G Loo** The University of Auckland, New Zealand
- J Lourenco** Universidade do Minho, Portugal
- J E Luco** University of California at San Diego, USA
- H Lui** State Seismological Bureau Harbin, China

C J Lumsden University of Toronto, Canada
L Lundqvist Division of Transport and Location Analysis, Sweden
T Lyons Murdoch University, Australia
Y-W Mai University of Sydney, Australia
M Majowiecki University of Bologna, Italy
D Malerba Università degli Studi di Bari, Italy
G Manara University of Pisa, Italy
B N Mandal Indian Statistical Institute, India
Ü Mander University of Tartu, Estonia
H A Mang Technische Universität Wien, Austria
G D Manolis Aristotle University of Thessaloniki, Greece
W J Mansur COPPE/UFRJ, Brazil
N Marchettini University of Siena, Italy
J D M Marsh Griffith University, Australia
J F Martín-Duque Universidad Complutense, Spain
T Matsui Nagoya University, Japan
G Mattrisch DaimlerChrysler AG, Germany
F M Mazzolani University of Naples "Federico II", Italy
K McManis University of New Orleans, USA
A C Mendes Universidade de Beira Interior, Portugal
R A Meric Research Institute for Basic Sciences, Turkey
J Mikielawicz Polish Academy of Sciences, Poland
N Milic-Frayling Microsoft Research Ltd, UK
R A W Mines University of Liverpool, UK
C A Mitchell University of Sydney, Australia
K Miura Kajima Corporation, Japan
A Miyamoto Yamaguchi University, Japan
T Miyoshi Kobe University, Japan
G Molinari University of Genoa, Italy
T B Moodie University of Alberta, Canada
D B Murray Trinity College Dublin, Ireland
G Nakhaeizadeh DaimlerChrysler AG, Germany
M B Neace Mercer University, USA
D Neculescu University of Ottawa, Canada
F Neumann University of Vienna, Austria
S-I Nishida Saga University, Japan
H Nisitani Kyushu Sangyo University, Japan
B Notaros University of Massachusetts, USA
P O'Donoghue University College Dublin, Ireland
R O O'Neill Oak Ridge National Laboratory, USA
M Ohkusu Kyushu University, Japan
G Oliveto Università di Catania, Italy
R Olsen Camp Dresser & McKee Inc., USA
E Oñate Universitat Politècnica de Catalunya, Spain
K Onishi Ibaraki University, Japan
P H Oosthuizen Queens University, Canada
E L Ortiz Imperial College London, UK
E Outa Waseda University, Japan
A S Papageorgiou Rensselaer Polytechnic Institute, USA
J Park Seoul National University, Korea
G Passerini Università delle Marche, Italy
B C Patten University of Georgia, USA
G Pelosi University of Florence, Italy
G G Penelis Aristotle University of Thessaloniki, Greece
W Perrie Bedford Institute of Oceanography, Canada
R Pietrabissa Politecnico di Milano, Italy
H Pina Instituto Superior Técnico, Portugal
M F Platzer Naval Postgraduate School, USA
D Poljak University of Split, Croatia
V Popov Wessex Institute of Technology, UK
H Power University of Nottingham, UK
D Prandle Proudman Oceanographic Laboratory, UK
M Predeleanu University Paris VI, France
M R I Purvis University of Portsmouth, UK
I S Putra Institute of Technology Bandung, Indonesia
Y A Pykh Russian Academy of Sciences, Russia
F Rachidi EMC Group, Switzerland
M Rahman Dalhousie University, Canada
K R Rajagopal Texas A & M University, USA
T Rang Tallinn Technical University, Estonia
J Rao Case Western Reserve University, USA
A M Reinhorn State University of New York at Buffalo, USA
A D Rey McGill University, Canada
D N Riahi University of Illinois at Urbana-Champaign, USA

- B Ribas** Spanish National Centre for Environmental Health, Spain
- K Richter** Graz University of Technology, Austria
- S Rinaldi** Politecnico di Milano, Italy
- F Robuste** Universitat Politecnica de Catalunya, Spain
- J Roddick** Flinders University, Australia
- A C Rodrigues** Universidade Nova de Lisboa, Portugal
- F Rodrigues** Poly Institute of Porto, Portugal
- C W Roeder** University of Washington, USA
- J M Roesset** Texas A & M University, USA
- W Roetzl** Universitaet der Bundeswehr Hamburg, Germany
- V Roje** University of Split, Croatia
- R Rosset** Laboratoire d'Aerologie, France
- J L Rubio** Centro de Investigaciones sobre Desertificacion, Spain
- T J Rudolphi** Iowa State University, USA
- S Russenchuck** Magnet Group, Switzerland
- H Ryssel** Fraunhofer Institut Integrierte Schaltungen, Germany
- S G Saad** American University in Cairo, Egypt
- M Saiidi** University of Nevada-Reno, USA
- R San Jose** Technical University of Madrid, Spain
- F J Sanchez-Sesma** Instituto Mexicano del Petroleo, Mexico
- B Sarler** Nova Gorica Polytechnic, Slovenia
- S A Savidis** Technische Universitat Berlin, Germany
- A Savini** Universita de Pavia, Italy
- G Schmid** Ruhr-Universitat Bochum, Germany
- R Schmidt** RWTH Aachen, Germany
- B Scholtes** Universitaet of Kassel, Germany
- W Schreiber** University of Alabama, USA
- A P S Selvadurai** McGill University, Canada
- J J Sendra** University of Seville, Spain
- J J Sharp** Memorial University of Newfoundland, Canada
- Q Shen** Massachusetts Institute of Technology, USA
- X Shixiong** Fudan University, China
- G C Sih** Lehigh University, USA
- L C Simoes** University of Coimbra, Portugal
- A C Singhal** Arizona State University, USA
- P Skerget** University of Maribor, Slovenia
- J Sladek** Slovak Academy of Sciences, Slovakia
- V Sladek** Slovak Academy of Sciences, Slovakia
- A C M Sousa** University of New Brunswick, Canada
- H Sozer** Illinois Institute of Technology, USA
- D B Spalding** CHAM, UK
- P D Spanos** Rice University, USA
- T Speck** Albert-Ludwigs-Universitaet Freiburg, Germany
- C C Spyarakos** National Technical University of Athens, Greece
- I V Stangeeva** St Petersburg University, Russia
- J Stasiak** Technical University of Gdansk, Poland
- G E Swaters** University of Alberta, Canada
- S Syngellakis** University of Southampton, UK
- J Szymd** University of Mining and Metallurgy, Poland
- S T Tadano** Hokkaido University, Japan
- H Takemiya** Okayama University, Japan
- I Takewaki** Kyoto University, Japan
- C-L Tan** Carleton University, Canada
- E Taniguchi** Kyoto University, Japan
- S Tanimura** Aichi University of Technology, Japan
- J L Tassoulas** University of Texas at Austin, USA
- M A P Taylor** University of South Australia, Australia
- A Terranova** Politecnico di Milano, Italy
- A G Tjihuis** Technische Universiteit Eindhoven, Netherlands
- T Tirabassi** Institute FISBAT-CNR, Italy
- S Tkachenko** Otto-von-Guericke-University, Germany
- N Tosaka** Nihon University, Japan
- T Tran-Cong** University of Southern Queensland, Australia
- R Tremblay** Ecole Polytechnique, Canada
- I Tsukrov** University of New Hampshire, USA
- R Turra** CINECA Interuniversity Computing Centre, Italy
- S G Tushinski** Moscow State University, Russia
- J-L Uso** Universitat Jaume I, Spain
- E Van den Bulck** Katholieke Universiteit Leuven, Belgium

D Van den Poel Ghent University, Belgium

R van der Heijden Radboud University,
Netherlands

R van Duin Delft University of Technology,
Netherlands

P Vas University of Aberdeen, UK

R Verhoeven Ghent University, Belgium

A Viguri Universitat Jaume I, Spain

Y Villacampa Esteve Universidad de
Alicante, Spain

F F V Vincent University of Bath, UK

S Walker Imperial College, UK

G Walters University of Exeter, UK

B Weiss University of Vienna, Austria

H Westphal University of Magdeburg,
Germany

J R Whiteman Brunel University, UK

Z-Y Yan Peking University, China

S Yanniotis Agricultural University of Athens,
Greece

A Yeh University of Hong Kong, China

J Yoon Old Dominion University, USA

K Yoshizato Hiroshima University, Japan

T X Yu Hong Kong University of Science &
Technology, Hong Kong

M Zador Technical University of Budapest,
Hungary

K Zakrzewski Politechnika Lodzka, Poland

M Zamir University of Western Ontario,
Canada

R Zarnic University of Ljubljana, Slovenia

G Zharkova Institute of Theoretical and
Applied Mechanics, Russia

N Zhong Maebashi Institute of Technology,
Japan

H G Zimmermann Siemens AG, Germany

Environmental Health & Biomedicine

Editors

C. A. Brebbia

Wessex Institute of Technology, UK

M. Eglite

Riga Stradins University, Latvia

I. Knets

Riga Technical University, Latvia

R. Miftahof

Arabian Gulf University, Bahrain

V. Popov

Wessex Institute of Technology, UK

WITPRESS Southampton, Boston



Editors:

C. A. Brebbia

Wessex Institute of Technology, UK

M. Eglite

Riga Stradins University, Latvia

I. Knets

Riga Technical University, Latvia

R. Miftahof

Arabian Gulf University, Bahrain

V. Popov

Wessex Institute of Technology, UK

Published by

WIT Press

Ashurst Lodge, Ashurst, Southampton, SO40 7AA, UK

Tel: 44 (0) 238 029 3223; Fax: 44 (0) 238 029 2853

E-Mail: witpress@witpress.com

<http://www.witpress.com>

For USA, Canada and Mexico

Computational Mechanics Inc

25 Bridge Street, Billerica, MA 01821, USA

Tel: 978 667 5841; Fax: 978 667 7582

E-Mail: infousa@witpress.com

<http://www.witpress.com>

British Library Cataloguing-in-Publication Data

A Catalogue record for this book is available
from the British Library

ISBN: 978-1-84564-524-3

ISSN: 1747-4485 (print)

ISSN: 1743-3525 (online)

The texts of the papers in this volume were set individually by the authors or under their supervision. Only minor corrections to the text may have been carried out by the publisher.

No responsibility is assumed by the Publisher, the Editors and Authors for any injury and/or damage to persons or property as a matter of products liability, negligence or otherwise, or from any use or operation of any methods, products, instructions or ideas contained in the material herein. The Publisher does not necessarily endorse the ideas held, or views expressed by the Editors or Authors of the material contained in its publications.

© WIT Press 2011

Printed in Great Britain by Martins the Printers.

All rights reserved. No part of this publication may be reproduced, stored in a retrieval system, or transmitted in any form or by any means, electronic, mechanical, photocopying, recording, or otherwise, without the prior written permission of the Publisher.

Preface

This book contains most of the papers presented at a meeting held in Riga on two important topics, i.e. the study and modelling of Environmental Health Risk and Biomedical problems.

While some of the sessions were specifically aimed at one of these two streams of the meeting, there were several joint sessions of common interest. The interdisciplinary nature of the conference helped to achieve a better understanding of the health problems facing our society and how they can be solved using modern technology.

We live in a world of unprecedented changes. Life on the Earth is fragile, and every living being can continue to exist only in the environmental conditions optimal for its life. There is a common view that the progress of the human civilization is measured by, among other indicators, progress in science, urbanization, ability of the agriculture, industry, and transportation to provide means for more comfortable life. This is understandable and many choose urban over rural life because of the various advantages that the life in cities offers. However, in many cases, the closer one is to the cities, the risks to health due to air pollution, traffic, radiation fields, noise, and many other factors increase. This observation underlines the impact of the industrialization, urbanization and other anthropogenic activities on the environment. There is now a growing awareness of the negative effects of the technological development on the environment and on human health due to exposure to environmental contaminants. One of the highest current priorities of society is to create a more sustainable way of future development with less detrimental impacts.

The field of environmental health is defined by the problems faced and by the specific approaches used. These problems include, amongst many others, the treatment and disposal of liquid and airborne wastes, the elimination or reduction of stresses in the workplace, purification of water supplies, the impacts of overpopulation and inadequate or unsafe food supplies, and the development and

use of measures to protect the population from being infected with a variety of diseases.

Related topics included in the first part of this volume deal with sessions on environment problems such as air and water contamination; health effects associated with buildings, toxicology and disease studies. Of special interest are the papers on food safety and occupational hazards. The contributions also include research presentations on risk prevention and monitoring.

The second part of the book deals with the development of computational tools for the solution of medical and biological problems. The use of mathematical ideas, models and techniques is rapidly growing and is gaining prominence through the biosciences. The field of computational biology emerged from the need to integrate multicomponent biological systems and establish missing functional links among them. Applied mathematicians and bioengineers working alongside bioscientists provide a quantitative description to intricate processes at the subcellular, cellular and tissue levels and integrate them in “viable” models. Such models uphold gnostic properties, offer an invaluable insight into hidden and experimentally inaccessible mechanisms of organ function and allow the researcher to capture the essence of dynamic interactions within it.

Studies are presented on the solution of physiological processes and the very important case of the simulation of cardiovascular systems. One of the most successful areas of bioengineering has been biomechanics and orthopaedics, which are topics studied in several of the papers contained in the volume. The book ends with a section on data acquisition and analysis.

This book is aimed at scientists and engineers working in the challenging area of biomedicine and health. It comprises a series of state of the art presentations which describe some of the many advances made in these fields.

The Editors are grateful to the members of the International Scientific Advisory Board for their help to select the papers and in particular to all authors for their outstanding contributions.

The Editors,
Riga, 2011

Contents

Part 1 – Environmental Health

Section 1: Air pollution

Vegetation fires and release of radioactivity into the air <i>F. P. Carvalho, J. M. Oliveira & M. Malta</i>	3
Assessment of diesel particulate matter exposure among underground mine workers <i>D. Bertolatti, K. Rumchev & B. Mullins</i>	11
An investigation into the association of ozone with traffic-related air pollutants using a quantile regression approach <i>S. Munir, H. Chen & K. Ropkins</i>	21
A choice experiment approach to the valuation of air pollution in Mashhad, Iran <i>M. Ghorbani, S. Kulshreshtha & A. Firozarea</i>	33

Section 2: Risk prevention and monitoring

Multiscale comparison of air quality modeling for an ozone occurrence during the 1996 Paso Del Norte Ozone Campaign <i>D. Lu, R. S. Reddy, R. Fitzgerald, W. R. Stockwell, Q. L. Williams & P. B. Tchounwou</i>	47
---	----

Breaking the connections: reducing and removing environmental health risk in the Canadian nuclear power industry <i>J. Eyles & J. Fried</i>	59
Disaster management and generational complacency: five crucial lessons <i>E. G. Bianchi</i>	69
Generic mapping of human activity-based exposure scenarios to petroleum hydrocarbon contaminants in an oil producing area of the Niger Delta region of Nigeria <i>W. J. Shittu, C. P. Nathanail & R. J. Abrahart</i>	79
The development of a model of pandemic preparedness planning utilizing critical success factors from the United States and the European Union <i>Y. Draine, J. Johnson, M. Levy & W. Sumrall</i>	91

Section 3: The built environment and health

Thermal comfort in operating rooms: a case study <i>F. Patania, A. Gagliano, F. Nocera & A. Galesi</i>	105
Modeling vapor intrusion processes and evaluating risks using subslab data <i>E. M. Suuberg, Y. Yao, R. Shen, O. Bozkurt & K. G. Pennell</i>	115
Assessment of fungal contamination in a Portuguese maternity unit <i>C. Viegas, R. Sabino, C. Veríssimo & L. Rosado</i>	127
Respiratory toxicity of <i>Aspergillus versicolor</i> : the most common indoor mould in Slovakia <i>E. Piecková, M. Hurbánková, S. Černá, M. Majorošová, Z. Kováčiková & D. Pangallo</i>	135
Environmental health issues in the wake of a major earthquake in West Sumatra, Indonesia <i>D. Fanany</i>	147

Section 4: Toxicology analysis

Breath odor characteristics after drinking alcoholic beverages and health monitoring <i>T. Oyabu</i>	161
---	-----

Cell-based bioassay for compounds with prooxidant activity <i>M. Thomas & L. Benov</i>	171
---	-----

Synthetic musks fragrances in the aquatic environment: <i>in vitro</i> toxicological studies of their biotransformation and potential negative effects <i>S. Focardi, C. Della Torre, M. Monti, T. Biagini & I. Corsi</i>	183
--	-----

Section 5: Food safety

Evaluation of QMRA performance for <i>Listeria monocytogenes</i> in cold smoked salmon <i>V. Popov, H. L. Lauzon, M. N. Haque, F. Leroi & R. Gospavic</i>	197
---	-----

Study of mutagenic effects of a packaging system with oxygen absorbers on sweet bakery products <i>R. A. Sueiro, M. J. Garrido & M. Araujo</i>	209
--	-----

Section 6: Occupational health

Work conditions and occupational morbidity in Latvia <i>M. Eglite, I. Vanadzins, L. Matisane, M. A. Bake, D. Sprudza, Z. Martinsone, I. Martinsone, J. Reste, J. Cirule & A. Seile</i>	221
---	-----

Occupational exposure to volatile organic compounds in the Portuguese printing industry <i>S. Viegas</i>	233
--	-----

Dioxins in remediation workers <i>C. Winder & G. Smith</i>	241
---	-----

Section 7: Ecology and health

Eco-biosociocultural H5N1 disease model in Egypt <i>S. L. Wilson & N. Oushy</i>	255
--	-----

Some aspects of reproductive health and metabolic disturbances in pregnant women and their newborn in ecologically injurious conditions of an industrial city in the Urals <i>L. A. Kovalchuk, A. E. Tarkhanova & A. A. Tarkhanov</i>	267
--	-----

Section 8: Water quality issues

Groundwater quality on a waste disposal area due to sand mining activities in São Paulo State, Brazil
D. M. Bonotto & E. G. de Oliveira 279

Ecological effects of underwater destruction of detonators in Lake Ormtjärn, Sweden: the impact from lead
B. E. Liljedahl, U. Qvarfort, R. Berglind & J. Sjöström 291

Part 2 – Biomedicine

Section 9: Cardiovascular system

Correlation of morphological parameters with likelihood of thrombus formation in intracranial aneurysms
K. Shimano & Y. Nakagawa 309

Dominant EEG frequencies of patients undergoing dobutamine stress test
A. K. Macpherson, S. Neti, M. Averbach, P. A. Macpherson & C. Chutakositkanon 323

Numerical evaluation of the slope and intercept of end-systolic pressure-volume relation
R. M. Shoucri 333

Modelling of embolus transport and embolic stroke
I. D. Šutalo, A. Bui, K. Liffman & R. Manasseh 347

Section 10: Biomechanics

Indoor motion analysis of a subject wearing prosthesis for adaptive snowboarding
L. Gastaldi, S. Pastorelli, M. Caramella & U. Dimanico 361

Do lateral dominance, body mass, body height and direction of perturbation influence the Lehr's damping ratio, which characterizes the balancing ability on an unstable oscillatory platform?
R. M. Kiss 373

Synthetic organs for transplant and bio-mimic reactors for process intensification using nano-structured micro-porous materials
E. M. Akay, Z. Okumus, O. S. Yildirim, M. A. Bokhari & G. Akay 383

Section 11: Simulation of physiological processes

A dynamic model of the pregnant myometrial fasciculus
R. Miftahof & N. Akhmadeev..... 397

Inverse dynamic model of the pupil muscle plant in the simulation of
response to sound, stimuli and hippus
E. Suaste Gómez & H. Reyes Cruz..... 407

Section 12: Orthopaedics and bone mechanics

Identification of landmarks on lower limb joint from CT images for
kinematics studies: a totally semi-automatic procedure
M. Giorgi, B. Innocenti, L. Labey, A. Audenino & C. Bignardi..... 417

The effect of time on the results of children's spine examinations
M. Takács, E. Rudner & R. M. Kiss..... 427

Section 13: Data acquisition and analysis

Association rule derivation for side effects of medical supplies and
its application
H. Shiroyama, Y. Zuo & E. Kita 439

Estimation of biophysical and functional properties of artery walls
from pulse wave measured by photoplethysmography
M. Huotari, K. Määttä & J. Kostamovaara..... 449

Statistical parameter estimation and signal classification in
cardiovascular diagnosis
S. Bernhard, K. Al Zoukra & C. Schütte..... 457

MRI: a tool for measuring turbulent intensities in flow systems
O. Adegbite, L. Kadem & B. Newling..... 471

Author index 483

This page intentionally left blank

Section 1

Air pollution

This page intentionally left blank

Vegetation fires and release of radioactivity into the air

F. P. Carvalho, J. M. Oliveira & M. Malta

Nuclear and Technological Institute,

Department of Radiological Protection and Nuclear Safety, Portugal

Abstract

Naturally-occurring radionuclides, such as those of the uranium and thorium series, as well as artificial radionuclides, are accumulated in plants generally in low concentrations. Summer vegetation fires release these natural and man-made radionuclides into the atmosphere. Concentrations of uranium isotopes ^{238}U , ^{235}U , ^{234}U , ^{232}Th , ^{230}Th , ^{226}Ra , ^{210}Pb and ^{210}Po were measured in smoke from wild vegetation fires. It is shown that radionuclide concentrations in smoke particles are enhanced about 100 times in comparison with the vegetation of the area and with reference aerosols. Smoke particles were particularly enriched in ^{210}Po , and displayed $^{210}\text{Po}/^{210}\text{Pb}$ activity concentration ratios always above unity and up to 12, while in common aerosols $^{210}\text{Po}/^{210}\text{Pb}$ is always <1 . Inhaled smoke particles from vegetation and forest fires may contribute to enhanced radiation doses in the human lung.

Keywords: naturally-occurring radionuclides, polonium, radioactivity in plants, vegetation fires.

1 Introduction

Every year, especially in the inter-tropical and temperate regions a high number of wild forest and vegetation fires causes loss of property and natural resources. The wild vegetation and forest fires release into the atmosphere large quantities of volatilized substances and particulate matter, aggravated by those from man made fires either for combustible control, agriculture fires, and plant biomass burning for heat production, all of them with an impact on atmospheric chemistry and a potential impact on climate change [1, 2]. Recent studies have increasingly focused on the impact of fire emissions on human health and



especially on the diseases of the respiratory tract in firemen and on the population at large [3].

More than 200 substances have been identified in the composition of smoke from forest and vegetation fires [3, 4]. Amongst them were investigated as health damaging substances the carbon monoxide, respirable particles, formaldehyde, acrolein, benzene, and toluene. NO_x compounds and metals are also released into the air by the bush fires, although not much information on these has been obtained as yet [3]. The burn of wood and other plant materials (e.g., tree bark) for heat production both at industrial scale as well as in fireplaces at home have been investigated as sources of exposure to toxic compounds in the indoor air [5].

Radionuclides are a group of elements that were addressed rarely in the studies related to fire smoke exposure, with the exception of concerns with radioactive caesium, mainly ¹³⁷Cs, from the Chernobyl accident and deposited in soils in Ukraine and Belorussia [6]. Forest fires occurring in Spring and Summer in those regions of the Eastern Europe, have re suspended ¹³⁷Cs formerly deposited on soils and allowed for atmospheric transportation and the detection of enhanced ¹³⁷Cs activity peaks in the air at neighbour countries [6, 7].

Besides artificially produced radionuclides, such as ¹³⁷Cs, the bush vegetation and forest trees (tree trunks and leaves) contain naturally-occurring radionuclides that they absorb from the soil and from the surface air. Although these concentrations are generally low, the burning of plant biomass has tremendously increased in recent years in Europe. In Portugal alone, during the last decade wild fires burned in average 150 000 ha per year, which represented 50% more than the annual average area burned in the previous decade. This has been the common trend around the Mediterranean basin, creating an extended exposure of large populations to smoke from vegetation and forest fires in the region.

This paper reports on naturally occurring radionuclides present in smoke particles from vegetation fires in Portugal and makes a comparison with the cigarette smoke as a preliminary step to the health risk assessment of exposure to smoke from vegetation fires.

2 Materials and methods

2.1 Sampling methods

Wild vegetation fires were sampled in September 2010 in collaboration with firemen in the rural areas of the North of Portugal (Montalegre, Trás os Montes). The surveyed fires burned wild bush areas with reduced forest (soil cover by trees less than 10%), but with dense Mediterranean “maquis” vegetation type. Several fires were monitored and surface air samples collected at around 1 m above the ground, either near the fire front (flames) or in areas several hundred meters away from the fire front in the smoke plume.

The aerosol samples from the fire front, naturally comprising mainly smoke particles and fly ash, were collected using a portable battery powered vacuum pump (F&J Specialty, USA) with digital control of flow rate, total volume and



sampling time. Aerosol samples were collected on Whatman microfiber glass filters (average 0.7 μm pore size) of 5 cm diameter.

Aerosol samples away from the fire front were collected with high volume samplers from F&J Specialty and Andersen. Typically, each sample corresponded to about 100 m^3 of air volume filtered. Air samplers were used as fixed monitoring stations and powered with a portable electric generator. Filters used were respectively circular filters with 9 cm diameter and rectangular filters of 20x25 cm, microfiber glass (Whatman). All filters were pre weighted and weighted again after the sampling and oven drying at 60°C in order to determine the amount of particulate material collected. This enabled to calculate the radionuclide concentrations per weight of aerosol particulates and per unit of air volume filtered.

In the same region monitored for vegetation fires, vegetation samples, including thorny bush, leafy green vegetation, and leaf litter were collected. These samples were dried, homogenized and sample aliquots analyzed for radionuclide concentrations.

2.2 Analytical methods

Radionuclide analysis targeted the alpha emitting radionuclides of the uranium and thorium series, namely ^{238}U , ^{235}U , ^{234}U , ^{232}Th , ^{230}Th , ^{226}Ra , ^{210}Po and ^{210}Pb . In the beginning of the analytical procedure, to each sample were added isotopic tracers (^{232}U , ^{229}Th , ^{224}Ra , ^{209}Po , and stable Pb^{2+}) to allow the quantification of the radiochemical yield. After separation and purification, each radioelement was electroplated onto a stainless steel disc (replaced by an Ag disc for polonium) and the radioactivity emitted from the disc measured with ion implanted silicon detectors and an alpha spectrometer OctetePlus (Ortec EG&G). The methods used were previously described and validated [8, 9]. The quality assurance of the results was regularly controlled with the analysis of certified reference materials and participation in international intercomparison exercises organized by the International Atomic Energy Agency with good results [9].

3 Results

Figure 1 shows the results for two radionuclides, ^{210}Pb and ^{210}Po in aerosol particles collected on small diameter microfiber glass filters near the fire front. One aerosol reference sample was collected in the absence of fires and the particle load recorded, mainly made of re-suspended soil dust, was the lowest, 0.21 mg/m^3 . The radionuclide concentrations and the $^{210}\text{Po}/^{210}\text{Pb}$ activity concentration ratio in this reference sample, 0.30, was in the range of $^{210}\text{Po}/^{210}\text{Pb}$ ratios in surface air (average ratio 0.19, range 0.03-0.78), previously reported for the Lisbon area [10]. The other aerosol samples were collected very close to the vegetation fires. The particulate concentration in the air varied from sample to sample, as smoke does in the fire zones. Concentrations of both radionuclides in the smoke samples increased in average by a factor of about 100 compared to the reference sample. Moreover, in all these smoke samples the ^{210}Po concentrations



were systematically higher than those of ^{210}Pb , with $^{210}\text{Po}/^{210}\text{Pb}$ ratios up to 12. Radionuclides were clearly associated with the smoke and fly ash particles produced by the vegetation fire and the activity concentration ratios were the reverse in comparison with the reference aerosol sample (<1) due to much higher ^{210}Po concentrations in the smoke compared to those of ^{210}Pb .

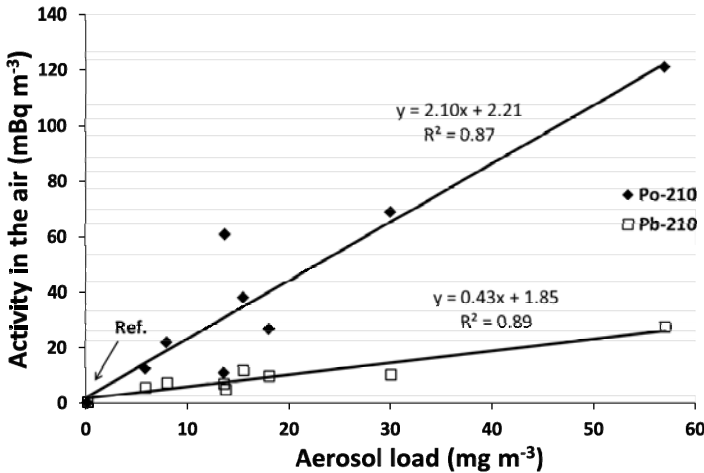


Figure 1: Polonium (^{210}Po) and radioactive lead (^{210}Pb) concentrations in the surface air and their increase with the load of smoke particles from vegetation fires, near the fire. The first sampling point (included in the regression fits) is from a reference aerosol. Correlations are statistically significant at $p < 0.001$.

Filters with large volume samples were analyzed for the entire set of alpha emitting radionuclides targeted in this study. Results are partly displayed in Figure 2. Concentrations of all radionuclides per unit of air volume ($\mu\text{Bq}/\text{m}^3$) increased in the smoke of vegetation fires in comparison to the reference aerosol sample. Specific activity of radionuclides (Bq/kg aerosol particulates) increased also in the smoke particles in comparison with the reference aerosol. This increase in aerosol specific activities was in average 10 times higher for uranium isotopes, ^{230}Th , and ^{226}Ra . ^{232}Th , the parent radionuclide of the thorium series, which is a good indicator of soil dust re-suspension, was present in the smoke in specific activities either similar or slightly higher than in the reference aerosol. A slight increase may be due to dust re-suspension in the fire zone caused by the hot air and atmospheric turbulence. Nevertheless, ^{232}Th in smoke particles was always lower than ^{238}U , ^{230}Th , and ^{226}Ra released from the vegetation by the combustion. Specific activities in smoke particles were higher for ^{210}Po and ^{226}Ra than for other radionuclides, such as uranium and thorium isotopes. This is likely related to the lower volatilization temperature of polonium and radium in comparison with the other radioelements.

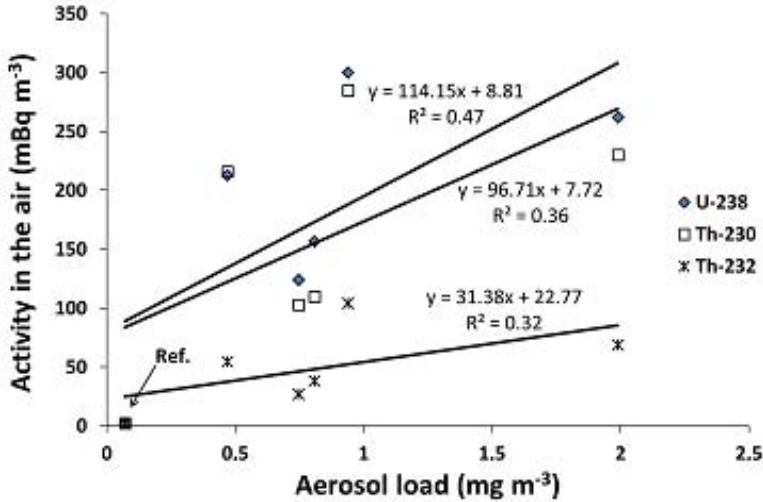


Figure 2: Increase of activity concentrations of radionuclides ^{238}U , ^{230}Th , ^{232}Th , in surface air with the increase of the load smoke particles from vegetation fires in the region. The first sampling point (included in the regression fits) is from a reference aerosol. Correlation fits are statistically significant at $p < 0.20$ only.

Data for several types of vegetation and leaf litter from the region of surveyed fires are shown in Table 1. Concentrations of radionuclides were all low and, on a mass basis, much lower in vegetation than in smoke particles released by the vegetation fires.

Table 1: Radionuclide concentrations (Bq kg^{-1} dry weight) in the vegetation and leaf litter of the region investigated. Uncertainties of concentrations are about 5%.

	^{238}U	^{235}U	^{234}U	^{230}Th	^{226}Ra	^{232}Th
Thorny bush #1	0.00142	5.90E-05	0.00144	0.0016	0.066	0.00089
Leaf litter #2	6.1	0.27	6.0	7.2	56.1	2.9
Grasses #4	0.94	0.044	0.94	0.90	5.3	0.40
Ferns #5	0.25	0.016	0.22	0.21	13.4	0.097
Leaf litter #6	0.88	0.032	0.89	0.86	7.3	0.42

4 Discussion and conclusions

The vegetation fires release the naturally-occurring radionuclides contained in the vegetation and, although part of them may remain on the ground associated with the ashes, important radionuclide amounts become associated with smoke particles and fly ash released into the atmosphere. From a radiation protection point of view, the naturally occurring radionuclides more relevant to the radiation dose are the uranium series decay products, particularly the alpha emitting radionuclides such as ^{210}Po and ^{226}Ra . On a mass basis (Bq/kg), the smoke from vegetation fires displayed radionuclide concentrations about 100 times higher than a reference aerosol collected in the absence of smoke. The smoke particles were clearly enriched in ^{210}Po and ^{226}Ra in comparison with the reference aerosol and in comparison with non burned bush and leaf litter from the same region.

Inhalation of smoke particles may be harmful by a number of physical-chemical mechanisms as shown by several studies. Evidence was provided that asthma and other respiratory diseases are positively correlated with the exposure to high suspended particulate loads in the air, including smoke from forest fires [11]. The results presented herein indicate that inhalation of smoke from vegetation fires increases the lung exposure to radioactivity, and especially to alpha emitting radionuclides such as the ^{210}Po .

The ^{210}Po concentrations measured in smoke sampled near the vegetation fire front are representative of the smoke inhalation by firemen during fire fighting operations. For ^{210}Po concentrations of 120mBq/m^3 and assuming a one day exposure to the fire smoke, the inhalation of 20 m^3 of air will correspond to the ^{210}Po inhalation rate of 2.4 Bq/day . This value may be compared with the average ^{210}Po inhalation in Lisbon area, of about $6.62 \times 10^{-4}\text{ Bq/d}$, and with the ^{210}Po inhalation of a one-pack-a-day cigarette smoker, 30 mBq/d [10]. The inhalation exposure to the smoke from vegetation fire over a one day may represent for a fireman a ^{210}Po inhalation about 80 times higher than a cigarette smoker and about 4000 times higher than inhalation of atmospheric background ^{210}Po by a member of the public.

These findings clearly show that vegetation fires increase the radioactivity levels in the atmosphere. Smoke particles from vegetation fires may also increase the lung exposure to enhanced levels of alpha emitting radionuclides and, thus, the respiratory tract protection of firemen is needed because also of the presence of carcinogenic radionuclides. The effect of radioactivity in smoke from the vegetation fires on the population at large shall be assessed namely with the support of aerosol particles characterization and measurement of the inhalable fraction.

Acknowledgements

This work was funded by “Fundação para a Ciência e Tecnologia”, Portugal, Research Contract Nr. PTDC/AMB/65706/2006.



References

- [1] Jayasekher, T., Aerosols near by a coal fired thermal power plant: Chemical composition and toxic evaluation. *Chemosphere*, 75, 1525 – 1530, 2009.
- [2] Lazaridis, M., Latos, M., Aleksandropoulou, V., Hov, Ø, Papayannis, A., Tørseth, K., Contribution of forest fire emissions to atmospheric pollution in Greece, *Air Quality, Atmosphere and Health*, 1:143 – 158, 2008.
- [3] Johnston, F.H., Rosalind, J. W., Pilotto, L., Bailie, R.S., Parry, D. L., Halpin, S., Vegetation fires, particulate air pollution and asthma: A panel study in the Australian monsoon tropics. *International Journal of Environmental Health Research*, 16(6): 391 – 404, 2006.
- [4] Vos, A.J.M.D., Reisen, F., Cook, A., Devine, B., Weinstein, P., Respiratory Irritants in Australian Bushfire Smoke: Air Toxics Sampling in a Smoke Chamber and During Prescribed Burns, *Archives of Environmental Contamination and Toxicology*, 56: 380 – 388, 2009.
- [5] Gonçalves, C., Alves, C., Evtugina, M., Mirante, F., Pio, C., Caseiro, A., Schmidl, C., Bauer, H., Carvalho, F., Characterisation of PM10 emissions from woodstove combustion of common woods grown in Portugal. *Atmospheric Environment*, 44 (35), 4474 – 4480, 2010.
- [6] Paatero, J., Vesterbacka, K., Makkonen, U., Kyllonen, K., Hellen, H., Hatakka, J., Anttila, P., Resuspension of radionuclides into the atmosphere due to forest fires. *Journal of Radioanalytical and Nuclear Chemistry*, 282, (2): 473 – 476, 2009.
- [7] Jargin, S., Forest fires in the former Soviet Union: no reasons for radiophobia. *Journal of Environmental Radioactivity*, 102, 218 – 219, 2011.
- [8] Oliveira, J.M., Carvalho, F.P. A Sequential Extraction Procedure for Determination of Uranium, Thorium, Radium, Lead and Polonium Radionuclides by Alpha Spectrometry in Environmental Samples. (Proceedings of the 15th Radiochemical Conference). *Czechoslovak Journal of Physics* 56 (Suppl. D): 545-555, 2006.
- [9] Carvalho F.P., Oliveira, J.M. Alpha emitters from uranium mining in the environment. *Journal of Radioanalytical and Nuclear Chemistry* 274: 167-174, 2007.
- [10] Carvalho, F.P. Origins and concentrations of ^{222}Rn , ^{210}Pb , ^{210}Bi and ^{210}Po in the surface air at Lisbon, Portugal, at the Atlantic edge of the European continental landmass. *Atmospheric Environment* 29 (15): 1809-1819, 1995.
- [11] Carvalho, F.P. ^{210}Po and ^{210}Pb intake by the Portuguese population: the contribution of seafood in the dietary intake of ^{210}Po and ^{210}Pb . *Health Physics* 69(4): 469-480, 1995.



This page intentionally left blank

Assessment of diesel particulate matter exposure among underground mine workers

D. Bertolatti, K. Rumchev & B. Mullins

Curtin Health Innovation Research Institute and

The School of Public Health, Curtin University, Australia

Abstract

Diesel motor emissions are a major source of ultrafine particles as research shows that the particulate fraction of diesel exhaust consists mainly of very small particles, which rapidly agglomerate to form clumps of particles with $<1 \mu\text{m}$ aerodynamic size. Substantial scientific evidence supports that inhalation of emissions from diesel exhaust particulates is associated with a range of adverse health effects. Measurements have shown that underground miners can be exposed to over 100 times the typical environmental concentrations of diesel particulate matter (DPM) and over 10 times the concentration measured in other work environments where diesel engines are common. This paper reports personal and environmental exposures to DPM in an underground mine in Western Australia. The findings demonstrated that the DPM concentration exceeded the provisional 8-hour time weighted average exposure standard of 0.1 mg/m^3 for most of the assessed locations. The elemental analysis indicated high concentrations of silica and iron in DPM which could be potentially associated with some adverse health effects including respiratory illnesses and irritating effects. Thermal comfort underground was also assessed and the results showed non compliance with the standards of the American Society of Heating, Refrigerating and Air-Conditioning Engineers (ASHRAE).

Keywords: diesel exhaust, diesel particulate matter, fine and ultrafine particles.

1 Introduction

Exhaust particles emitted from in-use diesel vehicles in underground mining operations are a major source of ultrafine carbonaceous particles, which have the potential to produce adverse health effects. The particulate fraction of diesel



exhaust consists of fine particles (typically aerodynamic diameter $< 2.5 \mu\text{m}$) including a high number of ultrafine particles (diameter $< 0.1 \mu\text{m}$) that include reactive organic and transition metal components [1].

Particles in the ultrafine size range have attracted significant scientific and medical attention since research shows that for equivalent masses of inhaled particles, ultrafine particles provide a greater surface area for adsorption of potentially toxic substances and metal agents. Further to this, ultrafine particles have also a higher deposition probability particularly in small airways and the alveolar region of the lungs than coarse particles. With regards to health outcome, the small particle size of diesel particulate matter (DPM) is considered a significant health issue as such particles can penetrate deep in the lungs [2–4]. In 1988, the National Institute of Occupational Safety and Health (NIOSH) [5] recommended that diesel exhaust be regarded as a “potential occupational carcinogen”. Similarly, in 1989, the International Agency for Research on cancer declared that “diesel engine exhaust is probably carcinogenic to human” [6]. Measurements have shown that underground miners can be exposed to over 100 times the typical environmental concentrations of diesel particulate matter (DPM) and over 10 times the concentration measured in other work environments where diesel engines are common [7–9].

Based on the current research evidence, the US National Research Council has concluded that the NIOSH Research Mining Program, related to exposure of DPM and related health effects, is considered as a high priority with a rating of four on a five-point scale [10]. Furthermore, evidence is increasingly being accumulated which suggests that nanoparticles (such as diesel soot which typically has a primary particle size $< 50 \text{ nm}$) affect health as a function of surface area rather than mass [11].

The study assessed personal and environmental exposures of diesel particulate matter (DPM) in an underground mine using various sampling system that included, low pressure cascade impactor (Nano-MOUDI-II) and scanning mobility particle size (SMPS) measurements. This research forms part of a wider study with the major milestone to reduce exposure levels of diesel particulate matter (DPM) and improve the air quality underground.

2 Methods and materials

The study was undertaken in a large underground mine in north-western Australia. The experimental method was designed to: (a) accurately measure DPM in real-time at representative locations, (b) collect size-fractionated DPM and other particulate for gravimetric measurement and analysis, (c) determine worker exposure levels.

2.1 Apparatus

The experimental apparatus consisted of, a NanoMOUDI 125B multi-stage low pressure impactor (MSP, Shoreview, MN, USA), a Scanning Mobility Particle Sizer (SMPS) consisting of a TSI 3081 Differential Mobility Analyzer (DMA)



and TSI 3775 Condensation Particle Counter (CPC) (TSI, Shoreview, MN, USA), a TSI DustTrak 8533 DRX, with a TSI P-Trak, TSI Velocicalc-Plus used to obtain air velocity, temperature and humidity measurements. Four SKC air pumps and filters were utilized for personal monitoring of mine-worker exposures. NIOSH method 5040 (Elemental Carbon) was applied to quantify elemental carbon (EC) via thermal-optical analyzer. Samples collected using the NanoMOUDI were analysed for elemental composition of by Scanning Electron Microscopy (SEM) Analysis and performed by the ChemCentre of WA. Analysis of organic species and PAHs was also undertaken.

2.1.1 Methods

Measurement sites were established at 4 representative locations within the mine:

Site 1 – The main fresh air inlet (baseline measurement) for the mine.

Site 2 – A dead-end passage at the base of the tunnel network with no airflow.

Site 3 – An active area of the mine where material extraction was actively occurring.

Site 4 – A site near the main air outlet from the mine.



Figure 1: Sampling equipment located on mine vehicle, in location at site 1.

Samples were taken at a height equivalent to the roof level of the vehicle. Sampling commenced at least 30 minutes after the vehicle was placed into position. The NanoMOUDI is not visible in image. Measurements were also taken above ground to compare with the fresh air inlet values.

At each site 1-4, measurements were taken continuously for a period of 6–14 hours. During each measurement, the NanoMOUDI, DustTrak and P-Trak were set to measure continuously. The SMPS was set to perform repeated scans between 15 nm and 950 nm at intervals of approximately 15 minutes. At the end of each measurement the equipment was taken to a clean laboratory on the surface where samples/filters could be removed and weighed, and data

downloaded, etc. At the start of each working shift, three workers were fitted with personal samplers, selected based on their proximity to the sampling location. The samplers were collected after 8 hours and the filters removed for analysis. For the time period where samples were being collected, information on vehicle movements and vehicle locations were obtained from the mine telemetry/logistics system. This made it possible to track vehicle movement past the sampling location.

3 Results and discussion

Table 1 shows the airflow, temperature and humidity values recorded at each sampling location.

Table 1: Environmental conditions at each sampling location.

Site	Location	Mean Temp (°C)	Mean R.H. (%)	Mean Air Vel. (m/sec)
1	Fresh air inlet	11.7	75%	2.01
2	Dead end tunnel	36.5	98%	0.17
3	Active extraction	30.2	83%	0.18
4	Near air exhaust	31.1	90%	0.57
Recommended range (ASHRAE 2004)		21–26	30–70	0.1–0.2

It will be noted that humidity levels are extremely high. This was due to a combination of evaporative cooling of the mine intake air, water sprays for dust suppression within the mine, and also artesian water which enters the mine and evaporates. It will be noted that relative humidity and temperature in the dead end tunnel were both exceptionally high. During the time of the measurement campaign, the mine was operating at approximately 30% of its typical operating capacity, due to the global financial crisis reducing demand/value of the mine production. Therefore particulate levels measured during this campaign could be expected to be near the lower levels of typical worker exposure.

3.1 Personal monitoring

Table 2 shows the results for personal monitoring, for sites 1, 3 and 4, averaged over 8 hours. Site 2 did not have any workers in the area while sampling was conducted, hence no data was possible.

The samplers were fitted to workers at the start of each shift. Workers would typically spend the first hour or more of each shift above ground, and then may come above ground for lunch and other breaks (though this is not enforced and underground refuge areas are often used for breaks). The vehicle operators have air conditioned vehicle cabins; however some choose to operate their vehicles with the windows open. The drill vehicles are the only electric vehicles in the



Table 2: Personal exposure to DPM (measured as elemental carbon).

Site	Worker	Elemental Carbon (mg/m ³)
1	Loader (“Bogger”) driver	0.06
	Truck driver	0.03
	Fixed position	<0.002
3	Assistant driller	0.03
	Drill vehicle driver	0.03
	Fixed position	0.05
4	Explosives technician	0.078
	Service/breakdown mechanic	0.11
	Fixed position	0.085

mine, which accounts for the low exposure of the driller and assistant driller. The underground service/maintenance mechanics and the explosives technicians are the only workers who are usually required to spend extended periods out of a vehicle in the mine, which accounts for the elevated readings for these workers. However these latter two types of workers drive between tasks in air conditioned 4x4 vehicles.

3.1.1 Stationary sampling results

Table 3 below shows the PM 1 levels measured by NanoMOUDI. This was selected as it is the size range which includes almost all DPM. EC values have also been determined from the total gravimetric measurements of PM 1. The aerosol in the mine was found to be bimodal. There existed a sub-micron peak, which consisted almost entirely (>99% by mass) of DPM, and a super-micron peak (at approximately 2-5 microns), which consisted of crustal materials from the mine, combined with high levels of silica (likely from the spray-concrete used to secure the ceiling and walls of the mine).

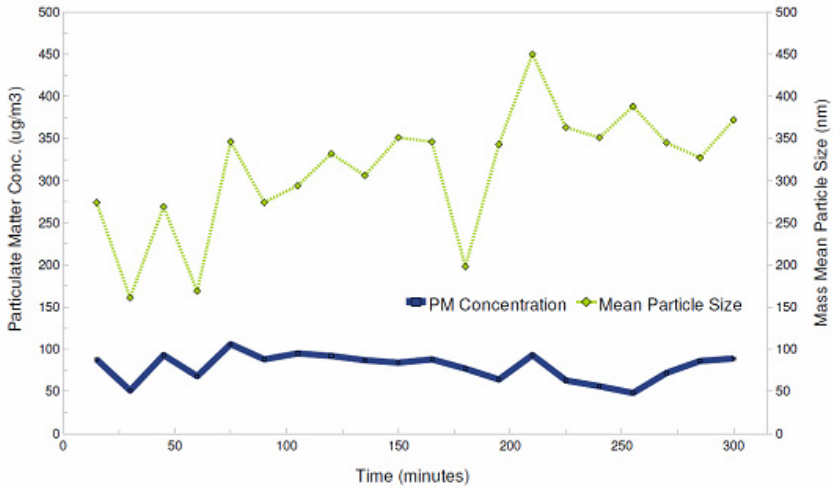
Table 3: PM1 and DPM levels as measured by NanoMOUDI.

Site	Sampling Time (hours: mins)	Average PM1 conc. (mg/m ³)	EC (mg/m ³)
1	6:00	0.08 mg/m ³ *	0.03 mg/m ³ *
2	8:50	0.11 mg/m ³	0.09 mg/m ³
3	6:55	0.16 mg/m ³	0.13 mg/m ³
4	14:10	0.12 mg/m ³	0.10 mg/m ³

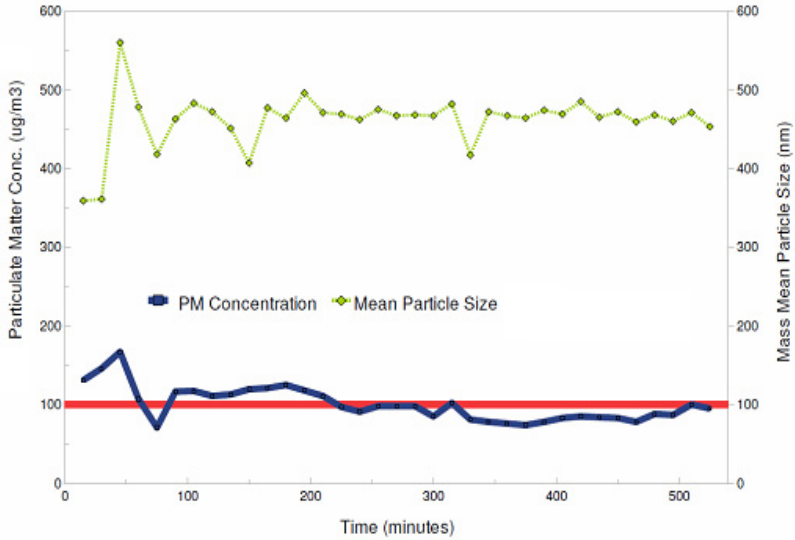
*A high level of elemental carbon was present in the intake air due to wildfires in the vicinity of the mine preceding the sampling period.



It can be observed that a nontrivial proportion of the (clean) intake air was elemental carbon. This was believed to largely be due to recent wildfires, rather than vehicle movement on the surface. It will be noted that the average levels are very high, despite the fact that the mine was operating at approximately 30% of normal production levels.



(a)



(b)

Figure 2: Time dependent mass and size of PM 1 (DPM) as measured using the SMPS. (a) Site 1, (b) Site 2, (c) Site 3. The red line denotes the time weighted DPM exposure limit of 0.1 mg/m³.



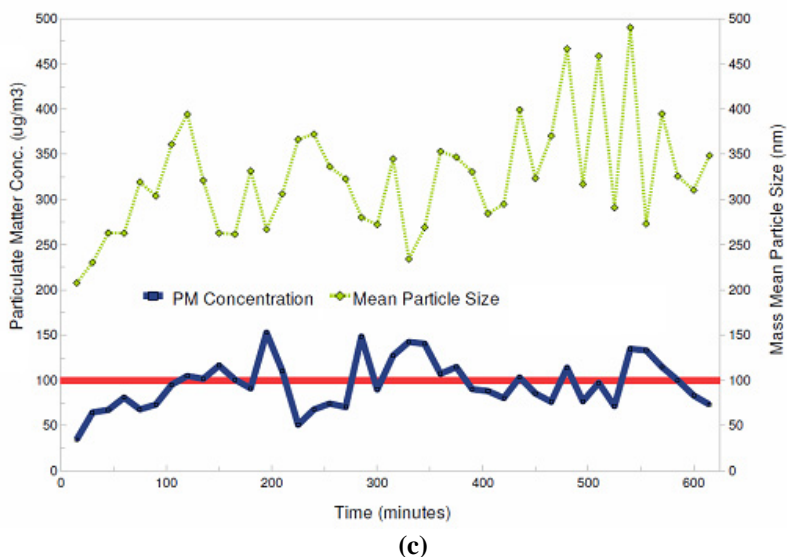


Figure 2: Continued.

Figure 2(a-c) shows the temporal evolution of PM 1 at sites 1–3. It can be observed that at sites 1 and 2 the values were relatively stable, as site 1 has a constant airflow of air which has passed through a filtration and conditioning system, and Site 2 has a low airflow and a very low air exchange rate. Site 3 however, had a mine vehicle (loader/bogger) working in close proximity to the sampling apparatus. It will be observed that an increase in particle mass often corresponds to a decrease in particle size. The mine telemetry data showed that these samples coincided with the loader passing by the sampling location, resulting in a high concentration of smaller particles which had just been emitted from the exhaust, and had not had sufficient time to dissipate or agglomerate.

3.1.2 Elemental composition of PM

An elemental analysis of the PM collected by the NanoMOUDI was also performed. The total particulate matter values for all size classes have been combined. Over 50% of the inorganic contaminants were found in the PM 2.5 fraction.

It can be observed that high levels of Silica and Iron were present, with levels of vanadium also elevated. The Silica is likely due to the concrete which is sprayed onto the walls and ceiling of the mine to ensure structural integrity. Overall, both the DPM and inorganic levels in the mine particulate are of concern. Overall TSP and PM10 levels were not significant, as the mass of larger particles is kept low due to water sprays, gravitational settling and the humidity in the mine.

Table 4: Inorganics found in PM10. Site 1–4 values are averages over the sampling period in mg/m³.

Element	TWA (NIOSH)	Site 1	Site 2	Site 3	Site 4
Magnesium (mg/m ³)	10 mg/m ³	0.002	0.005	0.002	0.005
Nickel (mg/m ³)	0.015 mg/m ³	0.001	0.003	0.004	0.005
Silica, (mg/m ³)	0.05 mg/m ³	0.050	0.044	0.071	0.073
Vanadium dust (mgV/m ³)	0.05 mgV/m ³ (15 min)	0.001	0.002	0.005	0.005
Iron (mg/m ³)	0.23 mg/m ³	0.056	0.127	0.202	0.195

In general, both the DustTrak and the SMPS showed a reasonably good agreement with each other and with the SMPS, generally within 10%. However both the DustTrak and especially the SMPS showed elevated mass levels at sites 2 and 4, likely due to condensed water on the aerosol particles. This was not a problem for NanoMOUDI samples were weighed and analysed in a dry state.

Direct reading instruments such as the DustTrak should always be calibrated against a gravimetric standard. For the mine in question, it would be advisable to fit a diffusion dryer before the sample inlet, so as to remove excess moisture, allowing the dry particle mass to be measured. The work showed that a P-Trak is unsuitable for DPM measurement as DPM mass was often inversely proportional to number concentration.

As mentioned, the mine was operating at only 30% of its usual capacity while the measurements were performed. It could be expected that the DPM values could triple once production is scaled back up at the mine. However, the ventilation and air conditioning system (or at least the fans which supply the air) were reportedly operating at 100% capacity. Due to the humidity, temperature and DPM problems which were found, significant remedial action is required.

4 Conclusion

This work provided a comprehensive evaluation of the DPM and PM levels in an underground mine, including the spatial and temporal information, as well as composition analysis.

Very high levels of DPM were found in the mine, which are likely to only increase once production levels are increased. There was however a slight disconnect between mine average DPM and worker exposure, as worker practices differ, and some workers spend most of their time in air conditioned cabs.

For the mine in question, optimisation of the ventilation system would be advisable, couples with engineering controls such as additional filtration or particulate removal/agglomeration technology. Further study into DPM levels in Australian mines and the formulation of binding exposure limits is warranted.

References

- [1] Wichmann, H.E., Diesel Exhaust Particles. *Inhalation Toxicology*, **19(Suppl.1)**, pp. 241-244, 2007.
- [2] Mühlfeld, C., Rothen-Rutishauser, B., Blank, F., Vanhecke, D., Ochs, M. & Gehr, P., Interactions of Nanoparticles With Pulmonary Structures and Cellular Responses. *American Journal of Physiology - Lung Cell Molecular Physiology*, **294(5)**, pp. L817-L829, 2008.
- [3] Diesel Exhaust: A Critical Analysis of Emissions, Exposures, and Health Effects. A Special Report of the Institute's Working Group; Health Effects Institute Web Site, pp. 294, 1995. [pubs.healtheffects.org/view.php?id= 11](http://pubs.healtheffects.org/view.php?id=11)
- [4] Pope, A., Burnett, R., Thun, M., Calle, E., Krewski, D., Ito, K. & Thurston, G., Lung Cancer, Cardiopulmonary Mortality, and Long-Term Exposure to Fine Particulate Air Pollution. *Journal of the American Medical Association*, **287(9)**, pp. 1132-1141, 2002.
- [5] Carcinogenic Effects of Exposure to Diesel Exhaust; National Institute of Occupational Safety and Health (NIOSH), Current Intelligence Bulletin 50, 1988, Cincinnati, Ohio, www.cdc.gov/niosh/88116_50.html
- [6] Monographs on the Evaluation of Carcinogenic Risks to Humans Diesel and Gasoline Engine Exhausts and Some Nitroarenes; World Health Organisation, International Agency for Research on Cancer website, 46, p. 458, 1989, Lyon, France. monographs.iarc.fr/ENG/Monographs/vol46/volume46.pdf
- [7] Cantrell, B.K. & Watts, W.F., Diesel Exhaust Aerosol: Review of Occupational Exposure. *Applied Occupational and Environmental Hygiene*, **12(12)**, pp 1019-1026, 1997.
- [8] Cash, D. & Baughman, W., DPM exposure in metal and nonmetal mines in the United States 2002-2005 and the 2005 Final Rule on the Interim Limit. *Proceeding of Mining Diesel Emissions Conference (MDEC)*, Markham, Ontario, October 12-14, 2005.



- [9] Bugarski, Schnakenberg & Patts, Implementation of Diesel Particulate Filter Technology in Underground Metal and Nonmetal Mines; National Institute for National Safety and Health, Centre for Disease Control Web Site, Pittsburgh, USA, www.cdc.gov/niosh/mining/pubs/pdfs/iodpf.pdf
- [10] Mining Safety and Health Research at NIOSH: Reviews of Research Programs of the National Institute for Occupational Safety and Health. NISBN: 0-309-66636-8, National Academies Press: Washington DC, 2007.
- [11] Biswas, P. & Wu, C. Nanoparticles and the environment. *Journal of the air & waste management association*, **55(6)**, pp. 708-746, 2005.



An investigation into the association of ozone with traffic-related air pollutants using a quantile regression approach

S. Munir, H. Chen & K. Ropkins

Institute for Transport Studies, University of Leeds, UK

Abstract

Ground-level ozone (O_3) is one of the most harmful air pollutants due to its adverse effects on human health, agricultural crops, biodiversity and materials. Ozone is a secondary air pollutant and interacts with meteorological variables as well as with many other air pollutants such as nitric oxide (NO), nitrogen dioxide (NO_2), particles ($PM_{2.5}$), and carbon monoxide (CO). This paper intends to investigate the relationship of ozone with these air pollutants and lagged ozone (previous day ozone) at a roadside monitoring site in Leeds UK. A quantile regression approach has been applied, which is suitable for the non-normal ozone distribution and capable of handling nonlinearities in the associations of ozone with its predictors; as it examines the entire distribution of the variables rather than a single measure of central tendency (mean or median). Our results show that lagged ozone has positive, whereas NO, NO_2 and CO have negative associations with ozone. $PM_{2.5}$ is negatively correlated with ozone at lower quantiles (below 0.6) and the relationship becomes positive at upper quantiles (0.6 and above), perhaps indicating more complex interactions. Also, it is shown that the effect of explanatory variables on ozone concentrations is a function of quantiles and hence the behaviour and interaction of the covariates with ozone change at different regimes of ozone concentrations, information which is normally hidden in the traditional regression models. Further statistical analysis demonstrates that for some air pollutants the nature of relationship (negative or positive) between ozone and its predictors remains unchanged and only the strength changes, for others nature and strength both change at different quantiles. The study explores the impacts of traffic-related air pollutants on ground level ozone concentrations and suggests the use of quantile regression



approach for ozone and air quality data analysis as an alternative to traditional regression models.

Keywords: quantile regressions, ozone, air pollutants, NO_x, CO, PM_{2.5}, lagged ozone.

1 Introduction

Background ozone concentrations over the last 20 years (1987 to 2007) have increased [1–3]. This increase in baseline concentrations is attributed to long distance migration of ozone from across the North Atlantic [2]. At the same time Jenkin [3] reported that local-scale removal of ozone by direct reaction with emitted NO has gradually decreased, a trend that is now widely attributed to ongoing improvement in vehicle NO_x emission regulations and associated progressive policy practices. This combination has resulted in a general increase in ozone concentrations since about 1990, which is most apparent at urban sites, but which to a less extent also influences the observations at the majority of rural locations. Air Quality Expert Group [2] has expressed their concerns that ozone levels in urban areas are increasing at comparatively faster rate than the surrounding rural areas, which in future may result in urban ozone levels as high as in the surrounding rural areas. If that happens it may increase ozone related health and environmental risks due to higher human exposure. Therefore it is vital to understand uncertainties in ozone predictions and quantify accurately the relationship of ozone with its sources and sinks.

Ozone is a regional pollutant and affects human health, agricultural crops, biodiversity and materials globally and exhibits distinct regional trends. Ozone concentrations also vary spatially from place to place within the UK considerably. Roadsides, urban centres, rural areas and remote sites all show different characteristics in terms of ground-level ozone. Ozone concentration at a given location is not only dependent on meteorological variables, but also on the concentrations of other air pollutants, e.g. NO_x, CO, hydrocarbon etc. Several scientists have investigated the relationship of ozone with different air pollutants (e.g. [2, 4, 5]) and have reported that these air pollutants play a vital role in ozone formation (e.g. ozone precursors i.e. NO_x and HC) and destruction (e.g. NO). Therefore, for accurate ozone prediction it is important to understand their mutual interaction and the role they play in controlling ozone concentrations.

Different techniques (models) have been used to study ozone and its associations with meteorological factors as well as with other air pollutants. Models have been used to predict ozone concentrations, establish long or short term ozone trends, understand underlying mechanisms in the formation and destruction of ozone, and study the health and environmental impacts of ozone [6, 7]. Multiple linear regressions are the most widely used methodologies for modelling the dependence of ozone on several independent variables (predictors). Soja and Soja [8], Tidblad et al. [4], Paschalidou et al. [5] and Pont and Fanton [9] all applied multiple regressions for ozone modelling. Linear regressions explicitly assume normality and linearity of the data, which are not



met by ozone and other air pollutants data. This study uses a quantile regression approach that is applicable to both normal and non-normal distributions and is capable of handling the non-linearities in ozone and other air pollutants data. Quantile regression model is especially useful when extremes values are important, such as air quality studies where upper quantiles of air pollutant (e.g. ozone) levels are critical from a public health perspective.

2 Methodology

This study is mainly based on the statistical analysis of ozone, NO_x, CO, lagged ozone, and PM_{2.5} data measured at Kirkstall roadside monitoring site in Leeds UK for a 2 year period. The data is divided into two subsets: training (Nov 2007 to Oct 2009, except May 2009) and test dataset (May, 2009). The study is applying a quantile regression approach, which has been explained in section 2.2.

2.1 Monitoring sites

Most of the data used in this study are taken from Kirkstall roadside monitoring site, which is part of the facilities available at Institute for Transport Studies (ITS) University of Leeds for the monitoring of air pollution, traffic and meteorological variables. The monitoring station lies between 53°48'31.38"N and 1°35'21.40"W, with Kirkstall Road (A65) running North-West to South-East adjacent to the site. The road is a busy thoroughfare with nearby petrol pump (20 meters) and used car garage (50 meters) to the South. In addition to ozone, the site monitors CO, NO_x and hydrocarbons (HCs) using certified gaseous analysers. This site also has facilities for monitoring wind speed, wind direction, temperature, humidity and solar radiation. Data from Harwell air quality monitoring station have also been analysed, which is a rural site and is part of the UK AURN (automatic urban and rural network), see [10] for the details of AURN sites.

At ITS every effort is made to ensure the quality of data is maintained. Automatic nightly calibrations of gaseous analysers, and fortnightly 'manual' zero and span calibrations using calibration gases CO, NO, NO₂ and Benzene are performed routinely. After collection the data go through verification, a process to clean-up the initial data. The data from AURN go through a proper 'data verification and ratification process' before it is marked as 'Ratified' data. All the data from AURN have a standard Quality Assurance and Quality Control (QA/QC).

2.2 Quantile regression model

This study applies quantile regression model (QRM) proposed by Baur et al. [6] for ozone and air quality data analysis and has certain advantages over other methods. QRM can be used for both parametric and nonparametric regression methods, as this model does not depend on the single measure of the central tendency (mean or median) of the data distribution only; instead it examines the



entire distribution of the data and hence is robust to departures of the data from normality and skewed tails. QRM allows the covariates to have different impacts at different points of the data distribution and is, therefore, capable of handling the non-linearities in the association of dependent and independent variables.

The linear regression model (LRM) focuses on modelling the conditional mean of a response variable (in our case ozone) without addressing its full distribution, whereas the quantile regression model accommodates analysis of the full distribution of the response variable. The QRM estimates the potential differential effect on various quantiles of the data distribution. In general form the QRM is presented as below [11]:

$$y_i = \beta_0^{(p)} + \beta_1^{(p)} x_i + \varepsilon_i^{(p)} \quad (1)$$

$$y_i = \beta_0^{(p)} + \sum_{k=1}^k \beta_k^{(p)} x_{ik} + \varepsilon_i^{(p)} \quad (2)$$

where p shows the p th quantile and $0 < p < 1$, y represent the response variable, x the explanatory variable, β_0 (constant) the intercept, β_1 the slope (gradient) and ε the error term. ε the error term in LRM is assumed to be independent of the value of the covariates (homoscedasticity). In contrast, quantile regression models allow for the variance of the error term to vary (heteroscedasticity) and make no assumptions about the variance structure. Moreover, the p th quantile of the error term conditional on the regressor is assumed to be zero i.e. $\varepsilon_i^{(p)} = 0$, which make equation 2 as:

$$Qy_i(p|x_{i1} \dots x_{ik}) = \beta_0^{(p)} + \sum_{k=1}^k \beta_k^{(p)} x_{ik}.$$

The constant β_0 and the coefficients β_1 are estimated for 99 different quantiles ($p=0.01, \dots, 0.99$) using each time the entire dataset. The 0.5th quantile represent the median, half of the data occur above the median and half below the median.

R (2.12.0) and two additional packages ‘openair’ and ‘quantreg’ were used to perform the statistical analysis presented in this report.

3 Results and discussion

The distributions of ozone and the other air pollutants were studied and it was established that their distributions were non-normal, and therefore Spearman correlation was applied which is a distribution free method for finding the correlation between two variables. Ozone concentrations have been shown to have strong correlation with these covariates. The Spearman correlation coefficients (R) for hourly mean data between ozone and other air pollutants were -0.64, -0.70, -0.68, -0.51, -0.53, 0.47 for NO, NO_x, NO₂, CO, PM_{2.5} and lagged-ozone respectively. The correlation between ozone and other variables was negative, except lagged-ozone which showed a positive correlation with ozone.

The outputs of quantile regression model are shown in Figure 1, using ozone as a response variable and lagged-ozone, NO, NO₂, CO and PM_{2.5} as explanatory



variables. The Barrodale and Roberts (br) algorithm method for computing the fit has been adopted here. The ‘br’ method has been described in details in Koener and d’Orey [12] as an efficient technique for large datasets (e.g. up to several thousand observations). In Figure 1 alongside quantile regression, the outputs of ordinary least square regression have also been visualised. In ordinary least square regression, only one regression coefficient represents the entire distribution of the explanatory variable (indicated by solid line along with its 95% confident interval); whereas in quantile regression generally several coefficients are given depending on the number of quantiles chosen. In Figure 1 regression coefficients have been given for 0.1, 0.2, 0.3, 0.4, 0.5, 0.6, 0.7, 0.8, 0.9, and 0.99 quantiles (represented by dashed-dotted line with their 95% confident intervals). In Figure 1 the top left panel shows the intercepts of the model. The values of intercept (constant) are higher for higher quantiles and vice versa. For instance, the intercept value for 0.1 quantile is about 17; whereas it is about 40 for quantile 0.99. Detailed analysis of the model outputs is described in the following sections.

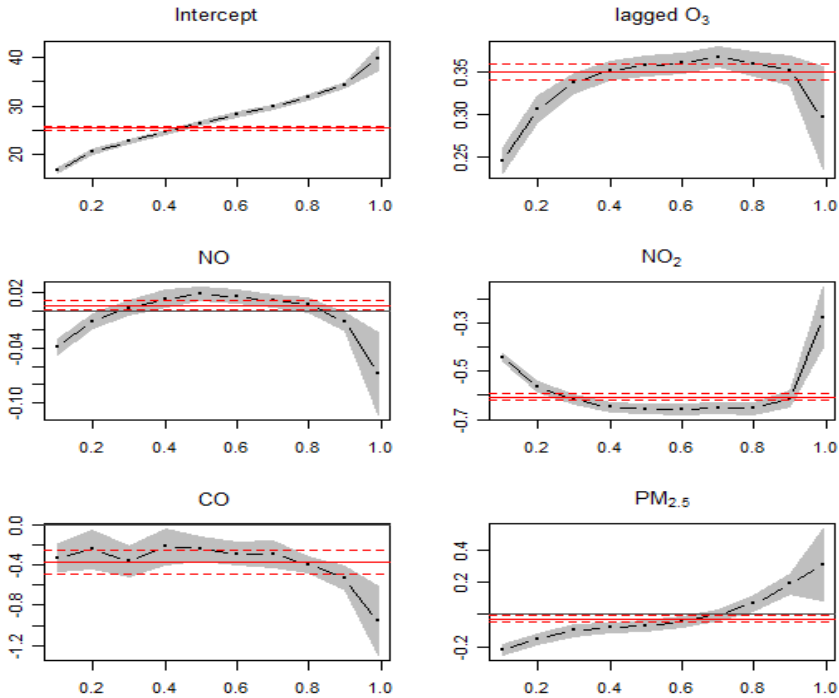


Figure 1: The outputs of quantile regression model showing the effect of lagged-ozone, NO, NO₂, CO and PM_{2.5} on hourly mean ozone concentrations. Quantile regression coefficients (dashed-dotted line) and ordinary least square regression coefficients (solid line) are presented with 95% confidence interval. Various quantiles are shown on x-axis, whereas their coefficients are shown on y-axis.



3.1 Auto-regression analysis ozone vs. lagged ozone

Lagged ozone (previous-day hourly mean ozone ppb) has positive effect on ozone mixing ratios. Figure 2 shows a scatter plot between ozone and lagged-ozone data from Kirkstall site for May, 2008. Ten estimated quantile regression lines for different values of Quantiles (0.1, 0.2, 0.3, 0.4, 0.5, 0.6, 0.7, 0.8, 0.9, and 0.99) have been superimposed on the scatter plot. The median (0.5 quantile) is indicated by bold broken line and the least squares estimate of the conditional mean function by bold solid line. There is a clear positive correlation between ozone and lagged-ozone, i.e. increasing lagged-ozone results in increasing ozone mixing ratios. The effect of lagged-ozone varies with quantile, as depicted in Figure 1 (top, right). The strength of relationship increases with increasing quantile values until quantile 0.7 and decreases afterward. At higher quantiles the lower coefficient values shows low persistence of ozone at extreme concentrations. The confidence bands are wider at higher quantile (0.99) showing less accurate modelling at these concentrations. On the other hand ordinary least square regression gives only one regression coefficient, which is represented by a straight line, as it considers only the mean value of the data and therefore hides the rest of the details.

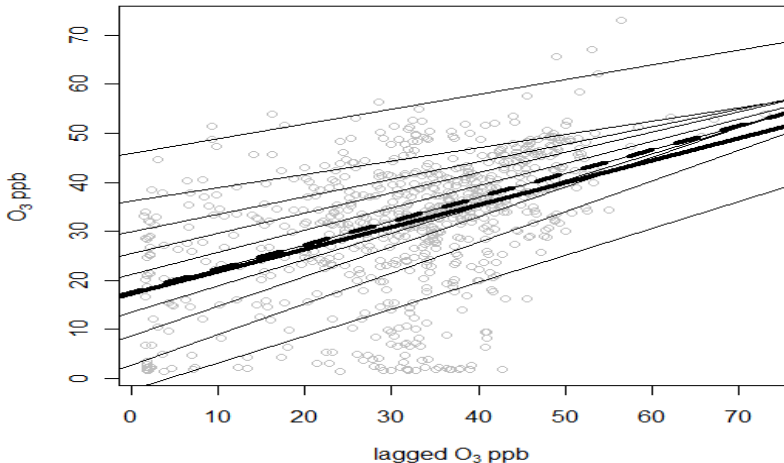


Figure 2: Scatter plot of ozone vs. lagged (previous day) ozone hourly mean data (May, 2008 from Kirkstall site in Leeds). Ten estimated quantile regression lines for different values of quantiles (0.1, 0.2, 0.3, 0.4, 0.5, 0.6, 0.7, 0.8, 0.9, and 0.99) have been superimposed on the scatter plot. The median (quantile 0.5) is indicated by bold broken line; the least squares estimate of the conditional mean function is indicated by bold solid line.

3.2 Ozone and nitrogen oxides

NO and NO₂ are collectively known as NO_x because they are rapidly inter-converted during the day. NO and NO₂ are both generated by combustion processes in the atmosphere, which mainly produce NO with a small proportion of NO₂ (~ 5%) [13]. Most of NO₂ is formed in the atmosphere by oxidation of NO, for example, by reaction with ozone. Therefore NO₂ is considered as a secondary (formed in the atmosphere) and NO as a primary pollutant (directly emitted). In the UK over 50% nitrogen oxides are produced by transport. NO₂ is split up by UV light to give NO and an oxygen (O) atom, which combines with molecular oxygen (O₂) to make ozone. In rural air, away from sources of NO, most of the nitrogen oxides in the atmosphere are in the form of NO₂, whereas near a source (e.g. a busy road) NO is the dominant species. Figure 3 shows the ratios of NO and NO₂ (NO/NO₂) at both Kirkstall (roadside) and Harwell (rural) monitoring site and confirms that the level of NO is more than NO₂ at the roadside monitoring site, whilst the opposite is true for the rural site. The reason is clear that at roadside traffic vehicles produce NO_x which is mostly consists of NO and by the time these gases reach rural areas most of the NO is oxidised into NO₂.

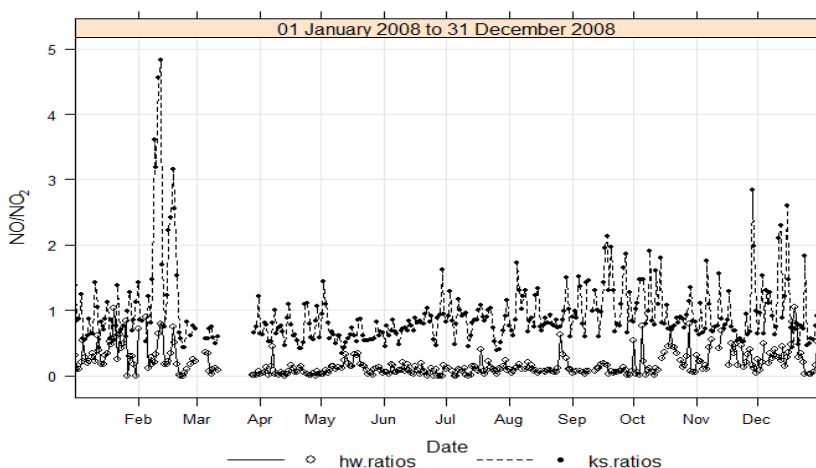


Figure 3: NO/NO₂ ratios for the year 2008 at Kirkstall (ks) roadside and Harwell (hw) rural site.

Quantile regression exhibits considerably stronger effect of NO₂ than NO on ozone mixing ratios. The quantile regression coefficients range from about '-0.06 to +0.02' for NO and '-0.3 to -0.7' for NO₂. It can be clearly seen in Figure 1 that the strengths of coefficients for NO and NO₂ follow opposite trends, i.e. for NO the highest correlation coefficients (absolute values) are observed at quantiles 0.1 and 0.99, whereas for NO₂ the weakest coefficients were recorded for these two quantiles. In other words, NO shows maximum effect whereas NO₂

shows minimal effect on ozone concentrations at extreme values (minimum and maximum). When ozone is modelled using only NO or NO₂ as explanatory variables with exactly the same quantiles, NO present a different picture (making a bowl shape as NO₂ does in Figure 1), whereas NO₂ behave almost in the same way (Figure not shown here).

3.3 Ozone vs. CO and PM_{2.5}

In this section the association of ozone with CO (Figure 1, bottom-left) and PM_{2.5} (Figure 1, bottom-right) is investigated using quantile regression model. CO has negative effect on ozone mixing ratios and the effect becomes stronger at quantile 0.9 and 0.99. The CO effect on ozone at different quantiles is not significantly different from the mean effect (as the confident intervals overlaps), except at 0.9 quantile and above. The effect of PM_{2.5} on ozone mixing ratios is negative below 0.6 quantile and positive above. The magnitude of estimated coefficients (absolute value) of PM_{2.5} decreases gradually from 0.1 to 0.6 quantile and become positive above 0.6 quantile. The effect gradually increases and reached a maximum value at 0.99 quantile. The negative coefficients of CO are most probably due to the fact that the data come from a roadside monitoring site and therefore almost all of CO is emitted by road traffic. Higher mixing ratios of CO pollutants indicate higher traffic volume and hence higher NO which depletes ozone.

4 Goodness of fit for quantile regression

The goodness of fit in ordinary least square regression is measured by the coefficient of determination (R^2), which is based on least squares criterion. R-squared values range from 0 to 1. Larger value of R-squared indicates a better model fit. In quantile regression the goodness of fit is represented by $R^1(\tau)$ and its values, like R^2 , lies between 0 and 1 [14]. R^2 measures a global goodness of fit over the entire conditional distribution, whereas $R^1(\tau)$ measures the local performance of model for a given quantile. Koenker and Machado [14] suggest measuring $R^1(\tau)$ by comparing the sum of weighted distance for the model of interest with the sum in which only the intercept is used (for details see [11] and [14]). $R^1(\tau)$ and R^2 have different nature, as the former is a local whereas the latter is a global measure of performance and therefore are not directly comparables. $R^1(\tau)$ values for different quantiles have been shown in Figure 4, which are relatively weaker as compared to global goodness of fit.

To estimate a global goodness of fit (R^1) for quantile regression model, this study adopts the approach suggested by Baur et al. [6] and is called amalgated quantile regression model (AQRM). AQRM approach for estimating the performance of the model is simple and can be directly compared with R^2 for the linear regression. To estimate R^1 , firstly quantile regression coefficients were determined for 10 quantiles (.1, .2, .3, .4, .5, .6, .7, .8, .9, .99) using ozone as variate and NO, NO₂, lagged-O₃, CO and PM_{2.5} as covariates for the whole dataset. The test dataset (May, 2009) was divided into 10 equal subsets



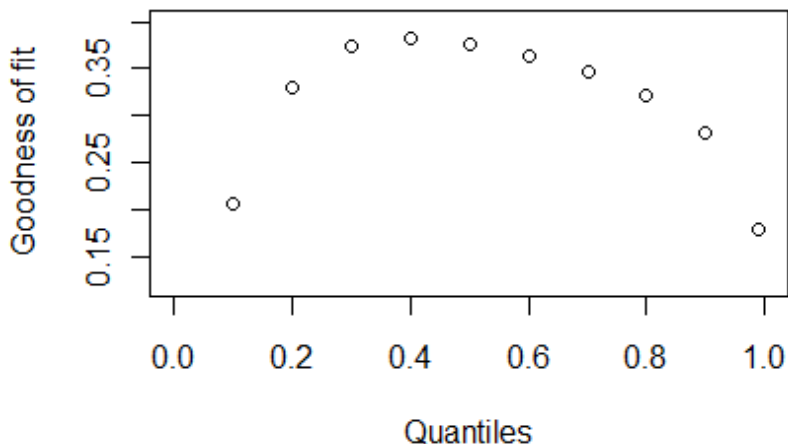


Figure 4: Local goodness of fit R^1 (τ) as a function of the ozone quantiles for the quantile regression model at Kirkstall site Leeds.

according to the above quantile values of ozone data. Using quantile regression coefficients of each quantile, ozone was predicted for each subset. For the estimation of quantile regression coefficients the whole dataset was used as training data, except May 2009, which was used as test data for prediction purposes. Finally predicted and observed ozone were compared for the test data (Figure 5 and Figure 6).

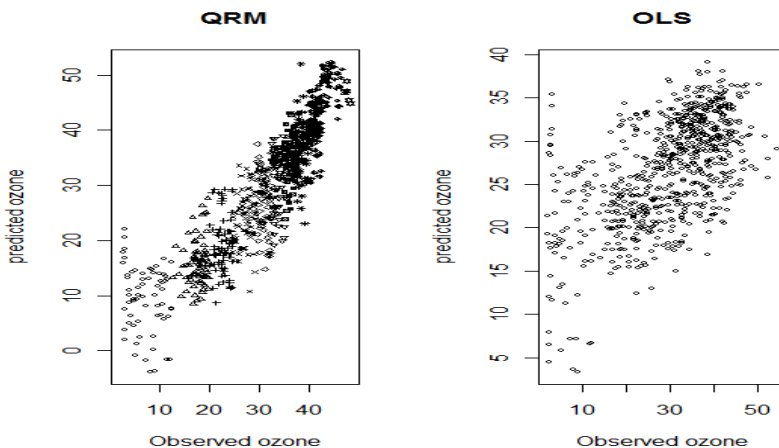


Figure 5: Predicted versus observed ozone concentration at Kirkstall site using AQRM (amalgated quantile regression mode) $R^1=0.80$ (left) and OLS (ordinary least square) model, $R^2=0.53$ (right) for May 2009.



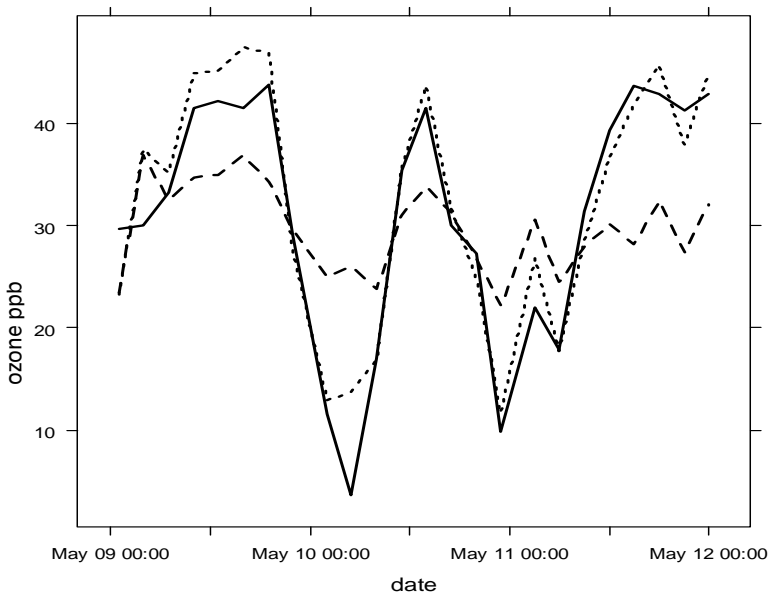


Figure 6: Observed (solid line) vs. predicted ozone, using AQRM ($R^1=0.80$, dotted line) and OLS model ($R^2=0.53$, dashed line) for 9 to 11 May 2009 at Kirkstall site.

Figure 5 depicts predicted ozone versus observed ozone mixing ratios at Kirkstall site. The scatter plot of observed ozone versus predicted ozone by Quantile Regression Model (QRM) is shown in the left, whereas the scatter plot of observed ozone versus predicted ozone by Ordinary Least Square model (OLS) is shown in the right panel of Figure 5. AQRM explains more of the ozone variations showing R^1 -value of 0.80 in comparison to OLS which gives R^2 -value of 0.53. This indicates that AQRM is explaining significantly more ozone variation than OLS. QRM model was more efficient in predicting ozone mixing ratios than OLS model, particularly at extreme values as shown in Figure 6, where the dotted line (QRM) closely follows the line of observed ozone.

5 Conclusion

This study explores the impacts of traffic-related air pollutants (NO , NO_2 , CO , $\text{PM}_{2.5}$) and lagged ozone on ground level ozone and suggests the use of quantile regression approach for ozone and air quality data analysis as an alternative to traditional regression models. Quantile regression model is suitable for non-normal ozone distribution and is capable of handling nonlinearities in the associations of ozone with its predictors; as it examines the entire distribution of the variables rather than a single measure of central tendency (mean or median).

It is shown that the effect of explanatory variables on ozone mixing ratios is better explained by quantiles and hence the behaviour and interaction of the variables with ozone changes at different regimes of ozone concentrations, which is normally hidden in the traditional regression models. Statistical analysis demonstrates that for some air pollutants the nature of relationship (negative or positive) between ozone and its predictors remains unchanged and only the strength changes, for others nature and strength both change at different quantiles, possibly indicating more complex interactions. Quantile regression model explains significantly more variations in ozone ($R^1= 0.80$) as compared to ordinary least square regression ($R^2=0.53$) and is therefore better suited for ozone data analysis and prediction.

Acknowledgement

We gratefully acknowledge Economic and Social Research Council (ESRC) for providing funding for this study, which is a part of my PhD project.

References

- [1] Derwent, R.G., Simmonds, P.G., Manning, A.J. and Spain, T.G., Trends over a 20-year period from 1987 to 2007 in surface ozone at the atmospheric research station, Mace Head, Ireland, *Atmospheric Environment*, 41, pp. 9091–9098, 2007.
- [2] Air Quality Expert Group (AQEG). Ozone in the UK, the fifth report produced by air quality expert group (AQEG), 2009. DEFRA publication London, 2009AQEG, 2009
- [3] Jenkin, M.E., Utembe, S.R. and Derwent, R.G., Modelling the impact of elevated primary NO₂ and HONO emissions on regional scale oxidant formation in the UK, *Atmospheric Environment*, 42 (2), pp. 323–336, 2008.
- [4] Tidblad, J., Mikhailov, A.A., Henriksen, J. and Kucera, V., Improved Prediction of Ozone Levels in Urban and Rural Atmospheres, 40 (1), pp. 67–76, 2002.
- [5] Paschalidou, A.K., Kassomenos, P.A. and Bartzokas, A., A comparative study on various statistical techniques predicting ozone concentrations: implications to environmental management, *Environmental Monitoring and Assessment*, 148 (1-4), pp. 277–289, 2008.
- [6] Baur, D., Saisana, M. and Schulze, Modelling the effects of meteorological variables on ozone concentration-a quantile regression approach, *Atmospheric Environment*, 38 (28), pp. 4689–4699, 2004.
- [7] Gardener, M.W. and Dorling, S.R., Meteorologically adjusted trends in the UK daily maximum surface ozone concentrations, *Atmospheric Environment*, 34, pp. 171–176, 2000
- [8] Soja, G., and Soja, A.M., Ozone indices based on simple meteorological parameters: Potentials and limitations of regression and neural network models, *Atmospheric Environment*, **33**, pp. 4299–4307, 1999.



- [9] Pont, V. and J. Fontan, Comparison between weekend and weekday ozone concentration in large cities in France, *Atmospheric Environment*, 35, pp. 1527–1535, 2000.
- [10] UK automatic urban and rural network (AURN). Department for Environment, Food and Rural Affairs. www.aurn.defra.gov.uk. Accessed October 12, 2010
- [11] Hao, L., Naiman, D.Q., *Quantile regression: Series-Quantitative applications in the social sciences*, Sage Publications, 2007 (Series NO. 07-149)
- [12] Koenker, R.W. and d'Orey, Computing regression quantiles, *Applied Statistics*, 36, pp. 383–393, 1994
- [13] Air Quality Expert Group (AQEG). Trends in primary nitrogen dioxide in the UK, the fourth report prepared by the air quality expert group, DEFRA Publication London, 2007.
- [14] Koenker, R. and J. Machado, Goodness of fit and related inference processes for quantile regression, *American Statistical Association*, 94, pp. 1296–1310, 1999



A choice experiment approach to the valuation of air pollution in Mashhad, Iran

M. Ghorbani¹, S. Kulshreshtha² & A. Firozzarea¹

¹*Department of Agricultural Economics,
Ferdowsi University of Mashhad, Mashhad, Iran*

²*Department of Bioresource Policy, Business and Economics,
University of Saskatchewan, Saskatoon, Canada*

Abstract

This study describes the results of a survey carried out in Mashhad, Iran. The survey was designed using choice-modeling techniques and intended to discover what valuation Mashhad residents placed on air pollution and the abatement of air pollution. The survey results were analyzed using a nested logit (NL) model. This analysis then allowed a consideration of the improvements in household welfare that might be expected under different scenarios of air pollution control. Researchers sampled two populations: inhabitants of areas with high air pollution and inhabitants of areas of moderate pollution. The results indicated that the inhabitants of the areas suffering the worst air pollution had the highest willingness to pay (WTP) for a reduction in pollution.

Keywords: air pollution, choice modeling approach, nested logit model, household welfare, Iran.

1 Introduction

Ever since the start of the Industrial Revolution, economic development and environment have been at odds with each other. According to the WCED [1], current environmental trends, if continued, will radically alter the planet and threaten the lives of many species upon it. As awareness of the danger has grown, environmental protection has been increasingly recognized as a principle concern (Gurluk [2]).

One alarming environmental trend in Iran is an increase in air pollution in major cities and the surrounding countryside. This has led to an increased public



awareness of the problems resulting from air pollution. Much pollution is due to automobiles, factories, and household cooking fuels. In many densely populated areas this pollution is a cause of poor health (due mainly to high particulate count in the air and foul odours) and reduced visibility (Dagsvik et al. [3]).

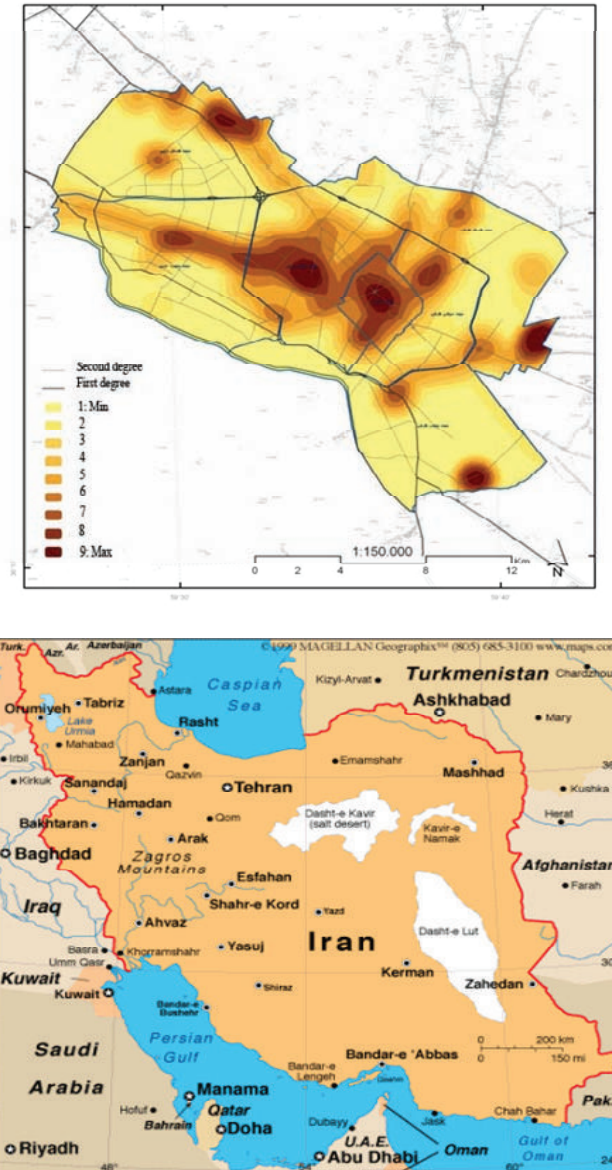


Figure 1: Distributions of air pollution in Mashhad zones (top); map of Iran showing location of Mashhad (bottom).



One of the reasons for the lack of policies to protect the environment is the lack of understanding by decision-makers of the social impact of environmental degradation. This is partly a result of a lack of information available on the economic value of the environment, since it is not recognized by the usual market-based valuations. Such valuations are not easily ascertainable. However, in recent years, a number of methods have been developed to assign economic values to environmental resources, and to integrate those values in the decision-making process. Choice experiment approach (CEA) is one of these methods (Gurluk [2]).

Pollution is a major problem in Iran in general and in the city of Mashhad in particular. Mashhad is located in Khorasan Razavi province, in the northeastern corner of Iran (Figure 1). It is Iran's second-largest city, second in size only to Tehran, Iran's capital. It is a center of pilgrimage (to the shrine of Imam Reza) and of industry. The city and its suburbs cover an area of approximately 204 km². The city is located on a plain between two long ridges: Binalood to the south and southwest and Hezarmasjed to the north and northeast. It is 985 meters above sea level and has a semi-temperate climate. For some 270 to 300 days of the year, it is subject to temperature inversions that hold smog over the city Mousavi [4]. Mashhad's air pollution is primarily a result of human activities and is caused mainly by emissions from motor vehicles. There are 294,608 motor vehicles in the city, of which 272,137 are powered by gasoline. The remaining 42,462 vehicles operate on diesel fuel (Mousavi [4]). There are also natural sources of pollution, such as dust and pollens.

The primary objective of our research is to estimate the willingness to pay (WTP) of the Mashhad population for reduction of air pollution.

2 Study methods

2.1 Environmental valuation methods and the choice modeling approach

Although not typically monetized, ecosystem goods and services do contribute to an individual's utility and they therefore have value. This value can be measured by the individual's maximum willingness-to-pay (WTP) for such goods and services (Loomis et al. [5]). The only methods that are capable of estimating non-use values of air pollution effects are the contingent valuation method (CVM) and the choice experiment approach (CEA) (Gurluk [2]). The latter approach has some advantages over CVM, as it can be used to value a selection of possible outcomes and to assess the tradeoffs between outcomes that individuals might be willing to make.

Choice experiments are one example of the stated preference approach to environmental valuation, in as much as they involve eliciting responses from individuals to researcher-constructed, hypothetical markets and do not require the study of actual behavior. The CE approach is based on random utility theory (RUT) and the characteristics theory of value. Environmental goods are valued by reference to their *attributes* (instruments of choice set definition), which are evaluated by applying probabilistic models to choices between different possible



scenarios. Our decision to use the CE approach was driven by the desire to estimate values for different aspects of air quality. These aspects constitute the attributes of interest in the CE design detailed below.

In a CE, the status quo and a number of alternatives are described (Muller and Diener [6]). Respondents are asked to state which of the alternatives they most prefer. Using appropriate statistical techniques, one can infer an index function from the responses. This function is the best predictor of the observed choices (Green [7]). This technique builds on the conjoint metric analysis methodology developed in the field of marketing and introduced into the environmental economics literature by Adamowicz et al. [8].

2.2 Study site

The current study is focused on air pollution issues in Mashhad. This city is a big populated city and located in north-east of Iran on a plain between Binalood and Hezar-Masjed heights. This city is home to more than 2.5 million people. In addition to this, this city receives over 14 million religious pilgrims annually. Table 1 reports the priorities of air pollutant sources of Mashhad.

Table 1: Sources of pollutants, ranked by output.

Source	Priority
Vehicles	1
Indoor	1
Commercial	1
Industries (inside the city)	1
Filling stations (inside the city)	1
Trains	2
Planes	3
Filling stations(outside the city)	4
Industries (outside the city)	4

In addition to thermal inversion, air stability and lack of rain, we should acknowledge that the most important factor of Mashhad air pollution is man-made pollutions like automobiles, factories and other pollutants. Based on statistics of environment office of Khorasan Razavi province about 72 percent of Mashhad air pollution is because of motor-vehicles traffic. In this metropolis about 800 thousands motor-vehicles are in traffic. Moreover, there are many polluting units like factories, compost plants, in Mashhad suburbs which are not compatible with dominant winds.

It is worth noting that distribution of air pollution in Mashhad differs in various times and zones of the city. Air pollution measurement through 12 measurement stations which are observing and registering Mashhad air pollution status shows that air pollution is more critical in Qale-sakhteman,



Panjrah, Shohada and Sajad regions. Furthermore, early morning hours of a day due to lack of ascending currents in big and industrial cities like Mashhad are more polluted. Thermal inversion and air stability bring about more air pollution in fall and spring rather than other seasons.

According to many physicians the reason of many diseases including gastrointestinal, heart, respiratory and vascular diseases in Mashhad is breathing polluted air. For this reason, some people with heart and respiratory diseases are advised not to leave their homes. Air pollution in Mashhad is responsible for a number of negative effects. It has been proved that air pollution can affect human health. These health effects include increased hospital admissions due to the exacerbation of cardiac and respiratory diseases, as well as increased mortality. In addition to adverse health effects, air pollution here creates poor visibility, black fallout and bad odours.

2.3 Data collection plan

Based on consultation with staff of environment office of Khorasan Razavi province, this study stratified Mashhad into two regions; high-polluted region and medium-polluted region. Stratified random sampling method was used to select sample residents. The main survey consisted of 160 and 126 households in the high polluted and medium polluted split samples, respectively.

2.4 Choice experiment design

In consultation with the staff of the Khorasan Razavi Environment Office, researchers chose four important measures of air pollution damage, called *attributes*, or instruments of choice set definition. They are outlined in Table 2. Measures included health effects (increase in hospital admissions due to cardio-respiratory diseases and increased mortality) and the numbers of days that

Table 2: Attribute levels used in choice experiment design.

Attribute	Current situation	About 30 percent better	About 30 percent worse
Health effects	18 extra hospital admissions and 2 extra deaths per month, compared to figures expected if the air were perfectly clean	12 extra hospital admissions and 1 extra death per month	24 extra hospital admissions and 3 extra deaths per month
High particulate count	3 days per month	2 days per month	4 days per month
Foul odors	4 days per month	3 days per month	5 days per month
Reduced visibility	3 days per month	2 days per month	4 days per month



Mashhad residents were warned of heavy particulate load, foul odours, or reduced visibility. In order to estimate WTP, survey respondents were asked to choose between possible changes in monthly taxes. These constitute the fifth *attribute*.

The survey was designed to elicit responses to three levels of each attribute. The middle level was based on the current level of pollution or property tax. The other two levels were based on a 30 percent reduction or a 30 percent increase in pollution levels; each level was paired with an increase, a decrease, or no change in monthly property taxes. The final survey comprised twenty-seven different choices; alternatives were combined with the baseline, the current state of affairs, into nine separate choice sets.

2.5 Statistical model

Although the logit-based models are based on RUT (Ortuzar and Willumsen [9]), the majority of past studies have not progressed beyond using the simple multinomial logit (MNL) model. While the independently and identically distributed (IID) assumption and the behaviorally comparable assumption of Independence of Irrelevant Alternatives (IIA) allow for ease of computation, violations of both of these assumptions can and do occur. When violations do occur, the cross-substitution effects observed between pairs of alternatives are no longer equal, given the presence or absence of other alternatives within the complete list of available alternatives within the model (Hensher et al. [10]). This property (IIA) states that the relative probabilities of two options being selected are unaffected by the introduction or removal of other alternatives. This property follows from the independence of the error terms across the different options contained in the choice set. If a violation of the IIA hypothesis is observed, then more complex statistical models are necessary. The model that relaxes some of the assumptions is the nested logit model. Furthermore, there are numerous formal statistical tests that can be used to test for violations of the IIA assumption, with the test developed by Hausman and McFadden [11].

One way to relax the homoscedasticity assumption in the conditional logit model (one which also provides an intuitively appealing structure) is to group the alternatives in subgroups that allow the variance to differ across the groups while maintaining the IIA assumption within the groups. This specification defines a Nested Logit model. Thus, it is useful to think of this specification as a two-level choice problem. Suppose that the J alternatives can be divided into L subgroups such that the choice set can be written as follows:

$$[c_1, \dots, c_J] = (c_{1/1}, \dots, c_{j/1}), \dots, (c_{1/L}, \dots, c_{jL/L}) \quad (1)$$

Logically we may think of the choice process as that of choosing among the L choice sets and then making the specific choice within the chosen set. This method produces a tree structure.

Suppose as well that the data consists of observations on the attributes (used in the technical sense) of the choice $X_{j/1}$ and attributes of the choice sets Z_l . In order to derive the mathematical form of the model, we begin with the unconditional probability:



$$prob[twig_j, branch_l] = p_{jl} = \frac{e^{\beta'x_{j/l} + \gamma'z_l}}{\sum_{l=1}^L \sum_{j=1}^{J_l} e^{\beta'x_{j/l} + \gamma'z_l}} \tag{2}$$

Now write this probability as:

$$p_{jl} = p_{j/l}P_l = \left(\frac{e^{\beta'x_{j/l}}}{\sum_{j=1}^{J_l} e^{\beta'x_{j/l}}} \right) \left(\frac{e^{\gamma'z_l}}{\sum_{l=1}^L e^{\gamma'z_l}} \right) \left(\frac{\sum_{j=1}^{J_l} e^{\beta'x_{j/l}}}{\sum_{l=1}^L \sum_{j=1}^{J_l} e^{\beta'x_{j/l} + \gamma'z_l}} \right) \left(\frac{\sum_{l=1}^L e^{\gamma'z_l}}{\sum_{l=1}^L \sum_{j=1}^{J_l} e^{\beta'x_{j/l} + \gamma'z_l}} \right) \tag{3}$$

Define the inclusive value for the l^{th} branch as:

$$I_l = \ln \sum_{j=1}^{J_l} e^{\beta'x_{j/l}} \tag{4}$$

Then after canceling terms and using this result, we find:

$$p_{j/l} = \frac{e^{\beta'x_{j/l}}}{\sum_{j=1}^{J_l} e^{\beta'x_{j/l}}} \tag{5}$$

$$P_l = \frac{e^{\gamma'z_l + \tau_l I_l}}{\sum_{l=1}^L e^{\gamma'z_l + \tau_l I_l}}$$

The new parameters τ_l must equal 1 to produce the original model (conditional logit model). The coefficients in this model are not directly interpretable Green [7]. The estimated coefficients of the attributes can be used to estimate the tradeoffs that respondents would be willing to make between various attributes. The price attribute can be assessed in conjunction with the other attributes to determine the WTP of respondents for gains or losses of selected attribute levels. This monetary value is called the implicit price of the attribute (Bergman et al. [12]) and can be expressed as:

$$WTP = - \left[\frac{b_{non-market \ attribute}}{b_{monetary \ attribute}} \right] \tag{6}$$

2.6 Economic surplus

One of the advantages of choice experiments is that estimated coefficients of the attributes may be used to estimate the economic value of different attribute combinations. In order to determine the change in economic surplus from



possible alternative scenarios in a multi-attribute nested logit model, a utility difference is calculated as:

$$\text{Economic surplus} = -\frac{1}{b_y} \left(V_i^1 - V_i^2 \right) \quad (7)$$

where, b_y is the marginal utility of income and V_i is the indirect utility associated with alternative i . The superscript 1 represents the current situation and superscript 2 represents other scenarios.

3 Results

3.1 Results of estimation

In order to test the violation of the IIA assumption, the Hausman test was used for both highly-polluted and moderately-polluted areas. The IIA was firmly rejected in both heavily and moderately polluted areas. This suggests that constructing the model as a simple conditional logit could generate misleading results. For this reason, researchers used nested structures.

Results from the nested logit models are presented in Table 3. The coefficients are parameters of the indirect utility function, notwithstanding the fact that they are confounded with a scale parameter. This makes it possible to interpret them directly. Coefficient signs show the influence of attributes on choice probabilities.

Table 3: Nested logit model results for combined area.

Descriptor	Areas with high air pollution			Areas with moderate air pollution		
	Coefficient	Std. error	Significance level	Coefficient	Std. error	Significance level
Health effects	1.6716	0.1527	P < 0.001	1.9175	0.2137	P < 0.001
High particulates	0.9489	0.1273	P < 0.001	1.6666	0.2566	P < 0.001
Foul odors	0.7810	0.0961	P < 0.001	0.7854	0.1085	P < 0.001
Reduced visibility	1.5872	0.1641	P < 0.001	1.0588	0.1504	P < 0.001
Taxes	-0.0104	0.0009	P < 0.001	-0.0132	0.0017	P < 0.001
Nest A	1.0142	0.1159	P < 0.001	0.7979	0.1179	P < 0.001
Nest B	0.5739	0.0680	P < 0.001	0.5095	0.0653	P < 0.001
Nest C	0.6916	0.0845	P < 0.001	0.4447	0.0700	P < 0.001
Goodness of fit criteria						
McFadden's LRI	0.7708			0.7280		
Veall-Zimmermann	0.9565			0.9460		
Estrella	0.9997			0.9993		
Adjusted Estrella	0.9997			0.9992		
Cragg-Uhler(1)	0.9861			0.9823		
Cragg-Uhler(2)	0.9899			0.9862		



As is evident, all attribute coefficients have the expected signs. The signs of all attributes, except the price attribute, are positive. This, as consumer preference theory predicts, suggests that any improvement in these attributes would cause an improvement in air pollution, which leads to increased utility. The coefficient for the price attribute is negative, and is also consistent with standard economic theory. All of the air pollution attributes are significant determinants of utility well below the one-percent level. The health effects of air pollution have the largest coefficient in highly polluted areas. Reduced visibility, high particulate counts, and foul odours are ranked second, third, and fourth, respectively. In areas of moderate air pollution, the health effect of air pollution also has the largest coefficient. However, in this case high particulate count, reduced visibility, and foul odours are ranked second, third, and fourth, respectively.

Because it is not possible to interpret the coefficients directly, marginal rates of substitution between non-market attributes and the monetary attribute were estimated. These are reported in Table 4. These values represent the amount of money individuals would be willing to pay for the specified improvement (as shown in Table 2). Mashhad residents are willing to pay IRR 1,607 (Iranian rials) per month for improvements in health measures if they live in highly-polluted areas and a slightly lower amount, IRR 1,453 per month, if they live in the moderately-polluted areas.

Table 4: Willingness-to-pay for improvement in several aspects of air pollution.

Attribute	Areas with high air pollution		Areas with moderate air pollution	
	Willingness-to-pay (rials month ⁻¹)	Index	Willingness-to-pay (rials month ⁻¹)	Index
Health effects	1607.30	100	1452.60	100
High particulates	912.40	56	1262.60	86
Foul odours	751.00	46	595.00	40
Reduced visibility	1526.10	94	802.10	55

Approximately 9500 Rials= 1 U.S. dollar.

According to the estimates in Table 4, residents of Mashhad living in the areas with high air pollution are willing to pay, on average, IRR 751, IRR 912, IRR 1,526, and IRR 1,607 per household per month for 30% improvements in foul odours, high particulate counts, reduced visibility, and health effects of air pollution, respectively. Comparable estimates of WTP for the moderately-polluted neighbourhoods are relatively lower for all four attributes. It is clear that residents of areas subject to moderate air pollution do not consider health improvements to have the same high value that is given to them by residents of heavily-polluted areas.



3.2 Comparison of scenario results

Researchers used the results of equation (7) to estimate improvement in household welfare, for both high pollution and moderate pollution neighborhoods, under each possible scenario (as shown in Table 5). For the baseline scenario (that is, current conditions), the welfare change is zero. Scenario 3, which postulates a 30% improvement in all four measures of air pollution, yields an estimate of strong positive change in household economic welfare. Under this scenario, Mashhad residents are better-off by IRR 24,950 per household per month in areas with high air pollution, and IRR 21,390 per household per month in areas with moderate pollution (Table 6). Both scenario 5 and 6 show household welfare decreasing, due to health measures 30% lower than baseline. All these results demonstrate the prominent role of air pollution's health effects in determining the economic well-being of Mashhad households.

Table 5: List of possible outcomes presented to interviewees.

Possible changes	Outcomes					
	1 *	2	3	4	5	6
Health effects:						
Extra hospital admissions per month	18	18	12	12	24	18
Extra deaths per month	2	2	1	1	2	2
Pollution effects:						
High particulate count (days per month)	3	3	2	3	4	4
Foul odours (days per month)	4	4	3	5	4	5
Reduced visibility (days per month)	3	3	2	2	4	4
Taxes (IRR per household per month)	10,400	12,480	10,400	5,200	10,400	14,560

* Baseline.

Table 6: Improvements in household welfare under various scenarios.

Particulars	Scenarios					
	1 *	2	3	4	5	6
	Areas with high air pollution					
Change in welfare (IRR household ⁻¹ month ⁻¹)	0	-2,087	24,950	17,600	-21,050	-20,750
	Areas with moderate air pollution					
Changes in welfare (IRR household ⁻¹ month ⁻¹)	0	-2,085	21,390	13,830	-18,280	-18,000

* Baseline.



4 Conclusions

Residents of the city of Mashhad, Iran, were surveyed to determine what values they would assign to local air pollution. They were asked to evaluate the following scenarios: 30% increases or decreases in foul odours, heavy particulate concentrations, reduced visibility, and impaired health, against a baseline of current conditions. By using a choice experiment approach and analyzing survey results with a Nested Logit (NL) model, researchers determined the value that Mashhad residents placed on the environmental effects of air pollution. In addition, researchers estimated the probable changes in household welfare under different possible outcomes associated with different levels of air pollution.

The results of this research indicate that the total economic value gained as the result of a thirty percent improvement in the four measures of air pollution could be estimated at IRR 6,732 million per month (equivalent to US\$708,632) in the areas with high air pollution. In the areas with moderate air pollution, a thirty percent improvement in these pollution measures was estimated as adding IRR 4,571 million per month (equivalent to US\$481,158) to economic value. Assuming common preference functions and shared utility of reduced air pollution in the two types of areas, the total value of a thirty percent improvement in Mashhad's air pollution would amount to close to IRR 11,303 million per month (equivalent to US\$1.19 million).

How could this money be raised and spent? The city could levy various green taxes, including cap-and-trade system (a program to cap emissions and set up a market for exchangeable pollution permits). The city could use these revenues to set up programs to teach Mashhad residents about pollution and how to curb it. It could invest in infrastructure that could reduce air pollution, such as subways, electric cars, dedicated safe bicycle lanes. Any such initiatives should of course be studied thoroughly before implementation.

References

- [1] WCED—World Commission on Environment and Sustainability. 1987. *Our common future*. Oxford University Press, New York.
- [2] Gurluk, S. 2006. The estimation of ecosystem services' value in the region of Misi rural development project: Results from a contingent valuation survey. *For. Pol. Econom.* 9, 209–218.
- [3] Dagsvik, J.K., Wennemo, T., Wetterwald, D.G., Aaberge, R. 2002. Potential demand for alternative fuel vehicles. *Transp. Res. Part B* 36, 361–384.
- [4] Mousavi, M. 2003. *Mashhad air pollution program*. Environment Office of Khorasan Razavi.
- [5] Loomis, J., Kent, P., Strange, L., Fausch, K., Covich, A. 2000. Measuring the total economic value of restoring ecosystem services in an impaired river basin: Results from a contingent survey. *Ecol. Econ.* 33, 103–117.



- [6] Muller, R.A., Diener, A.A. 1997. *Economic valuation of air quality in regional municipality of Hamilton-Wentworth*. Department of Economics, McMaster University, Hamilton, Ontario, Canada.
- [7] Green, W.H. 1993. *Econometric Analysis*. Second Edition. New York: Macmillan Publishing Company.
- [8] Adamowicz, W., Louviere, J.J., Williams, M. 1994. Combining revealed and stated preference methods for valuing environmental amenities. *J. Environ. Econom. Management* 26, 271–92.
- [9] Ortúzar, J. de D., Willumsen, L.G. 2001. *Modelling Transport*. Third Edition. John Wiley and Sons, Chichester.
- [10] Hensher, D.A., Rose, J., Greene, W.H. 2004. *Applied choice analysis: A primer*. Cambridge University Press: Cambridge.
- [11] Hausman, J.A., McFadden, D. 1984. Specification tests for the multinomial logit model. *Econometrica* 52, 1219–1240.
- [12] Bergmann, A., Hanley, N., Wright, R. 2006. Valuing the attributes of renewable energy investments. *Ener. Po.* 34, 1004–1014.



Section 2
**Risk prevention and
monitoring**

This page intentionally left blank

Multiscale comparison of air quality modeling for an ozone occurrence during the 1996 Paso Del Norte Ozone Campaign

D. Lu¹, R. S. Reddy¹, R. Fitzgerald², W. R. Stockwell³,
Q. L. Williams¹ & P. B. Tchounwou⁴

¹*Department of Physics, Atmospheric Science & Geoscience,
Jackson State University, USA*

²*Physics Department, University of Texas at El Paso, USA*

³*Program of Atmospheric Sciences, Howard University, USA*

⁴*NIH-RCMI Center for Environmental Health,
Jackson State University, USA*

Abstract

An air quality modeling has been applied to investigate an ozone event occurring during the period of 1996 Paso del Norte Ozone Campaign. An examination of model sensitivity to horizontal grid resolutions has been performed. The modeling results show that grid resolution evidently influences the simulations of ozone formation, dispersion, transportation and structural distribution. The 36-, 12-, 4- and 1-km models captured the diurnal variation of surface ozone, but with a few hours lag for simulated peak ozone. The coarser the spatial resolution of the model, the more the peak ozone lag occurs. All models underpredicted the peak ozone concentration where the 1-km model produced the best while the 36-km model yielded the worst. This study suggests that the problems of maximum ozone underprediction and minimum ozone overprediction can be mitigated by increasing the spatial resolution of the model. Compared to fine models, coarse models provided rather simple and smooth structures with many detailed and complex structures being lost. The frequency distribution analysis also revealed that the high ozone event occurring over the complex terrain area such as El Paso, TX can hardly be captured by using coarse spatial resolution models, and the high resolution model (i.e., grid spacing is no greater than 4-km) is necessary.



Keywords: air quality modeling, multiscale comparison, high ozone event, CMAQ, SMOKE, WRF.

1 Introduction

Ozone is formed from a series of chemical reactions among its precursors. The major precursors of ozone are oxides of nitrogen ($\text{NOX} = \text{NO} + \text{NO}_2$) and volatile organic compounds (VOCs). These precursors are emitted primarily from fossil fuel combustion and automobile sources and are subsequently oxidized to produce ozone through a complex series of interactions involving various chemical and physical processes [1]. Because of the complexity of ozone formation it is difficult to predict ozone episodes and impossible to understand its mechanism solely by direct experimental studies and field observations. Air quality modeling, however, provides a good alternative to study the physical and chemical mechanism of ozone formation due to model capabilities which provide a high temporal and spatial resolution study for a wide variety of pollutants. Most air quality models have adopted the three-dimensional Eulerian grid modeling framework which represents reasonable physical realism and predicts concentrations of the species throughout the entire model domain. When grid-based air quality models are used, the selection of grid cell size becomes important because the characteristics of species are regarded as uniform in each grid cell and chemical species are mainly denoted by concentration (i.e., mass per volume). Using coarse grids would cause the model to resolve emission strengths that are too low, especially in major source areas [1].

Additionally, the subgrid processes that regulate species transformations are assumed to be uniform in each grid cell, and certain characteristics of subgrid processes and their interactions may be lost as the size of the model grid cell increases. The U.S. Environmental Protection Agency (EPA) has recommended that the air quality modeling in support of the state implementation plan (SIP) may benefit from increased grid resolution [2]. An increased grid resolution model provides a more detailed and accurate representation of key factors such as complex terrain features, emission sources and urban characteristics. Jang et al. [1] found that, while the average transport of non-reactive species does not show sensitivity to grid resolution, reactive pollutants are sensitive. This suggests a nonlinear relationship between chemistry and horizontal grid size. Some studies have shown that increasing grid resolution does not always give better performance due to the challenge of the complexity in chemistry and meteorology and their nonlinear interactions and responses to grid size [3–5]. More studies and further analyses for the sensitivity of model predictions to horizontal grid resolutions are needed. The purpose of this study is to determine what spatial resolution is needed to successfully capture a high ozone event with a sufficient accuracy of intensity and detailed structure.



2 Case selection and observational data

The case, August 13 1996 ozone episode, was selected from a major field study, the Paso del Norte Ozone study, which was conducted during the summer of 1996 for the purpose of providing sufficient data to support photochemical ozone air quality. The campaign was conducted from July to September of 1996. During this period, a local intensive observation network of air quality and meteorological monitoring sites was operated and contained a sounding site and 20 surface meteorological stations in El Paso, Ciudad Juarez and its surrounding communities [6]. Data from routine network monitoring provided hourly surface observations of chemistry species and meteorological parameters including temperature, relative humidity, wind speed, wind direction, ozone, nitric oxide (NO), the sum of nitric oxide and nitrogen dioxide (NO_x), carbon monoxide (CO), and particulate matter (PM) [6, 7]. During the campaign period, 13 August 1996 was the only day which exceeded a 1-h NAAQS (National Ambient Air Quality Standard) of 0.12 ppm in El Paso/Juarez area [7].

3 Description of modeling system, input data and numerical design

3.1 Model system

In our previous publication [8], we provided a detailed description of air quality model system that we used. There are three major components in this system: a meteorology model, a chemistry and transport processor, and an emission model. The meteorological model used is the Weather Research and Forecasting (WRF) [9], version 3.0. WRF is a next-generation mesoscale weather forecasting system designed to serve both operational and research needs. It is a limited-area, nonhydrostatic, primitive-equation mode with multiple options for various physical schemes. The Community Multiscale Air Quality Model (CMAQ) version 4.6 [10] has been used in this study as the chemical transport model. CMAQ is a comprehensive, three-dimensional, multiscale, Eulerian-based, atmospheric chemistry, transport and deposition model for multiple air pollutants including tropospheric ozone, acid deposition, particulate matter, visibility and air toxins. CMAQ has been served as a flexible and comprehensive modeling tool in various applications such as urban and regional air quality evaluations, formulating state implementation plans for non-attainment areas, and investigating atmospheric processes [11]. The emission inventory model used in this study is the Sparse Matrix Operator Kernel Emissions (SMOKE) Modeling System developed by Carolina Environmental Program at the University of North Carolina at Chapel Hill [12]. The SMOKE was used to convert the source-level emissions (county total emissions) reported on a yearly basis to spatially resolved, hourly emissions, with detailed speciation information. SMOKE can



generate the speciated, gridded emission inventory inputs for various air quality models, including CMAQ. SMOKE is able to process the point, area, biogenic, and mobile emission sources: point source emissions are gridded according to the physical location of emitting facilities; area and mobile source emissions are gridded according to the spatial allocation factors; biogenic emissions are calculated using Biogenic Emission Inventory System Version (BEIS) version 3.13 along with meteorological data such as surface solar irradiation and temperature. The version of SMOKE2.3 was used in this study.

3.2 Input data

The data incorporated into the WRF model as initialization and lateral boundary conditions are obtained from NCEP/NCAR Reanalysis with a 6 hour interval. This is the global dataset in the format of grib with the resolution of 2.5×2.5 degree. The emission inventory data used in this study are EPA's NEI99 (final version 2). The inventoried emissions in NEI99 include nitrogen oxides (NO_x), sulfur dioxide (SO₂), volatile organic compounds (VOCs), carbon monoxide (CO), ammonia (NH₃), and particulate matter (PM) for point, area, non-road and on-road mobile emissions. Since the modeling domain includes both US and Mexico, the latest released Mexico emission dataset (Mexico NEI99. <http://www.epa.gov/ttn/chief/net/mexico.html>), which include six northern border states of Mexico, has also been obtained as the supplementation for NEI99. All emission species were adjusted by running the SMOKE model from the year of 1999 to 1996.

3.3 Design of numerical simulations

As addressed in Lu et al. [8], the WRF model was run over a one-way nested modeling domain centered at the location of El Paso (31.70N, 106.40W) with the spatial resolution of 36-, 12-, 4- and 1-km for the outer, two middle and inner domains (Fig. 1). The use of high spatial resolution simulation such as 1-km was expected to resolve the unique weather phenomena occurring over the complex area like El Paso [6]. This is because mountainous topography produces regional circulation resulting in wind in the mountains and valleys which consequently affects the local pollutant transportation and dispersion. We used 35 sigma vertical levels in WRF with 15 layers within the planetary boundary layer (PBL) (less than 1500 m) where the lowest sigma level is at the height of 12m. This way helps resolve the emission and chemical reactions of pollutants occur within PBL. For WRF model simulation, the analysis nudging scheme, Four Dimensional Data Assimilation (FDDA) [13], was applied during the first 6 hour simulation in all domains in order to improve meteorological parameters forecasted qualities.



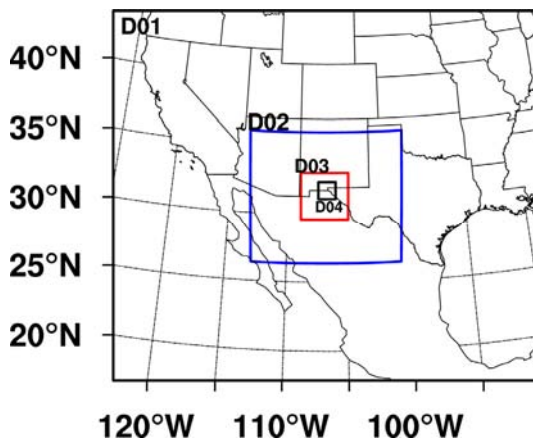


Figure 1: Nested domains used for WRF, SMOKE and CMAQ models. D01, D02, D03 and D04 are the outer, two middle and fine domains with the grid distances of 36-, 12-, 4- and 1-km respectively. The windows used by SMOKE and CMAQ are the maximum input of meteorological windows from WRF.

4 Results and discussions

4.1 Temporal evolution

One observational station, the site of Downtown El Paso, was selected to examine model performance in temporal variation of ground ozone concentration. Fig. 2 shows hourly surface ozone concentration comparisons between observations and model simulations at 1-, 4-, 12- and 36-km resolutions, respectively. It is found that all models provide a clear diurnal variation of surface ozone concentration. The maximum ozone appeared during the daytime and the minimum ozone occurred in the nighttime. For all models, the occurrences of peak ozone were noted to have a few hours lag between the simulations and the observation. The observed peak ozone was around 10:00 MST August 13 1996 while simulated peak ozone occurred around 13:00 MST from the 1-km model, 12:00 MST from the 4-km model, 15:00 MST from the 12-km model and 16:00 MST from the 36-km model. This suggests that the coarser the model spatial resolution, the more the lag of peak ozone occurs. In accordance with the peak value of surface ozone, the 1-km model yielded the best result with a reasonable agreement between simulation and observation being observed. For example, the peak value of 101 ppb was simulated with the 1-km model, 87 ppb with 4-km, 67 ppb with 12-km and 49 ppb with 36-km models while the observed value was 134 ppb [14]. All models underestimated the surface peak ozone concentration at this station. The 1-km model predicted 75% of the observed peak ozone concentration, 4-km model of 65%, 12-km model of 50%, and 36-km model of 37%. An evident overprediction of ozone

concentration occurring during nighttime was noted at each of the 12- and 36-km models while two fine resolution models (1- and 4-km) provided the comparable minimum ozone concentrations compared to the observations. The possible contribution for simulated ozone errors in coarse domains may originate from the simulation errors of surface temperature, wind speed or humidity, as well as from the uncertainties of emission distribution and intensity. Since all models run with the same physical and chemical processes, the spatial resolution is clearly the key factor producing model errors. For the grid-based model such as CMAQ, grid size is important because the characteristics of species are treated uniformly in each grid cell and chemical species are denoted by concentration instead of by mass itself [1]. If the grid cell size is relatively large compared to the spatial distribution of source areas, the intense emission sources could be artificially smeared throughout the entire grid cell. Consequently, coarse grid models tend to produce emission strengths that are too low when compared to physical measurements, especially in those major emission source regions. Because the processes that regulate species transformations are assumed to be uniform in each grid cell, certain characteristics of subgrid processes and their interactions may also be lost as the size of the model grid cell increases. Due to the nonlinear effect of ozone chemistry, an averaged treatment of subgrid processes in a large grid cell may not adequately represent the subgrid interactions of ozone, its precursors and their important processes. Therefore, the surface ozone concentration turns out to be underestimated.

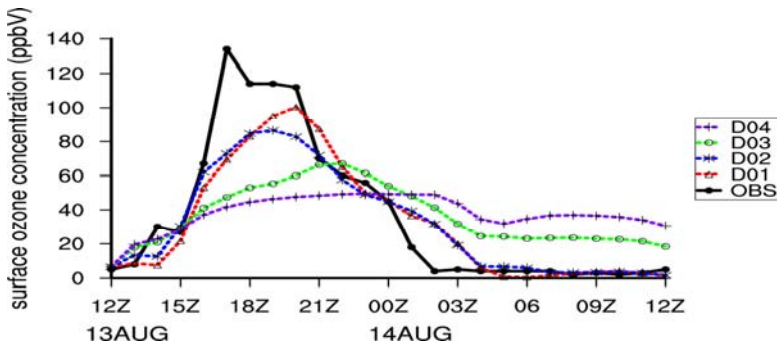


Figure 2: Hourly surface ozone concentration comparison between models at various spatial resolutions (1-, 4-, 12- and 36-km) and observation at the location of Downtown El Paso during the period from 12:00 UTC August 13 to 12:00 UTC August 14, 1996.

4.2 Spatial distribution

The model spatial resolution significantly influences the spatial pattern and central intensity of surface ozone concentration [1]. Fig. 3 shows the simulated surface ozone concentration at 20:00 UTC (13:00 MST) August 13 1996. Two coarser resolution models (36- and 12-km) produced the evident underestimates at most parts of the domain. The surface ozone centers are located at those areas

that are discernible at the major cities and their downwind areas (Fig. 3(a) and (b)). The central strengths at those major emission source areas are obviously enhanced as the spatial resolution increases. Compared to two coarse models, the higher resolution models (4- and 1-km) provided much more detailed and complex structures of the surface ozone simulations. Regarding the El Paso area, although all models underpredicted the peak surface ozone concentration, higher resolution models significantly reduced the problem of underestimation. It is seen that maximum surface ozone concentrations at the time of 13:00 MST August 13 1996 in El Paso area are 80 ppb in 4-km model (Fig. 3(c)) and 110 ppb in 1-km model (Fig. 3(d)). From an observational report [14], the average surface ozone concentration at El Paso / Juarez area at that time was around 114 ppb. The 1-km model of the CMAQ approximately captured the peak surface ozone while the 4-km model reproduced 72%, the 12-km model reproduced 63%, and the 36-km model reproduced 44%. Close examining the surface ozone

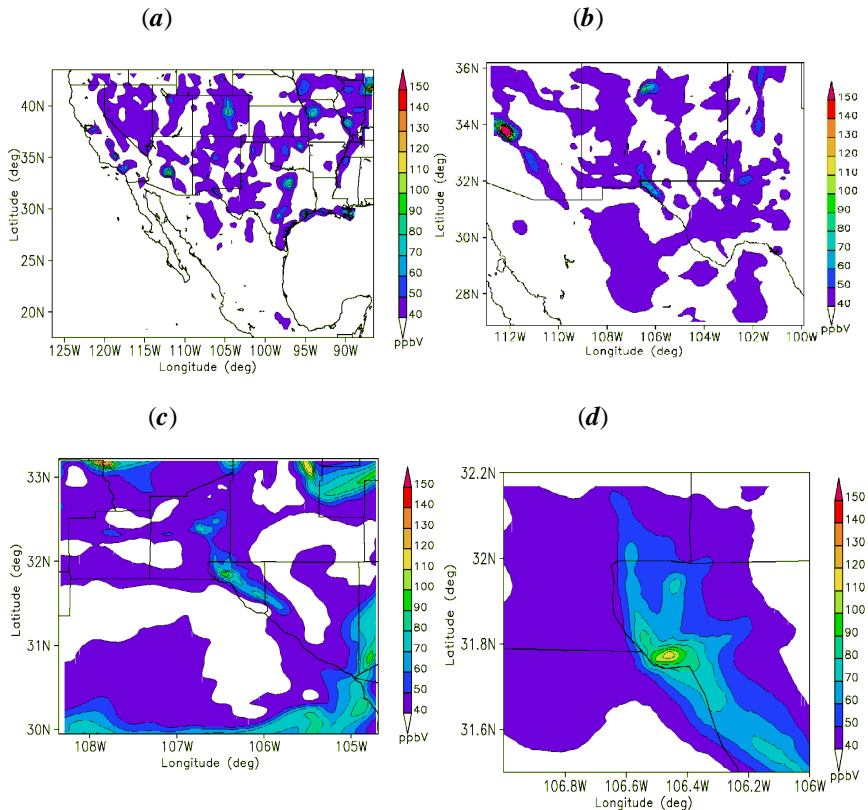


Figure 3: Surface ozone concentration (ppbV) at 13:00 MST August 13 1996 from CMAQ modeling with grid spacing of (a) 36-, (b) 12-, (c) 4- and (d) 1-km, respectively.

concentration distributions in the same region as the 1-km domain coverage from 36-, 12- and 4-km domains reveals that the coarse model (36-km) provided surface ozone distributions that were rather simple and smooth. The interested region was labeled with two lines of 40 ppb and 50 ppb contours (not shown). Many locally associated features were not captured. From 12- and 4-km domains it is found that (not shown) the higher the spatial resolution, the more detailed structures the model produced.

In addition, all models successfully captured the spatial evolution of surface ozone concentration (not shown). Simulations showed that, in the morning, high ozone concentration areas were located along Rio Grande River Valley. The distribution of surface ozone featured a spatial pattern of southeast-to-northwest direction. At the time of local noon, the center of surface ozone concentration moved northwestward and ended-up at the southwestern part of El Paso. Then, the surface ozone area moved westward along the US-Mexico border. This special pattern from model simulation is consistent with the local observations. Roberts et al. [14] reported that that an ozone cloud formed over the urban areas of Juarez and El Paso and flowed towards the northwest by the prevailing southeasterly winds. This unique track is mainly associated with the local topography distribution [7], especially under the ozone favorable condition where a calm weather dominates. The main geographical features of El Paso/Ciudad Juarez area are the Franklin Mountains, which run north-to-south and end abruptly just north of downtown El Paso; the Juarez Mountains, which lie to the west of Ciudad Juarez; and the Rio Grande River valley that divides the Franklin and Juarez Mountains and runs generally northwest-to-southeast through the domain. During summer, light northwesterly winds are prevailing under the condition of large-scale high pressure systems dominating in this area. Surface ozone will be advected through the prevailing winds northwestward. However, the Franklin Mountains stop further movement of the winds and turn them westerly, resulting in the spatial pattern of simulated surface ozone distribution.

4.3 Frequency distribution

To quantitatively describe the underestimation of surface ozone concentration from all models, the frequency distribution of hourly ozone concentration versus various concentrations at 13:00 MST August 13 1996 has been established (Fig. 4). The frequency is defined as the percentile fraction of the grid cells occupied by a given concentration threshold. It was calculated by considering all grid cells in each model. The range of surface ozone concentration corresponding to the peak frequency shifted to the higher ozone concentrations as model spatial resolution increases from 36- to 4-km. The peak frequency occurred at the range of surface ozone concentration between 30 - 40 ppb for the 36-km model, 40–50 ppb for the 12-km model, and around 50 ppb for the 4-km model. This indicates that the decrease in grid cell size will increase the number of places that exhibit higher surface ozone concentrations. However, the 1-km model simulation exhibited an exception in that the peak frequency of simulated surface ozone is located at the place of the concentration of 40 ppb. Closer inspection of



frequency distribution at high concentration thresholds (not shown) reveals that for the thresholds higher than 60 ppb, the frequencies of model outputs from two coarse grid resolutions, 36- and 12-km, were all zeros. In contrast, two fine grid resolution models, 4- and 1-km, provided the frequencies that were at the range from 1% to 5% at these high thresholds.

Figure 5 shows frequency distributions from all models where the frequency of each model was calculated by only considering those grid cells located within the coverage of the 1-km domain. With the focus being on such a small area, the

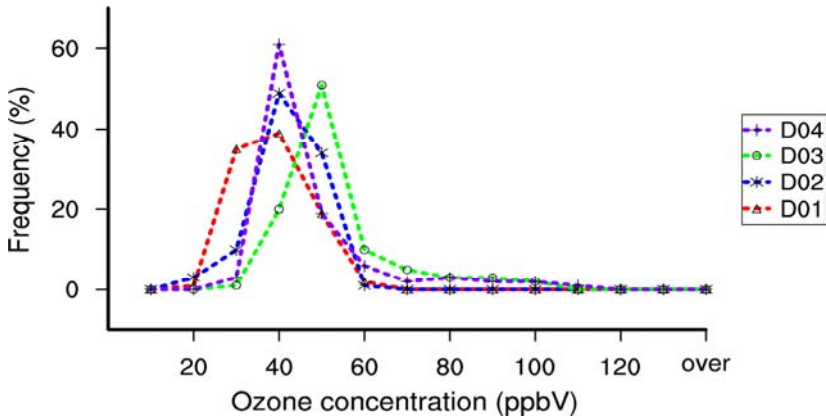


Figure 4: Comparison of the frequency distributions of hourly surface ozone concentration at 13:00 MST August 13 1996 from model outputs at 36-km (D01), 12-km (D02), 04km (D03) and 1-km (D04). There are 14 thresholds from 0–130 ppb.

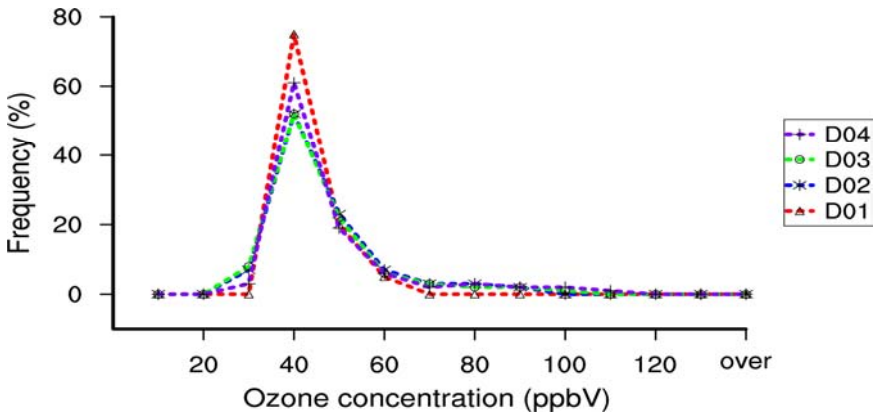


Figure 5: Same as Fig. 4 but with the frequency of each model calculated by only considering those grid cells located within the coverage of the 1-km domain.

threshold shifting among different spatial resolution models shown in Fig. 4 has not been found. The peak frequencies of all models occurred in the range of 40–50 ppb for surface ozone concentration. The 36-km model failed to capture the high ozone event because the frequency was approximately zero at threshold greater than 70 ppb. In contrast, two fine grid resolution models, 1- and 4-km, predicted some grids in this region with the surface ozone concentration exceeding 100 ppb. This mitigation of the surface ozone underestimation problem could be attributable to the capability of the high resolution models to resolve the fine information for the mountainous topography such as El Paso/Ciudad Juarez area.

5 Summary and conclusions

A modeling study was performed for a high ozone occurrence during the 1996 Paso del Norte Ozone campaign by incorporating meteorological model (WRF), emission model (SMOKE) and air quality chemical reactive and transport model (CMAQ) to investigate the sensitivity of model spatial resolution to surface ozone concentration. The results showed that grid resolution significantly affects the simulation of ozone formation, dispersion, transportation and structural distribution. Although all models captured the diurnal variation of surface ozone, a few hours lag of peak ozone concentration occurred for each model. The coarser the spatial resolution of model, the larger the lag of peak ozone. It is found that all models underpredicted the peak ozone concentration. The 1-km model produced the best result while the 36-km model yielded the worst. In addition, the coarser models (36- and 12-km) tended to overpredict the minimum ozone concentration in the nighttime. The problems of maximum ozone underprediction and minimum ozone overprediction are related to the spatial resolution model used. The minimum ozone overestimation may be attributed to the excessive predicting on the mixing process during nighttime. Excessive vertical mixing will result in upper-level ozone. The application of the high resolution model tends to suppress the excessive mixing process. Although previous studies have shown limited benefit with a higher grid resolution in ozone simulation and found that higher grid resolution simulation does not always enhance model performance, our studies revealed that increasing the horizontal spatial resolution is one way to reduce the problem of maximum ozone underprediction and minimum ozone overprediction. All models captured the evolution of the high ozone event. But the coarse resolution application (36- and 12-km) provided rather coarse textured spatial fields compared to the fine models (1- and 4-km). Many detailed and complex structures were lost from the coarser models. In contrast, the 1-km model provided an areal surface ozone concentration that is in very good agreement with that observed in the sense of central strength. The analysis of the frequency distribution revealed that the range of surface ozone concentration corresponding to the peak frequency shifted to the higher ozone concentration thresholds as the model spatial resolution increased from 36- to 4-km. But further increases in spatial resolution to 1-km did not draw the similar conclusion. The 36- and 12-km models failed to provide



the frequency that is greater than zero at the thresholds above 70 ppb. This suggests that the high ozone event can hardly be captured by using coarse spatial resolution models. Therefore, to successfully capture the high ozone occurrence, such as the event occurring on 13 August 1996, with the acceptable accuracy of central strength and sufficiently detailed structural distribution, a high resolution model (i.e., grid spacing is no greater than 4-km) is necessary.

Acknowledgements

This research was supported by the NOAA Educational Partnership Program with Minority Serving Institutions (EPP/MSI) under grant # NA06OAR4810172 through the NOAA Center for Atmospheric Sciences (NCAS). The authors want to express their gratitude to Dr. Paul Roberts, from Sonoma Tech, for providing them with important data collected during the 1996 ozone campaign performed in El Paso, TX. The support of NIH RCMI grant # G12RR013459-12 is also acknowledged.

References

- [1] Jang, J.C., Jeffries, H.E., Byun, D., Pleim, J.E, Sensitivity of ozone to model grid resolution: I. Application of high-resolution regional acid deposition model. *Atmos. Environ.* **29**, pp. 3085-3100, 1995.
- [2] US EPA. Guidance on the Use of Model and Other Analyses for Demonstrate Attainment of Air Quality Goals for Ozone, PM2.5, and Regional Haze, EPA-454/B-07-002, April, 2007.
- [3] Zhang, Y., Liu, P., Pun, B., Seigneur, C., A comprehensive performance evaluation of MM5-CMAQ for the Summer 1999 southern oxidants study episode, Part-I. Evaluation protocols, database and meteorological predictions. *Atmos. Environ.*, **40**, pp. 4825-4838, 2006.
- [4] Zhang, Y., Liu, P., Queen, A., Misenis, C., Pun, B., Seigneur, C., Wu, S.-Y., A comprehensive performance evaluation of MM5-CMAQ for the Summer 1999 southern oxidants study episode, Part-II. Gas and aerosol predictions. *Atmos. Environ.*, **40**, pp. 4839-4855, 2006.
- [5] Wu, S.-Y., Krishnanb,S., Zhang, Y., Aneja, V., Modeling atmospheric transport and fate of ammonia in North Carolina—Part I: Evaluation of meteorological and chemical predictions. *Atmos. Environ.*, **42**, pp. 3419-3436, 2008.
- [6] Brown, M.J., Muller, C., Wang, W., Costigan, K., Meteorological simulations of boundary-layer structure during the 1996 Paso del Norte Ozone Study. *Sci Total Environ.*, **276**, pp. 111-133, 2001.
- [7] MacDonald, C.P., Roberts, P.T., Main, H.H., Dye, T.S., Coe, D.L., Yarbrough J., The 1996 Paso del Norte Ozone Study: analysis of meteorological and air quality data that influence local ozone concentrations. *Sci. Total Environ.*, **276**, pp. 93-109, 2001.
- [8] Lu, D., Reddy, R.S., Fitzgerald, R., Stockwell, W.R., Williams, Q.L., Tchounwou, P.B., Sensitivity modeling study for an ozone occurrence



- during the 1996 Paso del Norte Ozone Campaign. *Int. J. Environ. Res. Public Health*, **5**, pp. 181-203, 2008.
- [9] Skamarock, W.C., Klemp, J.B., Dudhia, J., Prototypes for the WRF (Weather Research and Forecasting) model. In *Proceedings of Ninth Conference on Mesoscale Processes*, Fort Lauderdale, FL, USA. 2001.
- [10] Byun, D.W., Ching, J.K.S., Science Algorithms of the EPA Models-3 Community Multiscale Air Quality Model (CMAQ) Modeling System. EPA/600/R-99/030, US Environmental Protection Agency, 1999, Office of Research and Development, Washington DC, USA. 20460.
- [11] Lin, C.J., Ho, T.C., Chu, H., Yang, H., Mojica, M.J., Krishnarajanagar, N., Chandru, S., Krishnarajanagar, N., Chiou, P., Hopper, J.R., Sensitivity analysis of ground-level ozone concentration to emission changes in two urban regions of southeast Texas. *J. of Environ Manag.*, **75**, pp. 315-323, 2005.
- [12] Houyoux, M.R., Vukovich, J.M., Coats, C.J., Emission inventory development and processing for the Seasonal Model for Regional Air Quality (SMRAQ) project. *J. Geophys. Res.* **105**, pp. 9079-9090, 2001.
- [13] Stauffer, D. R., Seaman, N.L., Multiscale four-dimensional data assimilation. *J. Appl. Meteor.*, **33**, pp. 416-434, 1994.
- [14] Roberts, P.T, MacDonald, C.P., Main, H.H., Dye, T.S., Coe, D.L., Haste, T.L., Analysis of meteorological and air quality data for the 1996 Paso del Norte Ozone Study. Final report prepared for the U.S. Environmental Protection Agency, Region 6 Dallas, TX, by Sonoma Technology Inc. Santa Rosa, CA under subcontract to Science Applications International Corporation McLean, VA, 1997.



Breaking the connections: reducing and removing environmental health risk in the Canadian nuclear power industry

J. Eyles & J. Fried

*School of Geography and Earth Sciences, McMaster University,
Hamilton, Canada*

Abstract

In this paper, we examine how over the past twenty five years the nuclear industry has used various strategies to diminish or remove any environmental health risks that emanate from its practice and activities. Using both industry and critical website materials, we demonstrate how risk is removed by emphasizing its own safety culture in a complex process, its 'clean energy' credentials, its role in producing national energy options, close co-operation with its regulators, the ignorance of its critics, the suppression of opposing views and a narrowing risk assessment approach to potential environmental and health hazards. We suggest that the same strategies will be used after the recent Japanese nuclear disaster.

Keywords: branding, Canada, elimination of risk, environmental health, narratives, nuclear industry, power generation.

1 Introduction

Until the March 2011 catastrophe in Japan, the nuclear power industry seemed to have turned the corner from stagnation in the sector to widespread indications of growth. Since its dark days of 'nuclear winter' and the Chernobyl disaster, the industry has become a vital partner in the production of energy in many jurisdictions. Many countries are gearing up to assess the economic and political consequences of new reactors. Environmental and health concerns appeared of little importance in political decision-making as they had seemingly been dealt with by nuclear technological developments and safety standards. In this paper, we examine how the nuclear industry has reached this point. Paying special



attention to Canada and Ontario, we will comment on the industry's likely response to the 2011 crisis.

Ramana [1], in a review of nuclear power challenges, notes a widespread talk of nuclear revival, strengthened by 33 new reactors being constructed worldwide. Three main problems are identified, with nuclear weapons proliferation only mentioned as a side note: the high cost of nuclear electricity, the risk of a catastrophic accident and dealing with nuclear waste. Other studies point to elevated health impacts found among those living close to nuclear facilities. Yet the industry worldwide has worked diligently to ensure greater safety through technological and cultural changes within the industry and has addressed public concerns by communicating reassuring information with respect to energy production and nuclear waste. Fears of catastrophic events were dealt with by presenting statistically low probabilities of occurrence, often described as being once in a million years. Engineering standards were established to further better these odds, e.g. with the future Kincardine (Ontario) deep-geologic repository for low- and medium-level waste having an estimated safety factor ten times greater OPG [2]. Farsetta [3] notes that in the United States "the campaign to sell nuclear" has had great success. The industry has a set of varying approaches depending on which 'audience' is being addressed. This nuanced approach is likely to be seen in response to the Japanese nuclear problems. In this paper, we chart these approaches for the main industrial players and their associations and regulators as they use technological knowhow, the idea of fail-safe operations, and local economic power to attempt to remove environmental health risks from public discourse.

2 Responses of the nuclear industry: a theoretical interlude

Until March 2011, therefore, the nuclear industry had essentially cemented itself as a key element in the continued economic development of virtually all industrial nations. As Sundquist and Elam [4] argue, the nuclear renaissance has been framed in terms of ensuring security of the energy supply and the need to reduce CO₂ emissions.

Hudson [5] perceptively argues that some organizations must overcome core as well as event stigma. Event stigma emerges from specific events that may cast doubt on the legitimacy of an organization. Core stigma arises from the very attributes of the enterprise, *i.e.* what it is, what it does and who it serves with what. We do not, however, see these as discrete states. We suggest that for the nuclear industry, event stigma was transformed into core stigma as the fear of nuclear winter became linked not to weaponry but to power production, too. How then does the nuclear industry respond to this stigma? How do they legitimize their activities? We will show how the nuclear industry has changed its approach over time and for different audiences by pointing to its social relevance with key audiences, by pointing to the vital nature of its core activity to society in general, by demonstrating the illegitimacy of those who criticize it, by developing an organizational image of social worth and by enhancing its local and national reputation in terms of recognized parameters (such as scientific



validity and local community relations). Indeed, it has developed strategies and narratives to enhance its legitimacy and remove core stigma.

Hudson [5] suggests several strategies, some of which seem relevant to the nuclear industry. These strategic responses include specialized ones (where the organizations see themselves as specialized, complex entities), open ones (in which activities are broadly communicated with a normalizing narrative which stresses their societal importance), and network ones (in which the activities of the organizations are seen as linked to those of more legitimized bodies – regulators, governments – and/or expressed as part of a network of related companies). Some of these strategies have been noted in the narratives of the nuclear sector. The nuclear industry sees itself as a network of experts which can assist in the management of risk (while providing benefit) and permit the development and enhancement of ontological security. Hazards and insecurities can be managed by these expert systems.

In sum, the nuclear industry has adopted an interpretive strategy in which metaphor and communication are dominant in the development and maintenance of legitimacy (see Chaffee [6]). The nuclear industry has thus played down risk narratives, these being largely ‘fact sheets’ or reactive responses. Its strategy has been to minimize risk and hazard as it communicates its image and brand. As Loseke [7] notes, the power of the narrative of organizations is to tell convincingly the ‘right’ story to, we would add, the ‘right people in the ‘right’ way. In this paper, then, we illustrate the sophistication of the industry response to the stigma around its core activities by ignoring, trivializing or minimizing the often unspoken risk.

3 Data sources, methods and analytic approach

This paper explores the changing portrayal of environmental health risk by key nuclear companies in Ontario (Atomic Energy of Canada Limited (AECL), Bruce Power, Cameco, Ontario Power Generation (OPG)), their industry associations (Canadian Nuclear Association (CNA), World Nuclear Association (WNA)), and their national and international regulators (Canadian Nuclear Safety Commission (CNSC), International Atomic Energy Agency (IAEA)). These organizations form a complex array of production, regulatory and promoting institutions in Ontario.

The main data collection strategy to obtain material for our analysis utilized the websites of these organizations. As others have observed, public discourses are now best observed in technological media with annual reports and incident data seldom being widely circulated in print (Muhlhauser and Peace [8]).

Furthermore, a wide range of search terms was used and analysed. Analysing texts provides insight into how particular organizations present their image, reputation and brand over time and to different audiences as well as the views of their critics. Through quotations, this paper documents divergent images of the nuclear industry in Ontario.



4 Findings

We now turn to the narratives of the Canadian nuclear industry not only in response to its critics but also in how it communicates with governments and publics in general. We assert these responses try to break or minimize the connection between environmental health risk and industry actions or processes. First, there is the statistical removal of risk, often seen in terms of other exposures being far more dangerous to the environment and human health than plant or company activities.

An example here is the WNA-published and frequently cited comparison of deaths (per TWy electricity) due to major accidents among different production forms, with nuclear (8) having a lower number than electricity produced by hydropower (885), coal (342) or natural gas (85) WNA [9]. Interestingly, not included in this report are numbers related to wind or solar produced energy, perhaps due to the lack of major accidents.

In a press statement after the release of filtered water, OPG [10] commented that the (demineralised) water contained trace amounts of tritium, leading to a maximum potential increase of .56 Becquerel per litre but staying well below the Ontario standard for tritium in drinking water (7,000 Becquerel per litre). From a regulatory perspective, this was a very low level event. However, there is no comment that there is some degree of arbitrariness in such regulatory standards, with Ontario's seventy times greater than that of the U.S. CNSC [11].

In an often-cited, twenty year old book, Cohen [12] examined radiation exposure after accidents and noted that releases are usually minor and only very rarely have been as high as 5-10 millirem (mrem). So Cohen asks how dangerous is 1 mrem of radiation and uses a comparison with natural radiation for his answer. On average, people receive a total dose of about 85 mrem per year from natural sources, or 1 mrem every four days. Thus, an additional 1 mrem of radiation, according to Cohen, increases the risk of dying from cancer by about one in four million and results in a (statistical) reduction in life expectancy by two minutes. To further illustrate the risk associated with such additional radiation, Cohen compares it to daily activities and states that statistically it is as risky as crossing streets five times [12]. Arguments like these, however, do not consider all additive effects, risks related to inhalation of radioactive particles or the foregone investments in public resources that have to be used for clean-up after an 'accident'.

Furthermore, it is argued by proponents, that while there may be minimal risks from radiation, these are outweighed by the benefits nuclear technology provides, namely clean energy, nuclear medicine, and social protection. Small doses are seen as harmless WNA [9] and – as the IAEA [13] states – risks are everywhere and cannot be removed.

Another benefit often cited as advantage of using nuclear energy is the provision of a pollution-free (*i.e.* without environmental health risk) energy option in a world affected by climate change. Thus, the IAEA [14] has argued that the production of nuclear power produces virtually no greenhouse gas emissions. Following a similar argument, Ontario-based Bruce Power [15]



promotes its proposed new nuclear power plants to the provincial government in Saskatchewan by describing it as promising for developing clean energy and attracting significant private investment, while addressing an urgent environmental issue.

These arguments ignore any counterclaims that nuclear power is not the climate change panacea. In an exhaustive review, Savacool and Cooper [16] argue, for example, that electricity generation itself is only responsible for forty percent of global greenhouse gas emissions; that nuclear plants cannot easily adjust to load variations; and that nuclear power has higher costs than competitors per unit of net carbon dioxide displaced.

Social protection is also utilized as an argument for enhancing nuclear production (see Committee on Foreign Relations [17]), especially with respect to energy security. Wesley [18] makes a strong case for a worldwide concern about such security, while also flagging some potential problems, such as proliferation of nuclear elements across the world. The anticipated fossil energy depletion and the instability of their supply drive many countries to consider nuclear energy as their alternative energy source for the enhancement of their national energy security. 'Social protection' has been taken up by the nuclear industry and broadened to include citizen and environmental protection.

The nuclear industry also argues that environmental health costs may not exist as their critics are politically motivated or, more importantly, carry out poor or junk science, which then raises the concerns of a scientifically challenged public. For example, Cameco responded to a cancer epidemiologist's publicly raised concerns by criticising the "uninformed view of a biased outsider" for making many unsubstantiated claims (Thorne [19]).

It is interesting to note how science critical of nuclear activities is treated by the industry and is often portrayed as junk science (McGarity [20]). Examples of comparison between good and junk science can be found on the trade organisation's website CNA [21]. Another commonly employed way to marginalise critical voices is the immediate and concerted response to any academic studies or reviews reported in the media through letters to the editor and opinion pieces, e.g. Boreham [22, 23]; Moore [24–26].

According to the nuclear industry, it carries out sound science based on engineering principles and quantitative assessments, unlike its critics. Yet the industry is only an accident away from being accused of living in a glasshouse. Critics point to the problems of its 'fail-safe' branding. As Choo [27] points out, structural impediments may lead to failure, but the 'mentality' of fail-safe may lead to epistemic blind spots and risk denial. Still nuclear advocates, as we have seen, remain optimistic that technological innovation can minimize risk further and insist that critics simply incite fear with their commentaries. Thus, the nuclear 'brand' must be continuously protected in all responses.

Critics do not, the industry claims, understand how it operates and should thus accept that there are only limited environmental health risks due to nuclear technology's in-built operational redundancies in its fail-safe technology. The nuclear industry admits that minimal or theoretical risks exist but emphasises that these are completely controlled through expertise and government



regulation. The nuclear power sector claims to be the most regulated industry in Canada. So, as was noted about a public inquiry into the deep geologic repository in Kincardine, technical uncertainties are presented by advocates as either already or soon to be solved (Durant [28]). During the inquiry, claims were made “that expert groups could be trusted to have made the right judgments; that sufficient evidence was available to move to siting, because the disposal concept itself was a do-able scientific and engineering problem, and because regulatory bodies were providing adequate oversight [28, p.151].”

Bruce Power [29], on their public website, emphasises that they report to many different levels of government and their agencies and list several of these. In 2006, the company announced its restart plan for two mothballed reactors at the Bruce A Generating Station after receiving CNSC’s environmental approval that stated that the restart is “not likely to cause significant adverse environmental effects” (Algie [30]). Interestingly, the renewed operating license for Bruce B also permitted a pilot project for the use of enriched uranium fuel in place of natural uranium [30].

Cameco [31] also described its regulatory environment on its website, noting that the CNSC has lead responsibility for regulating activities at both its Ontario facilities, but detailing also other avenues of monitoring and reporting.

IAEA has also given its approval after inspection of nuclear facilities in Canada. So while well run, some question the arms-length nature of the companies from the regulators. CNSC has been criticized for having an industry and technical mind set. Its budget is provided in significant measure by the companies it regulates. IAEA is also dependent on country-based funding as well as operating in the political climate of the U.N. and its drivers.

From the nuclear sector’s perspective, benefits can also be maximized and costs and risks minimized at the local level. In some ways, this is where the nuclear sector can respond easiest to a particular audience and where high paying local jobs and investments are provided and can bolster support. Perceived risks are diminished as benefits are invoked – through local investments in public goods (e.g. clinic), greening, local environmental protection, and sharing the profits (e.g. giving to local community organisations). For example, Bruce Power [32] has “provided \$500,000 to upgrade diagnostic equipment at the Southampton and Owen Sound hospitals and pledged \$400,000 to the Women’s House Serving Bruce & Grey to help build transitional housing for women and children in need in four local communities.” An economic impact study shows direct and indirect spending in Port Hope by Cameco’s two local facilities totalled almost \$63 million in 2005, accounting for 9% of the total economic activity in the municipality during that year [31].

5 Discussion and conclusion

All the above described removals of risk are encapsulated in the ‘nuclear brand’. There is positivity in the nuclear communication responses whether pro- or re-active. This can be best seen in its branding. Yet the nuclear sector has a specific problem, namely its core stigma. Horlick-Jones *et al.* [33] note the extent to



which a nuclear label is able to generate a sense of stigma for the technology in question, exerting a powerful influence on the lay imagination.

Nuclear agencies use all the described ideas related to climate change, energy supply security and sound technology in their claims and communications about their role. Reference is made to the natural world, clean production spaces, children as a metaphor for the future and innocence, and blue sky for unlimited thinking and openness. To generalise from CNA, the brand is clean, affordable, future-oriented, attentive of families and their ways of life and mindful of its critics. All they require is the truth to be told.

We have shown how nuclear energy in Canada tried to overcome the tipping point of Three Mile Island and Chernobyl. With its appeals to fail-safe technofixes related to energy security and climate change, the sector placed itself close to government and seemed to be the answer for future energy needs. Through its response strategies to criticisms and its proactive communication styles and images, it reshaped its organizational identity. It was a corporate citizen, giving back to local communities in particular for the right to operate. It had shown resilience and seemed to have overcome core stigma as there were no episodes to produce event stigma. It is become a transparent industry run by dedicated professionals acting rationally on the bases of sound science. And then something happened. Soon after a massive earthquake and tsunami on 11th March 2011, six reactors at the Fukushima Daiichi nuclear power plant in Japan reached various critical levels. Now, the accident is being classified by the IAEA [34] at the highest level 7 of the International Nuclear and Radiological Event Scale, and thus the same as Chernobyl. So after twenty five years of actively breaking the connection between the sector and environmental health risks, they appear to be reconnected. It is too early to know the long-term response, but the usual ones are being put forward – safety flaws; given the catastrophic events, denial that such an event could happen in most nuclear jurisdictions; alternative energy production methods are more deadly, foreign oil dependability grows more fraught, the next generation of nuclear technology will be better. Many sound like arguments still played out to address the concerns of the 1970s and 1980s: déjà-vu all over again.

References

- [1] Ramana, M.V., Nuclear Power: Economic, Safety, Health, and Environmental Issues of Near-Term Technologies. *Annual Review of Environment and Resources*, **34**, pp. 127-52, 2009.
- [2] OPG, *The Deep Geologic Repository*. <http://www.opg.com/power/nuclear/waste/dgr/>, 2011.
- [3] Farsetta, D., The campaign to sell nuclear. *Bulletin of the Atomic Scientists*, **64(4)**, pp. 38-41, 2008.
- [4] Sundquist, G. and Elam, M., Public involvement designed to circumvent public concern? The “Participatory Turn” in European nuclear activities. *Policy Studies Organization*, **1(4)**, pp. 203-29, 2010.



- [5] Hudson, B.A., Against all odds: a consideration of core-stigmatized organizations. *Academy of Management Review*, **33**(1), pp. 252-666, 2008.
- [6] Chaffee, E.E., Three models of strategy. *Academy of Management Review*, **10**(1), pp. 89-98, 1985.
- [7] Loseke, D.R., The study of identity as cultural, institutional, organizational, and personal narratives: theoretical and empirical integrations. *The Sociological Quarterly*, **48**, pp. 661-88, 2007.
- [8] Muhlhausler, P. & Peace, A. Environmental discourses. *Annual Review of Anthropology*, **35**, pp. 457-79, 2006.
- [9] WNA, *Safety of nuclear power reactors*. <http://www.world-nuclear.org/info/inf06.html>, 2011.
- [10] OPG, *Low impact filtered water release to environment*. <http://www.opg.com/news/releases/110316lowlevelwaterrelease.pdf>, March 16th, 2011.
- [11] CNSC, *Standards and guidelines for tritium in drinking water*. http://nuclearsafety.gc.ca/pubs_catalogue/uploads/info_0766_e.pdf, CNSC Ottawa, 2008.
- [12] Cohen, B.L., *The nuclear power option*. University of Pittsburgh Press: Pittsburgh, 1990.
- [13] IAEA, www.iaea.org, 2011.
- [14] IAEA, *Climate change and nuclear power*. http://www.iaea.org/Publications/Booklets/ClimateChange/climate_change.pdf, 2000.
- [15] Bruce Power. *Bruce Power launches Saskatchewan 2020 initiative*. <http://www.brucepower.com/pagecontent.aspx?navuid=1212&dtuid=83768>, June 18, 2008.
- [16] Sovacool, B.K. and Cooper, Chr., Nuclear nonsense: Why nuclear power is no answer to climate change and the world's post-Kyoto energy challenges. *William & Mary environmental law and policy review*, **33**(1), pp. 1-119, 2008.
- [17] Deutch, J. & Schlesinger, J.R., *National security consequences of U.S. oil dependency*. Independent Task Force Report No. 58, www.cfr.org/content/publications/attachments/EnergyTFR.pdf.
- [18] Wesley, M., *Power Plays: Energy and Australia's Security*. Canberra: Australian Strategic Policy Institute, 2007.
- [19] Thorne, A., Standing with the people of Port Hope. www.cameco.com/fuel_services/common/.../Cameco_-_Caldicott-ml-lk.pdf, 2010.
- [20] McGarity, T., 2003. Our science is sound science and their science is junk science: Science-Based Strategies for Avoiding Accountability and Responsibility for Risk-Producing Products and Activities, *Kansas Law Review*, **52**, pp. 897.
- [21] CNA, Canadian Studies. http://www.cna.ca/english/studies_reports/canadian_studies.html, 2011.
- [22] Boreham, D., Opinion: Selective data led to one-sided report *The StarPhoenix*, 10 July, A6, 2009.



- [23] Boreham, D., The Lemstra nuclear health study is flawed, *Northumberland Today*. 2009.
- [24] Moore, P., Selective citation in Lemstra report. *Northumberland Today*, 7 July, 4, 2009.
- [25] Moore, P., Letters to the Editor, *The Calgary Herald*. 1 April, 2009.
- [26] Moore, P. (2009c). Renewables won't solve all our energy needs, *The Toronto Star*, 9 July, A18, 2009.
- [27] Choo, C.W., Organizational disasters: why they happen and how they may be prevented, *Management Decision*, **46(1)**, pp. 32-45, 2007.
- [28] Durant, D., Responsible action and nuclear waste disposal. *Technology in Society*, **31**, pp.150-57, 2009.
- [29] Bruce Power, Safety and environment. Regulatory reporting, <http://www.brucepower.com/pagecontent.aspx?navuid=602>, 2011.
- [30] Algie, J., Bruce A project gets go ahead, *Owen Sound Sun Times*, July 6 2006.
- [31] Cameco, *Frequently asked questions*. http://www.cameco.com/fuel_services/faq/, 2011.
- [32] Bruce Power, *Bruce Power Celebrates Safety Record with \$15000 donation to children in need*. Press Release August 28 2009, <http://www.brucepower.com/pagecontent.aspx?navuid=1212&dtuid=84053>.
- [33] Horlick-Jones, T., Prades, A. & Espluga, J., Investigating the degree of “stigma” associated with nuclear energy technologies: a cross-cultural examination of the case of fusion power, *Public Understanding of Science*, <http://pus.sagepub.com/content/early/2010/07/20/0963662510371630>.
- [34] IAEA, *Statement to International Conference on Chernobyl: Twenty-Five Years On - Safety for the Future*, by IAEA Director General Yukiya Amano, <http://www.iaea.org/newscenter/statements/2011/amp2011n010.html>, 2011.



This page intentionally left blank

Disaster management and generational complacency: five crucial lessons

E. G. Bianchi

Group Manager, Noel Arnold & Associates, Australia

Abstract

The World has suffered major disasters in the last 24 months. What have we learnt from natural disasters in the past, and what can we do differently in the management of critical disasters to minimise their impact on life, property and the environment? From a realistic and practical perspective, this paper will challenge conference attendees to consider the relationship between historical events and generational complacency, a learning from history, in measures to manage disasters, from devastating floods (which regularly flood the major Australian state of Queensland and city of Brisbane), to bushfires in 2009 which killed almost 200 hundred people.

Australia has a unique history of natural disasters, ranging from extremes in high temperature, to floods and cyclones. The impacts of these are highly destructive, and Australia, like some countries, has partly learnt from the past, and has developed extensive capability and strategic approaches for pre-empting and managing such events, lessons which have world wide application and benefit. Techniques for pre-planning as well as dealing with the aftermath of a disaster are critical in ensuring that the confidence of the public is restored and/or maintained to ensure the effective “normalisation” of communities post the disaster.

A simple risk management philosophy will be proposed to define the 5 lessons to manage such disasters, which all too often are a victim of generational complacency resulting in ineffective emergency management.

The paper will provide a summary of mistakes from the past, Australia’s current initiatives and techniques in addressing emergency needs, including prevention, communication, response and recovery. Conference delegates will



gain a unique and valuable insight into learning from the past, and the pro-active disaster management processes and techniques which must be formalised and enabled into the future.

Keywords: risk, fire, disaster, flood, resilience, prevention, Australia, system, generation, complacency.

1 Introduction

The management of past disasters in comparison to the approaches of today, has provided governments, authorities and community groups, including crisis and critical incident management personnel, a wealth of knowledge and data. One must ask, with an abundance of information and technologies that we still see major incidents being ineffectively managed and poorly planned for, placing huge social, physical and economic burdens on countries. This paper will challenge global thought patterns and community expectations to learn from history, and explore how generational change and complacency has played a contributing factor to ineffective disaster management.

Major natural disasters in Australia are generally predictable, however despite the best intentions of most governments and community groups, have been poorly managed and controlled. Worldwide, we continue to repeat the errors of the past. The five crucial lessons that need to be understood and communicated to current and future generations are as follows:

Lesson 1: Learn from the past – History repeats

Lesson 2: Evaluate the Impact of Incidents

Lesson 3: Legislate Change – Policy and Governance

Lesson 4: Design and Communication

Lesson 5: Future Proofing

This paper will focus on a number of recent and past natural disasters in Australia, which will provide the framework for the above lessons.





2 Lesson one: learn from the past: history repeats

Australia, like many countries around the world has a unique natural risk profile, being that it is susceptible to extreme heat, droughts, fires, cyclones and floods. As a result the country experiences extremes of weather and environmental events. Major fire and flood events continue to affect Australia. In the last two years Australia has once again suffered major floods and fires, events which are cyclic in nature and are generally predictable. Once again, these events have proven that there is one very important lesson that it is not being learnt (in Australia and globally for that matter) – learn from the mistakes of the past and do not fall not into the trap of generational complacency. Subsequently allowing the effects of time and years post disaster to reduce drive, engagement and resourcing in an attempt to implement preventative risk controls. Risk management methodologies need to address generational complacency as a real contributory factor.



2.1 Floods

The area of Brisbane located in Queensland has experienced major flooding over the centuries. Recent floods have occurred in 1974 and 2011 both similar in nature, with economic impact measured at approximately 6 billion dollars [1] each (refer Figures 1 to 4). In 1974 the lesson learnt was the need to mitigate the damage of future floods, and as a result the Wivenhoe Dam was built. The dam was completed in 1984 and located approximately 80km upstream from the City of Brisbane.

	
<p>Figure 1: 1974 Brisbane (State of Queensland) flood waters covering much of the city and metropolitan areas.</p>	<p>Figure 2: 2011 Brisbane city entertainment inundated by 10m floods.</p>
	
<p>Figure 3: 2011 Brisbane River engulfs foyers and first floor areas of city skyscrapers. Flood waters inundate entire city blocks and much of the metropolitan area.</p>	<p>Figure 4: 2011 Wivenhoe Dam releasing water in an attempt to mitigate flood damage. Areas downstream flooded. Water levels within the dam are at capacity.</p>

(Photos: Fairfax digital newspapers, State Library of Queensland, and Brisbane Times.)

In 2007 the Wivenhoe Dam was at 17% capacity. In 2011 it was at 190% capacity [2] (refer Figure 4). A massive storm system and rain deluge over a few weeks, influenced by a strong La Nina, dramatically broke the drought in Queensland which had lasted for many years. This dam was to play a major role in controlling the massive water influx into the Brisbane river catchment area and surrounds, but its effectiveness to do so was compromised due to a failure of Authorities to act on Bureau of Meteorology advice to release water from the dam early. A number of questions were posed to why the government and authorities not act early enough?:

- Was it due to generational complacency and minimal first hand experience or memory of the floods that occurred approximately 35 years earlier?
- Was there a failure to effectively communicate the need to release water?
- Was the State's emergency crisis preparedness not really ready?
- Fear of public reaction to release so much water when the state of Queensland was on water usage restrictions?
- Was it not known that a full dam holds no more water!

The Bureau of Meteorology has maintained a detailed history and trend of flood events in Queensland [2]. The impacts are predictable if measures are not taken to reduce the effect of these natural disasters. The answers to the above questions are currently being investigated by government enquiries and commissions. There is however an element of generational complacency and in particular of a failure to learn from the past, knowing that the dam was designed to mitigate flood damage, which required early intervention.

2.2 Fire





Fires within Australia are common and part of our landscape and history as is evident from the fires of 1926, 1939, 1967, 1983 and 2009.

These fires and in particular the events in 1983 [3] and 2009, were almost identical in nature, spaced almost 30 years apart, as per the Brisbane floods. The photos G and H show a very similar theme. The lessons of 1983 and 2009 were not implemented and despite various enquiries and investigations into the fires, the following prevailed:

- Fuel loads were not reduced in forest, urban and residential areas;
- Buffer zones and clearances around properties were not adhered to nor maintained;
- Design codes and recommendations for residential properties in fire prone areas were not effectively addressed and implemented;
- Realistic and well communicated emergency plans were weak and not effectively activated; and



- The use of animal stock to help reduce fuel loads and forest undergrowth (as had occurred for over a hundred years prior), was prevented due to vocal conservative groups.

	
<p>Figure 5: 1939 Victoria, Australia – Towns devastated.</p>	<p>Figure 6: 1967 Tasmania, Australia – Towns devastated.</p>
	
<p>Figure 7: 1983 Victoria Australia “Ash Wednesday” – Massive fires, causing many fatalities and devastating many towns are only stopped by the oceans. Ash Wednesday.</p>	<p>Figure 8: 2011 Victoria Australia “Black Saturday”. Almost 200 people killed and thousands of homes burnt to the ground.</p>

(Photos: “Burn” by Paul Collins, and Dept. Sustainability and Environment.)

2.3 Generational complacency

The impact from of disasters has evolved over time from a local to a national issue to one where global live coverage is the norm, with potential impacts on financial markets and global welfare organisations. Countries are not learning from the past, particularly with the technology today that enables greater scrutiny with widespread global media coverage. Complacency, generational change,



memory, and bureaucracy have all played a part. The CSIRO [4, 5] and many other reputable research organisations in Australia have known for a long time that fires, floods and natural disasters are not unpredictable and are not a matter of “if” they occur, but “when” they will occur.

Very quickly the world is realising that with the aid of globalisation, live TV coverage, internet and communications technology, natural disasters are telecast live within homes all around the world. This has immediate social, economic and political impact, unlike in the past, and can have catastrophic consequences. The common theme that stems from Australian natural disasters, and indeed global natural disasters, is that pre-1980’s, there were limited scrutinised approaches to the management of the events. The current processes attempt to apply pro-active management systems to control the risk. There is also greater legislative impetus on countries to manage these events, with building and design changes, and legislative change.

The frequency of the Australian natural disasters is on average 30 years apart, coincidentally a generation apart. What has been learnt to manage these events and their impact on society? Despite a concerted effort to address the root cause immediately following the events, and after the “dust” had settled, the initial impact of the tragedy had worn off, editorials in the newspapers and headlines had disappeared, the urgency and need to drive change had slowed down. Governments and authorities change, and new faces and generations are left to realise this change. A common failure is not learning from the past and not factoring in generational change in the risk matrix.

3 Lesson two: evaluate the impact of incidents

Consistent with criteria defined in ISO31000 Risk Management, one must clearly identify the areas of vulnerability and/or exposure in any disaster management plan. When looking at natural disasters, one can identify 5 areas of exposure and impact of an incident as follows:

- Physical;
- Social;
- Political;
- Environmental; and
- Economic.

The challenge in a pro-active risk management program is the effective quantification of the impact of a major disaster, and today this is often seen live globally (as seen in recent events including the recent earthquakes and Tsunami’s in Japan and Thailand). In an effort to provide a broad summary of the 5 key parameters, the following Table has been developed which shows the impact on the various criteria and the comparative effect on a time scale. As can be seen from Table 1 below, natural disasters are providing mechanisms and knowledge to effectively manage events into the future with key initiatives going forward. The expectations of the community in the future will be closely aligned to risk elimination and mitigation.



Table 1: Chronological natural disaster impacts.

Impact	Historic	Current	Predicted
	Pre-1980	1980—2011	2011-2040
Physical	Property damage. Temporary local reactive media coverage. Minimal evaluation of social/psychological impact on affected people.	Quantification of infrastructure damage. Risk profiling. Live global pictures and video. Personal and community group accounts of negative aspects of physical impact.	Physical impact pre-empted. Construction plans in place to re-build appropriately.
Social	Impact on communities, culture, history not fully quantified limited, and mostly lost.	Impact on social wellbeing controlled and measures taken to control negative impacts via counselling, forums, global support. Indigenous impact a consideration.	Prompt and pre-emptive intervention Aspects of social impact that are critical to maintaining positive culture and drive maintained and encouraged.
Political	Reactive response to disasters. Leadership minimal, and mostly taken up by emergency response personnel. Criticism of political parties lively but limited in impact owing to lack of importance placed on pro-active risk management	Leadership taken from political heads of government, supported by emergency personnel and advisors. Potential for responsible parties to be liable. Community expectation of government heightened with leaders being judged and critiqued.	Leadership is expected of their politicians. Litigation, whilst not eliminated is minimal, as due diligence and pre-emptive risk management policies are realised. Politicians will drive change.
Economic	Minimal knowledge on how to effectively quantify. Actual impact \$ estimated, but the final costs are rarely known.	Economic cost considered in global spheres, impacting on share markets. Rebuild costs are quantified. Insurance is generally in place. Global assistance usually reactive.	Economic evaluation is the norm. Global assistance packages are pre-empted. Insurance companies assign to global catastrophic insurance.
Impact	Historic	Current	Predicted
	Pre-1980	1980—2011	2011-2040
Environmental	Minimal consideration of environmental impact.	Environmental considerations are part of pro-active risk management plan. True impact on environment is critiqued by vocal environmental groups.	Impact is known and effective measures promptly implemented to manage the environment in a sustainable way.



4 Lesson three: legislate change – policy and governance

The need to legislate compliance with new initiatives and lessons learnt from previous events is continually evolving; however their effectiveness is once again impacted by generational complacency to remember events, their route cause and to drive change. In 2003 the Council of Australian Governments (COAG) [5] ‘Review of Natural Disaster Relief and Mitigation’, recommended:

- National risk assessment of natural disaster prone areas;
- Improved community awareness and instruction on risk; and
- Improved land use planning and gathering the data to convince governments on real positive return on investment.

Whilst positive change is improving, the recent events in Australia (the widespread floods in Brisbane and devastating bushfires in Victoria) are classic examples of the failure to engender and value change. We still continue to build vulnerable homes in bushfire prone areas [6], and build commercial, residential properties and many 50 storey skyscrapers in areas that will flood again. We continue to stumble in achieving effective pro-active emergency preparedness and risk mitigation systems. What is even more alarming is the fact that the Queensland Government had not taken up its insurance to cover the loss of public assets in the event of a flood, in an attempt to save \$50m per annum in insurance cover [1]. This alone has almost made the state bankrupt, necessitating the creation of special taxes and levies imposed on all Australians.

The 1983 bushfires in Victoria have provided the drive to identify the need for state based disaster plans, with emergency management authorities all playing a key part. Red tape and bureaucracy have contributed to major failures in risk control and disaster preparedness, despite the best intentions of legislators since 1983 [7]. So what are we looking at in terms of legislating change? It is clear that ownership and endorsement of the need for change from our regulators and authorities is essential. Cultural change and generational engagement is needed.

5 Lesson four: design and communication

A necessary part of the legislative change is to put into effect the requirements of all the parameters impacting on engineering design and maintenance. Reforms are already occurring with regulatory obligations now placed on various contracting parties involved in planning and design. This includes:

- Obligations of designers, planners, builders and authorities;
- Business continuity and resilience plans; and
- Communication protocols for leaders and advisors including live telecommunications, web updates, disaster zone and mobile phone emergency warnings.



The obligations are simple – ascertain your risk profile and minimise and/or eliminate that risk. This will ensure that due diligence obligations are met. It is important to do a “health” check of your risk management program and to test the program on a regular basis. If the system is not challenged, your emergency preparedness will be exposed, as demonstrated by recent events within Australia and globally. Engineering solutions are available to mitigate the impact of fires and floods, and it is worth noting that the design of residential properties in Brisbane and more broadly in the State of Queensland pre 1980’s, were flood resistant, with open flow though areas below, and living areas above – very different to the way residential properties are built in these same areas today.

6 Lesson five: future proofing

If we continue to not adhere to the lessons learnt from the past, then exposure to major disasters impacting adversely (and unnecessarily) on our lives will continue. Being prepared for an undesirable but known event is an important step in ensuring that we are not being negligent in the exercise of powers and effective risk control. The question could be asked whether the authorities and powers at the time of the above events were negligent, or did they just fall into the trap of generational complacency. The answer to whether negligence played a part is still being played out in the courts today. The general trend into the future is the anticipation of events and pre-empting their occurrence, impact and their management [8]. The lesson will be to know how these events will impact on a country, how to effect risk minimisation and control, and to test plans and their resilience into the future, based on past, current and anticipated scenarios. If the answer to all of the following questions is yes, then one can say that they are well prepared to engage and mitigate impending disasters:

- Is reliable data, including events of the past, and information accessible and being used by authorities to predict natural disasters?
- Have risk control and recovery plans been tested and proven effective for anticipated risk scenarios?
- Have responsibilities been allocated to authorities and tested in order to take effective control?
- Has infrastructure and building design risk evolved?
- Has generational complacency been addressed?

7 Conclusion

Heading towards 2040, approximately 30 years from now, we can expect the pre-empting and future proofing, as far as is practicable, of natural disasters. The key lessons for the management of future natural disasters are to learn from the past, apply the technology of today, implement real risk mitigation controls, and to beware of generational complacency.



References

- [1] Xenophon, N., Federal Senator, Editorial, 1 March 2011.
- [2] Australian Geographic, Journal, Brisbane Floods, January 2011, www.australiangeographic.com.au.
- [3] Department of Sustainability & Environment, Victoria, Fire & Other Emergencies, Bushfire History, Ash Wednesday Bushfire 1983, www.dse.vic.gov.au.
- [4] Braganza, K. & Church, J. A., Observations of Global & Australian Climate, CSIRO, 2011.
- [5] Lloyd, G., The Australian, Facing a Climate of Uncertainty, April 5, 2011.
- [6] Cary, G. & Lindenmayer, D. and Dovers, S., Australia Burning, Fire Ecology & Policy Mgt Issues, pp. 34-105, 2008.
- [7] Teague, B. & McLeod, R. & Pascoe, S., 2009 Victorian Bushfires Royal Commission, August 2009.
- [8] Standards Australia, AS/NZS ISO 31000:2009, Risk Management - Principles and Guidelines, Part 5, Process.



Generic mapping of human activity-based exposure scenarios to petroleum hydrocarbon contaminants in an oil producing area of the Niger Delta region of Nigeria

W. J. Shittu, C. P. Nathanail & R. J. Abrahart
School of Geography, University of Nottingham, UK

Abstract

Oil spills worldwide may occur during production and transportation by accident, equipment failure and error. However, the common cause in the Niger Delta region of Nigeria has been attributed to pipeline sabotage and vandalism. Over the past 50 years a total of 6,817 oil spill incidents have been recorded resulting in the discharge of more than 9 million barrels of crude oil into the environment of which over 70 per cent remains unrecovered. The negative impact of such oil spills on human health and the environment can be severe. Most of the oil spills in the region occur from pipeline discharge in or near rural communities where people survive mainly on naturally available resources, engaging daily in traditional activities like hunting, fishing, farming and gathering even at the risk of exposure to oil contaminated media.

This paper identify traditional rural activities in the region and map areas vulnerable to risk of exposure to petroleum hydrocarbon contaminants, base on a relative risk ranking model for traditional activities undertaken by the people. It indicates traditional activity with the highest risk according to age/gender following an average daily exposure scenario. To achieve this, oil spill site datasets from 1985 – 2008; spatial location of 354 rural communities; several kilometres of pipeline network digitised from SPOT satellite imaging was inputted into a GIS to map community proximity to oil pipeline routes and historic spill sites. Map overlay, buffering and Boolean operations were performed to determine community vulnerability to oil spill releases using proximity to pipelines and rivers, and land use type. The map will be beneficial



to oil companies, communities and government agencies in assessing the size of sites becoming polluted for remediation/management/compensations.

Keywords: risk, contaminants, exposure, pathway, oil spill, pollution.

1 Introduction

The Niger Delta covers an area of about 70,000km². It contains more 800 oil producing communities, 1000 oil producing wells, in addition to flow stations, gas plants and about 4,315km multi-product pipelines which criss-cross the delta [2]. In 1956 when the first oil-well was drilled by Shell in Oloibiri Bayelsa state, large quantities of crude was spewed into the environment and the people celebrated with a football match against the Shell staffs [3]; little did they know that oil spill will one day become a major environmental problem to confront them. Over the past 50 years more than 6,817 oil spill incidents have been recorded resulting in the discharge of about 9million barrels of crude with more than 70 per cent unrecovered [4]. This figure is nearly twice the quantity spilled in the Gulf of Mexico from BP's Macondo well in 2010. Amnesty International [5] pointed out that many polluted sites in the region have not been cleaned-up; as a result, the quality of the local water, food and livelihood has been compromised.

The majority of the oil spills in this region occur from pipeline discharge caused by equipment failure, operational error, sabotage and or vandalism. However, [1] claimed that oil theft and sabotage accounted for 98% of oil spill incidents in 2009, leading to the discharge of at least 14,000 metric tonnes or about 100,000 barrels of crude oil into the environment. This claim was collaborated by [6] indicating a total of 1,453 pipeline incidents attributed to vandalism in the same year.

Several International Oil Companies (IOCs) like Shell, Mobil, Chevron, Texaco, Total E&P, Pan-Ocean and NAOC/Phillips operate joint venture agreements with the Nigerian Government through the Nigerian National Petroleum Corporation to produce about 2.2million barrel of crude per day [6] from onshore and offshore fields. The majority of onshore oil production takes place in the Niger Delta region comprise Abia, AkwaIbom, Bayelsa, Cross River, Delta, Edo, Imo, Ondo and Rivers States (see Figure 1: insert). Of the 70,000km² total land mass of the region, about 31,000km² accommodates oil production facilities. The entire Niger Delta is inhabited by several traditional historic communities with a total population of 42.6 million [7].

The implications of oil production in this area are the taking over of common traditional land use space and high rate of pollution from incessant oil spills. In this paper risk related areas to actual and potential petroleum pollution are mapped using GIS to identify source of oil spill, type of land use activities, communities within and around historic oil spill sites. The basic aim of this paper is to identify traditional rural activities synonymous with the region and map areas vulnerable to risk of exposure to petroleum hydrocarbon contaminants using a traditional activity-based relative risk ranking model.



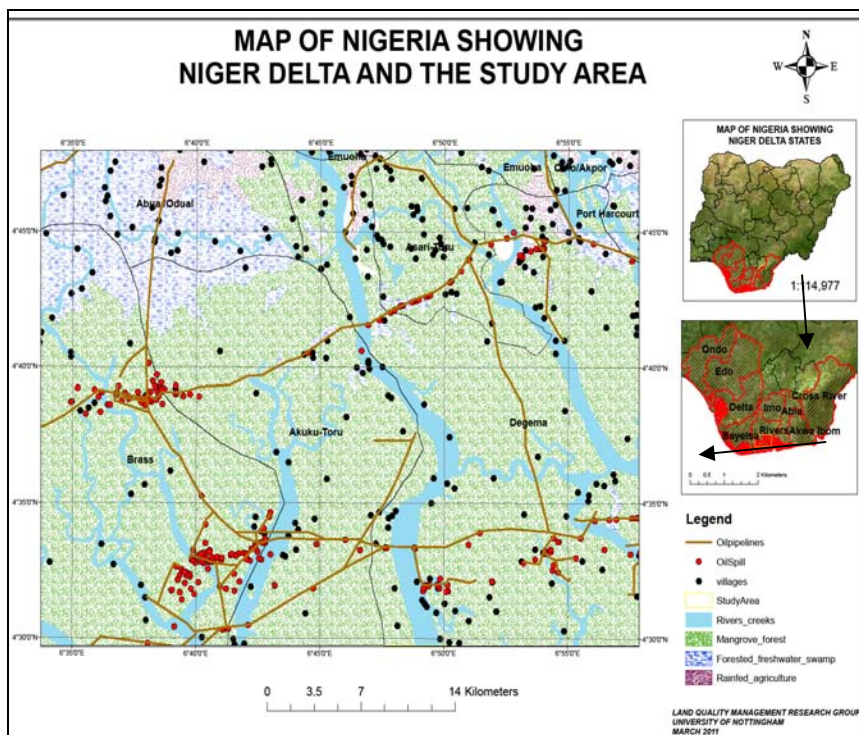


Figure 1: Study area in rivers state of Nigeria.

1.1 Study area

The study area consists of 354 communities in nine Local Government Areas in Rivers State and one in Bayelsa state covering approximately 1,939.8Km² with a population of about 1.36million (NPC 2002 projection) (see Figure 1). The area is dissected by several river tributaries and creeks flowing towards the Atlantic Ocean to the south. The vegetation is a typical deltaic environment, made up of mangrove forests and fresh water swamps, with poorly to moderately drained soils consisting of sand, loamy sand, clay and sometimes gravels subsoil. The average annual rainfall is 3000mm with 90% occurring between March and November with peak in July through September; as a result the area becomes inundated during the rainy seasons. The mean Temperature is 34°C during the hottest period around February and March while the coolest period is in August with a mean Temperature of 28°C [8]. Most of the communities in the area are fishing and farming hamlets located along river routes. Some 44.9% of the communities are located within 1.5km of a river. The people are mostly associated with subsistent lifestyles like small scale farming, fishing, and animal herding and hunting. The study area is transverse by 314.3km of pipeline network used for gathering and transporting crude from oil wells belonging to one or more oil companies. From the data collected, a total of 443 oil spill

incidents have been recorded between 1985 and 2008, thus 129,578 barrels of crude oil has been discharged in the area with the greatest amount of pollution occurring in the period 2003-07.

2 Traditional activities

The communities are agrarian in nature depending on naturally occurring resources by engaging in activities like fishing, hunting, farming (crop cultivation), and animal herding at subsistence level. Other activities include fuel wood gathering for energy, water collection from local streams, lakes or ponds for domestic use. In carrying out these activities, the people travel long distance and spend a lot of time in the process, perhaps due to distance or because things are done manually [10; 11].

2.1 Land use activities

Farming is a form of agricultural land use involving crop production. Kassali et al. [10] observed that farmers often walk approximately 6km a day to their farms, perhaps due to population pressure, land tenure system or availability of fertile soils close to the settlements [12]. **Fishing** is a major activity supplying more than 80% of animal protein [13, 14], as a result, most communities are classified as fishing hamlets established to take advantage of fishing opportunities presented by the riverine ecosystem [15]. **Animal herding** is another practice in which families keep and rear sizable numbers of domesticated animals such as cattle, goat, pig and sheep [17]. The animals are usually taken out for grazing at locations where green pasture is available and to prevent animals from straying into farms or cultivated fields. **Hunting activity** deals with killing or capturing of wild animals for consumption as bush meat. While some hunt for subsistence purposes (i.e. for family consumption) others do it as a full time occupation where the objective is to satisfy market demand for bush meat [18]. Hunting is unrestricted in most forests in the region [19]. **Fuelwood gathering** is an activity synonymous with most rural communities; it serves as the cheapest source of energy for low income families who cannot afford alternatives e.g. kerosene stove, gas cooker or electric cooker [20]. Fuel wood remains the dominant energy source utilised in over 50% of rural households for cooking, heating and food processing [21]. Women and children traditionally collect fuel wood for household usage, according to Ikurekong et al, [21] women walk more than 4km a day in search of fuel wood, sometimes because of access restrictions imposed on communal and family trees which compel them to gather from unrestricted marginal fields far away. **Water collection** is common activity requiring fetching water from natural sources for household needs. Women and children perform this role by undertaking multiple round trips over long distance carrying containers of water filled from different sources every day [23]. Nkwocha [23] claim that people travel a mean distance of approximately 5km to fetch water, thus spending averagely between 2-5hrs daily.



2.2 Land use potential exposure scenarios and pathways

In most African societies especially in the rural setting, day to day activities are designated among members according to culture and tradition. Over the years tradition has been used as a basis for assigning certain activities to specific genders or age groups. This way it is easy to identify the particular group or gender assigned to a specific activity and the type of land use associated with it. Such activities can be matched against western methods of contaminated land assessment where human health risk is assessed based on type of land use [25]. Land use activities help to understand how people behave; for instance frequency and duration of visits to a site, how and when the activity is performed. Thus the possibility of direct/indirect contact with contaminants can be determined especially where activity is performed on or near a contaminated source.

2.3 Exposure pathways

Human exposure to contaminants can occur through inhalation of dust and vapour, ingestion of soil or food grown on contaminated soil and dermal contact with contaminated media while performing an activity [26, 27]. The process of exposure begins with the introduction of a contaminant (agent) into the environment, where it is either transformed or transported through environmental media air, water, soil and dust and taken up through inhalation, ingestion and or dermal contact [26].

2.3.1 Inhalation

involves human respiration associated with air intake during breathing processes measured in cubic meters per hour (m^3/h). The amount of airborne contaminant inhaled (measured in micrograms per cubic meter ($\mu\text{g}/\text{m}^3$)) is depended on the concentration of the contaminant, time spent at a specific location, the body weight of the receptor and the intensity of activity [28].

2.3.2 Ingestion

is a means of introducing substances into the body system through the mouth and can be categorised into dietary and non-dietary exposures. Dietary exposure is the intake of contaminated substances in food, drinking water and beverages. Non-dietary on the other hand is the consumption of food items contaminated by substances through contact with polluted hands or surfaces, as well as ingestion of residues while mouthing hands and objects. Pollutants adhering to hands, toys, food and other objects are easily transferred to the mouth and ingested [29]. Contamination can occur to food during processing, distribution, storage, preparation and consumption.

2.3.3 Dermal

exposure on the other hand can occur during contact with contaminated media like water, soil, sediment, liquid, vapours/fumes while performing activity [30]. Dermal exposure can emanate from volatile substance deposition on skin directly



or indirectly through surface/cloth transfer to skin and absorption into the body system [31].

3 Methodology

The vector shapefiles used are GPS position of the 443 oil spill sites collected by the Department of Petroleum Resources (DPR) Lagos, Nigeria. Land use map dataset was obtained from the Department of Geography in the University of Lagos. 354 gazetted rural communities were also sourced from the University of Lagos to augment towns on the DPR's legacy map. The communities are represented by points due to lack of polygon shapefiles. 2002 projected population data was collected from the National Population Commission (NPC) Abuja, because the 2006 village population data has not been published yet. A SPOT[®] satellite imaging was used to digitise the pipeline network via onscreen digitisation.

3.1 Data analysis and result

The datasets were first projected to UTM_Zone32N in meters from decimal degrees; secondly the community shapefile was updated with the population data, and then further converted to geodatabase to facilitate automatic update of parameters like shape (area) and length. Proximity analysis performed to determine the distance of communities to pipeline gave a mean distance of 2.35km (SD= 1.99km), indicating the closeness of the communities to pipelines. Further proximity assessment performed for distance of communities to rivers and creeks gave a mean distance of 0.57km (SD= 0.58km). For the communities proximity to oil spill sites, gave a mean distance of 4.47km (SD= 3.72km). The population data gave a mean of 3,858.9 (SD= 8,104.4) persons per community. Since 1985 to 2008 a total of 129,578 barrels of crude oil have been spilt, giving a mean value of 292.5 (SD= 511.8). About 314.3km pipeline representing 7.28% of the 4,315km multi-product pipelines in the Niger Delta was digitised within the study area.

4 Discussion: risk assessment

The activities identified are performed out-doors with environmental media that may serve as vectors for contaminants. Because the people walk a great distance across the area, there is the chance of having contact with contaminants along their path, e.g. polluted river or ruptured pipeline. This is justifiable since the mean distance of communities to pipelines, rivers and oil spill sites is 2.35km, 0.5km and 4.47km respectively. Therefore those involved in any of these activities are at risk because of their proximity to pipelines and river which might convey contaminants. In Figure 3, pipeline intersection with river was buffered at an interval of 0.5km, 1km and 1.5km to demonstrate the extent to which a spill may spread along the river overtime, though this will depend on quantity,



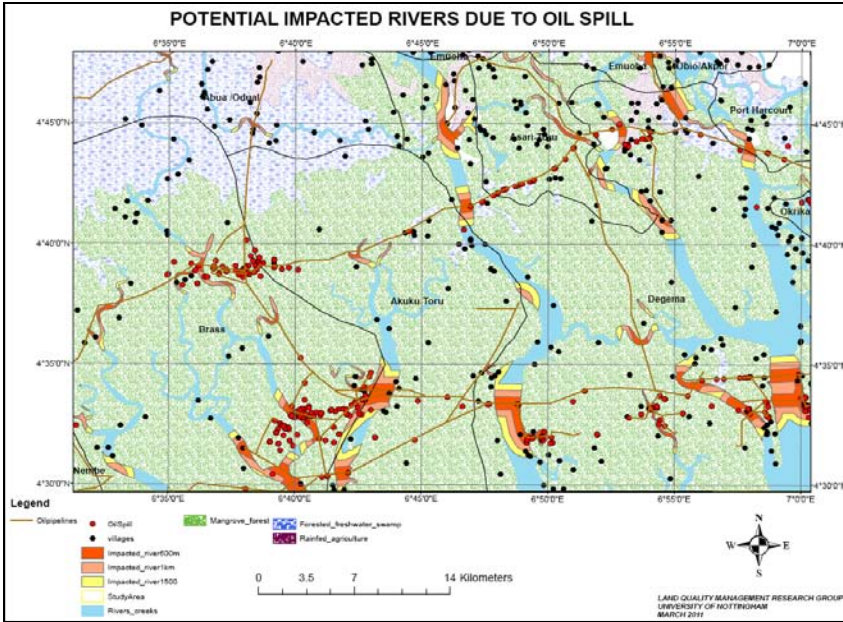


Figure 2: Potential impacted site at pipeline and river intersection.

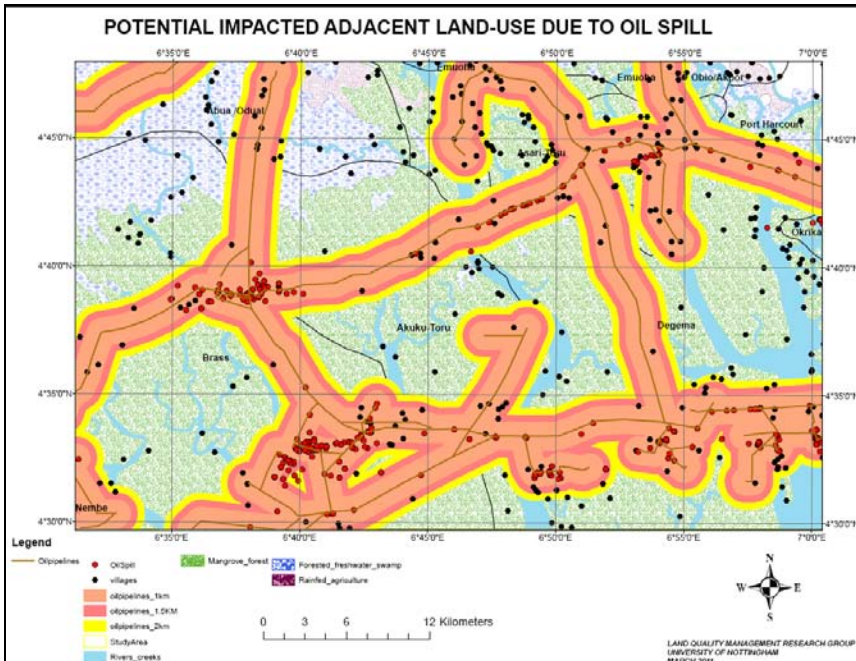


Figure 3: Potential impacted land use by oil spill.



pressure, duration of discharge and most importantly behaviour of the river at the time of discharge [32]. The extent of spread can be detrimental to water based-activities in the area.

Figure 4, on the other hand is a buffer of pipeline network with relation to land use and community location. The buffer distance of 1km, 1.5km and 2km was used as criterion to determine the difference in community and population sizes with increases in distance to the pipeline. The following were identified within the buffer zones i.e. 1km = 114 communities, mean population 3877.1 (SD= 7133); 1.5km = 159 communities, mean population 4420.1 (SD= 11007.1) and 2km =188 communities, mean population of 4266.2 (SD= 10212.5). It is assumed that since the primary cause of oil spill is due to pipeline rupture caused by vandalism/sabotage, discharge can occur from any part of the network. Thus any activities within these areas might be susceptible to exposure.

4.1 Exposure assessment

This employ the use of models to estimate the degree of exposure to specific environmental contaminants by assessing exposure duration, exposure frequency, magnitude of exposure, concentration of contaminant and pattern of activity undertaken by the receptor. It also takes into account bodyweight and gender of the receptor at risk through established exposure pathways [33]. Thus by relating a receptor to a possible exposure pattern, an average daily exposure can be estimated as in Table 1, where exposure duration (ED) and averaging time (AT) have been assumed for each activity according to age and gender. The ED is determined in year (i.e. hours/day/year) while AT is the assumed exposure duration given in days. A 50 years life expectancy at birth of has been assumed for the benefit of this work, although the CIA [34] and UNHDR [35] have published 47.56 and 48.4 years respectively. These parameters can be used in the Average Daily Exposure equation while others may be adopted from recommended values in USEPA [29] and Environmental Agency [27].

Although different countries and organisations have developed different models for estimating exposure through ingestion, inhalation and dermal contact, the Average Daily Exposure (ADE) model developed by [28] in Contaminated Land Exposure Assessment (CLEA) for assessing exposure through contaminated soil (see equation 1) has been found to be appropriate for the Niger delta in our research for the following reasons: a) it combine the three exposure routes, b) the variables can easily be modified using parameters developed for other countries, c) it can take care of lack of indigenous data from Nigeria. The ADE can be used for exposure to chemicals with non-carcinogenic effects. However, for compounds with carcinogenic or chronic effects, the lifetime average daily dose (LADD) can be evoked “*The LADD is the dose rate averaged over a lifetime*” [36, 37].

$$ADE = \frac{(IR_{ing} \times EF_{ing} \times ED_{ing})}{BW \times AT} + \frac{(IR_{inh} \times EF_{inh} \times ED_{inh})}{BW \times AT} + \frac{(IR_{derm} \times EF_{derm} \times ED_{derm})}{BW \times AT} \quad (1)$$

where: ADE = the average daily human exposure to chemical from soil ($\text{mg kg}^{-1} \text{bw day}^{-1}$), IR = the chemical intake/uptake rate (mg/day^{-1}), EF = the exposure



frequency (days year^{-1}), ED= the exposure duration (year), BW= the human body weight (kg), AT= the averaging time (days), **Note:** ing, inh and derm stands for ingestion, inhalation and dermal contact.

Table 1: Exposure duration and averaging time for specific activity according to age.

Receptor Age Group	Fishing	Animal herding	Fetching Water	Fuelwood Gathering	Hunting	Farming
Adult male 20-50 years	ED= 6hrs/dayx365 AT=365x50 (18,250 days)	ED= 8hrs/dayx365 AT=365x50 (18,250 day)	N/A	N/A	ED= 6hrs/dayx365 AT=365x50 (18,250 days)	ED= 8hrs/dayx365 AT=365x50 (18,250 day)
Adult female 18-50 years	N/A	N/A	ED= 6hrs/dayx365 AT= 365x50 (18,250 days)	ED= 6hrs/dayx365 AT= 365x50 (18,250 days)	N/A	ED= 6hrs/dayx365 AT= 365x50 (18,250 days)
Boy child 7-19 years	ED= 6hrs/dayx365 AT=365x19 (6,935 days)	ED= 8hrs/dayx365 AT=365x50 (18,250 day)	N/A	N/A	ED= 4hrs/dayx365 AT=365x19 (6,935 days)	ED= 4hrs/dayx365 AT=365x19 (6,935 days)
Girl child 7-17 years	N/A	N/A	ED= 6hrs/dayx365 AT= 365x17 (6,205 days)	ED= 6hrs/dayx365 AT= 365x17 (6,205 days)	N/A	ED= 4hrs/dayx365 AT=365x17 (6,205 days)
Infant child (boy/girl) ≤6 years	N/A	N/A	ED= 6hrs/dayx365 AT= 365x6 (2,190 days)	ED= 6hrs/dayx365 AT= 365x6 (2,190 days)	N/A	ED= 6hrs/dayx365 AT= 365x6 (2,190 days)

Note: it is assumed that the infant child spend time with their mother while they perform their activity.
ED = Exposure duration, AT = Averaging time, N/A = Not Applicable.

4.2 Relative risk ranking

According to the activity-based relative risk ranking in Table 2, the receptor most susceptible are children, because of their bodyweight and the fact that they are more easily tempted to interact with contaminated media than adults. The relative risk ranking used weighting system to qualify involvement in each activity according to age and sex. After ranking the normalised weight, the result shows infants to be higher because they are always accompany their mothers or grandparents; who might be involved in all or most of the activities, followed by the male child; who may perform similar tasks alongside their female siblings, then the female child; who may not necessarily be engaged in young male tasks like hunting, animal Herding and fishing. Child exposure through hand-to-mouth, soil ingestion and general attraction to contaminated media on play ground, clearly distinguished them as the receptors of greatest concern.

5 Conclusion

The possible continuing opportunities for human contact with contaminated media in everyday rural activities should be a concern to stakeholders in the oil industry. For example, opportunities that enable hand-to-mouth scenarios in children and adults or tracking of contaminants outdoors may cause long lasting



Table 2: Relative risk ranking of receptors with respect to activities.

Potential receptor	Farming	Hunting	Water collection	Fuelwood gathering	Fishing	Animal rearing	Total	Rank
Adult male (20-50yrs)	1(0.067)	4(0.267)	1 (0.067)	1 (0.067)	1(0.067)	4(0.267)	12(0.133)	5
Male Child (7-19yrs)	2 (0.133)	5(0.333)	2 (0.133)	2 (0.133)	5(0.333)	5(0.333)	21(0.233)	2
Adult Female (18-50yrs)	4 (0.267)	3(0.200)	3 (0.200)	3 (0.200)	2(0.133)	2(0.133)	17(0.189)	4
Female Child (7-17yrs)	3 (0.200)	2(0.133)	4 (0.267)	4 (0.267)	3(0.200)	3(0.200)	19(0.211)	3
Infants \leq 6yrs	5 (0.333)	1(0.067)	5 (0.333)	5 (0.333)	4(0.267)	1(0.067)	21(0.233)	1
Total	15(1.000)	15(1.000)	15(1.000)	15(1.000)	15(1.000)	15(1.000)	90(1.000)	

Note: Rating, (normalised value).

exposure and pose serious health risks [31]. According to [33] there are “no reliable quantitative data to support Human Health Risk Assessment for activities associated with receptors living in rural areas, or for lifestyles and occupations such as farming, where there is the potential for high exposures”. Lifestyles in rural areas predispose people to different exposure pathways because they conduct their activities under environmental conditions that guarantee the likelihood of intake/uptake of contaminated substances. As a result, exposure estimates for rural population associated with traditional land use practices are limited to qualitative assessments which are based on data extrapolated from other studies like [33].

While discussing the basic elements considered in assessing exposure to environmental contaminants, it is obvious that exposure during activities may occur simultaneously through several routes while in some cases only one may be available. This is because contaminants are not equally distributed spatially due to dispersion, diffusion and other mechanism responsible for loss of concentration, therefore the closer a receptor is to the source the higher the chances of multiple exposure routes.

Finally, in view of lack of data from the area, information from the Environmental Protection Agency (USA) and the Environment Agency (UK) has been adopted. Such exposure models can serve as a trigger for further research and development of a human health risk criteria for petroleum hydrocarbon contaminants in the Niger Delta. This study has provided a basis for further investigation into petroleum hydrocarbon contamination and its potential exposure pathways in the area.

References

- [1] Royal Dutch Shell PLC Sustainability Report 2009, www.shell.com
- [2] ONUOHA, F., Poverty, pipeline vandalisation /explosion and human security: Integrating disaster management into poverty reduction in Nigeria. *African Security Review* 16.2, www.iss.co.za



- [3] Akpan, W.N., Between that “Sectional” and the “National” oil, Grassroots discontent and civic discourse in Nigeria. *PhD thesis submitted to Rhodes University*, 2005, <http://eprints.ru.ac.za/249/1/Akpan-PhD.pdf>
- [4] This Day, Shell Faces Dutch Parliament over Nigeria. <http://www.thisdayonline.com>
- [5] Amnesty International., Nigeria: Petroleum, Pollution and Poverty in the Niger Delta. Amnesty International Publications 2009, www.amnesty.org
- [6] Nigerian National Petroleum Corporation, Annual Statistical Bulletin, www.nnpcgroup.com
- [7] National Population Commission of Nigeria, *Facts and Figures*, www.population.gov.ng
- [8] Omo-Irabor, O.O., Olobaniyi, S.B., Oduyemi, K. and Akunna, J., Surface and groundwater quality assessment using multivariate analytical methods: A case study of the Western Niger Delta, Nigeria. *Physics and Chemistry of the Earth*. **33**, pp.666-673, 2008.
- [9] Togunde, D. and Richardson, S., Household size and composition as correlates of child labour in urban Nigeria. *African Development*, Vol. **XXXI(1)**, pp.50-65, 2006.
- [10] Kassali, R., Ayanwale, A.B. and Williams, S.B., Farm location and determinants of agricultural productivity in the Oke-Ogun area of Oyo state, Nigeria. *Journal of Sustainable Development in Africa*. **11(2)**, pp.1-18, 2009.
- [11] Ismaila, U., Gana, A.S., Tswana, N.M. and Dogara, D., Cereals production in Nigeria: problems, constraints and opportunities for betterment. *African Journal of Agricultural Research*. **5(12)**, pp.1341-1350, 2010.
- [12] Baker, L.R. and Olubode, O.S., Correlates with the distribution and abundance of endangered sclater’s monkeys (*cercopithecus sclateri*) in southern Nigeria. *African Journal of Ecology*. **44**, pp.365-373, 2007.
- [13] Jamabo, N.A., and Ibim, A.T., Utilization and protection of the brackish water ecosystem of the Niger Delta for sustainable fisheries development. *World Journal of Fish and Marine Sciences*. **2(2)**, pp.138-141, 2010.
- [14] Tawari, C.C. and Davies, O.A., Impact of multinational corporations in fisheries development and management in Niger Delta Nigeria. *Agriculture and Biology Journal of North America*, **1(2)**, pp.146-151, 2010.
- [15] United Nations Development Programme., Niger Delta human development report. UNDP, UN House, Abuja, Nigeria. 2006.
- [16] Achudume, A.C., Environmental health, development and economic empowerment of rural women in Nigeria. *Environment Development and Sustainability*. **11**, pp.459-469, 2009.
- [17] Kuehi, H.S., Nzeingui, C., Yeno, S.L.D., Huijbregts, B., Boesch, C. and Walsh, P.D., Discriminating between village and commercial hunting of apes. *Biological Conservation*, **142**, pp.1500-1506, 2009.
- [18] Greengrass, E., Chimpanzees are close to extinction in southwest Nigeria. *Primate Conservation*, **24**, pp.77-83, 2009.



- [19] Adebayo, A.G., Oyun, M.B. and Kadeba, O., Access of rural women to forest resources and its impact on rural household welfare in North Central Nigeria. *Forest Policy and economics.* **12**, pp.439-450, 2010.
- [20] Adeoti, O., Idowu, D.O.O. and Falegan, T., Could fuelwood use contribute to household poverty in Nigeria. *Biomass and Bioenergy.* **21**, pp. 205-210, 2010.
- [21] Ikurekong, E. E., Esin, J. O. and Mba, A. C., Rural fuelwood exploitation in Mbo local government area- A Nigerian coastal settlement. *Ethiopian Journal of Environmental Studies and Management.* **2(3)**, pp.44-55, 2009.
- [22] WaterAid. Women's issues. 2009, www.wateraid.org
- [23] Nkwocha, E.E., Water supply deficiency and implications for rural development in the Niger-Delta Region of Nigeria. *Soc Inic Res.* **90**, pp.409-418, 2008.
- [24] DEFRA Environmental Protection Act 1990: Part 2A. Contaminated Land Circular 01/2006. Defra: London, 2006
- [25] Elert, M., Bonnard, R., Jones, C., Schoof, R.A., and Swartjes, F.A., Human Exposure Pathways. Swartjes, F.J. (ed) *Dealing with Contaminated sites.* **3**, pp.455-515, 2011.
- [26] Swartjes, F.A., and Cornelis, C., Human Health Risk Assessment. Swartjes, F.J. (ed) *Dealing with Contaminated sites.* **3**, pp.209-259, 2011.
- [27] Environment Agency Science Report: SC050021/SR3. Updated technical background to the CLEA model. Environment Agency UK, 2009.
- [28] US-EPA. Child-specific exposure factors handbook (final report). United States Environmental Protection Agency. EPA/600/R-06/096F. National Center for Environmental Assessment office of Research and Development, Washington, DC 20460. 2008, www.epa.gov/ncea.
- [29] US-EPA. Exposure Factor Handbook., United States Environmental Protection Agency, Washington, www.epa.gov/ncea
- [30] Kimbrough, R.D., Krouskas, C.A., Carson, M.L., Long, T.F., Bevan, C., and Tardiff, R.G., Human uptake of persistent chemicals from contaminated soil: PCDD/Fs and PCBs. *Regulatory Toxicology and Pharmacology.* **57**, pp.43-54, 2010.
- [31] Fingas, M., *The Basics of Oil Spill Cleanup.* Edited by Jennifer Charles; Second Edition. Lewis Publishers London, 2000.
- [32] International Programme on Chemical Safety (IPCS). Human Exposure Assessment. Environmental Health Criteria; 214. Geneva, World Health Organisation. 2000.
- [33] Doyle, J.R., Blais, J.M. and White, P.A., Mass Balance soil ingestion estimation methods and their application to inhabitants of rural and wilderness areas: a critical review. *Science of the Total Environment.* **408**, pp.2181-2188, 2010.
- [34] CIA World Fact book , www.cia.gov/library/publications/the-world-factbook/geos/ni.html
- [35] UNHDR, <http://hdrstats.undp.org/en/countries/profiles/NGA.html>



The development of a model of pandemic preparedness planning utilizing critical success factors from the United States and the European Union

Y. Draine¹, J. Johnson¹, M. Levy² & W. Sumrall³

¹*Department of Health Administration,
Central Michigan University, USA*

²*Public Health Program, University of Memphis, USA*

³*School of Business, Belhaven University, USA*

Abstract

Many countries were not prepared for a pandemic on June 11, 2009, when the World Health Organization (WHO) declared an Influenza Pandemic. Although Pandemic Influenza Preparedness Planning activity for 2011 has declined compared to 2009, we cannot take preparedness planning off the radar due to future potential pandemics. Unless countries develop model Pandemic Influenza Preparedness Plans, the consequences of being unprepared could be devastating to all of humankind.

This study identified Critical Success Factors (CSFs) necessary at all levels (local, state, and national) to achieve model Pandemic Influenza Preparedness Planning. Pandemic Influenza Preparedness Planning involves developing a plan in the event of the emergence of an influenza virus that causes serious illness and is spread easily and is sustainable among humans. Once the WHO issues a pandemic influenza alert, all countries should be prepared. Data was collected through surveys, interviews, and benchmarking methods. The goal of identifying CSFs is to provide those factors to countries as well as authorities on a local, state, and national level in order to develop model Pandemic Influenza Preparedness Plans.

Several CSFs were identified, they included the following: strong leadership support, plan development, having logical response plans, exercising plans, clear operations and implementation policies, adequate budget/resources, effective



public communications and outreach, and staff training. Clearly, there are benefits to providing CSFs for Pandemic Influenza Preparedness Planning. Being prepared can save the lives of millions around the world and as well as reduce economic and social impact. Pandemic Influenza Preparedness Planning should remain a high priority.

Keywords: influenza, preparedness, biological threats, pandemic, public health.

1 Introduction

For many years, there has been considerable international concern regarding the possibility of pandemics occurring in the United States as well as other countries. The World Health Organization (WHO) describes a pandemic using three conditions: the emergence of a disease to the population; the agent infects humans, causing serious illness; and the agent spreads easily and sustainably among humans. The WHO strongly recommends that all countries develop and prepare pandemic plans in advance to prevent and control the next influenza pandemic.

The WHO [1] developed a checklist for influenza pandemic preparedness planning for the benefit of its Member States worldwide. The checklist reflects international expert opinion and includes the following essential elements in the checklist:

- Preparing for an emergency
- Surveillance
- Case investigation and treatment
- Preventing spread of the disease in the community
- Maintaining essential services
- Research and evaluation
- Implementation, testing and revision of the national plan

The capacity of countries for influenza pandemic planning varies, and they may be at different stages of the planning process. The aim of the pandemic preparedness checklist is primarily to provide an outline of the essential minimum elements of preparedness, as well as elements of preparedness that are considered desirable. It is recommended that responsible authorities or institutions in countries that are in the process of planning should consider the specific aspects of the checklist for which they are responsible. Countries that already have a national pandemic preparedness plan in place may use the checklist to evaluate the completeness of the current plan.

The WHO posed the question: Are you prepared? Are you prepared to prevent or minimize the human morbidity and mortality, the social disruption, and the economic consequences caused by an influenza pandemic?

1.1 Global perspective

Garrett [2] stated that the world has rapidly become much more vulnerable to the eruption, and most critically, to the widespread and even global spread of both new and old infectious diseases. This new and heightened vulnerability is not



mysterious. The dramatic increase in worldwide movement of people, goods, and ideas is the driving force behind the globalization of disease. For not only do people travel increasingly, but they travel much more rapidly, and go to many more places than ever before. A person harboring a life-threatening microbe can easily board a jet plane and be on another continent when the symptoms of illness strike. The jet plane itself and its cargo can carry insects bringing infectious agents into new ecologic settings. Few habitats on the globe remain truly isolated or untouched, as tourists and other travelers penetrate into the most remote and previously inaccessible areas in their search for new vistas, business, or recreation.

Such a devastating disease would clearly have profound implications for international relations and the global economy. With death tolls rising, vaccines and drugs in short supply, and the potential for the virus to spread further, governments would feel obliged to take drastic measures that could inhibit travel, limit worldwide trade, and alienate their neighbors. It is even doubtful that any of the world's wealthy nations would be able to meet the needs of their own citizenry, much less those of other countries. Domestic vaccine purchasing and distribution schemes currently primarily assume that only the very young, the elderly, and the immunocompromised are at serious risk of dying from the flu. Every year the United States plans for 185 million vaccine doses, trusting that the flu will kill only the usual risk groups. If that guess were wrong, if all Americans were at risk, the nation would need at least 300 million doses. That is what the entire world typically produces each year. There would thus be a global scramble for vaccine (Garrett [3]).

1.2 Critical success factors (CSFs)

There is a need for public and private sectors to take action with pandemic preparedness activities. The identification of Critical Success Factors (CSFs) for pandemic preparedness planning will set a precedent for successful planning of these activities on a local, state, and national level.

CSFs are those few things that must go well to ensure success for a manager or an organization. They represent those managerial or enterprise areas that must be given special and continual attention to bring about high performance. CSFs include issues vital to an organization's current operating activities and to its future success (Friesen and Johnson [4]).

In the case of pandemic preparedness planning, the CSFs would be things and/or tasks that should be identified by organizations to ensure the creation of a successful pandemic preparedness plan. Essentially, highlighting the areas that must be given special and continual attention in order to have a high performing pandemic preparedness plan would constitute the identification of CSFs.

2 History and current state of Avian Influenza

Influenza A (H5N1) virus, also called "H5N1 virus", is an influenza A virus subtype that occurs mainly in birds and is highly contagious among birds, and



can be deadly to them. The H5N1 virus does not usually infect people, but infections with these viruses have occurred in humans. Most of these cases have resulted from people having direct or close contact with H5N1 through infected poultry or H5N1 contaminated surfaces. Avian Influenza is also known as “Bird Flu” (Key facts about Avian Influenza (Bird Flu) and Avian Influenza A (H5N1) Virus [5]).

According to Osterholm [6], Avian influenza caused by H5N1 initially received widespread attention in 1997 due to an outbreak in poultry in Hong Kong subsequently spread the virus to humans. There were eighteen human cases recognized; six of the patients died (there was no evidence of person-to-person transmission). In the fall of 2003, H5N1 avian influenza appeared in domestic poultry farms in Asia. It resurfaced in the summer of 2004 after subsiding briefly, appearing in Cambodia, China, Laos, Thailand, and Vietnam, where it persists today despite the prevalent vaccination of poultry. Studies of recent H5N1 isolates in Southeast Asia have indicated that the virus’ predominant lineage today originated in southern China. Other lineages are believed to have emerged in Southeast Asia, which suggests that the virus has been present in the region for a long time. A report by the UN Food and Agricultural Organization published in September 2004 found that existing reservoirs of the H5N1 influenza virus in ducks, wild birds, and potentially pigs, are already resilient enough to pose a severe challenge to eradication (Osterholm [6]). More recently, Woodward [7] indicated that according to the World Health Organization, as of March 6, 2006, 175 people in seven countries had contracted the H5N1 disease, and 95 people had died. Most of these infections were as a result of people having direct or close contact with H5N1-infected poultry or contaminated surfaces.

Osterholm [6] stated further that, similar to earthquakes, hurricanes, and tsunamis, influenza, pandemics are recurring natural disasters. The natural reservoir of the influenza virus is wild aquatic birds. Therefore, for a human influenza pandemic to occur, a strain of an avian influenza virus must develop to which humans have no pre-existing immunity and undergo critical genetic changes that allow it to be readily transmitted from person to person. The H5N1 strain of the influenza virus has had a limited impact on human health so far, but a human influenza pandemic could occur and be devastating if a current strain underwent the right genetic changes.

For several years, scientists believed that the only way for an avian influenza virus to become transmittable between humans was through a process known as reassortment. Reassortment takes place when an avian virus and a human virus both infect the same cells of an animal or a person and swap genes, producing a new virus adapted to humans. This is how the 1957 and 1968 influenza pandemics began (Osterholm [6]). The Asian Flu of 1957–58 killed 1 million to 2 million worldwide; and the Hong Kong Flu of 1968–69 killed more than 700,000 worldwide (Green [8]). Over the past couple of years, however, the potential development of a human influenza pandemic similar to that of 1918 (due to Spanish influenza) has been a paramount concern. The observation of two of the three key criteria that characterized the pandemic of 1918–1919 has



already been fulfilled in the present epidemic: (1) the ability of the virus to infect humans resulting in high mortality and (2) a global immunologically naïve human population. The third criterion, efficient human-to-human transmission, has yet to be observed. The adaptation that would result in human-to-human transmission might involve changes in the receptor properties or improved viral replication efficiency. This type of adaptation might be achieved by mutation of an avian virus genome or by mixing segments of an avian virus with segments from a virus already adapted to humans (genetic reassortment), paving the way to the emergence of a new influenza subtype with pandemic potential (Trampuz et al. [9]). According to (Garrett [3]) the 1918-19 Spanish flu killed 50 million people in 18 months; however, Avian Flu is far more dangerous. It kills 100 percent of the domesticated chickens it infects and among humans the disease is also lethal.

Although it is impossible to know for certain whether H5N1 will ever evolve into the next human pandemic virus, more and more of the genetic changes documented in the 1918–1919 Spanish flu have also been found to have occurred in recent H5N1 strains affecting both birds and people. Meanwhile, the spread of H5N1 infections to more avian species and to more humans continues to point to H5N1 as a likely strain of the next pandemic (Osterholm [6]).

3 History and current state of pandemic influenza preparedness planning

According to the World Health Organization [10], in the previous years, new strains of influenza have generated pandemics causing extensive death rates and paramount social disruption. In the 20th century, the greatest influenza pandemic occurred in 1918–1919 and caused an estimated 40–50 million deaths all over the world. Although health care has seen some significant improvements in the last decades, epidemiological models from the Centers for Disease Control and Prevention (CDC), Atlanta, USA project that today a pandemic is likely to result in 2 to 7.4 million deaths globally. In high income countries alone, which account for 15% of the world's population, models project a demand for 134–233 million outpatient visits and 1.5–5.2 million hospital admissions. However, the impact of the next pandemic is likely to be the greatest in low income countries because of different population characteristics and the already strained health care resources.

If an influenza pandemic occurs, the following can be anticipated:

- Given the high level of global traffic, the pandemic virus may spread rapidly, leaving little or no time to prepare.
- Vaccines, antiviral agents and antibiotics to treat secondary infections will be in short supply and will be unequally distributed. It will take several months before any vaccine becomes available.
- Medical facilities will be overwhelmed.
- Widespread illness may result in sudden and potentially significant shortages of personnel to provide essential community services.



- The effect of influenza on individual communities will be relatively prolonged when compared to other natural disasters, as it expected that outbreaks will reoccur [10].

The World Health Organization (WHO) indicated further that continuous global surveillance of influenza is critical. The WHO has a network of 112 National Influenza Centers that monitors influenza activity and isolates influenza viruses in all continents. The National Influenza Centers will report the emergence of an “unusual” influenza virus immediately to the WHO Global Influenza Programme (a network comprised of 4 WHO Collaborating Centers, WHO CCs, and 122 institutions in 94 countries), or to 1 of the 4 WHO Collaborating Centers (located in Australia, Japan, England and the United States). Rapid detection of unusual influenza outbreaks, isolation of possible pandemic viruses and immediate alert to the WHO system by national authorities is paramount to a timely and efficient response to pandemics (The WHO Global Influenza Surveillance Network [10]).

(Osterholm [6]) indicated that slacking off on preparedness activities today could lead to very bad news in the future. The warning that another pandemic could occur at any time and at a staggering cost to human health and the world economy was direct. These facts remain incontrovertible as many public health scientists believed that the outbreaks of the H5N1 influenza virus in birds in Asia, Europe, and Africa, with occasional infections in humans, were precursors to the next pandemic. Experts have recently noted that it would take only one to six months from the time a human transmitted form of the virus is detected in the United States (U.S.) for it to spread across the country, leaving a short window for hospitals to make preparations. The U.S. government health care agencies have informed businesses to be prepared for a pandemic that might spread to as much as 30 percent to 40 percent of the work force (Green [8]).

4 Global pandemic influenza preparedness planning

Mercer [11] invited organizations globally to participate in the Mercer Avian Flu Pandemic Preparedness Survey online. The online survey represented a critical first step in conducting an inventory of the organization’s current level of preparedness for a pandemic crisis from a Human Resources (HR) perspective. The findings consisted of data gathered from 450 respondents across 38 countries and 26 industries with respondents from Australia, Canada, People’s Republic of China, Hong Kong, Singapore, United Kingdom and the United States comprising 75 percent of total respondents. The top six industries, comprising 60 percent of participants, were manufacturing, finance, professional services, computer services, insurance, and education.

There were five key indicators that Mercer [11] utilized to gauge organizational pandemic preparedness. When observed individually, each of the indicators provided insight into the priorities that organizations have established in their pandemic preparedness planning. When grouped, they provide a broader review of the overall state of an organization’s preparedness for an Influenza Pandemic. The key indicators were:



- Establishment of a budget for pandemic preparedness
- Formation of a crisis leadership management team
- Development of a pandemic business continuity plan
- Workforce planning (including skills inventory)
- Development of an employee communication strategy

There were 11 questions that covered a comprehensive range of topics which included:

- Impact on organizational success factors
- Crisis leadership
- Employee communication
- Skills inventory for workforce planning
- Remote working procedures
- International assignees and corporate travelers
- Compensation and leave policies
- Insurance coverage
- Hygiene, quarantine and preventive health measures
- Employee assistance
- Business continuity planning

The survey report was formulated by identifying themes and issues that evolved from the responses and provided insight into the current state of organizational preparedness for a pandemic. Mercer [11] also believed that the report would provide companies with the ability to benchmark their capability to respond to a pandemic crisis and formulate necessary business continuity planning strategies.

The critical themes that emerged from the report are as follows:

- There is a considerable gap between organizational concern about the impact of a pandemic and organizations' current state of pandemic preparedness.
- Those countries that endured the Asian SARS crises of 2003 are generally more advanced in the pandemic preparedness planning.
- Conversely, for the United States and other economies that were not impacted by SARS and have not had direct exposure to the Avian Flu, planning is in its relative infancy.
- Labor intensive industries have recognized the profound consequences that a pandemic may inflict.
- Although results differ considerably by region and industry type, organizations globally are predicting that a pandemic will result in financial hardship.

5 Progress report 2008: H5N1/bird flu

According to the Responses to Avian Influenza and State of Pandemic Readiness, Fourth Global Progress Report [12], a global analysis of the current state of the H5N1 Virus indicates that as recent as mid to late 2008, there have been fewer of the following: outbreaks in poultry, newly infected countries,



human cases, and deaths compared to the same in 2006 and 2007. Over 50 of the 61 countries that have experienced an H5N1 Virus outbreak have successfully eliminated the disease. However, the H5N1 Virus remains deeply rooted in several countries and the threat of further outbreaks of the virus in poultry (and random cases in humans) persists. This is a confirmation that the threat of an H5N1 (Avian/Bird Flu) influenza pandemic remains imminent.

5.1 Progress report 2009: H1N1/swine flu

While the H5N1 Virus remains somewhat dormant, the H1N1 Virus has become more prevalent since April 2009. According to the World Health Organization [13], as of April 26, 2009, the United States Government had reported 20 laboratory confirmed human cases of swine influenza A/H1N1 at that time (8 in New York, 7 in California, 2 in Texas, 2 in Kansas and 1 in Ohio). All 20 cases had mild Influenza-Like Illness with only one requiring brief hospitalization and no deaths reported. All viruses had the same genetic pattern based on preliminary testing. The virus was being described as a new subtype of A/H1N1 not previously detected in swine or humans. The WHO reported further that on April 26, 2009, the Government in Mexico had reported 18 laboratory confirmed cases of swine influenza A/H1N1. Investigation was continuing to clarify the spread and severity of the disease in Mexico. There were suspect clinical cases reported in 19 of the country's 32 states at that time.

The World Health Organization (WHO) declared an influenza pandemic on June 11, 2009. The level of influenza pandemic alert was raised from phase 5 to phase 6 (pandemic period). At that time, nearly 30,000 confirmed cases had been reported in 74 countries. This particular H1N1 strain was entirely new and had not circulated previously in humans. It was indicated further that it was contagious and easily spreading from one person to another (WHO [13]).

The World Health Organization (WHO) informed that countries should prepare to see cases, or the further spread of cases, in the near future. Countries where outbreaks appear to have peaked should prepare for the second wave of infection. The WHO stated further that guidance on specific protective and precautionary measures had been sent to ministries of health in all countries (WHO [13]).

5.2 Progress report 2010: H1N1/swine flu

According to the World Health Organization [14], more than 209 countries and overseas territories have reported laboratory confirmed cases of the H1N1 2009 flu; this includes 14,142 deaths worldwide as of January 22, 2010. At that time, the most concentrated transmission of the virus continued to occur in North America, South Asia, and in limited areas of Eastern Europe. Overall, pandemic influenza activity in the temperate northern hemisphere reached a peak between late October and late November and has continually declined since. However, the Global Influenza Surveillance Network (GISN) continues global circulation of influenza viruses.



More recently, as of May 21, 2010, the World Health Organization continues to report deaths from laboratory confirmed cases of the 2009 H1N1 flu. These deaths are an under-representation of true numbers in that many deaths are not tested or confirmed as influenza related. The more active areas of transmission are in the tropical regions of the Caribbean, South America, and Southeast Asia (CDC [15]).

According to the Washington Post [16], the Obama Administration's fast and effective response to the 2009 H1N1 flu outbreak last year was the payoff of preparedness efforts since 2005. The government issued a strategy to prepare for a potential pandemic flu in 2005 and there have been significant improvements in the following areas: surveillance, coordination, communications, treatment capabilities and stockpiles, vaccine manufacturing capacity, and ensuring that every state now has a pandemic plan. However, the H1N1 flu has not truly tested the limits of the response plan in that the potential of what could be quite devastating has not taken place.

The Washington Post (2009) stated further that a number of key areas still need improvement including full funding for research to produce a vaccine against a novel virus, building stockpiles of anti-viral medication, so that every state is equally protected, supplying enough annual resources to support ongoing state and local response capacity, managing mass hospitalizations if there is a surge in patients, and the public health workforce during this time of downsizing and layoffs. There are challenges yet to be addressed in anticipation of the next influenza pandemic.

6 Data analysis and results

The following research question was addressed in this study: What are the Critical Success Factors (CSFs) in Pandemic Influenza Preparedness Planning? The first research objective of this study was to identify CSFs that are necessary to enhance and implement a Pandemic Influenza Preparedness Plan. The second objective was to increase the awareness and the current knowledge of Pandemic Influenza Preparedness Planning. The final objective of this study was to further necessary research on Pandemic Influenza Preparedness Planning.

The research question for this study was answered by the use of a multi-method approach which utilized the concept of triangulation. The triangulation concept involved combining surveys, interviews, and benchmarking data in order to create meaningful information. Existing information was gathered from current model pandemic influenza preparedness plans and was analyzed and related to primary data collected from this study where appropriate.

Five subject matter experts (panel of experts) from organizations that are responsible for pandemic influenza preparedness planning provided their top five Critical Success Factors (CSFs) and definitions for each CSF they indicated. The participants' open-ended responses were analyzed for content. All of the participants' CSF definitions were compiled and analyzed in random order so that the participant's affiliation would not bias the researcher. First, open coding was performed as a first attempt to condense participants' open-ended responses



into conceptual categories. Emerging themes were brought to surface during this process and initial codes were assigned. A second analysis led to a re-conceptualization of themes and reassigning of codes. This analysis revealed eight different reoccurring themes among the CSFs that were mentioned. These conceptual categories included the following: (1) strong leadership support; (2) plan development; (3) having logical response plans; (4) exercising plans; (5) clear operations and implementation policies; (6) adequate budget/resources; (7) effective public communications and outreach; and (8) staff training.

6.1 Summary of key findings

The present research drew on various sources to determine what factors at the local, state, national (provided by the experts), and international levels are critical to pandemic influenza preparedness planning. The information obtained from literature reviews (model plans), expert panelists, and the benchmark organization (World Health Organization) suggests that there seems to be some agreement across these various organizations in terms of what are those factors. As shown in Table 1, all agree that having *clear operations and implementation policies, staff training, plan development, effective public communication and outreach, and logical response plans* are important CSFs for pandemic influenza preparedness planning.

Table 1: Critical success factors common across local, state, national, and international organizations.

Critical Success Factors	Experts	State and Local Model Organizations	Benchmark Organization: World Health Organization
Clear Operations and Implementation Policies	✓	✓	✓
Effective Public Communications and Outreach	✓	✓	✓
Staff Training	✓	✓	✓
Plan Development	✓	✓	✓
Having Logical Response Plans	✓	✓	✓
Adequate Budget/Resources	✓		✓
Exercising Plans	✓	✓	
Strong Leadership Support	✓		

7 Conclusion

The research question answered by this study was, “What are the critical success factors in pandemic influenza preparedness planning?” The first objective was to identify the CSFs necessary to enhance and implement a pandemic influenza preparedness plan. The second objective was to increase the awareness and the current knowledge of pandemic influenza preparedness planning. The final objective was to further necessary research on pandemic influenza preparedness



planning. The research question was answered and the three research objectives were achieved for this study.

While the study answered questions, it raised many questions as well. Questions have been raised still for some, regarding the lack of planning or progress of influenza preparedness planning. There is a considerable gap between concern about the impact of a pandemic and the current state of pandemic preparedness. How can lessons be learned from model pandemic influenza preparedness planning and applied to invoke the urgency in planning on all levels (local, state, and national)?

The consequences of being unprepared for an influenza pandemic can be devastating to all of human-kind. The timeliness of this study is critical with the recent influenza pandemic alert that occurred in June 2009. As we approach another influenza season in 2011, all levels (local, state, and national) of planning should be considered an urgent priority in preparedness of the next potential influenza pandemic. With the identification of the CSFs revealed in this study, preparedness planning on all levels can be fully developed or further enhanced for successful pandemic influenza preparedness planning.

References

- [1] WHO checklist for influenza pandemic preparedness planning. (2005). Retrieved July 28, 2008, from http://www.who.int/csr/resources/publications/influenza/WHOCDS_CSR_GIP_2005_4/en/
- [2] Garret, L. (1994). *The coming plague*. New York, New York: Penguin Books.
- [3] Garrett, L. (2005). The next pandemic? *Foreign Affairs* 84,(4), 3-23.
- [4] Friesen, M. E. and Johnson, J. A. (1995). *The success paradigm*. Westport, Connecticut: Quorum Books.
- [5] Key facts about avian influenza (bird flu) and avian influenza A (H5N1) Virus. (2007). Retrieved March 18, 2008, from <http://www.cdc.gov/flu/avian/gen-info/facts.htm>
- [6] Osterholm, M. (2007). Unprepared for a pandemic. *Foreign Affairs* 86, (2), 47-57.
- [7] Woodward, N. H. (2006). Pandemic. *HR Magazine*. 51, (5), 46-52.
- [8] Green, E. (2006). Pandemic flu preparations taking shape at area hospitals. *Business First* (June).
- [9] Trampuz, A., Prabhu, R., Smith, T., and Baddour, L. (2004). Avian influenza: a new pandemic threat? *Mayo Foundation for Medical Education and Research*. 79, 523-530.
- [10] World Health Organization. (2008). *The WHO global influenza surveillance network*. Retrieved July 28, 2008, from <http://www.who.int/csr/disease/influenza/influenzanelwork/en/>
- [11] Mercer. (2006). *Avian Flu Pandemic Preparedness Survey Report*. New York, NY.
- [12] UN System Influenza Coordinator and the World Bank. (2008). Responses to Avian Influenza and State of Pandemic Readiness Fourth Global



- Progress Report. Retrieved February 4, 2009, from http://siteresources.worldbank.org/EXTAVIANFLU/Resources/3124440-1172616490974/Fourth_progress_report_second_printing.pdf
- [13] WHO Swine flu illness in the United States and Mexico – update 2. (2009). Retrieved April 27, 2009, from http://www.who.int/csr/don/2009_04_26/en/index.html
- [14] WHO Pandemic (H1N1) 2009 - update 84. (2010). Retrieved May 24, 2010, from http://www.who.int/csr/don/2010_01_22/en/index.html
- [15] Centers for Disease Control and Prevention 2009 H1N1 Flu: International Situation Update. (2010). Retrieved May 24, 2010, from <http://www.cdc.gov/h1n1flu/updates/international/>.
- [16] Levi, J. (2009). Is America Prepared for a Pandemic. *The Washington Post*. (April).



Section 3
The built environment
and health

This page intentionally left blank

Thermal comfort in operating rooms: a case study

F. Patania¹, A. Gagliano¹, F. Nocera^{1,2} & A. Galesi¹

¹*Energy and Environment Division of D.I.I.M.,*

Engineering Faculty of University of Catania, Italy

²*Faculty of Architecture of University of Catania, Italy*

Abstract

This paper focuses on thermal comfort in hospital operating rooms (ORs).

Thermal comfort depends on several factors such as temperature conditions of the operating room, insulation of protective clothing, stress, rate of metabolism and safety mechanisms in the body to keep core temperature stable. The modification of any of these elements triggers defense mechanisms which in extreme cases may lead to serious disturbances in the body. The maintenance of recommended standards (ISO 7330) concerning thermal conditions in operating rooms ensures the highest possible physical capabilities of the personnel while providing maximum safety for the patients. The purpose of the present work is to report the results obtained during an experimental campaign carried out at the Umberto I Hospital in Enna in order to improve efficiency of HVAC installations to secure thermal comfort in the operating rooms.

Keywords: operating rooms, thermal stress, thermal comfort.

1 Introduction

A person produces thermal energy through the oxidation of glucose from what they have consumed. This process is named metabolism. A great part of this energy (80%) is used for the maintenance of the body, while 20% is expended in work. Oxidation can increase in some situations, for example, with increased activity level or increased body temperature. Indoors, the temperature of the human body remains constant. The normal temperature is about 37°C. Outside these limits, a person is considered to be sick. However, they can survive at a minimum temperature of 32°C and at a maximum of 42°C [1]. Heat transfers



between the person and the environment. The body uses thermo-regulatory mechanisms to compensate the gain or loss of heat to keep body temperature in equilibrium. This system is known as the hypothalamic thermostat, which “tells” the body to increase or decrease the temperature, in accordance with thermal needs. A person is in thermal comfort when he/she is satisfied with the thermal environment [2, 3] and does not need to use their thermo-regulator mechanism. Factors which affect the thermal comfort include physiological perception, climate, the level and type of physical activity, and the types of clothes used. Thermal comfort in relation to environmental factors depends on environment temperature, radiant temperature, relative humidity, air velocity, level and type of activity, metabolic rates, and clothing [2]. Hospital operating rooms (ORs) require efficient HVAC installations to secure the highly demanding indoor environmental conditions for patients and medical personnel.

Understanding and managing the thermal comfort in Operating Rooms (ORs) is complex because each surgery can present different levels and types of activities of the staff, different patient requirements and so on. Figure 1 shows a typical configuration of one OR. The “thermal risks” of the patient is more difficult to resolve, because the patient is anesthetized and, therefore, his/her thermo-regulatory mechanisms are not in action and an inadequate environment temperature could cause hypothermia. A temperature between 24°C and 26°C is suitable, while temperatures below 21°C put the patient at risk of becoming hypothermic [4]. Consequently, it is an extremely interesting study and analyzes the ORs in order to ensure the recommended standards concerning thermal conditions and so to guarantee the highest possible physical capabilities of the personnel while providing maximum safety for the patients. The purpose of this paper is to evaluate the thermal comfort in the Enna Hospital Operating Rooms, considering all parameters necessary to verify the respect of the recommended standards of ISO EN 7730, 2005 and CR 1752, 1998.

2 Investigation methodology

The authors carried out a monitoring analysis, during the period from 1 July 2008 to 6 August 2008, of the thermal comfort in the Operating rooms at the Hospital “Umberto I” in Enna. The research was developed in two contemporaneous steps: an “objective investigation” and a “subjective” one.

The “objective investigation” pointed at calculating the thermal comfort Fanger’s indices: Predicted Mean Vote (PMV), Predicted Percentage dissatisfied (PPD) and Draft Risk (DR), by means of the measured value of the air temperature, mean radiant temperature, air relative humidity, air velocity and water vapor pressure.

The “subjective investigation” was carried out giving a questionnaire to the staff members (two surgeons, two assistants and two nurses) to determine their sensations of comfort or discomfort felt in the operating room.



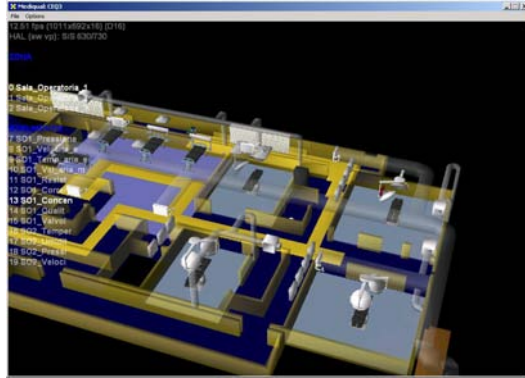


Figure 1: 3D view of the monitored operating rooms.

2.1 The “objective investigation”

The thermal environment was analyzed by means of field measurement campaigns. The CEQ (Controlled Environment Qualification) system of Keita srl was used to perform the measurements of air temperature, mean radiant temperature, air relative humidity, air velocity, water vapor pressure, flow rate of supply and return air, and so on. The CEQ system has a network of transducers that transmit their signals to a central computer which acquires the signals and converts them into data, charts and reports alarms. The three operating rooms were monitored continuously and simultaneously all the year around. The recorded data processed in the period from 1 July 2008 to 6 August 2008 were elaborated in order to evaluate the thermal comfort Fanger’s indices, PMV, PPD and DR according to the International Standard ISO 7730 [5]. The Predicted Mean Vote (PMV) is the mean vote expected to arise from averaging the thermal sensation vote of a large group of people in a given environment. PMV is derived from the physics of heat transfer combined with an empirical fit to sensation. PMV establishes a thermal strain based on steady-state heat transfer between the body and the environment and assigns a comfort vote to that amount of strain. The PMV is a complex mathematical expression involving activity, clothing and the four environmental parameters. It is expressed by equation:

$$PMV = (0,303xe^{-0,036M} + 0,028)L \quad (1)$$

in which M is metabolic rate (W/m^2) and L (W) is thermal load defined as the difference between the internal heat production and the heat loss to the actual environment for a person hypothetically kept at comfort values of skin temperature and evaporative heat loss by sweating at the actual activity level. The term Predicted Percentage Dissatisfied (PPD) is a quantitative measure of the thermal comfort of a group of people at a particular thermal environment. The PPD is related to the PMV as follows:

$$PPD = 100 - 95e^{-(0,0353PMV^4 + 0,2179PMV^2)} \quad (2)$$



The term Draft Risk (DR) is the predicted of people dissatisfied due to unwanted local cooling of the body caused by air movement and it is expressed by the following equation:

$$DR = (34 - t_a)(V_a - 0.05)^{0.62} (0.37V_a T_u + 3.14) \quad (3)$$

where t_a is the air temperature, V_a is the air velocity and T_u is the turbulence intensity. In the evaluation of such indices the metabolic rate was fixed at 1.4 met while the actual people's clothing came from the questionnaires.

2.2 The “subjective investigation”

A subjective investigation has been carried out to determine the wellbeing or discomfort sensations of the operating staff. Each surgical staff member was given a questionnaire concerned their physical characteristics (age, sex, weight, etc...), the job and the clothing they wore and the subject's judgment on the thermal environment, the overall comfort sensations and requests of eventual changes of the microclimatic characteristics of the operating room. The questionnaire was divided in three sections concerning: general information; thermal comfort; air quality. The questions in the section of thermal comfort concerned how the thermal environment was felt. In particular, surgical staff members gave a judgment about its acceptability and preference, answering the following questions:

- 1) “How do you consider the thermal environment in the operation room?”
- 2) “Would you prefer to feel warmer, cooler or no change?”
- 3) “Do you feel unpleasant air currents on some areas of your body?”

The judgments about the thermal environment have been compared with the results of the field measurements. Moreover, the subjective mean votes have been compared with the thermal environment perceptions in terms of acceptability and preference.

3 Results analysis

The thermal environment was analyzed by means the CEQ (Controlled Environment Qualification) system of Keita srl to measure air temperature, mean radiant temperature, air relative humidity, air velocity, water vapor pressure, flow rate of supply and return air, and so on.

During the monitored period the Air changes was always more or less 20 Vol/h

The analysis of this graph shows that the OR temperature is always between the values of 21°C and 23°C and only for a few days the temperature goes below the value of 21°C.

This condition could put the patient at risk of becoming hypothermic [6], so it is necessary to increase the air supply temperature considering that in operating



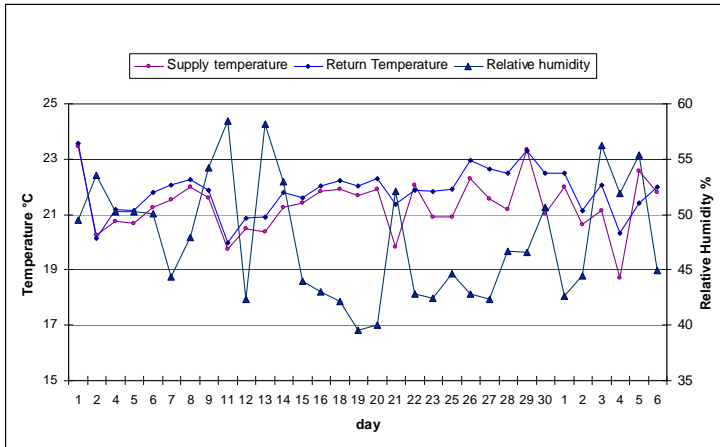


Figure 2: Variation of the air temperature and the RH in the OR.

rooms the thermal environment for the patient is prioritized over the staff. However, a temperature of $>23^{\circ}\text{C}$ is usually intolerable for the surgical staff [6, 7].

For each day of investigation the hourly value of thermal Fanger indexes have been calculated. The measured data indicate that all the parameters vary during the duty period, so for each day of monitoring the minimum and the maximum value for each parameter have been pointed out.

The acceptable PMV range for these typologies of environment has been fixed between -0.2 (slightly cool sensation) and +0.2 (slightly warm sensation) [8]. Figure 3 shows the variation for PMV index during the whole period of monitoring. Overall, it was noticed a similar trend of all the indices calculated for all three operating rooms.

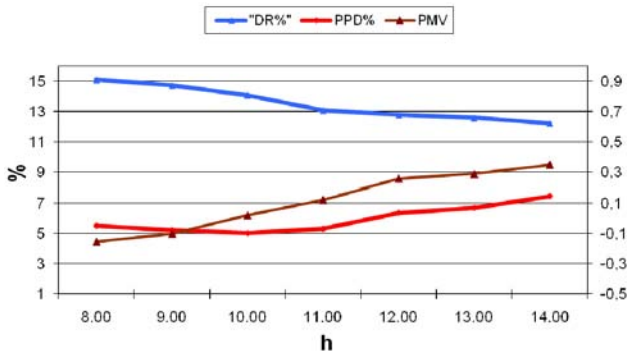


Figure 3: Daily variation of PMV, PPD and DR during a monitored day.



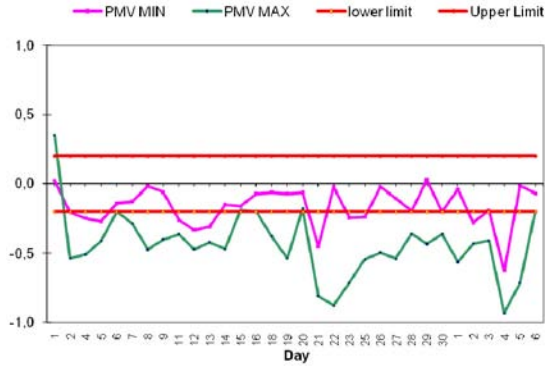


Figure 4: Trend of PMV index and law limit in OR n.1.

As shown in Figure 3, the minimum daily value of PMV remained substantially in the range of ± 0.2 except for some days, while the maximum daily value of PMV is always less than -0.2 and does not exceed the value of -0.5 except for some critical days (see Table 1).

Globally, these results indicate that the member of staff would felt “slightly cool” or cool. By means equation (2) the correlated PPD values have been calculated. Therefore for a value of PMV_s of ± 0.2 the correlated PPD result of 6%, while for a PMV_s of -0.5 result of 10%. This “objective analysis” has been compared with the questionnaire responses. Figures 5 and 6 show the summary of the responses to the questions nn. 1) and 2). It is possible to notice that the responses to the two questions are in perfect agreement. In fact 27% of persons are in neutral conditions (D1 and B1), 33% or 39% of person feels slight discomfort (E1 and B2), 27% or 22% of persons felt discomfort (F1+B1 and C2); 11% of persons felt high discomfort (A1+G1 and D2). With reference to the PPD the value of 10% calculated by Fanger theory more or less is in accordance with the 11% of person feeling high discomfort (A1+G1 and D2). We can also

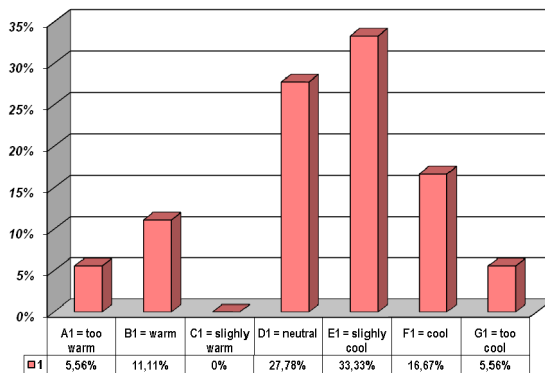


Figure 5: Responses to the Qs n.1.



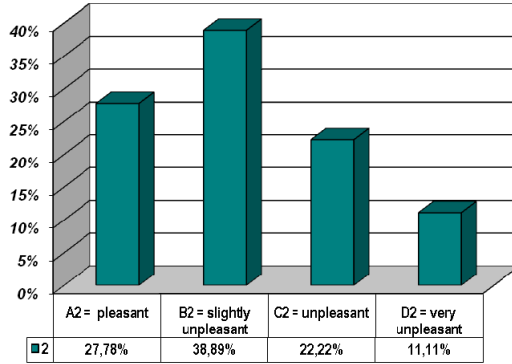


Figure 6: Responses to the Qs n.2.

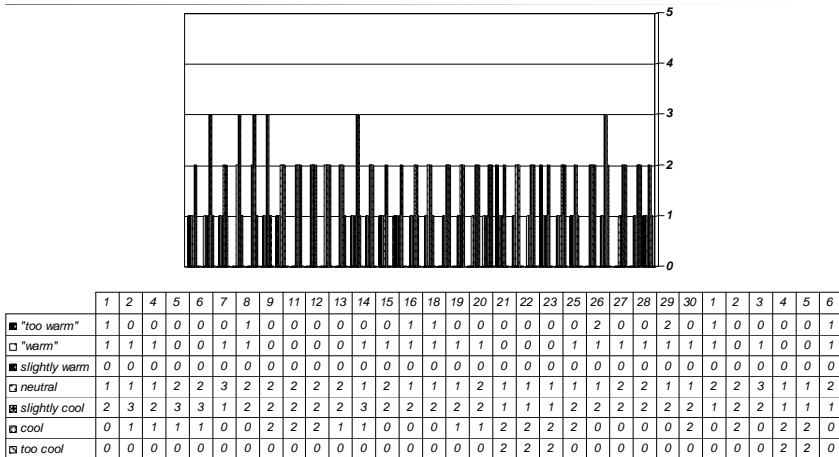


Figure 7: Typologies of responses of each member of the staff.

observe that globally the 55,5% of the responses indicate a thermal sensation of slightly cool or cool, the 28% indicate a thermal sensation of neutrality and the 16,5% indicate slightly warm or warm. The 16,5% of responses that indicate slightly warm or warm appear in contrast with the calculated values of PMV that do not indicate these typologies of sensations.

The reason of these discrepancies could be found out by observing the responses of each member of the staff as shown in figure 7. It is possible to observe that each member of the staff gives a different answer in respect of his thermal sensation. These variabilities could depend on the different levels and types of activities of the staff and by the clothes worn by the person in the OR that are different in function of the activities of each member of the staff. It usually happens that the thermal sensation of the surgeon is warm, while the anaesthesiologist and nurse feel the thermal sensation of cool. Table 1 summarizes the more critical thermal conditions registered during the campaign

of survey. For these days, characterised by PMV of less than -0.5, it is possible to notice the good correlation between the values of Fanger indexes and the answer of the member staff, in fact almost all the people feel a thermal sensation of cool. These results indicate that it is impossible to specify a thermal environment that will satisfy everybody. There will always be a percentage of occupants who perceive thermal discomfort.

Table 1: Critical values of PMV and PPD

Date	OR	PMV max	PPD max
21 July	1	-0,81	16.46
22 July	1	-0,88	18.12
23 July	1	-0,71	14.15
4 August	1	-0,93	19.32
5 August	1	-0,71	14.15

Moreover, as shown in figure 8, the minimum value of DR assumed a value of 15% in all three OR while the daily maximum value was always higher than the value of 15%.

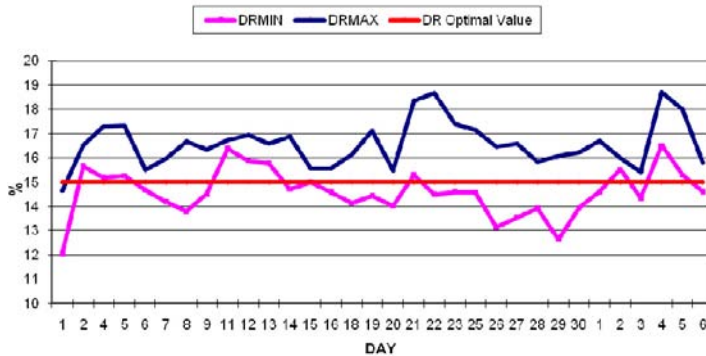


Figure 8: Trend of DR index and optimal value in OR n.1.

These values, according to the UNI EN ISO 7730, indicate a situation of discomfort due to air current (draft), as confirmed in the questionnaire responses: all the members of staff perceived air currents on the neck and the head as predicted by the DR index.

These results indicate the necessity to properly locate the supply outlets and extraction ports in optimal locations to reduce the air currents. The recommended ventilation system has to deliver air from the ceiling in a downward movement to several exhaust inlets located on opposite walls and barriers dividing the ceiling of the diffuser. Anyway, globally the environment has been considered “acceptable” for more than 70% of the occupants and the main complaints concern: low temperature, presence of annoying cold. 11% of the occupants have defined the environmental condition “comfortable” while 16% of the occupants have defined the environmental condition “poorly tolerable”.

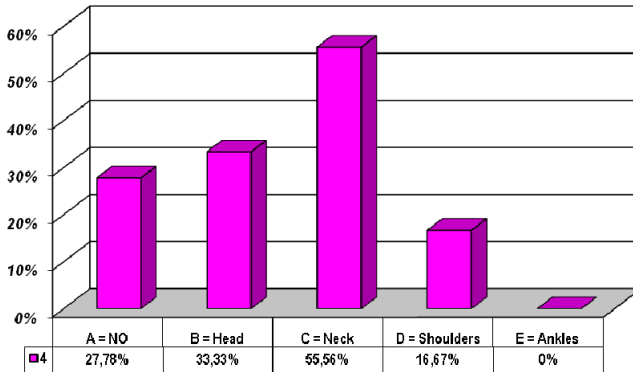


Figure 9: Responses to the Qs n.3.

4 Conclusions

In this paper an in-field investigation methodology on thermal comfort was applied.

The environmental parameters influencing thermal comfort were measured while, at the same time, the subjective judgments of the people about the thermal environment were expressed and significant tendency and correlation were found out.

The developed investigations highlighted the key findings as follow:

- the calculated Fanger indexes are in agreement with the subjective judgments of the people
- the acceptable range of PMV for the OR have to maintain in the range of ± 0.2
- the member of the staff reported different thermal sensation during surgery in relation to their function; often the thermal sensation of the surgeon and nurse is hot, while the anaesthesiologist sometimes feels the thermal sensation of cold
- the DR is the index that indicate the more negative judgments

So it is really important to concentrate the effort in two directions:

- 1) optimize the thermal comfort for the Staff, and at the same time ensure an adequate environment temperature for the patient, while preventing hypothermia, maintaining the ambient temperature in the range of 22 – 23°C
- 2) reduce the air currents on the neck and the head adopting air supply system that minimize harmful effects like short-circuit among air supply and air expulsions, the local undercooling caused by a too high residual speed of the air supply.

References

- [1] A. C. Guyton, 1988. "Fisiologia Humana", Guanabara Koogan, Rio de Janeiro.
- [2] American Society of Heating Refrigerating and Air-conditioning Engineers (ASHRAE), 2004. "Thermal Environment Conditions for Human Occupancy". Atlanta.
- [3] Nederlands Normalisatie-instituut (NEN-ENISO 7730, 2005. "Ergonomics of the thermal environment – Analytical determination and interpretation of thermal comfort using calculation of PMV and PPD indices and local thermal comfort". Delft
- [4] Johnston, I.D.A and Hunter, A. R., 1984. 'The design and utilization of operating theatres'. The Royal College of Surgeons of England.
- [5] ISO. Moderate thermal environments—determination of the PMV and PPD indices and specification of the conditions for thermal comfort. ISO 7730. Geneve: International Organization for Standardization;1998
- [6] Leslie, K. and Sessler, D.I., 2003. "Perioperative Hypothermia in the high-risk surgical patient". Best Practice & Research Clinical Anaesthesiology. Vol.17, n4, pp. 485-498
- [7] Wildt, M., 1996. "Pressure Hierarchy and Indoor Climate of Hospital Rooms". M. Maroni (ed.). Ventilation and Indoor Air Quality in Hospitals, 219-225. Kluwer Academic Publishers.
- [8] Ilona Frohner and László Bánhidi – Comfort Ranges Drawn up Based on the PMV Equation as a Tool for Evaluating Thermal Sensation Proceedings of Clima 2007 WellBeing Indoors



Modeling vapor intrusion processes and evaluating risks using subslab data

E. M. Suuberg¹, Y. Yao¹, R. Shen¹, O. Bozkurt¹ & K. G. Pennell²

¹*School of Engineering, Brown University, Providence, USA*

²*Department of Civil and Environmental Engineering,
University of Massachusetts, Dartmouth, USA*

Abstract

This paper considers the significance of observed subslab contaminant concentrations on the vapor intrusion process. In field measurements, there is observed wide variability in the ratio of indoor air contaminant concentration to subslab contaminant concentration. Here various aspects of the relationship of subslab concentrations to indoor contaminant levels are explored using a three-dimensional fluid dynamics model of the process. Subslab concentrations are determined mainly by diffusional processes and they are reasonably uniform across the subslab for buildings on homogeneous soils (with no significant advective subsurface disturbance). Also, subslab concentrations do not determine the main mode of contaminant entry into a structure (advection or diffusion), and widely different contaminant entry rates can be obtained with very similar subslab concentrations, depending upon whether the soil type supports advection or not.

Keywords: vapor intrusion, numerical modeling, subslab.

1 Introduction

One of the indoor air quality issues currently receiving increasing worldwide attention is that of vapor intrusion. The vapor intrusion problem is similar to that posed by radon, except that the source of the vapor in this case is anthropogenic, as opposed to natural. This also leads to differences in the nature of the phenomena. In non-radon vapor intrusion, the source is typically groundwater, and the problem is therefore often related to a plume of contaminated groundwater. Contaminants of concern include both chlorinated hydrocarbons



and petroleum compounds. In the latter case, the problem may be partially naturally mitigated by biological activity.

This paper will describe some results obtained from a full three-dimensional fluid dynamics analysis of prototypical situations. A commercially available finite element code (COMSOL) is used to capture the essential physics of the problem. The results of modelling to date have shown that such quantitative modeling is necessary in order to understand the problem at a particular site, since quite often, real results contradict intuition [1, 2]. The significance of soil geology, surface capping, “preferential pathways” and dynamic processes has all been illustrated. With such a code, it is possible to propose both better site investigation strategies as well as subsequent mitigation methods for existing or proposed buildings on contaminated sites.

Here, the focus is on the use of model results to inform the process of site investigation. Specifically, what are considered are the utility of so-called subslab contaminant vapor concentrations. These are generally obtained from within a structure suspected of being subject to a vapor intrusion impact. Figure 1 schematically shows the location of a subslab sample. Subslab measurements ordinarily involve boring a hole through the foundation slab of the structure, and taking a soil vapor sample from directly beneath that structure. Such measurements are clearly quite intrusive, particularly when residences or small commercial properties are the subject of investigation. Hence there is a desire to be judicious in their use and to make the most of these measurements. Among the argued advantages of such measurements is that they are the most indicative of the hazardous vapor concentration at a point immediately before entry to a structure in which measurement of concentrations can be confounded by factors such as variations in air exchange rates within the structure or background sources of the contaminant which have nothing to do with the vapor intrusion process itself.

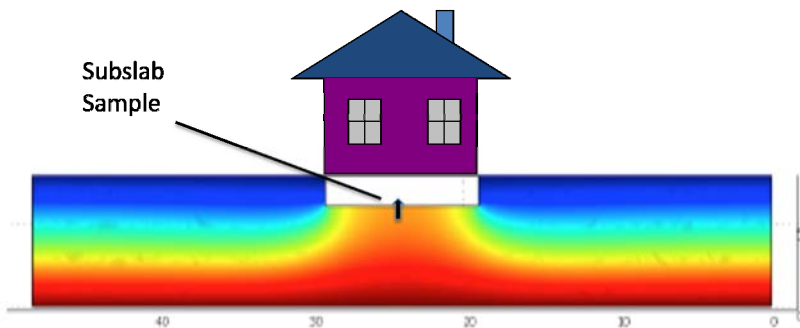


Figure 1: Structure sitting atop a homogeneous contaminant source in an otherwise open field. Colors indicate modelled contaminant concentration profiles, from high concentration at the source to zero concentration at the open surface.

It is well established that contaminant concentration in soil gas sampled at a particular depth beneath a non-permeable cap on the soil (such as a foundation slab or a parking lot) would generally be higher than a sample taken at the same depth beneath open ground [2–4]. This is because the contaminant concentration profile in the subsurface is determined mainly by diffusion [e.g., 5, 6], and that inward advection into a structure mainly serves to enhance the entry of the underlying contaminant into the building, but does relatively less to distort the concentration profile in the soil. The contaminant concentration profile beneath the building is, however, very much that which would be expected from interposing an impermeable barrier somewhere in a diffusion field between a sink (the atmosphere) and the contaminant vapor source (the groundwater). Such a barrier “bottles up” the contaminant beneath it, and the concentration at that point begins to approach the concentration at the (groundwater) source; the only way for contaminant to escape from beneath the barrier is via slow lateral transport in the soil, governed by a small gradient. Thus the subslab contaminant vapor concentrations are normally expected to be the highest near-surface concentrations, and therefore, represent in some sense the highest potential indoor air concentrations. This result is seen in Figure 1.

The U.S. Environmental Protection Agency (USEPA) has assembled a significant database of vapor intrusion field measurements from a range of sites throughout the United States. This database (which may be freely accessed via the internet at http://www.epa.gov/oswer/vaporintrusion/vi_data.html) includes various types of contaminant vapor concentration measurements at many different sites. The data, for various contaminants of concern, include measurements of indoor air concentrations, subslab vapor concentrations, other soil gas concentrations and measurements and estimates of groundwater source concentrations. A preliminary evaluation of these data is available at [http://www.envirogroup.com/publications/oswer_database_report_combined_3-4-08_\(2\).pdf](http://www.envirogroup.com/publications/oswer_database_report_combined_3-4-08_(2).pdf).

For present discussion purposes, it was interesting to examine this database in a way that is similar to that used by the USEPA, but with different constraints and representation of results. The values in the database were culled, choosing only at the data for one contaminant of concern, trichloroethylene (TCE). This was done to ensure that no artefacts are introduced by comparing across different compounds. The data were examined separately for structures built atop basements, slab on grade and crawlspaces.

Figure 2 shows the indoor air concentration in ratio to subslab concentration as a function of the particular structure's subslab concentration of TCE. This ratio of indoor to subslab concentrations clusters in a zone between 0.01 and 0.001, once the subslab concentrations are above a range of about $100 \mu\text{g}/\text{m}^3$. The data in Figure 2 were plotted in the subslab concentration range from 20 to $2000 \mu\text{g}/\text{m}^3$ to emphasize the portion of the dataset that represents the bulk of the field data. At lower concentrations, the reported ratio was often greater than unity, indicating either a problem of data consistency or possibly the influence of background sources. The choice to emphasize midrange concentrations should not be taken to imply that there is no interest in lower ranges of concentration



(which might still represent some health concern), but the focus here is in characterizing the transport aspects of the phenomenon, and the higher concentration level data afford this opportunity better than do the lower concentration level data where the above noted artefacts could play more of a role. The plot also demonstrates that the ratio of indoor to subslab concentrations is not materially dependent upon whether the data were taken from structures with basements or those involving slab-on-grade construction. While not shown here, data for crawlspaces were generally of the same order of magnitude as other indoor values.

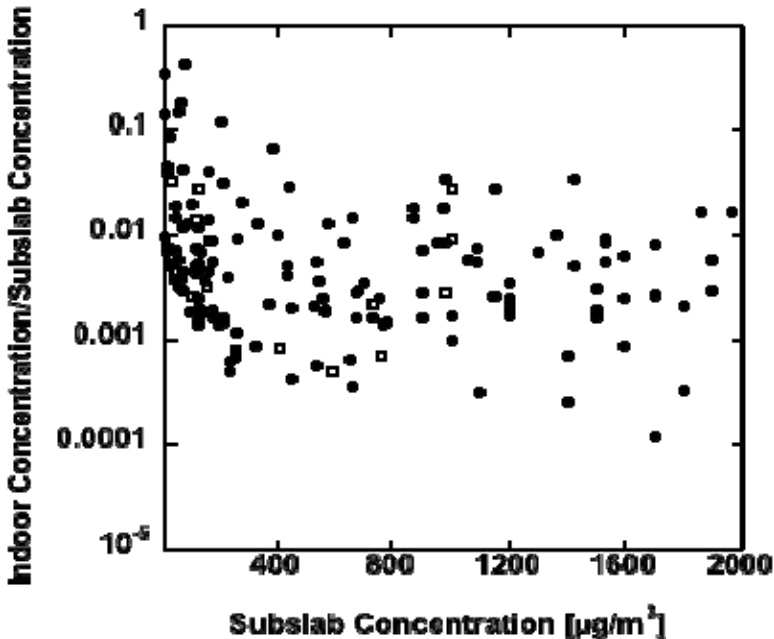


Figure 2: The ratio of measured indoor air contaminant concentration to measured subslab concentration (the “attenuation factor”) as a function of subslab concentration.

The above indicates that there is a general similarity of results, to within an order of magnitude around a mean, for a wide range of buildings and sites. This is true over a great range of different soil and construction types. One critical factor that could not be well controlled in such studies was the indoor air exchange rate, and surely some portion of the variability must be attributable to that, as well as to a related building ventilation parameter, the negative interior pressure (from the so-called “chimney effect”) that drives the inward advection of soil gas.

There are numerous anecdotal reports of order of magnitude or greater variations in subslab contaminant concentrations, either when the same building is sampled at the same time at a number of points, or when the same building is sampled a number of different times at the same point, or when nearby buildings are sampled at the same time. Thus some portion of the variability of Figure 2 can likely be attributed to spatial variability due to heterogeneity in the underlying geology, but it is less likely that temporal variations are responsible, since in many cases, the data were taken concurrently.

The calculation of the entry rate of contaminant from the subslab into a structure needs to take into account a combination of diffusion and advection rates. The resulting indoor air concentration of contaminant is determined by what is shown as Equation 4 in Table 1 below, and depends upon the combined advective plus diffusive entry rate divided by the overall air entry rate into the relevant volume of the structure. The latter is determined by both the building air exchange rate and effective mixed volume of the structure in the area in which the contaminant is sampled. The air exchange rate is normally independent of the actual process of vapor intrusion, though it could be linked to the driving force for advective entry into the structure. There can in practice be quite large ranges in the values of both mixing volume and air exchange rate. As an illustration of the potential consequences of this fact, if both values were to be characterized by a factor of three variability, then almost an order of magnitude variability in the ordinate of Figure 2 would result. It is not claimed that the full variability of results in Figure 2 derives from this source alone, but it must be viewed as a potential key contributor, apart from any uncertainty regarding actual contaminant entry rates into the structure.

The remainder of this paper considers how results of subslab contaminant measurements can relate to the resulting indoor air concentrations. It does so by drawing upon the results of simulations of the vapor intrusion process, utilizing the full three-dimensional fluid dynamics simulation that has been presented in detail elsewhere [1,2].

The present paper is only concerned with steady state conditions in cases where contaminant biodegradation plays no role. Clearly, transient processes can impact observed behavior, and the modeling work performed in this laboratory is considering these influences as well. Examples of factors that need to be considered in transient analyses include variations in source concentration with time, variations in groundwater character (e.g., the height of the water table, variations in soil moisture content), and variations in factors influencing vapor advection in the soil (such as changes in building pressure, effect of winds). Likewise, with certain classes of contaminants (especially petroleum-derived materials) there might be an impact of biodegradation processes on both steady state and transient contaminant vapor concentrations. Again, these processes are not considered here.



Table 1: Working equations for model.

<p>Equation 1: Soil Gas Continuity</p> $q = \frac{k\rho_g \nabla \phi}{\mu_g}$ $\phi = gz + \int \frac{\nabla p}{\rho_g}$	<p>q = Gas velocity (L/t) k = Intrinsic permeability (L²) ρ_g = Density of soil gas (M/L³) μ_g = Dynamic Viscosity soil gas (M/L/t) g = gravitational acceleration (L/t²) p = Pressure of soil gas (M/L/t²) z = elevation (L)</p>
<p>Equation 2: Pressure Drop Across Foundation Crack</p> $\Delta p_{ck} = \frac{12Q_{ck}\mu_g d_{ck}}{w_{ck}}$	<p>where: Δp_{ck} = pressure drop across crack (assumes parallel plates) (M/L/t²) w_{ck} = Width of crack (L) d_{ck} = Length of crack through foundation depth (L) Q_{ck} = Soil gas flow rate through crack into building (L³/t)</p>
<p>Equation 3: Contaminant Transport</p> $J_T = qC - D_i^g \nabla C$ $D_i^g = D_i^{air} \frac{\eta_g^{10/3}}{\eta_T^2} + \frac{D_i^w \eta_w^{10/3}}{K_H \eta_T^2}$	<p>where: J_T = Bulk mass flux of “i” (M/L²/t) C = Concentration of “i” in soil gas (M/L³) D_i^g = effective diffusivity of “i” in soil gas phase (L²/t) D_i^{air} = molecular diffusion coefficient for “i” in air (L²/t) D_i^w = molecular diffusion coefficient for “i” in water (L²/t) K_H = Air:water partition (Henry’s) coefficient (unitless) η = porosity; T=total, g=gas-filled, w=water-filled (L³/L³)</p>
<p>Equation 4: Indoor Air Concentration</p> $C_{indoor} = \frac{A_{ck} J_T}{A_e V_b + Q_{ck}}$	<p>Contaminant transport across foundation: $J_T = qC_{ck} - D_i^{air} \nabla C_{ck}$ $= \frac{q(C_{indoor} - C_{ck} (\exp(qd_{ck} / D_i^{air})))}{1 - \exp(qd_{ck} / D_i^{air})}$ C_{indoor} = Concentration of “i” in the indoor air (M/L³) C_{ck} = Concentration of “i” entering foundation crack (M/L³) A_e = Air exchange rate of building (1/t) V_b = Volume of basement (L³)</p>



2 Modeling approach

The modelling approach used here has been presented in more detail elsewhere [1, 2], and various results from this model have been published previously [3, 4]. Other three-dimensional models of the vapor intrusion process have also been developed [6], and the results from these different approaches are in agreement on all key points. There are significant differences between the nature of, and predictions from, other widely used one-dimensional models of the process [7]. Reviews of various models of the vapor intrusion process have recently been published [8–10].

In the present finite element computational scheme, the first step is to define a domain, and represent it using a mesh that allows finer spacing at key points. Figure 3 shows a typical example of that which has been used in these studies. The equations that have been solved are shown in Table 1. The computational scheme here allows separate solution of Darcy's law for soil gas advection, and then subsequent solution of the contaminant diffusion-advection model. Further details are given in [2].

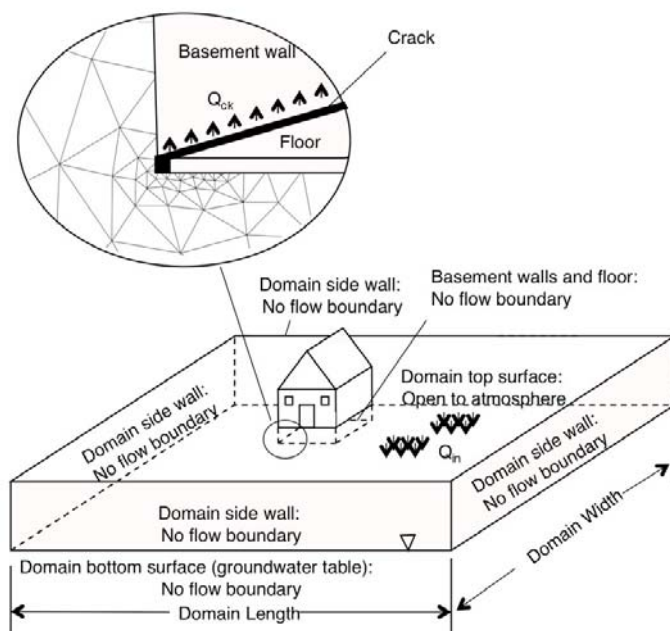


Figure 3: Simplified vapor intrusion model domain, showing domain boundary conditions. The model situation portrayed is a “perimeter crack” where the foundation walls meet the foundation slab. The inset figure shows the reduction in mesh size as the critical crack area is approached. Adapted from Pennell et al. [2].

3 Results

In the cases of interest here, the soil permeability (k) was explored in a “typical” range of 10^{-10} to 10^{-14} m², diffusivities (D^s_i) were in the range of 4×10^{-7} to 1×10^{-6} m²/s. Water filled porosities (η_w) were in the range 0.03 to 0.19 for soils with total porosities (η_T) in the range 0.35 to 0.45. A foundation size of 10 m x 10 m, with an in-ground depth of 2 m was taken as the base case.

Figure 4 shows the ratio of the predicted contaminant concentration at a perimeter crack of the foundation, as compared with the concentration of the contaminant at the center of the slab. The values are shown for three typical soil

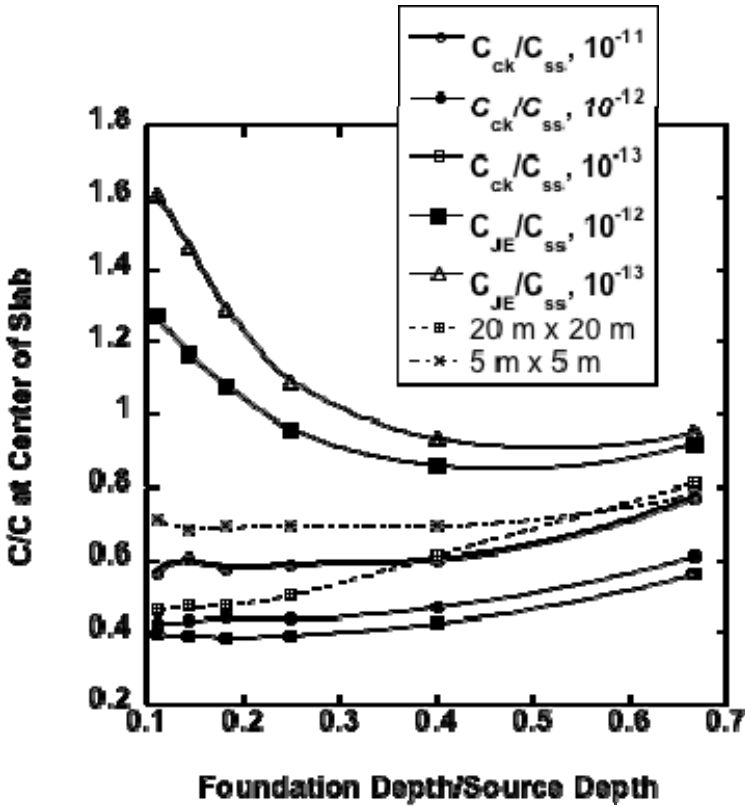


Figure 4: A comparison of the subslab concentrations at a perimeter crack and subslab center, for different soil permeabilities and source depths. Also shown is a comparison of the subslab concentrations from the Johnson-Ettinger model to the subslab center concentrations from the full three-dimensional model, for two soil permeabilities. All results are for 10 m x 10 m footprint except as noted.

permeabilities of 10^{-11} , 10^{-12} and 10^{-13} m^2 . The significance of these results is that the subslab concentrations are not particularly sensitive to the subslab location, to within a factor of two or three. These results were obtained for a constant contaminant vapor soil diffusivity of 1×10^{-6} m^2/s . This is true for a fairly wide range of source depth to foundation depth ratios. Also shown are results for 20 m x 20 m and 5 m x 5 m footprint structures ($k=10^{-11}$ m^2), and these confirm that the conclusion is not sensitive to building size for typical residential/small commercial buildings. In other words, in an area characterized by homogeneous soil, there would not be an expectation of orders of magnitude variation in subslab contaminant concentrations. This is entirely consistent with pictures such as Figure 1 that show generally uniformity of concentration beneath structures built atop homogeneous soils.

The implication of the above finding is that the prediction of contaminant entry rates through the foundation should not depend very strongly upon where the cracks in the slab may be located. Rather, the contaminant entry rate will depend more upon the pressure driving force, the total area of the cracks and how those cracks are distributed, because these determine the soil gas entry rate that carries the contaminant into the structure.

Again, the above is not intended to disregard the occasional field observations of widely varying subslab concentrations under the same structure. What this does mean is that such findings should only be expected where there are major subsurface features that create heterogeneity in the diffusion field, or that there exist variations in how well ventilated the subslab is.

It has recently been shown that the Johnson-Ettinger one-dimensional screening tool can often provide estimates of indoor air concentrations that are in reasonable agreement with the full 3-D analysis employed here. Figure 4 shows a reason why this is the case. The estimate of subslab contaminant concentration is quite close to that from the full 3-D analysis.

A separate calculation has been performed to illustrate the impact on contaminant entry rates of advection to diffusion. Sample results are shown in Figure 5, for a 10 m x 10 m structure with and without a 5 m wide impermeable paved apron around the building. All calculations are for homogeneous soil with a source at 8 m depth.

These results confirm that in high permeability soils, advection of contaminant with soil gas dominates the entry into the structure, whereas in low permeability (clay-type) soils, diffusional processes determine entry rates. Their relative contributions are similar, despite the fact that the structure with the surrounding paving has a 25% higher entry rate of contaminant at $10^{-12}m^2$ permeability. It is the slightly higher average contaminant concentration near the perimeter crack that determines this, which is an indication of the magnitude of impact of subslab concentration variations due to surrounding capping.

One additional point may be made when considering the results for the structure without surrounding paving. While not shown explicitly on Figure 5, at 10^{-14} m^2 permeability, the contaminant entry rate is half that at $10^{-12}m^2$ permeability. This is because diffusion is a much slower process than advection, and the process has moved to completely diffusion controlled at $10^{-14}m^2$.



The contaminant entry rate results for 10^{-11}m^2 are an order of magnitude higher than those for 10^{-14}m^2 , which would lead to an order of magnitude higher indoor air concentration for the former compared to the latter. This difference has nothing to do with subslab concentrations, which are comparable in all the cases; it is merely a consequence of the well known fact that where advection is significant, much higher entry rates will be observed despite the similarity of subslab concentrations.

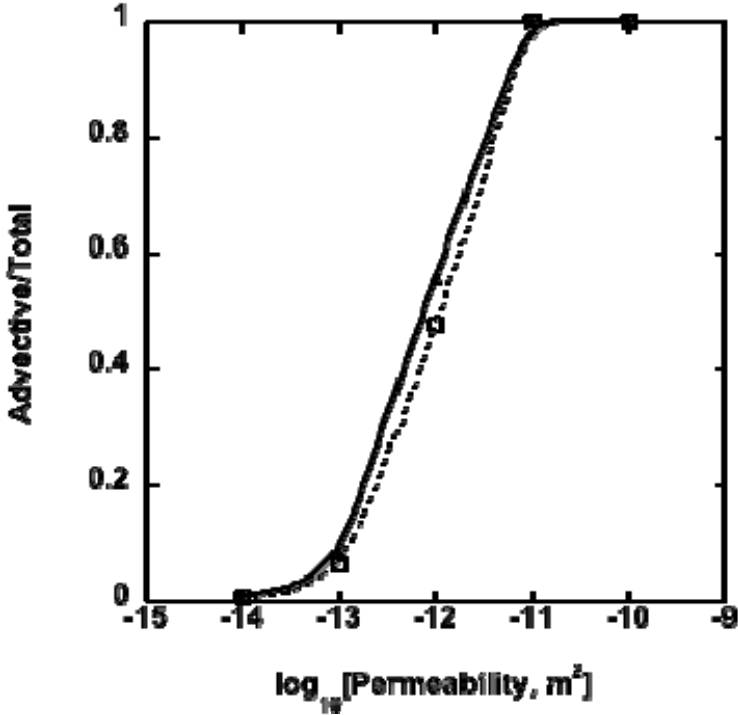


Figure 5: The relative contribution of advective contaminant transport to diffusive transport into a 10 m x 10 m structure with (squares and dotted line) and without (triangles and solid line) a 5 m wide paved apron around the structure. Contaminant entry is through a perimeter crack.

4 Conclusions

The results of numerical modelling of the vapor intrusion process suggest that for structures built atop homogeneous soils, there should be little variation in subslab contaminant concentrations immediately beneath the building footprint, and that sampling at any one point should be as good as sampling at any other

point. Existence of wide subslab concentration variations immediately implies complexity in the subsurface. Subslab concentrations by themselves do not indicate the potential for significant entry rate into a structure; advection greatly enhances the entry rate relative to diffusion, which may be the only mechanism of relevance in low permeability (clay-like) soils.

References

- [1] Bozkurt, O., Pennell, K. G., Suuberg, E. M., Simulation of the vapor intrusion process for nonhomogeneous soils using a three-dimensional numerical model. *Ground Water Monitoring and Remediation*, **29** (1), pp 92-104, 2009.
- [2] Pennell, K. G., Bozkurt, O., Suuberg, E. M., Development and application of a 3-D model for evaluating site-specific features on vapor intrusion rates in homogenous geologies. *Journal of Air and Waste Management Association*, **59**, pp 447-460, 2009.
- [3] Yao, Y., Pennell, K.G., Suuberg, E.M., Vapor intrusion in urban settings: effect of foundation features and source location. *Procedia Environmental Sciences*, **4**, pp 245-249, 2011.
- [4] Pennell, K.G., Suuberg, E.M. Vapor transport from soil and groundwater: numerical modeling approach (Chapter 4). *Vapor Emission to Outdoor and Enclosed Spaces*, ed. S. Saponaro, E. Sezenna, L. Bonomo, Nova Science Publishers, Inc.: New York, 2010.
- [5] Johnson, P.C. Identification of critical parameters for the Johnson and Ettinger (1991) vapor intrusion model. American Petroleum Institute (API), Washington, D.C., Publication #17, 2002.
- [6] Abreu, L.D., Johnson, P.C., Effect of vapor source-building separation and building construction on soil vapor intrusion as studied with a three-dimensional numerical model. *Environmental Science and Technology*, **39**, pp 4550-4561, 2005.
- [7] Yao, Y., Shen, R., Pennell, K.G., Suuberg, E.M., Comparison of the Johnson-Ettinger vapor intrusion screening model predictions with full three-dimensional model results. *Environmental Science and Technology*, **45**, pp 2227-2235, 2011.
- [8] Provoost, J., Bosman, A., Reijnders, L., Bronders, J., Touchant, K., Swartjes, F., Vapor intrusion from the vadose zone- seven algorithms compared. *Jl. Soils Sediments*, **10**, pp 473-483, 2010.
- [9] Provoost, J., Reijnders, L., Swartjes, F., Bronders, J., Seuntjens, P., Lijzen, J., Accuracy of seven vapor intrusion algorithms for VOC in groundwater. *Jl. Soils Sediments*, **9**, pp 62-73, 2009.
- [10] Turczynowicz, L., Robinson, N.I., Exposure assessment modelling for volatiles- towards an Australian indoor vapor intrusion model. *Jl. of Toxicology and Environmental Health, Part A*, **70**, pp 1619-1634, 2007.



This page intentionally left blank

Assessment of fungal contamination in a Portuguese maternity unit

C. Viegas¹, R. Sabino², C. Veríssimo² & L. Rosado²

¹Higher School of Health Technologies of Lisbon,
Polytechnic Institute of Lisbon, Portugal

²National Institute of Health Dr. Ricardo Jorge,
Mycology Laboratory, Portugal

Abstract

A descriptive study was developed to monitor air fungal contamination in one Portuguese maternity. Sixty air samples were collected through impaction method. Air sampling was performed in food storage facilities, kitchen, food plating, canteen, pharmacy, sterilization areas, gynecology wards, intensive care unit, operating rooms, urgency and also, outside premises, since this was the place regarded as reference. Besides air samples, forty three samples were collected by swabbing the surfaces using a 10 by 10 cm square stencil. Simultaneously, temperature, relative humidity and particles counting (PM10) were registered. Twenty three species of fungi were identified in air, being the two most commonly isolated the genera *Penicillium* (41,5%) and *Cladosporium* (28,4%). Regarding yeasts, only *Rhodotorula* sp. (45,2%), *Trichosporon mucoides* (51,6%) and *Cryptococcus neoformans* (3,2%) were found. Thirteen species of fungi were identified in surfaces, being the most frequent the *Penicillium* genus (91,6%). Concerning yeasts found in surfaces, four species were identified being *Rhodotorula* sp. (29,1%) the most frequent.

There was no coincidence between prevailing genera indoors and outside premises. Moreover, some places presented fungal species different from the ones isolated outside. In the inside environment, *Aspergillus* species were isolated in air and surfaces. There was no significant relationship ($p > 0,05$) between fungal contamination and the studied environmental variables.

Keywords: air, surfaces, fungal contamination, environmental variables, maternity.



1 Introduction

The hospital environment is a potential source of infections and for this reason, knowledge of the fungal contamination in clinical settings is important for understanding possible types of nosocomial infections that may emanate from them [1]. Moreover, hospital-wide surveillance studies have shown the presence of various potentially pathogenic fungal species in health care settings [2].

The presence of fungi requires ideal conditions of temperature, humidity, oxygen, carbon sources, nitrogen and minerals. Their biological activities of biodegradation and biodeterioration depend on their enzymatic activity, environmental conditions, competition phenomenon's and nature of the substrate [3]. Regarding particles, they can be vehicle for fungal dispersion [4], favoring the spread of fungi to larger areas.

Fungal health effects are dependent on the species present, the metabolic products, the concentration and exposure duration and individual susceptibility [5], being fungal exposure in hospitals of particular interest due to the possible patient's susceptibility.

Culturing air samples is usually the only parameter used to assess indoor fungal contamination [6]. However, surfaces analysis complements the air characterization and is used in order to identify contamination sources. It may also be used in order to evaluate the efficacy of surface cleaning and disinfection [7]. Although some studies have shown differences in the frequency of fungal species isolated between air and surfaces samples, a longitudinal fungal surface survey, even if performed only two or three times a year, in definite appropriate locations and areas, can detect minor contamination and can serve as a good marker for lack of cleaning or filtration. The surveillance strategy – air and surfaces – permits the control of maintenance and cleaning procedures, the education of healthcare workers regarding infection control protocols and the definition of acceptable levels of contamination in order to introduce immediate corrective measures [8, 9].

Therefore, it is important to contribute to the increase of knowledge regarding to air and surfaces fungal contamination in hospitals indoor spaces in order to identify most effective preventive measures to avoid such contamination. This investigation was designed to describe environmental fungal contamination in a Portuguese maternity and to allow, if necessary, the implementation of corrective measures.

2 Materials and methods

A descriptive study was developed to monitor fungal contamination in the biggest Portuguese maternity during a month period. Sixty air samples were collected through impaction method. Air samples were collected at 140 L/minute, at one meter tall, on to malt extract agar with the antibiotic chloramphenicol (MEA), in the facilities – food storage facilities, kitchen, food plating, canteen, pharmacy, sterilization areas, genecology wards, intensive care unit, operating rooms, urgency – and also, outside premises, since this is the



place regarded as reference. The volume of air collected indoor was 500 l and outdoor 250 l.

Besides air samples, forty three samples were collected by swabbing the surfaces of the same indoor places, using a 10 by 10 cm square stencil disinfected with 70% alcohol solution between samples according to the International Standard ISO 18593 – 2004.

Simultaneously, two environmental parameters – temperature and relative humidity – were monitored, using the Babouc equipment, (LSI Systems), according to the International Standard ISO 7726 – 1998. Particles counting (PM10) were also registered.

After laboratory processing and incubation of the collected samples, quantitative (CFU/m³ and CFU/m²) and qualitative results were obtained, with identification of isolated fungal species. Whenever possible, filamentous fungi were identified to the species level, since adverse health effects vary according to fungal species [10, 11]. Identification of filamentous fungi was carried out on material mounted in lactophenol blue and achieved through morphological characteristics listed in illustrated literature [11] and yeasts were identified through biochemical API test [12].

Tables with frequency distribution of isolated fungal species were made with the obtained data. Fungal concentration dependence in the three monitored environmental parameters – temperature, relative humidity and particles – was also analyzed.

3 Results

Twenty three species of fungi were identified in the collected air samples, being *Penicillium* and *Cladosporium* the two genera most commonly found, with 41,5% and 28,4% of frequency. Regarding yeasts, only *Rhodotorula* sp. (45,2%), *Trichosporon mucoides* (51,6%) and *Cryptococcus neoformans* (3,2%) were found. Thirteen species of fungi were identified in surfaces, being *Penicillium*

Table 1: Most frequent fungi identified in the maternity air and surfaces.

Air	Frequency (%)
<i>Penicillium</i> sp.	41,5
<i>Cladosporium</i> sp.	28,4
<i>Chrysonilia</i> sp.	10,8
<i>Aspergillus</i> sp.	9,1
Others	10,2
Surfaces	Frequency (%)
<i>Penicillium</i> sp.	91,6
<i>Aspergillus</i> sp.	2,7
<i>Chrysonilia</i> sp.	2,0
Others	3,7



genus (91,6%) the most frequent genera. Concerning yeasts found in surfaces, four species were identified being *Rhodotorula* sp. (29,1%) the most frequent.

There was no coincidence between prevailing genera indoor and outside premises. Moreover, some places presented fungal species different from the ones isolated outside. In inside environment, there were isolated *Aspergillus* species in air – *A. ochraceus*, *A. versicolor*, *A. candidus*, *A. fumigatus* and *A. niger* – and also in surfaces *A. glaucus*, *A. terreus* and *A. fumigatus*.

Regarding comparison of concentrations found in air, for indoor and outdoor environments, several places showed higher contamination indoor.

Concerning the influence of the monitored environmental variables – temperature, relative humidity and particles – no significant correlation ($p > 0,05$) was revealed.

4 Discussion

The mere presence of fungi in hospital air is a concern motif because many spores can be released leading to an incidence of nosocomial and occupational infections [1].

Concerning *Penicillium*, the predominant genus in the air and surfaces analyzed, there are different potential risks associated with their inhalation of their different species due to different the toxins release [13].

It is suggested that fungal levels found indoors should be compared, quantitatively and qualitatively, with those found outdoors, because the first are dependent on the last [5]. Nevertheless, when it comes to fungal levels, it should be taken into account that indoor and outdoor environments are quite different which, by itself, justifies diversity of species between different spaces. However, the fact that there is no stipulated limit, with regard to fungal contamination, makes it essential to compare fungal levels indoors and outdoors. Thus, indoor air quality that significantly differs from the outside air could mean that there are infiltration problems and the potential risk for health effects exists. It is worth mentioning that as outdoor air is a major source of the fungi found indoors, nonetheless there was no coincidence between prevailing genera indoor and outside premises. Moreover, some places presented fungal species different from the ones isolated outside and several places showed more contamination indoor, suggesting, all the three situations, fungal contamination from within [14], maybe due to the natural flowers and food brought for the patients [15].

Faure *et al.* [16] used the acceptability threshold for hospital settings > 2 CFU/room without *A. fumigatus* [16]. This threshold was used to interpret air results and to perform, as soon as possible, corrective measures in the contaminated areas. Considering this threshold, from the 31 indoor environments that were monitored, 61,3% showed more than 2 CFU/room and 6,5% presented the species *A. fumigatus*. Another threshold used for hospital settings, proposed by Krzysztofik in 1992, is 200 CFU/m³ [17]. Regarding this threshold 9,7% of indoor places exceed this value. Macher [18] also recommended concentrations for hospital environments, such as: a) for ultra clean areas like laminar airflows a value of < 4 CFU/m³ (viable particle count); b) for air-conditioned areas a value



of $< 18 \text{ CFU/m}^3$; c) for operation theatres and patient isolations rooms a value of $< 15 \text{ CFU/m}^3$ for saprophytic fungi and $< 0,1 \text{ CFU/m}^3$ for opportunistic fungal pathogens [18]. Regarding Matcher *et al.* recommendations, sterilization areas presented more than 4 CFU/m^3 and some areas belonging to the intensive care unit presented more than 18 CFU/m^3 .

Although there is no reference for surfaces we must consider that species found in surfaces – *A. glaucus*, *A. terreus* and *A. fumigatus* – can be aerosolized depending on several variables, such spores dimensions [19], biological characteristics [20, 21], air temperature, oxygen availability, nutrients presence [22] and also, surface vibrations [23].

Filamentous fungi were more frequent than yeasts in the maternity air and surfaces, such as in Kordbachehn *et al.* [24] study, made also in hospital wards [24]. However, in another studied setting – gymnasium with swimming pool – was found that in surfaces the CFU counts were higher for yeasts than for fungi, which may be due to the fact that yeasts are more difficult to disseminate in the air or because they are more resistant to the products used on surfaces during the cleaning procedures [25].

Results related to environmental variables are not consistent with what is expected, because several authors showed a strict correlation between indoor fungal load and temperature, humidity and particles [4, 26]. It was found that the relationship between the fungal air contamination and temperature, relative humidity and particles counting was not statistically significant ($p>0,05$). This may be justified by the effect of other environmental variables also influencing fungal spreading, namely workers, visitors, food, who may carry a great diversity of fungal species [27], as well the developed activities that may also affect fungal concentration [28].

5 Conclusions

With this study it was possible to characterize fungal distribution in this maternity, identify eventual risk sources and most effective preventive measures to avoid such contamination.

Unlike other studies, environmental variables monitored (temperature, relative humidity and particles) did not show the expected association with fungal concentration, which may possibly have resulted from other variables not investigated in this study.

We also conclude that fungal contamination was found within the maternity wards, being this hospital setting a potential source of infections for the patients.

References

- [1] Sudharsanam S., Srikanth P., Sheela M. & Steinberg R., Study of the indoor air quality in hospitals in South Chennai, India. Microbial profile. *Indoor and Built Environment*, 15, 5, pp. 436–441, 2008.



- [2] Sarica S., Asan A., Otkun M. & Ture M., Monitoring indoor airborne fungi and bacteria in the different areas of Trakya University Hospital, Edirne, Turkey. *Indoor Built Environment*, 11, pp. 285–292, 2002.
- [3] Bursykowski T., Molenberghs G. & Abeck D., High prevalence of foot diseases in Europe: results of the Achilles Project. *Mycoses*, 46, 11-12, pp. 496–505, 2003.
- [4] Kim K., Park J., Kim C. & Lee K., Distribution of airborne fungi, particulate matter and carbon dioxide in Seoul Metropolitan Subway Stations. *J Prev Med Public Health*, 39, pp. 325–330, 2006.
- [5] Goyer N., Lavoie J., Lazure L. & Marchand G., *Bioaerosols in the Workplace: Evaluation, Control and Prevention Guide*. Institut de Recherche en Santé et en Sécurité du Travail du Québec, 2001.
- [6] Srikanth P., Sudharsanam S. & Steinberg R., Bio-aerosols in indoor environment: composition, health effects and analysis. *Indian Journal of Medical Microbiology*, 26, 4, pp. 302–312, 2008.
- [7] Stetzenbach L., Buttner M. & Cruz P., Detection and enumeration of airborne biocontaminants. *Current Opinion in Biotechnology*, 15, pp. 170–174, 2004.
- [8] Lebeau B., Pinel C. & Grillot R., Infections nosocomiales fongiques et parasitaires: intérêt et limite des méthodes de désinfection. *Pathologie-Biologie*, 46, 5, pp. 335–340, 1998.
- [9] Brocard-Lemort C., Normes et recommandations en hygiène environnementale hospitalière. *Annales de Biologie Clinique*, 58, 4, pp. 431–437, 2000.
- [10] Rao C., Burge H. & Chang J., Review of quantitative standards and guidelines for fungi in indoor air. *J Air Waste Manage Assoc.*, 46, pp. 899–908, 1996.
- [11] Hoog C., Guarro J., Gené G. & Figueiras M., (2th ed). *Atlas of Clinical Fungi*. Centraalbureau voor Schimmelcultures, 2000.
- [12] Ghannoum M., Hajeh R., Scher R., Konnikov N., et al., A large-scale North American study of fungal isolates from nails: The frequency of onychomycosis, fungal distribution and antifungal susceptibility patterns. *J. Am. Acad. Dermatol*, 43, pp. 641–648, 2000.
- [13] Kemp P., Neumeister-Kemp H., Esposito B., Lysek G. & Murray F., Changes in airborne fungi from the outdoors to indoor air; Large HVAC systems in nonproblem buildings in two different climates. *American Industrial Hygiene Association*, 64, pp. 269–275, 2003.
- [14] Nevalainen A., Bio-aerosols as exposure agents in indoor environment in relation to asthma and allergy. *Section 3 Asthma and allergy. Proceedings of the First ENVIE Conference on Indoor Air Quality and Health for EU Policy, Helsinki, Finland, 2007.*
- [15] Ekhaïse F., Ighosewe O. & Ajakpovi O., Hospital indoor airborne microflora in private and government owned hospitals in Benin City, Nigeria. *Word Journal of Medical Sciences*, 3 (1), pp. 19–23, 2008.



- [16] Faure O., Fricker-Hidalgo H. & Lebeau B., Eight-year surveillance of environmental fungal contamination in hospital operating rooms and haematological units. *Journal of Hospital Infection*, 50, 2, pp. 155–160, 2002.
- [17] Augustowska M. & Dutkiewicz J., – Variability of airborne microflora in a hospital ward within a period of one year. *Annals of Agricultural and Environmental Medicine*, 13, 1, pp. 99–106, 2006.
- [18] Macher J., Bioaerosols: assessment and control. Cincinnati, OH: *American Conference of Governmental Industrial Hygienists*, 1999.
- [19] Aydogdu, H., Asan A. & Otkun M., Monitoring of fungi and bacteria in the indoor air of primary schools in Edirne city, Turkey. *Indoor and Built Environment*, 14, 5, pp. 411–425, 2005.
- [20] Gomes J., Contaminação do ar interior por bioaerossóis. *Revista Portuguesa de Pneumologia*. VIII, 6, pp. 689–694, 2002.
- [21] Lugauskas A. & Krikstaponis A., Microscopic fungi found in the libraries of Vilnius and factors affecting their development. *Indoor and Built Environment*, 3, 3, pp. 169–182, 2004.
- [22] Becker R., Fungal disfigurement of constructions analysis of the effects of various factors. In Samson R, Flannigan B. & Flannigan M., Air quality monographs. Vol 2: Health implications of fungi in indoor environments. Amsterdam: *Elsevier*, pp. 361–380. 1994.
- [23] Górný R., Reponen T. & Grinshpun S., Source strength of fungal spore aerosolization from moldy building material. *Atmospheric Environment*, 35, 28 pp. 4853–4862, 2001.
- [24] Kordbacheh P., Zaini F. & Kamali P., Study on the sources of nosocomial fungal infections at intensive care unit and transplant wards at a teaching hospital in Tehran. *Iranian Journal of Public Health*, 34, 2, pp. 1–8, 2005.
- [25] Viegas C., Alves C., Carolino E., Rosado L. & Silva Santos C., Occupational exposure to fungi in gymnasiums with swimming pools. *Fifth International Conference Environmental Health Risk*, 2009.
- [26] Kakde U., Kakde H. & Saoji A., Seasonal Variation of Fungal Propagules in a Fruit Market Environment, Nagpur (India). *Aerobiologia*, 17, pp. 177–182, 2001.
- [27] Scheff P., Pulus V., Curtis L. & Conroy L., Indoor air quality in a middle school, Part II: Development of emission factors for particulate matter and bioaerosols. *Applied Occupational and Environmental Hygiene*, 15, pp. 835–842, 2000.
- [28] Buttner M. & Stetzenbach L., Monitoring Airborne fungal spores in an experimental indoor environment to evaluate sampling methods and the effects of human activity on air sampling. *Applied and Environmental Microbiology*, 59, pp. 219–226, 1993.



This page intentionally left blank

Respiratory toxicity of *Aspergillus versicolor*: the most common indoor mould in Slovakia

E. Piecková¹, M. Hurbánková¹, S. Černá¹, M. Majorošová¹,
Z. Kováčiková¹ & D. Pangallo²

¹Slovak Medical University, Bratislava, Slovakia

²Institute of Molecular Biology, Slovak Academy of Sciences,
Bratislava, Slovakia

Abstract

A mould *Aspergillus versicolor* clearly dominates in damp and mouldy indoor environments under Slovak dwelling/public building conditions (up to 1/3 of all isolates during the last decade's surveys). Nearly all of its isolates are able to synthesize a mycotoxin sterigmatocystin (detected by LC/MS-MS), that showed severe *in vitro* as well as *in vivo* toxic potential in animal experiments (after intratracheal instillation to rats). *In vitro* toxicity of complex chloroform-extractable endo- and exometabolites of 10 indoor, and related outdoor, *A. versicolor* isolates from a heavily mouldy kids' fashion store in Slovakia with complaints from the occupants of irritation of their airways has been evaluated by a bioassay with tracheal organ cultures of one-day old chicks (20 microg of toxicants per mL of cultivation medium). In the *in vivo* experiments, respiratory toxicity of the same metabolite mixtures was tested in Wistar rats during three days. The inflammatory and cytotoxic biomarkers were then analyzed in bronchoalveolar lavage fluid. Searching for the fungus possible source, molecular epidemiological study of the isolates was performed using RAMP PCR. Strains colonizing the indoor walls of the shop were the highest correlated to the outdoor airborne ones (Pearson correlation 97%). While indoor airborne isolates correlated to the strains growing on retailled clothes at the levels of 90 or 86% according to Pearson. All micromycetes produced secondary metabolites that ceased ciliary beating in tracheal epithelium in the organ cultures already in 24 hrs of the activity, i.e. in the sense of the method used, they belong to strong toxicants. Two of the isolates tested also produced extrolites without toxic effects detectable by the method. The metabolites also showed certain cytotoxic



and inflammation-inducing effects that were in concentration depending on the animal experiments. It has been proven that toxin production in fungi depends not only on the species but may vary between every single isolate as well. The most important outcome of the study is that microscopic filamentous fungi present in the dwelling indoor environment under Slovak (Central European) building/housing conditions might produce compounds even with the potential to damage the airways of occupants, while children remain the most vulnerable population.

Keywords: dwellings, dampness, fungal toxic metabolites, airways, intratracheal instillation.

1 Introduction

While there remain many unresolved scientific questions, we do know that exposure to high levels of mould causes some illnesses in susceptible people. Sick building syndrome (SBS) is a term used for symptoms, such as runny nose, itchy eyes, sore throat, headaches, commonly associated with staying in buildings with poor indoor air quality. The importance of indoor fungal growth in this phenomenon continues to be evident and indoor fungi are not only a scientific issue anymore but they are also becoming the social one [1]. Recently, research is more focused on non-allergic mechanisms that may be inducing adverse health effects of indoor fungi stemming from such fungal metabolites as beta-D-glucan, mycotoxins and fungal volatile organic compounds (VOCs) [2, 3]. Humidity indoors is a major factor relating to symptoms of SBS [4].

Tuomi *et al.* [5] analyzed 17 mycotoxins from 79 bulk building materials collected from water-damaged buildings. Their results showed sterigmatocystin was present in 24% of the samples, trichothecenes in 19% of the samples, and citrinin in 3 samples. *Aspergillus versicolor* was found on most sterigmatocystin-containing samples, and *Stachybotrys chartarum* were found on the samples in which satratoxins were present. Residents who were exposed to toxigenic fungi in water-damaged buildings might suffer from many nonspecific symptoms, although the health effects of indoor molds can be inconsistent [6, 7].

The mould *A. versicolor* develops yellow, orange–yellow to yellow–green compact colonies, sporulation might be often poor. The optimal growth temperature ranges between 25 and 27 minimal is found at 6–9°C, optimal water activity (a_w) of the cultivation medium 0.78–0.98. *A. versicolor* fungal cells have an antigen structure similar to that of *Penicillium glabrum*. After one-month's inhalation of the spores, laboratory rats showed granulomatous lesions in lung tissue, localized mainly near to the bronchi [8]. Most of the relevant papers dealing with *A. versicolor* discuss the production of carcinogenic mycotoxin sterigmatocystin. The frequency of toxigenic strains in the fungus population is rather high, about 74%, under various laboratory conditions. Indoor *A. versicolor* isolates cultivated on plasterboard at 25°C in wet chambers for 3 months released into the material chloroform extractable endo- and exometabolites able to cease tracheal ciliary beating in chicks similar to the effect of strigmatocystin [9]. From the indoor environment quality point of view, this mould belongs to



so-called first colonizers, i.e. its common air-borne microorganism found in non-sterile spaces. For example, it was found in 32% of examined houses (air, walls) and in 50% of schools in Western Europe, but also in house dust in Saudi Arabia (15,000 colony forming units/g, 7.66% of mycoflora) [10]. *A. versicolor* clearly dominates in damp and mouldy indoor environments under Slovak dwelling/public building conditions (up to 1/3 of all isolates during last decade's surveys) [11]. Nearly all of the isolates are able to synthesize sterigmatocystin (detected by LC/MS-MS) [12].

In vitro toxicity of complex chloroform-extractable endo- and exometabolites of 10 indoor, and related outdoor, *A. versicolor* isolates from a heavily mouldy kids' fashion store in Slovakia with complaints from occupants of irritation of their airways has been evaluated by a bioassay with tracheal organ cultures of 1-d-old chicks'. In the *in vivo* experiments, respiratory toxicity of the same metabolite mixtures was tested after intratracheal instillation in Wistar rats while the inflammatory and cytotoxic biomarkers were analyzed in bronchoalveolar lavage fluid. Searching for the possible source of the fungus, molecular epidemiological study of the isolates was performed.

2 Material and methods

2.1 Moulds and their molecular characterization

The indoor/outdoor air of the building tested was sampled by the aeroscope (A-AIR 010, Agea, Ltd., Prague, Czech Republic) to obtain its particular mycoflora. Isolated *A. versicolor* strains (airborne – 5 indoor, 1 outdoor as well as from mouldy indoor surfaces' swabs – 3 and 1 from an air-co filter), 10 in total, tab. 1, were cultivated in the liquid Sabouraud medium with 20% sucrose and 2% yeast extract at 30°C for 10 d. Chloroform extracts of the biomass and the cultivation medium yielded crude fungal endo- or exometabolites for toxicological experiments [11].

Table 1: *Aspergillus versicolor* isolates used in the study.

Isolate Nr.	Origin
393	Indoor air (by the air-co system)
394	Dtto
382	Indoor air (next to W.C.)
383	Dtto
426	Indoor air (meeting room)
372	Outdoor air (roof)
366	Indoor wall
400	Goods (coat)
403	Goods (trousers)
413	Air-co filter



To find the probable source of fungal contamination, the molecular epidemiological method of RAMP PCR was explored. It is the new PCR method and the special PCR program, using two primers (T14 and K7) for the analysis, enabling more precious identification of microorganisms than other PCRs (RAPD, AFLP, REP, etc.). Fungal DNA was isolated from the biomass, grown as given above, by the DNeasy Tissue Kit (QIAGEN, Hilden, Germany). PCR products were analyzed electrophoretically and UV visualized. The program GelCompare II software (Applied Maths, Kortrijk, Belgium) helped to establish Pearson's correlations of the fungal genome similarity [13].

2.2 *In vitro* toxicity of fungal metabolites

The bioassay based upon the ability of toxicants (20 microg/mL cultivation Eagle's medium with Earl's salts) – endo-, exometabolites of all *A. versicolor* isolates characterized, a mycotoxin sterigmatocystin (Sigma, Ltd., St. Louis, USA) commonly produced by *A. versicolor* as positive control, and a solvent dimethylsulphoxid (DMSO) 2% as negative one, to cease ciliary beating in the tracheas of one-d-old chicks at 37°C and 5% CO₂ after 24, 48, 72 hrs, resp., was employed [14].

2.3 *In vivo* toxicity of *A. versicolor* metabolites after intratracheal instillation

Groups of 6 male Wistar rats (Velaz, Prague, Czech Republic), at about 200 g were exposed per toxicant – endo- and exometabolites (Aend, Aex) of *A. versicolor* Nr. 366. Animal treatment followed the Guidelines of the European convention for the Protection of Vertebrate Animals for Experimental Purposes. Each rat was intratracheally instilled with 4 microg of the metabolite in 0.2 mL of 0.2% DMSO. Animals in the negative control group received only the solvent, or sterigmatocystin (StDAS) in the positive one. After 3-day's exposure, the animals were killed by exsanguination under thiopental anaesthesia (150 mg/kg b. w.). Bronchoalveolar lavage was performed (5x), the pooled fluid (BALF) centrifuged and BALF cells isolated. Cytotoxic (phagocytic activity and viability of alveolar macrophages – AMs, the lactate dehydrogenase and acid phosphatase activities) and inflammatory response biomarkers (total BALF cell and AM counts, and white blood cells' differentials) were measured [15, 16].

3 Results and discussion

3.1 Molecular epidemiology of *A. versicolor* strains

The fungal isolates from indoor walls and outdoor air were highly correlated (Pearson's correlation 97%). Indoor airborne isolates showed 90 or 86% correlation with those from mouldy textile or between different sampling positions (fig. 1).



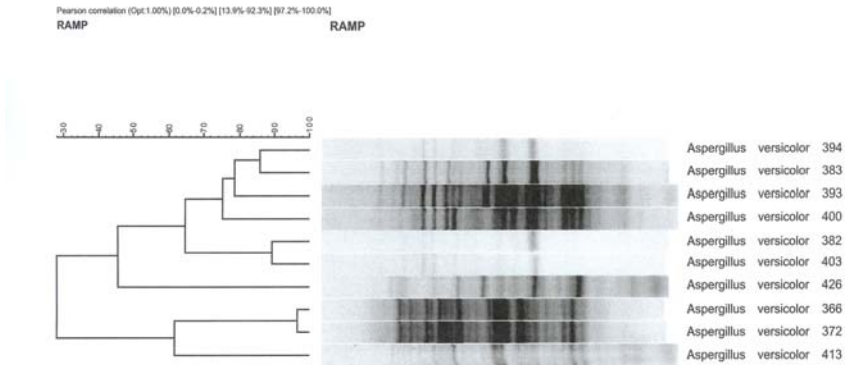


Figure 1: Pearson's correlation of *Aspergillus versicolor* isolates.

The highest correlation of 97% between *A. versicolor* strains could point to a mixing of out- and indoor air in the course of ventilation, while the outdoor air was apparently the source of the fungus later colonizing the walls inside the building examined.

On the other hand, mouldy textile items (trousers) could be seen as vectors carrying other, molecularly different, fungal strains into the indoor atmosphere as those correlated very well (90% according to Pearson). It might be stated indoor and outdoor mycoflora clearly affects each other and it is impossible to distinguish between them precisely in terms of present fungal propagules [17].

4 *In vitro* toxic potential of *A. versicolor* metabolites

All fungal isolates tested produced mixtures of secondary chloroform-extractable metabolites able to stop movement of chicken tracheal cilia in 24 hrs, i.e., according to the method performed, they might be pronounced as strongly toxic. In previous studies (e.g. [12]), *A. versicolor* was recognized as the almost absolute producer of the mycotoxin sterigmatocystin and its derivatives. Sterigmatocystin was able to break down the ciliary beating in any such experiment formerly (e.g. [18]). So, this mycotoxin was also supposed to be the active toxic principle in chemically non-characterized mixtures of fungal products studied now.

Two indoor airborne strains (Nr. 383 and 394) also produced extrolites not damaging tracheal epithelium detected by the bioassay used. Therefore, it was again proven that toxin production does not belong to fungal species necessarily, but it may vary among single isolates. *A. versicolor* was found on most sterigmatocystin containing samples that represented 24% of building materials collected from water/damaged buildings and analyzed for mycotoxin content [5].

4.1 Analysis of acute pulmonary toxicity of *A. versicolor*

Pulmonary exposition to fungal exo- and endometabolites during 72 hrs after intratracheal instillation to the rats did not cause statistically significant changes in some inflammatory parameters detected in bronchoalveolar lavage fluid (BALF). Though, total cell count and alveolar macrophages' (AMs) count in 1 mL BALF were elevated in the group of animals exposed to aspergillus metabolites (endo- and exometabolites – Aend, Aex in the graphs) comparing to the positive control group (exposed to the standard mycotoxin – StDAS in the graphs) (figs. 2 and 3). Differential counts of inflammation activated cells (AMs, lymphocytes and polymorphonuclears) were not altered by toxicants vs. controls in this experiment (figs. 4–6). Young monocytic AMs and binuclears were relatively depressed by fungal metabolites when compared to the positive control (fig. 7 and 8).

Results also indicated just very mild cytotoxic damage expressed as viability and phagocytic activity of AMs that were lowered only comparing to the negative control (DMSO in the graphs) (figs. 9 and 10). Activity of a cytoplasmatic enzyme lactate dehydrogenase (LDH) and the lysosomal ones acidic phosphatase (ACP) and cathepsin D (CATD) slightly increased in absolute numbers while the changes remained statistically insignificant, (figs. 11–13).

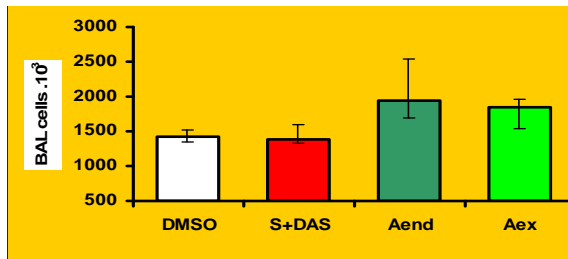


Figure 2: Total cells' count in bronchoalveolar lavage fluid (BALF).

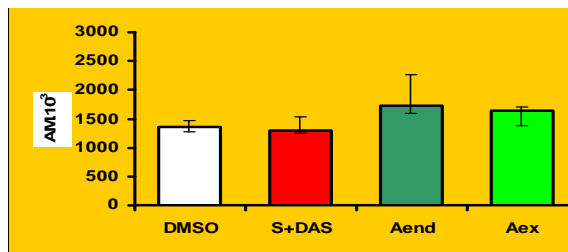


Figure 3: Alveolar macrophage (AM) count in BALF.

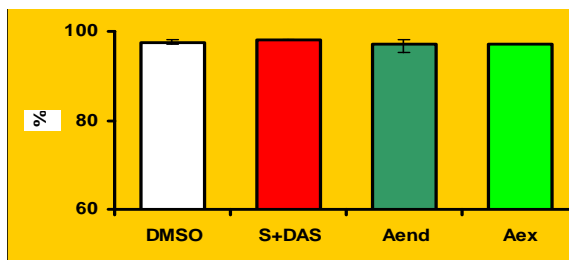


Figure 4: Proportion of AMs in total BALF cells.

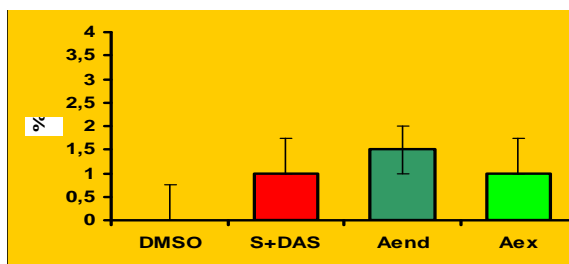


Figure 5: Proportion of lymphocytes in BALF cells.

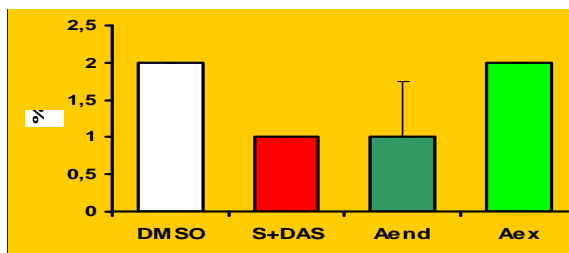


Figure 6: Proportion of polymorphonuclears in BALF cells.

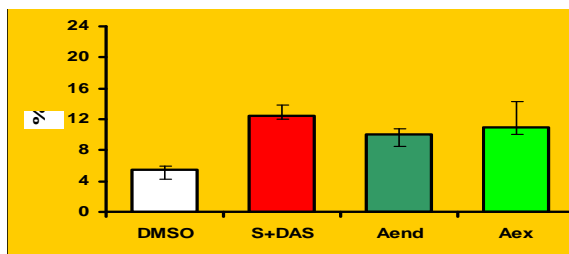


Figure 7: Proportion of young AMs in BALF cells.

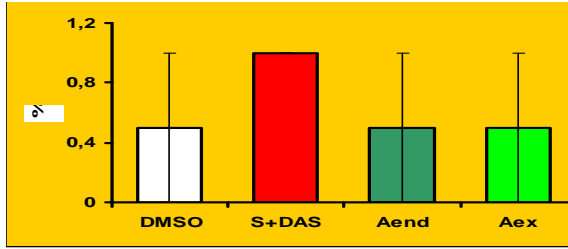


Figure 8: Proportion of binucleate cells in BALF cells.

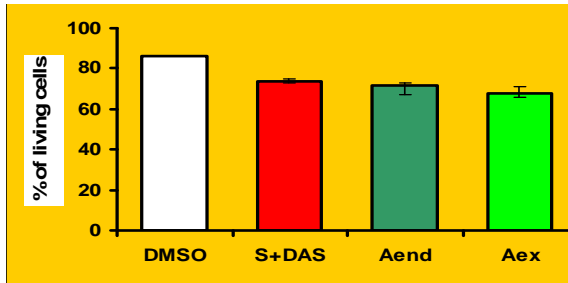


Figure 9: Viability of AMs.

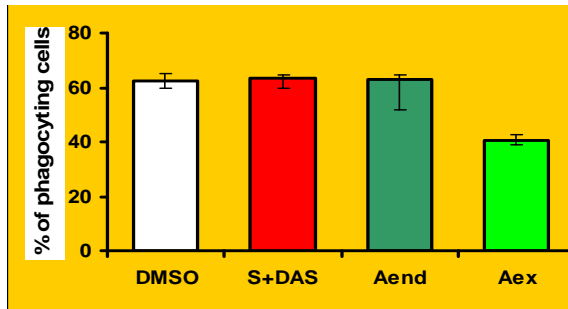


Figure 10: Phagocytic activity of AMs.

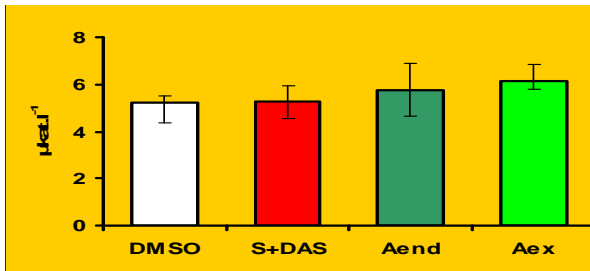


Figure 11: Activity of lactate dehydrogenase in cell free BALF.

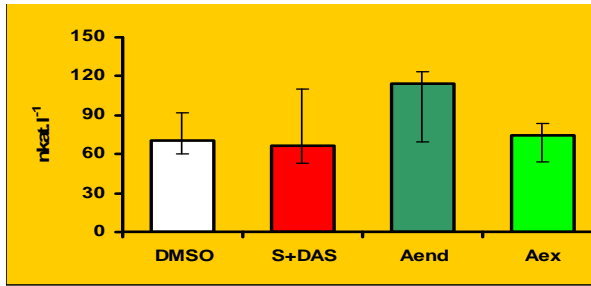


Figure 12: Activity of acidic phosphatase in cell free BALF.

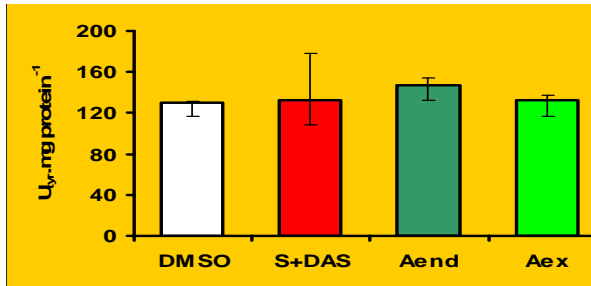


Figure 13: Activity of cathepsin D in cell free BALF.

It seems that *A. versicolor* metabolites tested possess less strong toxic – proinflammatory and cytotoxic potential than similar complex mixtures produced by *Stachybotrys chartarum*, which were analyzed under identical experimental conditions prior to them: when the exposed rats showed significant remarks of cytotoxic damage – higher lactate dehydrogenase and acidic phosphatase activities in the cell free BALF, higher phagocytic activity and lower AMs viability as well as increased total BALF cell count, indicating inflammation, lower AM count and depressed granulocyte count related to the BALF cells. The significant increase in young AM proportion was probably related to significantly lower AM viability, which was either a secondary effect of inflammation or the consequence of metabolite cytotoxicity. Binucleate cell count may rise after long-term exposure to some environmental toxicants (tobacco smoke, some dusts etc.) and along with multinucleate cell count in lung suspension may well reflect chronic inflammation. In all of our studies so far the changes in these cell counts were not pronounced very well as the experiments took only 3 d and the inflammation was still acute [15, 16].

5 Conclusion

Physiological effects *in vivo* of sterigmatocystin or complex mixtures of *A. versicolor* metabolites following direct respiratory intake have not been described yet. We found they were able to initiate certain non-specific

inflammatory response in the complex airways of experimental animals based on toxic reactions. Such response in the lungs may also cause systemic effects because of the spread of inflammatory cytokines in the blood to other organs of the entire body. Thus, it cannot be said yet that mycotoxin production in the buildings infested by fungi is definitely responsible for the ill health of their occupants, but it is clear that exposure to these chemicals should be avoided maximally.

References

- [1] Straus, D.C., Consequences of mold exposure in buildings. *Texas Journal of Rural Health*, **19(1)**, pp. 8–13, 2001.
- [2] Li, D.-W. & Yang, C.S., Fungal contamination as a major contributor to sick building syndrome. *Advances in Applied Microbiology*. Vol. 55, ed. D.C. Straus, Elsevier: San Diego, pp. 31–112, 2004.
- [3] Shelton, B.G., Kirkladen, K.H., Flanders, W.D. & Morris, G.K., Profiles of airborne fungi in buildings and outdoor environments in the United States. *Applied and Environmental Microbiology*, **68(6)**, pp. 1743–1753, 2002.
- [4] Wieslander, G. & Rylander, R., Humid buildings. *Indoor Building Environment*, **12(2)**, pp. 209 – 262, 2003.
- [5] Tuomi, T., Reijula, K., Johnson, T., Hemminki, K., Hintikka, E.-L., Lindroos, O., Kalso, S., Koukila-Kahkola, P., Mussalo-Rahamaa, H. & Haahtela, T., Mycotoxins in crude building materials from water damaged buildings. *Applied and Environmental Microbiology*, **66(6)**, pp. 1899–1904, 2000.
- [6] Ammann, H.M., ACGIH TLV Statement on bioaerosols; American Council of Government Industrial Hygienists. *Bioaerosols, fungi and mycotoxins: health effects, assessment, prevention and control*, ed. E. Johanning, ENYOEH: Albany, pp. 520–521, 1999.
- [7] Hessel, P.A., Klaver, J., Michaelchuk, D., McGhan, S., Carson, M.M. & Melvin, D., The epidemiology of childhood asthma in Red Deer and Medicine Hat, Alberta. *Canadian Respiratory Journal*, **8(2)**, pp. 139–146, 2001.
- [8] Piecková, E., *Aspergillus* sp. in dwellings and health implications of indoor fungi, www.aspergillus.man.ac.uk, 2001.
- [9] Piecková, E. & Jesenská, Z., Indoor fungi in dwellings. (In Slovak). *Hygiena*, **43(4)**, pp. 174–187, 1998.
- [10] Piecková, E. & Jesenská, Z., Microscopic fungi in dwellings and their health implications in humans. *Annals of Agricultural and Environmental Medicine*, **6(1)**, pp.1–11, 1999.
- [11] Piecková, E. & Kolláriková, Z.: *In vitro* toxicity of indoor moulds from Slovak dwellings. *Environmental Toxicology II*, eds. A.G. Kungolos, C.A. Brebbia & M. Zamorano, WitPress: Southampton, pp. 227-234, 2008.
- [12] Bloom, E., Bal, K., Nzman, E., Must, A. & Larsson, L., Mass spectrometry/based strategy for direct detection and quantification of some mycotoxins produced by *Stachybotrys* and *Aspergillus* spp. in indoor



- environments. *Applied and Environmental Microbiology*, **73(5)**, pp. 4211-4217, 2007.
- [13] Pangallo, D., Chovanová, K., Šimonovičová, A. & Ferianc, P., Investigation of microbial community isolated from indoor artworks and air environment: Identification, biodegradative abilities, and DNA typing. *Canadian Journal of Microbiology*, **55(1)** pp. 1-11, 2009.
- [14] Jesenská, Z. & Bernát, D., Effects of mycotoxins on *in vitro* movement of tracheal cilia from one-day-old chicks. *Folia Microbiologica*, **39(4)**, pp. 155-158, 1994.
- [15] Piecková, E., Hurbánková, M., Černá, S., Pivovarová, Z. & Kováčiková, Z., Pulmonary cytotoxicity of secondary metabolites of *Stachybotrys chartarum* (Ehrenb.) Hughes. *Annals of Agricultural and Environmental Medicine*, **13(2)**, pp. 259-262, 2006.
- [16] Piecková, E., Hurbánková, M., Černá, S., Líšková, A., Kováčiková, Z., Kolláriková, Z. & Wimmerová, S., Inflammatory and haematotoxic potential of indoor *Stachybotrys chartarum* (Ehrenb) Hughes metabolites. *Archives of Industrial Hygiene and Toxicology*, **60(4)**, pp. 401-410, 2009.
- [17] Piecková, E. & Pivovarová, Z., Indoor air fungal contamination in Slovak dwellings vs. outdoor aero-mycroflora. *Proc. of the 11th Int. Conf. Cold Climate, HVAC –ABOK: Moscow*, pp. 230–234, 2006.
- [18] Piecková, E. & Kunová, Z., Indoor fungi and their ciliostatic metabolites. *Annals of Agricultural and Environmental Medicine*, **9(1)**, pp. 59–63, 2002.



This page intentionally left blank

Environmental health issues in the wake of a major earthquake in West Sumatra, Indonesia

D. Fanany

School of Public Health, La Trobe University, Melbourne, Australia

Abstract

The 2009 earthquake in Padang, the capital city of the province of West Sumatra in Indonesia, devastated the city's physical landscape, causing material and economic damage that has yet to be repaired. Environmental health issues arising from the earthquake also remain mostly unresolved. Many of the earthquake's most devastating effects were exacerbated by the lack of effective contingency planning and responses in place. This paper presents the events relating to reconstruction efforts in the year following the earthquake and the environmental health issues that emerged, including problems related to the water supply and a serious outbreak of dengue fever. Four features of the Indonesian political landscape that affected the response to the disaster and the reconstruction process are identified: corruption; regional autonomy; technological leapfrogging; and the concept of *pembangunan* [development].

Keywords: West Sumatra, earthquake, environmental health, reconstruction.

1 Introduction

On September 30, 2009, an earthquake measuring 7.6 on the Richter scale struck the Indonesian province of West Sumatra. The earthquake's epicenter was in the region of Pariaman, on the coast just north of the provincial capital of Padang. While earthquakes are not uncommon either in Indonesia as a whole or in West Sumatra specifically, it had been relatively unusual for the epicenter to be in such close proximity to a major city. As such, little attention had been given to earthquake-resistant construction or city planning, and authorities had little in the way of contingency preparation for such an event. Official records reported 1,115 deaths and nearly 3,000 serious injuries as a result of the quake [1]. The city of Padang suffered severe and extensive damage, with many buildings either



destroyed outright or damaged so badly they needed to be demolished, and damage to gas and electricity lines that resulted in fires.

2 Post-disaster reconstruction

Severe disruption to the city's daily routine and operations followed the earthquake. According to the Departemen Sosial [Department of Social Affairs], many government and commercial buildings either sustained major damage or were entirely leveled, notably the Dinas Kelautan Perikanan Provinsi Sumatera Barat [Provincial Office of Maritime Affairs]; several shops and office buildings in the Sawahan neighborhood; several hotels including Hotel Ambacang, Hotel Ina Muara, and Bumi Minang; major shopping centers such as Plaza Andalas and Matahari; the state courthouse in Siteba; and the Muhammadiyah mosque in Simpang Haru [2]. The central offices of many banks that were located in the main market area were severely damaged, including Bank Indonesia (BI), the Padang branch of the nation's central bank [3]. Not only did this require the setup of emergency procedures to meet the public's pressing need for cash, BI was unable to conduct any government business, a major problem considering the number of people employed by the government (health care personnel, police and military officers, public school teachers, employees of government offices, and others). In the older Pondok neighborhood, many businesses' premises collapsed outright, trapping employees in the rubble [4].

Schools were particularly hard hit by the earthquake – 1078 were reported damaged in the disaster. Despite the existence of funds for this aspect of the reconstruction coming from Dana Alokasi Khusus Bencana [Special Allocation of Funds for Disaster] which are released as part of the national and regional budgets, the national newspaper *Republika* [5] reported that only 402 schools had been rebuilt or repaired one year after the disaster. The local government is hoping for more international aid to speed the reconstruction.

In the wake of the earthquake, the government has put a number of contingency plans and responses into place. For example, in September 2010, construction began on an earthquake “escape building” behind the governor's office. The escape building is intended to provide shelter for both provincial-level officials and members of the public in the event of another earthquake and was constructed with the assistance of Japanese experts [6]. The Andalas Bridge was also designated a tsunami evacuation route, with upgrades planned. The local government encountered a number of problems with this, most notably difficulties in reaching an agreement with residents to purchase land required for the upgrade [7]. This has been particularly vexing to local authorities, considering the periodic panics and fear of tsunamis and earthquakes apparent among the public.

Approaching two years after the earthquake, reconstruction efforts have proceeded slowly and remain far from complete. Many buildings have not been rebuilt, including large parts of the main market, and many restaurants and smaller stores have closed permanently. Much of the rubble resulting from the quake has not been cleared, and a large number of lots remain abandoned especially in older parts of the city. Both of these last two observations present



clear environmental health hazards, as they serve to multiply the number of potential breeding places for mosquitoes and other vectors.

3 Public services

The immediate aftermath of the earthquake saw Padang's public services reduced to nearly zero. There was no electricity at all in the city, although other population centers farther from the epicenter such as Bukittinggi, Solok, and Payakumbuh were relatively unaffected [8]. Electricity was restored to much of the city relatively quickly – about 85% of Padang was back on the grid within five days. The reconstruction effort aimed to fully restore electricity within 10 days of the earthquake, and the National Electric Company [Perusahaan Listrik Negara = PLN] sent 450 extra technicians from North Sumatra, Riau, Jambi, Bengkulu, Palembang, Lampung, Jakarta, and Bandung to work on this [9].

Communications were, overall, not impacted as much as might be expected given the severity of the earthquake. This was largely due to the popularity and ubiquity of mobile phones among the residents of Padang; while landlines were entirely disabled by the earthquake, some mobile users did not lose service at all [10]. In the aftermath, PT Excelcomindo Pratama Tbk was providing free mobile phone and wi-fi service in Padang. Their network was mostly undamaged, and they brought in generators to maintain services in the worst affected areas [11]. The fuel supply was also restored very quickly, with 22 gas stations in Padang, eight in Pariaman, and seven in Gunung Kerinci back in service by October 8, 2009 [9]. Additional fuel was brought by truck from Dumai, Siak, Sibolga, and Jambi, all located in neighboring provinces, which helped prevent severe shortages.

By contrast, the disruption to the city's water supply was extensive and long-lasting. Damage to installations belonging to PDAM Padang [Perusahaan Daerah Air Minum Padang = Padang Regional Drinking Water Company], the city's water company, was estimated at 45 billion rupiah resulting from destruction of water mains and reticulation systems, including underground piping originally installed during the Dutch era which was very difficult to access [12]. By the end of October 2009, most of the water plants were fully operational, but much of the reticulation system had to be replaced, and some parts of the city were being supplied by tanker truck. The director of PDAM Padang, Azhar Latif, predicted that it would take six months to fully restore water to the city [13]. Despite this issue being no less a priority than any other and the government's seeking assistance both within Indonesia and from outside the nation (such as the donation of water purifiers from two Dutch companies as reported by Radio Nederland Wereldomroep [14]), little progress was made in restoring service in the following weeks and, indeed, years. Radio Republik Indonesia [15] reported that many residents of Padang still had inadequate city water, with some locations having none at all during the day and a very limited supply at night. Many residents have attempted to adapt by buying tanks to collect rainwater [16], while anecdotal evidence suggests extremely high levels of dissatisfaction but also resignation to the situation.



4 Dengue fever

Dengue became a pressing issue in the aftermath of the earthquake, as the widespread destruction combined with heavy rainfall resulted in many new breeding sites for mosquitoes, while waste water disposal, water services, and toilet and bathing facilities broke down in many parts of the city leading to even more water present in the living environment. Despite warnings from authorities about environmental health risks and suggestions to the public that they take precautions and attempt to clean up their immediate environment, the number of cases of dengue reported in Padang rose dramatically in the days following the quake [17]. At the end of October 2009, the Indonesian Red Cross was planning to fog a number of neighborhoods where high numbers of cases had been reported. Some of these locations had reported more than a hundred new cases of dengue in a period of less than four weeks [18].

By early 2010, various estimates of the extent of the upsurge in cases of dengue were published. One regional hospital, RSUD Dr Rasidin, reported in February 2010 that most of the cases it had seen were in children and that the number had been increasing every month since the earthquake [19]. According to *Republika* [20], the official total number of cases in early 2010 was 1586, of whom 8 had died while 277 had been placed in intensive care. Because of widespread damage to Puskesmas [Pusat Kesehatan Masyarakat = public health centers] and general underreporting, the actual number of cases may be higher. Dengue and other fever diseases are endemic in Padang, and many people do not bother to go to doctors, feeling that little can be done. Those from higher SES levels tend to seek medical treatment for children suspected of having dengue, but adults may treat themselves until or unless their condition becomes critical.

It is worth noting that vector borne disease is a major issue in Padang and West Sumatra at all times, not just in the wake of natural disaster. There are periodic outbreaks and, at times, the media has reported epidemics. Nonetheless, most residents do not fully appreciate the connection between the presence of mosquito vectors and dengue and malaria. Many people view mosquitoes as a nuisance, which they ignore or attempt to kill by spraying bedrooms with Baygon (carbamate propoxur) or using combustible mosquito coils. All houses have multiple mosquito breeding sites inside or in the immediate vicinity as water for bathing and other uses is stored in open tubs filled occasionally from a tap. Ditches containing slow moving or stagnant water line all streets (there is no sewer system), and yards generally contain potted plants that may retain small amounts of water. The local authorities occasionally fog residential areas, but vector control tends to be sporadic and unsystematic.

5 Public response

In the wake of the earthquake, a great deal of public discussion was observed as residents attempted to understand the events they had witnessed. Some of this discussion was religious in nature, with particular focus on God's plans which cannot be comprehended by mortals and the need to accept the unchangeable



will of God [21, 22]. Others focused on the scientific view of the event, attempting to explain the earthquake in terms of geology and offer a method for predicting similar future incidents.

However, even this scientific view of the disaster was formulated by the public and proved relatively resistant to input from actual experts or authorities on geology. Reflecting Padang's increasing connection to global culture and internet sources (at least partially made possible by extensive mobile phone use), these interpretations clearly drew on existing trends and tropes in pseudoscience and scientifically questionable material available on the internet. An excellent example of this is the events surrounding a halo around the sun observed in October 2010, which was widely interpreted as a natural sign of an impending earthquake and tsunami, albeit one without a clearly-defined link or mechanism of causation. Although this phenomenon was easily explainable, likely being the result of the presence of reflective particles in the air after the eruption of Mount Merapi near Yogyakarta, fear of another disaster spread rapidly by word of mouth, leading to large numbers of people leaving work and school and avoiding public places [23].

Some of the discussion of the earthquake took on an almost conspiratorial tone. For example, another story circulated that Fauzi Bahar, the mayor of Padang, had been warned by a panel of Japanese geologists that a cataclysmic earthquake would occur around November 25, 2010. Supposedly, this earthquake would break the island of Sumatra in half, creating a new body of water, in an event similar to the Black Sea deluge theory which is widely available online [24]. This theory suggests that the level of the Black Sea rose abruptly and catastrophically around 5600 BC due to the level of the Mediterranean Sea rising, which caused large amounts of water to pour over a sill in the Bosphorus, leading to dramatic landscape changes on the Black Sea's shores and devastation to communities in the region. It is now generally accepted that the basic scenario probably did occur, but both the extremity and suddenness in the rise of the Black Sea's level is disputed, with some experts suggesting that smaller flows of water may have moved in both directions over a period of centuries. There are many references to the Black Sea deluge theory in pseudo-scientific sites on the internet, claiming it as a historical event that inspired myths of a great flood, as in the stories of Noah, Gilgamesh, or Deukalion. Fears of the supposed November 25th earthquake were amplified and perpetuated by viral media, including anonymous text messages which contained details of the impending disaster, said to be coming on "the date of the full moon when the earth's gravitational field with the moon is aligned with the planet Venus" [25]. This story had a profound impact on the public's mood in Padang, with many people reluctant to travel far from their homes or visit public places like the main marketplace, despite other news sources reporting that the mayor never in fact met with any such experts and was never told anything of this type [26, 27].



6 Discussion

There are four interrelated phenomena that significantly affected the response to the earthquake that occurred in Padang, West Sumatra on September 30, 2009, and that are significant in understanding Indonesian society in general. They are corruption; regional autonomy; technological leapfrogging; and the Indonesian concept of *pembangunan* [development] that became a central feature of planning and policy during the New Order and still features prominently in the government's approach to facilities and services provision.

Corruption, which has been a hot-button issue in Indonesia since the end of the New Order government in 1997, was blamed for both exacerbating the effects of the earthquake and hindering the reconstruction effort. Accusations of corruption in the distribution of aid, both from the government and from other sources, also emerged very quickly and even became the subject of an investigation at the national level [28]. The level of destruction also led to speculation that serious corruption was involved in the construction of schools and public buildings. West Sumatra's then-governor, Gamawan Fauzi, commented that public buildings are supposed to be able to withstand quakes measuring 8 on the Richter scale [29]. However, enforcement of this type of regulation has historically been lax. Additionally, the director of PDAM Padang is on trial for the alleged corruption of 2.5 billion rupiah from the company's funds during the period from 2005 to 2009 [30], the implication being that these funds should have been used to upgrade the water system in the city.

It was hoped that Regional Autonomy would lessen the incidence of corruption and that the resulting decentralization would allow for greater transparency and public involvement in government. While it is perhaps the case that there it is more possible for members of the public to influence their local administration, corruption has, in fact, increased dramatically across Indonesia under Regional Autonomy. What seems to have occurred is a multiplication of existing patterns of misuse and personal enrichment throughout the lower levels of administration. In other words, it has been suggested that a decentralization of government authority has also led to a decentralization of corruption (see [31]). The main difference that has emerged during the period of Regional Autonomy is that the public is more sensitized to the issue of corruption such that the nation has seen a series of highly publicized prosecutions of public officials for abuse of power. One such example is the case of Azhar Latif of PDAM Padang mentioned above. The then governor of West Sumatra, Zainal Bakar, was similarly charged with corrupting 6.4 billion rupiah from the regional budget in 2002, as was a former governor of Aceh, Abdullah Puteh, who was accused of corrupting 30 billion rupiah [32].

Under the rubric of *pembangunan* [development] that became the catch cry of the New Order government, development efforts that would bring Indonesia up to the standard of the west were the main focus. One element of the five year development plans of the New Order was the electrification of much of the nation. The availability of power in rural areas, which in West Sumatra occurred during the late 1970s and early 1980s, changed the nature of people's experience,



especially in that it allowed them to watch television and develop different patterns of work and employment. Electricity was difficult for individuals to develop on an individual basis because of the cost and difficulty of running generators such that this kind of development was not only welcomed but seen to be of enormous benefit. In this context, the contrast with the provision of water is marked. It is easy for improvements to water systems to receive less consideration, publicity, and attention, even from the government, compared to electricity. While water is no less critical to modern life and economic activity and to the successful functioning of a city, electricity is closely associated in the popular imagination with modernity and is the force behind many obvious symbols of progress such as television and the internet. Improvements to water systems require extensive planning and work that is often felt to be less “glamorous” than electrification; and the health and economic improvements bestowed by a functional water system may take years to be fully realized, while the results of a new or upgraded electrical grid can often be literally pointed to.

West Sumatra is a tropical region (the equator passes through the northern part of the province at the town of Bonjol) with very heavy rainfall. While there is a rainy season occurring from about October to February, there is no time of year when it does not rain. It is estimated that average rainfall is almost 400 mm per month with an average 17 days of rain per month [33]. Historically, the public has had ample access to water, albeit often of poor quality, and there are few parts of the province where water availability is a problem. Thus it has been relatively easy for the provincial government during the New Order and now for local governments under Regional Autonomy to overlook the need to upgrade aging water systems because the public has a historical capability to manage its own water. However, West Sumatra, like most of Indonesia, has experienced rapid urbanization and, especially for residents of Padang, is no longer a mostly rural society. As the earthquake demonstrated, a large number of people in cities and towns are now dependent on city water and do not have access to their own wells or sources of surface water as they did several decades ago when city living often resembled urban villages, rather than western-type housing complexes. Despite this, authorities have felt less pressure to repair the water system because many city residents still do have private wells or are prepared to collect rainwater. This willingness to provide their own water is probably partly historical but also an effect of the relative abundance of water for free.

The difference between the provision of electricity and water underscores the problem of technological leapfrogging in West Sumatra and Indonesia in general. National development efforts have often focused on the more visible aspects of technology, rather than those that are important but largely invisible to the public. The result has been a patchwork of innovation ranging from pre-industrial conditions (no sewers and only open ditches for wastewater drainage) to the latest technology of the globalized mainstream (Blackberry service). The earthquake in Padang exposed several significant examples of this phenomenon. The most interesting of these is the situation regarding mobile phones and communication in general. For years, the popularity of mobile phones has been increasing in Padang, partly for the precise reason that landlines have been



notably unreliable and very expensive. The advent of cheap prepaid phones and instantaneous recharge for small amounts has meant that almost everyone, regardless of SES, education or employment status, now has a phone and potential access to the internet. It has been estimated that some 30 million Indonesians use the internet regularly, often on mobile telephones, and most of this use seems to consist of social networking, surfing topics of interest, and e-mail, rather than more serious academic or business purposes [34].

Mobile phone service is provided largely by private companies that have been licensed to operate since the end of the New Order. Prior to this, all telephone service was provided by Telkom Indonesia. At present, the national government is still the majority stockholder in PT Telekom, but it has diversified its services considerably in the last decade in order to compete with private providers, including in the cable TV market. According to PT Telekom itself, it currently has 8.4 million customers using landlines, 15.1 million using wireless telephones, 81.6 million mobile customers [35]. These statistics clearly illustrate the impact of technological leapfrogging in that much greater emphasis (and consumer demand) is placed on the more technologically advanced forms of communication, while more traditional elements of the system, such as telephone cable networks, remain surprisingly underdeveloped. This has been a major problem for offices and institutions in the context of computer use, even though most institutional users have now switched to wireless networking.

The proliferation of technology, largely through the private sector, accelerated greatly following the end of the New Order government. Prior to that, there was a much higher level of government involvement through Badan Usaha Milik Negara [government owned businesses = BUMN], guaranteed monopolies for industries in which high ranking members of the national government or military had an interest, and strict limitation of the private sector [36]. These restrictions began to be eased in the 1990s, but the majority of private providers emerged after 2000 in the context of Regional Autonomy which gave local governments the power to manage many sectors that had been controlled by the central government (education, health, business) and also to make laws and regulations that reflected the local context.

It soon became apparent that experience was lacking in many regions to handle the wide range of services that were now the responsibility of the local government. For the three decades of the New Order, the highly centralized system drew the best educated and capable individuals to Jakarta where there were many more opportunities for career advancement. Local governments were seen as merely implementing orders from the top and were not viewed as milieus where talent was likely to have an outlet. Under Regional Autonomy, however, it was vital for regional governments to attract experienced individuals back to their regions or origin. This gave rise to the phenomenon often referred to in Indonesia as *daerahisme* [regionalism]. *Daerahisme* has led to preferential hiring of individuals who come from the region in question, often to the exclusion of others who are more qualified or experienced but who come from other areas. The basis for this practice seems to be the resurgence in ethnic identity that accompanied Regional Autonomy, perhaps as a response to the imposition of a



national culture across the country by the New Order government that conflicted with traditional practices in many regions. It is also the case that the relatively low level of government at which Regional Autonomy was implemented means that many regions are quite homogenous, as their boundaries coincide with traditional divisions between linguistic/cultural groups. This heightened interest in ethnic identity has also been apparent in the election of local government officials in many regions where local laws have been used to institutionalize religious practices (syariah law) or local customs (see Erb et al. [37]). As a result, there has often been less attention paid to general issues of health and development that the public has come to expect will continue in the same way as before.

In hindsight, the ongoing devastation resulting from the 2009 earthquake seems almost inevitable. The political milieu in Padang makes implementing any type of environmental health or contingency planning extremely difficult. While some changes have been seen in these areas since the end of the New Order government, corruption and the culture of personal enrichment remain, and the political will to enact policies whose benefit is not immediate is still lacking. Combined with the lack of consistency in infrastructure, these problems greatly exacerbated the effects of the earthquake and the environmental health problems that arose from it. The 2009 earthquake in Padang was a perfect storm, a cautionary confluence of factors whose shadow will hang over the city, the province, and the nation for a long time to come.

References

- [1] Antara (2009) "Number of Fatalities in West Sumatra Quake Now 1115," Antara News, October 14, 2009. <http://www.antaranews.com/en/news/1255472809/number-of-fatalities-in-w-sumatra-quake-now-1-115>
- [2] Kristanti, EY (2009a) "Daftar Gedung Bertingkat yang Rusak di Padang," VivaNews, October 1, 2009. http://us.nasional.vivanews.com/news/read/93650-daftar_gedung_bertingkat_yang_rusak_di_padang
- [3] Detik Finance (2009) "Gedung Rusak Berat, Kanti BI Padang Beroperasi Terbatas," October 2, 2009. <http://us.detikfinance.com/read/2009/10/02/140953/1213785/5/gedung-rusak-berat-kantor-bi-padang-beroperasi-terbatas>
- [4] Tempo Interaktif (2009) "Akibat Gempa, Ratusan Warga Padang Terjebak di Gedung Bertingkat," 30 September 2009. <http://www.tempointeraktif.com/hg/nusa/2009/09/30/brk,20090930-200134,id.html>
- [5] Republika (2010) "Baru Sebagian Jumlah Sekolah Rusak Akibat Gempa Padang Direhabilitasi," September 29, 2010. <http://www.republika.co.id/berita/breaking-news/nusantara/10/09/28/136964-baru-sebagian-jumlah-sekolah-rusak-akibat-gempa-padang-direhabilitasi>
- [6] Rinaldi, I (2010) "Padang Punya Gedung Tahan Gempa," Kompas, September 30, 2010. <http://regional.kompas.com/read/2010/09/30/22432777/Padang.Punya.Gedung.Tahan.Gempa>



- [7] PadangTV (2010) "Pelebaran Jembatan Andalas Terkendala Harga Ganti Rugi," PadangTV, December 14, 2010. <http://newspadangtv.blogspot.com/2010/12/pelebaran-jembatan-andalas-terkendala.html>
- [8] Wahyuni (2009) "Pemulihan Listrik di Padang Lebih dari Seminggu," Detik Finance, October 1, 2009. <http://us.detikfinance.com/read/2009/10/01/192705/1213259/4/pemulihan-listrik-di-padang-lebih-dari-seminggu>
- [9] ESDMWatch (2009) "Gempa Padang: Listrik dan BBM Dijanjikan Normal 10 Oktober," October 8, 2009. http://esdmwatch.com/e1/index.php?option=com_content&view=article&id=4554:gempa-padang-listrik-dan-bbm-dijanjikan-normal-10-oktober&catid=57:ketenagalistrikan&itemid=73
- [10] Candra, A (2009) "Gempa Putuskan Jaringan Kabel Telpon di Padang," Kompas, September 30, 2009. <http://regional.kompas.com/read/2009/09/30/19362659/Gempa.Putuskan.Jaringan.Telepon.Kabel.di.Padang>
- [11] Gandhi, GS (2009) "XL Sediakan Telepon Umum Gratis di Padang," Tempo Interaktif, October 7, 2009. <http://www.tempointeraktif.com/hg/bisnis/2009/10/07/brk,20091007-201282,id.html>
- [12] Matanews (2009) "Gempa, PDAM Padang Rugi Rp45 M," November 8, 2009. <http://matanews.com/2009/11/08/gempa-pdam-padang-rugi-rp45-m/>
- [13] TVOne (2009) "Jaringan PDAM Padang Normal 6 Bulan Lagi," October 21, 2009. http://www.tvonenews.tv/www/berita/25975/jaringan_pdam_padang_normal_6_bulan_lagi.html
- [14] Radio Nederland Wereldomroep (2009) "Perusahaan Air Belanda Bantu Padang," October 12, 2009. <http://www.rnw.nl/bahasa-indonesia/article/perusahaan-air-belanda-bantu-padang-0>
- [15] Radio Republik Indonesia (2011) "Pasca Gempa 2009, Debit Air PDAM Kota Padang Minim," February 8, 2011. http://www.rri.co.id/index.php?option=com_content&view=article&id=2204:pasca-gempa-2009-debit-air-pdam-kota-padang-minim&catid=44:index-berita-terbaru
- [16] Tempo Interaktif (2009b) "PDAM Rusak, Korban Gempa Padang Tampung Air Hujan," October 1, 2009. <http://www.tempointeraktif.com/hg/nusa/2009/10/01/brk,20091001-200214,id.html>
- [17] Kompas (2010a) "Penderita Pascagempa Padang Melonjak," February 24, 2010. <http://nasional.kompas.com/read/2010/02/24/03483759/Penderita.Pascagempa.Padang.Melonjak>
- [18] PMI (2009) "Fogging Untuk Lima Wilayah Endemik DBD di Kota Padang," October 27, 2009. <http://pmicabangpadang.blogspot.com/2009/10/fogging-untuk-lima-wilayah-endemik-dbd.html>
- [19] Kompas (2010) "Penderita Pascagempa Padang Melonjak," February 24, 2010. <http://nasional.kompas.com/read/2010/02/24/03483759/Penderita.Pascagempa.Padang.Melonjak>
- [20] Republika (2010) "Daerah Waspada Wabah Demam Berdarah," February 8, 2010. <http://bataviase.co.id/node/87482>
- [21] Antara (2009) "Warga Padang Sebagian Mulai Mengungsi Akibat Gempa," Antara, October 26, 2009. <http://id.news.yahoo.com/antr/20101026/tpl-warga-padang-sebagian-mulai-mengungsi-cc08abe.html>



- [22] Metro TV News (2009) “60 Siswa terjebak di BimBel GAMA,” October 2, 2009. <http://www.youtube.com/watch?v=QbOh0E4RVM4>
- [23] Malau, ILF (2010) “Muncul Cincin Matahari Warga Padang Mengungsi,” Viva News, October 21, 2010. <http://nasional.vivanews.com/news/read/184159-halo-matahari-warga-padang-pilih-mengungsi>
- [24] Yanko-Hombach, V et al (2007) “Controversy Over the Great Flood Hypotheses in the Black Sea in Light of Geological, Paleontological, and Archaeological Evidence,” *Quaternary International*, 167-168: 91-113.
- [25] Fanany, R “Local and Cultural Response to Major Earthquake in Padang, West Sumatra,” paper presented at ‘Living on the Edge,’ the Fourth International Conference of the ISSRNC , University of Western Australia, Perth, December 16-19, 2010.
- [26] Harian Singgalang (2010) “Warga Ditakut-takuti dengan SMS,” November 15, 2010. <http://www.hariansinggalang.co.id/sgl.php?module=detailberita&id=1867>
- [27] Padang Today (2010) “Isu Gempa Semakin Menggelisahkan,” November 25, 2010. <http://www.padang-today.com/?today=news&id=23286>
- [28] Kompas (2009) “Bantuan Korban Gempa Sumatera Barat Diselewangkan,” October 30, 2009. <http://infokorupsi.com/id/korupsi.php?ac=3837&l=bantuan-korban-gempa-sumatera-barat-diselewangkan>
- [29] Kristianti, EY (2009) “Korupsi Perparah Dampak Gempa Padang?,” VivaNews, October 6, 2009. http://us.nasional.vivanews.com/news/read/94821-korupsi_perparah_dampak_gempa_padang_
- [30] Kompas (2010b) “Korupsi Dana representasi, Dirut PDAM Padang Diperiksa kejati Sumbar,” December 16, 2010. <http://infokorupsi.com/id/korupsi.php?ac=8158&l=korupsi-dana-representasi-dirut-pdam-padang-diperiksa-kejati-sumbar>
- [31] Tempo Interaktif (2004) “Desentralisasi Korupsi Melalui Otonomi Daerah,” November 4, 2004. <http://www.tempointeraktif.com/hg/narasi/2004/11/04/nrs,20041104-01,id.html>
- [32] Tempo Interaktif (2005) “Beringin dan Ka’abah di Dua Pengadilan,” February 21, 2005. <http://majalah.tempointeraktif.com/id/arsip/2005/02/21/LU/mbm.20050221.LU105472.id.html>
- [33] Pemerintah Kota Padang (2009) *Banyaknya Hari Hujan dan Curah Hujan di Kota Padang*. <http://www.padang.go.id/v2/content/view/3119/180/>
- [34] Internet World Stats, *Telecommunications in Asia: Special Report*, <http://internetworldstats.com/stats3.htm#asia>
- [35] Telkom Indonesia (2010) Profil Perusahaan. <http://www.telkom.co.id/info-perusahaan/index.html#telkom>
- [36] Tempo Interaktif (1998) “Monopoli, Stop di Sini,” October 20, 1998. <http://majalah.tempointeraktif.com/id/arsip/1998/10/20/HK/mbm.19981020.HK96098.id.html>
- [37] Erb, M, Sulistiyanto, P and Faucher, C, eds *Regionalism in Post-Suharto Indonesia*, Routledge Curzon, London and New York, 2005.



This page intentionally left blank

Section 4

Toxicology analysis

This page intentionally left blank

Breath odor characteristics after drinking alcoholic beverages and health monitoring

T. Oyabu

Kanazawa Seiryō University, Japan

Abstract

Alcohol concentration in the expiration of a subjective person after drinking was examined. Beer, Japanese sake, red wine and *shochu* were adopted as the alcoholic subjects. The sensor outputs after 1 hour and 2 hours of drinking were adopted in the technique. The concentration grade was indicated using three metal-oxide odor sensors. It became obvious that the alcoholic component in the expiration could remain over 3 hours after drinking. Japanese elderly people mostly prefer beer and sake according to a questionnaire survey which was carried out for the aged, and the number of people was 68. The survey was carried out by a mail correspondence method. The number of males was 37 and the female number was 31. Many persons who received the questionnaire preferred beer and sake to whiskey and wine. In this study, the sensor-output characteristic as a function of passage of time after drinking sake was investigated and the suitable amount could be indicated by a developed technique. This means an amount of alcohol from which the subject feels refreshment of mind and body. In the questionnaire, it became obvious that 61% of aged men habitually drunk and 18% of females drunk. Women also preferred wine, plum liquor and *shochu* cocktails. This system was developed to survey the aged life style and identify whether they drunk moderately or not. And it can be also applicable to health monitoring for the elderly person.

Keywords: odor sensor, gas sensor, sensory system, welfare, the aged.

1 Introduction

Various kinds of problems are arising together with aging in Japan as well as other advanced countries. The important thing for the aged is to make a life worth living in quality. It is necessary to draw on our resources first and last to



support the aged life style. Recently, it has been reported that the rate of illnesses are increasing due to drinking too much [1]. It is necessary from the health-care point of view that the aged limit themselves to moderate drinking. Many males drank both sake and beer. Over drinking could trigger off not only dementia and Alzheimer's disease but also hypertension and cerebrovascular accidents [2]. On the contrary, moderate drinking controls those diseases and has a positive effect on diabetes, heart disease, restraining cancer and health care [3]. It should be recommended that the aged keep a lifestyle of moderate drinking and it is also desired for the aged to live a full life [4]. However, the drinking amount has to be limited strictly and it is necessary to construct a system which can survey the drinking amount and the kind of alcohol.

In this study, an odor sensory system was constructed to check the alcohol concentration and its kind in the expiration using metal oxide odor-sensors [5]. Also the concentration and the kind of alcohol in the expiration were examined. As for the results, there were some distinctions in the odor characteristic of the expiration after drinking and the amount of sake could be estimated using the characteristics. The system can raise caution about drinking alcoholic beverages. To control drinking is to maintain one's good health. The system will work for healthcare.

2 Experimental

Three types of metal oxide odor sensors are adopted in this system to examine the odor components and the grade in the expiration of a subjective person. Those three sensors are called S1, S2 and S3. S1 and S2 are made from tin oxide. S3 is made from indium oxide [6]. These three sensors have different sensitivities to various types of reducing gases respectively. S1 and S2 have a high sensitivity to alcoholic gases. Especially S2 has higher sensitivity to the gases. S3 has a high sensitivity to hydrogen gas but has no sensitivity to alcoholic gases. The sensor is suitable to detect the strain and fatigue from a subjective expiration. These sensors were adopted to detect the fatigue after drinking. The three sensors are installed on the inside of the lid of a small glass container of 150ml. The photograph of the three sensors is shown in Fig. 1. The photograph of the container installing the sensors is also shown in Fig. 2. The expiration was introduced into the container through a Teflon tube. The calibre is 2mm. The container also has an exhaust pipe of the same calibre.

The sensor outputs are indicated as a dc voltage of 0 to 5V according to the odor grade and components in the expiration. The output becomes larger as the odor concentration becomes larger. The odor is a kind of reducing gas and the concentration is very low. In the experiment, the base levels of the three sensor outputs are measured for 30 seconds in the first stage. After that, the expiration is introduced into the container via the tube for five seconds. The sensor output increases immediately after the introduction. The output range between the base level and the level of 85 seconds later is called as "sensor output". It takes 120 seconds for each experiment. The time chart is indicated in Fig. 3. The sensor outputs show the characteristics one hour later after drinking sake. The output

characteristic of S3 is low and the one of S2 is higher. The levels are measured every second and the data are input into the data logger through an A-D converter. After that, the data are inputted into a mobile computer. The program is written by C-language.

A questionnaire was carried out to examine the relationship among the alcoholic volume, the kind and seniors' feelings of purpose in their life. The summary of questionnaire indicates that Japanese elderly people mostly prefer beer and sake. It was carried out for the aged and the number of people was 68.



Figure 1: The photograph of the adopted three sensors.



Figure 2: The glass container adopted in this experiment.

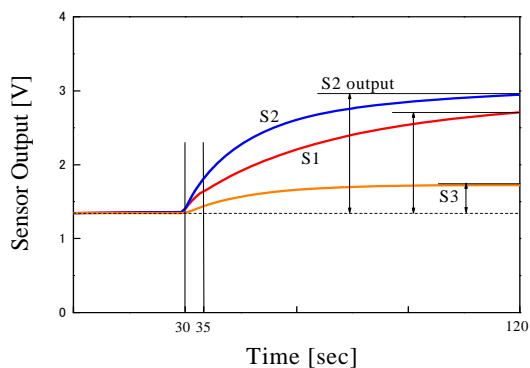


Figure 3: The experimental process for the detection of breath odor.

3 Results

3.1 Questionnaire for drinking

The number of males was 37 and the females were 31. The results for drinking habits are shown in Table 1. The person who drinks any kind of alcohol once or more a week belongs to “drinker”. “Non-drinker” includes people who drink only on social occasions and people who did not drink at all. In this questionnaire, the purpose was to examine the population of the aged drinker and their favorite liquors. When someone drinks two types or more, he or she must indicate the most favorite one. In a questionnaire which we sent out, it became obvious that 61% of elderly men and 18% of elderly women drank habitually. As a result, the number of male drinkers exceeded three times of females. The favorite drinks were beer and sake for male. Females like sake and beer but they also drink other kinds of alcohols such as wine and *shochu*. The results for the favorite drinks are shown in Table 2. The suitable quantity for one’s health was also surveyed and the results are shown in Table 3. The quantity of beer was a

Table 1: Drinking percentage by a questionnaire.

	Male (%)	Female (%)
Drinker	61	18
Non-drinker	39	82

Table 2: The percentage of the aged favorite alcohol.

	Male (%)	Female (%)
Beer	48	37
Sake	43	35
Whiskey	5	1
Other	4	27

Table 3: The suitable amounts of liquors declared by the aged.

	Suitable amount (ml)
Beer	250
Sake	180
Whiskey	90
Red wine	180
Shochu	90



volume of a regular-can of 250ml and the sake was one “go” which meant 180ml. In Japan, the quantity of sake and beer is measured using the unit of “go”. There were no sexual distinctions in the suitable quantity. It is thought that the quantity is fairly restricted according to their earnings and health care.

3.2 Breath odor characteristic for alcohol

Alcohol components are contained in expiration for over three hours after the subject drank liquor. The kind of liquor can be identified with the use of three sensor outputs. It can also check whether the drinking quantity is suitable or not. The system will adopt the amount based on Table 3. The breath odor experiments were carried out while referring to the results of the questionnaire. The subject was a poor drinking male of 55 years old. He was an acquaintance, having deep understanding and consciousness of the problems for the aged. He could operate the system.

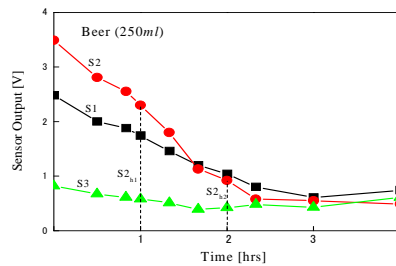


Figure 4: The sensor outputs for the expiration when the subject drank a beer of 250ml.

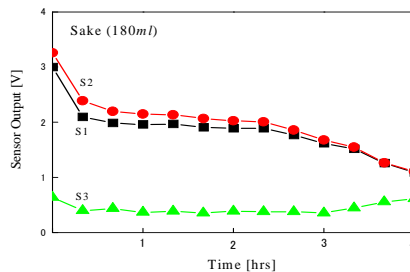


Figure 5: The sensor outputs for the expiration of the subject who drank a sake of 180ml.

The three sensor-output characteristics for expiration after the subject drank a beer of 250ml are indicated in Fig. 4. The horizontal axis means the passage of time and the vertical axis means the sensor output. The figure indicates that the outputs decrease gradually as the time progresses. The characteristic returned to the original level two and half hours later after drinking. The characteristics of

the sensor outputs when the subject drinks sake of 180ml are shown in Fig. 5. The characteristics differ from the ones in Fig. 4 and do not decrease over three hours. It took about four hours until they return to the original levels respectively. It takes a long time before the sensor level returns to the original level when the subject drinks sake. This is a feature of sake. The same feature appeared when the subject drank sake of 135ml but was not apparent in the case of 90ml and under. The result of whiskey is indicated in Fig. 6. The characteristics are very similar with the ones of Fig. 4. The characteristics for red wine of 120ml and *shochu* of 40ml are indicated in Figs. 7 and 8. The characteristics for popular drinks are shown in Figs. 4 to 8. In Japan, there is a tendency that the aged habitually drink sake. Therefore, the characteristics for the amount of sake were examined. The results are shown in Fig. 9. The experiments were carried out for the amounts of 45, 90, 135 and 180ml. In Fig. 9, figure (a) means S1 characteristics, (b) means S2 and (c) means S3. The S3 characteristics are unrelated to the drinking amount of sake. This sensor is used to detect fatigue and stress. In Fig. 9, the outputs at 1 and 2 hours become higher

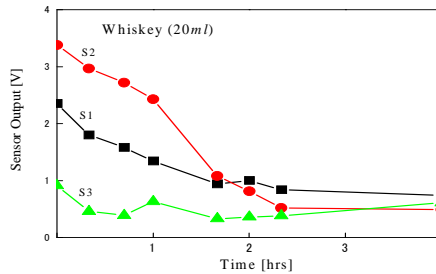


Figure 6: The sensor outputs for the expiration of the subject who drunk a whiskey of 20ml.

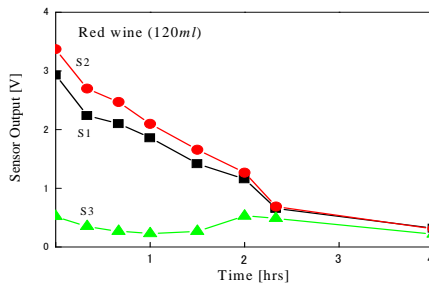


Figure 7: The sensor outputs for the expiration of the subject who drunk a red wine of 120ml.

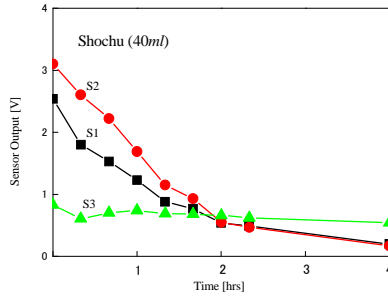


Figure 8: The sensor outputs for the expiration of the subject who drunk a shochu of 40ml. It is a clear distilled liquor.

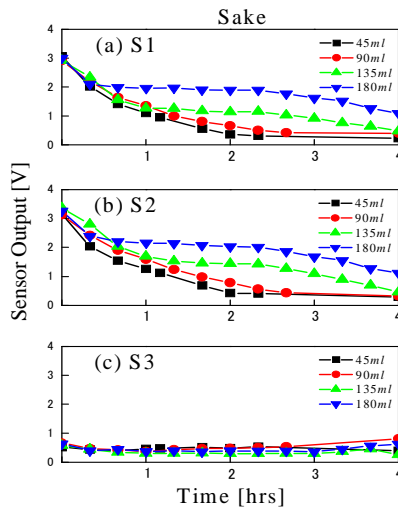


Figure 9: The three sensor outputs changes as a function of the sake quantity. (a) means S1 output, (b) means S2 output and (c) means S3 output.

when the subject drinks larger amounts of sake. There is a possibility to distinguish the drinking amount using their outputs. The S2 level reaches above 3V when the subject drinks alcohol. By examining the S2 level, the system can distinguish whether the subject drunk liquor or not. If the S2 level reaches over 3V, it is considered that the subject drunk liquor. The S2 outputs at 1 hour ($S2_{h1}$) and at 2 hours ($S2_{h2}$) were adopted as parameters to distinguish the kind of liquor.

3.3 Distinction of the alcoholic type and its amount

The distinctive possibility of alcohol type and its amount was already expressed in the section 3.2. In this section, we adopt a new parameter $w = S2_{h1} - S2_{h2}$. The scattering diagram between $S2_{h2}$ and w are exhibited in Fig. 10.



The horizontal axis is $S2_{h2}$ and vertical axis is w . The sensor output for whiskey and beer at one hour are high but remarkably reduce two hours later. In sake experiments for 135 and 180ml, the differences between $S2_{h1}$ and $S2_{h2}$ are small. So it is thought that the alcohol components are not lost in the expiration for three hours after drinking. According to the declaration, the subject felt himself warm when drinking sake of 135 and 180ml, and his thinking faculty slightly deteriorated. He felt relaxed with the drinking of red wine, sake of 45 and 90ml and *shochu* of 40ml. Therefore, it is thought that the suitable quantity range of the subject is $w=0.5$ to 1.25 . The w moves downwards as the sake quantity increases. It is thought that there is a correlation between the parameters

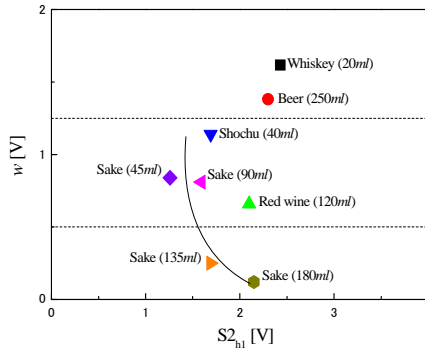


Figure 10: Scattering diagram of $S1_{h1}$ and w for the tested alcohol.

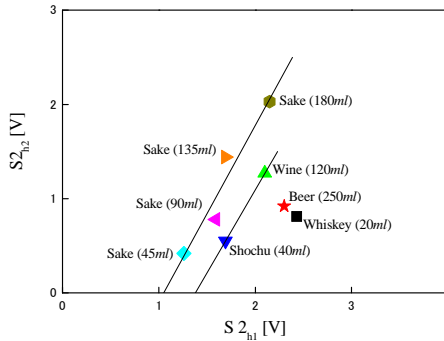


Figure 11: Scattering diagram of $S1_{h1}$ and $S2_{h2}$ for the tested alcohol.

$S2_{h1}$ and $S2_{h2}$ according to the amount of drinking. The scatter diagram of $S2_{h1}$ and $S2_{h2}$ for tested alcohol is shown in Fig. 11. As for the result, the plots for sake are on a straight line and the amount can be identified using this line. The plots for wine and *shochu* are also on a line. The plots for beer and whiskey had a different characteristic. Some plots are examined in addition.

3.4 Daily fluctuation of sensor outputs for human behaviors

The sensors have different responses to the expiration right after eating, drinking and teeth brushing. The breath odor grade becomes larger according to physical condition and illnesses. It is desirable for the aged to have a life worth living and moreover they spend a comfortable and healthy life. The system which can detect those conditions is very effective. In this study, the daily odor-sensor output changes for some human behaviors are examined. The results are shown in Fig. 12. The experiment was carried out on a holiday. The rising hour was 7:40 and bed time was 22:00. But he watched TV in the bed and slept at about 11:30. He played a tennis game from 9:15 to 10:30 and took a hot-spring bath from 18:50 to 19:20. He declared that he had spent a relaxed day. He drunk a sake of 90ml and the sensor responses for the behaviors were measured at 16:00, 17:00 and 18:00 respectively. Fig. 12(a) is for S1, (b) is for S2 and (c) is for S3. The breath odor is somewhat higher at awakening and S3 output is at a higher level than the average of 0.62. The averages for S1 and S2 are 0.99 and 1.13. These averages of S1 and S2 become higher when the subject drinks alcohol. When the subject did not drink, the one of S2 was about 0.8. S3 output is almost

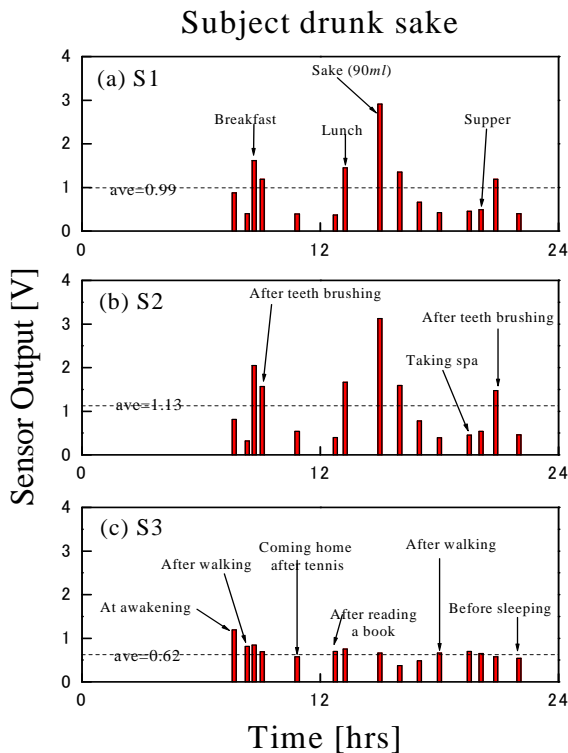


Figure 12: The daily fluctuations of the adopted three sensors for various kinds of human behaviors.

constant through the day, though it is somewhat higher at awakening. We can understand the living style of the aged at a distance by sending the data into the Internet. It is also necessary to establish the identification technique of the style using sensor output characteristics.

4 Conclusion

It has been reported that drinking a moderate amount of alcohol has a positive effect on the health of the aged. The questionnaire on drinking for the aged was sent out for this study. Especially the rate of drinking and their favorite kinds of alcohol were examined. As for the results, the rates were 61% for male and 18% for female. And the favorite liquors were beer and sake. Females, however, like various kinds of drinks, for instance wine, plum liquor and *shochu* cocktails. The expiration was examined after drinking beer, sake, whiskey, red wine and *shochu*. It became obvious that the adopted subject relaxed when he drunk sake of 90ml, red wine of 120ml and *shochu* of 40ml. He declared that his thinking ability fell off slightly when he drank sake of over 135ml, beer of over 250ml and whiskey of over 20ml. These ranges were plotted in Fig. 10 using sensor outputs.

The investigation on the relationship between health care and drinking customs will be studied hereafter. And an odor system, which can survey the life of the aged and support their living style, will be also built. This system can be connected to the Internet. The standardized sensor data which includes the bit size and assignment of data are also considered.

References

- [1] Kishi, R., Kono, S., Omae, K. & Koizumi, A., *NEW Preventive Medicine and Public Health*, Nanko-do: Tokyo, p146, 2006 (in Japanese)
- [2] Yanagawa, H., *Basic Learning of Health Management*, Nanko-do: Tokyo, p114, 2006 (in Japanese)
- [3] Muramatsu, T. & Kajimoto, M., *Public Health*, Kodan-sya: Tokyo, pp.56-57, 2005 (in Japanese)
- [4] Sawada, A., Oyabu, T., Seto, S. & Katsube, T., *Survey system for life styles of the elderly and to identify the consumption of food and drink*, Environmental Health Risk IV, WIT PRESS: Southampton, pp.61-70, 2007
- [5] Oyabu, T., Okada, A., Manninen, O. & Lee, Duck-Dong., *Proposition of a survey device with odor sensors for an elderly person*, Sensors & Actuators B, 96, pp.239-244, 2003.
- [6] Oyabu, T., Okada, A., Manninen, O., Lee, D. D., *Proposition of a survey device with odor sensors for an elderly person*, Sensors & Actuators B, 96, pp.239-244, 2003.



Cell-based bioassay for compounds with prooxidant activity

M. Thomas & L. Benov

*Department of Biochemistry, Faculty of Medicine,
Kuwait University, Kuwait*

Abstract

There is substantial evidence from epidemiological studies that the etiology of many 'modern' diseases is linked in part to environmental pollution. A number of observations suggest that an imbalance in cellular oxidants and antioxidants is a critical underlying factor. Many environmental pollutants, without being redox-active and capable of causing oxidation *in vitro*, are able to shift the oxidant/antioxidant balance of the cells, thus triggering pathological responses. It is difficult to assess the biological impact of mixtures of environmental pollutants because of their complexity. We propose the parallel use of normal (parental) and genetically engineered superoxide dismutase (SOD)-deficient *E. coli* strains, as a tool for the detection of prooxidant-acting environmental pollutants. Doubling time, viability, mutation rate, and induction of antioxidant regulons are used as parameters to assess the pollutants' toxicity and prooxidant action. SOD-deficient *E. coli* is highly sensitive to agents causing oxidative stress directly or indirectly. This sensitivity can be measured and is highly reproducible. Using *E. coli* is advantageous because the organism is well studied, can be stored at low temperatures for a very long time, and can be grown under standard, well-defined conditions. The parallel use of SOD-deficient mutants and SOD-proficient parents permits discrimination between compounds that exert general toxicity and compounds that act as prooxidants *in vivo*. The bioassay was used for fast screening of potentially hazardous chemicals with pro-oxidative action.

Keywords: prooxidant, environmental pollutants, superoxide dismutase-deficient, oxidative stress, bioassay.



1 Introduction

Increasing awareness that the environment is an important determinant of both individual and community health stimulates the search for a better understanding of the mechanisms of action of various environmental pollutants. There is substantial evidence from epidemiological studies that the etiology of a number of 'modern' diseases is linked in part to environmental pollution (Hennig et al. [1]). Many environmental contaminants, especially persistent organic pollutants, are risk factors for chronic diseases because they may exacerbate an underlying disease by altering gene expression patterns. Many mechanisms and signaling pathways associated with the pathology of 'modern' diseases are modulated by environmental pollutants. Pollutants have been found to contribute to the development of a wide range of diseases such as atherosclerosis (Hennig et al. [1], cancer (Brody et al. [2], Rumchev et al. [3]), diabetes (Yoshida et al. [4] Carpenter [5]), renal failure (Bertin and Averbeck [6]), cardiovascular (Prüss-Ustün et al. [7], Bjerregaard [8]), neurological (Grandjean and Landrigan [9]), and liver diseases (Yoshida et al. [4], Carpenter [5]), and can cause immunosuppression (Bertin and Averbeck [6]). Many genes induced in such diseases are oxidative stress-sensitive (Grandjean and Landrigan [9], Calabrese et al. [10], Watkins et al. [11]), suggesting that an imbalance in cellular redox status is a critical underlying factor (Hennig et al. [1]). Many environmental pollutants including heavy metals and various organic contaminants, without being redox active and prooxidative *in vitro*, are able to shift the oxidant/antioxidant balance of the cells, thus triggering pathological responses.

It is difficult to assess the biological impact of environmental pollutants acting as mixtures of individual compounds with different chemical properties and reactivities. More than 15,000 high volume production manmade chemicals are in use and hundreds more are introduced each year. More than half of them have never been tested for human toxicity (Landrigan et al. [12]), because the capacity to produce new chemicals exceeds the ability to test them (Chalupka [13]). This poses a demand for fast, easy and reliable methods for screening of potentially toxic chemicals. Whole-cell biosensors are finding increasing use in the detection of environmental pollution and toxicity (Ron [14]). Here we describe how the parallel use of normal (parental) and mutant, superoxide dismutase (SOD)-deficient strains (where the genes for the cytoplasmic SODs are deleted), can be used as a tool for the detection of prooxidant-acting environmental pollutants. We and others have demonstrated that the SOD-deficient *E. coli* is highly sensitive to various agents contributing directly or indirectly to oxidative stress (Carlioz and Touati [15], Benov et al. [16, 17]). Such sensitivity is manifested as retarded growth, increased mutation rates, induction of specific genes, and loss of viability. These responses can be easily measured and were found to be highly reproducible. Using *E. coli* as a biosensor is advantageous because the organism is well studied, can be stored at low temperatures for a very long time, and can be grown under standard, well-defined conditions. The parallel use of SOD-deficient mutants and SOD-



proficient parents provides a basis for discrimination between compounds that exert general toxicity and compounds that act as prooxidants in vivo.

2 Materials and methods

2.1 Strains

The strains of *E. coli* used were: GC4468 = parental; QC1799 = GC4468 Δ sodA3 Δ sodB-kan Touati et al. [18]. These strains were prepared by D. Touati, Institute Jacques Monod, CNRS, University Paris, France. To ensure that the responses are not a consequence of the genetic background, the following strains were used in parallel : AB1157 = parental; JI132 = AB1157 plus (sodA::MmdPR13) 25 (sodB-kan) 1- Δ 2 Imlay et al. [19]; These strains were provided by J. Imlay, University of Illinois, Champaign-Urbana, Urbana, IL.

2.2 Growth media

Luria-Bertoni (LB) medium contained 10 g Bacto-tryptone, 5 g yeast extract, and 10 g NaCl per liter and was adjusted to pH 7.0 with \sim 1.5 g of K_2HPO_4 . M9CA medium consisted of minimal A salts (6 g Na_2HPO_4 , 3 g K_2HPO_4 , 1 g NH_4Cl , and 0.5 g NaCl per liter (Maniatis et al. [20]); $MgSO_4$ and $CaSO_4$ were autoclaved separately and added to the cooled A salts to a final concentration of 20 mM and 100 μ M respectively), 0.2% casamino acids, 0.2% glucose, 3 mg pantothenate and 5 mg of thiamine per liter. Minimal medium consisted of minimal A salts supplemented with 0.2% glucose.

Starter cultures were grown overnight at 37°C, with shaking in air, in LB medium containing 50 μ g/ml kanamycin and/or 30 μ g/ml chloramphenicol where indicated. For monitoring growth, the overnight cultures were diluted 200 fold into M9CA medium not containing antibiotics. Freshly prepared filter-sterilized solutions of chemicals to be tested were added and cultures were grown at 37°C, with shaking in air. Respective controls not containing additives or containing solvents only were run in parallel. Growth was followed turbidimetrically at 600 nm. For survival and MTT assays M9CA cultures were grown to $A_{600nm} = 0.5 - 0.8$ and the cells were resuspended to the same density in minimal medium.

2.3 MTT assay

MTT (3-(4,5-dimethylthiazol-2-yl)-2,5-diphenyltetrazolium bromide) assay was performed using a modification of the original procedure of Mosmann [21]. Hundred μ l aliquots of the cell suspensions were transferred into a 96-well plate, graded concentrations of the tested chemicals or progressively diluted samples were added and the plates were incubated for 1 h at 37°C on a shaker at 200 rpm. After the completion of the incubation 10 μ l of MTT reagent (5 mg/ml) were added to all wells and the plates were incubated for 30 min at 37°C on a shaker. After 30 min, 100 μ l of 10% SDS in 10 mM HCl were added and plates were



incubated for 1 h at room temperature. The solubilized product was assayed at 570 nm, and the absorbance at 700 nm was used as a background value.

2.4 Mutagenesis

Mutagenesis was monitored by assaying the frequency of thymine-negative (Thy^-) mutants. Thy^- mutants are resistant to the drug trimethoprim and can be selected from a Thy^+ population (Miller [22]). The assay was performed as described by Farr et al. [23]. For counting Thy^- mutants, aliquots of the cultures were plated directly on LB plates containing thymine (50 $\mu\text{g}/\text{ml}$) and trimethoprim (15 $\mu\text{g}/\text{ml}$). For enumeration of cells, cultures were suitably diluted and plated on LB plates containing thymine, but not trimethoprim.

Where indicated, exogenous metabolic activation was performed as described by Ames et al. [24] Hydrophobic organic compounds were dissolved in DMSO. All samples were tested at different concentrations in triplicate, both with and without microsomal activation. The S9 mixture contained the hepatic S9 fraction (1 mg/ml of microsomal protein), and mid-log bacterial culture in M9CA medium.

All experiments were repeated 3–5 times with three replicates. Student t-test was used to determine statistical significance.

3 Results and discussion

E. coli contains three distinct SODs, CuZnSOD, FeSOD and MnSOD Touati [25]. Genes coding for MnSOD are designated as *sodA*, for FeSOD – *sodB*, and for CuZnSOD – *sodC* (Touati [26]). In *E. coli* both FeSOD and MnSOD are cytoplasmic, while the CuZnSOD is periplasmic (Benov et al. [27]). The *sodA sodB* strains are referred to as SOD-deficient even though they retain the periplasmic CuZnSOD, which is expressed in stationary phase and is practically not present during exponential growth (Benov and Fridovich [28]).

The *sodA sodB* mutants grow as well as the SOD-proficient parents anaerobically, but exhibit poor aerobic growth (Al-Maghrebi and Benov [29]), auxotrophy for certain amino acids (Benov et al. [30], Benov and Fridovich [31]), increased aerobic mutation rates (Farr et al. [23], Benov and Fridovich [32]), and hypersensitivity to H_2O_2 and redox-cycling agents (Carlioz and Touati [15]).

The hypersensitivity of the SOD-deficient mutants to compounds causing oxidative stress suggested that those mutants could be used as sensors for potentially prooxidant environmental contaminants. To test this idea, parental and SOD mutants were subjected to treatment with various potentially toxic chemicals, including known prooxidants, and physiological responses such as changes in growth rate, decrease in viability, acceleration of mutation rate, and overall changes in metabolic rate were determined.



3.1 Effect of toxic compounds on *E. coli* growth and viability

Growth of parental and SOD-deficient strains was followed in the presence of chemicals with prooxidant activity and compared to the growth with chemicals which are known to be toxic, but without known prooxidant activity. Fig. 1 A shows growth curves of SOD-proficient and SOD-deficient cultures and the effect of Cd^{2+} . The effect of graded concentrations of CdCl_2 on the growth of parental and mutant cultures is shown in fig. 1 B.

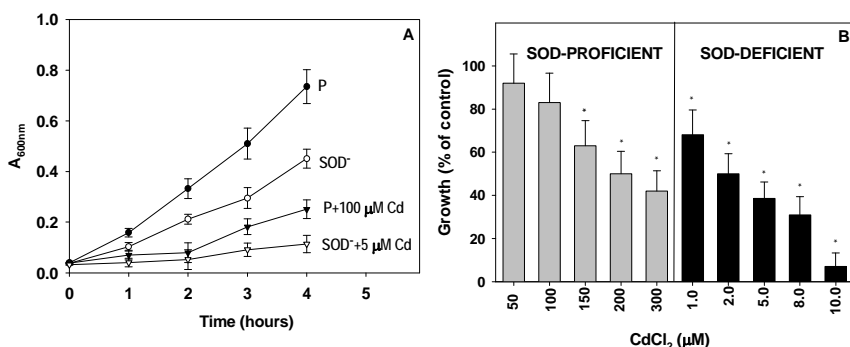


Figure 1: Effect of CdCl_2 on proliferation of SOD-proficient and SOD-deficient strains in M9CA medium. Panel A, growth curves; Panel B, growth rates. Growth was monitored as absorbance at 600 nm. The growth rate of control cultures (without toxic additions) was calculated as 100%. Values significantly different from control ($p < 0.05$) are indicated with a (*). Values are means of triplicates \pm SE and are representative of at least three independent experiments.

Fig. 2 illustrates the higher sensitivity of the SOD-deficient mutants to some heavy metals (Hg, Cd), paraquat (methyl viologen), phenazine methosulfate (PMS), peroxides, short-chain sugars, dicarbonyls, and even to ascorbate, which is considered an antioxidant.

No differences between parental and *sodAsodB* mutants were observed with respect to sensitivity towards pyridine (fig. 2 A), and similar effect was observed for arsenate, dimethylamine, formaldehyde, and chlorhexidine digluconate (not shown). Other compounds, considered potentially toxic (acrylamide, nitrate) had no effect at the tested concentrations.

The hypersensitivity of the *sodAsodB* cells towards heavy metals such as Cd and Hg has its explanation. Even though those metals are not redox active and cannot act as prooxidants *in vitro*, *in vivo* Cd was shown to increase the production of superoxide by interfering with the respiratory electron transport chain (Belyaeva et al. [33], Wang et al. [34]), while Hg being a sulfhydryl poison was shown to indirectly increase ROS production (Kovacic and Somanathan [35]) and to induce the $\text{O}_2^{\cdot-}$ -sensing *soxRS* regulon in *E. coli* (Fuentes and Amábile-Cuevas [36]). The prooxidant effect of otherwise considered antioxidants, for example ascorbate and cysteine, can be explained by coupled

redox-cycling with transition metals (Park and Imlay [37]), and that of paraquat and PMS, to intracellular redox-cycling, producing superoxide (Hassan and Fridovich [38]). Fig. 2 demonstrates that compared to the SOD-proficient parent, less *sodAsodB* cells survived in the presence of common metabolites such as triose-phosphates. The reason lies in O_2^- -dependent oxidation to α,β -dicarbonyl compounds (Benov et al. [16], Benov and Fridovich [17]), and their lower rate of elimination by the SOD-deficient cells (Okado-Matsumoto and Fridovich [39]).

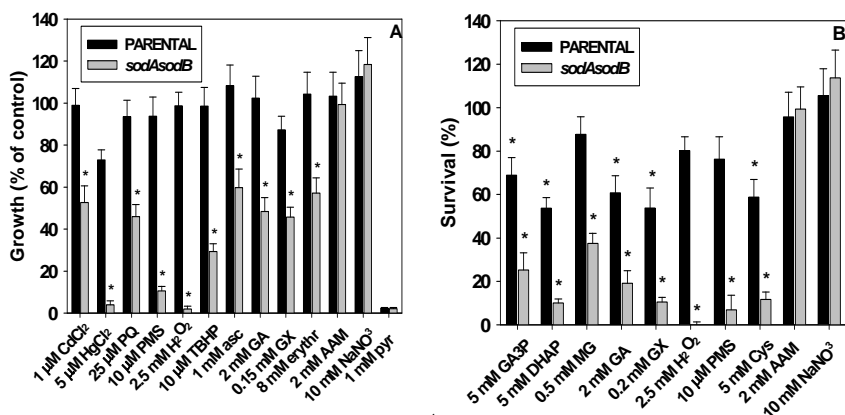


Figure 2: Effect of toxic compounds on growth (Panel A) and viability (Panel B) of parental and *sodAsodB* strains. To compensate for the volume added by the tested sample, an equal volume of the carrier was added to control cultures. Values significantly different from control ($p < 0.05$) are indicated with a (*). Means of triplicates \pm SE are shown and are representative of at least three independent experiments. PQ - paraquat; PMS - phenazine methosulfate; TBHP - tert-Butyl hydroperoxide; Asc - sodium ascorbate; GA - glycolaldehyde; GX - glyoxal; Erythr - erythrose; AAM - acrylamide; Pyr - pyridine; $NaNO_3$ - sodium nitrate; GA3P - glyceraldehyde-3-phosphate; DHAP - dihydroxyacetone phosphate; MG - methylglyoxal; Cys - cysteine.

3.2 MTT reduction test

Results shown above demonstrate that *E. coli* growth rate and viability can be used as relatively easily measurable parameters for assessment of toxicity and prooxidant effect. Growth, however, needs to be followed for relatively long time intervals and viability assessment requires plating and enumeration of colonies, which is time- and work-demanding. Methods based on reduction of tetrazolium salts to purplish-blue formazan products have become some of the most widely used tools for assessing cell viability and proliferation in cell biology. Since production of colored formazan depends on cell metabolism

(Berridge et al. [40]), the assay has been widely used for measuring the metabolic activity of cells ranging from mammalian to microbial. It has been proved suitable for assessing microbial cell proliferation (Tsukatani et al. [41]) and viability (Tsukatani et al. [42]), as well as bactericidal activity (Stevens et al. [43], Stevens and Olsen [44]). A comparison between the effects of prooxidant and non-prooxidant toxic compounds on cell proliferation and viability with MTT test, performed in a 96-well plate, demonstrated that MTT reduction can be used as a method for fast initial screening of a big number of samples (fig. 3).

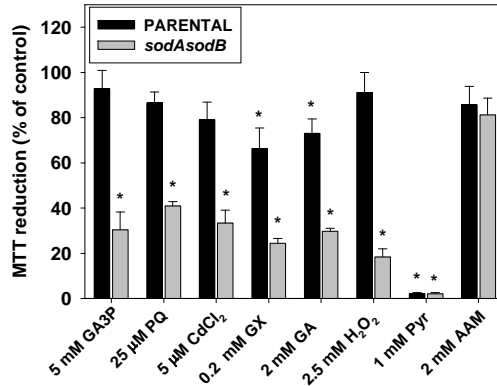


Figure 3: MTT reduction test. GA3P – glyderaldehyde-3-phosphate; PQ – paraquat; GX – glyoxal; GA – glycolaldehyde; Pyr – pyridine; AAM – acrylamide.

3.3 Mutagenesis

It is known that in aerobic environment, the *sodAsodB E. coli* cells mutate faster than the parental cells, which has been attributed to ROS-mediated DNA damage. This finding implies that compounds, which increase ROS production, i.e. act as prooxidants either directly or indirectly, would eventually further increase mutation rates, and SOD-deficient cells would be more sensitive. This is illustrated by the bigger number of mutants in SOD-deficient cultures treated with short-chain aldehydes (fig. 4).

Activation by rat hepatic S9 fraction, as described in the Ames' mutagenicity test, has been found to suppress the mutagenic effect of short-chain aldehydes, but potentiated the mutagenic effect of known mutagens such as benzpyrene (not shown). The assay was tested with samples of sea water, collected from different parts of Kuwait's coastal area. Fig. 5 shows increased mutagenicity of the SOD-deficient cells by S9-activated seawater samples (SW2 and SW3) collected from areas polluted as a result of a spill of sewage water from a malfunctioning sewage-treatment plant.

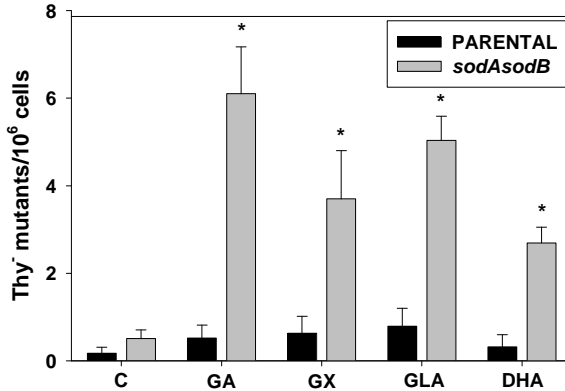


Figure 4: Prooxidant-acting compounds are much stronger mutagens for the SOD-deficient than for the parental strain. Overnight LB cultures of SOD-proficient and SOD-deficient strains were diluted 200 fold in M9CA medium and were grown aerobically at 37°C and 200 rpm to a density of $A_{600nm} \sim 0.5$. At this point compounds to be tested were added and the cells were kept for 2 h on the shaker. After the incubation, the cells were diluted and plated on LB plates containing thymine for assessing cell number or aliquots were plated without dilution on LB plates containing thymine and trimethoprim for counting Thy⁻ mutants. Bars represent mean \pm S.E.M. (n=3). GA – glycolaldehyde; GX – glyoxal; GLA – glyceraldehyde; DHA – dihydroxyacetone.

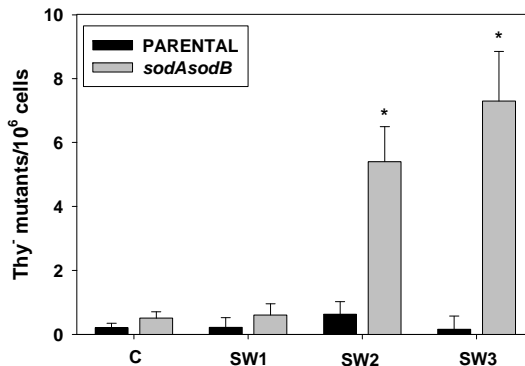


Figure 5: Mutagenicity of seawater samples collected from areas polluted with raw sewage (SW2 and SW3). Non-polluted seawater (SW1) was tested for comparison. Mutagenicity test was performed after activation by rat hepatic S9 fraction.

4 Conclusions

In conclusion, the data presented here indicate that the parallel use of SOD-proficient and SOD-deficient *E. coli* strains is a promising cell-based system for detection of environmental pollutants with potentially prooxidant action. Detailed studies with a bigger number of chemicals will be needed in order to assess the practical usefulness and the limitations of the proposed biosensor.

Acknowledgements

This work was supported by Kuwait University grants MB 03/07 and Research Core Facility grants GM01/01 and GM01/05.

References

- [1] Hennig, B., Oesterling, E. & Toborek, M., Environmental toxicity, nutrition, and gene interactions in the development of atherosclerosis. *Nutrition Metabolism & Cardiovascular Diseases*, **17**, pp. 162-169, 2007.
- [2] Brody, J.G., Rudel, R.A., Michels, K.B., Moysich, K.B., Bernstein, L., Attfield, K.R. & Gray, S., Environmental pollutants, diet, physical activity, body size, and breast cancer: where do we stand in research to identify opportunities for prevention? *Cancer*, **109**, pp. 2627-2634, 2007.
- [3] Rumchev, K., Brown, H. & Spickett, J., Volatile organic compounds: do they present a risk to our health? *Reviews on Environmental Health*, **22**, pp. 39-55, 2007.
- [4] Yoshida, T., Yamauchi, H. & Fan Sun, G., Chronic health effects in people exposed to arsenic via the drinking water: dose-response relationships in review. *Toxicology & Applied Pharmacology*, **198**, pp. 243-52, 2004.
- [5] Carpenter, D.O., Polychlorinated biphenyls (PCBs): routes of exposure and effects on human health. *Reviews on Environmental Health*, **21**, pp. 1-23, 2006.
- [6] Bertin, G. & Averbeck, D., Cadmium: cellular effects, modifications of biomolecules, modulation of DNA repair and genotoxic consequences (a review). *Biochimie*, **88**, pp. 1549-1559, 2006.
- [7] Prüss-Ustün, A., Vickers, C., Haefliger, P. & Bertollini, R., Knowns and unknowns on burden of disease due to chemicals: A systematic review. *Environmental Health: A Global Access Science Source*, **10**, pp. 1-15, art. no. 9, 2011.
- [8] Bjerregaard, P., Cardiovascular disease and environmental pollutants: the Arctic aspect. *Arctic Medical Research*, **1**, pp. 25-31, 1996.
- [9] Grandjean, P. & Landrigan, P.J., Developmental neurotoxicity of industrial chemicals. *Lancet*, **368**, pp. 2167-2178, 2006.
- [10] Calabrese, V., Guagliano, E., Sapienza, M., Mancuso, C., Butterfield, D.A. & Stella, A.M., Redox regulation of cellular stress response in neurodegenerative disorders. *Italian Journal of Biochemistry*, **55**, pp. 263-282, 2006.



- [11] Watkins, B.A., Hannon, K., Ferruzzi, M. & Li, Y., Dietary PUFA and flavonoids as deterrents for environmental pollutants. *Journal of Nutritional Biochemistry*, **18**, pp. 196-205, 2007.
- [12] Landrigan, P.J., Carlson, J.E., Bearer, C.F., Cranmer, J.S., Bullard, R.D., Etzel, R.A., Groopman, J., McLachlan, J.A., Perera, F.P., Reigart, J.R., Robison, L., Schell, L. & Suk, W.A., Children's health and the environment: a new agenda for prevention research. *Environmental Health Perspectives*, **3**, pp. 787-794, 1998.
- [13] Chalupka, S.M., Essentials of environmental health. Enhancing your occupational health nursing practice (Part I). *AAOHN Journal*, **49**, pp. 137-153, 2001.
- [14] Ron, E.Z., Biosensing environmental pollution. *Current Opinion in Biotechnology*, **18**, pp. 252-256, 2007.
- [15] Carlioz, A. & Touati, D., Isolation of superoxide dismutase mutants in *Escherichia coli* is superoxide dismutase necessary for aerobic life? *EMBO Journal*, **5**, pp. 623-630, 1986.
- [16] Benov, L., Beema, A.F. & Sequeira, F., Triosephosphates are toxic to superoxide dismutase-deficient *Escherichia coli*. *Biochimica et Biophysica Acta*, **1622**, pp. 128-132, 2003.
- [17] Benov, L. & Fridovich, I., Superoxide dependence of the toxicity of short chain sugars. *Journal of Biological Chemistry*, **273**, pp. 25741-25744, 1998.
- [18] Touati, D., Jacques, M., Tardat, B., Bouchard, L. & Despied, S., Lethal oxidative damage and mutagenesis are generated by iron in Δfur mutants of *Escherichia coli*: Protective role of superoxide dismutase. *Journal of Bacteriology*, **177**, pp. 2305-2314, 1995.
- [19] Imlay, J.A. & Fridovich, I., Isolation and genetic analysis of a mutation that suppresses the auxotrophies of superoxide dismutase-deficient *Escherichia coli* K12. *Molecular and General Genetics*, **228**, pp. 410-416, 1991.
- [20] Maniatis, T., Fritsch, E.F. & Sambrook, J., *Molecular Cloning: A Laboratory Manual*, Cold Spring Harbor Laboratory, Cold Spring Harbor, NY, 1982.
- [21] Mosmann, T., Rapid colorimetric assay for cellular growth and survival: Application to proliferation and cytotoxicity assays. *Journal of Immunological Methods*, **65**, pp. 55-63, 1983.
- [22] Miller, J.H., *Experiments in molecular genetics*, Cold Spring Harbor Laboratory 1972.
- [23] Farr, S.B., D'Ari, R. & Touati, D., Oxygen-dependent mutagenesis in *Escherichia coli* lacking superoxide dismutase. *Proceedings of the National Academy of Sciences of the United States of America*, **83**, pp. 8268-8272, 1986.
- [24] Ames, B.N., McCann, J. & Yamasaki, E., Methods for detecting carcinogens and mutagens with the *Salmonella* mammalian-microsome mutagenicity test. *Mutation Research*, **31**, pp. 347-364, 1975.
- [25] Touati, D., Molecular genetics of superoxide dismutases. *Free Radical Biology and Medicine*, **5**, pp. 393-402, 1988.



- [26] Touati, D., The molecular genetics of superoxide dismutase in E. Coli. An approach to understanding the biological role and regulation of sods in relation to other elements of the defence system against oxygen toxicity. *Free Radical Research Communications*, **8**, pp. 1-9, 1989.
- [27] Benov, L., Chang, L.Y., Day, B. & Fridovich, I., Copper, zinc superoxide dismutase in Escherichia coli periplasmic localization. *Archives of Biochemistry and Biophysics*, **319**, pp. 508-511, 1995.
- [28] Benov, L.T. & Fridovich, I., Escherichia coli expresses a copper- and zinc-containing superoxide dismutase. *Journal of Biological Chemistry*, **269**, pp. 25310-25314, 1994.
- [29] Al-Maghrebi, M.A. & Benov, L.T., Polyphosphate accumulation and oxidative DNA damage in superoxide dismutase-deficient Escherichia coli. *Free Radical Biology and Medicine*, **31**, pp. 1352-1359, 2001.
- [30] Benov, L., Kredich, N.M. & Fridovich, I., The mechanism of the auxotrophy for sulfur-containing amino acids imposed upon Escherichia coli by superoxide. *Journal of Biological Chemistry*, **271**, pp. 21037-21040, 1996.
- [31] Benov, L. & Fridovich, I., Why superoxide imposes an aromatic amino acid auxotrophy on Escherichia coli: The transketolase connection. *Journal of Biological Chemistry*, **274**, pp. 4202-4206, 1999.
- [32] Benov, L. & Fridovich, I., The rate of adaptive mutagenesis in Escherichia coli is enhanced by oxygen (superoxide). *Mutation Research*, **357**, pp. 231-236, 1996.
- [33] Belyaeva, E.A., Dymkowska, D., Wieckowski, M.R. & Wojtczak, L., Reactive oxygen species produced by the mitochondrial respiratory chain are involved in Cd²⁺-induced injury of rat ascites hepatoma AS-30D cells. *Biochimica et Biophysica Acta - Bioenergetics*, **1757**, pp. 1568-1574, 2006.
- [34] Wang, Y., Fang, J., Leonard, S.S. & Rao, K.M.K., Cadmium inhibits the electron transfer chain and induces reactive oxygen species. *Free Radical Biology and Medicine*, **36**, pp. 1434-1443, 2004.
- [35] Kovacic, P. & Somanathan, R., Unifying mechanism for metals in toxicity, carcinogenicity and therapeutic action: Integrated approach involving electron transfer, oxidative stress, antioxidants, cell signaling and receptors. *Journal of Receptors and Signal Transduction*, **30**, pp. 51-60, 2010.
- [36] Fuentes, A.M. & Amábile-Cuevas, C.F., Mercury induces multiple antibiotic resistance in Escherichia coli through activation of SoxR, a redox-sensing regulatory protein. *FEMS Microbiology Letters*, **154**, pp. 385-388, 1997.
- [37] Park, S. & Imlay, J.A., High levels of intracellular cysteine promote oxidative DNA damage by driving the Fenton reaction. *Journal of Bacteriology*, **185**, pp. 1942-1950, 2003.
- [38] Hassan, H.M. & Fridovich, I., Intracellular production of superoxide radical and of hydrogen peroxide by redox active compounds. *Archives of Biochemistry and Biophysics*, **196**, pp. 385-395, 1979.



- [39] Okado-Matsumoto, A. & Fridovich, I., The role of α,β -dicarbonyl compounds in the toxicity of short chain sugars. *Journal of Biological Chemistry*, **275**, pp. 34853-34857, 2000.
- [40] Berridge, M.V., Herst, P.M. & Tan, A.S., Tetrazolium dyes as tools in cell biology: New insights into their cellular reduction. *Biotechnology Annual Review* **11 (SUPPL.)**, pp. 127-152, 2005.
- [41] Tsukatani, T., Suenaga, H., Higuchi, T., Akao, T., Ishiyama, M., Ezoe, K. & Matsumoto, K., Colorimetric cell proliferation assay for microorganisms in microtiter plate using water-soluble tetrazolium salts. *Journal of Microbiological Methods*, **75**, pp. 109-116, 2008.
- [42] Tsukatani, T., Higuchi, T., Suenaga, H., Akao, T., Ishiyama, M., Ezoe, T. & Matsumoto, K., Colorimetric microbial viability assay based on reduction of water-soluble tetrazolium salts for antimicrobial susceptibility testing and screening of antimicrobial substances. *Analytical Biochemistry*, **393**, pp. 117-125, 2009.
- [43] Stevens, M.G., Kehrl Jr, M.E. & Canning, P.C., A colorimetric assay for quantitating bovine neutrophil bactericidal activity. *Veterinary Immunology and Immunopathology*, **28**, pp. 45-56, 1991.
- [44] Stevens, M.G. & Olsen, S.C., Comparative analysis of using MTT and XTT in colorimetric assays for quantitating bovine neutrophil bactericidal activity. *Journal of Immunological Methods*, **157**, pp. 225-231, 1993.



Synthetic musks fragrances in the aquatic environment: *in vitro* toxicological studies of their biotransformation and potential negative effects

S. Focardi, C. Della Torre, M. Monti, T. Biagini & I. Corsi
*Department of Environmental Sciences "G. Sarfatti",
University of Siena, Italy*

Abstract

The aim of the present study was to investigate the interaction of musk xylene (MX) and Tonalide (AHTN) with CYP1A by looking at gene transcription (*cyp1a*) and EROD activity in *Poeciliopsis lucida* hepatoma cell line (PLHC-1). MX and AHTN were studied individually and combined with classical inducer of CYP1A as B(a)P and PCB126. After 24h of exposure a different cytotoxicity has been observed with an LC₅₀ of 35.76µM for AHTN and LC₅₀ 123.6µM for MX. After 6h of exposure to MX, a dose-dependent reduction of *cyp1a* was observed respect to controls. At 24h, the same pattern was observed but with slight induction at the lowest concentration (2µM) and a dose-dependent reduction at the higher concentrations. Co-exposure to MX with B(a)P did not alter *cyp1a* transcription levels compared to the inducer alone. After 6h AHTN determined a slight induction of *cyp1a* transcription reaching maximum induction of 2.3 folds respect to controls at 2µM. No modulation of *cyp1a* transcription was observed after 24h. Co-exposure to AHTN with B(a)P and PCB126 at 6h determined a 55% reduction of *cyp1a* transcription respect to inducers alone which recovered at 24h. At 24h, MX caused a dose-dependent decrease of EROD activity. No modulation of EROD activity was detectable at 6h and 24h of exposure to AHTN. Co-exposure with both MX and AHTN did not alter EROD activity induced by B(a)P and PCB126. Results suggest different toxicological properties of MX and AHTN toward CYP1A in PLHC-1. MX reduced *cyp1a* basal transcription but did not alter *cyp1a* induction by B(a)P and PCB126. This suggests that MX cellular pathway is not mediated by AhR. On



the contrary AHTN did not alter significantly *cyp1a* basal levels but decreased *cyp1a* induction by B(a)P and PCB126. A potential role of AHTN as competitive antagonist of AhR could thus be hypothesized.

Keywords: synthetic musks, PLHC-1, CYP1A.

1 Introduction

In recent years, emerging organic contaminants known as pharmaceutical and personal-care products (PPCPs) have increasingly been released into the environment. PPCPs include many substances with a broad spectrum of uses, including musk fragrances [1]. They are divided into two categories, nitro- and polycyclic musks and are commonly added to detergents, perfumes, soaps and cosmetics. Nitromusks, as musk xylene (1-*tert*-butyl-3,5-dimethyl-2,4,6-trinitrobenzene, MX) are synthetic di- and tri-nitrobenzene derivatives, while polycyclic musks such as Tonalide (7-acetyl-1,1,3,4,4,6-hexamethyl-tetrahydroxaphthalene, AHTN) are indane and tetraline derivatives highly substituted by methyl groups.

Considered widespread environmental contaminants, MX and AHTN have been detected in the atmosphere, water, sludge and sediments. Levels in surface waters are in the ng- μ g/L range for both musks [1–5] so that exposure of aquatic biota is mainly related to waste water treatment plants.

The lipophilic nature of both compounds (log Kow MX = 4.90; log Kow AHTN = 5.70) suggests high bioaccumulation potential for aquatic biota, leading to levels in the μ g-mg/kg lipid basis range [4, 6].

With regards to their toxicity to aquatic species, MX and AHTN inhibits multixenobiotic resistance in mussel (*Mytilus californianus*) with IC₅₀ of 0.97 μ M for MX and IC₅₀ of 2.05 μ M for AHTN [7, 8]. MX has been reported to be embryotoxic in zebrafish (*Danio rerio*) [9] and AHTN induce alteration of hearth rate at 33 μ M [9]. Some studies describe the potential estrogenic/anti-estrogenic effects of MX and its metabolites as well as AHTN. MX metabolites 2-amino-MX and 4-amino-MX seem to bind oestrogen receptors (ER) competitively *in vitro* in rainbow trout (*Onchorynkus mykiss*) and in the South African clawed frog (*Xenopus laevis*) [10]. In zebrafish, antiestrogenic effects have been reported for AHTN mainly mediated by ER γ [11]. An induction of ER α and vitellogenin expression has been reported in males of *Oryzias latipes* at 500 μ g/L of AHTN [12]. Despite acute and chronic effects have been observed at doses exceeding environmental concentrations, the persistence in the aquatic environment and bioaccumulation by biota, suggest a potential concern for aquatic biota due to their presence in the aquatic environment.

The toxicological pathways of synthetic musks, in terms for instance of detoxification, are poorly understood in mammals and barely documented in aquatic organisms. Only a species-specific metabolization has been suggested for aquatic biota [4].

In this view, studies focusing on toxicological mechanisms of action of both compounds in fish species are needed, with particular regard to the interaction with major detoxification systems, such as cytochrome P450 responsible for



metabolism/detoxification of both endogenous and exogenous compounds. CYP1A in particular is a major enzyme subfamily involved in phase I of the detoxification response to various xenobiotics, well characterised in fish species [13].

The involvement of CYP450 in musks metabolism is supposed to be responsible for the species-specific accumulation of these compounds. In mammalian species, MX affects various CYPs, such as CYP1A1, CYP1A2, CYP2B and CYP3A. Rats exposed to high doses of MX (0.1 mM) show strong induction of CYP1A2, presumably by post-transcriptional induction [14]. Other studies in mice and rats showed that MX (up to 200 mg/kg/day) caused phenobarbital-like pretranslational induction of CYP2B mRNA and protein levels. Significant inhibition of the related pentoxyresorufin-O-deethylase (PROD) activity, probably related to MX amino metabolites, and no effects on CYP1A1 have also been reported [15, 16]. Long-term exposure of adult Long Evans rats to low doses of MX (0.7-0.8 mg/kg/day) showed increased CYP1A and CYP2B proteins and related resorufin activities [17], similar to those observed at higher doses of acute exposure. On the contrary AHTN resulted to be hepatotoxic, without altering CYPs activities [18].

The only study on fish indicated that among musks, MX was the strongest inhibitor of CYP1A activity *in vitro* ($IC_{50} 37 \pm 7 \mu M$) while AHTN determined a 30% inhibition [19]. Hence a different mechanism of interaction of MX and AHTN with CYP1A is likely.

The aim of the present study is to investigate the interaction of MX and AHTN with CYP1A by looking at gene transcription (*cyp1a*) and EROD activity in *Poeciliopsis lucida* hepatoma cell line (PLHC-1). PLHC-1 are commonly used in ecotoxicology to study toxicological pathways of chemicals, including PPCPs [20]. With regard to the biotransformation pathway, they are suitable by virtue of their high capacity to metabolize xenobiotics and they also express the gene for the aryl receptor AhR [21]. MX and AHTN were studied in short term exposure individually and combined with classical inducer of CYP1A as Benzo(a)pyrene (B(a)P) and 3,3'-4,4',5-pentachlorobiphenyl (PCB126).

2 Materials and methods

2.1 Cell culture

PLHC-1 cells (ATCC; LGC Promochem, Teddington UK) were kindly provided by Dr Tvrtko Smital of Ruder Boskovich Institute, Zagreb, Croatia. They were grown in 75 cm² plastic flasks (PBI International) at 30°C in 20 ml Dulbecco's Modified Eagles Medium (Sigma-Aldrich) supplemented with 5% FBS (Invitrogen). Cells were subcultured every 4 days by detaching with 1 ml per flask of 1:4 trypsin-EDTA solution (Gibco).

2.2 Neutral red assay

Cell viability was measured by neutral red assay [22]. Cells were grown in 200 µl/well of medium for 24 h. One hundred micro litres of medium was then



removed and replaced with the same volume of medium containing serial dilutions (range 0-250 μM) of MX and AHTN (LGC standards) or 0.1-2 μM B(a)P and 1nM PCB 126 (Sigma-Aldrich) dissolved in DMSO (maximum concentration 0.1%). Unexposed cells and DMSO-exposed cells were used as controls. The plates were incubated for another 24 h. The medium was then removed and the plates washed with 200 μl PBS, adding 100 μl neutral red medium, containing 40 $\mu\text{g/ml}$ Neutral Red dissolved in DMEM. Cells were incubated for 2 h under culture conditions. The medium was then removed and the cells washed with 150 μl PBS. Then 100 μl neutral red destain solution (50% ethanol, 49% deionized water, 1% glacial acetic acid) was added and the plate shaken for 10 min. The optical density (OD) of neutral red extract was measured by spectrophotometer at 540 nm. Each experiment was performed at least three times. The IC₅₀ for MX and AHTN were calculated by fitting the OD of a typical experiment to a classical sigmoidal dose-response model using GraphPad Prism5 software.

2.3 RNA extraction and Q-PCR

In order to evaluate CYP1A modulation at gene transcription by MX, AHTN, and the two known inducers B(a)P and PCB 126, singly and combined, cells were grown in 4 ml/well of medium for 24 h. Two millilitres of medium was then removed and replaced with 2 ml medium containing MX (2, 4 and 20 μM final concentrations) and AHTN (1 nM, 2 μM f.c.) singularly dissolved in DMSO 0.1%, B(a)P 2 μM f.c. and B(a)P 2 μM combined with MX 20 μM and 2 μM AHTN, PCB126 1 nM f.c. and PCB126 1 nM combined with 1 nM and 2 μM AHTN. The plates were incubated for another 6 and 24 h. The medium was then discarded and the plates washed twice with 1.2 ml PBS. Cells dissolved in PBS were recovered with a cell scraper and centrifuged 10 minutes at 1200 x g. Cell pellets were stored at -80°C.

Total RNA was isolated using Qiagen RNeasy MiniKit (Qiagen) according to the manufacturer's protocol. RNA was treated with DNase from RNase-Free DNase set (Qiagen) to avoid any traces of genomic DNA. RNA concentrations were measured using a Shimadzu spectrophotometer at 260 nm. 250 ng total RNA was transcribed to cDNA using i-script cDNA Reverse Transcription Kit (Biorad). Real-time PCR was used to evaluate *cyp1a* gene expression. Specific primers were designed using IDTDNA www.idtdna.com. 18S rRNA was used as housekeeping gene based on high stability in this cell line. Primer sequences for PLHC-1 *r18S* were kindly provided by Jovica Loncar from Ruder Boskovic Institute, Zagreb, Croatia.

The following primers were used:

cyp1a Fw: 5'-GCATTTGGCGTGCTCGAAGAAA-3',
 Rev: 5'-TTGCAGATGTGCTCCTCCAACA-3';
r18S Fw: 5'-CCTTTAACGAGGATCCATTGGA-3',
 Rev: 5'-CGAGCTTTTAACTGCAGCAACT-3'.

Each amplification reaction contained 12.5 μl SYBR green mix, 1 μl cDNA and 0.75 μl forward and reverse primers 10 μM , in 25 μl total volume. The

cycling parameters were: 3 min denaturing at 95°C, 40 cycles at 95°C for 15 s, annealing at 55°C for 45 s, elongation at 72°C for 1 min. All primer pairs gave a single peak of dissociation in all reactions, and no amplification occurred in reactions without template. PCR efficiencies for each primer were determined from a standard curve using dilutions of pooled cDNA ($r^2 > 0.97$ for all primers). Data was analysed by the $\Delta\Delta C_t$ method [23].

2.4 EROD activity

EROD activity was determined by microplate assay [24]. Cells were grown in 200 μ l/well of medium for 24 h. One hundred micro litres of medium was then removed and replaced with 100 μ l of medium containing serial dilutions (0-20 μ M) of MX, AHTN, B(a)P and PCB 126 and in combination, dissolved in DMSO (maximum concentration 0.1%). Unexposed cells and DMSO-exposed cells were used as controls. The plates were incubated for another 6 or 24 h and then washed with 200 μ l PBS, adding 100 μ l 2 μ M 7-ethoxyresorufin (7-ER) dissolved in phosphate buffer pH 8.0 to each well. The kinetics of resorufin production were monitored for 10 min using a Victor3 microplate reader (Wallak) at $\lambda_{\text{Excitation}} = 530$ nm and $\lambda_{\text{Emission}} = 590$ nm. Protein content was quantified by a photometric assay [25] using bovine serum albumin as standard (0-0.5 mg/L $r^2 = 0.9728$). Results of EROD assay shown in Tables 1 and 2 are expressed as mean \pm SD of at least three independent experiments.

3 Results

3.1 Citotoxicity

After 24 h of exposure, a different cytotoxicity has been observed for the two compounds with an LC_{50} of 35.76 μ M for AHTN and LC_{50} 123.6 μ M for MX. No cytotoxic effect was encountered at the concentration of 2 μ M of B(a)P and 1nM PCB126 (data not shown).

3.2 Interaction with CYP1A

After 6 h of exposure to MX, a dose-dependent reduction in *cyp1a* gene transcription was observed with respect to control. At 24 h, the same pattern was observed but with slight induction at the lowest concentration (2 μ M) and still a dose-dependent reduction at the higher concentrations of 4 μ M and 20 μ M (Fig. 1). Co-exposure to MX with B(a)P did not alter *cyp1a* transcription levels compared to cells exposed to B(a)P alone (Fig. 1).

On the contrary after 6 h AHTN determined a slight induction of *cyp1a* transcription reaching maximum induction of 2.3 folds respect to controls at 2 μ M. No modulation of *cyp1a* transcription was observed after 24 h (Fig. 2). Co-exposure to AHTN with PCB126 and B(a)P at 6 h determined a 55% reduction of *cyp1a* transcription respect to the inducers alone which seemed to recover at 24 h. No differences on *cyp1a* transcription were evident at 24h between single exposure to inducers and combined to AHTN (Fig. 2).



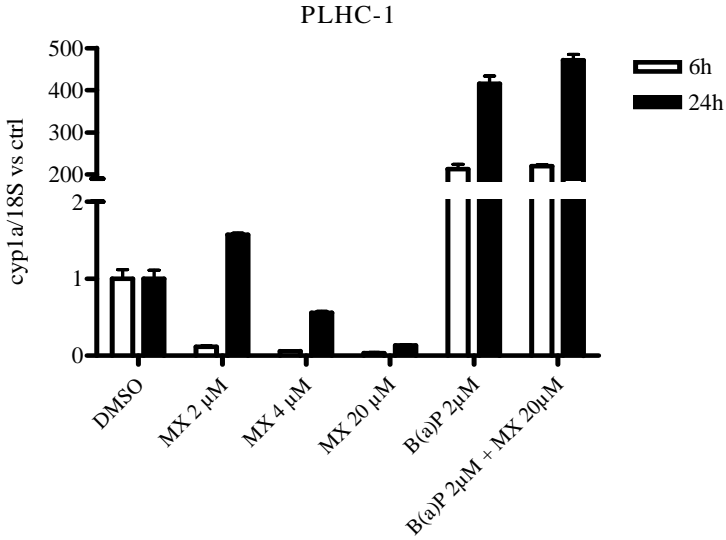


Figure 1: Transcription levels of *cyp1a/18S* of the cell line PLHC-1, exposed for 6 and 24 h to MX, B(a)P and B(a)P plus MX with respect to control (DMSO). Results are mean \pm SD (N=3).

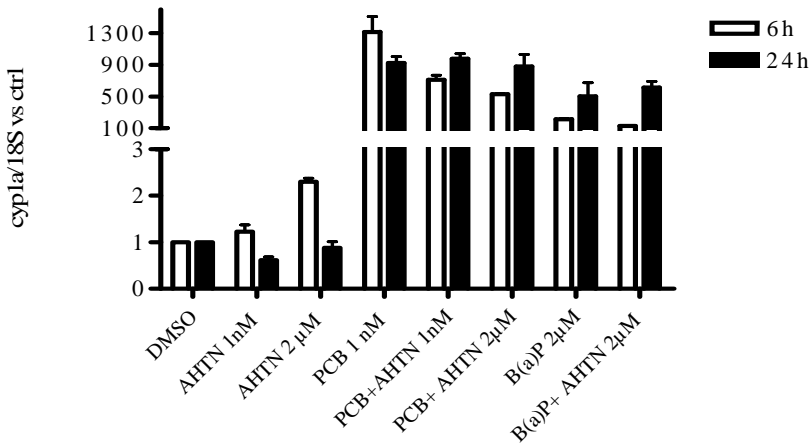


Figure 2: Transcription levels of *cyp1a/18S* of the cell line PLHC-1, exposed for 6 and 24 h to AHTN, B(a)P and PCB126 singly and combined with respect to control (DMSO). Results are mean \pm SD (N=3).

PLHC-1 cells exposed to MX for 6 h all showed increasing EROD activity, with maximum induction at the highest concentration of MX (20 μ M). On the



contrary, at 24 h, MX caused a dose-dependent decrease. Only a slight increase (about 2 folds vs ctrl) of EROD activity was detectable at 6 h and 24 h of exposure to AHTN (Tab. 1). Co-exposure with both MX and AHTN did not alter EROD activity induced by PCB126 and B(a)P (Tab. 2).

Table 1: Modulation of EROD activity by tested compounds at 6h and 24h. Indicated are maximal fold increase in activity \pm s.d. and the maximal concentration where the highest activity has been found.

	6h		24h	
	Max folds induction	conc Max	Max folds induction	conc Max
MX 6h	5.5 \pm 0.53	20 μ M	0.24 \pm 0.1	20 μ M
AHTN	2.32 \pm 0.79	2 μ M	2.18 \pm 0.01	4 μ M
B(a)P	80.35 \pm 37.75	0.2 μ M	79.15 \pm 1.10	0.2 μ M
PCB	40.53 \pm 3.55	1 nM	149.79 \pm 16.34	1 nM

Table 2: Induction of EROD activity by tested compounds in co-exposure at 24h. Indicated are fold increase in activity \pm s.d.

	EROD induction vs ctrl
PCB126 1 nM + AHTN 2 μ M	160.83 \pm 8.87
B(a)P 0.2 μ M + AHTN 2 μ M	67.11 \pm 5.31
PCB126 1 nM + MX 2 μ M	127.43 \pm 2.96
B(a)P 0.2 μ M + MX 2 μ M	88.85 \pm 10.07

4 Discussion

The different extent of MX and AHTN cytotoxicity observed in the present study has been already reported in liver rainbow trout cell lines (RTL-W1), in which a 30 folds lower LC₅₀ was measured for AHTN respect to MX [26]. These findings underline the need for more caution in the use of AHTN in household and personal care products. In Europe the use of AHTN is higher than nitromusk as MX with 358 tonnes per year for AHTN against 67 for MX (OSPAR data for 2000) [27].

Concerning CYP1A, results suggest that the MX and AHTN act differently in the PLHC-1 model.

MX seemed to affect CYP1A at transcriptional and enzymatic level with different profiles of *cyp1a* transcription after 6 h and 24 h of exposure. At 6 h, MX significantly reduced basal levels of transcription of the *cyp1a* gene in a dose-dependent manner. Partial recovery of the reduction but not dose-dependent occurred within 24 h. Positive feed-back involving amino metabolites, which act in the opposite manner to the parent compound, seems likely and reflects observations in mammals *in vivo* [15]. Although the cellular transformation pathways of MX are unknown, after 6 and 24 h of exposure our results suggest



that MX and its metabolites undergo different CYP1A biotransformation. Regarding the co-exposure experiment, MX reduced also *cyp1a* basal transcription but did not alter *cyp1a* induction by B(a)P. Other authors reported similar behaviour of rainbow trout hepatocyte cultures exposed *in vitro* to 17 β -estradiol (E2) and 17 α -ethinylestradiol (EE2), respectively [28,29]. In both studies, E2 and EE2 inhibited basal expression of the *cyp1a* gene and no interaction with induced levels of *cyp1a* by β NF (co-exposure) was observed. The effects on *cyp1a* expression found in the present study indicate that more research is needed into the behaviour of MX and its metabolites towards ER.

In mammals, it has been postulated that the MX cellular pathway is not mediated by AhR. A peculiar profile of drug-metabolizing enzyme induction by MX, not mediated by AhR, was suggested [14]. According to these authors, MX determined specific induction of CYP1A2 and phase II enzymes by a post-transcriptional induction mechanism. This hypothesis is in line with previous observations [30]. Under co-exposure conditions with 2-aminoanthracene (2-AA) or aflatoxin B₁ (AFB₁), MX caused an increase in genotoxicity of these compounds, whereas co-exposure with B(a)P did not cause any increase in toxicity. Thus the present results sustain the hypothesis of a distinct signalling pathway for MX not mediated by AhR.

On the contrary AHTN did not alter significantly *cyp1a* basal levels but decreased *cyp1a* induction by B(a)P and PCB126. A potential role of AHTN as competitive antagonist of AhR could thus be hypothesized. AHTN seems to interact with CYP1A similarly to other pollutants as PBDE (85) and PCB (105, 128) [31, 32].

The involvement of metabolites which act in the opposite manner to the parent compound, seems likely for both musks, due to the different profile of *cyp1a* transcription.

With regard to the effects of MX on EROD activity, a reduction was generally observed after 6 and 24 h of exposure, as observed for gene transcription, except for the increase at the highest concentrations (10-20 μ M). A similar inhibitory effect was reported in the microsomal fraction of carp *in vitro*, where MX reduced EROD activity by $71 \pm 5\%$ [19]. Besides clear evidence of inhibition of EROD activity by MX *in vitro*, the present results show temporal permanence of the inhibitory effect over 24 h. The large discrepancy between 6 and 24 h exposure to the higher concentrations suggests compensatory positive feedback in the first 6 h of exposure, seemingly cancelled out over 24 h. A possible explanation could be the observed significant reduction in *cyp1a* transcription.

With regard to AHTN, no interaction with EROD activity is observed both at 6 h and at 24 h, both in single and in co-exposure. Consequently, the alteration at the transcriptional level by AHTN does not seem to interfere with the catalytic function of CYP1A.

This observation is in agreement with what has been reported in carp [19], where a higher ability of nitromusk to interact with CYP1A compared to polycyclic musk has been observed. AHTN in fact determines only a slight inhibition of EROD activity compared to other musks while it has been reported



as the strongest inhibitor of CYP3A activity (BFCOD) [19]. Moreover in rat microsomes AHTN seems not altering EROD activity [18], thus confirming the hypothesis that it is not metabolized by CYP1A, but possibly by other enzymes as CYP3A.

Based on the overall results, it can be hypothesized that other enzymes could be responsible for rapid metabolism of MX and AHTN in PLHC-1.

First useful data have been thus obtained from the present study in order to understand toxicological pathways of MX and AHTN in relation to the CYP1A system in fish. Overall results of this study suggest a different mechanism of interaction with CYP1A of a nitro musk as MX and a polycyclic musk as AHTN. Therefore, both compounds seem to affect CYP1A detoxification of toxic compounds known inducers of the system as PAHs and PCBs. A reduction in the detoxification of toxic molecules could affect negatively fish cells with unexpected detrimental effects for aquatic organisms and the ecosystem.

5 Conclusions

The present study clarifies the interaction of MX and AHTN with the CYP1A system in fish both in single and co-exposure with classical CYP1A inducers.

Regarding MX, data suggests that it interferes with the biotransformation system but not involving AhR mediated pathway as confirmed by co-exposure with B(a)P. AHTN seems not to be metabolized by CYP1A but at the same time able to reduce the metabolization of classical toxic inducers as B(a)P and the dioxin-like PCB 126. Exposure to musks could thus result in reduced detoxification capacity of CYP1A and may also interfere with important physiological processes in the organism. Therefore, under conditions of chronic exposure unexpected adverse effects could occur, especially in areas chemically impacted by mixture of toxic pollutants. The use of co-exposure experiments confirmed a great investigative tool to clarify the interaction and behaviour of emerging contaminants in respect of important cellular defence systems.

Acknowledgements

The study was financed by the Italian Ministry for Universities and Research (MIUR) based on PRIN project 2007J23NNX_001 2007.

The authors are grateful to Roko Zaja and Jovica Loncar from the Ruder Boskovic Institute for setting up the PLHC-1 analysis and to Tvrtko Smital for great advice and support.

References

- [1] Daughton, C.G., & Ternes T.A., Pharmaceuticals and personal care products in the environment: agent of subtle change? *Environmental Health Perspectives*, **107**, pp. 907–938, 1999.



- [2] Rimkus, G., Polycyclic fragrances in the aquatic environment. *Toxicology Letters*, **111**, pp. 37-56, 1999.
- [3] Gaterman, R., Hühnerfuss, H., Rimkus, G., Attar, A., & Kettrup A., Occurrence of musk xylene and musk ketone metabolites in the aquatic environment. *Chemosphere*, **36**, pp. 2535–2547, 1998.
- [4] Gaterman R., Biselli S., Hühnerfuss H., Rimkus G., Hecker M., Karbe L., 2002. Synthetic musks in the environment. Part 1: Species dependent bioaccumulation of polycyclic and nitro musk fragrances in freshwater fish and mussels. *Archives of Environmental Contamination and Toxicology*, **42**, pp. 437–446, 2002.
- [5] Sumner, N.R., Guitart, C., Fuentes, G., & Readman, J.W., Inputs and distributions of synthetic musk fragrances in an estuarine and coastal environment; a case study. *Environmental Pollution*, **158**, pp. 215-22, 2010.
- [6] Rudel, H., Bohmer W., & Schroter-Kermani, C., Retrospective monitoring of synthetic musk compounds in aquatic biota from German rivers and coastal area. *Journal of Environmental Monitoring*, **8**, pp. 812-823, 2006.
- [7] Luckenbach, T., Corsi, I., & Epel, D., Fatal attraction: synthetic musk fragrances compromise multixenobiotic defense systems in mussels. *Marine Environmental Research* **58**, pp. 215-9 2004.
- [8] Luckenbach, T., & Epel, D., Nitromusk and polycyclic musk compounds as long-term inhibitors of cellular xenobiotic defence systems mediated through multidrug transporters. *Environmental Health Perspectives* **113**, pp. 17 – 24, 2005.
- [9] Carlsson, G., & Norrgren L., Synthetic musk toxicity to early life stages of zebrafish (*Danio rerio*). *Archives of Environmental Contamination and Toxicology*, **46**, pp. 102–105, 2004.
- [10] Chou, Y., & Dietrich, D.R., Interactions of nitromusk parent compounds and their amino-metabolites with the estrogen receptors of rainbow trout (*Oncorhynchus mykiss*) and the South African clawed frog (*Xenopus laevis*). *Toxicology Letters*, **111**, pp. 27–36, 1999.
- [11] Schreurs, R.H.M.M., Legler, J., Artola-Garicano, E., Sinnige, T.L., Lanser, H., & Van Der Burg B., In vitro and in vivo antiestrogenic effects of polycyclic musks in zebrafish. *Environmental Science and Technology* **38**, pp. 997-1002, 2004.
- [12] Yamauchi, R., Ishibashi, H., Hirano, M., Mori, T., Kim, J-W., & Arizono, K., Effects of synthetic polycyclic musks on estrogen receptor, vitellogenin, pregnane X receptor, and cytochrome P450 3A gene expression in the livers of male medaka (*Oryzias latipes*). *Aquatic Toxicology* **90**, pp. 261-268, 2008.
- [13] Goksøyr, A., & Förlin, L., The cytochrome P-450 system in fish, aquatic toxicology and environmental monitoring. *Aquatic Toxicology* **22**, pp. 287–312, 1992.
- [14] Iwata, N., Minegishi, K., Suzuki, K., Ohno, Y., Igarashi, T., Satoh, T., & Takahashi, A., An unusual profile of musk xylene-induced drug-metabolizing enzymes in rat liver. *Biochemical Pharmacology*, **45**, pp. 1659-1665, 1993.



- [15] Lehman-McKeeman, L.D., Caudill, D., Vassallo, J.D., Pearce, R.E., Madan, A., & Parkinson, A., Effects of musk xylene and musk ketone on rat hepatic cytochrome P450 enzymes. *Toxicology Letters*, **111**, pp. 105–115, 1999.
- [16] Lehman-McKeeman, L.D., Johnson, D.R., & Caudill, D., Induction and inhibition of mouse cytochrome P-450 2B enzymes by musk-xylene. *Toxicology and Applied Pharmacology*, **142**, pp. 169-177, 1997.
- [17] Suter-Eichenberger, R., Boelsterli, U.A., Conscience-Egli, M., Lichtensteiger, W., & Schlumpf, M., CYP 450 enzyme induction by chronic oral musk xylene in adult and developing rats. *Toxicology Letters*, **115**, pp.73–87, 2000.
- [18] Steinberg, P., Fischer, T., Arand, M., Park, E., Elmادfa, I., Rimkus, G., Brunn, H., Dienes, & H-P., Acute hepatotoxicity of the polycyclic musk 7-acetyl-1,1,3,4,4,6-hexamethyl-1,2,3,4-tetrahydronaphthaline (AHTN). *Toxicology Letters*, **111**, pp. 151-160, 1999.
- [19] Schnell, S., Martin-Skilton, R., Fernandes, D., & Porte, C., The interference of nitro- and polycyclic musks with endogenous and xenobiotic metabolizing enzymes in carp: an in vitro study. *Environmental Science and Technology*, **43**, pp. 9458 – 9464, 2009.
- [20] Fent, K., Fish cell lines as versatile tools in ecotoxicology: assessment of cytotoxicity, cytochrome P4501A induction potential and estrogenic activity of chemicals and environmental samples. *Toxicology in Vitro*, **15**, pp. 477 – 488, 2001.
- [21] Hahn, M.E., The aryl hydrocarbon receptor. A comparative perspective. *Comparative Biochemistry and Physiology C*. **121**, pp. 23 – 54, 1998.
- [22] Repetto, G., del Peso, A., & Zurita, J.L., Neutral red uptake assay for the estimation of cell viability/cytotoxicity. *Nature Protocols* **3**, pp. 1125-1132, 2008.
- [23] Pfaffl, M., A new mathematical model for relative quantification in real-time RT-PCR. *Nucleic Acid Research*, **29**, pp. 2002-2007, 2001.
- [24] Traven, L., Žaja, R., Lončar, J., Smital, T., & Mićović, V., CYP1A induction potential and the concentration of priority pollutants in marine sediment samples – In vitro evaluation using the PLHC-1 fish hepatoma cell line. *Toxicology in Vitro*, **22**, pp. 1648 – 1656, 2008.
- [25] Bradford, M., A rapid and sensitive method for the quantitation of microgram quantities of protein utilizing the principle of protein-dye binding. *Analytical Biochemistry* **72**, pp. 248-254, 1976.
- [26] Schnell, S., Bols, N.C., Barata, C., & Porte, C., Single and combined toxicity of pharmaceuticals and personal care products (PPCPs) on the rainbow trout liver cell line RTL-W1. *Aquatic Toxicology*, **93**, pp. 244-252, 2009.
- [27] OSPAR Commission. *Ospar Background Document on Musk Xylene and Other Musks*, Hazardous Substances Series; OSPAR Commission: London, pp. 45, 2004.



- [28] Navas, J.M., & Segner, H., Estrogen-mediated suppression of cytochrome P4501A (CYP1A) expression in rainbow trout hepatocytes: role of estrogen receptor. *Chemico – Biological Interactions*, **138**, pp. 285–298, 2001.
- [29] Grans, J., Wassmur, B., & Celander, M.C., One-way cross-talk between arylhydrocarbon receptor (AhR) and estrogen receptor (ER) signalling in primary cultures of rainbow trout hepatocytes. *Aquatic Toxicology*, **100**, pp. 263-270, 2010.
- [30] Mersch-Sundermann, V., Emig, M., & Reinhardt, A., Nitro musks are cogenotoxicants by inducing toxifying enzymes in the rat. *Mutation Research*, **356**, pp. 237–245, 1996.
- [31] Chen, G., Konstantinov, A.D., Joyce, E.M., Bols, N.C., and Bunce, N.J., Synthesis of polybrominated diphenyl ethers and their capacity to induce CYP1A by the Ah receptor mediated pathway. *Environmental Science and Technology*, **35**, pp. 3749-3756, 2001.
- [32] Hestermann, E.V., Stegeman, J.J., & Hahn, M.E., Relative contributions of affinity and intrinsic efficacy to aryl hydrocarbon receptor ligand potency. *Toxicology and Applied Pharmacology*, **168**, pp. 160-172, 2000.



Section 5

Food safety

This page intentionally left blank

Evaluation of QMRA performance for *Listeria monocytogenes* in cold smoked salmon

V. Popov¹, H. L. Lauzon², M. N. Haque¹, F. Leroi³ & R. Gospavic^{1,4}

¹Wessex Institute of Technology, Ashurst Lodge, Southampton, UK

²Matís ohf., Icelandic Food and Biotech R&D, Reykjavík, Iceland

³Ifremer, Laboratoire de Science et Technologie de la Biomasse Marine, Nantes, France

⁴Faculty of Civil Engineering, University of Belgrade, Serbia

Abstract

Food-borne listeriosis, caused by *Listeria monocytogenes* (*Lm*), is relatively rare but the relatively high rate of fatality (20–30%) compared to other food-borne microbial pathogens such as *Salmonella* makes it a serious disease. The foodstuff is recognised as the primary route of transmission for human exposure. A wide variety of food or raw material may become contaminated with *Lm* but the majority of listeriosis cases are related to ready-to-eat (RTE) food. The important factor related to food-borne listeriosis is that *Lm* can grow under low (refrigerated) temperatures when given sufficient time. Therefore, RTE products with long shelf life are under risk with respect to growth of *Lm* to critical concentrations.

A stochastic model for the growth of *Lm* with the inhibiting effect of lactic acid bacteria (LAB) in cold smoked salmon (CSS) was developed. An existing deterministic model for the growth of *Lm* was adapted by adding the Winner stochastic process in order to simulate the growth of *Lm*. The Poisson distribution is used to represent the initial count (occurrence) of *Lm*. A deterministic model for growth of LAB is used and the inhibiting effects of *Lm* and LAB on each other are taken into account. The Beta-Poisson model is used for estimating the dose response.

The model has been tested during field trials with CSS performed in August 2010. The salmon was slaughtered in Norway and transported to France where it was processed. The model, implemented within the QMRA module, indicated that growth of *Lm* would occur in the CSS samples investigated. However, the



data obtained during the field trial showed that microbial cell counts implied a reduction in the population of *Lm* with storage time, which means that a different model to describe the growth of *Lm* in presence of LAB may be required, especially for lower concentrations of *Lm*.

Keywords: QMRA, *Listeria monocytogenes*, cold smoked salmon, model evaluation.

1 Introduction

Illness caused by *Listeria monocytogenes* (*Lm*) is more rare but of more concern because of the seriousness of the illness which can cause death particularly in pregnant women, young children, elderly and immuno-compromised people [1, 2]. *Lm* is widely spread in the environment because it is resistant to different environmental conditions and it can grow in soil, water, fodder, straw, feed stuffs or faeces. The bacterium is therefore present in a wide variety of raw food. It is able to grow at refrigeration temperatures and survive in food for longer periods under adverse conditions [3]. Its ability to colonise food processing environments has been reported [4]. *Listeria* is able to attach itself to working surfaces creating biofilms that are difficult to remove [5, 6], and become a contamination source in food processing [7]. The contamination of the product in cutting and chilling areas is mainly due to cross contamination.

For RTE food the European Union (EU) regulations differentiate between products which cannot and those which can support growth of *Lm*. According to the EU regulations, the maximal allowed concentration of *Lm* in the products which cannot support the growth of *Lm* is 100 CFU/g (EC 2073/2005) [8].

A Quantitative Microbial Risk Assessment (QMRA) model was developed for estimation of the risk to the consumers expressed through the probability for illness due to consumption of CSS. The probability is obtained by using the probability density functions (PDF) for microbial concentration of *Lm* obtained from a stochastic growth model and a dose response model for *Lm*. The stochastic fluctuations in the growth rate are taken into account by using white noise and the Winner process [9]. The Poisson distribution is used as the initial concentration and occurrence of the pathogens in different food packages in a supply chain, where these are very low and rare, respectively.

High concentrations of LAB can inhibit growth of the *Lm* in lightly preserved seafood, and therefore the stochastic growth equation for *Lm* is coupled with the deterministic model for the growth of LAB to include the inhibiting effects of LAB on growth of *Lm* [10]. The Milstein algorithm was used to solve the stochastic differential equation numerically [11]. In the QMRA model the second order Monte Carlo simulation was used to simulate the stochastic process of microbial growth and random initial concentration of pathogenic microorganisms.

The model includes the influence of various parameters on the growth of *Lm* and LAB, such as: temperature, pH, water activity (a_w), salt content (NaCl), smoke components (phenols), undissociated lactic acid LAC_U , undissociated



diacetate – DAC_U , and concentration of dissolved CO_2 . More on the developed model can be found elsewhere [12, 13].

2 The mathematical model for microbial growth

2.1 Primary model

As the high concentration of the LAB can inhibit growth of Lm in lightly preserved seafood, such as CSS through the phenomenon known as Jameson effect, it is necessary to include this effect in the primary model for microbial growth of Lm [14, 15].

As the initial concentration of Lm is lower than the concentration of LAB this effect will restrict maximal concentration of Lm which will have great impact on the risk assessment of RTE products. The growth rate of LAB in lightly preserved food products generally is lower than the growth rate that would inhibit growth of Lm [16]. The microbial interaction between Lm and LAB could be described by the following equations:

$$\begin{aligned} \frac{dN_{Lm}}{dt} &= \alpha_{Lm}(t) \cdot \mu_{\max}^{Lm} \cdot \left(1 - \frac{N_{Lm}}{N_{\max}^{Lm}}\right) \cdot \left(1 - \frac{N_{LAB}}{N_{\max}^{LAB}}\right) \\ \alpha_{Lm}(t) &= \frac{q_{Lm}(t)}{1 + q_{Lm}(t)}; \quad \frac{dq_{Lm}}{dt} = \mu_{\max}^{Lm} \cdot q_{Lm}(t); \quad N_{Lm}(0) = N_{Lm0} \\ \frac{dN_{LAB}}{dt} &= \alpha_{LAB}(t) \cdot \mu_{\max}^{LAB} \cdot \left(1 - \frac{N_{LAB}}{N_{\max}^{LAB}}\right) \cdot \left(1 - \frac{N_{Lm}}{N_{\max}^{Lm}}\right) \\ \alpha_{LAB}(t) &= \frac{q_{LAB}(t)}{1 + q_{LAB}(t)}; \quad \frac{dq_{LAB}}{dt} = \mu_{\max}^{LAB} \cdot q_{LAB}(t); \quad N_{LAB}(0) = N_{LAB0} \end{aligned} \quad (1)$$

where $\mu_{\max}^{Lm/LAB}$ are maximal growth rate, $N_{\max}^{Lm/LAB}$ are maximal concentrations without microbial interaction, and $N_{Lm0/LAB0}$ are initial concentrations for Lm and LAB, respectively; $q_{Lm/LAB}$ are quantities which are related to critical substance necessary for growth and characterise the physiological state of the cells at the moment of inoculation and $\alpha_{Lm/LAB}$ are adjustment functions for Lm and LAB, respectively. The above model was extended using Baranyi and Roberts model for taking into account the lag phase [10, 17]. The above equations do not have analytical solution and could be solved numerically by discretisation in time [17].

2.2 Secondary model

The growth rate as a function of the temperature, water activity (a_w), pH, undissociated lactic acid (LAC_U), undissociated diacetate (DAC_U), smoked components (phenols, P), concentration of dissolved CO_2 , and nitrite (NIT), could be expressed by the following equation [18]:



$$\mu_{Lm} = b \cdot \left(\frac{T - T_{\min}}{T_0 - T_{\min}} \right)^2 \cdot \frac{a_w - a_{w\min}}{a_{w\text{opt}} - a_{w\min}} \cdot (1 - 10^{pH_{\max} - pH}) \cdot \left(1 - \frac{LAC_U}{MIC_{lac}} \right) \cdot \left(1 - \sqrt{\frac{DAC_U}{MIC_{dac}}} \right) \cdot \left(\frac{P_{\max} - P}{P_{\max}} \right) \cdot \left(\frac{CO_{2\max} - CO_{2eq}}{CO_{2\max}} \right) \cdot \left(\frac{NIT_{\max} - NIT}{NIT_{\max}} \right)^2 \cdot \zeta \quad (2)$$

The MIC_{lac} and MIC_{dac} are theoretical concentrations of undissociated lactate and diacetate, respectively preventing the growth of *Lm*. The pH_{\max} , P_{\max} , $CO_{2\max}$, NIT_{\max} , are maximal values for pH and concentration of phenols, CO_2 , and nitrite, respectively, which prevent growth of *Lm*. The $a_{w\min}$ and $a_{w\text{opt}}$ are minimal and optimal water activity for growth of *Lm*.

2.3 Stochastic model for microbial growth and initial concentration

The deterministic model for simultaneous growth of *Lm* and LAB gives only one single growth curve for both species which represents average value for microbial concentration. This type of model cannot be applied in microbial risk assessment and therefore a stochastic model for growth of *Lm* is used in this work [12]. On the other hand the model for growth of LAB was taken to be deterministic as it provides the inhibiting effect of LAB on the growth of *Lm*, for which the average value is sufficient, reducing this way the required central processor unit (CPU) time. The Poisson distribution was used as a most suitable for this kind of stochastic process [12].

2.4 Dose response model

Once the probability distribution for microbial concentration is obtained by using the dose response the probability for illness in consumers could be estimated. The dose response model is a cumulative density function (CDF) which gives the probability for infection or to get ill if a certain number of cells are inoculated. In this study the Beta-Poisson model is used for dose response [19, 20]. More on the developed model can be found elsewhere [12, 13].

2.5 Field trial experimental set-up and analysis of naturally *Lm*-contaminated CSS

Farmed salmon was slaughtered near Alesund in Norway (Aukra), and transported to Boulogne sur Mer, France, where it was processed into CSS fillets five days post-mortem. The sliced and vacuum-packaged product was ready two days later. The packages were assigned to 3 different treatments, aiming to study the effect of isothermal (3 and 10°C) or abusive temperature on the *Listeria* risk for these products. The abusive treatment implied shipping few packages to Paris during which high thermal load was applied twice (>20°C product temperature), followed by a low (3°C) temperature storage. Temperature of two packages was monitored every 10-min using temperature data loggers for each treatment investigated. The storage trial lasted for 27 days during which *Lm* and LAB analyses were performed regularly by a Cofrac-accredited French laboratory. Detection in 25 g (BRD-07/4-09/98) and enumeration (RLM-V9-13/10/06|BRD-



07/05-09/01) of *Lm* was conducted on duplicate samples for each treatment. Nitrite-Actidione-Polymyxin (NAP) agar [21] was used for LAB enumeration following incubation at 25°C for 3–5 days and confirmation by testing for the presence of catalase-negative colonies.

3 Results

The QMRA model for CSS was tested during the cold smoked salmon field trial in August 2010. The salmon was slaughtered near Alesund in Norway (Aukra), and delivered to Boulogne sur Mer, France, 5 days later where it was processed, sliced and vacuum-packaged by a processor. CSS products were stored at two temperatures (3 and 10°C) and a third treatment considered shipment of few samples to Paris, allowing a temperature abuse of few hours and brought back to laboratory storage at 3°C. The presence (detection and enumeration) of *L. monocytogenes* in the cold smoked salmon was regularly verified throughout the trial (27 days) and found to be naturally occurring from early post-packaging (25 h). The three different temperature profiles used in the study are shown in Figure 1, labelled as *Treatment 1*, *Treatment 2* and *Paris*. The laboratory results of microbial growth show that LAB reached high levels after 19 days of storage, being higher at 10°C than 3°C.

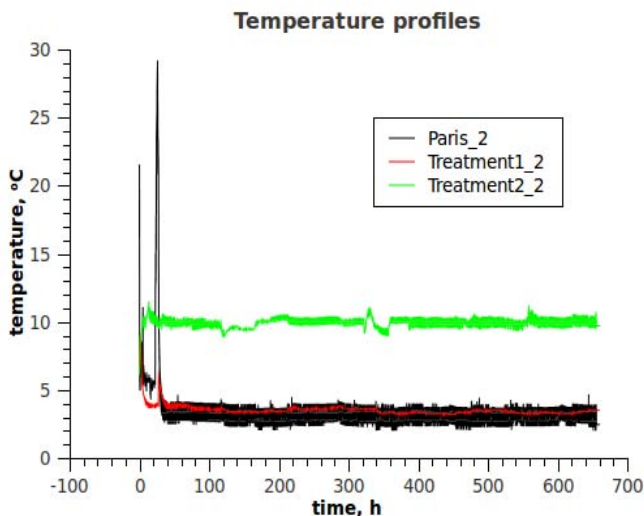


Figure 1: Temperature profiles applied to CSS products.

The experimental counts of the microbial population for Treatments 1 and 2 are shown in Tables 1 and 2, respectively. The presence of *Lm* was confirmed 25 h post-packaging and up to day 19. However, one of the samples was negative after 19 days of storage while all samples were negative on day 27. Up to day 19, the suspected *Lm* level ranged between 0.04 to just below 10 cells/g

while it had decreased to less than 0.04 cell per g on day 27. This demonstrates the very low *Lm* level in the product and even its sporadic incidence in the whole batch. It is also likely that the inhibitory activity of LAB may have contributed to the *Lm* growth control and, ultimately, the bactericidal effect observed towards the end of the storage life.

These results are not in agreement with the developed QMRA model. The model does not take into account reduction in number of colony-forming units (CFU) and therefore cannot predict the disappearance of *Lm* towards the end of the field trial.

Table 1: Laboratory results for the microbial population counts (log N CFU/g) of Treatment 1 group ($3.5 \pm 0.4^\circ\text{C}$) in duplicate samples (S1 and S2).

Time (h)	LAB counts		Lm detection*	
	S1	S2	S1	S2
25.02	3.90	2.65	+	+
119.75	3.67	3.40	+	+
290	4.30	4.84	+	+
462	5.11	5.56	-	+
658	5.64	4.18	-	-

*Detection in 25 g sample. Enumeration conducted always gave < 10 CFU/g.

Table 2: Laboratory results for the microbial population counts (log N CFU/g) of Treatment 2 group ($9.9 \pm 0.4^\circ\text{C}$) in duplicate samples (S1 and S2).

Time (h)	LAB counts		Lm detection*	
	S1	S2	S1	S2
25.02	3.90	2.65	+	+
119.75	3.52	5.15	+	+
290	>7.48	4.49	+	+
462	6.38	>8.48	+	+
658	8.15	8.48	-	-

*Detection in 25 g sample. Enumeration conducted always gave < 10 CFU/g.

Based on initial mean LAB load (log (N)=3.3 CFU/g), *Lm* and LAB growth were calculated under all three temperature profiles obtained (T1, T2, and P) assuming *Lm* counts of 0.04 cell/g and 10 cells/g. The lower level is based on the fact that detection of *Lm* in 25 g implies the presence of at least one living cell, hence 0.04 cell/g.

Figures 2 and 3 show the comparison between the laboratory counts for LAB and the corresponding model predictions for growth of LAB and *Lm* for initial

Lm count of 0.04 CFU/g for Treatment 1 and Treatment 2, respectively. The model performed calibration during the calculation of bacterial growth.

The results in Figure 2 show slow growth, however, the microbiological results suggest that *Lm* concentration is declining with storage time, perhaps due to interaction with LAB. At higher storage temperature, Figure 3 shows faster

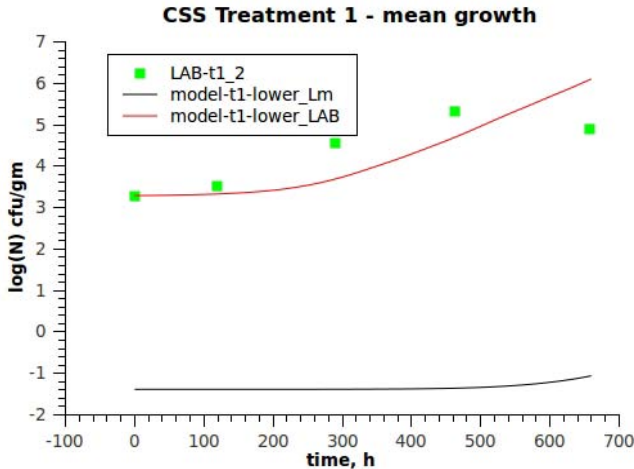


Figure 2: Comparison between observed counts of LAB (lactic acid bacteria) and predicted LAB growth along with the growth prediction for *Lm* (*L. monocytogenes*) for Treatment 1 profile. “lower” in the legend refers to 0.04 CFU/g.

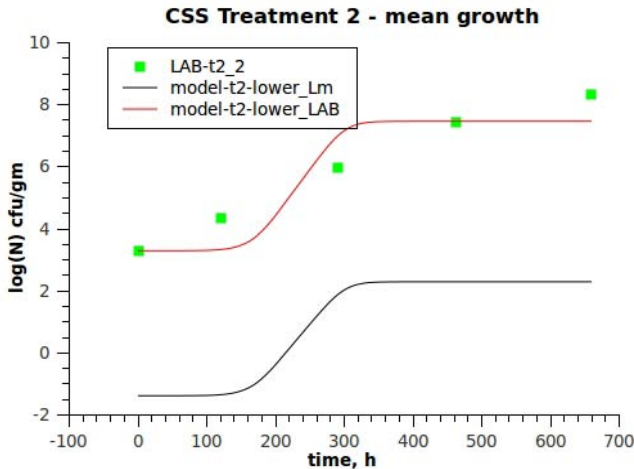


Figure 3: Comparison between observed counts of LAB (lactic acid bacteria) and predicted LAB growth along with the growth prediction for *Lm* (*L. monocytogenes*) for Treatment 2 profile and initial *Lm* count of 0.04 CFU/g.



Lm growth, in contrast to the data observed. The main conclusion is that the model reported by Mejlholm and Dalgaard [10], which has been modified to include automatic calibration for the lag phase and also stochastic element for growth and initial count, may not be applicable for low concentrations of *Lm*. The microbiological results show that the interaction with LAB reduces *Lm* concentration below the detection limit, while the model shows growth once the lag phase is finished and may stop the growth if LAB or *Lm* counts reach the maximum cell level, but cannot reduce the cell count under any conditions. This is not a characteristic of the dataset used to prepare the model. In fact, this is the characteristic of the model equations which do not allow for decrease in *Lm* concentration.

The QMRA model provides the risk to consumers due to consumption of the product. Table 3 shows the QMRA results for the three temperature profiles and two different initial *Lm* concentrations, 0.04 and 10 CFU/g. The calculated probability for illness in consumers for low initial concentration of *Lm* and lower average temperature results in a very low incidence, which is of order 2 to 3 cases of illness per 100 million portions, in this case each taken as 100 g. For the case of lower initial concentration and higher average temperature the probability for illness rises to 4,400 cases of illness per 100 million portions. This probability is of three orders of magnitude higher than for the case of lower average temperature, and one can argue that it might be high enough to allow establishing a link between the illness and the product. Due to the variability in response in humans to *Lm* it is still unlikely under such low probability to have two cases of illness in the same household or between the affected person and the close contacts, which is usually the easiest way of establishing link between food source and illness. Such low probability might not cause sufficient incidence of illness in an area to establish an outbreak, therefore the source may not be detected.

Under higher initial concentration and lower average temperature the probability for illness increases to approximately 10,000 cases of illness per 100 million portions. This is approximately twice as high probability as the one for lower initial concentration of *Lm* and higher average temperature. However, the above discussion on likeliness of establishing a link between illness and food source would still apply.

Table 3: Risk of illness in consumers, as influenced by *Lm* initial level and temperature conditions, according to the stochastic QMRA model.

Profile (Mean product temp.)		Treatment 1 (3.5 ± 0.4 °C)	Treatment 2 (9.9 ± 0.4 °C)	Paris (3.4 ± 1.0 °C)
Risk of illness	0.04 CFU/g	0.000002%	0.0044%	0.000003%
	10 CFU/g	0.0096%	0.5639%	0.0127%



For the case of higher initial concentration of *Lm* and higher average temperature the probability for illness rises to 5.6 cases of illness per 1 thousand portions (or 0.56% of a population). This incidence is high enough to establish a link between the food product and the illnesses in consumers which might result in an outbreak.

4 Conclusions

The model of Mejlholm and Dalgaard [10], implemented within the QMRA module, indicated that growth of *Lm* would occur in the investigated CSS samples. The field trial microbial cell counts implied a reduction in the population of *Lm*, which means that a different model to describe the growth of *Lm* in presence of LAB may be required, especially for lower concentrations of *Lm*. The inaccuracy in the predictions cannot be helped by the automatic calibration of the model [13] for two reasons: (i) the concentrations are on the detection limit and therefore the exact cell counts cannot be determined, which provides only information on whether *Lm* is detected or not detected; (ii) it is inherent property of the model not to be able to predict decrease of the microbial population of *Lm*.

To incorporate the reduction in cell counts of *Lm* in the model, in order to reflect the observed microbial counts, a model for the *Lm* growth in CSS in presence of LAB, which is based on the Lotka-Volterra type of equations can be used, as such model can predict both conditions; growth and decline in cell numbers of *Lm*.

Such model would require substantial amount of structured laboratory experiments in order to determine the model parameters. However, these results are indicative of the need for new models in order to describe the interaction of LAB with *Lm* at low contamination level.

Acknowledgement

The present study was supported by the CHILL-ON project, contract number: FP6-016333-2, as part of the Sixth Framework Programme, Priority 5, Food Quality and Safety.

References

- [1] Vellinga A. and Van Loock F., The dioxin crisis as experiment to determine poultry-related *Campylobacter enteritis*, *Emerging Infectious Diseases*, **8** (2002), 19–22.
- [2] McLauchlin J., Mitchell R.T., Smerdon W.J. and Jewell K., *Listeria monocytogenes* and listeriosis. A review of hazard characterization for use in microbiological risk assessment of foods, *International Journal of Food Microbiology*, **92** (2004), 15–33.



- [3] International Life Sciences Institute (ILSI) Research Foundation/Risk Science Institute, Expert Panel on *Listeria monocytogenes* in Foods, Achieving continuous improvement in reductions in foodborne listeriosis – a risk based approach, *Journal of Food Protection*, **68** (2005), 1932–1994.
- [4] Bell C and Kyriakides A., *Listeria. A Practical Approach to the Organism and its Control in Foods*, Blackie Academic & Professional, London (1998).
- [5] Blackman I.C. and Frank J., Growth of *Listeria monocytogenes* as a biofilm on various food-processing surfaces, *Journal of Food Protection*, **59** (1996), 827–831.
- [6] Spurlock A.T. and Zottola E.A., Growth and attachment of *Listeria monocytogenes* to cast iron, *Journal of Food Protection*, **54** (1991), 925–929.
- [7] Sammarco M.L., Ripabelli G., Ruberto A., Iannitto G. and Grasso G.M., Prevalence of Salmonellae, Listeriae and Yersiniae in the slaughterhouse environment and on work surfaces, equipment and workers, *Journal of Food Protection* **60** (1997), 367–371.
- [8] Regulation EC No 2073/2005 of 15 November 2005 on microbiological criteria for foodstuffs.
- [9] Gospavic R., Kreyenschmidt J., Popov V., Haque N., Bruckner S., Stochastic mathematical model for microbial growth in food under variable temperature conditions using the Monte Carlo Simulation, Proceedings of the *Cold Chain-Management*, 3rd International Workshop, Bonn, 2008.
- [10] Mejlholm O., Dalgaard P., Modeling and predicting the growth of lactic acid bacteria in lightly preserved seafood and their inhibiting effect on *Listeria monocytogenes*, *Journal of Food Protection*, **70/11** (2007), 2485–2497.
- [11] Kloeden P.E., Platen E., Numerical Solution of Stochastic Differential Equations, Springer-Verlag, Berlin Heidelberg, 1992.
- [12] Gospavic R., Haque M.N., Leroi F., Popov V. & Lauzon H.L., (2010) Quantitative microbial risk assessment for *Listeria monocytogenes* in cold smoked salmon. *Risk Analysis VII*, WIT Transactions on Ecology and the Environment, ISSN: 1743-3517; ISBN: 978-1-84564-472-7; 563-572.
- [13] Popov V., Gospavic R., Haque N. (2009) *D1.18 – Final report on risk assessments for microbial contamination and QMRA software module*, Chill-On (Project no.: FP6-016333-2), Sixth Framework Programme, Thematic Priority: Food Quality and Safety.
- [14] Augustin J.-C. and Carlier V., Mathematical modelling of the growth rate and lag time for *Listeria monocytogenes*, *International Journal of Food Microbiology*, **56** (2000), 29-51.
- [15] Ratkowsky D.A. and Ross T., Modelling the bacterial growth/no growth interface, *Letters in Applied Microbiology*, **20** (1995), 29-33.
- [16] Jorgensen L.V. and Huss H.H., Prevalence and growth of *Listeria monocytogenes* in naturally contaminated seafood, *International Journal of Food Microbiology*, **42** (1998), 127-131.



- [17] Baranyi J. and Roberts T.A., 1994. A dynamic approach to predicting bacterial growth in food, *International Journal of Food Microbiology*, **23** (1994), 277-294.
- [18] Dalgard P. and Jorgensen L.V., Predicted and observed growth of *Listeria monocytogenes* in seafood challenge tests and in naturally contaminated cold-smoked salmon, *International Journal of Food Microbiology*, **40** (1998), 105-115.
- [19] Haas C.N., Estimation of risk due to the dose of microorganisms: a comparison of alternative methodologies. *American Journal of Epidemiology*, **118** (1983), 573-582.
- [20] Haas C.N. and Thayyar-Madabusi A., Development and validation of dose-response relationship for *Listeria monocytogenes*, *Quantitative Microbiology*, **1** (1999), 89-102.
- [21] Davidson C.M. and Cronin F., Medium for the selective enumeration of lactic acid bacteria from foods, *Applied Microbiology*, **26** (1973), 439-440



This page intentionally left blank

Study of mutagenic effects of a packaging system with oxygen absorbers on sweet bakery products

R. A. Sueiro, M. J. Garrido & M. Araujo

*Lab. Microbiology (Instituto de Investigación y Análisis Alimentarios),
Universidad de Santiago de Compostela, Spain*

Abstract

In the present study, the potential mutagenic effects of a packaging system for food containing oxygen absorbers was evaluated on a popular sweet bakery product (glazed doughnuts) stored at 20°C along its extended self life by using the *Salmonella typhimurium* His⁺ test with the tester strains TA98, TA100, TA1535 and TA1537 and *Escherichia coli* Trp⁺ test with strains WP2uvrA and WP2uvrA pKM101. All samples were assayed in the presence and absence of an exogenous metabolizing system (S9 from rat liver). During the study, 3 lots were prepared and analysed: lot 1 consisted of control samples without absorber sachets. In lot 2 one oxygen absorber sachet was added into the package and in lot 3 two oxygen absorbers were used. All samples were packaged in high barrier pouches and stored at 20°C along the shelf life of the product, determined in other study as 4 days for control samples and 8 days for samples packaged with oxygen absorbers. As it was expected, the active concept itself did not show mutagenic activity. In addition, the control samples and samples in contact with the oxygen scavengers were also negatives in all sampling times (at days 0, 5 and 10). These results support the safe use of this type of active packaging to extend the shelf life of commercial doughnuts because the interactions between the bakery product and the package system did not represent a risk for the consumer health under the conditions tested.

Keywords: active packaging system, oxygen absorbers, sweet bakery products, *S. Typhimurium* his-test, *E. coli* Trp-test.



1 Introduction

Most bakery products stored at room temperature have a limited shelf-life. Between the main causes of deterioration are included oxidative degradation processes, changes in the content and distribution of water and microbial spoilage (Galić et al. [1]). Prolonging the shelf life of baked goods and pastries for alternatives ways to the use of additives, can be accomplished through the use of active packaging. Active packaging is an innovative concept that encompasses a collection of technologies in response to specific problems to improve the maintenance and extend the shelf life of foods (Vermeiren et al. [2]). Its use not only has the advantage of improving the conditions under which the food is supplied to the consumer, but it may also mean a lower cost of production and distribution as well as increased capacity of companies expansion since it has the potential ability to prolong the shelf life of packaged foodstuffs.

Due to the high potential of this technology, it has been developed and marketed a variety of concepts for use in active packaging of foods such as oxygen absorbers, carbon dioxide absorbers, ethanol emitters, ethylene absorbers and moisture absorbers (Rooney [3]). Oxygen absorbers are among the most suitable concepts for use in bakery products (Rooney [3]; Galić et al. [1]). They are often readily oxidizable chemicals commercialized in small pockets of oxygen permeable material that it is introduced into passive or conventional packaging with the food (Galić et al. [1]). Active packaging systems should not release their constituents if they are intended merely to absorb undesirable substances from the packaged foodstuff, such as oxygen. However, sachets containing active substances are often in contact with packaged foods, giving rise to the possibility that their migration into the foodstuff might be significant, especially in the case of moist, fatty and/or acid foodstuffs (López-Cervantes et al. [4]).

The European Union (EU), sensitive to many undesirable interactions that it can occur between the packaging and packaged foods, has developed the Framework Regulation (EC) no 1935/2004 [5] on materials and articles intended to come into contact with food where the active food contact materials were included in its field of application. Moreover, Regulation (EC) no 450/2009 [6] is a specific measure that lays down rules for active materials and articles to be applied in addition to the general requirements established in Regulation (EC) no 1935/2004 for their safe use. A community list of authorised substances shall be established after the European Safety Authority (EFSA) has performed a risk assessment on each substance including their toxicological properties (EFSA [7]) but to date it has not been published. With regard to materials and articles intended to come into contact with food, it has recently published the Commission Regulation (EC) no 10/2011 [8]. This latter Regulation supposes an update of applicable rules to such plastic materials which includes the list of authorized monomers and additives in the EU.

Despite numerous efforts by the EU to regulate the materials that come into contact with food, recent studies with other plastic materials authorized in the EU, such as epoxy resins based in bisphenol A, have shown that components of



this kind of resins and their derived products react with food components giving rise to formation of new and unknown compounds not subject to European legislation (Petersen et al. [9]; Coulier et al. [10]). Since oxygen absorber sachets are often in contact with packaged food, it cannot rule out the formation of new compounds when the passive plastic packaging, the active concept and the food interact. It is therefore necessary to check that their use does not represent a health risk for consumers under a toxicological point of view (Hotchkiss [11]).

Considering the absence of information available about that, the aim of the present study was to evaluate the potential mutagenic effects of a high barrier packaging system for food containing oxygen absorber sachets on a popular sweet bakery product (glazed doughnuts) stored at 20°C along its extended self life using the *Salmonella* His⁻ test and *Escherichia coli* trp⁻ test. The mutagenic effects of oxygen absorbers used in the present study were also evaluated with the same bacterial test systems. Both assays are between the most internationally agreed testing methods to identify and characterise potential hazard of new and existing chemical substances and chemical mixtures and they are used in regulatory safety testing (Organisation for Economic Co-operation and Development [12]). The assays are based on the ability of substances to induce point mutations in bacterial strains following DNA damage.

2 Materials and methods

2.1 Experimental conditions assayed

Doughnuts freshly prepared by a local manufacturer were packaged into polypropylene biaxially oriented film coated with acrylic and polyvinylidene chloride resin authorized for use in contact with foodstuff. Before sealing the packages, they were divided into 3 lots. In Lot 1 no active concept was incorporated within. In Lot 2 was added one iron-based oxygen-absorber sachet in each package and in lot 3 were added two absorber oxygen sachets. All lots were sampled at days 0, 5 and 10 in order to assess the mutagenic potential of packaged doughnuts. All samples were kept at 20°C during the study to simulate the conditions in which they are commercialized. Moreover, it was evaluated the mutagenic activity of oxygen absorbers used in the experiments. Lots from each sample type were collected each sampling day and they were submitted to extraction with dichloromethane-methanol (2:1, v/v). The organic extracts were dried over anhydrous sodium sulphate and concentrated to dryness under vacuum. Before performing the assays, they were dissolved in dimethyl sulfoxide (DMSO).

2.2 Mutagenicity assays

Sample extracts obtained from doughnuts and oxygen absorbers were tested using the plate incorporation method as described by Maron and Ames [13] for *S. typhimurium* and by Urios et al. [14] for *E. coli*. For experiments with *S. typhimurium* strains, the top agar was supplemented with 10 ml of 0.5 mM



histidine/biotin solution per 100 ml agar, and mutations to histidine independence were scored on minimal glucose agar plates (Maron and Ames [13]). For experiments with *E. coli* strains, mutations to tryptophan independence were scored on minimal glucose agar plates supplemented with 0.5 mg tryptophan per litre (Urios et al. [14]).

The S9 microsomal fraction from the livers of male Sprague-Dawley rats pretreated with a phenobarbital-methylcholanthrene mixture was purchased from Iffa Credo (L'Arbesle, France) and used as the external metabolic activation system. Both types of sample extracts were tested in the presence and absence of a mixture of 10% (v/v) S9 fraction in the S9 mix, which serves to convert mutagenic compounds in need of metabolic activation to their active mutagenic form. The concentrations of cofactors in the S9 mix (before adding them to the overlay) were 4 mM NADP, 5 mM glucose-6-phosphate, 33 mM KCl, 8 mM MgCl₂ and 100 mM sodium phosphate buffer (pH 7.4) (Maron and Ames [13]).

At least two complete assays were performed for each sample extract. All experiments were carried out in triplicate using a minimum of five doses. Positive and negative controls were included in each assay. Data from representative assays for the oxygen absorber extracts with the test doses evaluated are shown in Results and Discussion section where representative data for the doughnuts extracts along the period of study are also shown.

The statistical analysis of the data was based on biological mechanistic models proposed by Margolin et al. [15]. The SALM program (Kim and Margolin [16]) was used to fit Margolin's models to the data and select the model with the greatest likelihood. The Goodness of fit test calculated for each data set allows us to know if the data followed the fitted model. The estimated slope of the initial linear region (no. of revertants/mg sample equivalent) was used as a measure of mutagenic potency and for determining mutagenicity via a significance test. In this way, a positive response was obtained when the mutagenicity test p-value was less than 0.05. A sample was deemed to be mutagenic if at least one strain/activation combination yielded a reproducible positive response.

3 Results and discussion

Tables 1–3 present the mutagenic potential of the solvent extractable compounds recovered from oxygen absorber samples using *S. typhimurium* His⁻ and *E. coli* Trp⁻ tests in one independent mutagenicity assay. The dose levels assayed were between 0.313 and 5 mg sample equivalent/plate in all cases.

It can be seen the absence of mutagenic activity obtained with *S. typhimurium* strains TA98, TA100, TA1535 and TA1537 (Tables 1 and 2) either in the presence or absence of external metabolic activation. These results are indicative that oxygen absorber extracts did not induce frameshift mutations (detected with strains TA98 y TA1537), but neither have the ability to induce base pairs substitutions primarily affecting G-C base-pairs (detected with strains TA100 and TA1535) in the test system employed. No toxicity was evident at the highest dose assayed (5 mg/plate). Negative results were also obtained when *E. coli*



Table 1: Mutagenicity of oxygen absorber extracts in *S. typhimurium* strains TA98 and TA100.

Dose (mg/plate)	Number of revertants per plate			
	TA98		TA100	
	-S9	10% S9	-S9	10% S9
DMSO control	25 ± 5.3	29 ± 2.5	129 ± 7.4	121 ± 11.3
5	26 ± 4.4	36 ± 6.4	137 ± 4.2	124 ± 8.4
2.5	35 ± 9.1	29 ± 3.1	141 ± 10.2	123 ± 10.1
1.25	30 ± 4.6	31 ± 4.5	142 ± 6.7	126 ± 6.1
0.625	25 ± 4.0	33 ± 3.2	139 ± 5.9	126 ± 7.8
0.313	25 ± 3.1	31 ± 4.6	150 ± 7.9	124 ± 4.4
Slope ¹	0.60	0.87	0.00	0.04
H ₂ O control	-	-	124 ± 11.0	-
Positive control ²	226 ± 17.9	201 ± 14.4	450 ± 12.7	305 ± 17.0

Values are means ± SD of triplicate plates of one representative experiment. -, not tested. Revertants/mg of sample equivalent. ²Positive controls: TA98/-S9 (2,4,7-trinitro-9-fluorenone, 0.01 µg/plate; TA100/-S9 (sodium azide, 1 µg/plate), TA98 and TA100/4% S9 (1 and 2.5 µg/plate 2-aminofluorene, respectively).

Table 2: Mutagenicity of oxygen absorber extracts in *S. typhimurium* strains TA1535 and TA1537.

Dose (mg/plate)	Number of revertants per plate			
	TA1537		TA1535	
	-S9	10% S9	-S9	10% S9
DMSO control	10 ± 1.5	16 ± 3.5	9 ± 2.1	16 ± 1.5
5	12 ± 2.0	17 ± 3.1	11 ± 3.2	19 ± 3.2
2.5	10 ± 2.1	16 ± 4.0	12 ± 2.7	17 ± 2.7
1.25	13 ± 0.6	16 ± 4.0	11 ± 2.7	16 ± 2.7
0.625	13 ± 2.1	17 ± 3.1	10 ± 2.5	18 ± 2.0
0.313	11 ± 2.0	18 ± 3.0	10 ± 1.7	18 ± 2.5
Slope ¹	0.05	0.04	0.33	0.31
H ₂ O control	-	-	12 ± 2.5	-
Positive control ²	182 ± 14.3	90 ± 6.0	272 ± 8.5	181 ± 8.5

Values are means ± SD of triplicate plates of one representative experiment. -, not tested. Revertants/mg of sample equivalent. ²Positive controls: TA1537/-S9 (9-aminoacridine, 50 µg/plate; TA1535/-S9 (sodium azide, 0.5 µg/plate), TA1537 and TA1535/10% S9 (50 µg/plate 2-aminoanthracene, respectively).



strains WP2uvrA and WP2uvrA pKM101 were used in the assay at the same doses tested (Table 3), either with or without S9 fraction in the S9 mix. The latter data are indicative that active concept extracts analysed not induce base-pair substitutions affecting A-T base-pairs. Therefore, the results suggest that the use of such active concept itself does not represent a genotoxic hazard under the test conditions employed.

Table 3: Mutagenicity of oxygen absorber extracts in *E. coli* strains WP2uvrA and WP2uvrA pKM101.

Dose (mg/plate)	Number of revertants per plate			
	WP2uvrA		WP2uvrA pKM101	
	-S9	10% S9	-S9	10% S9
DMSO control	36 ± 5.7	37 ± 4.0	98 ± 4.6	105 ± 12.7
5	37 ± 4.0	40 ± 6.7	103 ± 5.0	105 ± 12.5
2.5	44 ± 4.2	38 ± 1.0	105 ± 8.4	116 ± 6.7
1.25	38 ± 7.8	45 ± 4.6	101 ± 4.4	108 ± 8.6
0.625	44 ± 4.0	47 ± 7.6	107 ± 5.3	112 ± 6.7
0,313	41 ± 10.2	43 ± 5.3	101 ± 2.5	111 ± 5.0
Slope ¹	0.00	0.00	0.52	0.00
H ₂ O control	-	-	122 ± 4.5	-
Positive control ²	178 ± 12.0	196 ± 13.4	449 ± 12.7	672 ± 21.0

Values are means ± SD of triplicate plates of one representative experiment. -, not tested. Revertants/mg of sample equivalent. ¹Positive controls: WP2uvrA and IC3327/-S9 (methyl methanesulfonate, 100 µg/plate; WP2uvrA and WP2uvrA pKM101/4% S9 (10 and 0.5 µg/plate 2-aminoanthracene, respectively).

These results could be expected considering the chemical composition provided by the supplier, which indicate that the oxygen absorber sachets used in the present study contained iron powder covered with sea salt and natural zeolith impregnated with a sodium chloride solution. The iron under appropriate humidity conditions uses up residual oxygen to form nontoxic iron oxide (Smith et al. [17]). Moreover, studies performed to know the behaviour of two commercial sachets of iron-based oxygen-absorber systems with respect to migration of active ingredients into foodstuffs showed that sodium chloride and iron were the compounds that migrate from the oxygen-scavenging system into solid foods (López-Cervantes et al. [4]). Therefore, it could be expected that these compounds interact with the packaged foodstuff along with those migrating from the plastic package.

To rule out the possible mutagenicity of doughnuts packaged with this active packaging system, mutagenicity assays of the product were performed along its extended self life. The doughnuts self lives were evaluated in other study as 4 days for control samples packaged without oxygen absorbers and 8 days for samples packaged with the active concepts based on sensorial and microbiological analyses (data not shown). The mutagenic potential of doughnut

extracts was also evaluated using *S. typhimurium* His⁻ and *E. coli* Trp⁻ tests. The five dose levels assayed for these sample extracts were between 1.25 and 20 mg sample equivalent/plate in all cases. Representative results of this part of the study are reported in the Figures 1–3 as reversion rates, which represent the total number of revertant colonies at a dose of 20 mg of doughnut extract per plate divided by the number of revertant colonies appearing for the negative DMSO control. Under this treatment of data, ratios greater than the numerical value of two are indicative of a mutagenic response. However, to determine if each sample extract was or not considered mutagenic the five doses tested were subjected to statistical analysis by using the SALM program, as indicated in Materials and Methods section.

Figure 1 show the reversion rate obtained with doughnut extracts along the period of study when *S. typhimurium* strain TA98 was used in the assay. Neither the control (lot 1) nor the bakery product packaged with one and two oxygen absorber sachets (lot 2 and lot 3, respectively) reached ratios greater than the numerical value of two, both with and without the addition of S9 fraction in the assay. The statistical analysis of the data obtained during the assays along the period studied confirmed the absence of mutagenic activity in all sample extracts analysed. No toxicity was evident at the higher doses tested, which was assayed at the maximum tolerated dose based upon its solubility limit in DMSO. In the same way, Figures 2 and 3 present data of reversion rates obtained for the sample extracts with strains TA100 and WP2*uvrA* pKM101, respectively. Again, it is shown that in no case the value of two was reached. Negative results were also obtained with TA1535, TA1537 y WP2*uvrA* (data not shown).

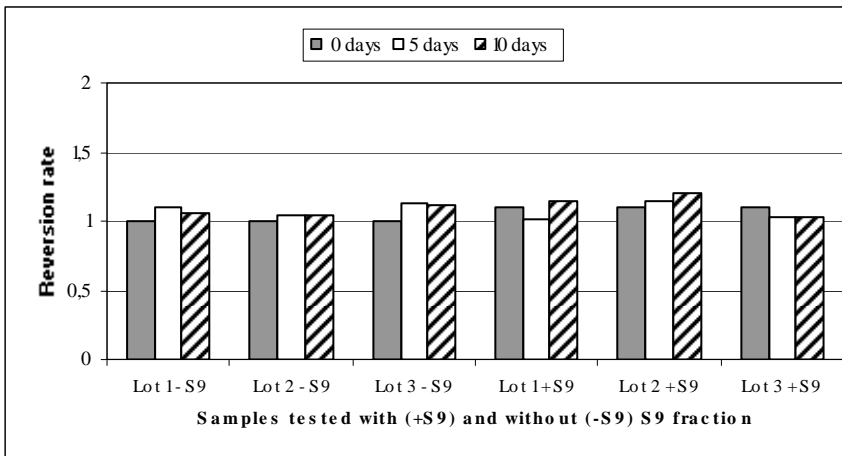


Figure 1: Reversion rates obtained for the doughnuts extracts in the mutagenicity assay with *S. typhimurium* strain TA98 in the presence and absence of S9 fraction at the higher dose assayed (20 mg/plate). Lot 1: doughnuts packaged without oxygen absorbers. Lot 2 and lot 3: doughnuts packaged with one and two oxygen absorbers, respectively.

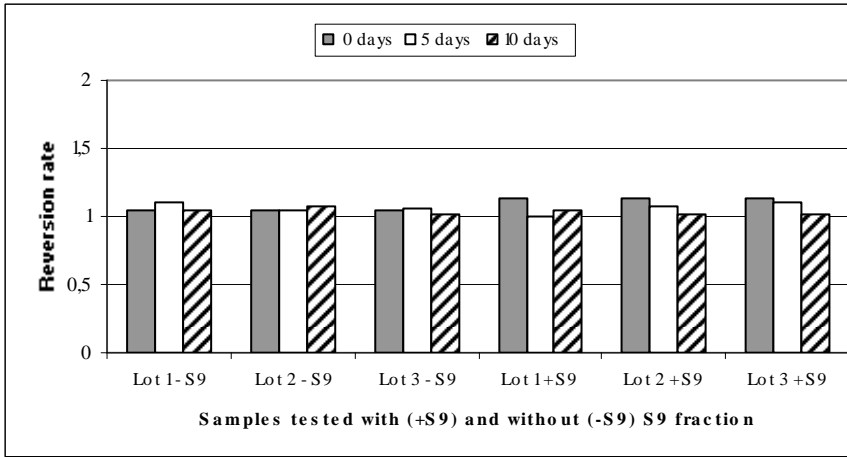


Figure 2: Reversion rates obtained for the doughnuts extracts in the mutagenicity assay with *S. typhimurium* strain TA100 in the presence and absence of S9 fraction at the higher dose assayed (20 mg/plate). Lot 1: doughnuts packaged without oxygen absorbers. Lot 2 and lot 3: doughnuts packaged with one and two oxygen absorbers, respectively.

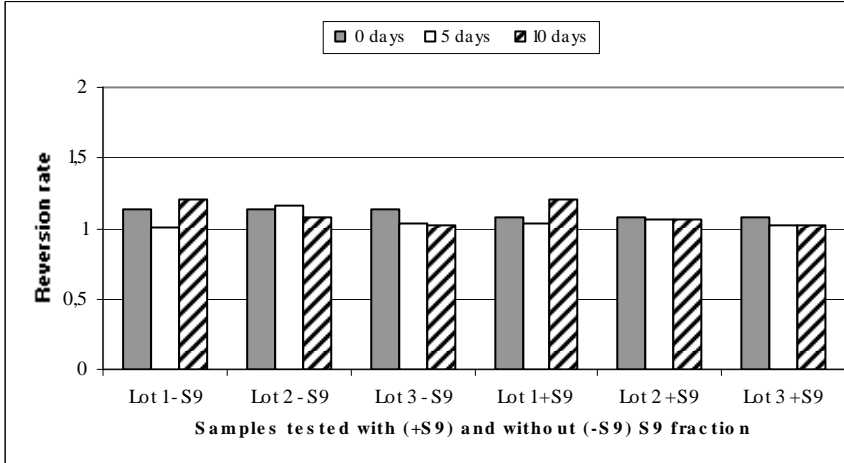


Figure 3: Reversion rates obtained for the doughnuts extracts in the mutagenicity assay with *E. coli* strain WP2uvrA pKM101 in the presence and absence of S9 fraction at the higher dose assayed (20 mg/plate). Lot 1: doughnuts packaged without oxygen absorbers. Lot 2 and lot 3: doughnuts packaged with one and two oxygen absorbers, respectively.

It can also highlight the lack of differences between the results obtained in the doughnuts packaged without oxygen absorbers (lot 1) and the use of one (lot 2) or two (lot 3) absorbers. These results support the safe use of this type of active packaging to extend the shelf life of commercial doughnuts because the interactions between the bakery product and the active packaged system (including the plastic package) did not represent a risk for the consumer health under the conditions tested. We consider that an important extension of the present work would include an examination for genotoxicity of these extracts in mammalian assay systems covering different end-points.

Acknowledgement

This work was partially funded by la Xunta de Galicia (PGIDT99PXI23701B and PGIDT00INN08E).

References

- [1] Galić, K., Ćurić, D., & Gabrić, D. Shelf life of packaging bakery goods. A review. *Critical Reviews in Food Science and Nutrition*. 49, pp. 405-426, 2009.
- [2] Vermeiren, L., Devlieghere, F., van Beest, M., de Kruijf, N. & Debevere, J. Developments in the active packaging of foods. *Trends Food Sci. Technol.* 10, pp. 77-86, 1999.
- [3] Rooney, M.L Active packaging in polymer films. *Active Food Packaging*, edited by M.L. Rooney (London: Blackie), pp. 74-110, 1995.
- [4] López-Cervantes, J., Sánchez-Machado, D.I. Pastorelli, S., Rijk, R. & Paseiro-Losada, P. Evaluating the migration of ingredients from active packaging and development of dedicated methods: a study of two iron-based oxygen absorbers. *Food Addit. Contam.* 20, pp. 291-299, 2003.
- [5] Regulation (EC) No 1935/2004 of the European Parliament and of the Council of 27 October 2004 on materials and articles intended to come into contact with food and repealing Directives 80/590/EEC and 89/109/EEC. *Official J. L* 338, pp. 4-17, 2004.
- [6] Regulation (EC) No 450/2009 on active and intelligent materials and articles intended to come into contact with food. *Official J. L* 135, pp. 3-11, 2009.
- [7] European Food Safety Authority (EFSA). Guidelines on submission of a dossier for safety evaluation by the EFSA of active or intelligent substances present in active and intelligent materials and articles intended to come into contact with food. *The EFSA Journal*. 1208, pp. 1-11, 2009.
- [8] Commission Regulation (EU) No 10/2011 on plastic materials and articles intended to come into contact with food. *Official J. L* 12, pp. 1-89, 2011.
- [9] Petersen, H., Biereichel, A., Burseg, K., Simat, T.J. & Steinhart, H. Bisphenol A diglycidyl ether (BADGE) migrating from packaging materials “disappears” in food: reaction with food components. *Food Addit. Contam.* 25, pp. 911-920, 2008.



- [10] Coulier, L., Bradley, E.L., Bas, R.C., Verhoeckx, K.C.M., Driffield, M., Harmer, N. & Castle, L. Analysis of reaction products of food contaminants and ingredients: Bisphenol A Diglycidyl Ether (BADGE) in canned foods. *J. Agric. Food Chem.*, 58, pp. 4873-4882, 2010.
- [11] Hotchkiss, J.H. Food-packaging interactions influencing quality and safety. *Food Addit. Contam.* 14, pp. 601-607, 1997.
- [12] Organisation for Economic Co-operation and Development. OECD Guidelines for the testing of chemicals, section 4: human effects. Test No 471: Bacterial mutation test. Available in http://www.oecd-ilibrary.org/environment/test-no-471-bacterial-reverse-mutation-test_9789264071247-en.
- [13] Maron, D.M. & Ames, B.N. Revised methods for the Salmonella mutagenicity test. *Mutat. Res.* 113, pp. 173-215, 1983.
- [14] Urios, A., Herrera, G. & Blanco, M. Detection of oxidative mutagens in strains of *Escherichia coli* deficient in the OxyR or Mut Y functions: dependence on SOS mutagenesis. *Mutat. Res.* 332, pp. 9-15, 1995.
- [15] Margolin, B.H. Kaplan, N. & Zeiger, E. Statistical analysis of the Ames Salmonella/microsome test. *Proc. Natl. Acad. Sci. U.S.A.* 78, pp. 3779-3783, 1981.
- [16] Kim, B.S. & Margolin, B.H. Statistical methods for the Ames Salmonella assay: a review. *Mutat. Res.* 436, pp. 113-122, 1999.
- [17] Smith, J. P., Ramaswamy, H. S. & Simpson, B. K. (1990). Developments in food packaging technology. *Trends Food Sci. Technol.* 1:112-119.



Section 6

Occupational health

This page intentionally left blank

Work conditions and occupational morbidity in Latvia

M. Eglite¹, I. Vanadzins¹, L. Matisane², M. A. Bake¹, D. Sprudza¹, Z. Martinsone¹, I. Martinsone¹, J. Reste¹, J. Cirule¹ & A. Seile¹

¹*Institute of Occupational Safety and Environmental Health of Riga Stradins University, Latvia*

²*Inspecta Prevention, Latvia*

Abstract

The aim of study was to analyse work conditions and occupational morbidity in Latvia during a 15-year period for recommendations to employment policy programmes. The study included the analysis of the database of occupational risk factor measurements in more than 7000 enterprises and companies performed in period 1995–2010 by the Laboratory of Hygiene and Occupational Diseases of the Institute of Occupational Safety and Environmental Health of Riga Stradins University. The analysis of registered occupational diseases according to the data from the Latvian State Registry of Occupational diseases run by the Centre of Occupational and Radiation Medicine of Pauls Stradins Clinical University Hospital for the same period was performed. Occupational diseases in Latvia are diagnosed and coded in accordance with the International Classification of Diseases.

Results of measurements showed that for one third of measured occupational risk factors values exceeded recommended limits. The traditional work risk factors (chemical, physical, biological etc.) have been partly replaced by new risks (ergonomic and psychosocial factors). The results of the study indicated that the following enterprises form a major risk group of non-compliance with legislation regarding occupational health and safety: small enterprises; enterprises of private and non-governmental sectors; enterprises of different industries (construction, metal processing and wood processing). The number of firstly diagnosed occupational diseases and patients has gradually increased. The total number of firstly diagnosed and registered occupational patients per 100,000 employees was 11.2 in 1995 and 140.5 in 2009. The structure of



occupational diseases shows musculoskeletal diseases (46.1%) as the leading group of diseases followed by diseases of the nervous system and organs of sense (29.3%), traumatic disorders and intoxications (11.7%).

Keywords: work risk factors, occupational morbidity, structure of occupational diseases.

1 Introduction

The rapidly changing living environment is closely related to changes in work environment – work becomes more intense and requires maximum attention and concentration, adaption of work with mental and physical capacity of an individual, as well as dealing with different managerial issues [1]. Occupational risk factors occur in all economic sectors and can affect large numbers of employees. Work makes our life reasonable, ensures our independency, affects mental and physical health and facilitates social welfare, however the work environment has a significant impact on the biological processes in the human body and, thus, can directly affect the safety, health and work ability of employees [2]. The health consequences of occupational risk factors, new technologies, unknown effects of existing technologies, create reasons for concern among the working population and people professionally involved in work and health.

It is impossible to maintain a working environment without any risk factors, therefore, reduction and control of risks is a main responsibility of every employer. The occurrence of health effects is often the first indication of occupational risks.

The aim of the study – to analyse work conditions and occupational morbidity in Latvia during a 15-year period for the characterisation of the general situation in the occupational health and safety system in Latvia and for recommendations to changes in employment policy programmes.

2 Materials and methods

The database of measurements of occupational risk factors in more than 7000 enterprises and companies performed in the period 1995–2010 by the Laboratory of Hygiene and Occupational Diseases of the Institute of Occupational Safety and Environmental Health of Riga Stradins University was analysed. The Laboratory is accredited for measurements of risk factors according to LVS EN ISO/IEC17025. The database comprises the assessment of 11 physical risk factors in 30,082 workplaces.

The following risk factors were most frequently measured: the noise level was measured in 4480 workplaces (according to 4 different parameters: 8h mean equivalent noise level, maximum noise, peak sound pressure, equivalent noise level); whole-body vibration – measurements were carried out in 1145 workplaces and hand-arm vibration measurements of 582 workplaces; microclimate (indoor air), including ventilation assessment were performed in 11,483 workplaces (4 different parameters: relative air humidity – in 3729



workplaces, air temperature in 3782 workplaces, air velocity – in 36,505 workplaces, ventilation in 322 premises); lighting – in 12,392 workplaces.

The database also comprises wide-ranging information on chemical substances – altogether 93 chemical substances (e.g., organic solvents in varnish, paint, synthetic detergents) and aerosols of dust (e.g., welding fumes, abrasive dust, wood dust) are included in the database, measurements of which were carried out in more than 5000 workplaces. Various ISO methods and modern measuring equipment were used, such as the detection of concentration of solvents and organic compounds in the working environment were performed using the gas chromatograph Varian 3800 with FID and ECD detectors and measurements of metals were done using the atomic absorption spectrophotometer (Varian Spectra AA) with graphite furnace and electrothermal atomisation with Zeeman background correction).

Altogether, organic solvent measurements were made in 2679 workplaces, in the breathing zone of worker, by using individual sample taking devices. The occupational exposure measurements of organic solvents were carried out in 290 companies and their branches of 22 sectors of economy (company codes according to NACE classification) [3]. To get more representative information, the measurements of occupational exposures of 30 organic solvents that are included in the database are analysed, joining them on the basis of similar structure in 8 groups: aromatic hydrocarbons, summary hydrocarbons, esters, ketones, petroleum distillates, celosolves, halogen hydrocarbons and alcohols.

For the assessment of probability of health risk caused by the occupational exposure to a chemical factor in the working environment, the exposure index (EI) is being used, which shows the degree of occupational exposure of a chemical substance and at the same time provides information on the probability of the effect of a chemical substance on workers' health [according to EN 689]. The exposure index is determined relating the actual concentration of chemical substance in the working environment to the occupational exposure limit value set out in the legislation for each substance (OEL). By applying the exposure index one can carry out an assessment of joint exposure risk of different chemical substances irrespective of their individual numerical values.

The exposure indexes of chemicals with low, medium and high exposure degrees are divided into three groups/classes. The first group with the exposure index less than or equal to 0.1 shows a low exposure probability of chemical substance. The second group ($0.1 < EI \leq 0.75$) shows a medium exposure probability. The third group ($EI > 0.75$) reflects a high exposure probability.

The following risk factors were assessed also: biologic factors (e.g., organisms causing tick-borne encephalitis, viral hepatitis B and C, HIV/AIDS); mechanic factors (e.g., work with equipment and with dangerous equipment, work at height, work in an explosive atmosphere); ergonomic factors (e.g., awkward posture, repetitive movements, lifting of heavy objects); psychosocial factors (e.g., shortage of time, overtime work, work at night, bad relationships with superiors and colleagues, conflicts).

The analysis of registered occupational diseases according to the data from the Latvian State Registry of Occupational Diseases run by Centre of



Occupational and Radiation Medicine of Pauls Stradins Clinical University Hospital for the same period was performed.

The term “occupational disease” in Latvia is defined as follows: Occupational diseases are diseases characteristic to certain categories of employees, which are caused by physical, chemical, hygienic, biological and psychological factors in the working environment. Occupational diseases in Latvia are diagnosed and coded in accordance with the International Classification of Diseases. Currently, the effective classification in Latvia is the 43rd International Statistical classification of Diseases and related Health Problems (ISC-10), which is confirmed with the decree No. 20 of January 17, 1996 of the Ministry for Welfare of Republic of Latvia. This classification has been adopted in Latvia without modifications, which allows for the comparison between countries.

The work analysed the absolute number of first time registered occupational diseases patients, as well as the absolute number of initially registered occupational diseases. In order to characterise the rate of cases of occupational diseases in dynamics, the sickness incidence ratio was used – cumulative incidence (CI). It is a quotient, which is calculated according to the following equation: $CI = \frac{\text{the number of persons suffering from occupational diseases as a first time occurrence within 1 calendar year}}{100,000 \text{ of the employed in Latvia at the beginning of the year}}$. Absolute numbers of new cases of occupational diseases were recalculated per 100,000 employees for adequate comparison of occupational morbidity in Latvia with that of other EU Member States.

The statistical processing of the study results was implemented by employing SPSS 14.0 software (company SPSS Ltd., USA). In the statistical data analyses, adequate methods were used [4].

3 Results

3.1 Analysis of database of measurements

Analysis of measurement database of the Hygiene and Occupational Diseases Laboratory of the Institute of Occupational and Environmental Health of the Riga Stradins University helped to assess compliance of the measured values with mandatory or recommended standards summarised in fig. 1. As reflected, more than one third of measured values of most occupational risks exceeded mandatory or recommended limits (norms). According to the database of work environment measurements, improper microclimate (inappropriate air temperature, too low or too high relative air humidity, as well as too low or too high air movement) should be considered as the most problematic issue. Bad microclimate itself causes neither occupational diseases, nor workplace accidents. However, it negatively affects subjective condition and work ability of employees, thus decreasing quantity and quality of the performed job, and could aggravate already prevalent diseases. For example, draught can worsen the course of musculoskeletal disorders. An inappropriate microclimate is mostly found in offices with bad air exchange and insufficient ventilation, in outdoor sheltered and semi-sheltered workplaces, as well as in workshops having



draught. Another essential occupational risk according to the database is dust, especially abrasive dust caused by abrasive tools (e.g., polishing equipment) and welding fumes.

More than a third part of the analysis of physical factors – vibration (36%), noise (44%), and lightening (46%) do not conform to corresponding mandatory or recommended values, fig. 1.

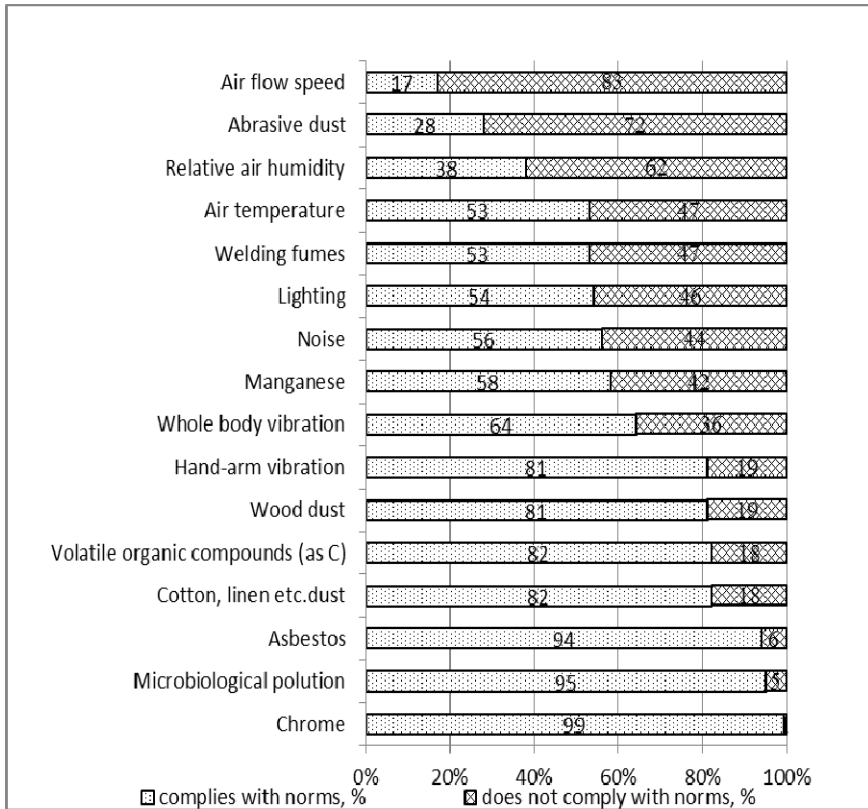


Figure 1: Compliance of occupational risk factors with norms or recommended standards (% of carried out measurements) in Latvia in the period 1995–2009.

The results of measurements on organic solvent groups showed that toluene, xylenes and benzene were the common pollutants (47% of measurements). 19% of measurements consist of determined aliphatic hydrocarbons as the sum calculated according to the amount of carbon mg/m^3 . Widespread alcohols from measurements were isopropanol, butanol and ethanol. In the 240 measurements of esters butyl acetate, ethyl acetate and methyl acrylate were predominating. The petroleum distillates were represented mostly by white spirit (lackbensin) or ligroin (a saturated hydrocarbon petroleum fraction) – 195 measurements. 75%

of measured halogenated hydrocarbons in the working environment were perchloroethylene in dry cleaning offices. The number of measurements of assessed workplaces for solvents according to the exposure indexes group (low, medium and high) is presented in table 1. The results show that 18% of measured solvents have high exposure levels (exposure index > 0.75).

Table 1: Number of measurements of assessed workplaces for solvents in definite (low, medium and high) exposure indexes group.

Solvent group	Exposure index		
	low	medium	high
Aromatic hydrocarbons	435	132	76
Cellosolves	36	9	28
Esters	89	37	14
Halogen hydrocarbons	12	17	74
Ketenes	77	11	4
Petroleum distillate	58	62	20
Alcohols	162	68	33
Summary hydrocarbons	146	114	76
Total	1015	450	325

The analysis of results of occupational exposure measurements of organic solvents carried out in different sectors according to NACE classification expressed by exposure indexes are presented in table 2.

The highest level of exposure indexes were revealed in these branches: leather processing and production of leather articles (74%), public, social and individual services (dry cleaning – 70%), manufacturing of equipment, mechanisms and machine tools (29%).

The traditional work risk factors (chemical, physical, biological) have been partly replaced by new risks (ergonomic – e.g. handling of heavy objects, awkward postures, work with computer, repetitive movements, psychosocial factors – e.g., shortage of time, overtime work, long working hours, conflicts). The analysis showed that improper indoor air quality also should be considered as a significant occupational problem. The results of the study indicated that the following enterprises form a risk group of non-compliance with legislation regarding occupational health and safety: small enterprises; enterprises of private and non-governmental sectors; enterprises of different industries (construction, metal processing and wood processing).

3.2 Occupational morbidity

Dynamics in morbidity with occupational diseases in Latvia during the period from 1996 till 2010 characterize the general situation in the occupational health and safety system in Latvia.



Table 2: Occupational exposure measurements (%) of organic solvents carried out in sectors of national economy (company codes according to NACE classification) expressed by classes of exposure indexes (EI).

NACE code	Type of economic activity	Number of measurements by classes of EI (%)		
		low	medium	high
A	Forestry, timber preparation and related services	60	40	0
DA	Foodstuff, beverage and tobacco production	50	50	0
DB	Textiles production	100	0	0
DC	Leather processing and production of leather articles	26	0	74
DD	Production of timber and wood articles	61	35	4
DE	Publishing and printing industry	65	23	12
DG	Production of chemical substances and chemical fibres	68	28	4
DH	Production of rubber and plastic material articles	40	34	26
DI	Production of non-metallic mineral articles	100	0	0
DJ	Production of metal and metal articles	59	30	11
DK	Manufacturing of equipment, mechanisms and machine tools	28	43	29
DL	Manufacturing of electric and optical equipment	62	19	19
DN	Furniture production	71	22	7
E	Power, gas and water supply	56	25	19
F	Construction	50	27	23
G	Repair of motorcars, motorcycles, household equipment and devices	57	22	21
I	Transport, rescue and communication	48	29	23
J	Financial mediation	0	100	0
K	Real estate transactions, lease, computer services, science and other commercial services	75	18	7
L	Public administration and defence; mandatory social insurance	75	18	7
N	Health and social care	59	28	13
O	Public, social and individual services	20	10	70



The number of occupational diseases and patients revealed for the first time during a year has been gradually increasing since 1996 until 2009. In 2010 there was a slight decrease in occupational morbidity connected with organisational reasons and changes in the registration system. The total number of firstly diagnosed and registered occupational patients per 100,000 employees was 11.2 in 1996 and 138.6 – in 2009, fig.2.

The number of first time patients in 2009 exceeded that of 1993 by 12 times, but the number of first time diagnoses – by 14.8 times.

In Latvia chronic forms of occupational diseases are most common. On very rare occasions acute or sub-acute cases of occupational diseases or chronic occupational diseases in the initial stages have been recorded.

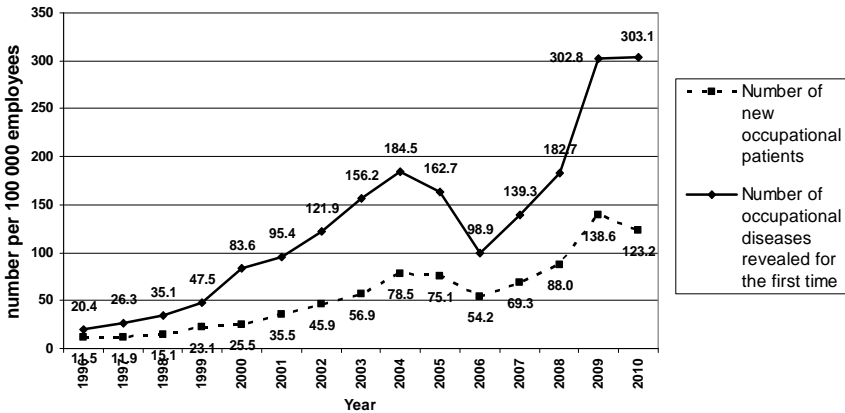


Figure 2: Total number of first time registered occupational diseases patients and occupational diseases in Latvia during 1996–2010 per 100,000 employees.

In Latvia quite often one occupational patient may have several occupational diseases caused by different occupational risks, fig. 3. For example, a carpenter may suffer from loss of hearing due to noise exposure and a respiratory disease due to dust exposure.

The structure of occupational diseases in 2009 shows musculoskeletal diseases (46.1%) as the leading group of diseases followed by diseases of the nervous system and organs of sense (29.3%) and traumatic disorders and intoxications (11.7%).

Similar to the situation worldwide, the structure of occupational diseases in Latvia has changed during 1993 and 2010. Since 1999 there was an increase in morbidity of diseases caused by physical overloads, such as musculoskeletal and connective tissue disorders, as well as carpal tunnel syndrome, but the occurrence of occupational diseases caused by chemical substances and dust has decreased.

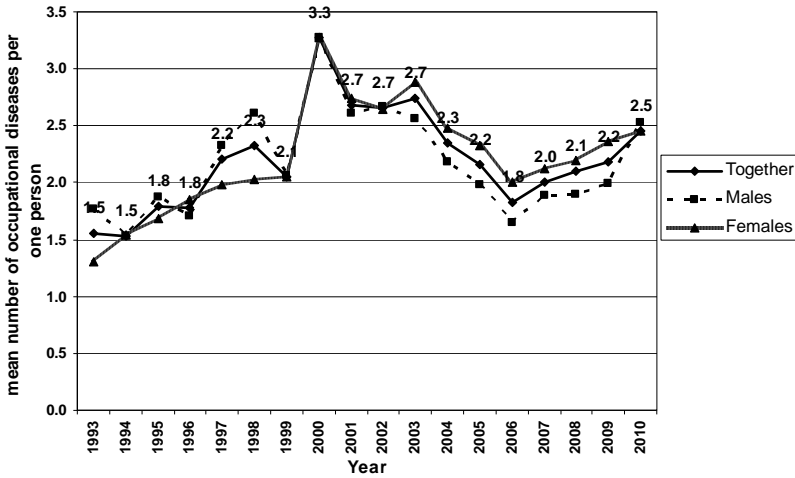


Figure 3: Mean number of occupational diseases per person.

In Latvia musculoskeletal and connective tissue disorders (ICD-10 code M00-M90) and carpal tunnel syndrome (ICD-10 code G560) are included in the list of occupational diseases caused by physical overloads (several types of so called ergonomic problems, including the lifting of heavy objects, awkward postures, repetitive movements etc.). The number of certified occupational physicians has increased in the last ten year period as well as the number of compulsory health examinations carried out has increased.

4 Discussion

The number of occupational diseases and patients revealed for the first time during a year has been gradually increasing since 1993 until 2010. This is only partly related to the current working environment. Many of the currently revealed health problems are still associated with exposure to occupational risk factors during the last 10–15 years. Supposedly, during the next 5 to 10 years the number of occupational diseases will still continue to grow reaching 250 cases per 100,000 employees. Then, stabilization and even a gradual, slight decrease are expected. Besides, the breakdown of occupational diseases by types has changed. At present musculoskeletal diseases are the most frequently diagnosed occupational diseases, building up to approximately one half of all registered diseases. This group of diseases requires special attention; therefore, it is necessary to build awareness of employers on ergonomic risks of the work environment.

There is a traditional opinion that in Latvian enterprises conventional occupational health problems, such as noise, vibration, dust, chemical substances etc., prevail while EU countries mostly deal with psychosocial, managerial and ergonomic risks. Information obtained during the study shows that at present



psychosocial factors and ergonomic factors are one of the most essential occupation risk factors in Latvia too. It means that conventional risk factors are substituted by modern ones. On the other hand, laboratory analysis shows that microclimate and dust (especially abrasive dust and welding fumes) should be considered as significant occupational problems. Taking into account that psychosocial and ergonomic risk factors, as well as microclimate, usually interfere with each other and even intensify the effects of one another, this group of factors should be treated with great care [1, 5, 6].

Measurements of the work environment are not carried out frequently enough. As a result, in most cases occupational risk assessment cannot be considered as being objective. The results of the study show that work environment measurement values exceed mandatory or recommended limit values in one third of cases. It could be explained by the fact that measurements are not carried out in all workplaces, but only in those indicated by the Client (for example, employer, competent specialist or competent authority), and, thus, the most “dangerous” or “hazardous” workplaces are selected

The Latvian State Occupational Diseases Registry mainly contains chronic forms of occupational diseases, which have developed within many years and do not correlate with exposure duration. Therefore, it can be assumed that an increase of occupational morbidity in Latvia is related not only to working conditions but to other factors too. The following other factors could be mentioned: for many years occupational morbidity in Latvia was lower than that of other EU states; therefore, it is probable that due to improved diagnosis and registration of occupational diseases the number of cases registered for the first time will still grow. However, considering amendments in legislation, it is hard to forecast the onset and speed of such an increase in the future. Employees become more aware of occupational risks and signs of occupational diseases; more and more employees are informed on the possibilities of receiving financial support in the case of occupational diseases.

The number of certified occupational physicians has increased and most probably the knowledge of physicians has improved as well. The number of compulsory health examinations carried out has probably increased.

Musculoskeletal diseases are a particular issue, and, according to the data of the Centre of Occupational and Radiation Medicine of Pauls Stradins Clinical Hospital, they belong to the most frequently found occupational disorders in Latvia. One should remember that musculoskeletal diseases are the so called “painful diseases”, which often have only short-term effects on working ability. On the other hand, the study reveals that ergonomic risk factors, which cause musculoskeletal problems, prevail in the working environment.

Supposedly, during the next 5 to 10 years the number of occupational diseases will still continue to grow, reaching 250 cases per 100,000 employees. Then, stabilization and even a gradual, slight decrease are expected. Nevertheless, due to amendments in legislation regarding the procedure of occupational diseases diagnostics, the number of occupational diseases could decrease during the next two to three years and after that increase again. This prognosis considers the maximum number of registered occupational diseases in



European Union countries during the last 15 to 20 years and the situation in Latvia, where occupational risk is still rather high (thus, the development of new occupational diseases are expected), the awareness level of employees is rather low (information of employees would raise their awareness on occupational diseases diagnostics and financial compensations) and diagnostics of occupational diseases will continue to improve [6].

Occupational morbidity in Latvia is considered coherent to occupational morbidity registered in other European countries. It should be noted that, during recent years, occupation morbidity tends to decrease in developed EU countries, while it is still increasing in Latvia. Working conditions in the European Union in general are improving and correspondingly lead to decreased occupational morbidity rates. However, in Latvia improved diagnosis of occupational diseases still outpace improvement of working conditions. The situation in Russia can be compared to that of Latvia in 1996 with no improvements in diagnostics.

5 Conclusions

1. Results of the study reveal that the following enterprises are in the at risk group of non-compliance with legislation regarding occupational health and safety, as well as legal labour relations: small enterprises; enterprises of private and non-governmental sectors; enterprises of different industries.
2. Results of measurements showed that one third of measured risk factors values exceed mandatory or recommended limits but the situation has improved in recent years. The results of surveys reveal insufficient assessment of risk factors in workplaces and the selection of the most hazardous or common ones only. However, occupational risk assessment is frequently carried out formally and disregarding legal requirements.
3. The traditional work risk factors (physical, chemical, biological) have been replaced with new ones risks (psychosocial – shortage of time, overtime work, long working hours; ergonomic – work with a computer, handling of heavy objects, awkward posture, and repetitive movements, microclimatic) in Latvia today.
4. The number of occupational diseases and patients revealed annually for the first time has been gradually increasing. The increase of registered occupational diseases is also related to growing awareness of employees, an increasing number of occupational physicians, as well as the possibility to receive monetary compensation.
5. Early diagnosis of occupational diseases during compulsory medical examinations is essential. This will reduce the necessity for compensations from the Special Budget for workplace accidents to be paid in the case of permanent loss of work ability. To facilitate returning of employees into the labour market after occupational illnesses, the focus should be switched to effective rehabilitation.
6. The study indicates that there is a need to improve occupational health and safety legislation, as well as a system for explaining such legal requirements



and building public awareness; to elaborate several occupational health and safety papers.

References

- [1] Kauppinen, T., Hanhela, R., Heikkilä, P., Kasvio, A., Lehtinen, S., Lindström, K., Toikkanen, J., Tossavainen, A. Work and Health in Finland. In: *Changes in work and working conditions in 1997–2006*, 2006. [http://www.ttl.fi/Internet/English/Information/Electronic publications/ pdf](http://www.ttl.fi/Internet/English/Information/Electronic%20publications/pdf).
- [2] Riedman, A., Bielenski, H., Szczurowska, T., Wagner, A. European Foundation for the Improvement of Living and Working Conditions, *Working Time and Work Life Balance in European companies*: Dublin, 70 p. 2006.
- [3] Glossary: Statistical classification of economic activities in the European Community (NACE) [http://epp.eurostat.ec.europa.eu/ statistics_explained/ index.php](http://epp.eurostat.ec.europa.eu/statistics_explained/index.php)
- [4] Altman, D.G. *Practical statistics for medical research*. Chapman and Hall: London, 606 pp. 2003.
- [5] Rantanen J., Kauppinen T., Lehtinen S., Mattila M., Toikkanen J., Kurpa K., Leino T. *Work and health country profiles of twenty two European countries*. Finnish Institute of Occupational Health: Helsinki, 444 p, 2002.
- [6] Rantanen J., Kauppinen T., Toikkanen J., Kurpa K., Lehtinen S., Leino T. Work and health country profiles and national surveillance indicators in occupational health and safety, In: *People and Work. Research Reports 44*. Finnish Institute of Occupational Health: Helsinki, 2001.



Occupational exposure to volatile organic compounds in the Portuguese printing industry

S. Viegas

*Escola Superior de Tecnologia da Saúde de Lisboa,
Instituto Politécnico de Lisboa (ESTeSL/IPL) CIESP,
Centro de Investigação e Estudos em Saúde Pública,
Escola Nacional de Saúde Pública,
Universidade Nova de Lisboa, Portugal*

Abstract

In the printing industry, volatile organic compounds main sources are the uses of organic solvents, fountain solutions and cleaning agents.

Nowadays, one circumstance which might confuse the exposure reality is that the majority of solvents which are often used have a faint odour. Therefore, the conditions at offset printing in regard to solvent exposure may seem acceptable to workers. Fortunately, general ventilation and local exhaust systems have also become more common, and new printing machines, often with automatic cleaning, have entered the market.

The health effects of volatile organic solvents are dependent on the chemicals involved but, normally, are associated with affecting the nervous system, the liver and also the kidneys.

The purpose of this study was to document the conditions regarding exposure to volatile organic compounds in an offset printing unit and to permit identify task with higher exposure and with priority for preventive measures application.

Exposure assessment was done before and after installation of general ventilation and local exhaust equipments and during printing and cleaning procedure. It was use portable VOCs measurement equipment with real-time measurements (MultiRAE, RAE Systems model) that allowed identify task with higher exposure.

The need and appropriateness of ventilation introduction is measured by the significant statistically difference ($p < .001$) in the concentration results before



and after installation, in ppm (Before: Mdn 50.1; St. Deviation 16.9; Min. 8.4; Máx. 85.5 / After: Mdn 11.2; St. Deviation: 7.2; Min. 0.3; Máx. 31).

The results of this study indicate that, actually, the most important source of volatile organic compounds exposure in this printing industry is the cleaning product and, probably, the conditions how this activity is develop promote exposure.

Keywords: volatile organic compounds, printing industry, occupational exposure, ventilation dispositive.

1 Introduction

Solvents are complex chemical mixtures containing many different hydrocarbon types, such as alkanes, alcohols, ketones, aldehydes, esters, ethers, and small aromatic molecules that evaporate and become incorporated into environmental air as volatile organic compounds (VOCs) [1].

In the printing industry, the main sources of VOCs are the use of organic solvents, inks, fountain solutions and, also, cleaning agents. Therefore, considerable amounts of vaporized toluene, xylenes, alcohols, and other airborne organic compounds are emitted to the indoor air [2].

Besides printing others processes and operations may cause serious VOC emissions, namely proofing, ink mixing, cleaning, binding, laminating, and chemical storage. Previous studies have reported occupational exposure to various VOCs during all these operations [2–6].

Since the late 1970s the use of organic solvents in the printing industry has been linked to acute intoxication and decreased performance in behavioural tests [3]. Evidence has also indicated a close relation between occupational VOCs exposure and consequential adverse health effects on workers in the printing industry in many countries [1–4, 7, 8]. Health effects include impairment of colour vision, liver dysfunction, hyperglycemia, some neurological symptoms, and cancers [2].

Meanwhile, since the early 1980s the printing industry has made efforts to reduce the exposure to VOCs [5]. Toluene, xylene and chlorinated hydrocarbons have been replaced by paraffins and cycloparaffins with high boiling points, and to some extent with water-based solvents and terpenes. However, despite these improvements, exposure to VOCs is still present in the printing industry [3].

The main purpose of this study was to understand the exposure conditions regarding VOCs in one offset printing unit before and after ventilation equipment installation. Additionally, more than comparing with reference values, the intention was to identify the task with higher exposure and, consequently, with priority for preventive and protective measures application.

2 Materials and methods

A printing facility located in south of Portugal was studied during four years. In order to obtain the details of occupational VOCs exposure in the industrial unit, field VOCs measurements were conducted in 27 measurement points during



printing (near printing machines) and in 1 point during printing machine cleaning. During the four years, two assessments were performed; first assessment was done before ventilation equipment installation and, the second, after installation of general and located ventilation.

In this research, real-time measurements of VOCs concentrations were performed using portable equipment ((MultiRAE, RAE Systems model – calibrated by isobutylene). The detection technique used in this equipment is Photo Ionization Detection (PID) (with 10.6 eV lamp). The use of this equipment permitted to identify worst case scenario (peak concentrations) concerning to VOCs exposure.

The PID equipment was zeroed outside the industrial unit in fresh air prior to start measurements. All measurements were done in the breathing zone of workers while they were performing their tasks, during 5 to 15 minutes. It was consider the highest concentration obtained in each measurement point. Only two tasks were studied, namely printing (before and after ventilation installation) and cleaning operations (only after ventilation installation).

Concerning statistical analysis, non-parametric Mann-Whitney U-test was used to evaluate differences between the two conditions, namely before and after ventilation equipment installation. Previous to that, deviation of variables from normal distribution was evaluated by the Kolmogorov-Smirnov test.

Data statistical analysis was performed with SPSS for Windows statistical package, version 17.0 for Windows® of Microsoft International®.

3 Results

The ventilation device adopted was designed by several hoods placed over the area of cylinders of the three printing machines existed in the printing facility (local ventilation). In addition three exhausted ventilation equipment were installed near the roof of the unit (general ventilation).

The results obtained during the two environmental monitoring actions (before and after installation of ventilation) revealed, in all measurement points, lower values after installing ventilation devices (on average, 9 times less). Before installation, concentration results varied between 20 ppm and 85 ppm. After ventilation installation, results varied between 0.3 ppm and 28 ppm (Table 1).

Statistical tests demonstrated that results obtained before ventilation installation ($Mdn = 50.1\text{ppm}$) were significantly different from results after installation ($Mdn = 11.2\text{ ppm}$), $W = 407$, $z = -5.81$, $p < .001$.

Concerning the task with the higher peak concentration, cleaning operation obtain highest value (146.6 ppm) even after ventilation devices installation. This operation was studied in normal conditions, namely with disconnected ventilation and without protective masks and gloves, considering that chemical absorption can occur by inhalation but, also, by dermal exposure. We have also to consider that frequency of doing this task depends on production exigencies.



Table 1: Results of VOCs concentration during printing.

Measurement point	Before ventilation installation (ppm)	After ventilation installation (ppm)
1	60	31.0
2	85	16
3	51.2	11.5
4	51.2	12.3
5	51.2	12.7
6	55	12.8
7	42.5	11.2
8	39	10.8
9	51.8	11.6
10	51	10.1
11	51.6	10.2
12	50	11
13	50.6	11.6
14	50.6	12
15	50.1	12
16	48.8	10.3
17	49.5	11.3
18	49	4.2
19	8.4	0.9
20	20.1	0.3
21	85	28
22	51.6	11
23	32	0.7
24	24.9	5.2
25	24.3	5.4
26	24.1	5.4
27	42	23.8
Stand Deviation	16.5	7.1



4 Discussion

Study developed not intent to obtain results to compare with reference value since there are no available specific exposure criteria for VOCs due to their different composition, depending basically of the emission source (paints or cleaning products for instance) and task performed.

Nevertheless, measurement of VOCs concentration in two different moments permitted, in this case, to assess protective measures efficacy (ventilation equipment). Obtained results demonstrate the ventilation importance in chemical exposures reduction, also confirmed in other similar studies, namely Ryan et al. [5] and Leung et al. [2].

In addition, in this research, the cleaning process was identified as the task with higher peak concentration, contributing to the increase of short-term workers exposure. Studies developed in the same occupational setting obtained similar results, indicating higher exposures in the cleaning process [2–4, 6, 9]. Moreover, this task is performed without ventilation and, therefore, VOCs can also be present after the cleaning and result in an overall increased VOCs level that can possibly promote the exposure of workers that are not involve in this task [4].

This study illustrates that worker in this industry use aerosol cleaning products under uncontrolled conditions. As a consequence, they receive an inhalation dose of VOCs during each cleaning action. However, in the case of cleaning actions, some factors have to be consider because can influence exposure, namely the distance from breathing zone to the surface (generally the cartridges of the printing machines) that depends of the length of the workers arms and the way of task performing; the vapor pressure of solvents used, which are normally high; and the air change rate near the breathing zone, which is minimal in the absence of ventilation working.

Peak exposures, intense exposures of short duration, are a special concern because the high concentration produces a high dose rate into the body and target tissue, which may alter metabolism, overload protective or repair mechanisms, and amplify tissue responses. As a result, a peak can produce more and different effects than the same administered dose given with less intensity over a longer time period [10–12]. Therefore, knowing the task with higher peak concentration is extremely important to define priorities for the appliance of preventive and protective measures.

Furthermore, development of real-time measurements offers the possibility of defining exposure distributions on time scales relevant to directly relate performance with exposure. This kind of measurement resource is well describe in a study performed by Viegas et al. [13] that also permitted to identify the tasks that involve higher peak exposure to formaldehyde in ten pathology and anatomy laboratories and one formaldehyde-based resins production factory [13].

VOCs characterization was not possible but, normally, one of the most present chemicals in this occupational setting is isopropanol [3]. Isopropanol has a known effect on the central nervous system and is irritating to mucous membrane. Moreover, when used in combination with chlorinated solvents, also



presented in the printing industry, isopropanol reinforces their effect on the liver [3]. Considering that recommend limit concentration for short-term exposures in Portuguese Norm 1796 (2007) is 400 ppm, none of the obtain results were above this reference value [14]. Meanwhile, and because we are dealing with exposure to a mixture of chemicals, risk assessment have to consider possible synergetic or additive effects in workers health.

5 Conclusions

Considering to preventive measures is important to use low-VOC paints in the printing industry but also, and take into account that cleaning operation obtains the highest peak concentration, low-VOC and low-toxicity cleanup products.

Also, in this study, was possible to demonstrate the importance of ventilation devices for reducing exposure to VOCs and, therefore, to protect workers health.

References

- [1] Mendoza-Cantú, A, Castorena-Torres, F, León, M, Cisneros, B, López-Carrillo, L, Rojas-García, A, Aguilar-Salinas, A, Manno, M, Albores, A, Occupational Toluene Exposure Induces Cytochrome P450 2E1 mRNA Expression in Peripheral Lymphocytes. *Environmental Health Perspectives*. 114 (2006) 494-499.
- [2] Leung, M, Chun-Ho, L, Han, A, Occupational exposure to volatile organic compounds and mitigation by push-pull local exhaust ventilation in printing plants. *Journal of Occupational Health*. 47 (2005) 540-547.
- [3] Svendsen, K, Rognes, K, Exposure to Organic Solvents in the Offset Printing Industry in Norway. *Annals of Occupational Hygiene*. 44 (2000) 119-124.
- [4] Wolkoff, P, Schneidera, T, Kildesoa, J, Degerthb, R, Jaroszewskic, M, Schunkd, H, Risk in cleaning: chemical and physical exposure. *The Science of the Total Environment*. 215 (1998) 135-156.
- [5] Ryan, T, Hart, E, M, Kappler, L, VOC Exposures in a Mixed-Use University Art Building. *American Industrial Hygiene Association Journal*. 63 (2010) 703-708.
- [6] Sutton, P, Wolf, K, Quint, J, Implementing safer alternatives to lithographic cleanup solvents to protect the health of workers and the environment. *Journal of Occupational and Environmental Hygiene*. 6 (2009) 174-187.
- [7] Muttray, A, Wolters, V, Jung, D, Konietzho, K, Effects of high doses of toluene on color vision. *Neurotoxicol Teratol*. 21 (1999) 41-45.
- [8] Kaido, T, Honda, Y, Kitamura, K, Association between liver dysfunction and hyperglycemia in Japanese male workers at printing and papermaking plants. *Journal of Occupational Health*. 44 (2002) 401-406.
- [9] Wadden, R, Scheff, P, Franke, J, Conroy, L, Javor, M, Keil, C, Milz, S, VOC Emission Rates and Emission Factors for a Sheetfed Offset Printing Shop. *American Industrial Hygiene Association Journal*. 56 (2010) 368-376.



- [10] Smith, T, Studying peak exposure: toxicology and exposure statistics. In: Marklund, S., ed. lit. – Exposure assessment in epidemiology and practice. Stockholm: National Institute for Working Life. (2001) 207-209.
- [11] Vyskocil, A, Thuot, R, Turcot, A, Peak exposures to styrene in Quebec fibreglass reinforced plastic industry. In: MARKLUND, S., ed. lit. – Exposure assessment in epidemiology and practice. Stockholm: National Institute for Working Life. (2001) 316-318.
- [12] Preller, L, Burstyn, I, De Pater, N, Characteristics of peaks of inhalation exposure to organic solvents. *The Annals of Occupational Hygiene*. 48 (2004) 643-652.
- [13] Viegas, S, Ladeira, C, Nunes, C, Malta-Vacas, J, Gomes, M, Brito, M, Mendonça, P, Prista, J, Genotoxic effects in occupational exposure to formaldehyde: A study in anatomy and pathology laboratories and formaldehyde-resin production. *Journal of Occupational Medicine and Toxicology*. (2010) 5-25. <http://www.occup-med.com/content/5/1/25>.
- [14] Instituto Português da Qualidade – NP 1796: 2007: segurança e saúde do trabalho: valores limite de exposição profissional a agentes químicos existentes no ar dos locais de trabalho. Caparica: IPQ, 2007.



This page intentionally left blank

Dioxins in remediation workers

C. Winder¹ & G. Smith²

¹*School of Risk and Safety Sciences, The University of New South Wales, Sydney, Australia*

²*AECOM, Gordon, NSW, Australia*

Abstract

A survey was conducted on workers involved in the remediation of a large, chemically contaminated site in Sydney, Australia. Workers were monitored for chlorinated dioxin and furan congeners in blood lipids over a two year period. Baseline levels of blood dioxins in workers starting at the site were similar to background dioxin levels in Australians (below 10 pg/g blood lipids). An action level of double the background levels (20 pg/g blood lipids) was used as an occupational health limit. As time progressed, blood lipid levels in workers increased, with the most likely source being exposure while working at the site. While levels of most congeners remain relatively even, most striking was the proportion of tetrachloro-congeners in exposed workers, which increased steadily. Worker exposure was above the action level in a small number of workers; these workers were transferred to other projects where the potential for dioxin exposure was absent. The role of congener profiling in occupational biological monitoring may provide additional information on workplace exposure to dioxins and related compounds.

Keywords: polychlorinated dioxins, worker exposure, environmental remediation, biological monitoring.

1 Introduction

The polychlorinated dioxins (CDDs) and furans (CDFs), are a group of materials that is often associated with wastes and waste disposal, and one particular member of this group, 2,3,7,8-tetrachlorodibenzo-*p*-dioxin (TCDD) is often incorrectly called “the most toxic chemical ever found” [1]. While 2,3,7,8-tetrachlorodibenzo-*p*-dioxin is the most toxic of the CDDs, the other CDD/CDFs also have varying toxicities, and the range of toxicities can differ by a factor of



10,000. Also, while there are a few CDDs and CDFs whose potency is well known, the toxicity of most are poorly characterised [2]. In addition, CDD/CDFs are most often found in mixtures of congeners rather than as single compounds in the environment. A shorthand method of assessing the toxicity of different mixtures of CDD/CDF congeners has been developed by comparing the toxicity of different individual congeners and homologues of CDD/CDFs to the toxicity of the most toxic congener, 2,3,7,8-TCDD. Using this system, a toxicity equivalence (TEQ) scale can be developed. By setting the toxicity of 2,3,7,8-tetrachlorodibenzo-p-dioxin arbitrarily at one, other CDDs and CDFs can be measured as the fraction of 2,3,7,8-tetrachlorodibenzo-p-dioxin's activity to the criteria [3]. The concentrations of CDDs and CDFs emitted from incinerator stacks can then be reported in terms of toxic equivalents (TEQ), or in terms of the known toxicity of 2,3,7,8-tetrachlorodibenzo-p-dioxin.

Most emission and environmental data post-1988 are generally reported solely as TEQs, as reporting total amounts of CDD/CDFs provides little data on toxicity. Reviews of the use of toxicity equivalency factors were published by the WHO in 1998 [4], and US EPA in 2000 [5]. These reviews conclude that the TEQ approach remains the most appropriate approach for estimating the toxicity of dioxin and furan mixtures.

Exposure to dioxins is predominantly in diet with 90-95% from this source. Well established foods with increased dioxin levels include dairy products, fish and meat. The risks to some groups of the population (for example breastfed babies) may be greater than can be predicted, because of increased relative levels of CDDs and CDFs in the diet of such individuals.

Dioxins have been reported to produce a number of health problems in humans. Workers exposed to high levels of dioxins develop a skin condition called chloracne, and workers exposed to very high levels of dioxins have a higher risk of developing cancers later in life. The available evidence suggests that 2,3,7,8-tetrachlorodibenzo-p-dioxin is a tumour promoter, not a tumour initiator [6-9]. Nevertheless, 2,3,7,8-tetrachlorodibenzo-p-dioxin is classified as a carcinogen [10-12].

Other studies at higher exposures show that dioxin exposure can lead to reproductive and developmental problems, increased heart disease and increased diabetes. Dioxin's ability to cause birth defects (teratogenicity) has not been established in humans but studies in mice have shown that dioxin and similar chemicals can produce congenital defects.

In 2002, the National Dioxins Program of the Australian National Medical Research Council (NHMRC) report that studies in dioxin dosed animals show effects on the immune system, nervous system, reproductive system, and during development. Workers exposed to high levels of dioxins develop a skin condition called chloracne, and workers exposed to very high levels of dioxins have a higher risk of developing cancers later in life. The NHMRC conclude: "However, the exact impact of dioxin on people's health is not yet known, and *there is currently no clear indication that dioxins are causing increased disease in the general population.*"



More critical is the dose response relationship for dioxins, and the possibility of establishing no effect levels and possibly recommendations for human exposure. Based on work of the National Dioxins Program of the Australian National Medical Research Council (NHMRC), and review of international evaluations of the WHO, US EPA, European Community and the Joint FAO/WHO Expert Committee on Food Additives, a tolerable monthly input (TMI) of 70 pg/kg body weight a month was proposed for use in Australia. This is equivalent to 4900 pg/person/month or 15 pg/person/day [13].

Based on a breath volume of 0.5 L, a respiratory rate of twenty breathes a minute; a person inhales about 11 m³ of air a day. Based on the NHMRC TMI of 15 pg/person/day, and adopting extremely conservative assumptions that all of this 15 pg is present in the air that a person inhales in a day, and assuming that all of the inhaled dioxin is absorbed, and assuming that there is no dioxin from any other source, a concentration of 15 pg/11 m³ calculates to a constant daily air concentration of about 1.4 pg/m³.

With regard to a value of a “normal” dioxin level, the Australian Government National Dioxins Program analysed dioxin levels in the over 9000 blood samples taken from Australian Population in 2004 [14]. Overall the levels in the Australian population are very low by international standards. The mean and median levels expressed as upper bound TEQ values for all pooled samples were 10.9 and 8.3 pg/g TEQ lipid, respectively. For males, and females the mean levels were 10.4 and 11.5 pg/g TEQ lipid, respectively. A direct relationship was also found of increasing dioxins in blood with increasing age, from about age 25, increasing from 6.2 at age 25 to 27.9 at 80.

Because of these phenomena, especially the age related changes, it is difficult to establish a baseline dioxin in blood level for use in Australia. However, from a practical perspective, the mean value reported in this study, of 10.9 pg/g blood lipids would seem suitable as a baseline level.

2 The site

The site was a former Chemical Manufacturing site in Sydney, first developed in the 1920's on a river embayment. A range of organic chemicals were manufactured for use in Australia, using local feedstocks (such as by-products from gas and coke processing at a nearby manufacturer to make wood preservatives such as creosote, and solvents, antiseptics, nitro-compounds and xanthates. By the 1940s additional chemicals manufactured for a large and rapidly growing agricultural sector included herbicides such as 2,4-D and 2,4,5-T and insecticides such as DDT. Further, factory and processing wastes from the manufacturing of these chemicals was used in land reclamation in nearby mangrove swamps along the embayment and produced substantial contamination of land. The company was purchased by a multinational company in 1955, and continued producing chemicals (and reclaiming land with its waste products) until 1985. The land reclamation activities were never fully documented and the scale of contamination is unknown but considered substantial. One problem was



the remediation carried out by the multinational company as it exited Australia in 1987 prior to vacating the site to an “industrial” (as opposed to a “residential”) standard. By the 1990s, the site had been vacated and the land had been cleared of built structures. However, the land was known to be contaminated and at the time, not suitable for residential development.

Migration of wastes off site had also occurred, with chlorinated wastes found in adjacent river embayment sediments and in marine organisms in the river. This resulted in a fishing ban being placed over the embayment in 1989 and downriver in 1990. As a result of leaching, sediments are heavily contaminated to a depth of one metre and stretch well out into the embayment.

By the mid 2000s, a decision was made to remediate the land. Part of this process was to process all the soil on the site through a thermal combustion facility. An Environmental Impact Assessment was prepared for the project, and an OHS program was developed for workers at the site, including risk assessments, training, and OHS risk controls. Baseline levels of dioxins in air, as stated in the 2002 Environmental Impact Statement for the project, was 0.1–2.5 pg/m³ TEQ. This is well within the suggested occupational exposure standard noted earlier, of 15 pg/m³ TEQ, although airborne levels of dioxins while remediation activities were being conducted are likely to be higher than this baseline.

Further, periodic blood dioxin monitoring was required of workers at the site. A benchmark blood dioxin level that was used as an action level for dioxin exposure was 20 pg/g TEQ blood lipids. This is about double the background level found in a survey of dioxin levels in Australians (10.9 pg/g TEQ blood lipids) carried out by the Commonwealth Government in 2004, and is consistent with baseline data for blood supplied by most workers before working at the site.

Workers from two contracting organisations (A and B) were employed on the site. Blood samples were collected at regular intervals, and shipped to a laboratory certified for dioxin congener analysis in Hamburg, Germany. Dioxins were measured in blood samples using high resolution mass spectrometry and reported as pg/g blood lipids. Some congeners/congener groups were reported as absolute values, others as estimates based on the detection limit (and expressed as “>value”. In the analysis of dioxin values used in this report, where such estimates were provided, a fraction of the estimated value was used in total TEQ calculations, of 10%.

Blood dioxin data was expressed in terms of 25 individual dioxin/furan congeners and grouped congeners, including 19 congeners which have toxicity equivalence factors (TEF). This provided individual values for all congeners, and multiplied by the relevant WHO TEF value, allowed calculation of a total TEQ value for each sample. The TEQ of the WHO were used.

3 Results

3.1 Blood dioxin sampling

Descriptive statistics for the monitoring data provided are shown in Table 1.



Table 1: Descriptive statistics: monitoring data: samples.

Parameter	Company A Data	Company B Data
Number of Employees/Contractors	71	72
Number of Employees/Contractors with No Samples	2	7
Number of Samples	153	135
Number of First Samples	72	62
Number of Second Samples	46	43
Number of Third Samples	26	23
Number of Fourth Samples	9	4
Number of Fifth Samples	0	2
Number of Sixth Samples	0	1

3.2 Baseline blood dioxin levels

Analysis of data from the first sample provided by all workers allows an examination of baseline dioxin levels in this group of workers. This analysis is shown in Table 2.

Table 2: Baseline dioxin data.

	Count	Mean	St Dev	Highest	Lowest
Company A Data	72	6.82	4.58	23.37	0.64
Company B Data	62	8.14	7.07	38.93	0.64

The “Highest” values in Table 2 are of interest, in that they indicate outlier baseline dioxin levels that may indicate an upper limit of normal values in this group of workers.

Congener profile data in all samples is shown in Table 3

Table 3: Baseline dioxin data.

Congener Group	Company A Data			Company B Data		
	Mean	% of Tot	St Dev	Mean	% of Tot	St Dev
Tetra-Cl	0.9	13%	± 1.00	1.4	18%	± 1.7
Penta-Cl	4.1	60%	± 2.9	4.3	54%	± 4.1
Hexa-Cl	1.5	22%	± 1.2	1.8	23%	± 2.3
Septa-Cl	0.3	4%	± 0.4	0.4	5%	± 0.7
Octa-Cl	0.03	0.4%	± 0.01	0.02	0.5%	± 0.01



There were six baseline values (two from Company A, four from Company B) that were above the action level of 20 pg/g, shown in Table 4.

Table 4: Baseline dioxin data: outliers above 20 pg/g.

Dioxin TEF											
Total	Tetra-Cl		Penta-Cl		Hexa-Cl		Septa-Cl		Octa-Cl		
	pg/g	%	pg/g	%	pg/g	%	pg/g	%	pg/g	%	
20.3	0.2	1	14.1	69	4.5	22	0.6	3	0.05	0.2	
38.9	2.3	6	19.0	49	15.3	39	0.9	2	0.04	0.1	
26.2	2.3	9	15.6	60	6.6	25	0.6	2	0.04	0.2	
24.7	0.4	2	15.8	64	6.5	26	1.0	4	0.04	0.2	
23.4	4.0	17	12.5	53	6.0	26	0.8	3	0.06	0.3	
20.4	2.5	12	12.1	59	4.9	24	0.4	2	0.06	0.3	

3.3 Blood dioxin results (all samples)

Data for all blood samples are shown in Figure 1 (Company A data) and Figure 2 (Company B data). For comparison purposes, these are drawn on the same axes.

3.4 Blood dioxin levels as a function of sample sequence

There was a steady increase in blood dioxin as the sample sequence increased (as shown chronologically in Figures 1 and 2). The number of samples fell as

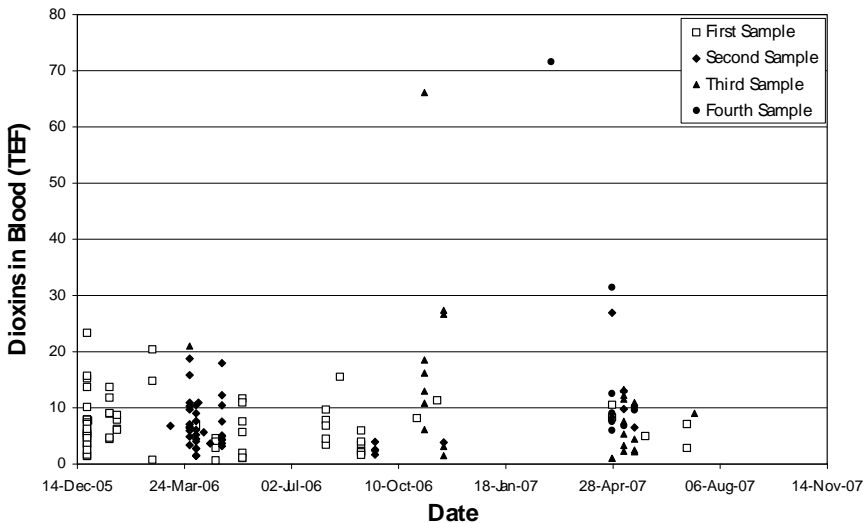


Figure 1: Total dioxin in blood (as TEF), company A data.

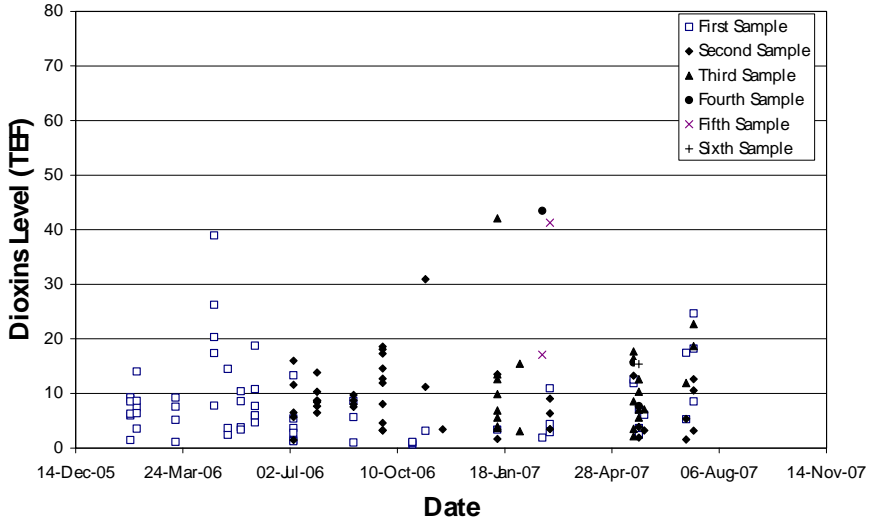


Figure 2: Total dioxin in blood (as TEF), company B data.

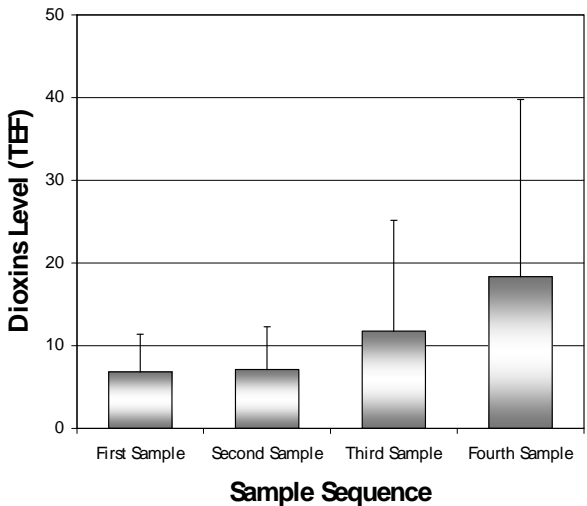


Figure 3: Total dioxin in blood (as TEQ), as sample sequence, company A data.

sampling continued (see Table 1), although these data vary considerably. How blood dioxin levels changed over time through the sampling sequence is shown in Figures 3 and 4.

The congener profile of these values (by sample) is shown in Figures 5 and 6 (again, drawn to the same scale for comparison purposes).

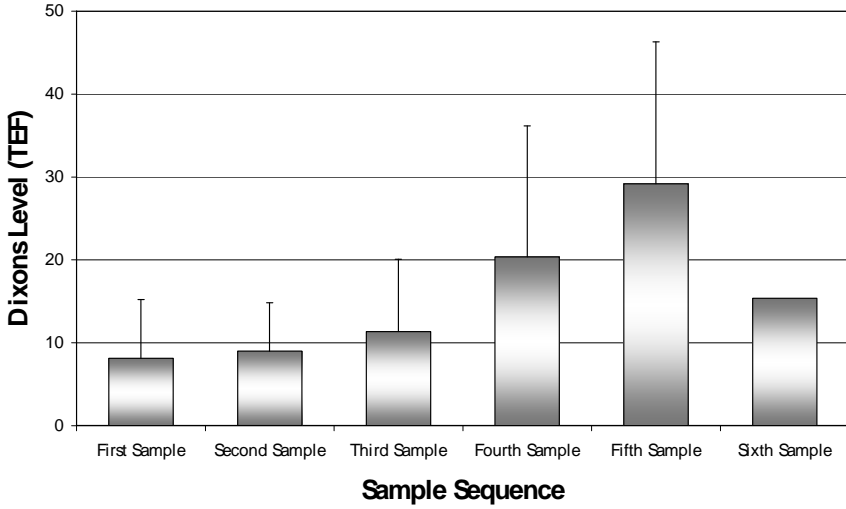


Figure 4: Total dioxin in blood (as TEQ), as sample sequence, company B data.

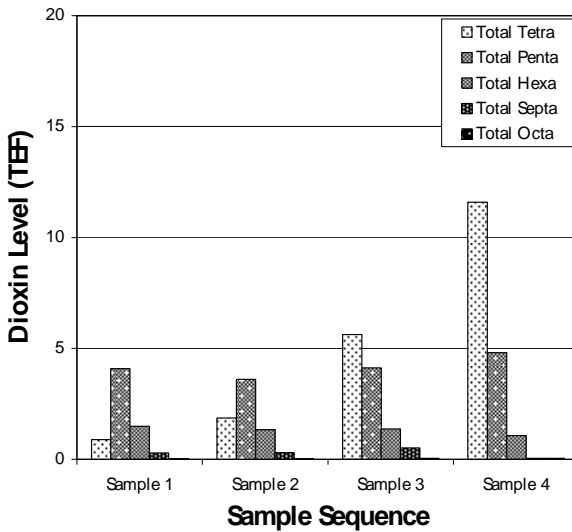


Figure 5: Total dioxin in blood (as TEF), as sample sequence, company A data, congener profile.

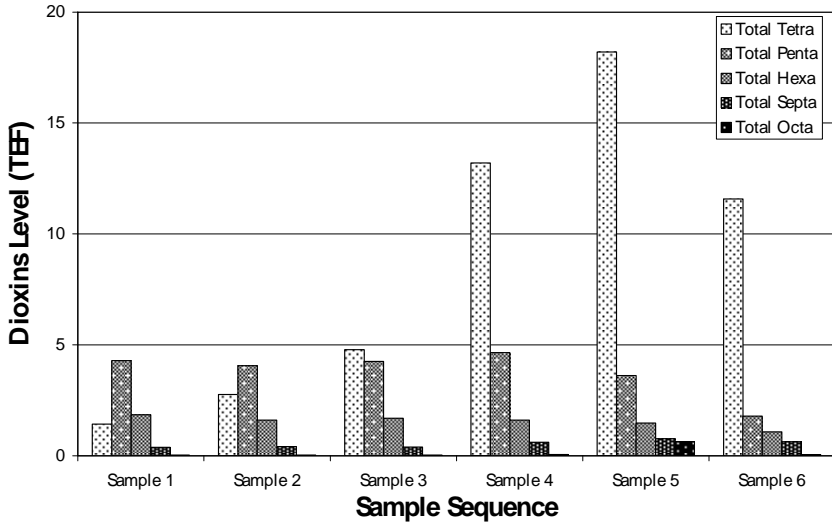


Figure 6: Total dioxin in blood (as TEF), as sample sequence, company B data, congener profile.

3.5 Data on outliers

On occasion, blood dioxins levels for a number of workers at the site exceeded 20 pg/g TEQ in blood lipids. Curves for individual workers are shown in Figures 7a and 7b.

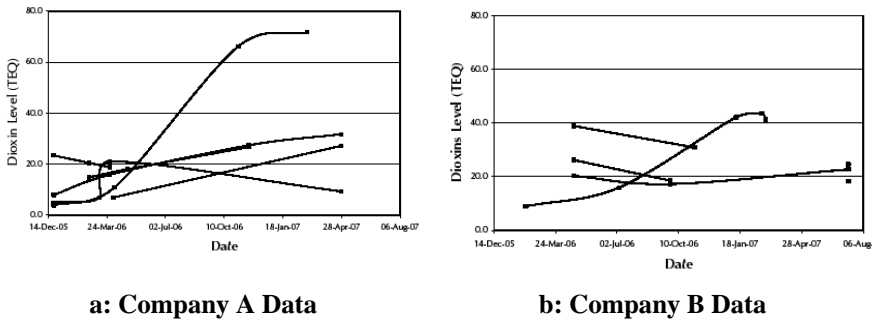


Figure 7: Total dioxin in blood (as TEF), outliers.

4 Discussion

Human biomonitoring of dose and biological effect nowadays has tremendous utility for providing an efficient and cost effective means of measuring human exposure to chemical substances [15]. While not preventive in approach, this method offers the means to identify and quantify human exposure and risk, to



gain information about toxicity and exposure, and to assess the adequacy of occupational health controls. In this study, biomonitoring of workers was used to identify trends in exposure to dioxins on a major remediation project of established dioxin contamination in Sydney, Australia. With an overall mean of 7.43 pg/g in baseline levels (that is, before working on the project; see Table 2) of blood dioxins in workers engaged on this project, it is apparent that these blood dioxin levels, compare favourably with those of the 2004 survey of Dioxins in Australian published the Commonwealth Government (of 10.9 pg/g).

The congener profile of these baseline values (see Table 3), shows that the main congeners contributing to baseline values are from the penta- (60% and 54% of total) and hexa- (22% and 23% of total) chlorinated dioxins and furans. The level of 20 pg/g TEF in blood lipids, being approximately double the baseline level for Australians, was suitable for use as an action level in the occupational environment.

Reviewing the congener profile data in six levels above 20 pg/g blood lipids, it is apparent even with the higher levels, the congener profile is proportionally similar to the other baseline values (see Table 4). For trends in the levels of blood dioxin in all samples (Figures 1–4), the majority of values were below 20 pg/g. For Company A data this is 144/153 samples (94.1%) and for Company B data this is 126/135 samples (93.3%).

Generally, blood dioxin levels increased as time progressed, indicating that working conditions were such that exposure to dioxin contaminated soil was sufficient to increase blood dioxin levels. Overall, blood dioxin levels to Company A workers were higher than Company B workers. It was not possible to identify any specific trends in the activities carried out by workers, as there was considerable flexibility in working arrangements across the site. These data indicate that a number of elevated values occurred during the period October 2006 to April 2007, suggesting that worker or site activities were such that increased exposure to dioxins occurred.

The congener profile data shown in Figures 5 and 6 suggests that while the dioxin/furan concentration (as TEF) of worker blood samples remains largely the same for penta-, hexa-, septa- and octa- congeners, there is a substantial increase in tetra- congeners as the sample sequence progresses. As the most obvious source of this increase is exposure to contaminated soil as part of working at the site, such an increase could be used to identify that component of body burden of dioxins in these samples arises out of industrial exposure. Other studies have suggested that employment history is an important determinant of dioxin levels, and this was identified in the present study [16].

Further, as this congener group contains the most toxic of the congeners (2,3,7,8-tetrachloro-para-dibenzodioxin) this raises issues that may need further attention, especially with regard to on site controls, control of occupational exposure and worker personal hygiene.



Acknowledgements

The authors gratefully acknowledge the support and contribution to this project by Thiess Services Pty Ltd.

References

- [1] Gaudet, B. *Risk Assessment of Dioxins*. VGM Verlag, Saarbrücken, 2009.
- [2] Lowe, J.A. Methods of estimating toxic equivalents for polychlorinated dibenzodioxins and dibenzofurans. Chapter 12 (pp 237-248) In: Hattemer-Frey HA and Travis C, editors. *Health Effects of Municipal Waste Incineration*. CRC Press, Boca Raton, 1991.
- [3] Mukerjee, D., Cleverly, D. Risks from exposure to polychlorinated dibenzo-*p*-dioxins and dibenzofurans emitted from municipal incinerators. *Waste Management Research* **5**: 269-273, 1987.
- [4] Van den Berg, M., Birnbaum, L., Bosveld, B.T.C., Brunstrom, B., Cook, P., Feeley, M., Giesy, J.P., Hanberg, A., Hasegawa, R., Kennedy, S.W., Kubiak, T., Larsen, J.C., van Leeuwen, F.X.R., Liem, A.K.D., Nolt, C., Peterson, R.E., Poellinger, L., Safe, S., Schrenk, D., Tillit, D., Tysklind, M., Younes, M., Waern, F., Zacharewski, T. Toxic equivalency factors (TEFs) for PCBs, PCDDs, PCDFs for humans and wildlife. *Environmental Health Perspectives* **106**: 775-782, 1998.
- [5] US EPA. *Exposure and Health Assessment for 2,3,7,8-Tetrachlorodibenzo-*p*-dioxin (TCDD) and Related Compounds*. NCEA Office of Research and Development, US Environmental Protection Agency, Washington, 2000.
- [6] Gough, M., Turnbull, D. Estimating the Cancer Risks of exposure to 2,3,7,8-tetrachlorodibenzo-*p*-dioxin. Chapter 7 (pp 131-146) In: Hattemer-Frey, H.A., Travis, C., editors. *Health Effects of Municipal Waste Incineration*. CRC Press, Boca Raton, 1991.
- [7] Hay, A. Identifying carcinogens. *Nature* **269**: 468, 1977.
- [8] Poland, A., Palen, D., Glover, E. Tumor promotion by 2,3,7,8-Tetrachlorodibenzo-*p*-dioxin in skin of HRS/J mice. *Nature* **300**: 217-272, 1982.
- [9] Pitot, H.C., Goldsworthy, T., Campbell, H.A., Poland, A. Quantitative evaluation of the promotion by 2,3,7,8-tetrachlorodibenzo-*p*-dioxin of hepatocarcinogenesis from diethylnitrosamine. *Cancer Research* **40**: 3616-3627, 1980.
- [10] IARC. *IARC Monographs on the Evaluation of Carcinogenic Risk to Humans: Polychlorinated Dibenzofurans and Polychlorinated Dibenzodioxins*, Volume 69. International Agency for Research on Cancer, Lyon, 1997.
- [11] Steenland, K., Bertazzi, P., Baccarelli, A., Kogevinas, M. Dioxin revisited: Developments since the 1997 IARC classification of dioxin as a human carcinogen. *Environmental Health Perspectives* **112**: 1265-1268, 2004.



- [12] Popp, J.A., Crouch, E., McConnell, E.E. A weight of evidence analysis of the cancer dose response characteristics of 2,3,7,8-tetrachlorodibenzodioxin (TCDD). *Toxicological Science* **89**: 361-369, 2006.
- [13] NHMRC. Dioxins: Recommendations for a Tolerable Monthly Intake for Australians. National Medical Research Council, Canberra, 2002.
- [14] Harden, F., Muller, J., Toms, L. *Dioxins in the Australian Population: Technical Report No 9*. National Dioxins Program, Department of Environment and Heritage, Canberra, 2004. At: <http://www.environment.gov.au/settlements/publications/chemicals/dioxins/report-9/pubs/report-9.pdf>
- [15] Angerer, J., Ewers, U., Wilhelm, M. Human biomonitoring: State of the art. *International Journal of Environmental Health* **210**: 201-228, 2007.
- [16] Burns, C.J., Collins, J.J., Humphry, N., Bodner, K.M., Aylward, L.L., McBride, D. Correlates of serum dioxin to self reported exposure factors. *Environmental Research* **110**: 131-136, 2010.



Section 7

Ecology and health

This page intentionally left blank

Eco-biosociocultural H5N1 disease model in Egypt

S. L. Wilson & N. Oushy

Department of Health Science, New Mexico State University, USA

Abstract

This paper explores environmental and behavioral interactions that facilitate human exposure to the highly pathogenic avian influenza (HPAI) H5N1/A virus (termed bird flu or H5N1 throughout this document) in Egypt. The approach used in this research integrates public health and anthropological methods to assess environmental and behavioral interactions that facilitate human exposure to bird flu. Four key elements of the H5N1 eco-biosociocultural model were identified: (1) the subsidized natural environment; (2) the built environment; (3) the socio-political and economic environment; and, (4) the cultural environment. Analysis of these elements resulted in development of an eco-biosociocultural disease model for H5N1 that addresses health disparities by incorporating the built and subsidized natural environments integrated with associated cultural beliefs, knowledge, and behaviors. Our results suggest that the disparate incidence and mortality pattern of H5N1 in Egypt is likely affected by increased exposure opportunities among women and children resulting from lack of knowledge, traditional daily activities, poultry practices, and child-rearing activities. Despite community based health education efforts, knowledge about poultry diseases and H5N1 transmission are not well understood among Egyptian women. In the absence of a perceived immediate bird flu threat, this research suggests that women tend to maintain traditional behaviors. The H5N1 epidemiologic footprint in Egypt differs from other countries, but the lessons learned provide a basis for health education action that may be transferable to other venues.

Keywords: ecology and health, social determinants of health, Bird Flu, Egypt, H5N1, ethnography, built environment, subsidized natural environment, health disparities, eco-biosociocultural, avian influenza.



1 Introduction and need

This research explores environmental and behavioral interactions that facilitate human exposure to the highly pathogenic avian influenza (AI) or HPAI H5N1 virus (termed bird flu or H5N1 throughout this document) in Egypt. Bird flu is considered a serious health threat worldwide and is a quarantinable communicable disease with a geographic range that includes Asia, Southeast Asia, Europe, the Indian subcontinent, and Africa [1]. Humans contract H5N1 by through primary or incidental (secondary) direct exposure, i.e., via inhalation of airborne effluents; ingestion of undercooked, infected meat; or by contact with excretions (e.g., saliva, feces, and contaminated feathers) [1]. Findings suggest that the virus has a much wider spectrum than originally thought; making it potentially more problematic than anticipated should it develop the capability to transfer easily from human-to-human [2]. As of March 2011, Egypt ranks second in the world in number of confirmed human H5N1 cases (behind Indonesia) and ranks third highest worldwide in total deaths (behind Indonesia and Viet Nam) [1].

Two main factors indicate the importance of addressing the human ecology of bird flu in Egypt from a holistic perspective: the epidemiologic footprint of bird flu in Egypt and a lack of behavioral data surrounding the disease. First, the epidemiological footprint of reported cases of human H5N1 in Egypt presents a distinct pattern disproportionately affecting young adult women and small children – a pattern different from that seen in other countries [1, 3–5]. No attempt was made to estimate the effects of underreporting. Of a total of 144 cases of Egyptian bird flu between 2006 and 25 March 2011, 44 (30.6%) died [1]. Most deaths (N=36, 81.8%) occurred among females. Women aged 15-44 years (N=33 deaths) were most likely to die from the disease, accounting for 91.6% of female deaths [1]. Children of both sexes (ages birth to 14 years) contracted the disease slightly less often than adults (N=70 or 48.6% of all cases); however, children were more likely to recover than adults (N= 65, 92.8% recovery among children compared to N= 21, 35.0% recovery among adults) [1].

The second main factor is that, to date, no studies have addressed specific behaviors or traditional cultural practices that affect exposure, though several have identified human behavior as a factor in the disease [1, 5]. Demonstrated need suggests developing greater insight into environmental milieu affecting the presence of disease. Exposure to poultry or infected poultry account for almost all cases (a few case sources are unknown) and no cases were attributed to wild birds exposure [1]. Therefore, analysis of the Egyptian human bird flu pattern indicates a need to consider the local epidemiologic footprint when developing policy and public health actions.

2 Methods

The approach used in this research integrates public health and anthropological methods to assess environmental and behavioral interactions that facilitate human exposure to bird flu [6–11]. Our approach incorporated a holistic,



bio-sociocultural ecological approach using progressive contextualization among the abiotic, biotic, and cultural environmental components [6, 10]. Researchers worked under the auspices of National Council for Childhood and Motherhood (NCCM) while in Egypt. The Institutional Review Board (IRB) at New Mexico State University reviewed and approved the research protocol, and all interview study participants signed an informed consent.

General knowledge, photographic data, observations, and personal journals based on extended participant observation and long-term social relationships (between 1989 and 2008), provided basic ethnographic background data, which were analyzed using traditional ethnographic methods [12, 13]. A grounded theory analysis [14] identified potential ecological and social determinants of health associated with bird flu. General inductive analysis established links between objectives and findings to develop a model regarding underlying structure or experiences or processes evident from the text data [15]. Cross verification triangulated interview data with nonreactive data.

A purposive sample of eight households in a rural village north of Aswan was selected for in-depth interviews during June 2008. In-depth interviews lasted 30 minutes to one hour each, followed by village and household tours. Each interviewee was female, maintained a small poultry flock, and had small children in and around the household. Researchers conducted each interview in the home of the interviewee in their native language (Arabic). A social worker from the Ministry of Health and Population (MOH-Aswan), served as an interview guide, suggested interviewees, and provided entrée to the local community. A second key informant from the Ministry of Agriculture assisted in interviews and Arabic translation. To ensure the validity of paraphrases, an independent translator assisted during household interviews. Interviews were recorded and transcribed. In addition to interviewee households, researchers visited numerous other households and villages to assess poultry practices and venues.

3 Results

3.1 Study community – the context

The principal study community was a rural village just north of Aswan, Egypt, with no direct access to the River Nile. Community development resulted from chain migration to an unpopulated area, where people subsequently built extended family housing and shops. No demographic figures are available for the village. A two-lane, paved road runs north and south through the village and other paved roads connect with the main road as one approaches Aswan to the south. Unpaved, dirt roads lead to housing areas that have branched off the main artery. Although designated as rural, the village closely resembles a chain periurban type (CPU) community, i.e., it is “geographically on an urban fringe, appears to be derived primarily from chain migration, and represents a



reconstituted institutional context” [16, p.8]. Although specific demographic data are not available for the village, the following represents rural, Upper Egypt [17].

- Most women are illiterate (62.5%) with a median education level of 0.3 years.
- Most people are poor: 72.8% in the two lowest quintiles and 42.7% in the lowest quintile.
- Most people have access to improved drinking water sources (93.5%).
- A small number of households (8.4%) pipe sewerage to a canal, groundwater, or have no toilet facility.

The following description typifies a common daily street scene in the village. Two-storied, mud brick buildings with brightly painted doors line the street where most doors are closed and windows are tightly shuttered. A few old cars and trucks are parked, while workers go about their daily chores. Men sit on a doorstep in front of a house talking. Most women are inside their homes, though a few venture out to purchase milk or vegetables from vendors who frequent the street with their donkey driven carts. Dressed in a traditional long dress or *galabea*, a barefoot young woman sips tea in her doorway, watching activities on the road. A young boy carries a small goat over to the shade by his front door. Children, some with sandals, others barefoot, ride bicycles, talk with each other, or roll an old tire down the street while laughing and chasing one another. In the shade, a water buffalo lounges lazily, while a rooster struts across the street to search for food scraps, and goats pick at tin cans and paper litter strewn about the street. Brightly colored baby clothes hang to dry on lines strung across balconies. Behind tightly closed doors lie living rooms, kitchens, and sleeping quarters and often a shared courtyard. Over the hum of human voices, poultry cluck from cages in secluded enclosures or from rooftop cages.

3.2 Ecological analysis

The need to consider the synergistic interaction of the avian, virus, and human environments at various levels of geography complicates evaluation of the H5N1 health and ecology system. Initially, Egypt appears largely unsuitable for H5N1 sustainability; however, the densely populated *green zone* along the Nile River valley and delta identify likely areas for H5N1 survival [18]. The green zone provides ample year-round habitat for large flocks of wild aquatic birds, supplemented by hundreds of thousands during winter months, many of which may shed viruses that contaminate the natural environment.

Our research identified four main recurring and overlapping environmental contexts that contribute to the H5N1 eco-biosociocultural system: (1) the natural environment; (2) the built environment; (3) the socio-political /economic environment; and, (4) the cultural environment. Each interacts synergistically with the others in complex ways to facilitate virus niches and, ultimately, disease exposure routes and occurrence. A microenvironment conducive to virus survival results, from which domestic birds (frequently) and humans (sporadically, but, so far with reasonable consistency) become infected in Egypt. Figure 1 represents main themes identified and interactions in an eco-biosociocultural H5N1 model for Egypt.



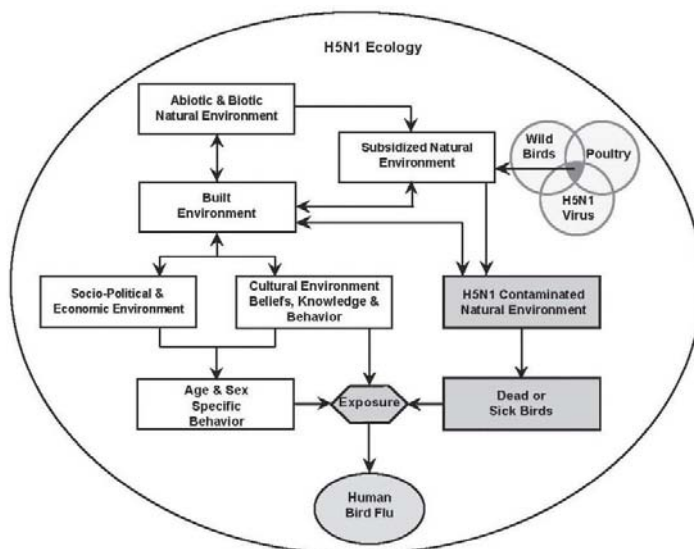


Figure 1: Eco-biosociocultural model of H5N1.

4 Discussion

4.1.1 The subsidized natural environment

The relationship between people and the H5N1 contaminated natural environment, especially the river and canals in rural areas, emerged as a recurring theme from analysis of field notes, literature, and interviews. As one person put it, “The canal has its own system. If you throw a dead donkey in the canal, it will be bones in a week.” Individuals encounter potentially contaminated soil and water daily because of occupation, traditional behavior, or leisure. The river and canals afford water for fishing, recreation, irrigation and household chores, such as dish or clothes washing. These same water sources may also serve as disposal sites for biotic and abiotic refuse and as impromptu, or in some areas, regular sewage collectors. Petrol/diesel driven pumps, as well as, traditional water wheels/buckets, lift water into tanks and smaller irrigation channels where barefooted or sandaled farmers and children work. Domestic animals and wild birds also contribute to water and soil pollution. Wherever Egyptians live, one frequently finds small household, rooftop, or backyard domestic flocks of chickens, ducks, pigeons, and occasionally turkeys. In summary, two processes make the transfer of the H5N1 to domestic poultry possible: (1) direct virus transfer from wild birds/ducks to domestic fowl, and (2) primary or incidental virus transfer to the household, principally through routine daily human activities in the endemically infected natural environment.

4.1.2 The built environment

Another recurring theme that emerged from data analysis reveals that the built environment facilitates virus transfer in several ways. Used here, the term built environment refers to that which "... comprises urban design, land use, and the transportation system and that encompasses human activity within the physical environment" [19, p.65]. Most H5N1 dispersion (estimated 78%) appears to have been through human action rather than natural biotic action [20]. Egypt is a country of people on the move: by water, on foot, and by bicycle, car, train, donkey, donkey cart, motorbike, bus, or camel. Movement of poultry, poultry products, and infected materials contributes to the inadvertent spread of H5N1 throughout the country [21, 22].

Egyptian policy makers initially focused on commercial producers, live markets, and macro-economic concerns following H5N1 identification in the country. In doing this, they failed to take into account customary practices and traditional exposure routes among small producers and average citizens. Both actions led to large-scale biosecurity lapses at the onset of the virus, which allowed the virus to go endemic. Subsequently, the free poultry vaccine program failed for two main reasons: (1) vaccine was ineffective [23] and (2) inadequate bio-security training of field technicians contributed to virus transference [24]. Securing perimeters, culling, and disinfecting major commercial farms proved easier than controlling the movement of traditional (backyard and household) producers' poultry. Upon learning of the government's culling initiatives, Egypt's small producers sought to save their flocks and their wealth by hiding or moving birds away from the of government's reach. When asked about children carrying roosters/chickens under their arms, one interviewee commented, "If it had feathers, the police killed it....but when they came here people hid their chickens under the bed or took them to a relative's house so they wouldn't be killed". These actions effectively thwarted government efforts to geographically isolate and eliminate the virus, which ultimately resulted in it becoming endemic in 2008 [25].

Rurality figures significantly in human exposure to H5N1. First, interviewees stated that they raise poultry mainly for personal consumption as eggs and meat, with some local marketing. This substantiates observations reported previously [26]. Second, women usually tend household flocks kept in yards, cages, on rooftops, or in secured areas around courtyards of their homes, though children frequently carry poultry from place to place. Third, household poultry flocks are more common among rural households than urban ones. Fourth, rural built environments tend to be less sophisticated than urban areas and have more undeveloped areas scattered with garbage and animal litter, including poultry litter. Finally, officials find it more difficult to enforce regulations in rural areas.

4.1.3 Sociopolitical and economic environments

Data identified three principal sociopolitical/economic themes associated with bird flu: relative status, lack of reciprocal social capital, and consumer protein consumption. Raising poultry provides a source of great pride among Egyptian women. It not only increases her relative social status among peers, but also, represents relative economic power for the owner and her household.



Intergenerational relationships, housing structure, and flock size contributed to deference behavior observed among households visited. Sale of excess poultry and eggs also increase a woman's economic independence. One woman stated, "I don't have to buy many eggs because I have my chickens." Therefore, owning poultry also provides a method adding protein to the diet through eggs and occasionally meat while elevating a woman's social status vis-à-vis her peers and relatives.

Reciprocal trust has been noted to be an important ingredient in development of rural social capital, [27, 28] and has been identified as a significant social determinant of health [29]. Rural Egyptian women distrust the government, government programs, and fear government will take actions against them and their poultry. Women do not trust the government to tell them the truth about the disease through the use of television, radio, or public service announcements (PSA's) to educate them about the disease. However, our results substantiate previous reports that women are aware of the bird flu [30]. Translating governmental information into daily life poses difficulty because rural women are not sure H5N1 constitutes a serious health threat to them since their birds are healthy. In addition, the fact that less attention to the topic appears in the news leads them to believe it either never existed or no longer poses a threat. Women expressed doubts that government actions to eradicate the disease are in their best interests, and, they frequently stated that the government is trying to take away their income in favor of large commercial enterprises. Some interviewees thought outside sources were responsible for trying to ruin the poultry industry, e.g., "Bird flu came from chicks imported from Turkey".

Bird flu has affected the diet and nutrition of average citizens as well as the macro-economy of Egypt. Before H5N1, the Egyptian poultry industry represented a LE (Egyptian pounds) 17 billion national investment, employed an estimated two-three million people either directly or indirectly, and accounted for 45 to 50 percent of animal protein consumed in Egypt, as compared to about 20 percent elsewhere in the world [31]. H5N1 resulted in the collapse of the Egyptian poultry industry [32, 33]. As a result, the price of available fresh and frozen chicken rose approximately 500% between 2006 and 2008.

Consumer preferences play a role in continuation of relatively invisible live markets. Egyptians strongly prefer live birds slaughtered at sale to consumers [26]. "The frozen chickens that we get now do not taste right," one participant reflected. Although the government outlawed live bird markets, these markets continue to operate in spite of legal restrictions [34]. Live poultry continues to be available throughout Egypt, more so in rural areas, and can be purchased in live bird markets although these markets are rarely visible [35].

4.1.4 Cultural environment

Various facets of the cultural environment affect human exposure to bird flu; however, this research will focus on two main themes: women's awareness and knowledge of bird flu and behavioral risk factors. Everyone we encountered had heard of bird flu. Women acquire much of their knowledge about bird flu from their personal social network, which revolves around intergenerational, informal



communication among women in the village or household. They also cited physicians, medical centers, and family planning clinics as health information sources. Women demonstrated a low level of personal empowerment regarding bird flu knowledge, voicing concern over information gaps about causation, transmission, procedures, and extent of the disease threat. As one informant asked, "How will I know if my chickens are sick?" Another stated, "I don't know who to call if my birds get sick". Discussions revealed that women had little or no understanding of bird flu etiology. When asked, "How do you think people get bird flu?" Answers ranged from "I don't know" to "handling sick chickens" to "handling wild or sick birds".

Community social workers conducted health education interventions targeting avian influenza throughout much of the country, including the study village. Interviewees cited washing hands, surfaces, and butchered birds as important for hygiene, but this was not new behavior stimulated by health education training. Village women appear to have selectively implemented prevention strategies into behavior change. It is not clear if they would implement prevention strategies in the presence of an immediate perceived risk such as sick birds in the area. For example, when displaying poultry sites, women did not change clothes, don gloves, cover their faces, or wear shoes when entering poultry pens or picking up poultry, although each of these practices were recommended in community based training. In addition, a single enclosure frequently housed chickens and ducks (although some were separated by wired dividers). One interviewee stated she did not understand how her ducks could give chickens bird flu. This perception is particularly problematic since ducks are asymptomatic when infected; yet, ducks shed more H5N1 virus than chickens when infected.

Proximal distance between people and poultry constitutes an important behavioral risk factor. When examining this particular risk factor, it is important to distinguish between primary and incidental direct virus exposure routes. The most direct primary exposure routes include handling infected birds, slaughtering/butchering, or food preparation. However, it is important that the virus also transfers from feces, feathers, and saliva to such items as bedding straw or soil on vehicles, equipment, cages, shoes, and clothes, providing an incidental direct exposure route. With the exception of a few roosters walking on the village streets, women we interviewed separated their poultry in small rooms, pens, or roof enclosures. It is not clear if this is new behavior or their tradition; however, this practice does reduce primary exposure opportunities to those in closest contact with enclosed poultry. However, many women do not always practice poultry isolation in spite of government educational efforts. For example, some women keep poultry in the yard during the day, but pen them over night, and some women allow poultry into the house, whereas, other do not.

Proximal distance between humans and poultry varies by age and sex in patterns similar to the disease occurrence. All ages and both sexes encounter incidental virus contaminated features of the environment. In the household environment, men may have infrequent direct contact with poultry, but commonly have incidental exposure at other venues. Women, who care for,



slaughter/butcher poultry, dispose of remains, clean contaminated areas, and cook poultry experience primary exposure risks.

Slaughtering/butchering/food preparation practices provide the most obvious primary behavior risks when the virus is present. The level of risk varies depending on where and how birds are prepared, and, of course, if the birds are infected. For example, it is easiest to de-feather birds after dipping them into boiling water, but not all women have hot water where they slaughter/butcher birds. In fact, some women dry-pluck dead birds; however, the frequency and effect of virus dispersion of this practice is not known and should be assessed. Following slaughtering/butchering of the bird in a bucket, women typically clean the bucket and area with regular soap or detergent and wash/boil the poultry for cooking. After learning about bird flu, village women indicate they do not allow children with them when they slaughter poultry and that slaughtering occurs more often on the roof or outside the house rather than in the kitchen. This needs to be verified by extensive observation.

Other practices that accompany slaughtering/butchering/food preparation activities afford both primary and incidental exposure routes. Until H5N1, women could process and eat or freeze sick or dead poultry to avoid waste, prevent further loss of assets, and to prevent sickness in other birds. However, H5N1 infected poultry can contaminate freezers, other frozen products, and any surfaces with which it comes in contact. The extent of this practice needs further investigation. Next, the slaughter/butcher bucket is rarely a single purpose container, e.g., women use it for washing dishes and clothes or for cooking. Depending on where slaughter/butcher practices occurs, other uses for the space include cooking, sitting, visiting, children's play, or sleeping. Also, disposal of bird remains into the trash, street, or canals represents other behavior risks for incidental virus transfer. Furthermore, tucking the end of a *hijab* or headscarf over the face, suggested by training materials, will not likely eliminate virus inhalation. However, the practice would potentially contaminate more cloth surfaces. To suggest that women maintain separate clothing for tending poultry is unrealistic considering the poverty level in rural communities. Furthermore, since they may have only one or two daily-wear galabeas, it is unlikely women change clothing, put on special shoes, or even wear gloves or plastic bags on their hands (which may be bulky and cumbersome) while going about their daily poultry duties. When the virus is present, women's clothing, shoes, hair, preparation environment, and furniture provide incidental exposure routes or potential transfer mechanisms for the virus to other parts of the environment.

Children's behavior presents a special case, because their behavior presents both primary and incidental virus transfer opportunities. Enclosing poultry away from living quarters may limit, but not eliminate, childhood exposure. Furthermore, children often assist in tending to poultry, especially chickens and ducks. Older children often develop an "owner-pet" affiliation with their poultry carrying them about with them from place to place in the village. Older children also participate in child-care activities for their younger siblings and relatives. Early childhood exposure risks are not limited to being in close proximity to persons who may have the virus on their clothing, hair, hands, or feet, but also



contaminated accessible household surfaces, both indoors and out, e.g., preparation tables, floors, furniture, and other surfaces that are not easily decontaminated. Small children and babies accompany their elders throughout the day. Like children everywhere, small children also crawl and walk about the home, often without shoes; climb on furniture; and, put hands and items in their mouths. Finally, older children or adults almost constantly hold babies and small children, a loving action that can be risky if the person holding the child has the H5N1 virus on their person.

5 Conclusions

Poultry flocks represent a source of income and nutrition for families living in rural Egypt. Importantly, poultry also represents a prestige value, i.e., a source of pride and status to families. H5N1 easily transfers through bio-security lapses across borders and even from house to house. Our results suggest that the disparate incidence and mortality pattern of H5N1 in Egypt is likely affected by increased exposure opportunities among women and children resulting from lack of knowledge, traditional daily activities, poultry practices, and child-rearing activities.

Despite community based health education efforts, Egyptian women do not know or understand enough about poultry diseases and H5N1 transmission. In the absence of a perceived immediate bird flu threat, this research suggests that women tend to maintain traditional behavioral patterns they learned from their mothers and grandmothers when they were children. Similarly, they pass this knowledge along to their children through their behavior. The majority of women at risk are in the preconception stage of change according to the Transtheoretical Model of Health Behavior [36], and, thus, do not recognize a need to change their risky behaviors. Therefore, it is suggested that future health education interventions initially focus on consciousness-raising and self-reevaluation associated with H5N1 among this population.

The observed value rural Egyptian women place on raising household, yard, and roof poultry may well be representative of the practice in communities and countries yet unaffected by the H5N1 virus. Therefore, the authors believe the model presented provides a starting point for assessing H5N1 in other geographical and cultural settings. Finally, the H5N1 epidemiologic footprint in Egypt may be different from other countries, but the lessons learned provide a basis for health education action and which may be transferable to other countries and diseases.

References

- [1] World Health Organization. Epidemic and pandemic alert and response (EPR): Avian Influenza. Online. http://www.who.int/csr/disease/avian_influenza/en/
- [2] Zhou L, Liao Q, Dong L, Huai Y, Bai T, Xiang N, et al. Risk factors for human illness with avian influenza A (H5N1) virus infection in China. *The Journal of Infectious Diseases*, 199(12), pp. 1726-1734. 2009.



- [3] Dudley J. Age-specific infection and death rates for human A (H5N1) avian influenza in Egypt. *Euro surveillance*, **14(18)**, pp. 1-2, 2009.
- [4] Fasina F, Ifende V, Ajibade A. Avian influenza A (H5N1) in humans: lessons from Egypt. *Euro surveillance*, **15(4)**, pp. 1-4, 2010.
- [5] Kandeel A, Manoncourt S, elKareem EA, Ahmed A-NM, El-Refaié S, Essmat H, et al. Zoonotic transmission of avian influenza virus (H5N1), Egypt, 2006-2009. *Emerging Infectious Diseases*, **16(7)**, 2010. Online. <http://www.cdc.gov/EID/content/16/7/1101.htm>
- [6] Vayda A. Progressive contextualization: Methods for research in human ecology. *Human Ecology*, **11(3)**:265-81, 1983.
- [7] McLeroy KR, Bibeau D, Steckler A, Glanz K. An ecological perspective on health promotion programs. *Health Education & Behavior*, **15(4)**, pp. 351-377, 1988.
- [8] Barbosa CS. Epidemiology and Anthropology: an integrated approach dealing with bio-socio-cultural aspects as strategy for the control of endemic diseases. *Memórias do Instituto Oswaldo Cruz*, **93**, pp. 59-62, 1998.
- [9] Reifsnider E, Gallagher M, Forgione B. Using ecological models in research on health disparities. *Journal of Professional Nursing*, **21(4)**, pp. 216-222, 2005.
- [10] McElroy A, Townsend P. *Medical Anthropology in Ecological Perspective*. Boulder, CO. 5th ed: Westview Press, 2008.
- [11] Scott A, Wilson R, Scott A. Social determinants of health among African Americans in a rural community in the Deep South: an ecological exploration. *Rural and Remote Health*, **11**, No. 1634, 2011. Online. <http://www.rrh.org.au>
- [12] Van Maanen J. Ethnography then and now. *Qualitative Research in Organizations and Management: An International Journal*, **1(1)**, pp. 13-21, 2006.
- [13] Birks M, Chapman Y, Francis K. Memoing in qualitative research. *Journal of Research in Nursing*, **13(1)**, pp. 68-75, 2008.
- [14] Strauss A, Corbin J. *Basics of qualitative research: Grounded theory procedures and techniques*. Sage publications: Newbury Park, CA, 1990.
- [15] Thomas DR. A general inductive approach for analyzing qualitative evaluation data. *American Journal of Evaluation*, **27(2)**, pp. 237-246, 2006.
- [16] Jaquinta D, Drescher A. Defining the peri-urban: rural-urban linkages and institutional connections. *Land Reform, Land Settlement and Cooperative*, **2000(2)**, pp. 8-26, 2000.
- [17] El-Zanaty F, Way A. *Egypt demographic and health survey 2005*. Cairo, Egypt: Ministry of Health and Population, National Population Council, El-Zanaty and Associates, and ORC Macro, pp. 377, 2006.
- [18] Williams R, Peterson A. Ecology and geography of avian influenza (HPAI H5N1) transmission in the Middle East and northeastern Africa. *International Journal of Health Geographics*, **8(47)**, pp. 1-11, 2009.



- [19] Handy SL, Boarnet MG, Ewing R, Killingsworth RE. How the built environment affects physical activity. *American Journal of Preventive Medicine*, 23(2S), pp. 64-73, 2002.
- [20] Kaoud HA. HPAI Epidemic in Egypt: Evaluation, Risk Factors and Dynamic of Spreading. *International Journal of Poultry Science*, 6(12), pp.983-988,2007.
- [21] Food and Agriculture Organization. Questions & Answers: The Facts of Bird Flu. Online. <http://www.fao.org/avianflu/en/qanda.html>.
- [22] World Health Organization, International Food Safety Authorities Network (INFOSAN). Highly pathogenic H5N1 avian influenza outbreaks in poultry and in humans: Food safety implications, 2005. Online. www.who.int/foodsafety/fs_management/No_07_AI_Nov05_en.pdf
- [23] Hafez MH, Arafa A, Abdelwhab EM, Selim A, Khoulosy SG, Hassan MK, et al. Avian influenza H5N1 virus infections in vaccinated commercial and backyard poultry in Egypt. *Poultry Science*, 89(8), pp.1609-1613, 2010.
- [24] Peyre M, Samaha H, Makonnen YJ, Saad A, Adbd-Einabi A, Galal S, et al. Avian influenza vaccination in Egypt: Limitations of the current strategy. *Journal of Molecular and Genetic Medicine*.v3(2), pp. 198-204, 2009.
- [25] World Organization for Animal Health. Update on highly pathogenic avian influenza in animals (Type H5 and H7). Online. http://www.oie.int/downld/AVIAN%20INFLUENZA/A_AI-Asia.htm.
- [26] Taha FA. *The Poultry Sector in Middle-Income Countgries and Its Fee Requirements: The case of Egypt*, United States Department of Agriculture, 2003.
- [27] Putnam RD, Leonardi R, Nanetti R. *Making Democracy Work: Civic Traditions in Modern Italy*, Princeton University Press, 1994.
- [28] Falk I, Kilpatrick S. What is social capital? A study of interaction in a rural community. *Sociologia Ruralis*, 40(1), pp. 87-110, 2000.
- [29] Scott AJ, Wilson R, Scott A. Social determinants of health among African Americans in a rural community in the Deep South: an ecological exploration. *Rural and Remote Health*. 11(1634), pp. 1-12, 2011.
- [30] El-Zanaty F, El-Ghazaly N. *Final Study Report: Avian Influenza Household Survey: Knowledge, Attitudes and Practices of the Egyptian Public*. Report. Cairo, Egypt: UNICEF, Egypt, 2007.
- [31] Leila R. Poultry industry collapses. *Al-Ahram Weekly*, 23 Feb–1 March, 2006.
- [32] GRAIN. Bird flu crisis small farms are the solution not the problem. Seedling. 2006. Online. <http://www.grain.org/seedling/?id=437#>
- [33] Khattab A. A Foul Business. *Egypt Today*. 2006. Online. <http://www.egypttoday.com/article.aspx?ArticleID=6448>
- [34] SAIDR. Homepage. Cairo, Egypt. 2010. Online. <http://www.saidr.org/>.
- [35] Sparks V. Personal Communication, 8 July 2010, Social Science Division, Brookhaven College, Dallas, TX, USA.
- [36] Rosenstock I. The health belief model: Explaining health behavior through expectancies. *Health Behavior and Health Education*, eds. K. Glanz, B. Rimer, & F. Lewis. Jossey-Bass: San Francisco, pp. 39-62: 1990.



Some aspects of reproductive health and metabolic disturbances in pregnant women and their newborn in ecologically injurious conditions of an industrial city in the Urals

L. A. Kovalchuk^{1,2}, A. E. Tarkhanova^{1,3,4} & A. A. Tarkhanov^{1,3,5}

¹*Middle Urals Scientific Center, Russian Academy of Medical Sciences, Laboratory of Adaptation Problems, Russia*

²*Institute of Ecology, Ural Branch Russian Academy of Sciences, Russia*

³*The Ural State Medical Academy, Russia*

⁴*Municipal Hospital 1, Russia*

⁵*Dispensary of Oncology, Sverdlovsk Region, Yekaterinburg, Russia*

Abstract

Medico-social aspects of the reproductive health of women are actual during the last decade in connection with the critical demographic tendency in Russia. Women of Ekaterinburg have disturbed reproductive functions and pregnancy complications (gestoses, danger of pregnancy break) Up to 80% of inspected women had somatic pathology. The leading among diseases are anemia, chronic infections inflammatory diseases, kidney and endocrine diseases and various forms of mastopathy.

Therefore, health protection, especially of women and newborn is of special importance in ecologically unfavourable regions, including the Urals. Considering the fact that technogenic pollution consequences instantly dangerously affect the health of a mother and a child, we investigated the “mother-placenta-fetus” biological system. In the blood serum and placenta tissue of all inspected pregnant women in Ekaterinburg concentration of trace elements (Cu, Zn, Cd, Pb, Ca, Cr, Ni ($p < 0,05$)) were higher compared with the data for other regions.

The deficiency of essential trace elements (Cu, Fe, Zn, Mg, Ca) and accumulation of toxic Cd and Pb in the umbilical cord blood were the reason for the intrauterine sufferings of a fetus responsible for the low body mass at birth,



retardation of growth and development. The disturbance of fetal and infant development frequently disturbed the early neonatal adaptation and underlied many subsequent diseases.

Keywords: reproductive health, pregnant women, newborn, blood serum, placenta, trace elements.

1 Introduction

Ecologically dependent pathologies of the population, including pregnant women and the newborn have grown in industrially developed countries during last decades. Numerous publications, including annual reports of the World Health Organization expert committees, show that 20–25% of the population's health depends on environmental conditions. It is known that in most industrial cities of the Russian Federation the environmental pollution with many harmful substances scores of times exceeds the maximum permissible concentration [1].

Medico-social aspects of the reproductive health of women have become urgent at present in connection with the extremely negative demography trend in Russia. It makes us pay special attention to the reasons for the increased instances of perinatal morbidity and mortality [2, 3].

The most important factors causing the high obstetric risk during pregnancy and influencing the demography are the ecological situation and population health in large industrial cities.

The Ural region long ago became a zone of ecological risk concerning heavy metals and radiation pollution [4–8]. The medico-ecological situation in this region is unfavourable. In Severdlovsk region every second pregnancy; in Ekaterinburg, every third has burdened obstetric and gynecologic anamnesis [9]. A good state of the fetoplacental complex is responsible for the bearing and birth of a healthy child [10–12].

As participation of essential (Fe, Mg, Mn, Ca, Cu, Zn, Ni, Cr,) and toxic (Cd, Pb) microelements in the course of pregnancy is doubtless, the problem of their toxicity for an embryo and fetus is very important. A growing number of women inhabiting megacities is affected by various combinations of these elements. Thus all districts of Ekaterinburg are polluted with heavy metals (HM).

At present there are many problems of trace element metabolism, there are no exact data on adaptation to them [13–16]. Shortage of facts does not allow us to uniformly explain underlying mechanisms of trace elements participation in homeostasis; theoretic discoveries are not introduced in clinical practice.

In conditions of environmental pollution with hazardous compounds responsible for the embryo – and gonado – toxic effects the decrease and prevention of fetoplacental insufficiency cases is impossible without early diagnostics and preventive measures [12, 17–19].

2 Cases and methods

The research was made in the obstetric clinic on the basis of the maternity hospital of the central hospital of №1 in Ekaterinburg. We made a complex



clinico-laboratory inspection of 156 pregnant women at the age of 17 to 42 and of their newborn, and a retrospective analysis of pregnancies, deliveries and newborn development,

A complex ultrasonic inspection of pregnant women included fetometry, evaluation of the fetal biophysical profile, dopplerometric estimation of the blood-stream in the umbilical cord arteries. For the echography and dopplerometry we used the "Aloka-1400" device. According to the ultrasonic and dopplerometric results, groups of inspected cases were formed,

The levels of microelements: Fe, Ca, Mg, Mn, Ni, Cr, Zn, Cu, Cd, Pb in the placenta, tissues, blood serum of women, and in the umbilical blood of the newborn were analyzed in triplicate and estimated by atomic absorption spectrophotometry (Perkin Elmer Analyst 1000, USA) and by atomic absorption ("AAS" spectrophotometer, Germany). Separate and disposable sterilized plastic syringes were used for blood collection. A blood sample was left standing for one hour to coagulate; serum was separated at 2000 rpm centrifugation for 10 minutes, transferred to a 5 ml polystyrene tube and stored at -18°C – -20°C until the analysis.

A statistical analysis was carried out with the program "Statistica & Microsoft Excel". Results were shown as a mean \pm standard error (SEM). Parameters showing Gaussian distribution were analyzed by Student's t-test. The Mann-Whitney U-test was used for parameters showing non-Gaussian distribution. The correlation between variables was evaluated by Pearson's correlation coefficients or Sperman's rank correlation coefficients were used to relate trace elements concentration, body mass and the fetal growth and medical data. The distinctions between the samples were considered to be statistically significant at $p < 0.05$.

3 Results and discussion

The object of the research was the biological system – "mother-placenta-newborn". The basic group was 117 pregnant women constantly living in Ekaterinburg and their 117 newborn. The control group was 26 women constant residents of nonindustrial areas in Sverdlovsk region and their 26 newborn. The basic and the control groups were formed by the method of random sampling, with the account of ecological conditions of residence. The composition of groups was heterogenous; there were no professions with harmful working conditions.

The analysis of the obstetric anamnesis revealed the following data. In the basic group (Ekaterinburg residents) 81,25% had complicated obstetric and gynecologic anamnesis, somatic pathology and pregnancy complications. 65% had various extragenital diseases of an infectious-inflammatory character. Anemia (50,4%), threats of pregnancy interruption (13,7%) and hypertension unconnected with pregnancy were noted in 16%. 18,8% of women had chronic pyelonephritis, 29,9% had hestosis.

In the control group (ecologically "safe" territories) physiologically proceeding pregnancy and delivery were observed in 69% of women. Complicated obstetric anamnesis and various complications of pregnancy were



marked in 30,8%. 100,0% of women from the control group had extragenital infections and noninfectious diseases. Complications of pregnancy were the following: Fe-deficit anemia – 50,0%; chronic pyelonephritis – 25,0%; hestosis – 25,0%; hypertension unconnected with pregnancy – 12,5%.

In the basic group the number of complicated pregnancies and deliveries exceeded the frequency of complications among the newborn, the last in its turn was above that in the control group: immaturity, a syndrome of respiratory disturbance predominated in the newborn. In the basic group 18,7% of children were born healthy, chronic hypoxia of various degrees was observed in 81,2%. Light hypoxia cases exceeded those in the control group 4,1 times; average degree cases – 2,0 times; every fifth child had heavy hypoxia. In the basic group 75,0% of children had proportional physical development; 25,0% – had intra-uterine growth restriction and 36,1% of them were born premature.

In the control group 92,3% of children had proportional physical development and 7,7% with intra-uterine growth restriction. Chronic hypoxia was observed in 30,8% of the newborn from the control group. In the control group there were no premature births.

Thus, considerably worse obstetric indices were observed in women living in ecologically unfavorable conditions in comparison with the women whose organisms were not affected by hazardous anthropogenous factors. Especially worse was the state of fetus and newborn – they exhibited the highest degree of hypoxia and intra-uterine growth restriction.

All sampled women, irrespective of the place of their residence, were subject to dopplerometry of placental blood circulation during physiological and complicated pregnancy.

In somatically healthy women without complicated pregnancy no pathological curves of the blood-current in the umbilical cord artery were registered (Fig. 1a). Pregnant women with prenatal fetal pathology exhibited a lower diastolic component of the blood flow in the umbilical cord artery, and apparition dicrotics dimple in the phase of early diastole (Fig. 1b).

In cases of heavy prenatal fetal pathology – zero and reverse diastolic component of the blood flow in the umbilical cord artery were registered – a characteristic sign of heavy disturbances of fetoplacental blood circulation (Fig. 1b, Fig. 1r.).

The analysis of haemodynamics in the umbilical cord artery revealed an increased sistolo-diastolic correlation in the group of pregnant city residents compared with the control group ($4,0 \pm 0,07$ and $2,4 \pm 0,03$ accordingly, $p < 0,05$). Resistance indices also revealed worse fetal blood circulation in the city residents: $0,75 \pm 0,08$ in the basic group and $0,58 \pm 0,07$ in the control group ($p < 0,05$). The research revealed considerably worse obstetric indices in the city residents: development of anaemia and the highest level of hypoxia and intra-uterine growth restriction of fetus.

Thus, in comparison with the data from other regions, all pregnant of Ekaterinburg residents had higher levels of trace elements: Cu, Zn, Cd, Pb, Sa, Cr, Ni in the blood serum and placenta tissue ($p < 0,05$). This corresponded to the results of other authors [20, 21]. The levels of the essential microelements Mn,



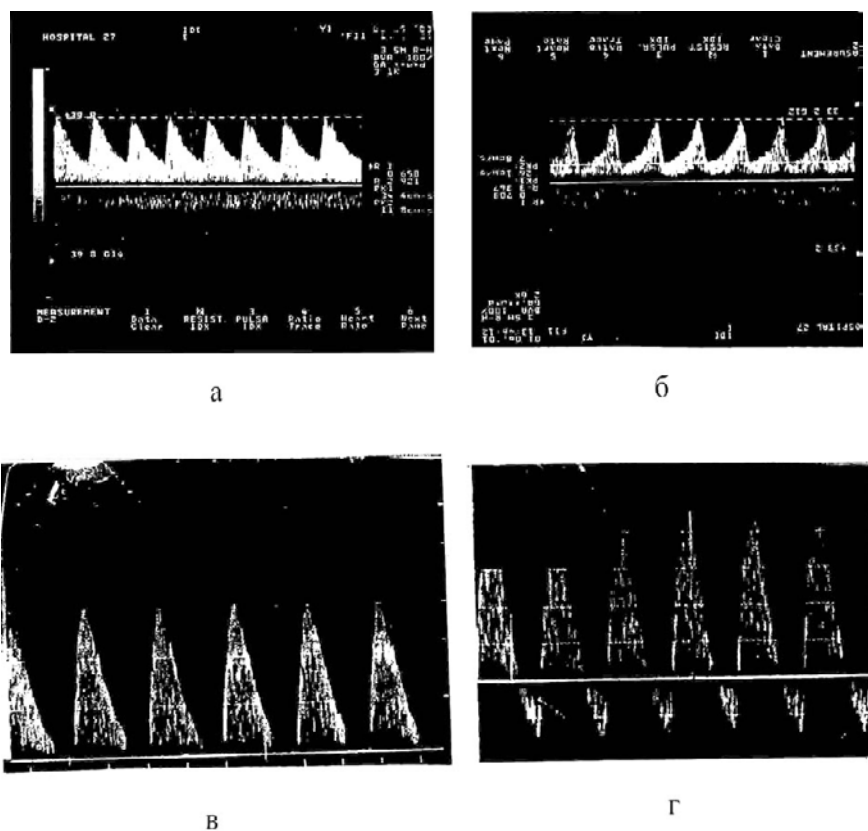


Figure 1: Dopplerometric indices of pregnant Ekaterinburg residents: **a** – healthy fetus; **б** – initial stage of placental insufficiency; **в** – absence of diastolic component in all heart cycles; **г** – reverse diastolic component of the blood flow in all heart cycles.

Mg and Fe were significantly lower ($p < 0.01$). Somatically healthy women of Ekaterinburg had significantly higher concentrations of heavy metals in placenta tissues, than somatically healthy women from the control group (Cu – 1,8 times, Zn – 2,4 times, Cd – 14,0 times, Pb – 12,4 times) (Table 1.).

A direct correlation was revealed between the levels of Cd in the city environment and in placentas of its pregnant residents ($r = 0.86$ $p < 0.05$). For Pb the relationship had average values ($r = 0.34$; $p < 0.05$). Concentrations of ecotoxic cadmium and lead in the blood ($Cd = 0.03 \pm 0.006$; $Pb = 0.31 \pm 0.07$) and placentas ($Cd = 0.084 \pm 0.014$; $Pb = 0.62 \pm 0.8$) of somatically healthy pregnant city residents exceeded those in other technogenic territories and the European standard [22-24]. Permeability of placental barrier to toxic lead was noted. At the same time placenta was a barrier for the penetration of raised concentrations of cadmium into the fetal organism, Cd a content in the umbilical blood of the newborn was lower compared to the mother's blood.

Table 1: Trace elements in placentary tissues of megapolis (basic group) and unindustrial area (control) residents.

Trace element, mkg/g	Group	M	m	P
Cu	basic	0.74	0.036	$T_{1-2}=7.9 > T_{0.99}=2.58$
	control	0.42	0.012	
Ca, Mmol/l	basic	8,82	1,05	$T_{1-2}=6.9 > T_{0.99}=2.58$
	control	1,42.	0,20	
Zn	basic	14.62	1.90	$T_{1-2}=4.3 > T_{0.99} = 2.58$
	control	6.10	0.28	
Fe	basic	1.01	0.28	$T_{1-2}=8.4 > T_{0.99}=2.58$
	Control	3.54	0.12	
Mn	basic	0.37	0.02	$T_{1-2}=4.05 > T_{0.99}=2.58$
	control	1.18	0.21	
Ni	basic	0.62	0.16	$T_{1-2}=0.9 < T_{0.99}=2.58$
	control	0.45	0.09	
Cr	basic	0.98	0.11	$T_{1-2}=6.3 > T_{0.99} = 2.58$
	control	0.27	0.03	
Cd	basic	0.084	0.01	$T_{1-2}=6.5 > T_{0.99} = 2.58$
	control	0.006	0.001	
Pb	basic	0.62	0.08	$T_{1-2}=7.1 > T_{0.99}=2.58$
	control	0.05	0.014	
Mg, Mmol/l	basic	0.61	0.14	$T_{1-2}=2.5 > T_{0.99}=1.96$
	control	1.22	0.20	

The distribution of H.M. in biosubstrata “mother-placenta-newborn” has the character of correlations of concentrations of industrial metals (Table 2.). Thus, concentrations of Cu, Pb, Zn ions quantitatively correlate; there is a direct relationship ($r = 0,613$; $r = 0,501$; $r = 0,609$ accordingly at $p < 0,05$) in their level between the mother’s and newborn’s blood (Kovalcuk et al. [8]). Correlation analysis shows that the distribution and accumulation of H.M. in the fetal and newborn organism is significantly dependent on the concentration of metals in the mother’s blood. Thus, for Cd levels there is a significant relationship between the blood serum and placenta tissue of pregnant women ($r = 0,567$ at $p < 0,05$) but no correlation in the system “mother’s placenta – newborn’s blood” ($r = 0,098$ at $p < 0,05$) and mother’s blood – newborn’s blood ($r = 0,140$ at $p < 0,05$).

The high extragenital morbidity among city residents, frequent complications during pregnancy and delivery, the observed imbalance of trace elements in

Table 2: Correlation of trace element concentrations in the biological system “mother-placenta-newborn”.

Trace element	Factor	Correlation coefficient, r	P
Cu	mother's blood –placenta	0.117	0.05
	placenta – newborn's blood	0.173	0.05
	mother's blood – newborn's blood	0.613	0.05
Zn	mother's blood –placenta	0.157	0.01
	placenta – newborn's blood	- 0.190	0.05
	mother's blood – newborn's blood	0.609	0.05
Pb	mother's blood –placenta	0.136	0.01
	placenta – newborn's blood	0.160	0.01
	mother's blood – newborn's blood	0.501	0.05
Cd	mother's blood –placenta	0.567	0.01
	placenta – newborn's blood	0.098	0.05
	mother's blood – newborn's blood	0.140	0.05

homeostasis showed that the system “mother-placenta-newborn” was a single functional structure depending on ecological environmental conditions and was responsible for the health of progeny.

We marked a spatial correlation between children's pathology and centres of environmental pollution with heavy metals ($r = 0.63$; $p < 0.05$). In the basic group placental insufficiency was accompanied by the deficiency of essential elements: Fe, Cu, Ca, Zn, Mg in blood of the newborn during the first hours after birth. In the blood of these children levels of Cd increased 5 times (0.02 ± 0.001 mkg/ml) concentrations of lead –1.9 times (0.29 ± 0.07 mkg/ml) against the background of lower levels of the essential microelements: Cu (0.68 ± 0.085 mkg/ml), Zn (1.4 ± 0.95 mkg/ml), Fe (0.81 ± 0.05 mkg/ml), and Mg (14.5 ± 0.06 mkg/ml) compared to children born by somatically healthy mothers.

The development of pathological processes causing embryo and fetus suffering significantly depended on the state of microelement metabolism which frequently affected other metabolic processes in an organism. Thus in the umbilical cord blood of children with prenatal hypoxia (81,2%), we observed increased levels of copper against the background of lower levels of the essential zinc, iron, calcium, magnesium ($p < 0.05$). Fe levels were up to 0.65 mkg/ml in the newborn suffering chronic hypoxia of a heavy degree ($p < 0.05$). The imbalance of trace elements in the blood of the newborn also resulted from the entry of toxic heavy metals cadmium and lead, concentrations of which correlated with the degree of hypoxia ($p < 0.05$).



Zn, Fe and Mg are known to induce the synthesis of metal thioneins which bond the excessive lead and detoxicating it. As the levels of these metals were low in the blood of the newborn this effect was absent. The deficiency of the essential elements (Cu, Fe, Zn, Mg, Ca) and the selective accumulation of toxic microelements (Cd, Pb) in the umbilical cord blood were the reason for prenatal fetus suffering, low body mass at birth, the child's growth development retardation. This conclusion was supported by our research on the physical development and health of the newborn of the city. The established correlation between the levels of heavy metals and physical development indices evidenced by the injurious complex effect of high concentration of Cu, Zn, Pb on the body mass ($r = -0.98$; $r = -0.98$; $r = -0.80$ accordingly, $p < 0.05$) and those of Cd on the fetal growth ($r = -0.79$; $p < 0.05$). This effect caused the failure of early adaptation of the newborn and subsequent health deviations. The disturbance of growth and development of the fetus and newborn was often the reason for the prenatal death, difficult early neonatal adaptation of children and many diseases in the future. The analysis of the material showed that in the basic group of the newborn 72,2% had the risk of prenatal infection, in the control group – 100% and 8,5% – had prenatal intoxication.

4 Conclusions

The polluted environment of Ekaterinburg is a constant source of a complex entry of xenobiotics – lead and cadmium – into organisms against the background of the deficiency of the essential trace elements (copper, zinc and iron). The analysis of our data allows us to state that increased levels of heavy metals in the environment have a combined effect on organisms of pregnant residents and cause a high risk of prenatal fetal suffering.

The ecologically unfavourable urban environment promotes changes in physiological and biochemical processes underlying prepathology and pathology. Women of Ekaterinburg have indices of ecological valency, disturbance of reproductive functions and pregnancy complication (gestoses, anaemia, threaten pregnancy interruption). 80% of the inspected woman had somatic pathology. Among diseases the leading were anaemia, chronic infectious-inflammatory diseases, kidney and endocrine diseases, various forms of mastopathy. Fetoplacental insufficiency, complicated pregnancy and delivery, postnatal complications unfavourably affect the newborn's state. Therefore, health protection, especially protection of health of women and the newborn in conditions of ecologically unfavourable regions including the Urals is priority.

References

- [1] Onishchenko G.G., The effect of environmental conditions on the population health, unsolved problems and aims. *Hygiene and sanitary*, **1**, pp. 3–8, 2003.



- [2] Rahmanin N.V., Revazova J.A., Ivanov S.I., Novikov S.M., The actual problems of human ecology and the environment hygiene. *Vest. Med. Acad. Sci. Ural. Div.*, **2**, pp. 18–23, 2005.
- [3] Oberlis D., Kharland B., Skalny A., The biological role of trace elements of a Man and animals, Nauka: St.-P-burg, 2008.
- [4] Avtsyn A.P., Zhavoronkov A.A., Rish M.A., Strochkova L.S., Microelements of a Man: an aetiology, classification, organopathology. Medicine: Moscow, 1991.
- [5] Agadzhanyan N.A., Adaptation medicine and health. *Vest. Med. Acad. Sci. Ural. Div.*, **2** pp. 10–18, 2005.
- [6] Bolshakov V.N., Mikshevich N.V., Peredery O.G., Ecological evaluation of the work of enterprises of nonferrous metallurgy, Manual – Poligrafist: Sverdlovsk, 1986.
- [7] Kovalchuk L.A., Ecologo-physiological aspects of adaptation to conditions of technogenic ecosystems, NISO Ural Div.RAN: E-burg, 2008.
- [8] Kovalchuk L.A., Satonkina O.A., Tarkhanova A.E., Heavy metals in the environment of the Middle Urals, their influence on an organism. *Ecology*, **5**, pp. 358–361, 2002.
- [9] Regional peculiarities of sanitary-and-epidemiological situation in Sverdlovsk region. GUSCMSR: E-burg, 2008.
- [10] Ailamazyan E.K., Savitsky G.A., Beljaeva E.V., Vinogradova E.G., The role of ecological and industrial factors in formation of a of reproductive function pathology in women. *Vest. Rus. Ass. Obst. and Gynec.*, **2**, pp. 13–16, 1996.
- [11] Skalny A., Odinayeva N., Lukoyanova O. Trace elements in the newborn and their mothers from different regions of Russia. *Proc. 2nd Int. Symp. on trace elements in human and new perspectives.* Athens, 1999.
- [12] Strizhakov A.N., Timohina T.F., Bayev O.R., Phetoplacental insufficiency: pathogenesis, diagnosis, treatment. *Problems of Gynec., Obst., and Perinatology*, **2(2)**, pp. 53–56, 2003.
- [13] Eichhorn G. L., Intra metal ions and genetic regulation. Metabolism of trace metal in man, Ed. O. M. Rennert., W. Y. Chan, Boca Raton, pp. 1–6, 1984,
- [14] Kirchgessner M., Underwood memorial lecture. Homeostasis and homeorhesis in trace element metabolism. *Trace elements in Man and animals* (Tema – 8). M. Anke., D. Meissner., C.F. Mills (eds). Dresden, pp. 4–21, 1993.
- [15] Schrauser G.N., The discovery of the essential trace elements: An outline of the history of biological trace elements research. *Biochemistry of the ultratrace elements.* Ed. E. Freiden, Plenum Press: New York, London, pp. 17–32, 1994.
- [16] Trakhtenberg I.M., A book about poisons and poisonings. Toxicology sketches.– Kiev: Naukova Dumka, 2000.
- [17] Diperman A.A., The .role of environment contaminants in the disturbance of embryonal development, Medicine: Moscow, 1980.



- [18] Tarkhanova A.E., The effect of anthropogenic factors on formation of fetus and newborn hypoxia of women dwelling in a big industrial center. A.R. Diss.: Samara, 2004.
- [19] Tarhanova A.E, Kovalchuk L.A., Peculiarities of spectrum of essential amino acids in the blood plasma in women with physiological pregnancy in conditions of an industrial city. *Vest. Med. Acad. Sci. Ural. Div*, **2(25)**, pp. 171–172, 2009.
- [20] Skalny A., Diagnostics and preventive of microelementoses based on the results of medico-ecological inspection. Bases of system analysis in ecologo-hygienic studies. St-P-burg, 2000.
- [21] Boev V.M., Environment and ecologically caused disbalance of microelements in the population of urbanised and rural territories. *Hygiene and Sanitary*, **5**, pp. 3–7, .2002.
- [22] National Integrated Programmes on Environment and Health in Countries of Central and Eastern Europe (CCEE) / Coddon D., Yoldsmith Y., Yedrichovski W. et al, Moscow, 1994.
- [23] Trakhtenberg I.M., Kolesnikov V.S., Lukovenko V.P., Heavy metals in an environment: Modern hygienic and toxicological aspects Наука і техніка: Minsk, 1994.
- [24] Shtabsky B.M., Xenobiotiks, homeostasis and chemical safety of people. Lviv, 1999.



Section 8

Water quality issues

This page intentionally left blank

Groundwater quality on a waste disposal area due to sand mining activities in São Paulo State, Brazil

D. M. Bonotto¹ & E. G. de Oliveira²

¹*Departamento de Petrologia e Metalogenia, Instituto de Geociências e Ciências Exatas-UNESP, Rio Claro, Brazil*

²*Departamento de Geologia Aplicada, Instituto de Geociências e Ciências Exatas-UNESP, Rio Claro, Brazil*

Abstract

This investigation reports the results of a study realized in an area related to the development of sand mining activities, which belongs to Sibelco Mineração Ltd. The site is located around Analândia municipality, nearly in the center of São Paulo State, Brazil. Hydrochemical analyses of groundwater were realized under different periods of time, with the aim of evaluating the possibility of release of several constituents to the liquid phase, which may be a source of pollution of the surface hydrological resources and of the deeper Guarani aquifer. This is because the site is located at the recharge area of Guarani aquifer and some tributaries from Corumbataí river may also be suffering contamination, implying on the impoverishment of the water quality that are very important resources in the region, as they are extensively used for drinking purposes, among others.

Keywords: sand mining activities, water quality, groundwater, elemental concentrations, trace and heavy metals, São Paulo State.

1 Introduction

The São Paulo State in Brazil, due to its advanced stage of agricultural and industrial growth, has a great diversity of problems related to the interaction between the society and the environment. The sand mining activities in Depressão Periférica geomorphological province are presently very important, because potentially they can be a source of anthropogenic impacts, since several



chemicals are used for the treatment of natural sand like HCl, H₂SO₄, NaOH and Na₂SiO₄, generating mine tailings that can pollute the surface and underground hydrological resources. This study focuses one area belonging to Sibelco Mineração Ltd., located about 5-6 km from Analândia city, nearly in the center of São Paulo State (Fig. 1). The knowledge of the concentrations of dissolved elements and compounds is needed in order to establish their background values and to predict their potential increase in future years. Thus, the purpose of this paper is to compare the values obtained for various parameters in groundwater from the studied area with those defined by the national standards for drinking water.



Figure 1: Location of the Analândia city at São Paulo State, Brazil, and simplified geological map of area studied. Modified from [1–3].

2 General features of the area studied

The area is situated within the Corumbataí river basin that occurs in an eroded belt in the cuestas zone of the Depressão Periférica geomorphological province [4]. The Corumbataí river basin extends over an area of about 1,581 km². It is a sub-basin of the giant Paraná sedimentary basin, whose area is about 1,000,000 km² in Brazilian surface [5]. Several stratigraphic units of the Paraná basin (Paleozoic - Cenozoic) crop-out in it as described by [3], where the main lithologies include: the Lower and Upper units from Pirambóia Formation, the Botucatu Formation and the weathered cover developed over Pirambóia Formation (red-yellow latosols).

The Lower unit from Pirambóia Formation consists of a consolidated whitish sandstone (after washing) with well-preserved sedimentary structures, whose thickness is more than 80 m, the retention after grinding is greater on the 0.125 mm-size sieve, and the Fe oxide mineral content is low. The occurrence of small clay lenses of variable lateral size is very common in this unit. The Upper unit from Pirambóia Formation is a light pink saprolite characterized by thin sedimentary structures and very brittle sandstone located above the water table, whose concentration of Fe oxide is also low and the dominant particle-size after milling is in the range 0.125-0.25 mm.

A 1-30 cm thick stone line profile [6] occurring as an irregular replica of the topography divides the Upper unit from Pirambóia Formation and the above located mantle of weathering, which is constituted by tabular blocks of sandstones cemented by black coloured limonite, dark red ferruginous concretions, small tablets of limonite cementing sandstone, SiO₂ pebbles, weathered yellowish sandstone and major concentration of heavy minerals (hematite, magnetite and ilmenite).

The Botucatu Formation is represented in the area by weathered sandstones with high content of Fe oxide and particle-size predominantly in the range 0.5-1 mm.

The weathered cover developed over Pirambóia Formation includes: peat soil, creep soil, and soil above the stone line. The peat soil is light grey-black colored, and occurs from the point of the discharge of the water table up to the contour level corresponding to that of the local streams. The creep soil is very clayey (12-20%), occurs on the steep ground, being characterized by a red-brownish color, values of Fe oxide content of about 5000 ppm, and presence of limonite concretions between 2 and 6 m depth. The soil above the stone line is yellow-orangish colored, its thickness may attain 18 m, occurs where the ground slope is smooth, has a clay content varying between 7 and 18%, and a higher Fe oxide content near the surface due to the laterization, which diminishes with increasing depth, rising again at the stone line position.

The area investigated in this study is inserted within the Taipas stream sub-basin of the Corumbataí river basin (Fig. 1). The Taipas stream is the main drainage in the area; its name changes to Ponte Funda current, about 1 km upstream from the sand mining area. Its general flow direction is NE-SW, flowing towards SW up to the confluence with the Corumbataí River. Its average



discharge is 337.49 L/s, decreasing approximately 10% during the drier months. It also controls the groundwater flow as demonstrates the piezometric lines direction characterized by a gradient increase at the channel position (Fig. 2).

The mean ground slope of Taipas stream is 2.0% and slightly lower (1.3%) in front of the sand mining area, where the groundwater flow lines exhibit the following characteristics (Fig. 2): a) hydraulic gradient ranging from 0.10 (10% or 6°) to 0.15 (15% or 8°); b) main direction of the flow vectors varying from N-S to NW-SE.

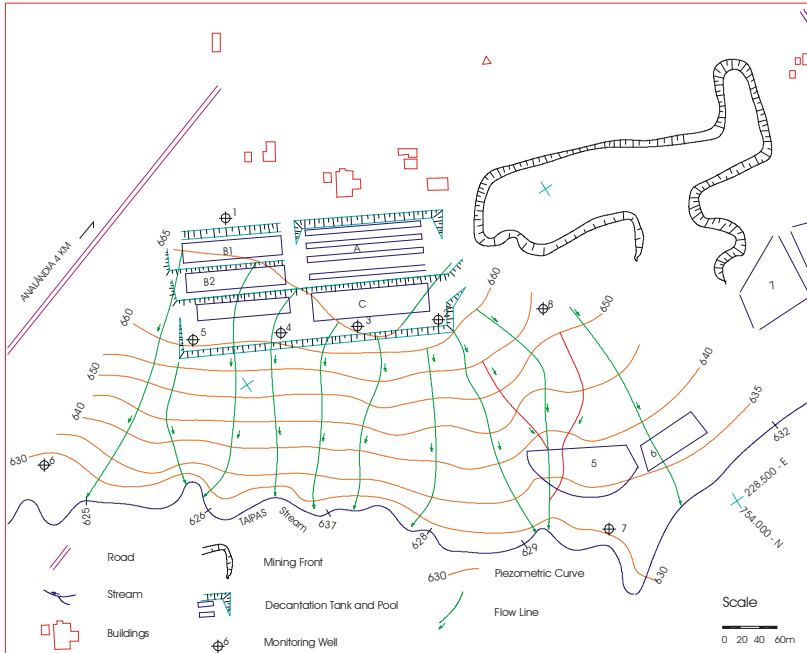


Figure 2: Piezometric map and location of decantation pools and tanks at the studied area.

However, some distortions occur in the groundwater flow lines, mainly between the monitoring wells 2 and 8, which are caused by two dominant factors:

1. Existence of a fault line that created a more permeable zone in this region, responsible by the water table lowering in monitoring well 8. Actually, such deformation extends from the area between wells 2 and 8 up to the monitoring well 7, along the fault. This faulting fits the regional pattern despite being masked by the weathered cover developed over Pirambóia Formation.
2. Sedimentary character of the flow net, i.e. it occurs in the Lower unit from Pirambóia Formation that controls its direction. Thus, there is no complete subordination to the hydraulic gradient, but also to the less permeable and more

compact characters of this unit. This aspect is reinforced by the lower inflexion of the flow lines towards Taipas stream, where occurs the groundwater discharge. The flow lines in Fig. 2 also indicate that the zones of lower altitude (630-650 m) exhibit higher permeability and lower hydraulic gradient than the areas situated at the more elevated altitudes (650-665 m).

3 Material and methods

The groundwater sampling was held in 8 monitoring wells drilled for characterizing the subsurface flow (Fig. 2 and Table 1). The first station was located up-flow of the waste disposal/treatment area, whereas all others were situated down-flow (Fig. 2). Three water sampling campaigns were realized (September 1993, March 1994 and October 1994) in which the samples were stored in polyethylene bottles, and depending on the requirements of the analysis, they were a) unfiltered and unpreserved, b) filtered through 0.45 μm membrane and unpreserved and c) filtered and preserved with different acids.

Table 1: Characteristics of the monitoring wells drilled at the studied area.

Parameter	Unit	1	2	3	4	5	6	7	8
Diameter	mm	100	100	100	100	100	100	100	100
Length	m	31.0	25.9	26.2	25.2	26.3	15.7	6.7	-
WTD1 ^a	m	13.99	10.38	6.17	9.62	10.01	5.41	1.25	-
WTD2 ^a	m	16.90	10.40	7.32	10.80	11.45	5.00	0.50	-
WTD3 ^a	m	18.90	11.70	8.80	12.70	13.70	5.80	1.15	18.30
WLT1 ^b	m	14.10	14.35	18.93	14.30	14.75	10.70	5.60	-
WLT2 ^b	m	12.10	14.20	17.45	12.50	12.60	9.90	5.55	-
Water Volume ^c	L	442.7	450.6	594.4	449.0	463.2	336.0	175.8	-

^aWTD = Water Table Depth (1-September 1993; 2-March 1994; 3-October 1994);

^bWLT = Water Layer Thickness (1-March 1994; 2-October 1994); ^cMarch 1994.

Portable meters were used for *in situ* measurements of temperature, pH, and dissolved oxygen (DO), with the equipment calibration being performed immediately before the analyses. The pH measurement was performed by a digital portable meter coupled to a combination glass electrode; buffer solutions equilibrated with the sample temperature were utilized to calibrate the equipment before the analyses. The DO was determined in a pointer meter recording the potential values generated by an O₂ sensible electrode consisting on a metallic wire covered by a thin layer of gold. A bench digital meter provided electrical conductivity readings obtained through a 1 cm² area platinum electrode calibrated with KCl standards.

The settleable solids in each sample were evaluated by a clear borosilicate glass Imhoff cone 0-1000 mL calibrated. The dry residue (DR) content was evaluated on evaporating the filtrate to dryness in a weighed flask that was dried



to constant weight at 180°C, with the increase in flask weight representing DR [7]. The BOD (Biochemical Oxygen Demand) was measured by the dilution method, employing high purity distilled water provided by Barnstead Mega-Pure One Liter Water Still. For this purpose, the dissolved oxygen (DO) content remaining in six portions of each well-mixed sample transferred to different 300-mL glass-stopped bottles was evaluated after a 5-day incubation period. The DO values measured potentiometrically by using a DO probe were plotted against the sample volume taken, yielding a straight line that allowed obtain the BOD data. The chemical oxygen demand (COD) was evaluated by the dichromate reflux method [7], using aliquots acidified to pH=2 with concentrated H₂SO₄.

Standard analytical techniques consisting on colorimetry and inductively-coupled plasma spectrometry were used for determining the following metals in the water samples: Fe, Al, Ca, Pb, Mg, Ni and Ag. The amount of Pb, Al and Fe in the samples collected in September 1993 and March 1994 was estimated colorimetrically by Hach DR/2000 spectrophotometer [8]. Lead ions in basic solution reacted with dithizone to form a pink to red lead-dithizonate complex, extracted with chloroform and read at 515 nm. The aluminon method that utilizes ascorbic acid provided the measurements for aluminum, read at 522 nm. The 1,10 phenanthroline indicator formed an orange color in proportion to the iron concentration, which was read at 510 nm. All other analyses were realized by inductively-coupled plasma spectrometry [9] that exhibits a lower detection limit than colorimetry. Tables 2-4 report the results of the measurements.

Table 2: Analytical data of the groundwater samples collected in 09/06/1993.

Parameter	Unit	1	2	3	4	5	6	7
Temperature	°C	30	27	29	29	30	30	26
DO	mg/L	2.6	7.6	8.9	6.5	4.0	7.7	4.1
pH	-	6.85	5.95	6.30	6.07	6.17	6.13	6.42
Conductivity	µS/cm	510.0	25.1	21.1	66.2	55.0	101.9	84.4
Iron	mg/L	3.00	0.02	0.06	<0.02	<0.02	<0.02	0.60
Aluminum	mg/L	3.30	<0.10	<0.10	<0.10	<0.10	<0.10	2.20
Calcium	mg/L	3.50	0.50	0.90	0.80	1.70	8.20	3.20
Lead	mg/L	<0.10	<0.10	<0.10	<0.10	<0.10	<0.10	<0.10
Magnesium	mg/L	1.50	0.20	0.30	0.20	0.70	2.30	0.60
Nickel	mg/L	<0.02	0.02	0.09	0.02	<0.02	<0.02	<0.02
Silver	mg/L	<0.10	<0.10	<0.10	<0.10	<0.10	<0.10	<0.10
COD	mg/L	36.80	18.40	9.20	9.20	9.20	27.60	9.20
BOD	mg/L	44.75	19.00	6.84	8.68	8.30	9.52	11.36
Dry residue	mg/L	364	46	28	568	44	62	118
Settleable solids	mg/L	47.72	<0.01	1.04	<0.01	1.20	0.03	382.93



Table 3: Analytical data of the groundwater samples collected in 03/31/1994.

Parameter	Unit	1	2	3	4	5	6	7
DO	mg/L	5.1	2.0	4.8	3.7	3.5	4.1	3.2
pH	-	6.51	5.65	5.97	6.30	6.37	5.86	6.31
Conductivity	µS/cm	356.0	33.2	27.6	89.0	69.7	105.1	79.5
Iron	mg/L	0.05	0.10	<0.02	0.03	<0.02	<0.02	<0.02
Aluminum	mg/L	<0.10	<0.10	<0.10	<0.10	<0.10	<0.10	<0.10
Calcium	mg/L	1.50	0.60	0.60	1.20	1.40	8.30	4.50
Lead	mg/L	<0.10	<0.10	<0.10	<0.10	<0.10	<0.10	<0.10
Magnesium	mg/L	0.70	0.30	0.30	0.30	0.70	2.50	0.80
Nickel	mg/L	<0.02	<0.02	<0.02	<0.02	<0.02	<0.02	<0.02
Silver	mg/L	<0.10	<0.10	<0.10	<0.10	<0.10	<0.10	<0.10
COD	mg/L	6.48	4.33	4.32	17.44	16.28	2.32	19.76
BOD	mg/L	6.11	0.94	3.29	5.64	4.23	1.87	3.29
Dry residue	mg/L	200	60	16	16	80	100	112
Settleable solids	mg/L	0.70	49.95	0.75	3.10	1.55	0.30	0.60

Table 4: Analytical data of the groundwater samples collected in 10/14/1994.

Parameter	Unit	1	2	3	4	5	6	7	8
Temperature	°C	27	26	25	25	25	25	24	25
DO	mg/L	3.2	5.8	7.3	7.3	6.4	7.4	7.0	7.0
pH	-	6.29	5.20	5.87	5.60	5.71	5.50	6.42	5.80
Conductivity	µS/cm	312.0	50.0	18.7	107.0	101.0	103.0	82.0	49.2
Iron	mg/L	0.80	0.01	<0.01	<0.01	<0.01	0.04	0.08	0.01
Aluminum	mg/L	1.07	0.02	0.01	0.03	0.02	0.05	0.37	0.06
Calcium	mg/L	1.77	0.92	0.66	0.90	1.74	8.05	5.12	1.66
Lead	mg/L	0.01	0.01	0.01	0.01	0.01	0.01	0.02	0.02
Magnesium	mg/L	0.74	0.48	0.27	0.29	0.82	2.57	0.91	0.82
Nickel	mg/L	<0.02	<0.02	<0.02	<0.02	<0.02	<0.02	<0.02	<0.02
Silver	mg/L	<0.10	<0.10	<0.10	<0.10	<0.10	<0.10	<0.10	<0.10
COD	mg/L	6.24	<1.00	<1.00	6.24	12.49	<1.00	6.24	<1.00
BOD	mg/L	<5.0	<5.0	<5.0	<5.0	12.5	<5.0	<5.0	<5.0
Dry residue	mg/L	216	40	26	102	67	90	48	32
Settleable solids	mg/L	0.10	<0.01	<0.01	<0.01	0.10	<0.01	0.10	<0.01



4 Discussion

The permissible concentration limits in Class 2 Brazilian fresh waters as established by National Register CONAMA 20 (published on 18 June 1986) is given in Table 5 and will be used as reference values to compare all data reported here.

Table 5: Permissible concentration limits in Class 2 Brazilian fresh waters established by national register CONAMA 20 published on 18 June 1986.

PARAMETER	UNIT	VALUE
pH	-	between 6 and 9
Settleable solids	mL/L	< 1 ^a
Total Dissolved Solids (~DR)	mg/L	< 500
DO	mg/L	> 5
BOD	mg/L	< 5
Lead	mg/L	< 0.03
Soluble Iron	mg/L	< 0.3
Nickel	mg/L	< 0.025
Silver	mg/L	< 0.01
Aluminum	mg/L	< 0.1

^aFor the release of effluents.

The highest value found for the settleable solids corresponded to 383 mg/L (Table 2). Under the most pessimistic assumption, if they would have the water density (1 g/mL), then, it would be possible estimate 0.38 mL/L for the settleable solids that is below the guidance value of 1 mL/L for this parameter (Table 5).

The total dissolved solids exceeded the CONAMA guideline values in one sampling campaign (September 1993) of monitoring well 4, however, it is within the analytical uncertainty of the technique (10-15%). The conductivity was always higher at bore 1 in all sampling campaigns. In general, higher total dissolved solids content also imply on more elevated conductivity values in water bodies and such trend was verified at bore 1 in the last two monitoring programs.

The National Register CONAMA 20 did not establish guidance levels for calcium and magnesium. The highest Ca and Mg contents were found at monitoring well 6, respectively, 8.0-8.3 mg/L and 2.3-2.6 mg/L. No health-based guideline value is proposed for hardness due to Ca and Mg in drinking-water by WHO [10]. Depending on the interaction of other factors, such as pH and alkalinity, water with hardness above approximately 200 mg/L may cause scale deposition in the treatment works, distribution system and pipework and tanks within buildings [10]. The data reported here are well below this value.

Some pH values are lower than the minimum of 6, as given in Table 5, and could be attributed to occasional anthropogenic inputs. The lowest value was 5.2 at monitoring well 2, whose sampling occurred in October 1994. However, the



low values of conductivity (50 $\mu\text{S}/\text{cm}$) and dry residue (40 mg/L) in this bore do not favor the enhanced presence of the cation Na^+ and anions SO_4^{2-} and Cl^- , which are potentially important to affect the area. On the other hand, this groundwater facies reflects the composition of rainwater with small amounts of silica added from contact with the aquifer. Such pattern of chemical data is not much amenable to plot on a standard Piper diagram [11], because there is a lack of the preponderance of typical anions and cations, and the mixed character is commonly identified. The rainwater interaction with the weathered mantle developed over Pirambóia Formation when it enters the aquifer by percolating through the unsaturated zone until it meets the water table constitutes a reasonable explanation for the low pH values, because the pH of several soil suspensions representative of horizons from three pedological profiles was determined both in water and in KCl solution and the most of the obtained values are strongly acid ($\text{pH} < 4.5$) or moderately acid (pH between 4.5 and 5.5) [12].

The CONAMA guideline level for dissolved oxygen was based on a criterion for the maintenance of the aquatic life in surface water bodies (Table 5). Several DO values are lower than the minimum of 5 mg/L, as given in Tables 2-4, demonstrating no pronounced aeration during sampling that is a typical situation expected in groundwater resources.

The BOD exceeded the CONAMA guideline value in the following circumstances: all bores (September 1993), monitoring wells 1 and 4 (March 1994) and bore 5 (October 1994). CONAMA did not establish guidance level for COD. Both the BOD and COD tests have been widely adopted as a measure of pollution effect based on the relative oxygen-depletion due to a waste contaminant. The BOD test measures the oxygen demand of biodegradable pollutants whereas the COD test measures the oxygen demand of biodegradable pollutants plus the oxygen demand of non-biodegradable oxidizable pollutants [13]. Despite there is no generalized correlation between BOD and COD, it is possible to develop it in some cases like verified for the groundwater samples collected in September 1993 (Fig. 3). Such relationship suggests that aerobic biological organisms are breaking down organic material present in the aquifer system following a proportion related to its abundance.

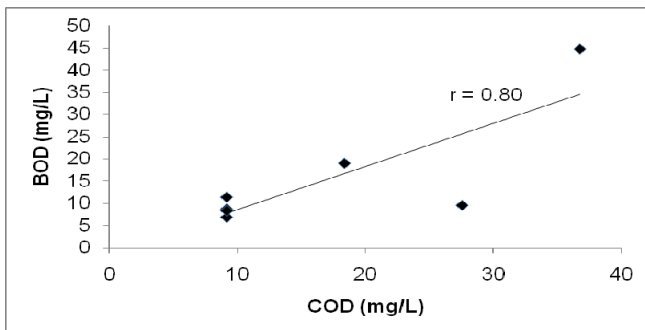


Figure 3: The relationship between BOD and COD in groundwater samples collected in September 1993.



The Ag detection limit (0.10 mg/L) in all sampling campaigns was above the CONAMA guidance level (0.01 mg/L). Ni exceeded the reference value in one sampling campaign (September 1993) of monitoring well 3, without a reasonable explanation. The Pb detection limit (0.10 mg/L) in the sampling campaigns held in September 1993 and March 1994 was above the CONAMA guideline value (0.03 mg/L). However, Pb was always below this reference value in the sampling campaign held in October 1994.

Fe always exceeded the CONAMA guidance level in monitoring well 1, the same occurring with Al in the sampling campaigns held in the wettest seasons (September 1993 and October 1994). Groundwater providing from this borehole often exhibited high turbidity possibly caused by some pre-filter leakage. Such assumption is reinforced by the enhanced Fe and Al contents in bore 1 relatively to others, as well by its location up-flow of the waste disposal/treatment area (Fig. 2). However, some anthropogenic inputs of these constituents are evidenced at monitoring well 7 during the sampling campaigns held in the wettest seasons, when the water table raised. This is supported by the fact that bore 7 was situated down-flow of the waste disposal/treatment area in a zone dominated by higher permeability and lower hydraulic gradient.

5 Conclusion

Hydrogeochemical monitoring held in eight bores drilled for characterizing the subsurface flow in a waste disposal/treatment area coupled to the development of Sand mining activities in São Paulo State, Brazil, allowed identify some anthropogenic inputs. BOD, Fe and Al contents in several groundwater samples have exceeded the permissible concentration limits in Class 2 Brazilian fresh waters as established by National Register CONAMA 20 published on 18 June 1986). The enhanced levels of these parameters is possibly related to the use of several organic and inorganic chemicals for the treatment of natural sand, which have generated mine tailings able to pollute the aquifer system occurring in the area. The BOD, Fe and Al levels decreased from September 1993 to October 1994 at a monitoring well situated in a zone dominated by higher permeability and lower hydraulic gradient. However, further monitoring programs would be needed for clarifying if the concentration decrease has been caused by natural attenuation processes, different rainfall regime, human action or others factors. This is because the site is located at the recharge area of Guarani aquifer and can also contaminate some tributaries from Corumbataí River, which are very important hydrological resources in the region.

References

- [1] IG (Instituto Geológico), *Formações geológicas de superfície-Folha Geológica de Corumbataí-Fl. SF-23-Y-A-12, 1:50000*. Instituto Geológico, São Paulo, 1984.
- [2] IPT (Instituto de Pesquisa Tecnológica do Estado de São Paulo), *Mapa Geológico do Estado de São Paulo*. São Paulo, Monografias, 1981.



- [3] Tandel, R.Y., *Caracterização do arenito Pirambóia da Fazenda São João em Analândia, SP, e sua utilização industrial*, USP, São Paulo, 75 pp., 1993.
- [4] Penteadó, M.M., Geomorfologia do setor centro-ocidental da Depressão Periférica paulista. *Série teses e monografias*, **22**, IGEOG/USP, São Paulo, 1976.
- [5] França, A.B. & Potter, P.E., Stratigraphy, Depositional Environment and Reservoir Analysis from Itararé Group, Paraná basin (Part 1). *Petrobrás Geosciences Bulletin*, **2** (2/4), pp. 147-192, 1988.
- [6] Lecomte, P., Stone line profiles: importance in geochemical exploration, *J. Geochem. Explor.*, **30**, pp. 35-61, 1988.
- [7] APHA (American Public Health Association), *Standard methods for the examination of water and wastewater*. 17th edn, Washington, 1989.
- [8] HACH, *Water Analysis Handbook*, 2nd edn, Hach Company: Loveland, 1992.
- [9] Nollet, L.M.L., *Handbook of Water Analysis*, 2nd edn, Taylor & Francis Group: New York, 2007.
- [10] Guidelines for drinking water quality; WHO (World Health Organization), Online. www.who.int/water_sanitation_health/dwq/gdwq3/en/
- [11] Piper, A.M., A graphic procedure in the geochemical interpretation of water analyses, *Trans.Amer.Geophysical Union*, **25**, pp.914-928, 1944.
- [12] Jiménez-Rueda, J.R., *Comments about some mineralogical data and pH values of soil suspensions from Pirambóia Formation*, 1994.
- [13] Sawyer, C.N., McCarty, P.L. & Parkin, G.F., *Chemistry for Environmental Engineering and Science*, 5th edn, McGraw-Hill: New York, 2003.



This page intentionally left blank

Ecological effects of underwater destruction of detonators in Lake Ormtjärn, Sweden: the impact from lead

B. E. Liljedahl, U. Qvarfort, R. Berglind & J. Sjöström
Swedish Defence Research Agency, CBRN Defence and Security, Sweden

Abstract

After the Second World War, dumping in lakes was a rational way to solve the security problem with the extensive amount of unused, aging ammunition. Most commonly the ammunition was dumped in sealed boxes or as pieces. In some cases the ammunition was deliberately detonated when dumped. In Ormtjärn, a small lake in central Sweden, very high levels of lead (1900 mg/kg dry weight Pb) were detected in the sediments indicating a possible need for remediation. The lead was expected to originate from years of underwater destruction of about 1.5 million detonators containing lead azide. The lake is unique in the sense that the lead levels are among the highest in Sweden, the boundary is well defined and that no other source of pollutant is present in the lake. It is also the only known major site for underwater destruction of detonators in freshwaters in Sweden. The aim of this study was to evaluate the environmental impact from underwater destruction of detonators containing lead azide in this natural forest lake.

Samples were taken of sediment, bottom water, surface water, bottom fauna and littoral and was analysed for Pb and physical parameters in order to investigate if a possible effect on biota could be demonstrated from the heavily polluted sediment. Acute toxicity of sediment was determined with a mouse cell assay.

Results showed high to very high lead content (1500-2000 mg/kg dry weight) in sediment down to 25 cm depth evenly distributed over the whole lake. Water showed low levels (surface water) to high levels (bottom water) of Pb. Disturbance on bottom fauna was observed for BQI-index but none for O/C-index. No effect on littoral fauna was found. Acute toxicity was low for bottom



water (*Daphnia magna*), and cytotoxicity (neutral red incorporation assay, L-929 mouse cell line) was low in the sediment.

Keyword: bottom fauna, detonators, ecological impact, lead (Pb), littoral fauna, sediment, underwater destruction.

1 Introduction

After the Second World War several amounts of ammunition were dumped in about 100 lakes in Sweden (Sjöström et al. [1]). The reason was to make a safe disposal of aging and malfunction ammunition which, if left in store, might self-explode. Dumping of ammunition was a legal disposal method until 1970s for the ammunition industry, resulting in that several lakes in Sweden today host large amount of ammunition. Some of the lakes were also used for underwater destruction of detonators. The possible needs for remediation of lakes with such ammunition deposits have been intensively discussed in Sweden i.e. as to safety issues and costs if all dumped ammunition should be removed in relation to the ecological impact if left in place. This set focus on the issue of possible long term leaching from dumped ammunition to sediment, water and biota. Lead impact on lake sediment and biota (Förstner and Kresten [2], Davis and Galloway [3], Riba et al. [4], Bäckström [5]) as well as the environmental impact from dumped ammunition (Sjöström et al. [6], Voie [7], U.S Geological Survey [8]) and underwater detonations (Karlsson et al. [9]) has been discussed in different studies. However, none of these studies could be used to predict the future effects of leaching of lead from underwater destruction of detonators. One problem is the well-known concern that an ecological impact studied in the field, often might origin from different pollutants and that it is difficult to define a strict pollutant – effect connection to the source of interest (Covello and Merkhofer [10], Tuvikene et al. [11]) in this case, the underwater destruction of detonators. Another concern is the internationally addressed need for increased ecological perspective in risk assessments (den Besten et al. [12]). In order to increase the knowledge regarding possible future ecological impact from destructed detonators, it has been of interest to find a lake with well-defined natural boundaries, where the sediments are polluted from lead azide or lead oxide, and where no other source of pollution can be expected. A study of such a well-defined lake might contribute with information on its present ecological status as well as with information on possible expected long term ecological effects from underwater detonation during which lead azide will form the product lead oxide in the explosion.

The objective of the study was to evaluate the environmental impact from underwater destruction of detonators containing lead azide, with special focus on lead and some ecological effects shown by bottom fauna in a natural forest lake. An attempt was also made to study the effects on the fish in the lake. Gillnetting resulted however only in four fishes. Analysis showed lead content in (*muscle*) up to 0,148 mg/kg for perches. Because of the limited number of fishes will the results not been included in the study but a follow-up study is however planned.



2 Experimental, material and methods

2.1 Lake Ormtjärn characterisation

Lake Ormtjärn is a small, natural forest lake located at a shooting field in the central part of Sweden. The shooting field is situated on a water dividing zone (200 m above sea level) with discharge in three directions. The lake area is 0.0085 km², average depth is 4 meter and the catchment area approx. 0.5 km². The water retention time of the lake is estimated to be 5 months. Oxygen level decreases from 6ppm in surface water to 2 ppm in the bottom water. The pH is close to 6 (6.1 in surface water and 5.9 close to the bottom), and the concentration of sulphate range from 4 ppm (surface) to 3.2 ppm (bottom). Alkalinity range from 0.7 mekv/L (surface) and to 0.3 mekv/L (bottom) and total organic carbon (TOC) from 7ppm (surface) to 11ppm (bottom). Upper sediment (0-5 cm) has an organic content of 48% (dry weight of 70%). Underlying sediment (20-25 cm) has an organic content of 43% (dry weight 58%) (Sjöström et al. [13]).

Lake Ormtjärn has no well-defined outlet or inlet. Water arrives from a small pine vegetated hill and from a well vegetated wetland. The lake is drained by percolation through a wetland. The geological conditions represent a typical Swedish forest area.

No nearby located lake were suitable as Reference Lake i.e. with regard to geochemical and ecological status, since all surface waters in the area had been more or less affected by dumping and/or shooting activities. For this reason, natural background reference levels and conditions have been compared with studies of lakes in middle Sweden (Sjöström et al. [13]). For specific geochemical background of pollution impact from day-to day activities at the shooting fields, comparison has been made with nine nearby lakes within the shooting field (Sjöström et al. [13]).

2.2 Pollution profile

About 1.5 million detonators containing 0.5 – 1.5 g lead per detonator (lead azide (Pb (N₃)₂) were dumped and destroyed in the lake between 1950s and 1990s. This corresponds to approximately 1500 kg pure lead. The detonators was dumped as pieces or packed in bags, sunk in the lake and destructed by underwater detonation. No other pollution source is known for the lake. A minor background impact might be expected from the day-today shooting at the field Waleij et al. [14]. The geological geochemistry in the area does not imply naturally increased levels of lead in sediment Swedish Geological Survey [15].

2.3 Impact scheme, lead conditions and some ecological effects

There are several methods for risk assessment within the framework of remediation, where consideration is given to the balance between type of pollutant, risk of leaching, sensitivity of surrounding environment and amount of pollution Swedish Environmental Protection Agency [16] (Covello and Merkhofer [10]). To facilitate the comparison of chemical impact (lead content)



and ecological impact, a simple scheme moderated from different Swedish EPA regulations has been developed within the study.

2.4 Sampling

A total of nine sediment samples were taken during three occasions in May 1999 (S23; 0-5 cm and 20-25cm) Sjöström et al. [13] (O1-O7; 0-5 cm and 10-15 cm respectively) (Qvarfort et al. [17]) and May 2000 (O8; 0-5 cm). Sediment cores from the water-sediment interface down to mineralised layers were sampled. The sediment cores were split into 5 cm layers onsite, and the samples were stored in plastic boxes at +4°C and dark until analysed.

Water samples were taken on three occasions; March 2000 (W1 at 0.5 m depth) (Qvarfort et al. [17]), May 2001 (W2 at 4m depth) and September 2001 (W3 at 0.5 m depth). Samples of surface and bottom water were taken by Rüttners sampler. Water samples were stored in 0.5 L acid rinsed plastic bottles (for metals) and in glass bottles (for analysis of explosives), and stored in darkness at +4°C until analysed. PH was measured on site.

Bottom fauna were collected at two sites with Ekman Bottom Grab Sampler by i.e. 10 samples respectively. Samples were sieved from coarse material and placed in plastic boxes filled with 98% ethanol, and stored dark at +4°C until analysed. Littoral fauna were collected along a spatial 20 m profile on the “long side” and “short end” of the Lake Ormtjärn by kick sampling according to method M42 Swedish Environmental Protection Agency [16]. Samples of emerging insects were collected on 3x5 occasions by butterfly net in surface water, air above surface water, and along the lake shore. Samples were collected in plastic boxes filled with 98% ethanol, turned over and stored dark at +4°C until analysed, figure 1.

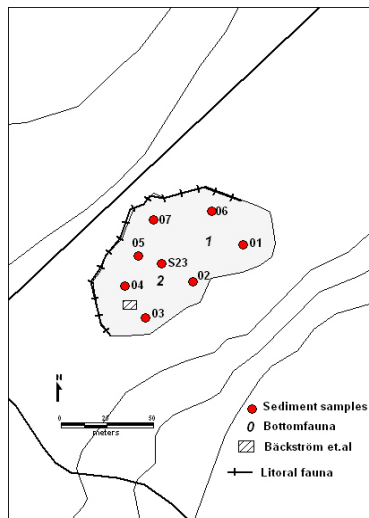


Figure 1: Sampling of Lake Ormtjärn.

2.5 Analysis

Sediment were analysed for metals according to EPA-method 200.7 and 200.8 (modified). Metals in water were analysed by ICP-SFMS. W represent water analysis and S sediment analysis.

Table 1: Sampling and analysis.

Sample	Date	Level	Total number	Analysis
W1	00-03	0.5 m	1	pH, conductivity, alkalinity
W2	00-05	4.0 m	1	As, Cd, Co, Cr, Cu, Hg, Mn, Ni, Pb, Zn, TNT and its degradation products, RDX, HMX, picric acid. Toxicity <i>Daphnia magna</i>
W3	00-09	0.5 m	1	NO ₃ /NO ₂ , Ntot, NH ₄ , Ptot, PO ₄ , pH and conductivity (mS/m), ToC, alkalinity, color
S 23	99-03	0-5/20-25 cm	1x2	As, Cd, Co, Cr, Cu, Hg, Mn, Ni, Pb and Zn, dry weight, Organic content
S1-S7	00-03	0-5/10-15 cm	7x2	
S8	00-05	0-5 cm	1	only TNT and its degradation products, RDX, HMX, picric acid. Toxicity <i>Daphnia magna</i> and Cytotoxicity

Water geochemistry data of Lake Ormtjärn has been provided by Bäckström [5]. Additional water analysis in this study was limited to three complementing analysis regarding explosives and water characterisation of relevance for the interpretation of fauna results. Explosives in sediment and water were analysed by HPLC and GC/MS according to Sjöström et al. [13].

Bottom fauna was analysed by abundance, and taxa. Additional analyses were made for BQI-index indicating nutrient and / or organic content in bottom water and for O/C index indicating oxygen saturation in bottom of the lake. Littoral fauna was analysed for Taxa, ASPT-index, Danish fauna index and Acidity index Swedish Environmental Protection Agency [18].

Acute water toxicity was assessed using *Daphnia magna*. The experiment was performed as a static acute toxicity test, following the procedure described in SS028180 (ISO 6341-1982: Water quality - Determination of the inhibition of the mobility of *Daphnia magna* Straus (*Cladocera*, *Crustacea*)). Five to ten animals, neonates < 24 h old, were added to 30 ml test solution in a 50 ml glass beaker. The exposure time was maximised to 48 h. Water temperature, pH, conductivity and dissolved oxygen were measured at the start and at the end of the test in controls and in the highest and lowest test concentrations. The number of immobilised animals was checked 24 and 48 h after test start. The water fleas



were considered as immobilised when their appendages or the body failed to move upon prodding.

The water fleas were cultured in 500 ml beakers filled with 300 ml reconstituted hard water prepared in untreated tap water according to Klüttgen et al. [19]. The animals were fed daily with algae, *Selenastrum capricornutum* (approx. 10^6 cells/ ml). The water hardness was about 275 mg CaCO_3 /l and the pH was between 7.9 and 8.2. The temperature was kept at $22 \pm 1^\circ\text{C}$ and the photoperiod was 16 h light and 8 h dark.

The test solution was prepared by diluting the water sample with the daphnia culture water. The test concentrations were prepared by serial consecutive diluting of the water sample giving a series with a diluting factor of study 1.5. Values for EC_{50} (probit analysis, SPSS soft ware) was calculated for the 24 and 48 hours of exposure.

Acute sediment toxicity, from sediment water extracts, was assessed by a growth inhibition assay using L-929 cells (mouse fibrocytes). Inhibition of cell growth were detected in a neutral red incorporation assay (NRI), initially described by Borenfreund and Puermer [20] and adapted to L-929 fibroblasts by Sauvart et al. [21]. Cells were grown in a cultivation medium containing EMEM (Eagles Minimum Essential Medium, Gibco), complemented with 10% FCS (Fetal Calf Serum, Gibco), 1% L-Glutamine (Gibco), 1% NEAA (Non Essential Amino Acids, Gibco) and 50 mg/ml Gentamycine (antibiotics, MERCK), and incubated in humidified atmosphere at 37°C and 5% carbon dioxide thus adjusting pH to 7.2. Toxicity measurements were performed as cell culture growth inhibition tests in 96 well microtiter plates (Becton Dickinson Labware, NJ, and USA). Cells were exposed for 72 h to a mixture of growth media and sediment extracts, produced by the extraction procedure (L/S ratio 2,5:1, shaking in 50°C for 14h), proposed by Wahle and Kördel [22] in proportions of 50, 25, 10 and 1 vol% respectively. Prior to exposure all extracts were filtered through 0, $22\mu\text{m}$ Millipor© as sterility is required.

2.6 Impact scheme, geochemical conditions and ecological effects

A coarse scheme has been developed summarizing the impact from underwater destruction of detonators. The impact level has been moderated from and related to Swedish regulations and recommendations approved by Swedish environmental protection agency [23], sediment, bottom fauna and littoral fauna Swedish Environmental Protection Agency [24], and toxicity (Daphnids and L-929, see 2.4) also linking to normally occurring follow up activity (“trigger for remediation / monitoring or other”). Five levels of impact were chosen for summarizing the observed effects;

1. Very low level little or none impact or background level – *no action*
2. Low level slight impact or near background level – *no action*
3. Medium level significant impact - *normally not causing action*
4. High level large impact - *might cause action if supported by other risk factors*
5. Very High level very large impact - *normally causing action*



3 Results

3.1 Sediment and water

Sediment samples showed high content of lead in all parts of Lake Ormtjärn. Lead content were highest at level 0-5 cm (2090-1570 mg/kg dry weight) with a slight decrease at level 10-15 cm (1970-1290 mg/kg dry weight). The sample at 25 cm depth had a lead content of 1940 mg/kg dry weight. Bottom water samples contained up to 3.4 µg/L for Pb. Other analysed metals showed low to moderate levels. No explosives or degradation products were detected in sediment or bottom water. Physical and nutrient conditions of the lake were good with pH at 6.1 and alkalinity of 17.8 mg/L CaCO₃, representing the natural conditions of one common type of Swedish soft water forest lakes. Results of geochemical analysis of water and sediment are shown in, tables 2a-c.

Table 2a: Geochemistry sediment Lake Ormtjärn. The metal contents in µg/L.

Sample	Level cm	Dry weight %	Organic content %	As	Cd	Cu	Hg	Pb	Zn
S23 0-5	0-5	70,1	48,7	0,588	0,349	14,9	0,263	2090	235
S24 20-25	20-25	57,9	43,3	0,812	0,281	13	0,252	1940	204
O1 0-5	0-5	4,6	48,3	1,05	0,366	13,4	0,49	1570	196
O1 10-15	10-15	10,5	33,1	0,611	0,232	9,55	0,212	1290	164
O2 0-5	0-5	7,8	39	0,458	0,168	9,82	0,109	1780	182
O2 10-15	10-15	10,9	35,3	0,412	0,178	10,4	0,0805	1500	185
O3 0-5	0-5	4,1	50,9	0,959	0,37	15,3	0,431	1910	238
O3 10-15	10-15	7,7	44,4	0,682	0,266	13,8	0,324	1890	201
O4 0-5	0-5	4	49,9	0,81	0,395	14	0,162	1820	246
O4 10-15	10-15	7,8	40,4	0,52	0,183	10,5	0,0963	1760	182
O5 0-5	0-5	5,5	48,9	0,753	0,332	15,7	0,162	1950	270
O5 10-15	10-15	7,2	46,8	0,447	0,245	12,2	0,114	1970	225
O6 10-15	10-15	10,5	34,4	0,333	0,186	9,14	0,0942	1310	157
O7 0-5	0-5	27,2	50,3	0,828	0,365	16	0,164	1750	239
O7 10-15	10-15	38,7	44,3	0,565	0,248	13,2	0,299	1670	190
O8 0-5	0-5	6		0,74	0,28	14,7	0,28	1810	213

Table 2b: Water chemistry Lake Ormtjärn.

Sample	Depth (m)	As	Cd	Cu	Hg	Pb	Zn
W2 bottom water	4	0.174	0.082	3.49	0.0026	3.43	22.9



Table 2c: Physical conditions Lake Ormtjärn.

Sample	Depth (m)	Temp	pH	Conductivity /mS/m	CaCO ₃	Alkalinity	N total	Nitrite-nitrate	P total	Phosphate
		°C			mg/L	mg/L	mg/L		ug/L	
W1 bottom water	4	6	6.1	42.0		17.8				
W3 surface water	0.5	10	6.19	3.3	53.4		0.4	<0.02	10	2

Analysed concentrations of the explosives (TNT) were all below the detection limit < 1ng/L.

3.2 Bottom fauna and littoral fauna

Bottom fauna showed a significant higher abundance and number of taxa along the shore of the lake (B1) compared to the centre of the lake (B2). Abundance/m² was average 1700 for (B1) and 200 for (B2). Total number of taxa at (B1) was 8 (*Potamothenis/Tubifex sp.*, *Chaoborus flavicans*, *Arctopelopia*, *Procladius sp.*, *Tanytus sp.*, *Chironomus sp.*, *Chironomus sp plumosus*, *Chironomus sp thummi*, *Polypedilum sp.*) compared to 2 taxa for (B2) (*Leuctra sp.* and *Chaoborus flavicans*). BQI –index and O/C index was low for both sites (0-1) respectively (0-0.3) indicating high content of nutrients and/or organic content and good oxygen saturation in bottom water and sediment. Both numbers of taxa as well as abundance was to be considered low for station (B2) and slightly less effected for (B1) Swedish Environmental Protection Agency [23] indicating a disturbed ecological status in the midst of the lake but less disturbed conditions along the shore, table 3.

Littoral fauna showed a total of 33 taxa from 9 families (*Bivalvia*, *Oligochaeta*, *Crustacea*, *Ephemeroptera*, *Odonata*, *Heteroptera*, *Coleoptera*, *Trichoptera* and *Diptera*). Number of taxa as well as abundance was indicating undisturbed ecological conditions at the shore of the lake. ASPT-index was 5.9; Danish fauna index 5 and Acidity index 4, table 4.

3.3 Toxicity

The bottom water of Lake Ormtjärn was not toxic to newborn *Daphnia magna*. The number of immobilised or mortal / total animals was zero after both 24 h and 48 h in undiluted samples of bottom water.

The toxicity of the sediment from Lake Ormtjärn was compared to toxicity of sediment taken from the nearby lake Svarta Sjön, which is of approximately the same size as Lake Ormtjärn. Results showed no significant toxic effect of extracts from Lake Svarta Sjön or Lake Ormtjärn in the cytotoxicity test, figure 2.





Table 3: Bottom Fauna Lake Ormtjärn (depth of sampling 4 meters).

Lake Ormtjärn	Sample no. B1										Statistics - Sample no. B1		
Local 1	1	2	3	4	5	6	7	8	9	10	Mean value	%	S.D.
Taxa													
Oligochaeta													
Potamothrix/Tubifex sp.	0	0	0	0	1	0	1	0	1	0	0,3	0,8	0,5
Chaoboridae													
Chaoborus flavicans	13	8	5	3	1	14	4	11	13	24	9,6	25,0	6,9
Chironomidae													
Arctopelopia-typ	0	1	0	0	0	0	0	0	0	0	0,1	0,3	0,3
Procladius sp.	0	0	1	0	1	1	3	2	0	1	0,9	2,3	1,0
Tanypus sp.	0	0	0	0	0	0	1	0	0	0	0,1	0,3	0,3
Chironomus sp.	1	5	1	0	5	4	3	2	9	3	3,3	8,6	2,6
Chironomus sp. plumosus- typ	10	6	35	0	7	37	43	23	33	41	23,5	61,2	16,3
Chironomus sp. thummi-typ	0	0	0	0	0	0	0	0	4	1	0,5	1,3	1,3
Polypedilum sp.	0	1	0	0	0	0	0	0	0	0	0,1	0,3	0,3
Organisms/sample	24	21	42	3	15	56	55	38	60	70	38,4		22,0
Organisms/m ²	1066,6	933	1866,5	133	667	2488,64	2444,2	1688,72	2666,4	3110,8	1706,5		979,7
Taxa/sample	3	5	4	1	5	4	6	4	4	4	4,0		1,3
Taxa total	8												
BQI-index	1												
O/C-index													

Table 3: Continued.

Ormtjärn	Sample no. B2										Statistics - Sample no. B2			
	Local 2	1	2	3	4	5	6	7	8	9	10	Mean value	%	Stdav
Taxa														
Plecoptera														
Leuctra sp.	0	0	0	0	0	0	1	0	0	0	0,1	2,2	0,3	
Chaoboridae														
Chaoborus flavicans	1	0	1	0	27	7	2	4	1	1	4,4	97,8	8,2	
Individuals/sample	1	0	1	0	27	7	3	4	1	1	4,5		8,2	
Individuals/m ²	44,44	0	44,44	0	1199,9	311,08	133,32	177,76	44,44	44,44	200,0		364,2	
Taxa/sample	1	0	1	0	1	1	2	1	1	1	0,9		0,6	
Taxa/ total	2													
BQI-index	0													
O/C-index														



Table 4: Littoral fauna; identified taxa, ASPT-index, Danish fauna index and Acidity index.

Littoral fauna Lake Ormtjärn				
Bivalvia	Odonata	Heteroptera	Trichoptera	Diptera/tvåvingar
Sphaeriidae	Coenagrionidae sp.	Notonecta glauca	Holocentropus dubius	Dixidae
Oligochaeta	Coenagrion hastulatum	Hesperocorixa linnaei	Oxyethira sp.	Ceratopogonidae
Tubifex/Potamothrix sp.	Aeshna juncea	Sigara sp.	Limnephilidae sp.	Chironomidae
Crustacea	Aeshna grandis	Coleoptera	Limnephilus sp. (L. rhombicus?)	
Asellus aquaticus	Corduliidae sp.	Gyrinus minutes	Limnephilus sp. (L. griseus?)	
Ephemeroptera	Leucorrhinia dubia	Haliplidae sp. (larv)	Nemotaulius punctatolineatus	
Cloeon inscriptum	Leucorrhinia rubicunda	Haliplus fulvus	Agrypnia sp.	
Leptophlebia vespertina	Libellula quadrimaculata	Porhydrus lineatus	Oligotricha striata	
		Ilybius sp. (larv)	Molannodes tinctus	

ASPT-index 5,9
 Danish faunaindex 5
 Acidity index 4

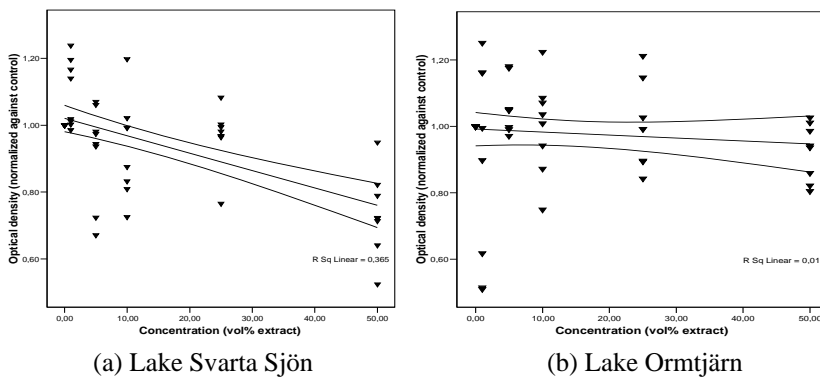


Figure 2: (a) Lake Svarta Sjön – dose-response for L-929 cell culture exposed to sediment water extract and (b) Lake Ormtjärn – dose-response for L-929 cell culture exposed to sediment water extracts. Data are presented with linear regression and 95% confidence interval.



4 Discussion

Very high levels of lead (2090-1240 mg/kg dry weight) were found in the sediment of the Lake Ormtjärn caused by underwater destruction of detonators. No other source of concern for heavy metal contamination was present. The background value for lead as well as possible impact from shooting field were within local background levels (30-197 mg/kg dry weight) and it could be concluded that the underwater destruction of detonators was the source of the high lead levels. The impact from the underwater destruction of detonations was summarized in a coarse impact scheme to facilitate the discussion of the lead conditions and ecological status in the environmental risk assessment of Lake Ormtjärn, table 5.

Table 5: Chemical impact of lead and ecological status.

Lake Ormtjärn level of impact	Very low level	Low level	Medium level	High level	Very High level
<i>Chemical impact of lead</i>					
Sediment Lead (Pb) content (0-25 cm)				X (all levels)	X (surface)
Water Lead (Pb) content			X (surface water)	X* (bottom water)	
<i>Ecological status</i>					
Water acute toxicity (<i>Daphnia magna</i>)	X				
Sediment acute toxicity (<i>Cytotoxicity</i>)	X				
Bottom fauna				X (detonators found in sediment core)	
Littoral fauna		X			

1. Very low level Background level – very low risk for biological effect
2. Low level Small impact or near background level – low risk for biological effect – no action
3. Medium level Noticeable impact – biological effect might occur – normally not causing action
4. High level High impact – increasing risk for biological effect - might cause action if supported by other risk factors
5. Very High level Very high impact – increased risk for biological effect even for short time exposure – normally causing action

The concentration of lead in sediment was high in all parts of the lake down to 25 cm level depth. The even distribution was explained by the effects of numerous detonations during the underwater destruction. The total content of



lead in the upper 25 cm of the sediment was calculated to be approximately 2000 kg. This is more than the expected 1500 kg from detonators known to be destructed in the lake. The difference may be caused by the fact that in practice more than 1.5 million detonators were destructed. The concentration of heavy metals including lead in the surface water samples was low. However but in the bottom water high lead concentration were found (3,4 µg/L). No explosives or other chemical anomalies were detected in water or sediment.

The results are consistent with an earlier investigation by Bäckström [5], who studied the chemical status as well as the mobility of lead and other trace elements in Lake Ormtjärn through analysis of surface water, pore water and the solid phases of the sediment (the later by use of sequential extraction). The sequential extraction by Bäckström [5] showed that that 2% (30 ppm) of total lead was ion exchangeable, between 43% and 32% of the total lead was extracted in the acid soluble and reducible fraction, respectively, 23% was ox disable and 1% residual. By using the PHEREQC-2 model it was also shown that the limiting phase for lead in the pore water was expected to be cerussite (PbCO₃). The calculated mobility of lead from the sediment was partly confirmed by pore water analysis and the content in the bottom water, (8µg/L) compared to lead in surface water (2µg/L). In surficial water, the concentration of lead was supposed to be mainly controlled by an internal iron-lead cycle.

The concentration of lead in the water (< 8µg/l) was not high enough to induce acute effects in *Daphnia magna*. The lead concentration was about 7500 times below measured 48 h acute EC₅₀ for lead in *D. magna* (Milan et al. [24]). However, the total concentration of lead in the water was at the level which would have induced toxic effects as inhibition of growth or reproduction in the water flea (Berglind [26]).

No acute toxicity (L-929 cytotoxicity) was found in the upper part of the polluted sediment of Lake Ormtjärn despite high levels of lead. It is suggested that only a small fraction bio available lead exists in the top sediment phase due to strong interaction with the matrix. High organic carbon content (48%) leads to the conclusion that lead is strongly bound to functional groups within the organic material. Cat-ion exchange between protons and divalent lead is also expected to be low at neutral pH. Furthermore, soluble lead in the water phase may have reduced bioavailability due to interaction with dissolved organic matter (Kördel [27]), but also with inorganic ligands e.g. carbonate, phosphate and mineral particles. According to Sauvant et al. [21], IC₅₀ for lead (Lead nitrate) in L-929 cells (24 h of exposure) is 580 mg/L. Hence, the extraction yield from 14 h shaking in 50°C did not exceed those levels of lead required for an acute response in L-929, even though the test is expected to be more sensitive with an exposure time of 72 h used in the present study.

The study showed that the *bottom fauna* in the centre of Lake Ormtjärn were disturbed with low abundance and number of taxa. In the centre of the lake, the most disturbed area, several detonators were found in the sediment samples. Closer to shore, bottom fauna showed a more normal abundance and taxa. The concentration of lead in the sediment was very high at both sites, so no obvious explanation for the significant difference in bottom fauna related to lead (Pb)



levels could be made. Oxygen saturation as well as nutrient conditions and depth (4 m) were normal and comparable at both sites. The littoral *fauna* in the lake was rich in abundance and taxa showing no obvious sign of impact. The fauna conditions were expected to be worse if not improved by the relatively high pH and high nutrient status of the Lake Ormtjärn.

It is concluded that underwater destruction of detonators containing lead azide can cause very high levels of lead at more than 25 cm depth in the sediment of a lake. Leaching of lead to the water phase and further exposure for e.g. bottom fauna can be expected over long time. If pH is high and if oxygen saturation and nutrient conditions are favourable the expected ecological effect by the lead contamination may be high in near vicinity of the sediment (bottom fauna, bottom water) but low in the remaining part of the lake. This is in accordance with international studies where lead has been identified to bio diminish through the food chain (Southward et al. [28]).

5 Recommendations and outlook

No remediation of Lake Ormtjärn is recommended at present. For the long-term assessment of impact in Lake Ormtjärn and from underwater destruction of detonators containing lead azide in similar typical Swedish forest lakes; pH, nutrient conditions and oxygen saturation has been identified as possible key “triggers” in an ecological chain of impact. Considering the high potential of pollution from the sediment and the regional natural acid conditions, monitoring of the conditions and pH, will be of key importance for a regularly update regarding any future need for remediation of the lake. Also, if remediation is considered, the hazard of unexploded ordnance and possible effect on human health and safety as well lake ecology must be addressed.

References

- [1] Sjöström J, Karlsson R-M., Qvarfort U (2004): Environmental risk assessment of dumped ammunition in Natural Waters in Sweden – a Summary. FOI-R—1307—SE
- [2] Förstner U, Kresten M (1988): Assessment of metal mobility in dredged material and mine waste by pore water chemistry and solid speciation. In: Salomon's, W. and Förstner U. (Eds.), Chemistry and biology of solid waste. Dredged material and mine tailings. Springer Verlag, 214-237
- [3] Davis A, Galloway J N (1993): Distribution of Pb between sediments and pore water in Woods lake. Adirondack State Park New York, U.S.A. Applied geochemistry 8, 51-65.
- [4] Riba I, Garcia-Luque E, Blasco J, DelValls T. A (2003): Bioavailability of heavy metals bound to estuarine sediments as a function of pH and salinity values. Chemical Speciation and Bioavailability, 15(4)
- [5] Bäckström M. (2002): Migration and mobility of lead and antimony from heavily polluted lake sediment in “On the chemical state and mobility of



- lead and other trace elements at the biosphere techno sphere interface” Örebro University ISBN 91-7668-313-3
- [6] Sjöström J, Liljedahl B, Forsman M (2004): Environmental risk assessment of dumped ammunition in Swedish lakes. Explosives and metals in water and sediments. FOA-R—99-01070-222—SE
 - [7] Voie A (2005): Bioavailability of metals from munitions. Norwegian Defence Research Establishment. FFI/Report 2005/00443
 - [8] U.S Geological Survey (2000): Survey of Lake Ontario bottom sediment off Rochester, New York, to define the extent of Jettisoned World War II materiel and its potential for sediment contamination. U.S Geological Survey Open-File report 99-237 and contribution number 1081 of the USGS Great Lake Science Center
 - [9] Karlsson R-M, Almström H, Berglind R (2004): Environmental effects of underwater blasts – a literature study. FOI-R-1193—SE
 - [10] Covello V, Merkhofer M (1993): Risk assessment Methods approaches for assessing health and environmental risks. ISBN 0-306-44382-1
 - [11] Tuvikene A, Huuskonen S, Koponen K, Mauer O, Lindström-Seppä P (1999): Oil Shale Processing as a source of Aquatic Pollution Monitoring of the Biologic Effects in Caged and Freshwater Fish. Environmental Health Perspectives Vol 107: 9
 - [12] den Besten P, de Decker E, Babut M, Power B, DelValls A, Zago C, Oen A, Heise S (2003): Biological Effect-based sediment Quality in ecological risk assessment for European waters. JSS- J Soils Sediments 3 (3) 144-162
 - [13] Sjöström J, Qvarfort U, Scott Å, Liljedahl B, Fällman Å, Hägglund L, Berglind R, Wiklund A (1999): Environmental risk assessment of areas for combustion, blasting and dumping at the artillery range at Bofors and the industrial area of Björkborn. FOA-R—99-01170-222—SE
 - [14] Waleij A, Karlsson R-M, Qvarfort U, Scott Andersson Å, Lackman T, Åkerman J, Wingfors H, Berglind R, Sjöström J (2003): Environmental Impact Assessment of Bofors Shooting field. Swedish report. FOI-R—1118—SE. ISSN 1650-1942
 - [15] Swedish Geological Survey (1991): Geochemical mapping Report No 68,
 - [16] Swedish Environmental Protection Agency (1999): Environmental Quality Criteria; Lakes and natural waters. Report 4913
 - [17] Qvarfort U, Sjöström J, Bäckström M, Forsman M (2000): Extended Environmental Risk Assessment of two lakes within the Bofors Artillery Range area. FOA-R—00-01455-222—SE
 - [18] Swedish Environmental Protection Agency (1999): Environmental Quality Criteria; Polluted areas. Swedish report. Report 4918
 - [19] Klüttgen B, Dülmer U, Engels M, Ratte HT (1994): ADaM, an artificial freshwater for the culture of zooplankton. Wat. Res. 28, 743-746.
 - [20] Borenfreund E, Puerner J.A, (1985): Toxicity determined in vitro by morphological alterations and neutral red absorption. Toxicology Letters 24, p 119-124



- [21] Sauvant M P, Pepin D, Bohatier J, Groliere C, Guillot J (1997): Toxicity of 16 inorganic pollutants by six bioassays. *Ecotoxicology and Environmental Safety* 37, p 131-140
- [22] Wahle U, Kördel W (1997): Development of analytical methods for the assessment of ecotoxicological relevant soil contamination. *Chemosphere*. Vol.35. No 1/2, p 223-237
- [23] Swedish Environmental Protection Agency (EPA) (2004): Swedish report. Sötvatten Årsskrift från miljöövervakningen 2004. ISSN 1652-3962
- [24] Milan B Arambasic, Sabrija Belie, Gordano Subakov (1995): Acute toxicity of heavy metals (Copper, lead, zinc), phenol and sodium on *Allium Cepa* L., *Lepidium Sativum* L. and *Daphnia Magna* St.: comparative investigations and the practical applications. *Wat. Res.* Vol 29, No 2 pp 497-503
- [25] Swedish Environmental Protection Agency (2004): Metaller I kust och havsmiljö
- [26] Berglind, R. (1985): Biotic and abiotic interactions on toxic effects in *Daphnia magna*. PhD Thesis, University of Göteborg, Sweden
- [27] Kördel W, (1997): Fate and effects of Contamination in soils as influenced by Natural Organic Material Status of information. *Chemosphere*, Vol. 35 Nos 1/2, pp. 405-411.
- [28] Southward LA, Marschall E, Stein R (2003): Trophic Transfer of heavy Metals to Top Predators: Quantifying the role of Non-native Species. Final Report Lake Erie Protection Fund Project number: SG 181-02



Section 9

Cardiovascular system

This page intentionally left blank

Correlation of morphological parameters with likelihood of thrombus formation in intracranial aneurysms

K. Shimano¹ & Y. Nakagawa²

¹*Department of Mechanical Systems Engineering,
Tokyo City University, Japan*

²*Graduate School, Tokyo City University, Japan*

Abstract

Accurate rupture prediction of intracranial aneurysms is crucial because not all aneurysms rupture. With past reports that aspect ratio (AR) and size ratio (SR) have significant correlations with rupture probability, these two morphological parameters are regarded as promising for rupture prediction: an aneurysm with a higher AR or SR is more likely to rupture than one with a lower AR or SR. However, 100% reliability of prediction is not guaranteed even with these parameters. It is necessary to clarify reasons for the high correlations of AR and SR with rupture status and what is responsible for unsuccessful predictions. In this paper, the authors discuss haemodynamic significance of the two parameters with a special focus on stagnant flow and resulting thrombus formation, which are considered to play important roles in the process of aneurysmal rupture. Results with computational fluid dynamics and a platelet aggregation model are also shown in order to demonstrate that stagnant flow and thrombus formation can be observed even in an aneurysm with low AR and SR.

Keywords: intracranial aneurysm, rupture prediction, thrombus formation, platelet aggregation, computational fluid dynamics.

1 Introduction

Intracranial aneurysms can cause fatal subarachnoid haemorrhages when they rupture. Unruptured aneurysms can be found by means of magnetic resonance imaging (MRI) or computed tomography (CT) before the patients have any symptoms, and there are neurosurgical treatments to prevent future rupture of



detected aneurysms, e.g. clipping and coiling. However, such a treatment is not applied to every aneurysm because it is known that not all aneurysms rupture and because the treatments are so invasive that the patients' lives could be jeopardised. It is, therefore, necessary to make a critical decision about whether to apply any treatment whenever an unruptured aneurysm is found. Although it seems reasonable to treat only aneurysms with high probabilities of future rupture, it is difficult with the present understanding to predict precisely which aneurysms are likely to rupture.

Aspect ratio (AR) [1–3] and size ratio (SR) [4–6] were reported to have significant correlations with probability of aneurysmal rupture, being recognised as promising reference parameters for rupture prediction. AR is a ratio of aneurysmal dome depth to neck width while SR is defined as a ratio of dome length to parent artery diameter. It is considered that an aneurysm with a higher AR or SR is more likely to rupture than one with a lower AR or SR. Nonetheless, there is still considerable uncertainty about rupture prediction based on these two morphological parameters. For development of a more reliable rupture prediction method, it is important to elucidate what causes aneurysms to rupture.

The authors have worked on modelling of blood flow and thrombus formation in cerebrovascular bifurcation aneurysms because it is considered that slow intra-aneurysmal flow and resultant thrombus formation play important roles in the process of rupture [7]. In this paper, a reason for probable mis-prediction with AR/SR is discussed by means of theoretical and numerical analyses. Firstly, significance of the two parameters is explained with a dynamic energy balance theory. Secondly, the platelet aggregation model by Shimano *et al.* [8, 9] is applied to three model aneurysms, one of which was constituted from multi-slice CT images.

2 Significance of AR and SR

Ujiiie *et al.* [1] showed a significant correlation of AR with probability of rupture: almost 80% of ruptured aneurysms had ARs larger than 1.6. Other researchers such as Weir *et al.* [2] and Nader-Sepahi *et al.* [3] concurred with the correlation between AR and rupture probability. On the other hand, Dhar *et al.* [4], Tremmel *et al.* [5] and Rahman *et al.* [6] reported a high correlation of SR with rupture status. Tremmel *et al.* suggested aneurysms with SRs larger than 2.0 could have a potential risk of rupture.

Significance of AR and SR is intra-aneurysmal flow speed: the larger AR and SR become, the more slowly internal blood flows. According to the theory of Ujiiie *et al.* [7], thrombi are considered to play an important role in degeneration of the aneurysmal wall and subsequent rupture because extremely slow blood flow and resultant thrombus formation are likely in aneurysms with high ARs. Fibrinolysis, in which thrombi are resolved, presumably causes damage to endothelia. Also Shojima *et al.* [10] pointed out that an extremely low level of wall shear stress (WSS) might contribute to degeneration of the artery wall. This



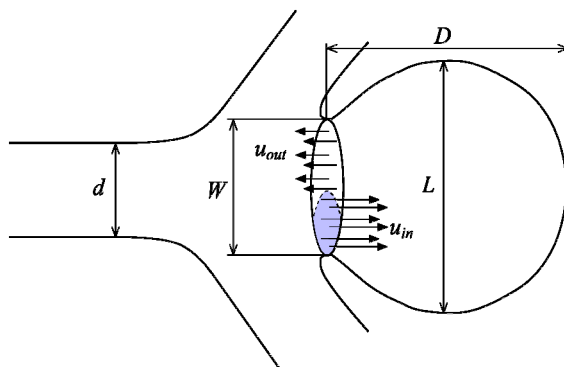


Figure 1: Hypothetical bifurcation aneurysm.

is true for aneurysms with high ARs because low WSS results from slow internal flow.

In this section, a haemodynamic reason for the high correlations of AR and SR with rupture probability is discussed. It is theoretically explained how AR and SR are associated with the intra-aneurysmal flow speed. It is also discussed why rupture prediction based on AR/SR is sometimes unsuccessful.

2.1 Energy balance theory

Energy conservation of blood in the hypothetical bifurcation aneurysm schematically shown in fig.1 is considered so that magnitude of intra-aneurysmal flow velocity can be approximately estimated. L , D and W respectively represent lateral length, depth and neck width of the aneurysm. $AR = D/W$ and $SR = D/d$ where d is parent vessel diameter. Deformation of the artery wall is neglected because results of past numerical studies (e.g. Torii *et al.* [11]) imply the rigid wall assumption does not cause dramatic change in the velocity magnitude. Effects of unsteadiness are also negligible because velocity averaged over the pulse period is considered here.

There are three fluid-dynamical mechanisms which affect the amount of energy kept in the dome: (a) convective energy transport by incoming flow velocity u_{in} which brings energy into the dome, (b) convective energy transport by outgoing flow velocity u_{out} which takes energy out of the dome and (c) energy loss caused by wall shear stress. All the three contributions should balance out: energy in the aneurysmal dome is increased by (a) and decreased by (b) and (c).

As shown in Fig. 1, the cross section at the neck is divided into the in-flow and out-flow regions, and u_{in} and u_{out} stand for averaged velocity components perpendicular to the cross sectional plain in the respective regions. On the assumption that inflation of the aneurysmal dome is negligible, the two velocity components satisfy the mass conservation law expressed by

$$A_{in}u_{in} = A_{out}u_{out} \quad (1)$$

where A_{in} and A_{out} represent in-flow and out-flow areas, respectively. Here, ratio κ is defined so that A_{in} and A_{out} can be calculated from the total cross sectional area A :

$$A_{in} = \kappa A \quad , \quad A_{out} = (1 - \kappa)A. \quad (2)$$

The amount of energy brought into the dome through A_{in} per unit time is evaluated by

$$E_{in} = A_{in} u_{in} \left(\frac{\rho V_{in}^2}{2} + p_{in} \right) \quad (3)$$

where V_{in} and p_{in} are flow speed and pressure averaged over the in-flow area. The amount of energy taken out of the dome through A_{out} per unit time can be calculated in the same manner:

$$E_{out} = A_{out} u_{out} \left(\frac{\rho V_{out}^2}{2} + p_{out} \right) \quad (4)$$

Angles formed by flow directions and the cross-sectional plain at the bottleneck, where the flow accelerates, are unlikely to deviate greatly from 90 degrees. Thus, we assume that $V_{in} \approx u_{in}$ and $V_{out} \approx u_{out}$. It is also assumed that $p_{in} \approx p_{out}$. These approximations and eqns. (1)-(4) lead to the following expression for energy change due to convection:

$$E_{in} - E_{out} \approx \rho A K u_{in}^3 \quad \text{where} \quad K = \frac{\kappa(1 - 2\kappa)}{2(1 - \kappa)^2}. \quad (5)$$

On the other hand, energy loss caused by WSS should agree with frictional work per unit-time W_{wall} , which can be approximated by

$$W_{wall} \approx S \tau_{wall} U \quad (6)$$

where S , τ_{wall} and U stand for area of the arterial wall surface within the dome, wall shear stress averaged over S and representative velocity within the aneurysmal dome. Equation (6) is rewritten into

$$W_{wall} \approx \mu D U^2. \quad (7)$$

using the following approximations to S and τ_{wall}

$$S \approx LD \quad (8)$$

$$\tau_{wall} \approx \frac{\mu U}{L} \quad (9)$$

where μ is blood viscosity. As E_{in} , E_{out} and W_{wall} are in equilibrium, eqns. (5) and (7) result in the following expression of energy balance:

$$\rho A K u_{in}^3 \approx \mu D U^2. \quad (10)$$



Lines over quantities in eqn. (10) mean that the quantities are averaged over the pulse period. Although $\overline{ab} = \bar{a} \cdot \bar{b}$ does not hold strictly true, the approximation $\overline{ab} \approx \bar{a} \cdot \bar{b}$ is still reasonable when only the scale of each quantity is concerned. It is also assumed that the magnitude of the incoming flow velocity u_{in} is comparable to the mean velocity of the main flow u . In addition, $A \approx W^2$ is obvious. Application of these approximations to eqn. (10) results in

$$\frac{\overline{U}}{\overline{u}} \approx \sqrt{\frac{\rho W^2 \overline{K} \cdot \overline{u}}{\mu D}}. \quad (11)$$

The left hand side of eqn. (11) represents ratio of the intra-aneurysmal flow speed U to the main flow speed u . The degree of flow stagnancy in the dome can be evaluated by this ratio. After some arrangements, the flow speed ratio can be associated with AR and SR:

$$\frac{\overline{U}}{\overline{u}} \propto \sqrt{\frac{\text{Re}}{\text{AR}}} \quad \frac{\overline{U}}{\overline{u}} \propto W \sqrt{\frac{\tau_{mv}}{\text{SR}}} \quad (12)$$

where Re is the Reynolds number based on the neck width and τ_{mv} is wall shear stress of the mother vessel approximated by $\tau_{mv} \propto \mu u / d$. Note that τ_{mv} does not change dramatically in normal cerebral arteries.

The relations in (12) clearly show that both AR and SR correlate with the degree of flow stagnancy. Although there are still other influential factors such as Re and W, it can be concluded that the intra-aneurysmal flow tends to be slower when AR or SR is larger. This is considered to be one of the primary reasons for high correlations of these parameters with rupture probability.

2.2 Limit to energy balance theory

In the energy balance theory, each basic physical quantity in the dome is represented by a single scale. For example, only U is used to represent the intra-aneurysmal velocity scale. This implies that fairly simple internal flow is assumed. However, in some conditions, internal flow is so complicated that the relations in eqn. (12) are not valid any more. A typical example of such complicated flow can be found in the case where flow separation occurs. In the presence of flow separation, flow speed in the separation bubble is much lower than in other regions and, consequently, WSS exerted on the separation bubble area is much lower than the estimation with eqn. (9). Another example of complicated intra-aneurysmal flow can be observed in a bulky aneurysm where kinetic energy brought by the incoming flow cannot spread fully within the aneurysmal dome. A lack of uniformity can cause slowdown in flow speed in a limited part of the dome. It should be emphasised that even “local” stagnancy of the intra-aneurysmal flow could induce thrombus formation and might lead to rupture. Rupture prediction based on AR/SR could be unsuccessful because AR and SR cannot represent any reduction in “local” flow speed caused by flow



separation or large aneurysmal volume: they are “global” parameters only accounting for overall morphological features.

Computational fluid dynamics (CFD) allows us to detect any “local” flow separation and slowdown in flow speed if spatial resolution of the computational grid is fine enough. This is one of the reasons why numerical simulation is regarded as a promising tool in this field.

3 Modelling of intra-aneurysmal flow and platelet aggregation

CFD and the platelet aggregation model by Shimano *et al.* [9] were applied to three model aneurysms so as to demonstrate that the “local” stagnancy discussed in Section 2.2 makes it impossible to estimate the internal velocity scale or the degree of thrombus formation from AR/SR.

The three model aneurysms shown in figs. 2–4 are named Bulky, Slim and Real Models, respectively. The maximum Reynolds number, Womersley parameter, AR and SR of each model are listed in Table 1.

Table 1: Haemodynamic and morphological parameters of the three model aneurysms.

Model	Max.Reynolds number	Womersley parameter	Aspect Ratio	Size Ratio
Bulky	485	2.39	2.3	3.2
Slim	728	2.25	2.0	1.6
Real	797	3.36	0.9	1.1

Bulky Model shown in fig. 2 is identical to the glass aneurysm experimentally tested by Takahashi *et al* [12]. They reported that thrombus formation was clearly observed in the glass aneurysm when it was embedded into a canine artery. Bulky Model has a larger SR than the other models because the mother vessel diameter d , which was presumably determined according to the canine artery, is smaller. Slim Model shown in fig. 3 is smaller in lateral length of the dome than Bulky Model, although ARs of the two models are comparable. More details of Bulky and Slim Models are available in Reference [13].

The aneurysm in Real Model shown in fig. 4 is located across the whole anterior communicating artery and regarded as an aneurysm with a low risk of rupture because it has an AR of 0.9 and SR of 1.1, each of which is much smaller than the corresponding criterion.

Real Model was constituted from multi-slice CT images of a real aneurysm. Constitution procedures of the 3-D computational model are depicted in fig. 5. In the beginning, a 3-D polygon model was made up by layering 184 CT images. At this point, two separate arteries were erroneously recognised as adhering to each other. The operator needed to do time-consuming manual work to correct this error using Rhinoceros and other software. More sophisticated software should be developed for reduction in the workload.

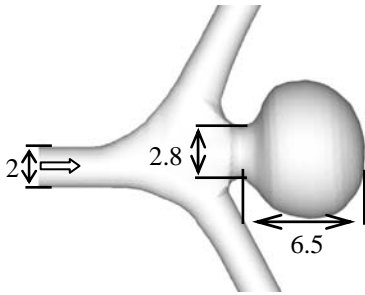


Figure 2: Bulky model.

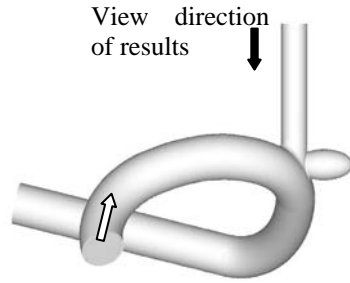


Figure 3: Slim model.

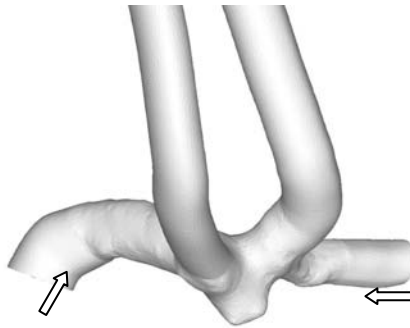


Figure 4: Real model.

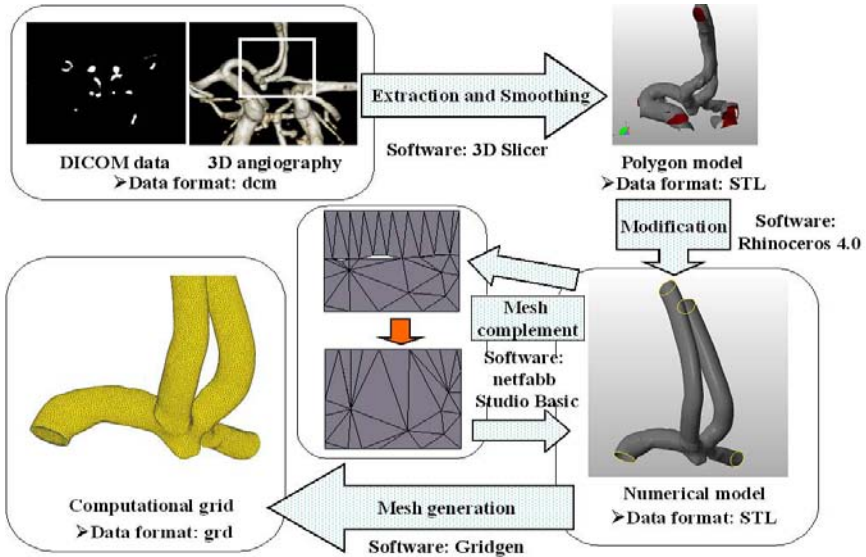


Figure 5: Procedures to constitute a computational model from CT images.

The unsteady incompressible Navier-Stokes equations and continuity equation were numerically solved. Blood was assumed to be a Newtonian fluid and flow was treated as laminar. It has been shown that the non-Newtonian effect of blood does not change significantly the intra-aneurysmal velocity distribution [13]. The cell-centred finite volume approach was used for spatial discretisation of the governing equations. Unstructured grid systems were employed so that the complicated geometry of each model could be properly expressed. The SIMPLE algorithm was used for coupling of pressure and velocity. It was confirmed that the authors' CFD code could produce flow patterns in Bulky model similar to those observed in the experiment of Takahashi *et al.* [12].

When the platelet aggregation model [9] was applied, flow velocity components calculated by CFD were used to evaluate transport by convection. In the aggregation model, transport equations were solved for three parameters: density of primarily aggregated platelets N_1 , that of secondly aggregated platelets N_2 and concentration of adenosine diphosphate (ADP) n_A . No effect of adhesion of platelets to artery walls or coagulation was taken into consideration.

ADP released from haemolysed red blood cells (RBCs) is considered to activate platelets and induce aggregation [13]. It was assumed in the present simulation that 20% of ADP contained in RBCs impinging against the wall was released into plasma in the region within a 1mm radius of the stagnation point. The impingement of the main flow is explained in Section 4.1.

4 Computational results

4.1 Flow patterns

Velocity vectors on the central plains of Bulky and Slim Models are compared in figs. 6 and 7 at the temporal point of the systole. The view direction of fig. 7 is shown in fig. 3 with a dark arrow. A reference arrow in each figure represents 50% of the maximum mean velocity of the main flow at the inlet.

It is observed in each model that the incoming main flow hits the protruding wall of the neck at the entrance to the dome and that some blood moves into the dome after the impingement against the neck. However, in Bulky Model, stagnant blood occupies a large part of the dome while low speed flow is only observed near the apex of the aneurysmal dome in Slim Model. This sharp contrast between flow patterns in the two models might be partly attributable to the larger SR of Bulky Model. It is, however, apparent from fig. 6 that a lack of flow uniformity caused by the too large volume of the dome is responsible: kinetic energy brought into the dome cannot spread fully within the dome. In such flow conditions, the estimation based on eqn. (12) is no longer valid. For this reason, flow patterns in the two models with comparable ARs are significantly different.

Velocity vectors in Real Model are depicted in fig. 8 at the systole and diastole. Incoming flow hits the wall near the entrance to the dome and some blood circulates inside before going out of the dome. This flow pattern in Real Model seems similar to that in Slim Model but the magnitude of flow speed in



Real Model is larger even near the deep end of the aneurysmal dome. The higher flow speed in the circulating flow in Real Model obviously results from smaller AR and SR.

The most important observation in fig. 8 is a small separation bubble at the apex of the dome. This separation bubble, in which flow speed is much lower than in the circulating flow, exists throughout the pulse cycle and is likely to give a good chance of thrombus formation. This stagnant flow in the small region cannot be detected by AR or SR as these two parameters are much smaller than respective criteria: $AR=0.9$ (<1.6) and $SR=1.1$ (<2.0).

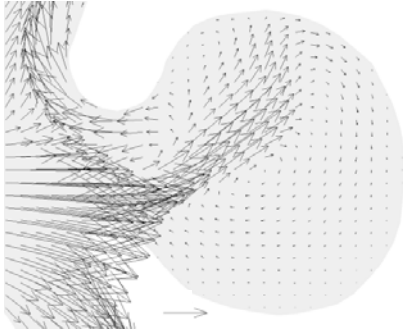


Figure 6: Velocity vectors on the central plain in bulky model at the systole.

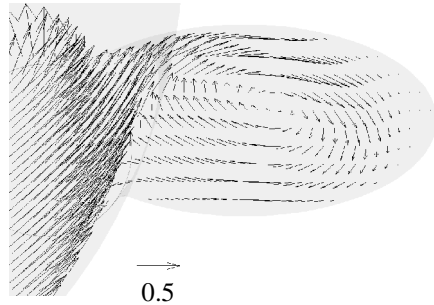
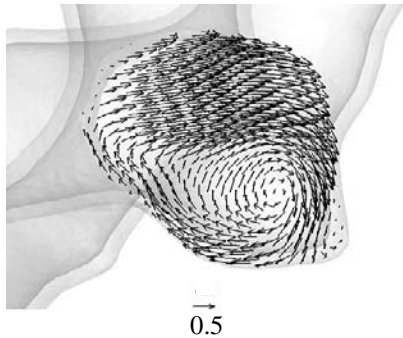
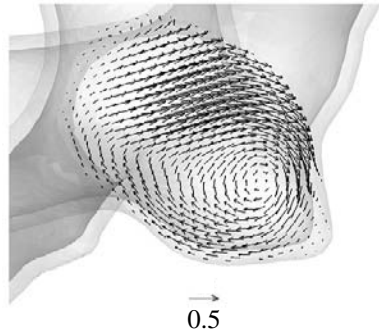


Figure 7: Velocity vectors on the central plain in slim model at the systole.



(a) Systole.



(b) Diastole.

Figure 8: Velocity vectors in real model at the systole and diastole.

4.2 Platelet aggregation

This section refers to density of primarily aggregated platelets N_1 , which was calculated by the platelet aggregation model. Here, density means the number of platelets per volume. For simplicity, N_1 is expressed as a percentage to the total



density of platelets contained in normal blood. Time t is also represented in a dimensionless being divided by the pulse period T .

Figure 9 shows instantaneous distribution of N_1 along the aneurysmal wall in Real Model at $t/T = 11.8$. The location of the highest N_1 is near the apex of the aneurysmal dome where the flow separation discussed in the previous section occurs. The low-speed flow in the separation bubble seems responsible for the highest N_1 because slow flow enables a long residence time of ADP which is necessary for active platelet aggregation.

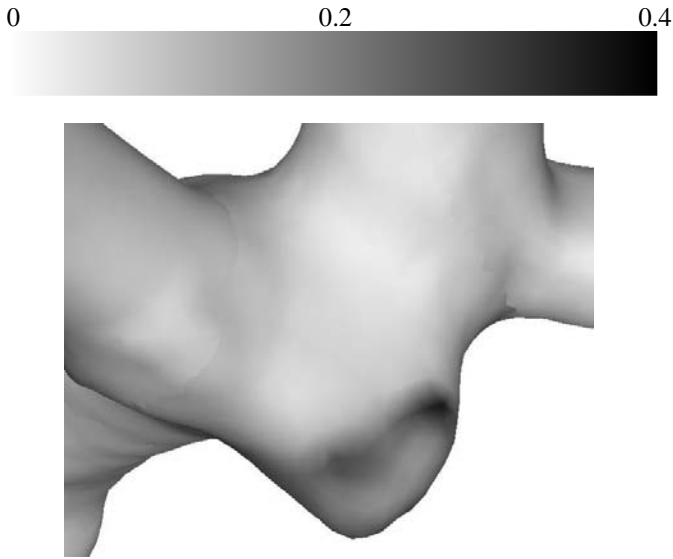


Figure 9: Instantaneous distributions of N_1 (density of primarily aggregated platelets) in the vicinity of the wall surface in real model at $t/T = 11.8$.

Figure 10 shows temporal changes in N_1 at the points where the maximum values of N_1 in the respective models are found at $t/T = 11.8$. At the observation point in Bulky Model, aggregation starts after $t/T = 2.0$ because it takes ADP two times the pulse period to move from the location of haemolysis to the observation point. A monotone increase in N_1 observed after the start of aggregation is fairly quick due to the extremely slow internal flow shown in fig. 6. On the other hand, cyclic changes in N_1 are found at the observation points in Slim and Real Models. Reduction in N_1 occurs at the systole because some aggregated platelets are flushed out by high speed flow at the systole. Despite the drop in N_1 , aggregated platelets stay near the observation points throughout the pulse cycle, keeping N_1 higher than 0.5% in Slim Model and approximately 0.1% in Real Model.

No effect of adhesion is included in the present aggregation model. However, adhesion of activated platelets to aneurysmal walls actually occurs because Tanahashi *et al.* [14] confirmed that activated platelets adhere to endothelia. The

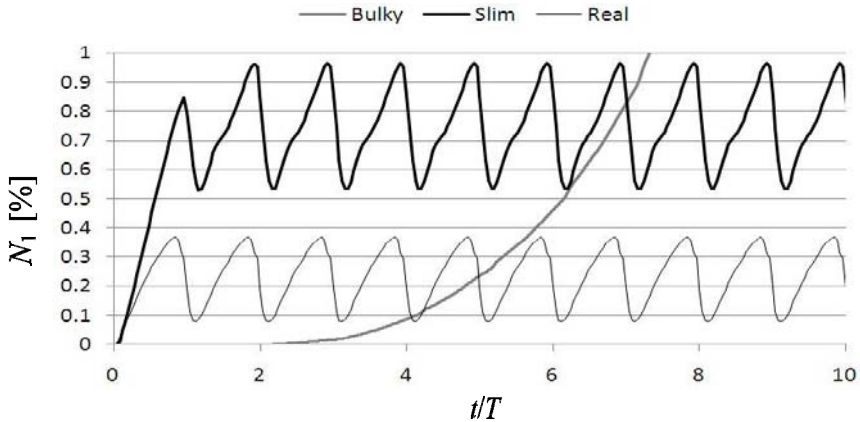


Figure 10: Temporal changes in N_1 (density of primary-aggregated platelets) at the points where the maximum values of N_1 in respective models are observed at $t/T=11.8$.

number of platelets adhering to the wall is, therefore, considered to keep increasing near the observation points in Slim and Real models. As platelets adhering to endothelia contribute to acceleration of the following coagulation, it seems a natural conclusion that probability of thrombus formation is comparably high in both models.

5 Conclusions

It is theoretically shown that AR and SR are linked with flow speed in aneurysms. This is presumably a reason for high correlations of the two parameters with rupture probability. However, the present numerical results demonstrate that AR and SR do not always reflect intra-aneurysmal flow status and, presumably, likelihood of thrombus formation. Although Bulky and Slim Models have comparable ARs, stagnant flow occupies a larger region of the dome in Bulky Model and platelet aggregation in the dome is more active. Real Model with much smaller AR and SR seems to have a good chance of thrombus formation due to flow separation. These findings might account for uncertainty about rupture prediction based on AR and SR. As the degree of thrombus formation is determined by not only stagnant flow or platelet aggregation, further studies are necessary for more detailed insights into intra-aneurysmal thrombus formation with adhesion and coagulation taken into account.

Acknowledgement

The authors thank Cybernet Systems Co., Ltd. for providing CT data.



References

- [1] Ujiie, H., Tamano, Y., Sasaki, K. & Hori, T., Is the aspect ratio a reliable index for predicting the rupture of a saccular aneurysm? *Neurosurgery*, **48(3)**, pp.495-503, 2001.
- [2] Weir, B., Amidei, C., Kongable, G., Findlay, J.M., Kassell, N.F., Kelly, J., Dai, L. & Karrison, T.G., The aspect ratio (dome/neck) of ruptured and unruptured aneurysms, *Journal of Neurosurgery*, **99(3)**, pp.447-451, 2003.
- [3] Nader-Sepahi, A., Casimiro, M., Sen, J. & Kitchen, N.D., Is Aspect Ratio A reliable Predictor of Intracranial Aneurysm Rupture? *Neurosurgery*, **54(6)**, pp.1343-1348, 2004.
- [4] Dhar, S., Tremmel, M., Mocco, J., Kim, M., Yamamoto, J., Siddiqui, A.H., Hopkins, L.N. and Meng, H., Morphology Parameters for Intracranial Aneurysm Rupture Risk Assessment, *Neurosurgery*, **63(2)**, pp.185-197, 2008.
- [5] Tremmel, M., Dhar, S., Levy, E.I., Mocco, J. and Meng, H., Influence of Intracranial Aneurysm-to-Parent Vessel Size Ratio on Hemodynamics and Implication for Rupture: Results from a Virtual Experimental Study, *Neurosurgery*, **64(4)**, pp.622-631, 2009.
- [6] Rahman, M., Smietana, J., Hauck, E., Hoh, B., Hopkins, N., Siddiqui, A., Levy, E.I., Meng, H. and Mocco, J., Size Ratio Correlates With Intracranial Aneurysm Rupture Status (A Prospective Study), *Stroke*, **41**, pp.916-920, 2010.
- [7] Ujiie, H., Tachibana, H., Hiramatsu, O., Hazel, A.L., Matsumoto, T., Ogasawara, Y., Nakajima, H., Hori, T., Takakura, K. & Kajiyama, F., Effects of size and shape (aspect ratio) on the hemodynamics of saccular aneurysms: a possible index for surgical treatment of intracranial aneurysms, *Neurosurgery*, **45(1)**, pp.110-130, 1999.
- [8] Shimano, K., Hayashi, T., Ujiie, H., Ono, T. & Enomoto, Y., Modelling of platelet aggregation in aneurysm, *Proc. of 7th Int. Conf. on Modelling in Medicine and Biology*, WIT Press, Southampton, pp.43-52, 2007.
- [9] Shimano, K et al. (2009) Modeling of platelet aggregation in cerebrovascular bifurcation aneurysms, *IFMBE Proc. vol. 25, World Congress on Medical Physics& Biomedical Engineering*, Springer, pp.495-498, 2009.
- [10] Shojima, M., Oshima, M., Takagi, K., Torii, R., Hayakawa, M., Katada, K., Morita, A. and Kirino, T., Magnitude and Role of Wall Shear Stress on Cerebral Aneurysms -Computational Fluid Dynamics Study of 20 Middle Cerebral Artery Aneurysms-, *Stroke*, **35**, pp.2500-2505, 2004.
- [11] Torii, R., Oshima, M., Kobayashi, T., Takagi, K. and Tezduyar, T.E., Influence of Wall Elasticity on Image-Based Blood Flow Simulations (in Japanese with English abs.), *Transactions of Japan Society of Mechanical Engineers, Series A*, **70(697)**, pp.1224-1231, 2004.
- [12] Takahashi, N., Ujiie, H., Yotoryama, T., Suzuki, Y., Hori, T. & Kaibara, M., Flow visualization study of the endothelialized glass aneurysm model



- implanting canine carotid artery (in Japanese with English abs.), *Journal of Japanese Society of Biorheology*, **18(4)**, pp.143-148, 2004.
- [13] Shimano, K., Kudo, T., Yoshimoto, S., Ujiie, H. and Enomoto, Y., A numerical study of blood flow patterns in cerebral aneurysms and the causal relationship with platelet aggregation. *International Journal of Design & Nature and Ecodynamics*, **5(2)**, pp.122-141, 2010.
- [14] Tanahashi, N., Fukuuchi, Y., Tomita, M., Yokoyama, M., Tomita, Y., Inoue, K. and Schiszler, I., Platelet adhesion to human brain microvascular endothelial cells in vitro (Observation with video-enhanced contrast microscopy), *Neuroscience Letters*, **274**, pp.199-202, 1999.



This page intentionally left blank

Dominant EEG frequencies of patients undergoing dobutamine stress test

A. K. Macpherson¹, S. Neti¹, M. Averbach², P. A. Macpherson³
& C. Chutakositkanon¹

¹*Institute of Biomedical Engineering and Mathematical Biology,
Lehigh University, USA*

²*Division of Cardiology, St Luke's Hospital, USA*

³*Department of Applied Technology, Rogers State University, USA*

Abstract

There has been considerable research and speculation that if the brain is under stress then it could affect the heart and lead to heart disease. The purpose of the present research was to examine the inverse problem of whether the heart could potentially cause undesirable reactions in the brain. One method to evaluate for underlying coronary artery disease is to perform stress testing. Often, myocardial stress is achieved by the patient walking on a treadmill while being monitored. In patients who are unable to exercise, pharmacologic stress testing is performed, either with vasodilatory agents (e.g. adenosine) or dobutamine, which is a pro-inotropic and chronotropic drug. During dobutamine infusion, the heart rate increases, but there is a negligible increase in blood pressure. Five patients who were undergoing dobutamine stress testing were instrumented with the standard 19 electrode EEG sensors to record brain activity. It was found that all patients showed resonance in the brain activity at frequencies around 10Hz. The signal strengths and the electrode locations where a resonance varied between patients. The one location where all of the patients showed resonance was at T5-O1; towards the back of the head and for this location, all patients showed an EEG resonance frequency at approximately 10Hz. Further analysis of the EEG data is needed to appreciate the consequences of this neurocardiological phenomenon.

Keywords: heart, brain, echocardiograms, neurocardiology, electroencephalographs.



1 Introduction

A review of how the brain regulates the cardiovascular system is given in [1]. A study [2] involved a patient on a bicycle undergoing a stress test that was instrumented with EEG electrodes on the patient's head. The object of the research was to construct a model for determining the effect of stress on patients in an industrial environment. Although **only** the output of the electrode on the top of the head is reported it is clear that more electrodes were used. The result was a clear indication of a relation between the heart activity and the electroencephalograph (EEG) reading. The regions of the brain which could clearly be identified as independent of blood pressure were the left temporal and the lateral frontal region. The brain activity correlated with the stress induced cardiac activity. The present work is in many ways an extension of that study. There were several aims in the present study. One was to eliminate the possibility that the increase in blood pressure may be the prime cause of any effect observed. A second aim was to use a standard 12 electrode EEG to locate where the signals arose on the brain surface. Finally the longer term objective was to seek relationships between the EEG output and the electrocardiograph (EKG) results.

2 Method of experimentation and calculation

In patients that are unable to exercise, pharmacologic stress testing is performed with the vasodilatory agent dobutamine, which is a pro-inotropic and chronotropic drug. During dobutamine infusion, the heart rate increases, but there is a negligible increase in blood pressure. The result is that the heart rate increases as a function of the dosage. The use of Dobutamine removes the possibility of blood pressure being the cause of the brain activity observed. There were 5 patients involved in the experiments and due to their health state there was a variation in the rate of Dobutamine injected. The highest dosage for a given patient varied dependent on the patient's tolerance and were in the 20 mics/kg/sec and 40 mics/kg/sec range. Some patients had a maximum of 35 mics. The general aim was to achieve a heart rate of 120 beats per minute.

While the dobutamine was being injected readings from the standard 19 electrodes were recorded. The location of the electrodes is shown in figure 1. A typical EEG output is shown in figure 2.

A significant difference between the present work and that reported in [4] is that in [4] analogue output was used to undertake the calculations whereas in the present work EEG digital data output has been used. This has had an impact on the reliability of the results. Fourier transforms were taken of each of the EEG signals. A very simplified explanation of a Fourier transform [3] which will serve to clarify the concept is as follows. The number the keys on a piano from 1 to 88 and play some music. There is a different frequency and hence different energy of the original overall sound associated with each key. The energy associated with each key is summed over the number of times it is struck during the playing of the music and plotted against the frequency. This is essentially a Fourier transform.



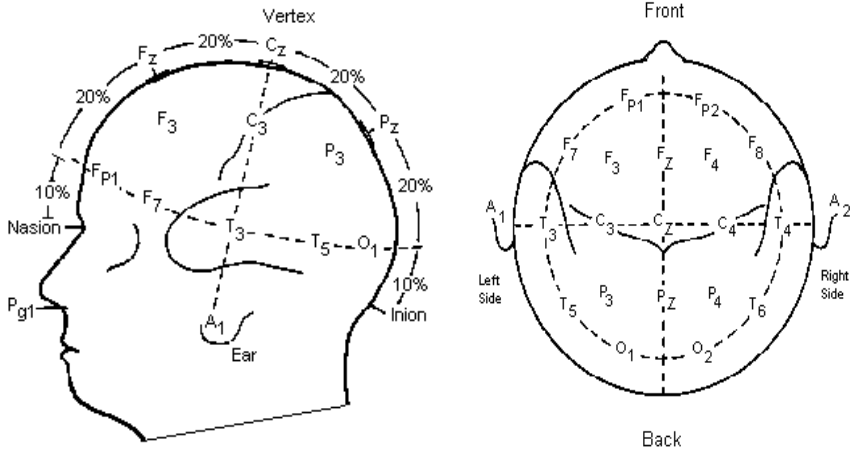


Figure 1: Electrode positions on skull. From web site by Eric Chudler, University of Washington.

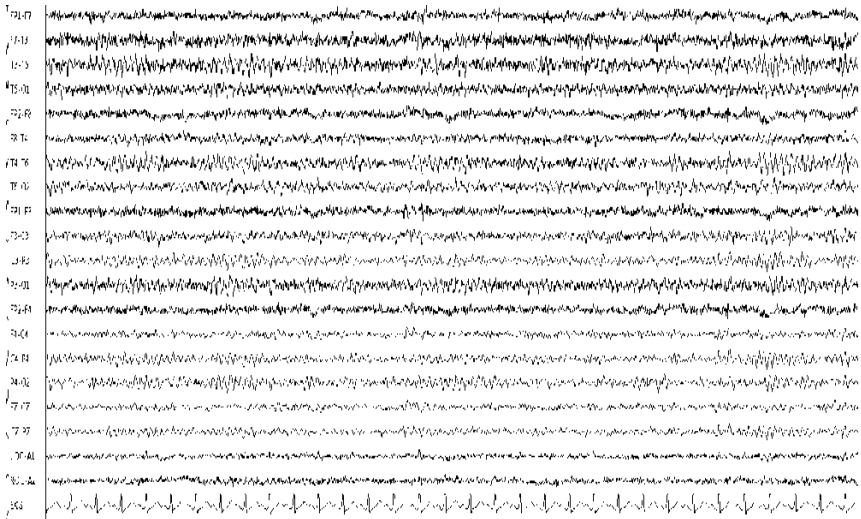


Figure 2: Sample EEG output for a patient.

At the same time as the EEGs were being taken, ECG (EKG) results were also obtained while the dobutamine was administered. The ECG was analyzed using a system known as wavelet analysis. Wavelet analysis shows the variation of various frequency bands with time. The piano analogy may be extended to wavelets. If the piano keys were divided into 5 energy groups for example, 1-20, 21-41, etc., then the wavelet analysis would at any given time account for the total energy for each group and plot it against time. Thus Fourier analysis



considers for a period of time how much energy is associated for a given frequency whereas wavelet analysis considers the time variation of frequencies.

The results were generated using the MATLAB code.

3 Results

Some preliminary results were published in [4] indicating that, using dobutamine to increase heart rate, Fourier transform resonances could be detected in the brain at approximately 10Hz. The locations where these resonances were found were at the CZ-PZ, C4-P4, T5-O1, T4-T6 and C3-P3 regions. In the present study it was found that resonance was found for EEG data obtained at CZ-PZ, F8-T4, C4-P4, T5-O1, T4-T6, F3-C3, F7-T3, P3-O1, P4-O2, T5-O1, T3-T5, T6O2 and C3-P3 as designated in Figure 1.

The present study extended earlier work [4] and involved 5 patients. All of the five patients showed varying responses of brain activity. The quality of the transforms varied between different patients as shown in figure 3.

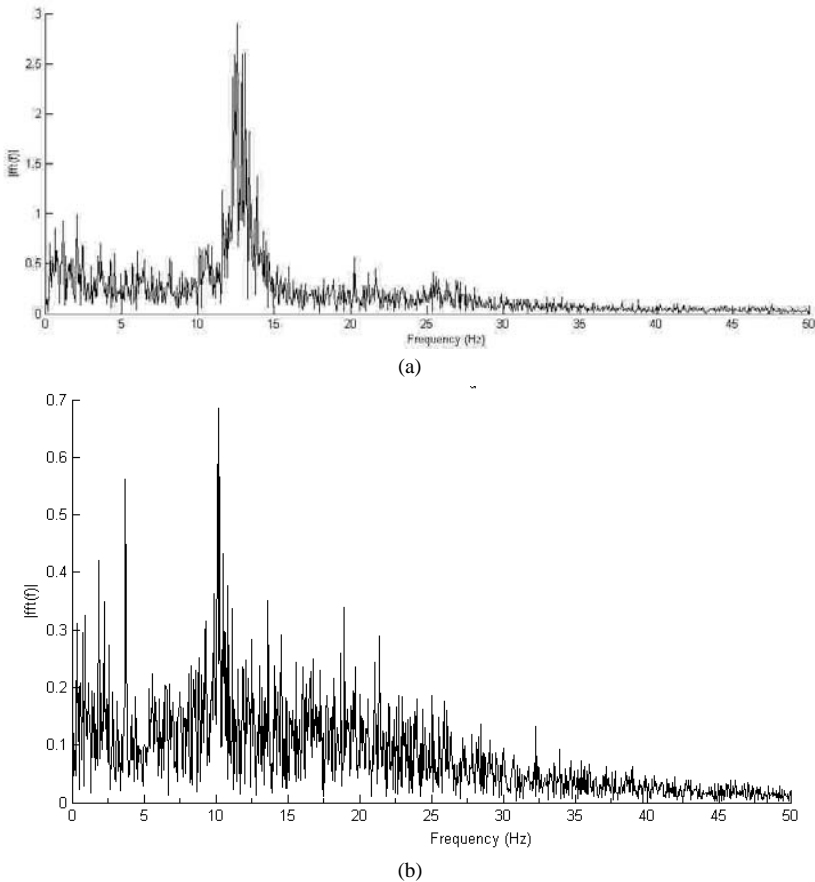


Figure 3: Variation of Fourier transforms between patients.

There is a significant variation in the magnitude of the response between patients. The detail shown is due to use of the digital signals from the EEG output. For example heart beats using (EKG) digital data are shown in figure 4.

As it is impossible to discuss all the results here, only the results are shown for patient 3 as representative of the patients who did show resonance at approximately 10 Hz. This patient was chosen as the clinical report on the results of the tests indicated there was no evidence of ischemia and systolic function was normal.

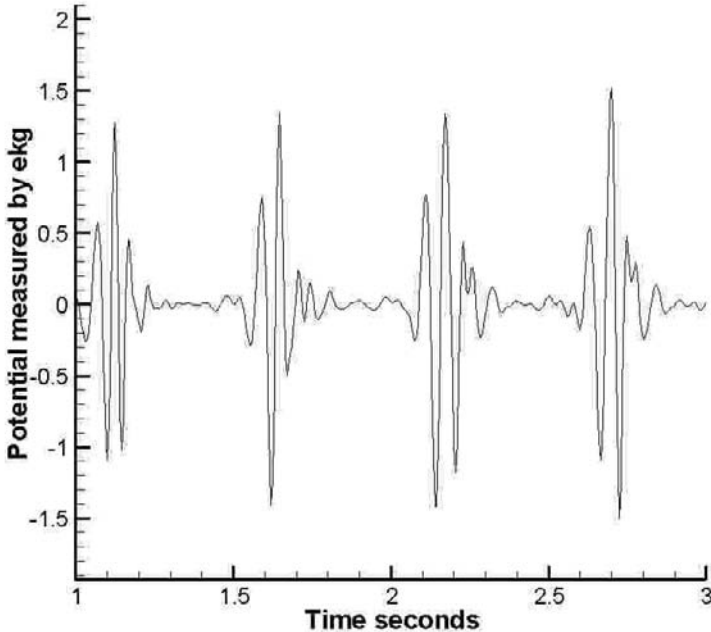


Figure 4: Heart beat from digital signal.

A typical Fourier transform from the EEG results for patient 3 is shown in figure 5. It shows a strong signal at 10 Hz. This persists over the entire time that the heart rate is elevated. When comparing with the rest EEG it is difficult to find extended periods where the patient is calm when undergoing the dobutamine testing.

The results are often similar to figure 3(b) without such a pronounced peak at 10 Hz. There are short periods where there is little brain activity at 10 Hz but the smallest disturbance will generate signals. For example if the doctor enters the room. This not the case in the elevated heart rate. In addition the heart rate is not constant even at a rest condition. The rest rate of patient 3 was 80bpm.

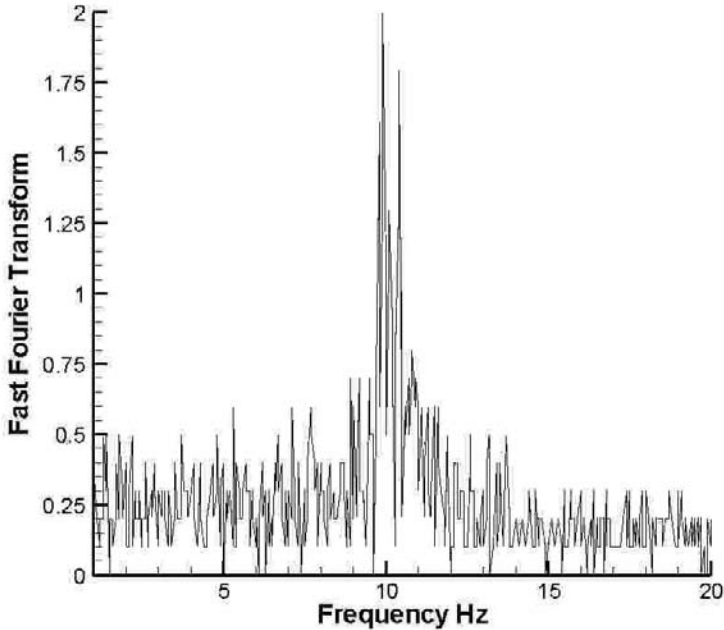


Figure 5: FFT at CZ-PZ.

An investigation was then undertaken to try and determine the cause of these resonances by the heart. Wavelet analysis was undertaken of the heart signals. The results are displayed in bands of different frequencies. The code to generate the wavelets was taken from [5]. A typical result is shown in figure 6.

The upper 4 bands on magnification are similar to figure 4 both at elevated and resting heart rates. The difference occurs in band 5 above. The magnified images of the resting waves is shown in figure 7 and the waves at a heart rate of 120 BPM is shown in figure 8.

It can be seen that there is an increase in frequency at the higher heart rate going from 4Hz to 5Hz. However a significant feature is that at the higher heart rate the signal is better organised. Further research is required to determine if this is the driving mechanism for the resonance in the brain.

4 Conclusions and future work

It has been shown that generally resonant frequencies in the brain EEG output appear as the heart rate is increased as part of a dobutamine stress test. The frequency of these resonances is around 10Hz for most patients. These resonances could be caused by low frequency waves and harmonics of these waves in the heart beat.

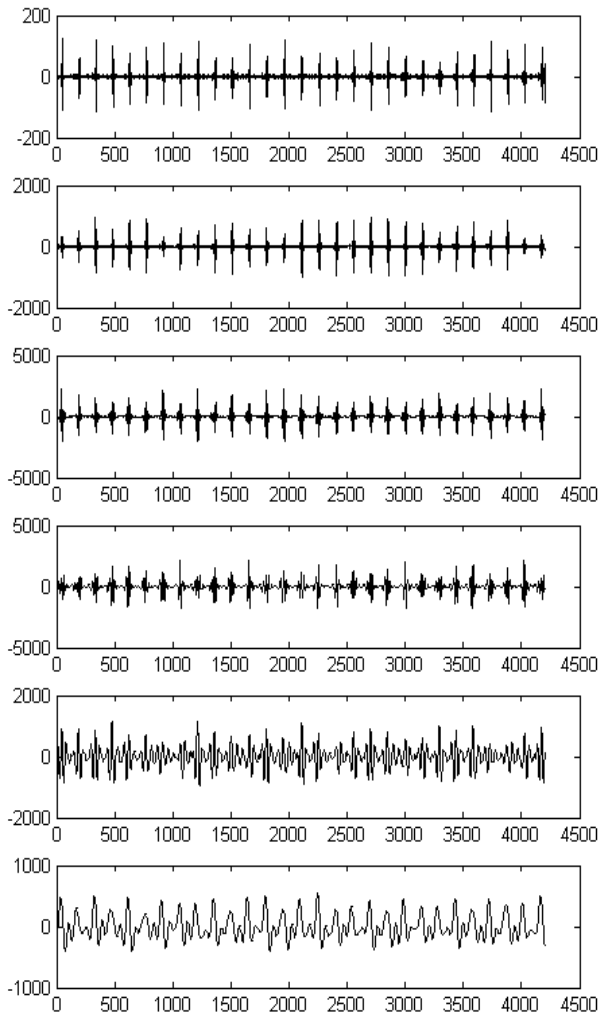


Figure 6: Six frequency bands generated using code from [5].



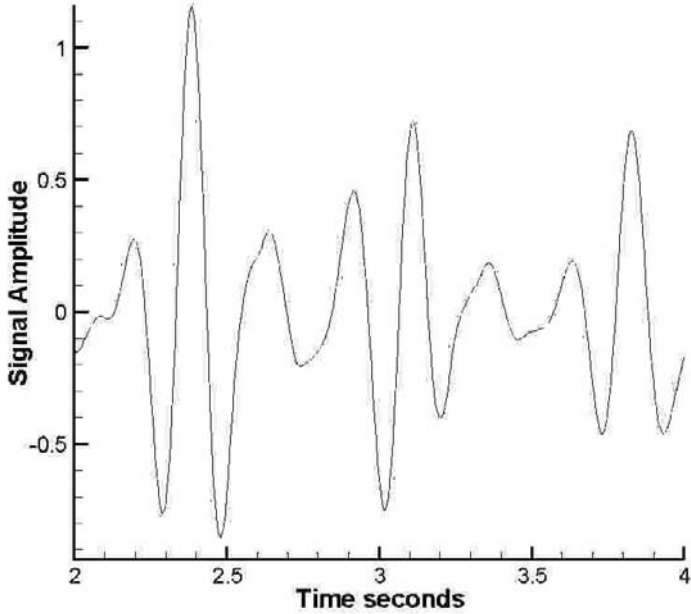


Figure 7: Low frequency wavelet at resting heart rate.

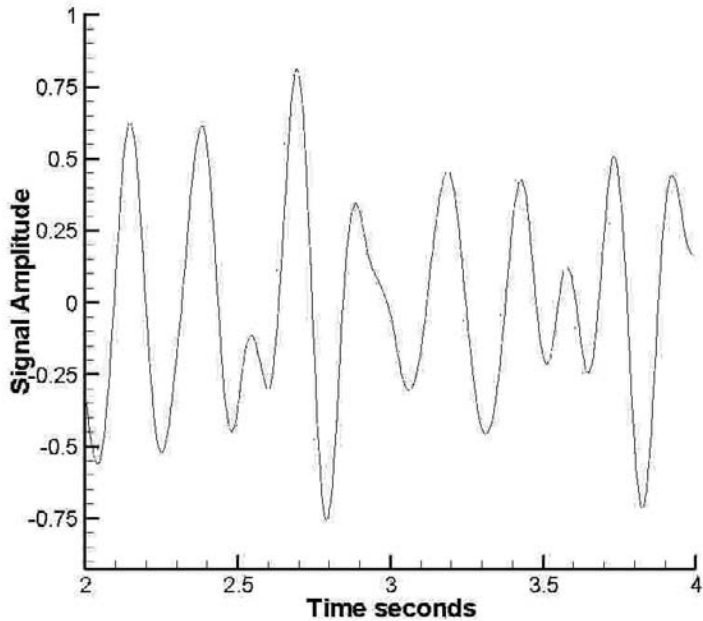


Figure 8: Low frequency wavelet at heart rate 120bpm.

There may be long term health issues involved with these repeated assaults on the brain due to low frequencies. Besides the possibilities involving disease there is a documented effect (trauma) due to low frequency waves known as wind turbine syndrome. Such trauma including headaches is experienced by people living close to wind turbine farms. Some reports have put that critical frequency at 8Hz and the 10 Hz resonances from the EEG signals reported above are not far from those. Further analyses might bring out the relationship between these two phenomena.

References

- [1] Coote, J.H. Landmarks in understanding the central nervous control of the Cardiovascular System. *Experimental Physiology*, 92(1), pp 3-18 2007
- [2] Ema, El-sd., Mahdi, M., Derick. A.L. A closed-loop hybrid physiological model relating to subjects under physical stress, *Artificial Intelligence in Medicine*, 38, pp 257-274, 2006.
- [3] This analogy is not original to this publication but we are unable to determine the origin of the analogy
- [4] Macpherson, A.K., Neti, S., Averbach, M. Macpherson, P.A., Chutakositkanon, C. and Nathanson, D. The Influence of Heart Stress on the Brain: A preliminary Study, *Design & Nature and Ecodynamics*, 5(2) 160-172, 2010.
- [5] Internet web site *M:\uvi_wave\Matlab Uvi_Wave Toolbox.htm*



This page intentionally left blank

Numerical evaluation of the slope and intercept of end-systolic pressure-volume relation

R. M. Shoucri

*Department of Mathematics & Computer Science,
Royal Military College of Canada, Canada*

Abstract

Numerical evaluation of two methods to calculate slope and intercept of end-systolic pressure-volume relation (ESPVR) in the left ventricle is presented. The mathematical formalism is based on results previously published in which the active force of the myocardium (also called isovolumic pressure P_{iso}) is introduced in the formalism describing the pressure-volume relation (PVR) in the left ventricle. The numerical calculation is simple and can be easily implemented in routine clinical work, only the ventricular pressure P_m near end-systole needs to be estimated. A thick-walled cylindrical model contracting symmetrically is assumed for the left ventricle.

Keywords: ventricular elastance, end-systolic pressure-volume relation, pressure-volume relation in the ventricles, peak isovolumic pressure, active force of the myocardium.

1 Introduction

In previous studies the author has stressed the importance of introducing the active force of the myocardium (also called isovolumic pressure P_{iso} by physiologists) in the formalism describing the pressure-volume relation (PVR) in the ventricles [1–5]. The mathematical formalism developed was used to calculate the stress in the myocardium by using linear elasticity [5] and large elastic deformation [1–4], in this formalism the active force of the myocardium is modelled as force/unit volume of the myocardium generated by the cardiac muscle (see fig. 1). In this study a relation derived in [2] is used to calculate the non-linear end-systolic pressure-volume relation (ESPVR). It is shown that this mathematical relation can be used to calculate in a non-invasive way the



intercept V_{om} of the ESPVR with the volume axis (see fig. 2), only knowledge of the volume of the myocardium V_o , the end-systolic volume V_{ed} and the ventricular cavity volume V_m near end-systole are required in order to calculate V_{om} . If the ventricular cavity pressure P_m near end-systole can be estimated in a non-invasive way, then the different slopes of the non-linear ESPVR (see fig. 2) and the peak isovolumic pressure P_{isom} can also be calculated in a non-invasive way. This study focuses on a comparison between a numerical approximation obtained by assuming that for small z , $\log(1 + z) \approx z$, with the exact expression using the logarithmic function. The interest of this approximation is that the calculations are much simpler.

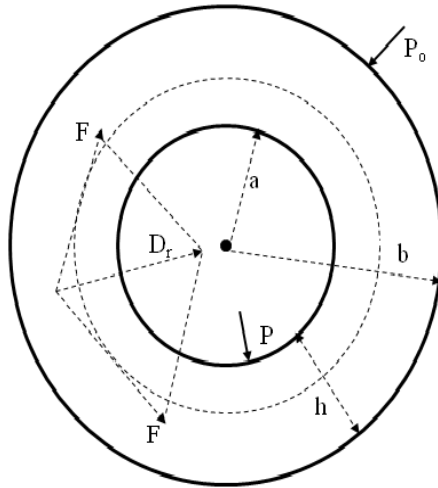


Figure 1: The left ventricle is represented as a thick-walled cylinder contracting symmetrically. P = ventricular pressure, P_o = outer pressure (neglected in the calculation), a = inner radius, b = outer radius, $h = b - a$ = thickness of the myocardium. A helical fibre is projected on the cross-section as a dotted circle. Because of the assumed symmetry of the contraction, a radial active force $D_r(r)$ (force/unit volume of the myocardium) is generated by the muscular fibre.

Although the cardiac pressure-volume loops at different loadings appear to define an almost linear relationship of end systolic values, the ESPVR is essentially a non-linear relation (see references [6–8]). Several approaches have been proposed to estimate the parameters of the ESPVR from single beat measurement [9, 10] (for a critical review see [10]), but none has the simplicity of the method presented in this study.

2 Mathematical model

As in previous studies a quasi-static approximation of the ventricular contraction is considered (inertia forces and viscous forces neglected). Figure 1 shows a cross-section of the left ventricle that is modelled a thick-walled cylinder contracting symmetrically, a helical myocardial fibre is projected on the cross-section as a dotted circle. It will generate a radial active force/unit volume of the myocardium $D_r(r)$, this force will develop an active pressure on the inner surface of the myocardium (endocardium) given by

$$\int_a^b D_r(r) dr = \bar{D}h \quad (1)$$

The thickness of the myocardium is given by $h = b - a$, a = inner radius of the myocardium, b = outer radius of the myocardium. \bar{D} is an average radial force/unit volume of the myocardium calculated by applying the mean value theorem. We shall follow the practice of physiologists and by writing $\bar{D}h = P_{iso}$, where P_{iso} is the isovolumic pressure developed in a non-ejecting contraction. Near end-systole when the myocardium reaches its maximum state of activation, the equilibrium of forces on the inner surface of the myocardium in a quasi-static approximation can be written as follows

$$P_{isom} - P_m = E_{2mx} (V_{ed} - V_m) \quad (2)$$

The left hand side is the resultant pressure applied on the inner force of the myocardium. The right hand side is the pressure resulting from the change of volume from V_{ed} (end-diastole when $dV/dt = 0$) to V_m when the cardiac muscle reaches its maximum state of activation ($V_m \approx V_{es}$ the end-systolic volume when $dV/dt = 0$), the corresponding ventricular pressure is P_m . From fig. 2, one can deduce that the elasticity coefficient $E_{2mx} = \tan\beta_2$. The outer pressure P_o in fig. 1 is neglected.

If P_{isom} is kept constant and (P_m, V_m) is varied in eqn (2), then the point (P_m, V_m) will describe the ESPVR represented by the curve BDC in fig. 2, as if a balloon is inflated against a constant P_{isom} .

Equation (2) can be split into two equations as follows

$$P_m = E_{1mx} (V_m - V_{om}) \quad (3)$$

$$P_{isom} = E_{mx} (V_{ed} - V_{om}) \quad (4)$$

The intercept V_{om} of the non-linear ESPVR with the volume axis is shown in fig. 2. From fig. 2, one can deduce that the coefficients $E_{1mx} = \tan\beta_1$ and $E_{mx} = \tan\alpha$. An interesting feature of the preceding equations is the introduction of the peak isovolumic pressure P_{isom} in the formalism describing the ESPVR.



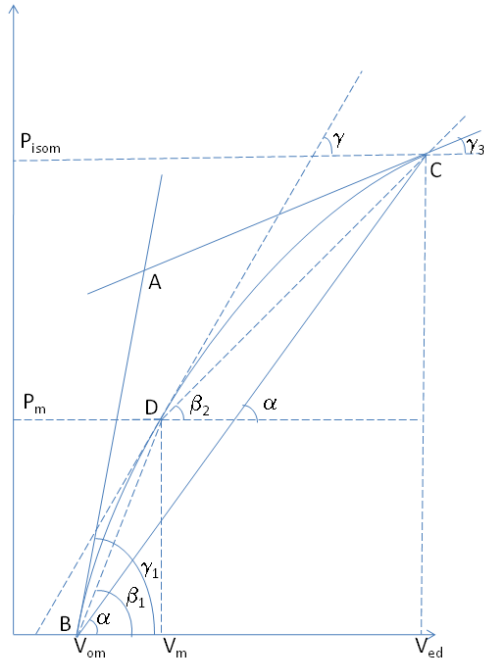


Figure 2: Non-linear ESPVR represented by the curve BDC, D has coordinates (P_m, V_m) . P_m is the left ventricular pressure (corresponding to the maximum state of activation of the muscle), P_{isom} is the peak isovolumic pressure. $E_{mx} = \tan\alpha$ slope of BC, $E_{1mx} = \tan\beta_1$ slope of BD, $E_{2mx} = \tan\beta_2$ slope of DC. The slope of the tangent to the ESPVR at D is $\tan\gamma$.

3 Slopes of the ESPVR

Unlike the linear ESPVR that is characterized by one slope, we have in fig. 2 several slopes that characterize the non-linear ESPVR. These slopes are

$$\tan\beta_2 = E_{2mx} = \text{slope of the line CD} \tag{5a}$$

$$\tan\alpha = E_{mx} = \text{slope of the line CB} \tag{5b}$$

$$\tan\beta_1 = E_{1mx} = \text{slope of the line DB} \tag{5c}$$

$$\tan\gamma = \frac{dP_m}{dV_m} = \text{tangent to the ESPVR BDC at point D } (P_m, V_m) \tag{5d}$$

$$\tan\gamma_1 = \text{tangent to the ESPVR BDC at point B } (0, V_{om}) \tag{5e}$$

$$\tan\gamma_3 = \text{tangent to the ESPVR BDC at point C } (P_{isom}, V_{ed}) \tag{5f}$$

We give in this section an exact expression of slopes based on the cylindrical model of the ventricular cavity as derived in [2], we then discuss in the next section the numerical calculation procedures.

a) From reference [2] we can write

$$\tan\beta_2 = k_w \left(\frac{1}{V_m} - \frac{1}{V_m+V_\omega} + \frac{\log\frac{V_m+V_\omega}{V_{ed}+V_\omega} - \log\frac{V_m}{V_{ed}}}{V_{ed}-V_m} \right) \tag{6a}$$

We use log to represent the natural logarithm, k_w is a constant coefficient calculated by applying the mean value theorem in [2]. For small z we can apply the relation $\log(1+z) \approx z$, we get the following approximate expression $\tan\beta_{2a}$

$$\tan\beta_{2a} \approx k_{wa} \left(\frac{1}{V_m} - \frac{1}{V_m+V_\omega} + \frac{1}{V_{ed}} - \frac{1}{V_{ed}+V_\omega} \right) \tag{6b}$$

The coefficient k_{wa} corresponds to the calculation carried out when the approximation $\log(1+z) \approx z$ is used.

b) When point D moves to point B, $V_m \rightarrow V_{om}$ and $\tan\beta_2 \rightarrow \tan\alpha$. We get

$$\tan\alpha = k_w \left(\frac{1}{V_{om}} - \frac{1}{V_{om}+V_\omega} + \frac{\log\frac{V_{om}+V_\omega}{V_{ed}+V_\omega} - \log\frac{V_{om}}{V_{ed}}}{V_{ed}-V_{om}} \right) \tag{7a}$$

By applying the approximation $\log(1+z) \approx z$ we get the following approximate expression $\tan\alpha_a$

$$\tan\alpha_a \approx k_{wa} \left(\frac{1}{V_{om}} - \frac{1}{V_{om}+V_\omega} + \frac{1}{V_{ed}} - \frac{1}{V_{ed}+V_\omega} \right) \tag{7b}$$

c) From eqns (4) and (7a) one can derive the following expression for P_{isom}

$$P_{isom} = k_w \left[\left(\frac{1}{V_{om}} - \frac{1}{V_{om}+V_\omega} \right) (V_{ed} - V_{om}) + \log\frac{V_{om}+V_\omega}{V_{ed}+V_\omega} - \log\frac{V_{om}}{V_{ed}} \right] \tag{8a}$$

and the approximate expression P_{isoma}

$$P_{isoma} \approx k_{wa} \left(\frac{1}{V_{om}} - \frac{1}{V_{om}+V_\omega} + \frac{1}{V_{ed}} - \frac{1}{V_{ed}+V_\omega} \right) (V_{ed} - V_{om}) \tag{8b}$$

d) We note that $P_m = P_{isom} - (P_{isom} - P_m)$, which can be written as

$$P_m = \tan\alpha (V_{ed} - V_{om}) - \tan\beta_2 (V_{ed} - V_m) \tag{9a}$$

By using eqns (6a) and (7a) we get

$$P_m = k_w \left[\left(\frac{1}{V_{om}} - \frac{1}{V_{om}+V_\omega} \right) (V_{ed} - V_{om}) - \left(\frac{1}{V_m} - \frac{1}{V_m+V_\omega} \right) (V_{ed} - V_m) + \log\frac{V_{om}+V_\omega}{V_{ed}+V_\omega} - \log\frac{V_{om}}{V_{ed}} - \left(\log\frac{V_m+V_\omega}{V_{ed}+V_\omega} - \log\frac{V_m}{V_{ed}} \right) \right] \tag{9b}$$

By combining the logarithmic terms, we get:

$$P_m = k_w \left[\left(\frac{1}{V_{om}} - \frac{1}{V_{om}+V_\omega} \right) (V_{ed} - V_{om}) - \left(\frac{1}{V_m} - \frac{1}{V_m+V_\omega} \right) (V_{ed} - V_m) + \log\frac{V_{om}+V_\omega}{V_m+V_\omega} - \log\frac{V_{om}}{V_m} \right] \tag{9c}$$



We notice that by using the approximation $\log(1+z) \approx z$ when z is small, eqns (9b) and (9c) give different results. We use eqn (9c) to obtain the approximation

$$P_{ma} \approx k_{wa} \left[\left(\frac{1}{V_{om}} - \frac{1}{V_{om}+V_{\omega}} \right) (V_{ed} - V_{om}) - \left(\frac{1}{V_m} - \frac{1}{V_m+V_{\omega}} \right) (V_{ed} - V_m) + \left(\frac{1}{V_m} - \frac{1}{V_m+V_{\omega}} \right) (V_m - V_{om}) \right] \tag{9d}$$

e) The slope $\tan\beta_1 = E_{1mx}$ is calculated from eqn (3) and eqn (9a), we get

$$\tan\beta_1 = \frac{P_m}{V_m - V_{om}} \tag{10a}$$

$$\tan\beta_1 = \frac{\tan\alpha (V_{ed} - V_{om}) - \tan\beta_2 (V_{ed} - V_m)}{V_m - V_{om}} \tag{10b}$$

By using eqn (9c) we get

$$\tan\beta_1 = k_w \left[\left(\frac{1}{V_{om}} - \frac{1}{V_{om}+V_{\omega}} \right) \frac{V_{ed} - V_{om}}{V_m - V_{om}} - \left(\frac{1}{V_m} - \frac{1}{V_m+V_{\omega}} \right) \frac{V_{ed} - V_m}{V_m - V_{om}} + \frac{\log \frac{V_{om}+V_{\omega}}{V_m+V_{\omega}} - \log \frac{V_{om}}{V_m}}{V_m - V_{om}} \right] \tag{10c}$$

By using the approximation $\log(1+z) \approx z$ for small z , we obtain the approximation

$$\tan\beta_{1a} \approx \frac{1}{V_{om}} - \frac{1}{V_{om} + V_{\omega}} + \frac{1}{V_m} - \frac{1}{V_m + V_{\omega}} + k_{wa} \left[\frac{1}{V_{om}} - \frac{1}{V_{om}+V_{\omega}} - \left(\frac{1}{V_m} - \frac{1}{V_m+V_{\omega}} \right) \right] \frac{V_{ed} - V_m}{V_m - V_{om}} \tag{10d}$$

f) In order to calculate the tangent to the ESPVR (see eqn (5d)), we calculate the derivative dP_m/dV_m from eqn (9c) to obtain

$$\tan\gamma = k_w \left[2 \left(\frac{1}{V_m} - \frac{1}{V_m+V_{\omega}} \right) + \left(\frac{1}{V_m} - \frac{1}{V_m+V_{\omega}} \right) \left(\frac{1}{V_m} + \frac{1}{V_m+V_{\omega}} \right) (V_{ed} - V_m) \right] \tag{11}$$

g) We obtain $\tan\gamma_1$ (see eqn (5e)) by letting $V_m \rightarrow V_{om}$ in eqn (11), we get

$$\tan\gamma_1 = k_w \left[2 \left(\frac{1}{V_{om}} - \frac{1}{V_{om} + V_{\omega}} \right) + \left(\frac{1}{V_{om}} - \frac{1}{V_{om}+V_{\omega}} \right) \left(\frac{1}{V_{om}} + \frac{1}{V_{om}+V_{\omega}} \right) (V_{ed} - V_{om}) \right] \tag{12}$$

We obtain $\tan\gamma_3$ (see eqn. (5f)) by letting $V_m \rightarrow V_{ed}$ in eqn. (11), we get

$$\tan\gamma_3 = k_w \left[2 \left(\frac{1}{V_{ed}} - \frac{1}{V_{ed}+V_{\omega}} \right) \right] \tag{13}$$

4 Numerical application

The numerical application is based on the experimental data published by Burns et al. [11] for experiments on dogs. The values of V_{ed} , $V_{es} \approx V_m$, V_{ω} are given in [11] as well as the maximum left ventricular pressure P_{max} . We have assumed that the pressure P_m near end-systole, corresponding to the maximum state of

activation of the muscle, can be estimated from $P_m \approx P_{max}/1.2$ approximately. These values are shown in Table 1.

Table 1: Result of the calculation of V_{om} and P_{isom} by two different methods.

	P_{max} mmHg	mass gr.	V_{ed} ml	V_m ml	Exact		Approximate	
					P_{isom} mmHg	V_{om} ml	P_{isom} mmHg	V_{om} ml
1	113	73	17.7	5.6	191.92	3.18	180.78	3.34
2	144		30.3	4.7	241.84	2.44	231.09	2.57
3	144		49.2	8.0	239.30	4.21	227.81	4.43
4	109	136.4	23.8	9.7	186.04	5.86	175.30	6.11
5	139		41.0	19.7	233.76	12.61	219.47	13.05
6	155		56.5	27.2	258.56	17.51	241.94	18.11
7	103	91.4	34.3	27.0	171.36	22.16	165.04	22.34
8	142		49.9	38.1	234.85	30.72	224.72	31.01
9	155		63.3	50.4	255.80	41.84	245.53	42.15
10	115	123	24.5	11.4	195.41	7.19	184.09	7.45
11	133		49.5	40.6	221.07	34.31	213.89	34.51
12	135	138.8	38.5	23.8	226.67	16.93	214.68	17.31
13	149		52.3	29.6	248.74	20.28	233.93	20.82
14	153		70.0	29.7	254.08	18.42	237.03	19.14
15	101	155.9	56.2	34.0	168.68	24.00	159.17	24.55
16	150.4		87.0	55.9	248.39	40.88	234.06	41.66

end-systolic pressure $P_m = \max.$ pressure $P_{max}/1.2$; myocardial volume in ml $V_o = \text{mass}/\text{density}$, density = 1.055 g/cm³; data for P_{max} , mass, V_{ed} and V_m taken from Burns et al. [11].

4.1 Calculation of V_{om}

The intercept V_{om} with the volume axis of the nonlinear ESPVR can be calculated from the three following approximate relations. At point B (coordinates (0, V_{om})) on the ESPVR (see fig. 2) we have

$$\tan\beta_1 \approx (\tan\gamma_1 + \tan\alpha)/2 \tag{14}$$

At point D (coordinates (P_m, V_m)) (see Fig. 2) we have

$$\tan\gamma \approx (\tan\beta_1 + \tan\beta_2)/2 \tag{15}$$

At point C (coordinates (V_{ed}, P_{isom})) (see Fig. 2) we have

$$\tan\beta_2 \approx (\tan\gamma_3 + \tan\alpha)/2 \tag{16}$$

It should be noticed that k_w simplifies on both sides of eqns. (14) to (16), so that only V_{ed} , $V_m \approx V_{es}$, and V_o are needed to calculate V_{om} . The calculation is done by using Newton-Raphson method (see Appendix). It has been verified that

the three equations give the same result for V_{om} . Figure 3 shows the result of calculating V_{om} by using eqn (16) with the exact expressions (eqns (6a), (7a) and (13)), and the approximate expressions (eqns (6b), (7b) and (13)), the maximum error between the two approaches is of the order of 5.5%.

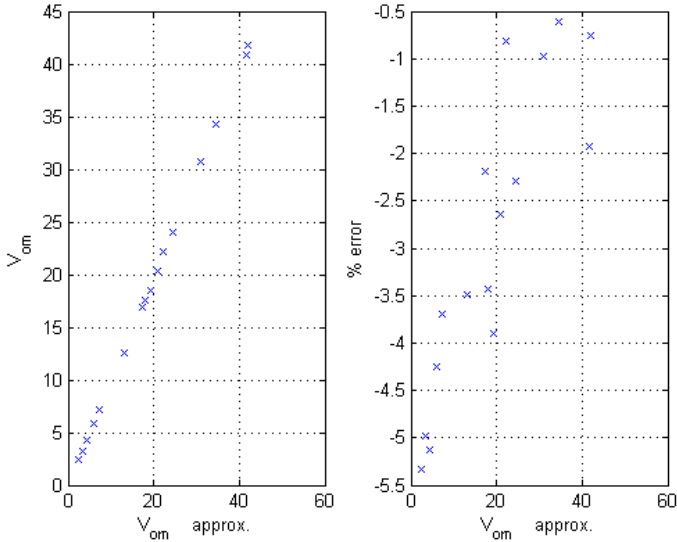


Figure 3: V_{om} (ml) is the intercept of the ESPVR with the volume axis, calculation of V_{om} is done by using the approximate relation $\log(1+z) \approx z$ (horizontal axis), and without using this approximation (vertical axis). The percentage relative error is shown on the right side (vertical axis).

4.2 Calculation of the coefficient k_w

The values of V_{ed} , $V_m \approx V_{es}$, V_{ω} , V_{om} and P_m are needed to calculate the coefficient k_w from eqns (9c) and (9d), the results are shown in fig. 4. The maximum relative error, due to the approximation $\log(1+z) \approx z$, for the calculation of k_w is of the order of 17% (see fig. 4).

4.3 Calculation of the tangents

Because of space consideration only the results of the calculation of the tangents $\tan\beta_1$ and $\tan\alpha$ are shown in figs. 5 and 6. On the horizontal axis we have the results obtained by using the approximation $\log(1+z) \approx z$, on the vertical axis we have the results obtained without using this approximation. The right hand side shows that the maximum error in all these cases is of the order of 10%.

The results for $\tan\alpha$ and $\tan\beta_2$ are similar.



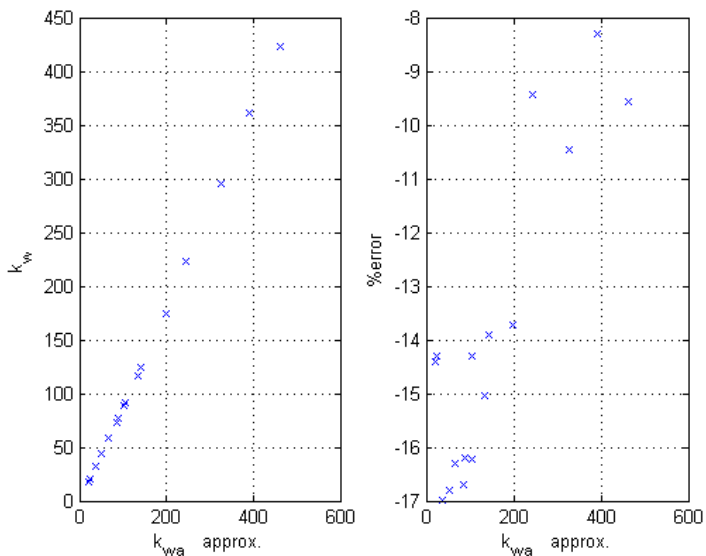


Figure 4: The coefficient k_w (mmHg) is calculated by using eqn (9d) (horizontal axis), and by using eqn (9c) (vertical axis); % error = $100*(k_w - k_{wa})/k_w$ is shown on the right side (vertical axis).

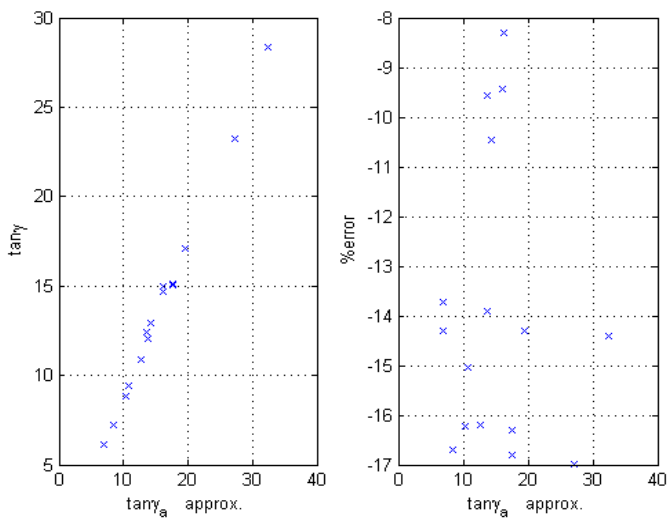


Figure 5: The tangent $tany$ is calculated by using eqn (6b) (horizontal axis), and by using eqn (6a) (vertical axis); % error = $100*(tany - tany_a)/tany$ is shown on the right side (vertical axis).



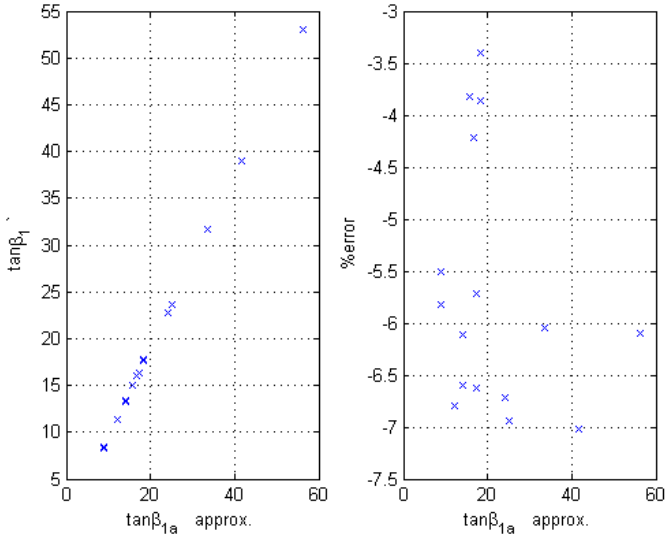


Figure 6: The slope $\tan\beta_1$ is calculated by using the approximate eqn (10d) (horizontal axis), and by using eqn (10c) (vertical axis); % error = $100 * (\tan\beta_1 - \tan\beta_{1a}) / \tan\beta_1$ is shown on the right side (vertical axis).

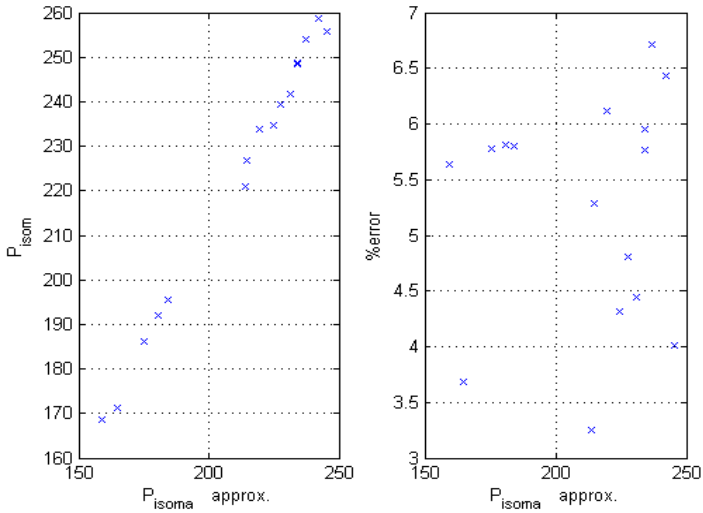


Figure 7: The peak isovolumic pressure P_{isom} (mmHg) is calculated by using the approximate eqn (8b) (horizontal axis), and by using eqn (8a) (vertical axis); % error = $100 * (P_{isom} - P_{isoma}) / P_{isom}$ is shown on the right side (vertical axis).



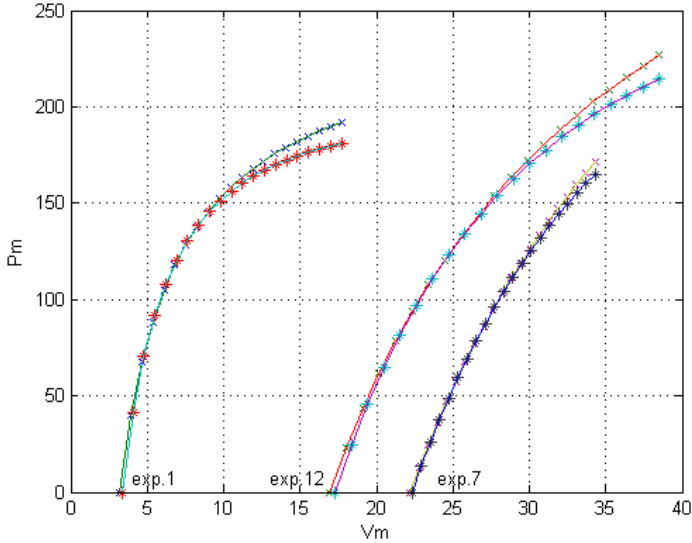


Figure 8: Variation of (P_m , V_m) along ESPVR using exact formula x (eqn. 9c) and approximate formula * (eqn. 9d) for three experiments taken from Table 1.

4.4 Calculation of P_{isom}

The calculation of the peak isovolumic pressure P_{isom} by using eqns (8a) and (8b) is shown in fig. 7. The maximum relative error in using the approximation $\log(1+z) \approx z$ for the calculation of P_{isom} is of the order of 7%.

4.5 ESPVR

The calculation of the ESPVR was done by using eqns. (9), eqn. (2) can be used to verify the results. In the calculation of Fig. 8, V_m is varied from V_{om} to V_{ed} and P_m is calculated by using eqn (9c) for the exact value (x) and eqn (9d) for the approximate value (*) corresponding to the approximation $\log(1+z) \approx z$. From Table 1 we see that we have

V_m varies from $V_{om} = 3.34$ ml to $V_{ed} = 17.7$ ml for experiment 1.

V_m varies from $V_{om} = 22.34$ ml to $V_{ed} = 34.3$ ml for experiment 7.

V_m varies from $V_{om} = 17.31$ ml to $V_{ed} = 38.5$ ml for experiment 12.

Only the results for three experiments are shown in a way not to overload the figure. The results of Fig. 8 show that the volume intercept V_{om} is not very much affected by the approximation $\log(1+z) \approx z$, and similarly for the peak isovolumic pressure P_{isom} .

5 Conclusion

We have investigated the possibility to use the approximation $\log(1 + z) \approx z$ for small z in the calculation of different parameters used to describe the non-linear ESPVR. The result of this study indicates that this approximation seems to have small effect on the calculation of V_{om} or P_{isom} , but the error in the calculation of the slope to the ESPVR is relatively larger.

Appendix

The Newton-Raphson Method is used to solve Equation (16). By using the approximation $\log(1 + z) \approx z$ we get

$$1 - \frac{V_m(V_m+V_\omega)}{V_{ed}(V_{ed}+V_\omega)} = \frac{V_m(V_m+V_\omega)}{V_o(V_o+V_\omega)} - 1 \quad (A1)$$

By writing

$$x = \frac{V_o}{V_m} \quad y = \frac{V_o+V_\omega}{V_m+V_\omega} \quad (A2)$$

then eqn. (A1) can be written in the form

$$f(x, y) = \left[2 - \frac{V_m(V_m+V_\omega)}{V_{ed}(V_{ed}+V_\omega)} \right] x y - 1 \quad (A3)$$

The two eqns (A2) combine to give

$$g(x, y) = y \frac{V_m+V_\omega}{V_\omega} - x \frac{V_m}{V_\omega} - 1 \quad (A4)$$

We start with an approximation x_o and y_o to the solution of Eqs A3 & A4. A new approximation x_n , y_n is calculated from the relation

$$\begin{bmatrix} x_n \\ y_n \end{bmatrix} = \begin{bmatrix} x_o \\ y_o \end{bmatrix} - J^{-1} \begin{bmatrix} f(x_o, y_o) \\ g(x_o, y_o) \end{bmatrix}, \quad \text{with } J = \begin{bmatrix} \frac{\partial f}{\partial x} & \frac{\partial f}{\partial y} \\ \frac{\partial g}{\partial x} & \frac{\partial g}{\partial y} \end{bmatrix} \quad (A5)$$

J^{-1} is the inverse of J . The MATLAB code is shown below, one can verify that the calculated values $vom1$ and $vom2$ representing V_{om} are equal.

```
function [vom1,vom2] = Calcul3Vo(ved,vm,vw)
% ved = end-diastolic volume; vm = end-systolic ventricular volume
% vw = volume of the myocardium; xo, yo initial approximations
xo = 2/vm; yo = (xo*vm + vw)/(vm + vw);
epsx = 1.0; epsy = 1.0; count = 0;
while ((epsx > 0.001) || (epsy > 0.001))
Ko = 2 - (vm/ved)*(vm + vw)/(ved + vw);
fxy = Ko*xo*yo - 1;
gxy = yo*((vm + vw)/vw) - (vm/vw)*xo - 1;
dfx = Ko*yo; dfy = Ko*xo;
dgx = -vm/vw; dgy = (vm + vw)/vw;
dlt = dfx*dgy - dfy*dgx;
```



```

xn = xo - (dgy*fx - dfy*gy)/dlt;
yn = yo - (-dgx*fx + dfx*gy)/dlt;
epsx = abs(xn - xo); epsy = abs(yn - yo);
xo = xn; yo = yn;
count = count + 1;
if (count > 15)
epsx = 0; epsy = 0;
end
end
vom1 = xo*vm; vom2 = yo*(vm + vw) - vw;

```

References

- [1] Shoucri, R.M., The pressure-volume relation and the mechanics of left ventricular contraction, *Japanese Heart Journal*, **31**, pp. 713-729, 1990.
- [2] Shoucri, R.M., Theoretical study of pressure-volume relation in left ventricle, *Am. J. Physiol Heart Circ. Physiol.*, **260**, pp. H282-H291, 1991.
- [3] Shoucri, R.M., Studying the mechanics of left ventricular contraction, *IEEE Engineering in Medicine and Biology Magazine*, **17**, pp. 95-101, May/June 1998.
- [4] Shoucri, R.M., Mathematical aspects of the mechanics of left ventricular contraction, *Int. J. of Design & Nature and Ecodynamics*, **5**, pp. 1-16, 2010.
- [5] Shoucri, R.M., Comparison between linear elasticity and large elastic deformation in the study of the contraction of the myocardium, *Modelling in Medicine and Biology VII*, ed. C.A. Brebbia, WIT Press: Southampton & Boston, pp. 3-13, 2007.
- [6] Kass, D.A., BeyarR., et al., Influence of contractile state on curvilinearity of in situ end-systolic pressure-volume relations, *Circulation*, **79**, pp. 167-178, 1989.
- [7] Claessens, T.E, Georgakopoulos, D., et al., Nonlinear isochrones in murine left ventricular pressure-volume loops: how well does the time-varying elastance concept hold?, *Am. J. Physiol Heart Circ. Physiol.*, **290**, pp. H1474-H1483, 2006.
- [8] Sato, T., Shishido, T., et al., ESPVR of in situ rat left ventricle shows contractility-dependent curvilinearity, *Am. J. Physiol Heart Circ. Physiol.*, **274**, pp. H1429-H1434, 1998.
- [9] ten Brinke, E.A., Klautz, R.J., Verwey, H.F., van der Wall, E.E., Dion, R.A., Steendijk, P., Single-beat estimation of the left ventricular end-systolic pressure-volume relationship in patients with heart failure, *Acta Physiol.*, **198**, pp. 37-46, 2010.
- [10] Kjorstad, K.E, Korvald, C, Myrmed T, Pressure-volume-based single-beat estimation cannot predict left ventricular contractility in vivo, *Am. J. Physiol Heart Circ. Physiol.*, **282**, pp. H1739-H1750, 2002.
- [11] J.W. Burns, J.W. Covell, R. Myers, J. Ross Jr, Comparison of directly measured left ventricular wall stress and stress calculated from geometric reference figures, *Circ. Res.*, **28**, pp. 611-621, 1971.



This page intentionally left blank

Modelling of embolus transport and embolic stroke

I. D. Šutalo^{1,2}, A. Bui³, K. Liffman^{1,2} & R. Manasseh^{4,5}

¹*Materials Science and Engineering, Commonwealth Scientific and Industrial Research Organisation (CSIRO), Australia*

²*Curtin Health Innovation Research Institute, Curtin University, Australia*

³*Idaho National Laboratory, USA*

⁴*Faculty of Engineering and Industrial Sciences, Swinburne University of Technology, Australia*

⁵*Mechanical Engineering, The University of Melbourne, Australia*

Abstract

Cerebral microembolism may lead to the restriction of blood supply due to damaged blood vessel tissue (focal ischemia) which is increasingly seen as the cause of cognitive deterioration including Alzheimer's disease and vascular dementia. The flow through fractal models of the peripheral vasculature of the Anterior Cerebral Arteries (ACA) and Middle Cerebral Arteries (MCA) was modelled. The multi-scale model of the cerebral vasculature was coupled with blood flow and embolus transport models. The model incorporated asymmetric bifurcation trees, embolus-vascular interactions and autoregulation. Simulations were carried out where the embolus deposition rate, embolus diameter and embolus introduction rate were varied. Increasing the embolus diameter and embolus introduction rate increased the number of blocked terminal arteries to a quasi steady-state. For a low embolus deposition rate the MCA and ACA territory had the same embolization dynamics, even though, the MCA was larger than the ACA. It was also found for a higher embolus deposition rate the MCA, due to its more expansive structure, was less prone to occlusion than the ACA. The results also showed the effect of a single blockage is expected to be less severe in asymmetric flow than symmetric flow. This model will assist in developing a better understanding into embolic stroke and effect of



microembolism and on the alteration of blood flow distribution in the circle of Willis.

Keywords: embolic stroke, microembolism, cerebral arteries, cerebral hemodynamics, ischemia, numerical models.

1 Introduction

Cerebral microembolism and microinfarction may be the reason for gradual degradation of brain functionality and cognitive impairment [1], including Alzheimer's disease (AD) and vascular dementia [2]. Microembolism has been investigated clinically [3], in animals [4, 5] and analytically [6, 7]. Chung *et al.* [7] established the mechanisms of embolic stroke and studied the relationship between embolic stroke and cerebral blood flow. The effects of embolus dissolution and interaction with a vascular bifurcating network were incorporated in a probabilistic Monte Carlo framework for embolic stroke prediction. However, they employed simplified fluid dynamics and cerebral vasculature models without taking into consideration the effect of autoregulation. Hague and Chung [8] subsequently carried out a basic fluid dynamics analysis of the vascular tree to justify their flow weighting scheme. They used symmetric bifurcations whereas they are usually asymmetric [7, 8].

Niimi *et al.* [6] modelled a small portion of a realistic cerebral microcirculation network and included an autoregulation mechanism based on wall shear variation. Variation of blood flow in the circle of Willis (CoW) during focal ischemia caused by occlusion of the MCA was examined in the numerical simulation by Hudetz *et al.* [9]. However, details of the flow in the arterial networks beyond the CoW were not considered. More advanced three-dimensional (3D) modelling studies have modelled flow and deformation of red blood cells in microvessels [10, 11].

The present study simulates flow and embolus transport through fractal models of the peripheral vasculature of the ACA and MCA to investigate the effect of embolus deposition rate, diameter and introduction rate on the percentage of blocked terminal arteries. This model is novel in that it combines models of cerebral vascular networks and the flows inside [12], with a statistical model of microembolic occlusion which includes embolus transport by blood flow and embolus-vasculature interactions, asymmetric bifurcation trees and autoregulation.

1.1 Fluid dynamics of embolus transport and cerebral microembolism

The transport of emboli in the cerebral microcirculatory system is mainly governed by the cerebral vasculature geometry, the blood flow characteristics, and the interactions of the emboli with the vascular system. These factors are interrelated and influenced by physiological and pathological variations and mechanisms including cerebral blood flow, autoregulation, metabolism, and ageing. Experimental observations have identified that the dominant geometry of the cerebral blood vessels with diameters larger than that of the capillaries



(approximately $10\ \mu\text{m}$) is the fractal tree-like structure with bifurcations dominating [13, 14]. The embolus-bifurcation interaction is a very important factor in the embolus transport in the cerebral vasculature.

The cerebral blood flow transporting the emboli is governed by the systemic pressure, vascular geometry, blood rheology and autoregulation. The Reynolds number in the cerebral microcirculation network is 10^{-1} - 10^{-3} [15] so the blood flow rate, Q , can be defined by Poiseuille's law:

$$Q = - \frac{\pi D_{\text{vessel}}^4}{128 \mu} \frac{\partial P}{\partial l} \quad (1)$$

The transport of emboli in the cerebral vasculature is a dynamic process with the emboli changing and sustaining various interactions while moving along the branching vascular network. The emboli can dissolve [16], interact with the blood vessel wall [17] or vascular network bifurcations [18]. These interactions are the most important factor which may lead to the narrowing of vascular lumen and possible blood vessel occlusion and brain infarction. Alzheimer's patients have deposits of Amyloid Beta ($A\beta$) which is a vasoconstrictor. The clinical study by Bateman *et al.* [19] found significant reduction of blood flow (as much as 18%) in AD patients and increase of flow resistance (up to 23%), which can be explained by both the effects of $A\beta$ vasoconstriction [20] and partial blockage of large number of arterioles by microemboli.

2 Methods

2.1 Cerebral vasculature and flow models

Using the fractal scaling concept, a branching tree model, which possesses physiologically meaningful morphology, can be created for the treelike part of the cerebral vasculature. In this work, a three-dimensional (3D) branching-tree model of cerebral vasculature has been constructed using the Constrained Constructive Optimization method (CCO) [21].

A model of pulsatile flow and pressure distribution in a vascular branching network which takes into consideration the effect of variable blood rheology and blood vessel compliance has been developed by Bui *et al.* [12]. They showed the flow and pressure distributions in a complex vascular branching network can be described by a system of differential algebraic equations (DAEs) representing the mass conservation at the branching points. For human cerebral blood vessel characteristics, this system of DAEs is generally stiff and can be solved by using the MATLAB or other stiff differential equation solvers. Following the work by Pries *et al.* [22], the blood viscosity is made a function of the vessel diameter and hematocrit level. The effect of $A\beta$ vasoconstriction on certain sections of the cerebral circulatory system is simulated by varying the diameter of the branches in the affected area, which leads to the localized increase of flow resistance defined as:

$$R = \frac{128 \mu L_{\text{vessel}}}{\pi D_{\text{vessel}}^4} . \quad (2)$$



2.2 Blood flow autoregulation

Autoregulation plays a very important role in maintaining constant supply of oxygen and other metabolic ingredients to the brain and maintaining constant blood flow in the capillary networks [23]. Consequently, the deterioration of neurovascular autoregulation can have a disruptive effect on cerebral blood flow, leading to brain dysfunction and potentially AD [24]. A few recent studies have coupled autoregulation and hemodynamic models at microcirculation level [22]. In the present work, the cerebral blood flow autoregulation was modelled through a vasodilation/vasoconstriction feedback in response to the change of wall shear stress, and was correlated to the relative blood vessel diameter [6].

2.3 Embolus transport and interaction models

The model of material transport developed in this work has been based on the detailed solution of pressure and flow distributions obtained for all components of the vascular branching tree. Inside a segment of a vascular branching tree model without diffusion, the mass transport of material is described by the Reynolds Transport Theorem:

$$\frac{d(\bar{c}V)}{dt} = Q_{in}c_{in} - Q_{out}c_{out} + \dot{m}_c \quad (3)$$

where \bar{c} is the average concentration of material, Q the volume flow rate, V the segment volume, c the concentration and \dot{m}_c is the generation/loss rate of material.

Generally, the material concentration varies along the segment length and a species transport model should take this into consideration [25, 26]. As a first approximation, the average concentration in the segment was assumed to be an average of material concentrations at the inlet and outlet of the segment, i.e.

$$\bar{c} = \frac{1}{2}(c_{in} + c_{out}) \quad (4)$$

Since the change of the segment volume can be described as:

$$\frac{dV}{dt} = Q_{in} - Q_{out} \quad (5)$$

a mass conservation of the material can be derived from eqn. (3) as follows:

$$V \frac{d(c_{in} + c_{out})}{dt} = (Q_{in} + Q_{out})(c_{in} - c_{out}) + 2\dot{m}_c \quad (6)$$

Eqn (6) has a form similar to the oxygen transport formulation given by Boas *et al.* [27]. Red blood cells with microvascular bifurcations can lead to a phase separation with subsequent variation of hematocrit level in the branches of different sizes. This phenomenon was termed as Fahraeus-Lindqvist (or plasma skimming) effect [28]. This effect can also explain the selective propagation of microemboli in the cerebral vascular network which may have a big implication for cerebral embolism [18].



At a bifurcation point shown in Fig. 1, the conservations of overall flow and embolus concentration dictate:

$$Q_o = Q_1 + Q_2 \quad (7)$$

$$Q_o c_o = Q_1 c_1 + Q_2 c_2 \quad (8)$$

The variations of c_1 and c_2 relative to c_0 are caused by phase separation at the bifurcation point as described above. The relationship between ratios c_1/c_0 and c_2/c_0 and flow rates are derived from eqns. (7) and (8) as:

$$Q_1 \left(1 - \frac{c_1}{c_0} \right) = -Q_2 \left(1 - \frac{c_2}{c_0} \right) \quad (9)$$

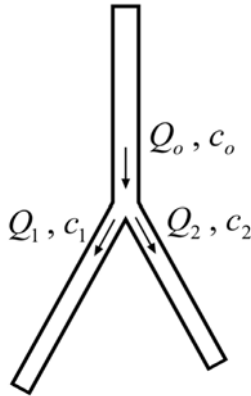


Figure 1: Flow and embolus concentration at a bifurcation point.

Experiments [18] conducted on microemboli with size ranging from 7 to 210 μm in an in-vitro flow system mimicking the human MCA, indicate that interactions of emboli of various sizes with microvascular bifurcations would lead to the preferential transport of the largest emboli along the main arterial trunks. Using these experimental data an empirical relationship between the relative concentration c_1/c_2 and branch size ratio D_1/D_2 can be correlated:

$$\frac{c_1}{c_2} = 1 - a \left(1 - \frac{D_1}{D_2} \right) \quad (10)$$

with $D_1 \leq D_2$ and the inclination coefficient a is defined by $a = 0.05 + 0.1823(d_e - 7)$ where d_e is the embolus diameter in μm .

Eqns. (9) and (10) define the effect of embolus separation at the vascular branching points. The interaction of emboli and the blood vessel wall, while potentially being a factor leading to gradual reduction of the arterial lumen and subsequent blockage and ischemia, may also be a major mechanism of removing the emboli from the blood flow [17]. This interaction is dependent on the distribution of the embolic particles across the flow. Alevriadou and McIntire [17] showed the steady-state flux of embolus deposition has the form:

$$J(x) = c / \left[\frac{1}{k} + 1.48 \left(\frac{4U\Gamma^2}{Dx} \right)^{-1/3} \right] \quad (11)$$

where c denotes the bulk embolus concentration, k the adhesion rate constant, Γ the embolus diffusivity, and U the flow velocity in the axial direction x . The embolic deposition is therefore driven by two mechanisms, namely adhesion reaction and cross-flow diffusion, which are defined by adhesion rate constant and embolic diffusivity, respectively. The diffusion coefficient can also be determined in terms of the local shear rate as: $\Gamma \approx \gamma^n$, with n being a constant [17]. In this work, only the effect of adhesion was considered and the adhesion rate coefficient was assumed to be equal to that of either activated platelets ($k = 3.5 \times 10^{-3}$ m/s) or unactivated platelets ($k = 2.5 \times 10^{-6}$ m/s) [29].

Based on the flow and embolus distribution in the vascular network, an occlusion probability map is computed and used to initiate blockages in the network at a specified rate. Occlusion probability is assumed to depend not only on the relation between embolus size and the local blood vessel size, but also on the embolus distribution, which, in turn, is determined by the flow and embolus-vasculature interactions as described above. In addition, the occlusion probability is reduced with the increase of embolus residence time, i.e. occlusion should happen to the branches close to the root first. The presence of blockages in the vascular network will alter the flow and embolus distribution and affect further creation of blockages in the network. Therefore, the flow and embolus distributions are recalculated each time when a new blockage appears or an old one clears. In each simulation case, the computation has been conducted until a statistical balance of blockage creation and clearance is established in the system.

2.4 Cerebral vascular geometry

Fractal models of the peripheral vasculature of the ACA and MCA were constructed [12] and have approximately 1400 and 2800 terminal points, respectively, with the total number of segments equal to 2800 and 5600, respectively. A constant cerebral perfusion pressure of 62.8 mmHg (8367 Pa) was used. Only spherical solid emboli were considered with a constant dissolution rate of 0.1 mm per hour [7]. The rate of embolus introduction into the ACA and MCA peripheral vascular was a function of total flow rate under normal conditions (i.e., without occlusion), so that the embolus concentration was assumed to be similar at the inlets to the cerebral vascular territories.

3 Results and discussion

3.1 Factors affecting blood flow and embolus transport

Simulations were conducted on branching fractal models of the peripheral vasculature of the ACA and MCA. Among the factors affecting the blood flow and embolus transport it was predicted that embolus separation at branching



points and flow autoregulation have small effects on embolic occlusion and embolization dynamics. For the ACA peripheral vasculature the activation of autoregulation was seen to marginally reduce the vascular blockage (Fig. 2(a)) from emboli of similar sizes entering the system at a similar rate. The effect of embolus deposition rate, embolus diameter and embolus introduction rate were also investigated.

3.2 Effect of embolus deposition rate

Embolus deposition in arteries larger than the embolus size was predicted to have much larger influence on embolization. The increase of embolus deposition rate from 2.5×10^{-6} m/s to 3.5×10^{-3} m/s for ACA peripheral vasculature significantly decrease the number of emboli available to block smaller arterioles (Fig. 2(b)) and resulted in an approximately 36% reduction in vascular blockage.

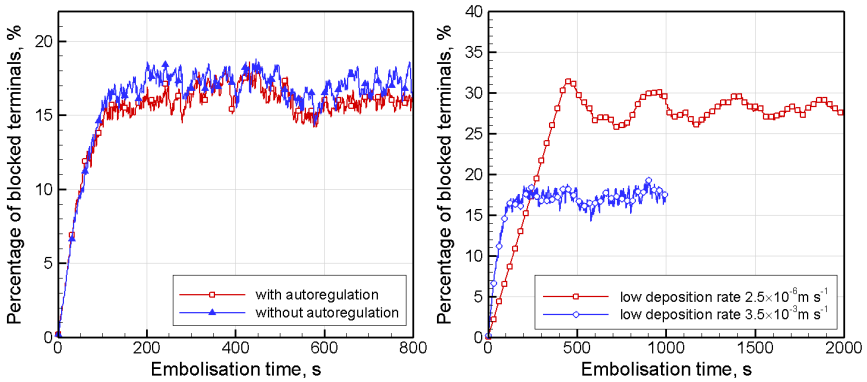


Figure 2: Effects of autoregulation and deposition rate on embolization on the ACA vasculature, 1 embolus per second.

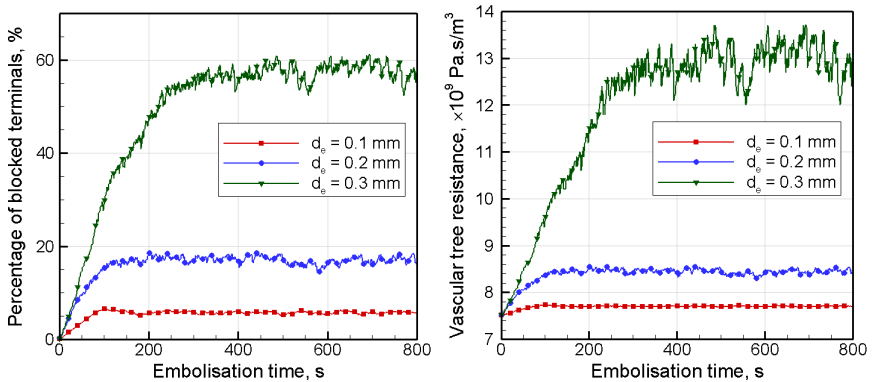


Figure 3: Percentage of blocked terminals and vascular tree resistance on the ACA vasculature, 1 embolus per second, deposition rate 3.5×10^{-3} m/s.



3.3 Effect of embolus diameter

Figure 3 shows the variations in time of the blocked terminal percentage and total vascular tree resistance. Similar to the investigation by Chung *et al.* [7], the portion of the blocked terminal arteries increases and reaches a quasi equilibrium state after a certain embolization time. Both this saturated blockage percentage and transition time were also found to be dependent on the embolus diameter (Fig. 3). Increase in embolus diameter from 0.2 to 0.3 mm increased the percentage of blocked terminals, so that embolus of 0.3 mm diameter had approximately three times higher percentage of blocked terminals compared to embolus of 0.2 mm. Chung *et al.* [7] also found that the percentage of blocked arteries increased with embolus diameter, especially for > 0.2 mm. The increase in embolus diameter also increased the vascular resistance which restricts blood flow and may lead to focal ischemia.

3.4 Effect of embolus introduction rate

Increase in embolus introduction rate from 0.5 to 3 embolus per second increased the number of blocked terminals fourfold (as shown in Fig. 4), to 40% at an embolus introduction rate of 3 embolus per second. Chung *et al.* [7] also found that increased embolus rate also increased the danger of blockage.

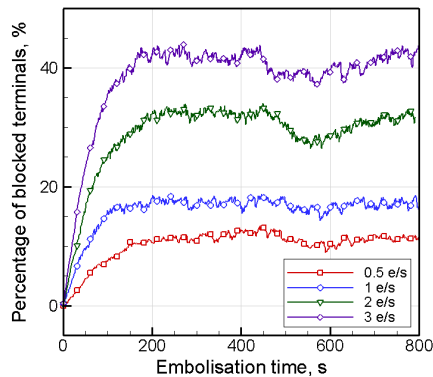


Figure 4: Effect of embolus introduction rate on embolization of the ACA vasculature, $d_e = 0.2$ mm, deposition rate 3.5×10^{-3} m/s.

3.5 MCA versus ACA cerebral vascular territory

Although the MCA territory is significantly larger than the ACA territory and the blood flow rates in them are different, they were predicted to have identical embolization dynamics, when emboli of similar size and concentration were introduced into the circulatory systems and a low embolus deposition rate of 2.5×10^{-6} m/s was assumed (Fig. 5). However, with a higher embolus deposition rate of 3.5×10^{-3} m/s, the MCA, due to its more expansive structure, had lower percentage of blocked terminals for a given embolus diameter. Hence, the MCA seemed to be less prone to occlusion and focal ischemia than the ACA (compare Fig. 3 and Fig. 6).

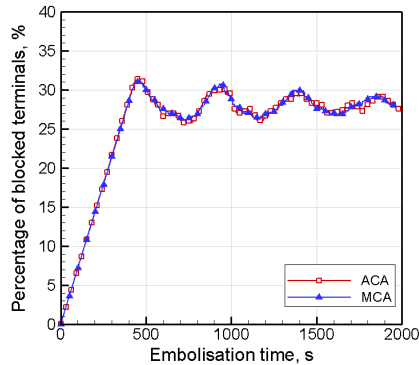


Figure 5: Embolization in ACA and MCA vasculature at low embolus deposition rate - $d_e = 0.2$ mm, deposition rate = 2.5×10^{-6} m/s.

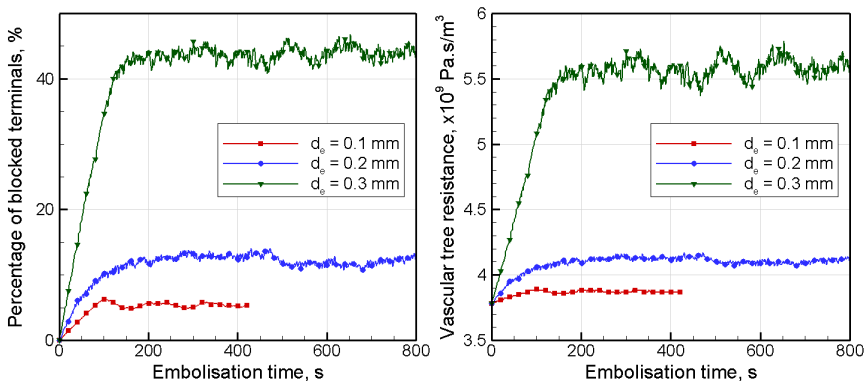


Figure 6: Percentage of blocked terminals and vascular tree resistance on the MCA vasculature, embolus introduction rate equivalent to 1 embolus per second in ACA, deposition rate 0.0035 m/s.

3.6 Effect of asymmetric versus symmetric bifurcations

Our model is different from the models by Chung *et al.* [7] and Hague and Chung [8] in that asymmetric bifurcation trees are considered rather than just symmetric. For a similar number of terminals, an asymmetric vascular branching tree will have more bifurcation levels compared to a symmetric one. The effect of a single blockage is therefore expected to be less severe in asymmetric flow system. Due to the effect of preferential transport of large emboli in the large vascular branch they have more opportunity to absorb before blocking terminals.

3.7 Current model and future model improvements

The current numerical model, which incorporates human cerebral vascular morphology, hemodynamics, blood flow autoregulation, physics of embolus



transport and interactions. It can assist in developing a better understanding into embolic stroke and effect of microembolism and associated focal ischemia on the alteration of blood flow distribution and increased resistance in the CoW. The model can also be used make comparisons with in-silico experiments.

Wijman *et al.* [30] showed that cerebral infarcts occurred more frequently in the MCA than the ACA main arteries. In future, the inlet embolus concentration at the inlet of the peripheral vasculature can be varied when comparing the ACA and MCA territory blockage.

Previously, Šutalo *et al.* [31] modelled the blood flow in a coupled computational fluid dynamics (CFD) model of the 3D patient-specific CoW and branching tree fractal model of the cerebral vascular networks [32]. In future, it is possible to couple this model of the embolus transport in peripheral cerebral vascular networks with embolus transport in the CoW. Such a coupled model of the embolus transport in the CoW and cerebral vasculature could be used to compare with experimental results by Chung *et al.* [33] from a patient-specific silicone model of the CoW showed the embolus trajectory through the cerebral arteries is dependent on embolus size and favours the MCA for large emboli (≥ 0.5 mm).

4 Conclusion

The blood flow and embolus transport through fractal models of the peripheral vasculature of the ACA and MCA were modelled to investigate the effect of embolus variables on the embolization of the terminals.

The model showed increased terminal embolization occurred with decrease in embolus deposition rate, increase in embolus diameter and increase in embolus introduction rate. Interestingly, due to the MCA's more expansive structure it was found, for a higher embolus deposition rate, the MCA was less prone to occlusion and focal ischemia than the ACA. However, for a lower embolus deposition rate they both had identical embolization dynamics.

The results can help us in our understanding of the dynamics of embolus transport including that the embolus diameter was important when comparing blockages in different vascular territories, and that asymmetric vasculature is expected to have less blockages compared to simplified symmetric vasculature. The activation of autoregulation in the model was only seen to marginally reduce the vascular blockage from emboli.

In future, we can couple this branching tree fractal model with 3D patient-specific CFD model of the CoW to see the trajectory and distribution of emboli through this system.

References

- [1] Russell, D., Cerebral microemboli and cognitive impairment. *J Neurol Sci*, **203-204**, pp. 211-214, 2002.
- [2] Purandare, N., Burns, A., Daly, K.J., Hardacre, J., Morris, J., Macfarlane, G. & McCollum, C., Cerebral emboli as a potential cause of Alzheimer's



- disease and vascular dementia: Case-control study. *Brit Med J*, **332**, pp. 1119-1124, 2006.
- [3] Vermeer, S., Jr, W.L. & Koudstaal, P., Silent brain infarcts: a systematic Review. *Lancet Neurol*, **6**, pp. 611-619, 2007.
- [4] Hossmann, K.A., Cerebral ischemia: models, methods and outcomes. *Neuropharmacology*, **55**, pp. 257-270, 2008.
- [5] Atochin, D., Murciano, J., Gürsoy-Özdemir, Y., Krajsik, T., Noda, F., Ayata, C., Dunn, A., Moskowitz, M., Huang, P. & Muzykantov, V., Mouse model of microembolic stroke and reperfusion. *Stroke*, **35**, pp. 2177-2182, 2004.
- [6] Niimi, H., Komai, Y., Yamaguchi, S. & Seki, J., Microembolic flow disturbances in the cerebral microvasculature with an arcadial network: A numerical simulation. *Clin Hemorheol Micro*, **34**, pp. 247-255, 2006.
- [7] Chung E.M.L., Hague, J.P. & Evans, D.H., Revealing the mechanisms underlying embolic stroke using computational modelling. *Phys Med Biol* **52**, pp. 7153-7166, 2007.
- [8] Hague J.P. & Chung E.M.L., Statistical physics of cerebral embolization leading to stroke. *Physical Review E*, **80(5)** Article Number: 051912, Part 1, pp. 051912-1-051912-9, 2009.
- [9] Hudetz, A., Jr, J.H., Horton, C., Conger, K. & Reneau, D., Mathematical simulation of cerebral blood flow in focal ischemia. *Stroke*, **13**, pp. 693-700, 1982.
- [10] Bagchi, P., Mesoscale simulation of blood flow in small vessels. *Biophys J*, **92**, pp. 1858-1877, 2007.
- [11] AlMomani, T., Udaykumar, H.S., Marshall, J.S. & Chandran, K.B., Micro-scale dynamics simulation of erythrocyte-platelet interaction in blood flow. *Ann Biol Eng*, **36**, pp. 905-920, 2008.
- [12] Bui, A., Šutalo, I.D., Manasseh, R. & Liffman, K., Dynamics of pulsatile flow in fractal models of vascular branching networks. *Med Biol Eng Comput*, **47**, pp. 763-772, 2009.
- [13] Cassot, F., Lauwers, F., Fouard, C., Prohaska, S. & Lawers-Cances, V., A novel three-dimensional computer assisted method for a quantitative study of microvascular networks of the human cerebral cortex. *Microcirculation*, **13**, pp. 1-18, 2006.
- [14] Lauwers, F., Cassot, F., Lauwers-Cances, V., Puwanarajah, P. & Duvernoy, H., Morphometry of the human cerebral cortex microcirculation: General characteristics and space-related profiles. *NeuroImage*, **39**, 936-948, 2008.
- [15] Schmid-Schönbein G.W., Biomechanics of microcirculatory blood perfusion, *Annu Rev Biomed Eng*, **1**, pp. 73-102, 1999.
- [16] Moser, K.M., Guisan, M., Bartimmo, E.E., Longo, A.M., Harsanyi, P.G. & Chiorazzi, N., In vivo and post mortem dissolution rates of pulmonary emboli and venus thrombi in the dog. *Circulation*, **48**, pp. 170-178, 1973.
- [17] Alevriadou, B. & McIntire, L., Rheology (Chapter 20). *Thrombosis and Hemorrhage*, Blackwell Sci Publ, Boston, pp. 369-381, 1994.
- [18] Pollanen, M., Behaviour of suspended particles at bifurcations: implications for embolism. *Phys Med Biol*, **36**, pp. 397-401, 1991.



- [19] Bateman, G.A., Levi, C.R., Schofield, P., Wang, Y. & Lovett, E.C., Quantitative measurement of cerebral haemodynamics in early vascular dementia and Alzheimer's disease. *J Clin Neurosci*, **13**, pp. 563-568, 2006.
- [20] Niwa, K., Porter, V., Kazama, K., Cornfield, D., Carlson, G. & Iadecola, C., A β -peptides enhance vasoconstriction in cerebral circulation, *Am J Physiol Heart Circ Physiol*, **281**, pp. H2417-H2424, 2001.
- [21] Schreiner, W., Karch, R., Neumann, M., Neumann, F., Szawlowski, P. & Roedler, S., Optimized arterial trees supplying hollow organs, *Med Eng Phys*, **28**, pp. 416-429, 2006.
- [22] Pries, A., Secomb, T. & Gaehtgens, P., Review - Biophysical aspects of blood flow in the microvasculature, *Cardiovasc Res*, **32**, pp. 654-667, 1996.
- [23] Davis, T., Alzaidi, S., Chatelin, R. & Farr, H., Coupled autoregulation models, in: IFMBE Proceedings - ICBME 2008, Springer, pp. 1896-1899, 2008.
- [24] Girouard, H. & Iadecola, C., Neurovascular coupling in the normal brain and in hypertension, stroke, and Alzheimer disease. *Journal of Applied Physiology*, **100**, pp. 328-335, 2006.
- [25] Vadapalli, A., Goldman, D. & Popel, A., Calculations of oxygen transport by red blood cells and hemoglobin solutions in capillaries, *Artif Cell Blood Sub*, **30(3)**, pp. 157-188, 2002.
- [26] Kavanagh, B., Secomb, T., Hsu, R., Lin, P., Venitz, J. & Dewhurst, M., A theoretical model for the effects of reduced Hemoglobin-Oxygen affinity on tumor oxygenation. *Int J Radiat Oncol*, **53**, pp. 172-179, 2002.
- [27] Boas, D.A., Jones, S.R., Devor, A., Huppert, T.J. & Dale, A.M. A vascular anatomical network model of the spatio-temporal response to brain activation. *NeuroImage*, **40**, pp. 1116-1129, 2008.
- [28] Pries, A.R., Leg, K., Claassen, M. & Gaehtgens, P., Red cell distribution at microvascular bifurcations, *Microvasc Res*, **38**, pp. 81-101, 1989.
- [29] Goodman, P., Barlow, E., Crapo, P., Mohammad, S., Solen, K., Computational model of device-induced thrombosis and thromboembolism, *Ann Biomed Eng*, **33**, pp. 780-797, 2005.
- [30] Wijman, C.A.C., Babikian, V.L., Winter, M.R. & Pochay, V.E., Distribution of cerebral microembolism in the anterior and middle cerebral arteries. *Acta Neurol Scand*, **101**, pp. 122-127, 2000.
- [31] Šutalo, I.D., Bui, A., Ahmed, S., Liffman, K. & Manasseh, R., Modelling of flow through the circle of Willis and cerebral vasculature, *Modelling in Medicine and Biology VIII*, WIT Transactions on Biomedicine and Health, Vol. 13., *BioMED 2009*, Crete, Greece, pp. 83-92, 2009.
- [32] Bui, A.V., Manasseh, R., Liffman, K. & Šutalo, I.D., Development of optimized vascular fractal tree models using level set distance function. *Medical Engineering and Physics*, **32**, pp. 790-794, 2010.
- [33] Chung, E.M.L., Hague, J.P., Chanrion, M.A., Ramnarine, K.V., Katsogridakis, E. & Evans, D.H., Embolus trajectory through a physical replica of the major cerebral arteries. *Stroke*, **41(4)**, pp. 647-652, 2010.



Section 10

Biomechanics

This page intentionally left blank

Indoor motion analysis of a subject wearing prosthesis for adaptive snowboarding

L. Gastaldi¹, S. Pastorelli¹, M. Caramella² & U. Dimanico²

¹*Department of Mechanics, Politecnico di Torino, Italy*

²*S.S.D. Neurofisiologia Riabilitativa ASL CNI, Fossano, Italy*

Abstract

The growing popularity of adaptive snowboarding has motivated the designs of new prostheses for lower limb amputees. In the paper the biomechanics of an amputee subject wearing an energy-storing trans-femoral prosthesis for snowboarding is investigated. Experimental motion analysis lab tests were conducted by two expert surfers, an amputee and an able body subject, in order to compare the different behaviours.

Results for the two subjects and for different working conditions are reported and analysed. A strong dependence of the prosthesis behaviour on working conditions, especially on working frequency, can be pointed out.

Keywords: adaptive snowboard, movement analysis, lower limb prosthesis.

1 Introduction

It is well known that sport activity is an excellent functional and psychological rehabilitation for subject with limb capacity compromised due to traumatic events, such as amputees or spinal cord injured. Besides sport can also be a mean to overcome their present physical limitations and more in general physical activity presents many benefits, including a decrease in pain, depression and an increase in the quality of life.

Still a redefinition of the sports is necessary to make them adaptive, defining rules and athletes' classification, and finally re-designing equipments. While rules and classification are under the jurisdiction of international organisation and they must be as general as possible to consider all the disabilities, equipment matter is a more delicate aspect, as it has to respect general rules and at the same



time it has to be personalised in order to fulfil functional and physical gaps that exist between athletes.

For amputees entry equipment encompasses also dedicated prostheses, as sport activity is more demanding, from a mechanical aspect, than every day activities. As a matter of facts even if we consider very sophisticated solutions, both from material or functions point of view, the prosthesis will never accomplish all the physiological tasks, such as providing shock absorption, knee stabilisation, limb length change in order to minimise the displacement of the centre of gravity, etc. Consequently, the necessity to understand the specific biomechanics of the sport and the physical characteristic of the remnant limb in order to design a specific solution and to enhance injured subjects to pursue athletic performances. The prosthesis is a tool that plays an important role in maximising performances, especially speaking of elite athletes.

Actually in the winter paralympic sports scenario adaptive snowboard is spreading more and more. National and International Federations are arising and the goal is the snowboard discipline debut in the next Winter Paralympic Games in 2014 and many snowboarders are dreaming about it. The introduction of this new sport discipline will also help to involve young people, which is a main task of all the disable committees.

Few studies can be found about biomechanics of the lower extremities in snowboarding, although no one is addressed to lower limb prostheses. Corresponding to the determination of kinematical parameters of the ankle joint complex, Delorme et al. [1] analysed this complex while on slope snowboarding. To improve safety aspects in skiing and snowboarding, Klous et al. [2] compared the loading at the knee and ankle joint in skiing and snowboarding. Interesting results about kinematics and kinetics are presented in [3], where ground reaction forces of jump landings in freestyle snowboarding are measured by means of a snowboard-mounted force platform. However, the mechanical characteristics (weight, standing height) of such a system can affect a snowboarder adversely. Finally, Krüger et al. in [4] present a pilot study to determine relevant kinematical and kinetic parameters using an inertial measurement suit in combination with a bilateral insole measurement system.

In skiing, several biomechanical studies roughly estimated joint loading in turning [5, 6] and on landing manoeuvres after a jump [7, 8], but none with sufficient accuracy.

Generally results show that loading is more evenly distributed between the legs in snowboarding than in skiing and that the highest moments were found in the rear leg in snowboarding.

As stated above the immense popularity of snowboarding has suggested the developmental designs of prostheses for trans-femoral amputees. The present study investigates performances of a trans-femoral prosthesis for snowboarding and in the paper biomechanical results from an indoor movement analysis are acquired and commented. These results are necessary for the further step that consists in an inverse dynamic study of the trans-femoral prosthesis and in evaluating forces in the joints and on the stump.



2 Adaptive snowboard

Adaptive snowboard events include male and female athletes with a physical disability such as spinal injury, cerebral palsy, amputation, and visual impairments. Athletes compete based on their functional ability, allowing participants with different disabilities to race against each other.

Adaptive snowboarding athletes compete and use the same venue as able-body snowboardcross events. The event format is also conducive to a classification process, which will be finalized by the adaptive snowboarding International Federation which is in working progress. Classification is a very delicate point, and it is undertaken to ensure that an athlete's impairment is relevant to sport performance and to ensure that the athlete competes equitably with all the other athletes. The process will held to define, for each category, a time factor that multiplies the real time achieved by the athletes. For non sever impairments the multiplier factor is equal to 1 and it decreases for severer impairments. The three macro-classes are: blind, standing and sitting, among which sub-categories are detected according to the disability level.

In general, snowboards are chosen on the basis of the rider's height, weight, and ability level. Some adaptive riders use outriggers to help balance themselves while they board, but many don't use any special equipment. Also bindings on the board can be moved to help with balance.



Figure 1: Adaptive snowboarding.

For the standing class, athlete must be able to keep her/his balance; this is possible moving conveniently the body center of mass and controlling the lower limb flexo-extension angles. The slow down phase is obtained by impressing a pressure with the front or rear part of the feet and concentrating the weight in the rear part of the snowboard. The breaking action is more effective as the snowboard axis and the course direction become more perpendicular. Pressure control is also used to control downhill velocity, while change of direction is managed rotating the upper part of the body.

The rider, as the able body one, can assume two different positions, called Regular and Goofy. This refers to the dominant way surfer points the board down the hill. Regular means left foot forward, while goofy means right foot forward.

Rotation movements are basic and they can be distinct in backside or frontside. When in the first part of the spin the front part of the body faces the mountain, then this is a frontside or toe-side turn, the opposite is a back or heel-side turn.

To surf it is necessary a prosthesis allowing a loaded, flexed knee and ankle position, as snowboarders are in bilateral dynamic hip, knee, and ankle flexion as they negotiate the hill.

3 Experimental tests

Due to the intrinsic difficulties in performing effective tests on the ski runs without influencing the natural surfing gesture, authors opted for a preliminary activity consisting in lab tests motion analysis. The indoor conditions do not allow us to reproduce exactly the surfing movement, thus a significant gesture has been taken into account to evaluate the biomechanics of the amputee athlete wearing the lower limb prosthesis with respect to an able-body subject.

Tests were carried out in a gait analysis lab in which kinematic and dynamic clinical analyses are usually performed.

3.1 Prosthetic device

The prosthesis used during tests is a commercial one specifically designed for snow sports. Knee and ankle joints are replaced by two planar cylindrical hinges that allow flexo-extension in the sagittal plane. To mimic the quadriceps and hamstring muscles a passive energy-storing system is present: a pneumatic spring and a hydraulic shock absorber are integrated into the prosthesis both at the knee and ankle level. The spring system stores energy when loaded during flexion and it returns it during extension to help the athlete to promptly regain an upright standing position. The damper provides an impact absorption capacity and it delivers less dangerous impact to the musculoskeletal system. The system stiffness is user-adaptable by changing spring air pressure and three damping sets are available.

To allow the user to wear a standard snowboard-boot and to use standard bindings, a customized foot is fixed to the prosthesis. During tests this had been replaced by a rigid insole as they were conducted by barefoot users.

3.2 Experimental protocol

Two subjects were selected, a left trans-femoral amputee and a healthy subject, in order to compare the different behaviours.

Subjects were request to repeat movements similar to the one performed on the ski slope; both are expert surfers and normally the amputee uses the



prosthesis to ride. Tests consist of squat exercises executed with three one-by-one changeable tests conditions:

- *feet position*. In figure 2 the reciprocal positions between feet axes and frontal plane are depicted. “Central position” corresponds to the physiological standing position in which feet are slightly externally rotated (about 7°) and they are symmetric respect to the sagittal plane. In “left position” subjects were requested to keep shoulders still, while feet were rotated about the vertical axis by 30° anticlockwise. Similarly for the “right position”, where rotation was 30° clockwise.
- *load*. Subjects hold a barrel on the shoulders and performed tests without loads on the barrel itself or with an additional load equal to 20% of the subject’s weight.
- *squat frequency*. Amputee subject was requested to squat at two self-chosen frequencies, a high (approx 140 beats/min) and a low (approx. 35 beats/min) one. The able-body subject fits his frequencies to the amputee’s ones. No restriction was imposed on the pelvis vertical displacements.



Figure 2: Feet position with respect to the frontal plane (*f.p.*) during experimental tests.

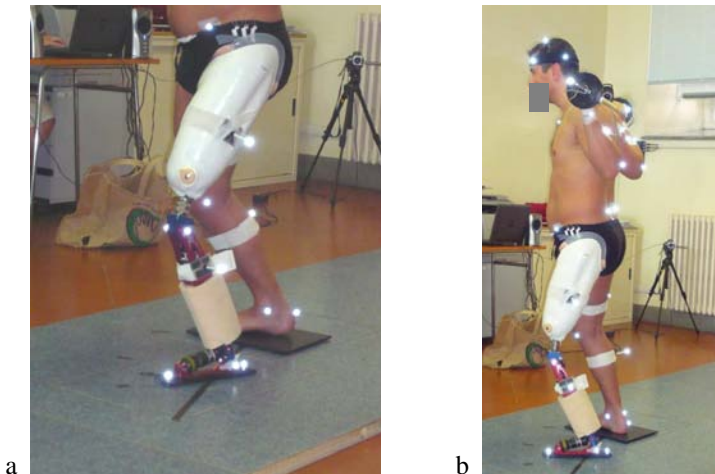


Figure 3: Experimental tests with the prosthesis.

3.3 Motion analysis system

Movements were acquired using a stereo-photogrammetric system (VICON 6 infrared cameras with a 100 frames/second) and ground reaction forces were recorded using two six components force plates.

Markers were placed according to the Plug-in-Gait protocol [9] for the healthy subject and according to a modified Plug-in-Gait protocol for the markers placed on the prosthesis, as it is pointed out in Figure 3a.

Markers were added also on the barrel and on the upper body in order to check the correctness of the squat movements (Figure 3b). Totally 51 markers were acquired and processed. After movements tests, from a full 3-D movement reconstruction kinematics of body and prosthesis is obtained.

4 Results

All the subjects' kinematics and ground reactions were analysed; however in the paper only main results are reported. For both limbs in the next figures following data trends are depicted:

- knee flexo-extension angles, ankle plantar and dorsi-flexion angles, which correspond to the degrees of freedom of the prosthesis;
- the vertical components of the ground reaction forces measured by the force platforms;
- the spatial position of the feet centre of pressure (COP) on the force plates; the diagonal line represents the subject frontal plane projection;
- picture of the subject during respective tests.

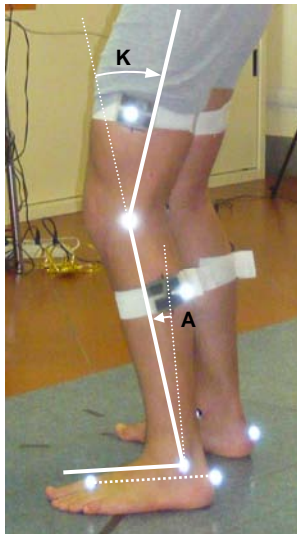


Figure 4: Convention to measure ankle (A) and knee (K) angles.

The ankle plantar and dorsi-flexion is measured between the line perpendicular to the foot axis and the shank long axis; while the knee flexo-extension angle is measured between the thigh and shank long axes. A 0° of plantar flexion corresponds to shank and foot right angled, while a 0° of knee flexion is measured when thigh and shank are aligned. In figure 4 the conventions adopted to measure knee (K) and ankle (A) angles are reported.

At first a comparison is made between the able-body and the amputee subject; then the prosthesis performances in different test conditions are analysed. In Figures 5 and 6 results of the test performed at high frequency, with no load and with the feet in central position respectively for the able-body and the amputee subject are reported. These test configurations will be taken as standard, and these conditions will be changed one at a time in order to evaluate the influence of the single parameters on the complete movement performances.

In the case of Figure 5a good symmetry both for the kinematics and for the Ground Reaction Forces (GRFs) can be pointed out. Knees and ankles angles ranges are respectively about 25° and 12°, while forces change between 280 and 700 N. The Centre of Pressure (COP) location is concentrated in the central part of the feet.

Considering figure 6, from the first graph it can be seen that the sound limb knee flexes for a greater angle (15°), the prosthesis knee angle has a more

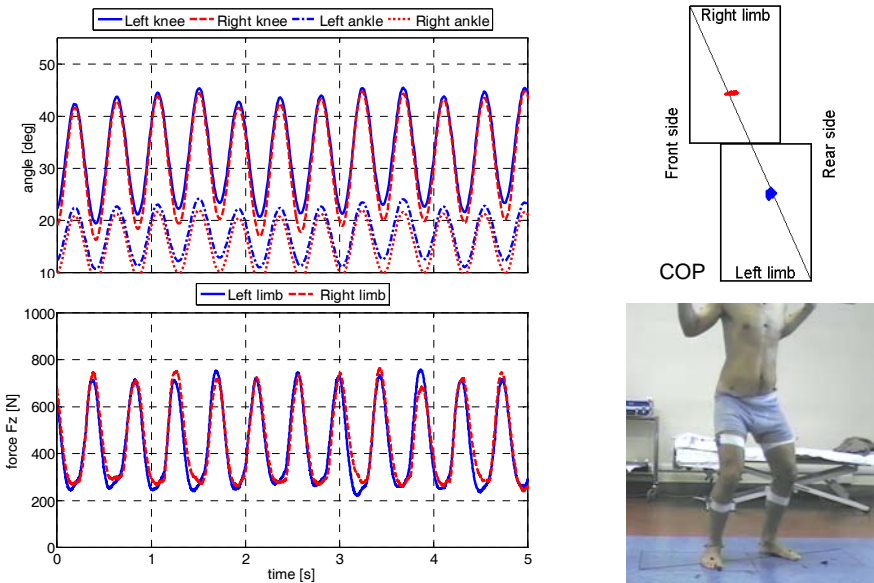


Figure 5: Able body subject. Test conditions: high frequency, no applied load and central feet position.

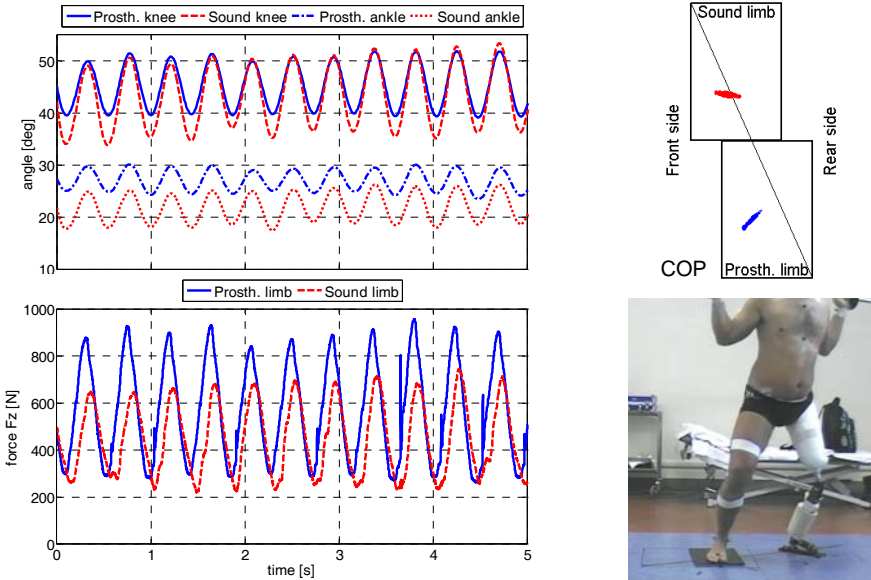


Figure 6: Amputee subject. Test conditions: high frequency, no applied load and central feet position.

limited range (approx. 10°), while the ankle flexion range is about 5° . For both joints it can be observed that the mean values of the flexion angles are higher for the prosthetic limb. This can be explained observing the GRFs, where the force exchanged with the ground is higher at the prosthesis and hence to unload the sound limb.

Moreover, considering the displacement of the COP, there is a distribution of the point in which reaction forces are applied on all the contact area for the sound limb, while for the prosthetic one a concentration on the tip can be noticed.

For the able body subject the COP is concentrated in the middle of the foot, in correspondence of the frontal plane projection line. The area swept from the COP is in any case smaller for the able body subject than the amputee.

Trends reported in figure 7 were recorded during a test with the same conditions of the previous one, except for the frequency that this time was the low one.

In this case there is a major mobility of the prosthetic limb respect to the sound one, but these data need to be correlated with the ground reaction forces trends. Firstly it can be observed that the total ground reaction force (given by the sum of the two reactions) is diminished. In fact the slower movement involves minimal inertia actions; practically the instantaneous total force corresponds to the subject's weight.

This requires a major translation of the body centre of mass on the prosthesis side. This is done by the subject and it can be seen from trends in Figure 6 where the two GRFs are in opposite phase. The effect is that the subject has his centre of mass totally unbalanced on the prosthesis and for these reasons the sound leg is in a more extended stance.

The COP is still concentrated on the tip of the sole and the area is more restricted than the previous case both for the sound and non sound limb.

The effect of foot position can be gather observing results reported in Figure 8. In this case foot are placed in a “left position” (Figure 2), corresponding to a regular rider, as the user effectively is.

In this case the body weight is naturally shifted on the front limb, which turns out also to be the more flexed one. This working configuration is particularly favourable for the prosthesis.

The knee joints excursion is almost the same for both legs, only the flexion angle is greater for the prosthetic limb. The minor flexion of the sound limb knee is compensated by the corresponding ankle that in this case is greater compared to the opposite one. For the GRFs it can be observed that a slight phase shift is present.

Interesting is the area swept by the COP. For the sound limb the area is reduced respect to the full footmark and the COP moves in the internal part of the foot, while concerning the prosthesis only the front part is loaded and the COP zone is smaller.

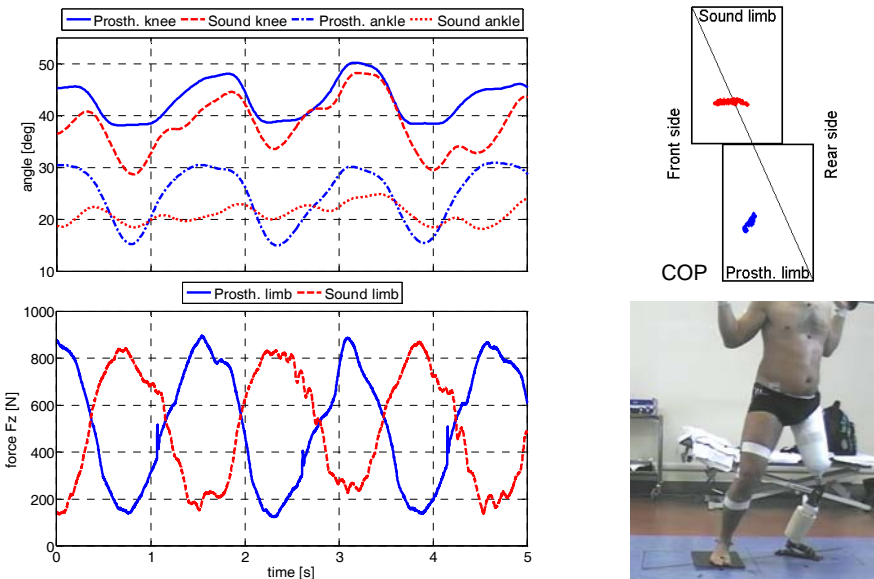


Figure 7: Amputee subject. Test conditions: low frequency, no applied load and central feet position.

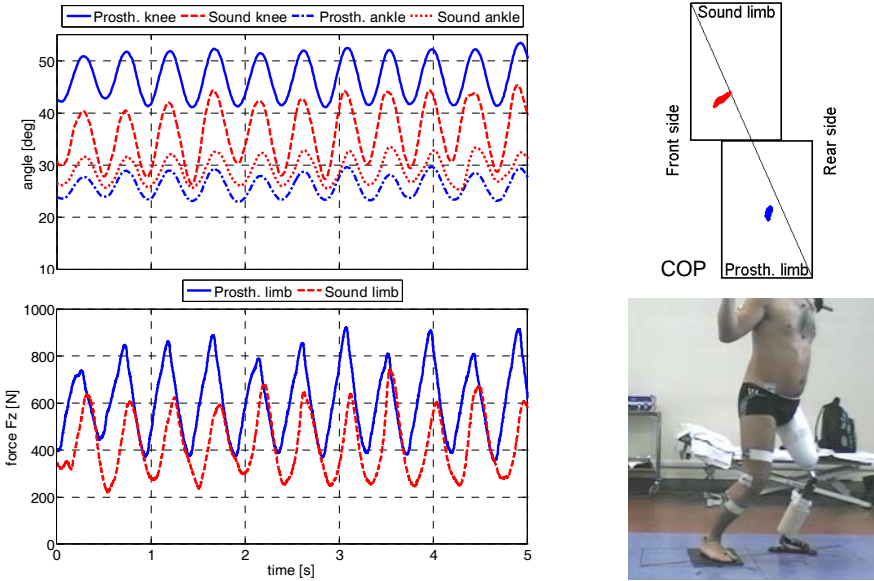


Figure 8: Amputee subject. Test conditions: high frequency, no applied load and feet in left position.

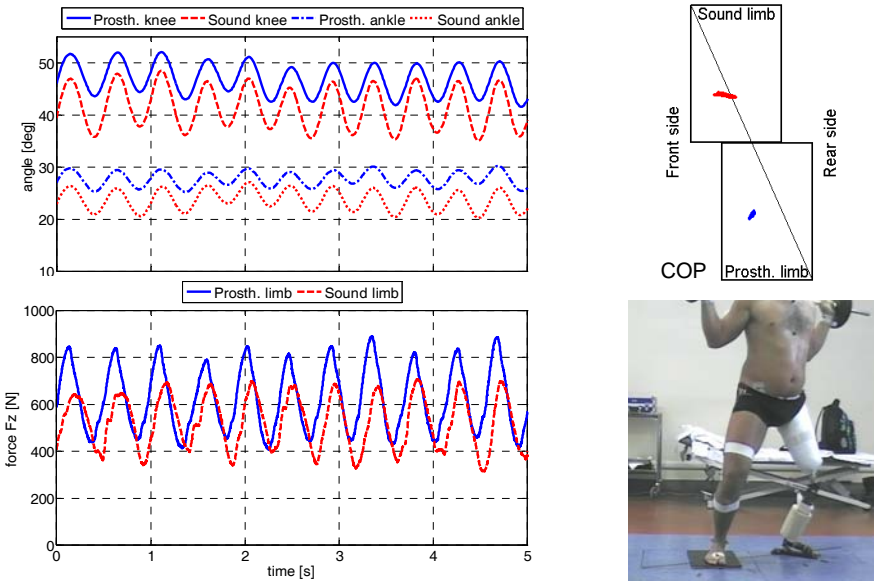


Figure 9: Amputee subject. Test conditions: high frequency, applied load and central feet position.

Test were performed also with the opposite feet position (Figure 2 “right position”); for sake of brevity results are omitted. However this position corresponds to a goofy one and is not favourable for the prosthesis as to load it is necessary to shift back the body weight. This force the subject to an unnatural posture, the rear limb rests only on the tip of the plate and balance is seriously jeopardised.

Last trends (Figure 9) are relative to an increased load of 180 N. Compatibly with the fact that in this case the subject squatted with a little lower frequency than in the standard test, no meaningful differences can be pointed out.

5 Conclusions

Test motion analysis results showed for the able body subject, both for the kinematic and force data, a good symmetry between the legs substantially in all the tests conditions. On the contrary trends obtained with the amputee wearing the trans-femoral prosthesis are affected by the working conditions.

Stating beforehand that the amputee normally uses this prosthesis to snowboard and hence he already had it tuned and aligned to fulfil his requirements; from test results a good kinematic symmetry can be observed for high frequency movements. Although the user had to maintain the load not equally distributed on the two limbs by throwing off centre the body centre of mass.

This behaviour is due to the fact that the user cannot control separately the knee and the ankle flexo-extension angles and hence the only way he has to flex them is to unbalance his body to load the prosthesis. The presence of the pneumatic system in the prosthesis has the task of helping the joint extension by returning the elastic energy stored during flexion. This explains the necessity of the user to load and unload the prosthetic limb; only for high frequency inertia actions help this process, while when moving at low frequency it is necessary to alternatively shift the centre of mass from one leg to the other. This behaviour is highlighted by the ground reaction forces trends, in which for low frequency they are in opposite phase while for high frequencies the ground reaction force on the sound limb is lower than the one measured on the controlateral.

Considering the centre of pressure graphs, generally the application point of the vertical forces on the prosthetic limb is concentrated in the anterior part of the sole. This is due to the design of the prosthesis, in fact loading it on the more tip allows to augmenting the force arm and hence the flexion moments.

Acknowledgements

The research was supported by the Fondazione Cassa di Risparmio di Torino. The authors would like to thank Gregory Leperdi and Bruno Larocca for their availability during tests.



References

- [1] Delorme S., Tavoularis S. and Lamontagne M. Kinematics of the Ankle Joint Complex in Snowboarding, *J. Appl. Biomech*, 21, 394-403, 2005.
- [2] Klous M., Schwameder H. and Müller E. Joint loading on the lower extremities in skiing and snowboarding: methodological procedure, *J Biomech* 39 Suppl. 1, S187, 2006.
- [3] McAlpine P.R. and Kersting U.G. Jump Landings in Snowboarding: An Observational Study. In *Proc. of 4th Int. Cong. on Science and Skiing, Austria, 2007*.
- [4] Krüger A. and Edelmann-Nusser J. Biomechanical analysis in freestyle snowboarding: application of a full-body inertial measurement system and a bilateral insole measurement system. *Sports Technology*, 1-2, 17-23, 2009.
- [5] Maxwell S.M. and Hull M.L. Measurement of strength and loading variables on the knee during Alpine Skiing *J. Biomech* 22, 609-624, 1989.
- [6] Quinn T.P. and Mote C.D. Jr. Prediction of the loading along the leg during snow skiing *J Biomech* 25, 609-625, 1992.
- [7] Read L. and Herzog W. External Loading at the Knee Joint for Landing Movements in Alpine Skiing. *Int. J. of Sports Biomech*, 8, 62 – 80, 1992.
- [8] Nachbauer W., Kaps P., Nigg, B.M, Brunner F., Lutz A., Obkircher G. and Mössner M. A video technique for obtaining 3-D coordinates in alpine skiing, *J. Appl. Biomech.*, 12, 104–115, 1996.
- [9] Davis 3rd R.B., Ounpuu S, Tyburski D., Gage J.R. A gait analysis data collection and reduction technique. *Human Movement Science*, 5, vol. 1991.



Do lateral dominance, body mass, body height and direction of perturbation influence the Lehr's damping ratio, which characterizes the balancing ability on an unstable oscillatory platform?

R. M. Kiss

Dept. of Structures,

Budapest University of Technology and Economics, Hungary

Abstract

An unstable oscillatory platform can be used as a simple measuring instrument for modelling balancing capacity. We sought to determine the effects of (1) lateral dominance, (2) body mass, (3) body height and (4) the direction of perturbation on the Lehr's damping ratio for characterizing the balancing ability of 80 healthy young participants on an unstable oscillatory platform. Tests were performed while standing on both limbs and on one limb (dominant or non-dominant), and the direction of oscillation was anterior-posterior and medial-lateral. The healthy patients were divided into four groups based on body height and into five groups based on body mass. The average value of the Lehr's damping ratio was significantly smaller for participants standing on their non-dominant limb compared to their standing on both limbs or on the dominant limb. The largest difference of the Lehr's damping ratio was 0.014 (2.5%) comparing the groups with different body mass, and it was 0.012 (2.1%) comparing the groups with different body height. A weak correlation was found between the Lehr's damping ratio and body mass ($r=0.14$) and between the Lehr's damping ratio and body height ($r=0.19$). There was a significant difference when comparing the Lehr's damping ratio determined from oscillation in the anterior-posterior direction to the Lehr's damping ratio determined from oscillation in the medial-lateral direction ($p<0.008$). Based in our results the



Lehr's damping ratio depends on lateral dominance and the direction of perturbation; however, it is independent of body mass and body height.

Keywords: ultrasound-based measuring, sudden perturbation, balance.

1 Introduction

The measurement of balancing capacity is an important question; most studies concerning balance control have focused mainly on measuring postural balance during quiet standing to be represented by COP (centre of pressure), or COM (centre of mass) position [1, 3–6]. A moving platform is a common method for studying perturbation in balance, and a few previous studies have examined the effect of sinusoidal moving platform translation on postural movement and stability [7–11]. These studies principally examined the linear motion of body segments and the movement of COP and COM relative to the perturbation and involved a wide range of experimental perturbations [12].

Falls regularly occur during gait or following a specific perturbation such as a jump or sudden stop. A high level of complex coordination is required to regain equilibrium after a sudden impulse or a change in direction, either with a static posture (standing, sitting) or during motion (walking, running) [13]. In everyday life, this phenomenon occurs when one is bumped while walking or standing. This effect can be modelled using the PosturoMed[®] (Haider-Bioswing, Weiden, Germany) device, with its moveable and adjustable unstable therapy plates, which is a widely used training and therapy device for neuro-orthopaedic rehabilitation and sports rehabilitation in Europe. The therapy platform can be locked outside of the resting position using the fastening/provocation units. By releasing the fastening/provocation units, the stance equilibrium will be suddenly perturbed [14]. The horizontal movements of the suspended oscillating platform are recorded in two orthogonal directions using a mechanical deflection device (Digimax, Mechatronic, Hamm, Germany) [15–17]. The length of the moving path characterizes balancing capacity, and the shorter moving path represents a better balancing capacity [15–17]. The oscillating platform with an individual on it is a damped system [15]. The motion of the damping system can be represented dynamically by the Lehr's damping ratio D [14]. The Lehr's damping ratio (damping factor) relates the actual damping to the critical damping value at which the system does not oscillate [18]. The Lehr's damping ratio D can be calculated from the movement of the plate recorded as a function of time. The individual balancing ability influences the Lehr's damping ratio. Our earlier research determined the good reliability of the measuring method and of the Lehr's damping ratio for both young and elderly volunteers, and a significant influence of age on the Lehr's damping ratio [14, 19]. The goal of this research was to determine the effects of lateral dominance, body mass, body height and direction of perturbation on the Lehr's damping ratio.



2 Materials and methods

2.1 Subjects

Inclusion criteria were age over 18 years and under 40 years for the healthy young group, and the ability to perform independent motion without aids. Each participant's motion range, joint stability, axial position, muscular strength, and muscular tension in the lower limbs were physiologically adequate. Exclusion criteria included any lesion or surgery affecting a lower limb or the lumbar spine in the clinical history; osteoarthritis affecting any joint of a lower limb; neurological alterations (Parkinson, dementia, vertigo, cerebral apoplexy); uncontrolled hypertension, unstable angina or involvement of the peripheral vestibular system.

The investigation included healthy young men ($n = 45$; average age: 24.8 ± 3.5 y; average height: 179.9 ± 14.8 cm; average body mass: 89.4 ± 9.2 kg, body mass index (BMI): 27.9 ± 3.4 kg/m²) and women ($n = 35$; average age: 27.9 ± 6.9 y; average height: 169.4 ± 10.1 cm; average body mass: 70.8 ± 13.5 kg; BMI: 24.8 ± 5.7 kg/m²). According to a physical examination performed before motion analysis, the healthy young people were not limited in their everyday motion and sports activities.

Before the test, the dominant side of each participant was determined by a balance recovery test. The subject was nudged off balance from behind by the tester. The perturbation was a nudge applied to the midpoint between the scapulae from directly behind the subject and sufficient to require the subject to respond by taking a step. The leg that the subject used to recover balance was considered the dominant leg for each of the 3 trials. This 3-test sequence was the same for all subjects [20]. In this research the dominant side was the left side for 12 young healthy subjects and it was the right side for 68 young healthy subjects.

To analyse the effect of body mass, the participants were divided into five groups: under 50 kg ($n=3$), between 50-65 kg ($n=22$), between 66-75 kg ($n=35$), between 76-100 kg ($n=16$) and over 100 kg ($n=4$). To analyse the effect of body height, the participants were divided into five groups: under 150 cm ($n=2$), between 150-170 cm ($n=43$), between 170-190 cm ($n=28$), over 190 cm ($n=7$). To analyse the effect of the body mass index, the participants were divided into four groups: normal group BMI between 20 and 25 kg/m² ($n=25$), overweight BMI between 25 and 30 kg/m² ($n=33$), obese I and II BMI between 30 and 40 kg/m² ($n=13$), obese II BMI over 40 kg/m² ($n=9$).

The tests were authorized by the Science and Research Ethics Committee of Semmelweis University (174/2005). Each volunteer provided informed written consent to participation in the tests.

2.2 Methods

Sudden changes in direction can be modelled using a commercially available PosturoMed© device, which has a rigid plate that is connected to a rigid frame by eight springs of identical strength (Fig. 1). In this research the easiest setting



is used for the provocation test, where four springs work and four springs are fixed (the spring constant of fixed springs is infinite) [14, 15, 17].

In this study, the motions of the rigid plate were recorded by single individual markers attached on the side of the rigid plate. The spatial coordinates of markers were measured using a ZEBRIS CMS10 (ZEBRIS, Medizintechnik GmbH, Germany) computer-controlled, ultrasound-based motion analysis system (Fig. 1). The measuring methods are detailed in Kiss [14].

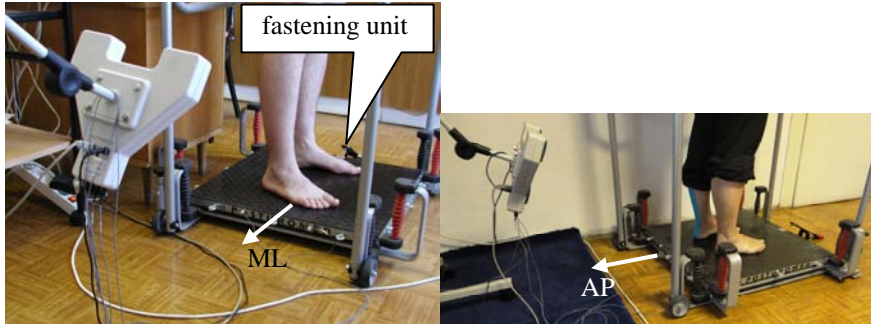


Figure 1: Measurement arrangement a) medial-lateral perturbation (ML) b) anterior-posterior perturbation.

The standardized double-limb stance position for the measurements involved arms hanging freely at the side, with the participant standing barefoot with feet slightly apart at the centre of the platform (position marked by tape). The standardized single-limb stance position for the measurement involved arms hanging freely at the side, the supporting leg barefoot in the centre of the platform (position marked by tape), and the non-supporting leg bent without contacting the supporting leg. Participants were instructed not to watch their motion but instead to look straight ahead. In addition, they were instructed not to hold on to anything but rather to balance with arm motion. They received no warning that the plate would shift. Each participant wore a safety harness, part of the PosturoMed device, that allowed natural arm motion. If a participant touched either a hand or the non-supporting leg to the guardrail or the platform or if the supporting leg was moved from the starting position, the trial was rejected.

The first measurement was carried out on the double-leg stance, followed by measurement on the dominant leg and then the non-dominant leg stance using medial-lateral perturbation. The platform was moved 20 mm in a medial-lateral direction towards the dominant side and locked by a fastening unit. All trials were then repeated under the anterior-posterior perturbation, where the platform was moved 20 mm in an anterior-posterior direction towards anterior side and locked by a fastening unit. The participants took up the standardized measuring position and stood for 2s, after which the fastening unit was released to perturb the stance equilibrium. Three 3s measurements were carried out for each measuring position. There were 60s rest intervals between measurements. The average value of successfully completed trials was taken as the value for each

measuring position, and a minimum of two successfully completed trials was required for each measuring position.

The oscillated PosturoMed[®] device with a participant on it is a damped system [14, 19]. The damped system can be characterized by the Lehr's damping ratio (damping ratio, ratio D , damping factor), which can be calculated from the measured damped curve (Fig. 2) [14, 19].

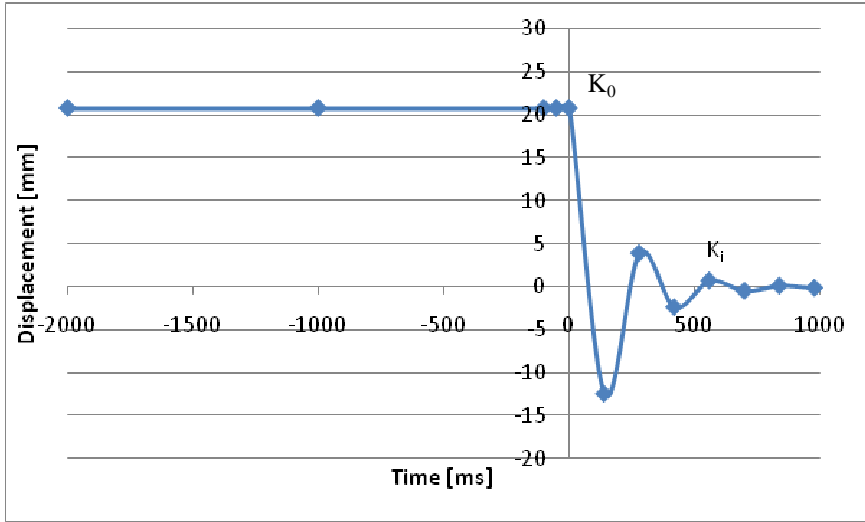


Figure 2: Measured damping curve.

$$D = \frac{\Lambda}{\sqrt{\Lambda^2 + 4\pi^2}}, \tag{1}$$

where π is 3.14;

$$\Lambda \text{ is the logarithmic decrement, } \Lambda_i = \frac{1}{i} \ln \frac{K_0}{K_i}, \tag{2}$$

where K_0 is the amplitude at time $t = t_0$, and K_i is the amplitude at time $t = t_{i,0}$ as measured by the ultrasound-based system.

The Lehr's damping ratios for individuals within a given group were statistically analysed using the MS Excel Analysis Tool Pak software. The average and standard deviation were calculated, and the homogeneity of variance was checked by an F-test. To analyse the influence of dominance and direction of perturbation on balancing ability, the one-sample t-test applying a symmetrical critical range was used. To analyse the effect of body mass, body height, and BMI on balancing ability, the two-sample t-test was used and the ratio - the two-tailed Pearson product-moment correlation coefficient (r) - was calculated between the Lehr's damping ratio and the body mass or body height. The significance level was $p \leq 0.05$.

3 Results

Each volunteer managed to complete all three parts of the tests; thus, no exclusions occurred for incomplete results. The F-test demonstrated the uniformity of standard deviations. The Lehr's damping ratio was between 0 and 1 in all cases where the motion of the rigid plate was a damping movement. Table 1 provides a summary of the results. There were no significant differences between the average values of the Lehr's damping ratio of male subjects and of female subjects ($p>0.14$); of the subjects with different body mass ($p>0.11$), and subjects with different body height ($p>0.19$) (Table 1).

No significant difference was found comparing the average values of the Lehr's damping ratio of subjects with different BMI ($p>0.09$), except for the values of subjects with normal BMI (20-25 kg/m²) compared to the values of subjects with obese III BMI (>40 kg/m²) ($p<0.03$) (Table 1). The Pearson correlation was very weak between the Lehr's damping ratio and body mass ($r=0.19$) and between the Lehr's damping ratio and body height ($r=0.14$).

The average value of the Lehr's damping ratio determined while the participants stood on their non-dominant limb was significantly smaller than it was while they stood on both of their limbs ($p = 0.006$) or standing on their dominant limb ($p = 0.001$) (Table 1). There was no significant difference between the average values of the Lehr's damping ratio determined while participants were standing on the dominant limb compared to those determined while participants were standing on both limbs ($p= 0.139$ for the young group) (Table 1).

The direction of perturbation significantly influenced the values of the Lehr's damping ratio; the value of the Lehr's damping ratio was significantly higher if the direction of perturbation was anterior-posterior ($p<0.008$) (Table 1).

4 Discussion

On the basis of the results above, it can be established that the effect of body mass, body height, BMI and sex was very low (Table 1). The Lehr's damping ratio increased with the increasing of body mass; however, the difference is not significant. This was confirmed by the weak correlation between the Lehr's damping ratio and body mass ($r=0.19$). The tendency is not linear between the Lehr's damping ratio and body height, which is confirmed by a very weak correlation ($r=0.14$). Maki and McIlroy [1] established that balancing capacity is a result of a complex control mechanism in which the effect of body mass and body height is negligible compared to neurological, proprioceptive parameters and to age. Blaszczyk et al. [22] established that postural control was significantly decreased only at female subjects with BMI over 40 kg/m². Our results agree with this trend, because a significant difference was found at male and female subjects with BMI over 40 kg/m² (Table 1).

Lateral dominance influenced balancing capacity on an unstable oscillatory platform after sudden perturbation. For both groups in the current work, the Lehr's damping ratio calculated during standing on both limbs did not differ



Table 1: Average \pm standard deviation of Lehr's damping ratio (D).

		Medial-lateral provocation			Anterior-posterior provocation		
		standing on			standing on		
		both limbs	dominant limb	non-dominant limb	both limbs	dominant limb	non-dominant limb
Sex	male n=45	0.543 \pm 0.031	0.530 \pm 0.027	0.418 \pm 0.015 ^{†,‡}	0.597 \pm 0.025*	0.590 \pm 0.020*	0.502 \pm 0.011 ^{†,‡,*}
	female n=35	0.539 \pm 0.029	0.525 \pm 0.023	0.417 \pm 0.017 ^{†,‡}	0.594 \pm 0.027*	0.588 \pm 0.019*	0.499 \pm 0.013 ^{†,‡,*}
Body mass	<50 kg n=3	0.535 \pm 0.030	0.523 \pm 0.026	0.415 \pm 0.014 ^{†,‡}	0.589 \pm 0.026*	0.584 \pm 0.021*	0.491 \pm 0.013 ^{†,‡,*}
	50-65 kg n=22	0.537 \pm 0.029	0.526 \pm 0.025	0.416 \pm 0.016 ^{†,‡}	0.593 \pm 0.024*	0.585 \pm 0.019*	0.494 \pm 0.011 ^{†,‡,*}
	66-75 kg n=35	0.541 \pm 0.027	0.527 \pm 0.023	0.417 \pm 0.019 ^{†,‡}	0.595 \pm 0.020*	0.587 \pm 0.017*	0.497 \pm 0.012 ^{†,‡,*}
	76-100 kg n=16	0.545 \pm 0.027	0.533 \pm 0.021	0.420 \pm 0.015 ^{†,‡}	0.598 \pm 0.027*	0.590 \pm 0.018*	0.500 \pm 0.013 ^{†,‡,*}
	>100 kg n=4	0.549 \pm 0.026	0.537 \pm 0.030	0.419 \pm 0.017 ^{†,‡}	0.599 \pm 0.028*	0.597 \pm 0.019*	0.502 \pm 0.015 ^{†,‡,*}
Body height	<150 cm n=2	0.541	0.528	0.420	0.596	0.592	0.497
	150-170 cm n=43	0.539 \pm 0.033	0.527 \pm 0.029	0.416 \pm 0.019 ^{†,‡}	0.593 \pm 0.024*	0.589 \pm 0.021*	0.501 \pm 0.012
	171-190 cm n=28	0.545 \pm 0.021	0.533 \pm 0.023	0.419 \pm 0.016 ^{†,‡}	0.601 \pm 0.022*	0.596 \pm 0.018*	0.503 \pm 0.011 ^{†,‡,*}
	>190 cm n=7	0.533 \pm 0.020	0.524 \pm 0.018	0.420 \pm 0.012 ^{†,‡}	0.588 \pm 0.023*	0.582 \pm 0.014*	0.506 \pm 0.011 ^{†,‡,*}
BMI	20-25 kg/m ² n=25	0.537 \pm 0.028	0.525 \pm 0.025	0.408 \pm 0.015 ^{†,‡}	0.587 \pm 0.020*	0.582 \pm 0.019*	0.492 \pm 0.012 ^{†,‡,*}
	25-30 kg/m ² n=33	0.540 \pm 0.033	0.530 \pm 0.030	0.416 \pm 0.017	0.595 \pm 0.023*	0.588 \pm 0.020*	0.497 \pm 0.014 ^{†,‡,*}
	30-40 kg/m ² n=13	0.549 \pm 0.031	0.538 \pm 0.028	0.420 \pm 0.019 ^{†,‡}	0.599 \pm 0.027*	0.592 \pm 0.021*	0.504 \pm 0.013 ^{†,‡,*}
	>40 kg/m ² n=9	0.564 \pm 0.037 [#]	0.540 \pm 0.036 [#]	0.424 \pm 0.020 ^{†,‡,#}	0.604 \pm 0.029 ^{*,#}	0.599 \pm 0.024*	0.507 \pm 0.016 ^{†,‡,*,#}

[†] Significant difference between the average values of parameters compared to parameters measured during standing on both limbs.

[‡] Significant difference between the average values of parameters compared to parameters measured during standing on the dominant limb.

* Significant difference between the average values of parameters measured with medial-lateral perturbation compared to the parameters measured anterior-posterior perturbation.

[#] Significant difference between the average values of parameters of subjects with normal BMI (20-25 kg/m²) compared to the parameters of subjects with obese III BMI (>40 kg/m²).

significantly from the value calculated during standing on the dominant limb. However, the results obtained during standing on the non-dominant limb did differ significantly from those of the other two tests. Boer et al. [16] and Müller et al. [15] showed that the total path of the moving plate representing balancing capacity on an unstable oscillatory platform depends on lateral dominance. Our measurement results provide further confirmation because the Lehr's damping ratio indicated a dependence on lateral dominance.



Another new finding from the current research is that the direction of perturbation significantly affects balancing capacity on an unstable oscillatory platform after sudden perturbation, as characterized by the Lehr's damping ratio. Boer et al. [16] demonstrated that the path length of an oscillatory platform after sudden disturbance standing on single limb was significantly decreased if the direction of perturbation was anterior-posterior. Our results confirmed these findings for standing on single and double limbs, because the values of the Lehr's damping ratio during standing on both limbs or on a single limb significantly increased if the direction of perturbation was anterior-posterior (Table 1). The difference can be traced back to a difference in neuromuscular control mechanisms of motion in the anterior-posterior and medial-lateral directions, which are discussed partly differently [15, 16]. Our results confirmed that the neuromuscular control mechanism is better in anterior-posterior motion.

The provocation test can model complex balancing capacity because after dislocation, the fastening unit locks the platform, and after release, the platform starts to return suddenly to its original position, representing a sudden perturbation [14]. The results in the current work show that lateral dominance and the direction of perturbation significantly affect balancing capacity on an unstable oscillatory platform after sudden perturbation; however, the effect of body mass and body height is negligible. On the basis of our results it can be established that the stabilization of the oscillated platform, characterized by the Lehr's damping ratio, is the result of the control mechanism of the neuromuscular system. Finally, this study extends knowledge because of its expanded study populations: different effects on the Lehr's damping ratio were determined by analysing data for 80 healthy young volunteers. Indeed, this method is used on a day-to-day basis at the Biomechanical Laboratory of MÁV Hospital at Szolnok and at the Department of Orthopaedics of Semmelweis University.

Acknowledgements

This work is connected to the scientific program of the "Development of quality-oriented and harmonized R+D+I strategy and functional model at BME" project. This project is supported by the New Hungary Development Plan (Project ID: TÁMOP-4.2.1/B-09/1/KMR-2010-0002). This work was supported by the Hungarian Scientific Fund T083650. Special thanks to Professor Kocsis for advice and help and to Árpád Illyés MD PhD, Zoltán Bejek MD, Gergely Holnapy MD, Maria Takacs MD and Ákos Pethes MD for their help in completing the measurements.

References

- [1] Maki, B.E. & McIlroy, W.E., Postural control in the older adults. *Clinics in Geriatric*, **12**, pp. 635-658, 1996.
- [2] Prieto, T.Y., Myklebust, J.B., Hoffmann, R.G., Lovett, E.G., & Myklebust, B.M., Measures of postural steadiness: differences between healthy young



- and elderly adults. *IEEE Transaction on Biomedical Engineering*, **43**, pp. 956-966, 1996.
- [3] Newell, K.M., van Emmerik, R.E.A., Lee, D. & Sparague, R.L., On postural stability and variability. *Gait and Posture*, **1**, pp. 225-230, 1993.
- [4] Yamada, N. Chaotic swaying of the upright posture. *Human Movement Science*, **14**, pp. 711-736, 1995.
- [5] Riley, M.A., Balasubramaniam, R. & Turvay, M.T., Recurrence quantification analysis of postural fluctuation. *Gait and Posture*, **9**, pp. 65-78, 1999.
- [6] Donker, S.F., Roerding, M., Greven, A.J. & Beek, P.J., Regularity of center of pressure trajectories depends on the amount of attention invested in postural control. *Experimental Brain Research* **181**, pp. 1-11, 2007.
- [7] Berger, W., Discher, M., Trippel, M., Ibrahim, I.K. & Dietz, V., Developmental aspects of stance regulation, compensation and adaptation. *Experimental Brain Research* **90**, pp. 610-619, 1992.
- [8] Buchanan, J.J. & Horak, F.B., Emergence of postural pattern as a function of vision and translation frequency. *Journal of Neurophysiology* **81**, pp. 2325-2339, 1999.
- [9] Corna, S., Tarantola, J., Nardone, A., Giordano, A. & Schiepati, M., Standing on a continuously moving platform: Is body inertia counteracted or exploited? *Experimental Brain Research*, **124**, pp. 331-341, 1999.
- [10] Diener, H.C., Dichgans, J., Bruzek, W. & Selinka, H., Stabilization of human posture during induced oscillation of the body. *Experimental Brain Research*, **45**, pp. 126-132, 1982.
- [11] Dietz, V., Trippel, M., Ibrahim, I.K. & Berger, W., Human stance on a sinusoidally translating platform: balance control by feed forward and feedback mechanism. *Experimental Brain Research* **93**, pp. 352-362, 1993.
- [12] Ko, Y.G., Challis, J.H. & Newell, K.M., Postural coordination patterns as a function of dynamics of the support surface. *Human Movement Science*, **20**, pp.737-764, 2001.
- [13] Winter, D.A., *ABC of balance during standing and walking*. Waterloo: Waterloo Biomechanics, 1995.
- [14] Kiss, R.M., Parameters of kinaesthesia during gaits derived from an ultrasound-based measuring system. *Modelling in medicine and biology VIII* eds. C.A. Brebbia, WIT Press: Wessex, pp. 171-180, 2009
- [15] Müller, O., Günther, M., Krauß, I. & Horstman, T., Physical characterization of the therapeutic device Posturomed as a measuring device-Presentation of a procedure to characterize balancing ability. *Biomedizinische Technik*, **49**, pp. 56-60, 2004.
- [16] Boer, J., Mueller, O., Krauß, I., Haupt, G. & Horstman, T., Reliability of a measurement technique to characterize standing properties and to quantify balance capabilities of healthy subjects on an unstable oscillatory platform (Posturomed). *Sportverletz Sportschaden* **24**, pp. 40-45, 2010.
- [17] Boer, J., Mueller, O., Krauß, I., Haupt, G., Axmann, D. & Horstman, T., Effect of a Sensory-motor exercise program for older adults with osteoarthritis or prosthesis of the hip using measurements made by



- Posturomed oscillatory platform. *Journal of Geriatric Physical Therapy*, **33**, pp. 10-15, 2010.
- [18] Hubbeler, R.C., *Engineering Mechanics: Dynamics*. Prentice Hall: New Jersey, 1999.
- [19] Kiss, R.M., A new parameter for characterizing balancing ability on an unstable oscillatory platform. *Medical Engineering and Physics*, (under publishing), 2011.
- [20] Hoffman, M., Schrader, J., Applegate, T. & Kocejka, T., Unilateral postural control of the functionally dominant and nondominant extremities of healthy subjects. *Journal of Athletic Training*, **33**, pp. 319-322, 1998.
- [21] Kiss, R.M., Kocsis, L. & Knoll, Z, Joint kinematics and spatial temporal parameters of gait measured by an ultrasound based system. *Medical Engineering & Physics* **26**, pp. 611-620, 2004.
- [22] Blaszczyk, J.W., Cielinska-Swider, J., Plewa, M., Zahorska-Markiewicz, B. & Markiewicz, A., Effects of excessive body weight on postural control. *Journal of Biomechanics*, **42**, pp. 1295-1300, 2009.
- [23] Morasso, P.G. & Schieppati, M. Can muscle stiffness alone stabilize upright standing? *Journal of Neurophysiology*, pp. 1622-1626, 1996.
- [24] Winter, D.A., Prince, F., Frank, J.S., Powell, C. & Zabjek, K.F., Unified theory regarding AP and ML balance in quiet stance. *Journal of Neurophysiology*, pp. 2334-2343, 1996.



Synthetic organs for transplant and bio-mimic reactors for process intensification using nano-structured micro-porous materials

E. M. Akay¹, Z. Okumus², O. S. Yildirim^{3,4}, M. A. Bokhari^{4,5}
& G. Akay^{5,6}

¹*North Middlesex University Hospital, University College London, UK*

²*Veterinary Faculty, Ataturk University, Turkey*

³*Medical Faculty, Department of Orthopaedic, Ataturk University, Turkey*

⁴*Medical Faculty (Orthopaedics), Newcastle University, UK*

⁵*Process Intensification and Miniaturization Centre, School of Chemical Engineering and Advanced Materials, Newcastle University, UK*

⁶*The Institute of Stem Cell Biology and Regenerative Medicine, Newcastle University, UK*

Abstract

In order to achieve Process Intensification through monolithic micro-reactors in bio- and chemical technology we examined the processing strategy in the human body, taking the liver as a typical organ. The macro- and micro-architectural structure can be mimicked by using nano-structured micro-porous polymers which were used as support in tissue engineering and bioprocess intensification. It was shown that these materials could be used as bone transplant and they are integrated into the body. Their integration could be predicted through in vitro experiments. Metallic versions of these structures with a hierarchy of pore size were produced in order to obtain catalytic bio- or chemical reactors operating at high temperature and/or pressure.

Keywords: bio-mimic materials, BioProcess Intensification, ChemicalProcess Intensification, nano-structured micro-porous materials.



1 Introduction

1.1 Process intensification

Process Intensification (PI) emerged as a novel process design philosophy in which the processing volume is deliberately reduced while the processing vectors (conditions) were enhanced in order to achieve the same levels of production rate. This resulted in the reduction of chemical plant/unit operation capital and processing costs [1]. Process Intensification is achieved via two routes [1]. Firstly, PI is a direct result of the imposition of enhanced and uniform processing fields (such as deformation rates, pressure, temperature, extended surface area) which are best realized through miniaturization with controlled micro-architecture of the intensified reactor providing accessibility for heat/mass transfer facilities. Secondly, (known as phenomenon based PI) PI results from an underlying inherent phenomenon which is only observed in the presence of enhanced processing field and/or miniaturization which in fact constitute the two prerequisite process conditions for PI.

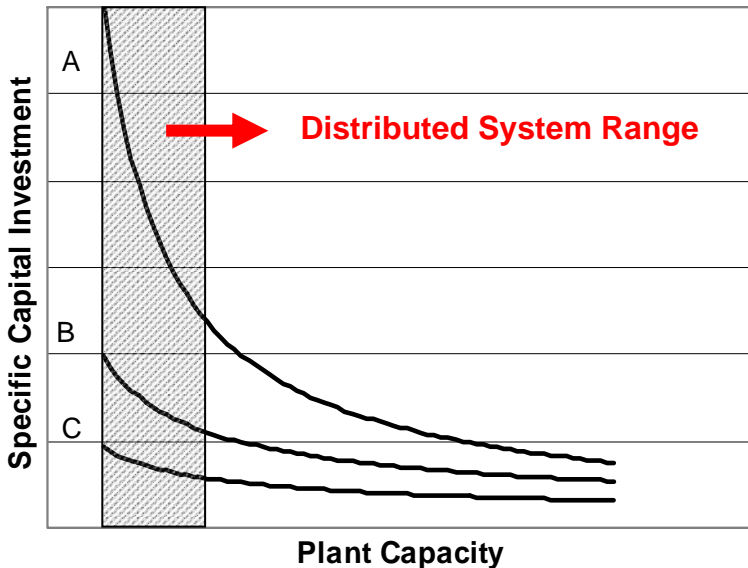


Figure 1: Variation of specific capital cost with plant capacity as a function of TAD: A: Current technology; TAD = $1\text{k m}^2/\text{m}^3$; B: Micro-capillary reactor technology (Intensified Process) with TAD = $10\text{k m}^2/\text{m}^3$; C: Micro-reactors using nano-structured micro-porous materials with applied intensification field (Intensified Hybrid Reactors) with TAD = $100\text{k} - 1000\text{k m}^2/\text{m}^3$.

1.2 Importance of PI in sustainable chemical and energy production

Phenomenon based PI, coupled with high throughput microreactor technology (Process Intensification and Miniaturization, PIM) is more powerful in delivering intensification above 10 fold or more; in some cases reaching 1000 fold compared with the existing technology. One of the effects of PIM is that, the specific capital cost of intensified processes has weak dependency on capacity. This technology does not have the burden of 'economies of scale', a defining characteristics commonly associated with large scale centralised production facilities such as refineries, chemical and power plants. It is possible to relate the specific capital cost of the centralised production plant with TAD (transfer area density which is area per unit volume for heat and/or mass transfer), of the reactors as shown in Figure 1 [2].

Figure 1 indicates why the current production plants must have large capacity in order to circumvent the burden of economies of scale. Intensified distributed production plants which consist of intensified unit operations do in fact deliver low specific capital and operating costs with short start up and shut down times. The distributed chemical and power generation through intensified integrated bio-refineries is essential for sustainability and in combating global warming using biomass and biomass waste as renewable feedstock instead of fossil fuels.

1.3 Nano-structured micro-porous materials for PI

Figure 1 also illustrates the importance of materials science, including the catalysis and reactor design to achieve PI in distributed production. By increasing the transfer area density for heat and mass transfer in reactors, capital cost is substantially reduced in distributed-intensified plants. Transfer area density can be enhanced by using monolithic high throughput micro-reactors in which the reaction media is made of nano-structured micro-porous materials. Nano-structure provides catalytic surface area while micro-porosity providing accessibility of the catalytic sites.

These materials can be made of polymeric, metallic or ceramic or in composite form fabricated into monolithic agro- bio- or chemical-reactors. It is also possible to add other process intensification fields to such reactors in order to achieve 'Phenomenon based process intensification'. Current examples of PI cover agro-processes, biotechnology, chemical and energy conversion processes [1, 3].

1.4 Processing strategy in the human body

The objective of this work is to utilize nature's (the human body) processing strategy in the design of micro-reactors for AgroProcess, BioProcess and Chemical Process Intensifications while designing micro-bioreactors for organ replacement in the form of transplants.

Due to its long evolution, we can assume that the human body is an intensified biochemical plant formed by the integration of unit operations in the form of organs and monitored and controlled by neural and hormonal systems. The macroscopic architecture of the plant is provided by the skeletal structure



which itself interact with the organs and connective tissue. The important elements of the body's processing strategy can be summarised as:

- 1) High surface area-to-volume ratio for heat–mass transfer. For example, for human adult lungs TAD is ca. $10^4 \text{ m}^2/\text{m}^3$.
- 2) Hierarchical length scale in organs involving flow such as lungs, liver and (millimeter; micro; nano connectivity) for simultaneous accessibility, continuous process and maintenance.
- 3) Mass transfer and communication (also quorum signalling by cells) across nano-size barriers (bilayers).
- 4) Monolithic unit operations with continuous product removal.
- 5) Physiological stress dependent response in 3-Dimensional cell culture with its own cell-support system.

The hierarchic length scale in the liver can be seen in Figure 2 [4].

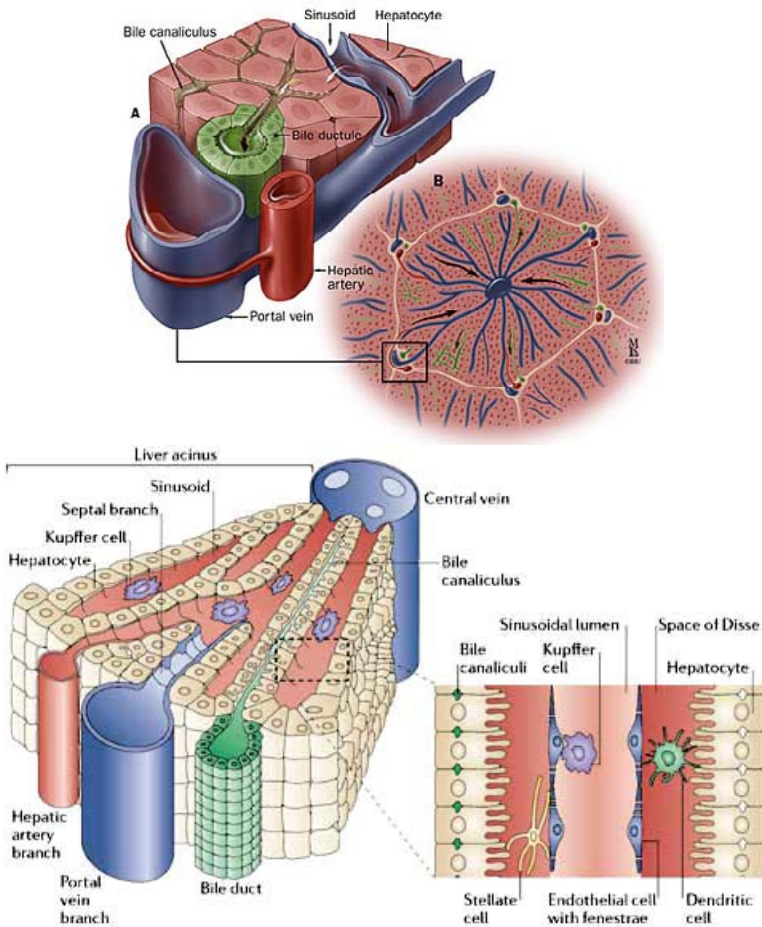


Figure 2: Macro- and micro-level structure of the liver showing the architecture of the unit operation.

The liver receives a dual blood supply from the portal vein and hepatic artery which join in the capillary bed of the liver and exit via central veins, coalescing into hepatic veins, then leave the liver. Anatomically, based on the blood supply, the liver is divided into two 'hemilivers' which further divide into eight segments which focus upon subdivisions of the hepatic and portal veins. Each of these segments is in turn divided into lobules which centre on central portal veins. The liver is divided microscopically into functional units called 'acini'. These centre around a vascular stalk (terminal branches of the portal veins and hepatic arteries) and bile ducts and are comprised of the functioning cells of the liver (hepatocytes). These highly organised functional units allow optimal productivity of the liver whilst forming a compact structure, reflecting the processing strategy cited above.

1.5 Significance of 3D culture and quorum signalling in BioProcess Intensification

During bioprocessing, micro-organisms undergo physiological stress which alters their metabolism and physiology. It is therefore not surprising that a number of scale-up responses are observed when the performance of bacteria in small and large bioreactors is compared. These differences include, biomass yield, recombinant protein accumulation and cell viability [5]. Strong production of recombinant proteins interferes with cellular processes and the cells readjust metabolic fluxes and enzyme composition which may result in inhibition of growth or low level of product accumulation [6]. It is then possible to adopt production schemes that enhance volumetric productivity and sustainability of the process.

Recently, we have shown that bioprocesses could be intensified (Bioprocess Intensification) through the immobilization of bacteria within the micro-pores (within certain size range) of nano-structured micro-porous polymers which alter the metabolic activity of the bacteria [7]. This phenomenon is similar to that we observed for mammalian cells whereby the cell proliferation, protein production rate and differentiation are dependent on the size of the micro-environment that they grow [8–11]. The observed bioprocess intensification is over 30 fold compared with the best of the existing technology. As a result, for a given bacteria or animal cell, an optimum pore size is present in order to maximise productivity and proliferation. We have also observed that bacterial growth under maximum productivity is in monolayer form without the formation of biofilm which occurs when the pore size of the support was large.

Another factor for enhanced in vitro protein production during 3D cell culture (in bone or cartilage cells) using micro-bioreactors in the form of cell support, is the chemical environment of the cell growth media. Both bone cells and cartilage cell growth rates and marker protein productions are enhanced by several hundred percent when bio-responsive coatings (such as hydroxyapatite) are used. These results indicate that the chemical and physical structure of the micro-environment affect cell viability, productivity and differentiation as observed for bacteria.



It is now well understood that the 3D *in vitro* culture of cells is essential in order to provide the necessary micro-architecture for the cell growth similar to that observed in nature. This micro-architecture provides cell-cell communication for collective function as cell complete autonomy will not result in tissue specificity. Isolated cells lose most functional differentiation when separated and placed in traditional cell cultures. There is now a growing opinion that cell function is regulated by microenvironment and tissue architecture [12]. The effect of micro-environment in bacteria is evaluated in terms of environmental stress as well as in terms of alteration of the metabolic pathway and it is suggested that the physiological stress should be controlled in order to control the metabolic activity, viability, differentiation and productivity, gene expression pattern including mRNA levels of molecular chaperons, proteases, lysis genes. However, in large scale fermentation reactors, or in supported bioreactors without a uniform or suitable pore micro-architecture and stressor field, the physiological response of the bacteria to the micro-environment is not collective due to the transient and variable nature of the stressor.. Therefore the phenomenon of micro-environment induced physiological response will be absent in the absence of quorum signalling.

2 Experimental

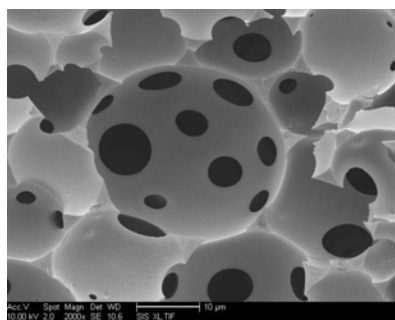
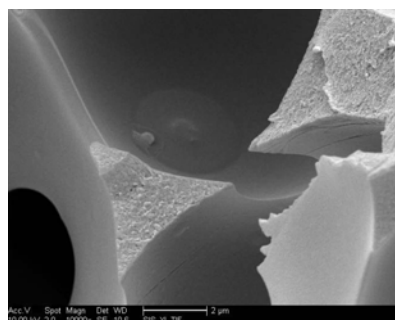
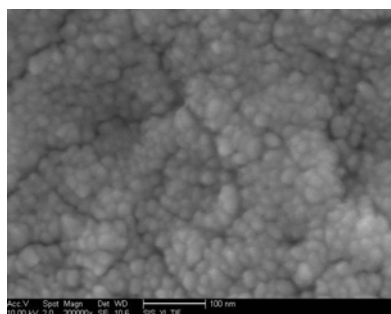
Experiments were conducted in 4 levels. Here, experimental details are not provided but we refer to our previous publications. They include: 1) Preparation of nano-structured micro-porous (NSMP) polymers [11, 13]; 2) NSMP-catalysts /catalyst support / monolithic reactors [14]; 3) *in vitro* bone growth [8–11].

3 Results

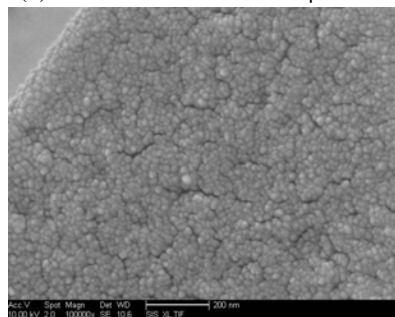
3.1 Nano-structured micro-porous polymers for tissue engineering and monolithic bioreactors with 3D-culture

As shown previously [1, 7–11] the pore and interconnecting hole sized as well as the pore volume are important in the growth, viability and differentiation of cells *in vitro*. While the architecture of the support provides a 3D-culture and cell-cell communication, biochemical compatibility or even biochemical activation of the cells can be achieved by the chemical composition of the nano-structured micro-porous support material. The in-situ coating of the NSMP-polymers has shown to enhance bone and cartilage growth similar to those observed for naturally occurring peptide coatings [10]. In tissue engineering or bioprocess intensification when the pore structure is important, the pore and interconnect size distributions should be narrow. Figure 3 illustrates the pore structure of a typical NSMP-polymer. Fig 3(a) illustrates the pore and interconnect structures while Fig 3(b) shows the wall structure. Figs 3(c), (d) illustrate the nano-porosity of the pore surface and wall.



(a) Pore structure, Bar 10 μm (b) Wall cross-section. Bar: 2 μm 

(c) Pore surface. Bar: 100 nm

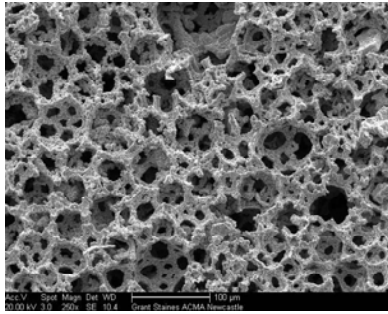


(d) Wall cross-section. Bar: 200 nm

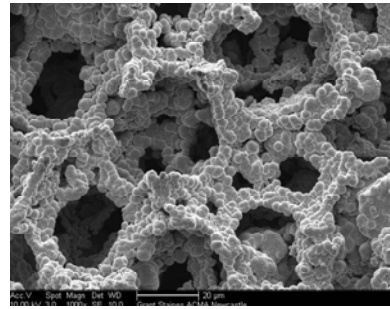
Figure 3: Typical NSMP-polymer structure suitable for monolithic bioreactors.

3.2 Nano-structured micro-porous metals for intensified reactors

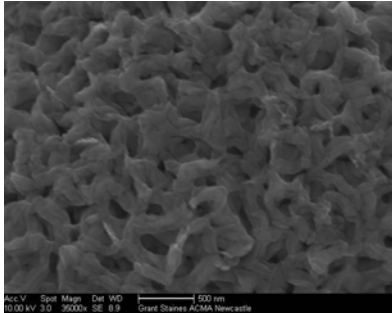
Nano-structured micro-porous metals with structures very similar to those NSMP-polymers have been developed as catalyst, catalyst support for use as monolithic microreactors. Chemical processes have the advantage of being carried out at high or very low temperatures, pressures, concentrations, deformation rates and hence are more suitable for intensification. Further intensification can be achieved through the superimposition of a process intensification field (such as electric field) in hybrid reactors which often need to be monolithic. It is once again necessary to have a hierarchic pore structure so that the catalytic surfaces are accessible to the reactants. Figure 4 illustrate the hierarchy of the pores in a typical metallic monolith where the pore range can be over 4–5 decades. In these materials, pores are made from grains (size range 10 μm – 0.1 μm) as seen in Figures 4(a,b). The grain surface have nano-porosity (Fig 4 (c)) which can be controlled (typically 100–10 nm). Inside the grains, pore volume and pore size can be variable as shown in Fig 4(d) where the pore size is illustrated in Fig. 4(e). The structure of the NSMP-metals can be varied depending on the method of manufacture and its composition [13, 14]. A variant structure is illustrated in Fig. 4(f).



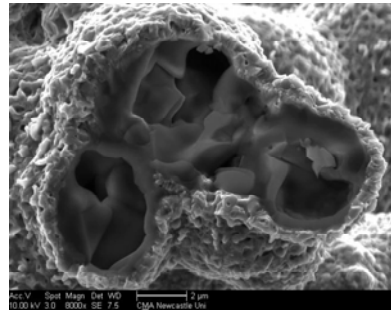
(a) General appearance (Bar: 100 µm)



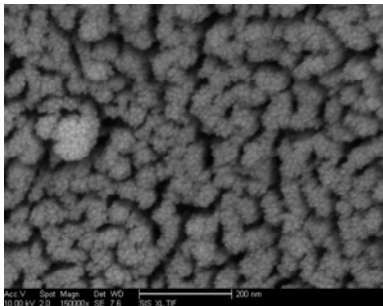
(b) Wall structure (grains) (Bar: 20 µm)



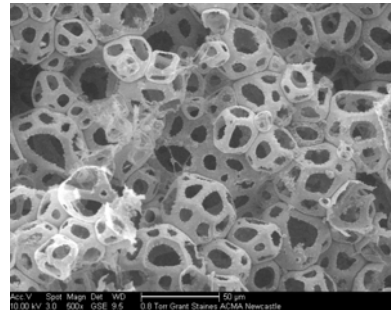
(c) Grain surface (Bar: 500 nm)



(d) Inner structure of the grains (Bar: 2 µm)



(e) Detail of the inner grains (Bar: 200 nm)



(f) A variant of pore structure (Bar: 50 µm)

Figure 4: Nano-structured micro-porous metal alloys with a hierarchy of pores.

3.3 Bone tissue engineering

The purpose of tissue engineering is to create artificial organs for *in vitro* testing or for transplant after growing of the tissue *in vitro*. It is also possible to graft the well characterised and optimised *in vitro* support. Here we optimise the chemical and physical structure of the support material for grafting. We used NSMP-polymers which were coated with hydroxyapatite. Figure 5 clearly shows

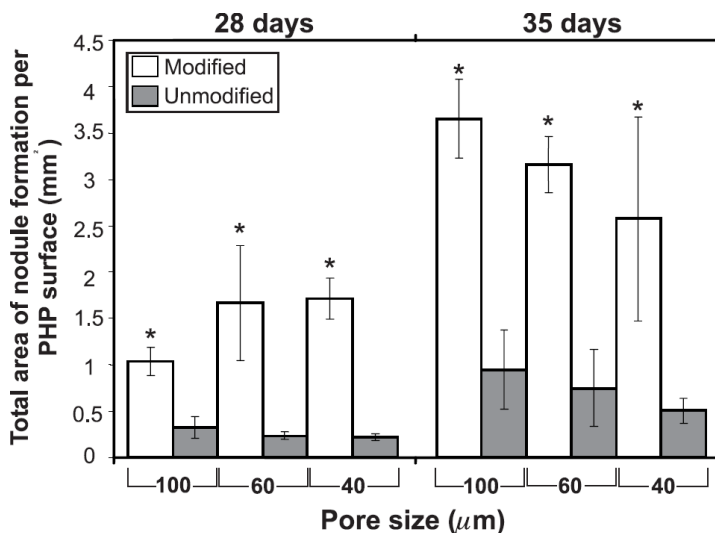


Figure 5: The effect of NSMP-polymer support pore size ($D = 100, 60, 40 \mu\text{m}$) on mineralized nodule formation of rat osteoblast cells cultured *in vitro* after 28 or 35 days using hydroxyapatite coated (modified) or uncoated (unmodified) styrene NSMP-polymer (PolyHIPE Polymer) cell supports.

that the coating of the polymer increases mineralized nodule formation of rat osteoblast cells cultured *in vitro* and that $100 \mu\text{m}$ pore support is more effective.

3.4 Bone graft

Repair of bone defects created by surgery, tumours, trauma, infections, and implant revisions may be enhanced by bone graft substitutes. Here we use NSMP-polymers also known as PolyHIPE Polymer (PHP) with pore size of 100 or $40 \mu\text{m}$. In our previous studies PHP has been found to be biocompatible with at several different cell types such as fibroblasts, osteoblasts, macrophages^{and} and chondrocytes. Biocompatibility studies demonstrated that there was no cytotoxic effect observed when cells were cultured within PHP in *in vitro*. The purpose of this investigation was to determine whether PHP is biocompatible and if the incorporation of HA in PHP scaffold would enhance the biological properties of living body response as compared to different pore sized PHP scaffolds. Extracellular matrix (ECM) production was examined by histological analysis and indicated new bone had been formed in PHP. Graft area morphology was also examined using environmental scanning electron microscopy (ESEM). The inflammatory response to PHP was negligible at both short (4 weeks) and long (12 weeks) time points. These results indicate that the addition of hydroxyapatite in PHP improves osteoblast response as compared PHP without hydroxyapatite. All PHP implants were tolerated; no necrosis or abscess formation was observed around either type of implants. Figure 6 shows the implant after 12 weeks within

the frontal section of rabbit iliac bone showing good integration between the implant (PHP) and bone (B). In this scanning electron micrograph, the implant is 100 μm pore size PHP coated with hydroxyapatite. In Figure 6(a) the connectivity of the bone and PHP implant is illustrated while Fig 6(b) shows osteoblast cell process (arrow) is present in the form of fibrillar collagen synthesized and organized by osteoblast. Heamatoxylin and Eosin (H&E) stained

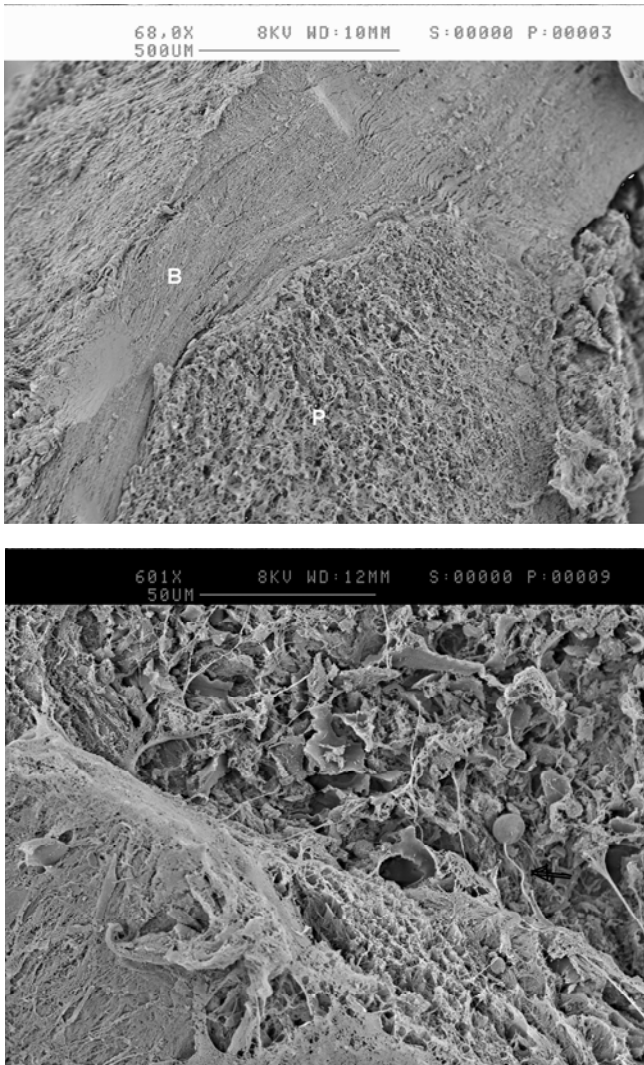


Figure 6: Scanning electron micrographs of bone implant showing: (a) their connectivity; (b) presence of osteoblast cell process (arrow) in the implant.

histological section of 40 μm hydroxyapatite coated PHP implant show the presence of vascularisation indicating that the implant was fully integrated into the body.

3.5 Model in vitro organ and intensified monolithic reactors

Figure 7 is a diagrammatic illustration of an intensified monolithic micro-reactor which can be used for biological or chemical conversion processes. It is made from nano-structured micro-porous materials, either polymeric (structure described in Figure 4) or metallic (structure described in Figure 5). The bulk of the monolith provides the surface area for bio- or chemical catalysis while the array of large (millimeter size) channels provide heat and mass transfer facility close the catalytic reaction sites. This reactor is very similar to the liver structure described in Figure 2 and hence can be used as a model for the liver. The porosity of the interface between the large channels and the micro-porous bulk can be controlled. When the interface is non-porous, pressures in the channels and the bulk can be controlled independently.

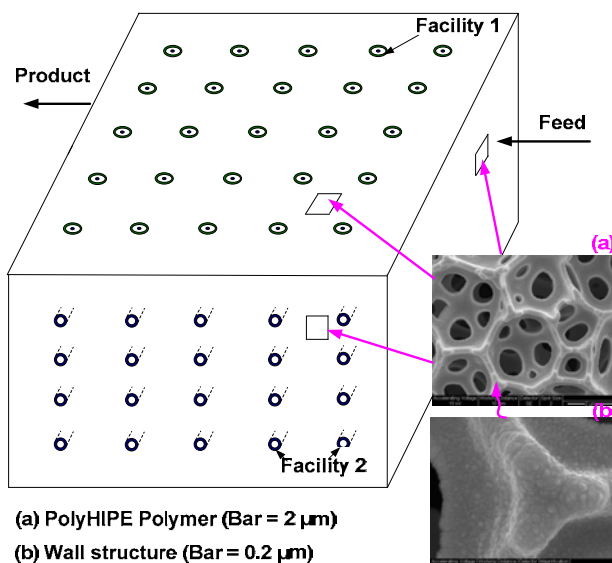


Figure 7: A model for an in-vitro organ or intensified micro-bioreactor.

References

- [1] Akay, G., Bioprocess and chemical process intensification. In: Encyclopedia of Chemical Processing, Ed: S Lee, Marcel Dekker, NY. pp. 185–198, 2006.
- [2] Akay, G., Renewable resources come together, The Chemical Engineer, 784, 27–30, 2006.



- [3] Akay, G., Burke, R.D., Synthetic symbiosis system as soil additives to deliver active ingredients through plant roots for enhanced plant and crop yield. PCT Patent Application PCT/GB09/02380, 2009. Also: J. Agricultural Sci., (accepted for publication).
- [4] Adams, D.H. & Eksteen, B., Aberrant homing of mucosal T cells and extra-intestinal manifestations of inflammatory bowel disease, *Nature Reviews Immunology*, **6**, 244-251, 2006.
- [5] Enfors, S-O., et al., Physiological responses to mixing in large scale bioreactors, *J. Biotechnology*, **85**, 175-185, 2001.
- [6] Hoffman. F., & Rinas, U., Stress induced by recombinant protein production in *Escherichia coli*, *Adv Biochem Engin/Biotechnol.*, **89**, 73-92, 2004.
- [7] Akay, G., Erhan, E., Keskinler, B., Bioprocess intensification in flow through micro-reactors with immobilized bacteria, *Bioengineering Biotechnology*, **90**, 180-190, 2005.
- [8] Bokhari, M. Birch M., and Akay, G., Polyhipe polymer: A novel scaffold for in vitro bone tissue engineering, *Advances in Experimental Medicine and Biology*, **534**, 247 – 254 (2003).
- [9] Akay, G., Birch, M.A., Bokhari, M.A., Microcellular Polyhipe polymer (PHP) supports osteoblastic growth and bone formation in vitro, *Biomaterials*, **25** 3991-4000, 2005.
- [10] Bokhari, M.A., Akay, G., Zhang S., and Birch, M.A., A hybrid biomaterial combining the peptide hydrogel RAD 16-1 with PolyHIPE Polymer (PHP) enhances osteoblast growth and differentiation *in vitro*. *Biomaterials*, **26** , 5198-5208, 2005.
- [11] Akay, G., Bokhari, M.A., Byron, V.J., and Dogru, M., Development of nano-structured materials and their application in bioprocess-chemical process intensification and tissue engineering. In: *Chemical Engineering Trends and Developments*, Ed: MA Galan and E.M. Del Valle, Wiley, London, pp. 171-196, 2005.
- [12] Bissell, M.A., Rizki, A., Mian, I.S., Tissue architecture: the ultimate regulator of breast epithelial function, *Curr. Opin. Cell Biol.*, **15**, 753-762, 2003.
- [13] Akay. G., Dawnes, S., Price, V.J., Microcellular polymers as cell growth media and novel polymers, EP 1183328, 2002.
- [14] Akay, G., Calkan, B., Hasan. H., and Mohamed R., Preparation of nano-structured microporous composite foams, PCT/GB09/02403, 2009.



Section 11
Simulation of
physiological processes

This page intentionally left blank

A dynamic model of the pregnant myometrial fasciculus

R. Miftahof¹ & N. Akhmadeev²

¹Arabian Gulf University, Manama, Kingdom of Bahrain

²Kazan Medical University, Russia

Abstract

A mathematical model of the pregnant myometrial fasciculus is proposed. It is based on real anatomical and physiological data of its structure and function. The model reproduces electromechanical wave phenomena in the myometrium under normal physiological conditions and after application of different classes of pharmacologically active compounds.

Keywords: human myometrium, fasciculus, electromechanical waves.

1 Introduction

In recent years the biomedical research on reproduction has been focused mainly on molecular, neuroendocrine and pharmacological aspects of uterine activity. A relatively small amount of work has been dedicated to modeling of the uterus *per se*. Various approaches have been developed for uterine mechanics modeling during parturition. The majority of them rely on assumptions of geometrical and physical linearity [1, 2]. Results of numerical simulations obtained for different values of parameters and constants resembled patterns of spontaneous contractility observed during normal labor and reproduced voltage–clamp traces recorded experimentally on pregnant rats and human non-pregnant myometrial cells. Although the existing models of the myometrium and the gravid human uterus are based on the accurate application of general principles of solid mechanics and incorporate some morphological data on the structure and function of the organ, these models remain of limited biomedical value. New integrative, biologically plausible models are needed to answer urgent questions related to clinical problems of labor and delivery.



The aims of this study were twofold: i) to formulate a biomechanical model of the pregnant human myometrial fasciculus, and ii) to study numerically the biological phenomena that underlie processes of electromechanical activity in it.

2 Model formulation

Consider a one-dimensional model of the dynamics of fasciculus (myofiber) - the functional unit of the human uterus. Let a fasciculus be embedded in the extracellular matrix of connective tissue. Our developments of a biomechanical model will be based on the following assumptions which are consistent with several lines of experimental evidence [3, 4].

- i) Smooth muscle cells in the fasciculus are connected by tight junctions to form a homogenous electromechanical continuum.
- ii) The myofiber possesses nonlinear viscoelastic properties; the mechanics of inactive smooth muscle cells, collagen, elastin fibers and the extracellular matrix define the “passive”, $T^p(\lambda, c_i)$, and intracellular contractile proteins describe the “active” component, $T^a(\lambda, Z_{mn}^{(*)}, [Ca_i^{2+}], c_i)$, of the total force, T^t

$$T^t = T^p(\lambda, c_i) + T^a(\lambda, Z_{mn}^{(*)}, [Ca_i^{2+}], c_i), \quad (1)$$

where λ is the stretch ratio, c_i are empirical material constants, $Z_{mn}^{(*)}$ is the “biofactor”, and $[Ca_i^{2+}]$ is the concentration of free cytosolic calcium.

- iii) Contractions of the fiber are isometric; deformations are finite.
- iv) Myogenic electrical events are a result of activity of an intrinsic autonomous oscillator; its function is defined by the fast (T-type) and slow (L-type) inward Ca^{2+} , BK_{Ca} , voltage dependent K_{v1}^+ and leak Cl^- currents.
- v) Each oscillator is in the silent state; the transformation to a firing state is a result of depolarization and/or stretch deformation of the cell that alters the conductance for L- and T-type Ca^{2+} channels, while the stretch affects permeability of L-type channels.
- vi) The myofiber possesses cable electrical properties; propagation of the wave of depolarization is a result of combined activity of the Na^+ , K_{v2}^+ , and leak Cl^- ion currents.
- vii) A smooth muscle cell or a group of cells within the fasciculus have intrinsic pacemaker properties; the transformation from a silent to a bursting state can occur spontaneously and is a result of “alterations” in electrical properties; additionally, an *a priori* defined “pacemaker” provides an excitation to the fiber.

Let the fasciculus of a length L be referred to a local Lagrange coordinate system α . Its equation of motion is given by

$$\rho \frac{\partial v}{\partial t} = \frac{\partial}{\partial \alpha} T', \quad (0 \leq \alpha \leq L) \tag{2}$$

where ρ is density, v is the velocity, and the meaning of other parameters are as described above. Following the working assumption ii), the total force T can be decomposed as

$$T' = k_v \frac{\partial(\lambda - 1)}{\partial t} + T^a(\lambda, Z_{mm}^{(v)}, [Ca_i^{2+}], c_i) + T^p(\lambda, c_i), \tag{3}$$

where the viscoelastic term has been added to Eq. (1). Here k_v is viscosity.

Substituting the above into Eq. (3) we obtain

$$\rho \frac{\partial v}{\partial t} = \frac{\partial}{\partial \alpha} \left(k_v \frac{\partial(\lambda - 1)}{\partial t} + T^a(\lambda, Z_{mm}^{(v)}, [Ca_i^{2+}], c_i) + T^p(\lambda, c_i) \right), \tag{4}$$

where the force-stretch ratio relationship yields

$$T^p = \begin{cases} c_1 [\exp c_2(\lambda - 1) - 1], & \lambda > 1.0, \\ 0, & \text{otherwise.} \end{cases} \tag{5}$$

and the active-force – intracellular Ca_i^{2+} relationship for the myometrium is given by

$$T^a = \begin{cases} 0, & [Ca_i^{2+}] \leq 0.1 \mu M \\ c_3 + c_4 [Ca_i^{2+}]^4 + c_5 [Ca_i^{2+}]^3 + c_6 [Ca_i^{2+}]^2 + c_7 [Ca_i^{2+}], & 0.1 < [Ca_i^{2+}] \leq 1 \mu M \\ \max T^a, & [Ca_i^{2+}] > 1 \mu M. \end{cases} \tag{6}$$

The system of equations for the oscillatory activity of the membrane potential V is

$$\lambda C_m \frac{dV}{dt} = - \sum_j \tilde{I}_j \tag{7}$$



where, $\tilde{\lambda}$ is the numerical parameter, C_m is the uterine smooth muscle cell membrane capacitance, and \tilde{I}_j is the sum of the respective ion currents

$$\begin{aligned} \tilde{I}_{Ca}^f &= g_{Ca}^f \tilde{m}_i^3 \tilde{h} (V - V_{Ca}), & \tilde{I}_{Ca}^s &= g_{Ca}^s \tilde{x}_{Ca} (V - V_{Ca}), \\ \tilde{I}_{K1} &= g_{K1} \tilde{n}^4 (V - V_{K1}), & \tilde{I}_{Ca-K} &= \frac{g_{Ca-K}^f [\text{Ca}_i^{2+}](V - V_{Ca})}{0.5 + [\text{Ca}_i^{2+}]}, \\ \tilde{I}_{Cl} &= g_{Cl} (V - V_{Cl}). \end{aligned} \quad (8)$$

Here V_{Ca}, V_{K1}, V_{Cl} are the reversal potentials, and $g_{Ca}^f, g_{Ca}^s, g_{K1}, g_{Ca-K}, g_{Cl}$ are the maximal conductances for the ion currents, $\tilde{m}, \tilde{h}, \tilde{n}$ and \tilde{x}_{Ca} are dynamic variables given by

$$\begin{aligned} \tilde{m}_i &= \frac{\tilde{\alpha}_m}{\tilde{\alpha}_m + \tilde{\beta}_m}, & \tilde{\lambda} \tilde{h} \frac{d\tilde{h}}{dt} &= \tilde{\alpha}_h (1 - \tilde{h}) - \tilde{\beta}_h \tilde{h}, \\ \tilde{\lambda} \tilde{h} \frac{d\tilde{n}}{dt} &= \tilde{\alpha}_n (1 - \tilde{n}) - \tilde{\beta}_n \tilde{n}, \\ \tilde{\lambda} \tau_{x_{Ca}} \frac{d\tilde{x}_{Ca}}{dt} &= \frac{1}{\exp(-0.15(V + 50))} - \tilde{x}_{Ca}, \\ \tilde{\lambda} \frac{d[\text{Ca}_i^{2+}]}{dt} &= \wp_{Ca} \tilde{x}_{Ca} (V_{Ca} - V) - [\text{Ca}_i^{2+}]. \end{aligned} \quad (9)$$

Here the activation $\tilde{\alpha}_y$ and deactivation $\tilde{\beta}_y$ ($y = \tilde{m}, \tilde{h}, \tilde{n}$) parameters of ion channels satisfy the empirical relations

$$\begin{aligned} \tilde{\alpha}_m &= \frac{0.1(50 - \tilde{V})}{\exp(5 - 0.1\tilde{V}) - 1}, & \tilde{\beta}_m &= 4 \exp \frac{(25 - \tilde{V})}{18}, \\ \tilde{\alpha}_h &= 0.07 \exp \frac{(25 - 0.1\tilde{V})}{20}, & \tilde{\beta}_h &= \frac{1}{1 + \exp(5.5 - 0.1\tilde{V})}, \\ \tilde{\alpha}_n &= \frac{0.01(55 - \tilde{V})}{\exp(5.5 - 0.1\tilde{V}) - 1}, & \tilde{\beta}_n &= 0.125 \exp \frac{(45 - \tilde{V})}{80}, \end{aligned} \quad (10)$$

where $\tilde{V} = (127V + 8265)/105$, $\tau_{x_{Ca}}$ is the time constant, \wp_{Ca} is the parameter referring to the dynamics of Ca^{2+} channels, \tilde{h} is a numerical constant.



The evolution of L- and T-type Ca^{2+} - channels depends on the wave of depolarization, V^s , and is defined by

$$g_{Ca}^s(t) = [\delta(V) + (\lambda(t) - 1)](\max g_{Ca}^s), \quad (11)$$

$$g_{Ca}^f(t) = (\lambda(t) - 1)g_{Ca}^f,$$

where

$$\lambda(t) \geq 1.0, \quad \delta(V) = \begin{cases} 1, & \text{for } V \geq V_p^s \\ 0, & \text{otherwise} \end{cases}.$$

Here V_p^s is the threshold value for V^s .

The propagation of the wave of excitation V^s is described by

$$C_m \frac{dV^s}{dt} = \frac{d_m}{R_s} \frac{\partial}{\partial \alpha} \left(\lambda(\alpha) \frac{\partial V^s}{\partial \alpha} \right) - (I_{Na} + I_{K2} + I_{Cl}), \quad (12)$$

where d_m is the diameter, R_s is the specific resistance of the fasciculus, and

$$I_{Na} = g_{Na} \hat{m}^3 \hat{h} (V^s - V_{Na})$$

$$I_{K2} = g_{K2} \hat{n}^4 (V^s - V_{K2})$$

$$I_{Cl} = g_{Cl} (V^s - V_{Cl}). \quad (13)$$

Here g_{Na}, g_{K2}, g_{Cl} are the maximal conductances, and V_{Na}, V_{K2}, V_{Cl} are the reversal potentials of $\text{Na}^+, \text{K}^+,$ and Cl^- membrane currents, respectively. The dynamics of the variables $\hat{m}, \hat{h}, \hat{n}$ are described by

$$\frac{d\hat{m}}{dt} = \hat{\alpha}_m (1 - \hat{m}) - \hat{\beta}_m \hat{m}, \quad \frac{d\hat{h}}{dt} = \hat{\alpha}_h (1 - \hat{h}) - \hat{\beta}_h \hat{h}, \quad \frac{d\hat{n}}{dt} = \hat{\alpha}_n (1 - \hat{n}) - \hat{\beta}_n \hat{n} \quad (14)$$

with the activation $\hat{\alpha}_y$ and deactivation $\hat{\beta}_y$ ($y = \hat{m}, \hat{h}, \hat{n}$) parameters given by

$$\hat{\alpha}_m = \frac{0.005(V^s - V_m)}{\exp 0.1(V^s - V_m) - 1}, \quad \hat{\beta}_m = 0.2 \exp \frac{(V^s + V_m)}{38},$$

$$\hat{\alpha}_h = 0.014 \exp \frac{-(V_h + V^s)}{20}, \quad \hat{\beta}_h = \frac{0.2}{1 + \exp 0.2(V_h - V^s)}, \quad (15)$$



$$\hat{\alpha}_n = \frac{0.006(V^s - V_n)}{\exp 0.1(V^s - V_n) - 1}, \quad \hat{\beta}_n = 0.75 \exp(V_n - V^s).$$

Here V_m, V_h, V_n are the reversal potentials for activation and inactivation of Na^+ and K_{v2}^+ ion currents of the myometrium.

In the following numerical experiments we assume that at the initial moment of time the functional unit is in unexcitable state

$$V^s(\alpha, 0) = 0, \quad v(\alpha, 0) = 0, \quad [\text{Ca}_i^{2+}] = [\text{Ca}_i^{2+}]^0, \quad (16)$$

$$\hat{m} = \hat{m}_\infty, \quad \hat{h} = \hat{h}_\infty, \quad \hat{n} = \hat{n}_\infty, \quad \tilde{h} = \tilde{h}_\infty, \quad \tilde{n} = \tilde{n}_\infty, \quad \tilde{x}_{Ca} = \tilde{x}_{Ca}^\infty.$$

It is activated by a series of discharges of action potentials by an intrinsic pace-maker cell

$$V^s(0, t) = \begin{cases} 0, & 0 < t < t^d \\ V^s, & 0 < t < t^d \\ 0, & t \geq t^d \end{cases}, \quad V^s(0, t) = V(t), \quad (17)$$

The ends of the myofiber are clamped and remain unexcitable throughout

$$V^s(0, t) = V^s(L, t) = 0, \quad v(0, t) = v(L, t) = 0. \quad (18)$$

Eqs. (4)–(15), initial and boundary conditions (16) –(18) constitute the mathematical formulation of the model of the electromechanical activity of the myometrial fasciculus. It describes:

- i) self oscillatory behavior and/or myoelectrical activity induced by discharges of a “pacemaker” cell;
- ii) generation and propagation of the wave of depolarization along the myofiber;
- iii) coupling of spatially distributed oscillators;
- iv) generation of action potentials;
- v) dynamics of the cytosolic Ca^{2+} transients;
- vi) active and passive force generation;
- vii) deformation of the fasciculus and the following excitation of the cell membrane with contractions.

The governing system of equations was solved numerically using *ABS Technologies*© software.

3 Results of numerical simulations

3.1 Physiological condition

The resting membrane potential of the fasciculus is $V^r = -59$ mV. Continuous fluctuations at low rate and amplitudes of the L-type -0.08 nA, T-type $\text{Ca}^{2+} - 0.48$ nA, respectively, an outward $\text{K}^+ - 0.03$ nA, the $\text{BK}_{Ca} - 0.62$ nA, and the small chloride -0.04 nA currents result in oscillations of the membrane potential



V known as slow waves. Their frequency, $\nu = 0.02$ Hz, and the amplitude, $V = 27$ mV, remain constant. The maximum rate of depolarization is calculated 9 mV/s and of repolarization -7.5 mV/s.

The slow wave induces the flux of Ca^{2+} ions inside the cell at a rate of 0.057 $\mu\text{M/s}$. There is a 20 sec time delay in the intracellular calcium transients as compared to the wave of depolarization. Free cytosolic calcium at max $[\text{Ca}^{2+}] = 0.44$ μM activates the contractile protein system with the production of spontaneous contractions, $T^a = 13.6$ mN/cm (Fig. 1). They follow in phase and time the dynamics of calcium oscillations and are normally preceded by slow waves.

High frequency discharges of an intrinsic pacemaker initiate high magnitude ion currents: $\tilde{I}_{Ca}^s = 0.4$, $\tilde{I}_{Ca}^f = 0.51$, $\tilde{I}_{K1} = 0.2$, $\tilde{I}_{Ca-K} = 1.0$, and $\tilde{I}_{Cl} = 0.5$ (nA), and the generation of action potentials of amplitudes $38 \div 45$ mV at a frequency of 2.7 Hz. A concomitant rise in intracellular calcium to 0.51 μM causes the

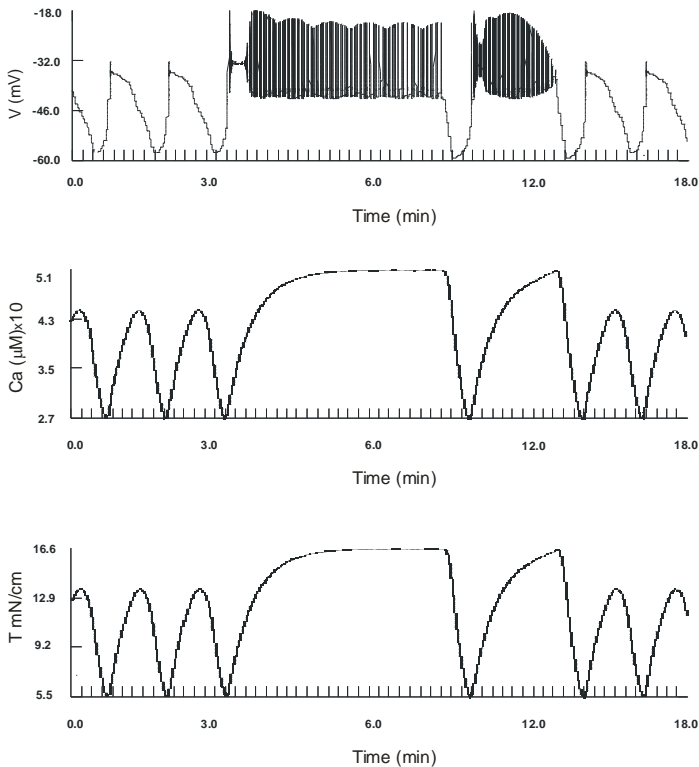


Figure 1: Dynamics of changes of the ion currents, membrane potential, cytosolic calcium and total force in the pregnant fasciculus at rest and during excitation.

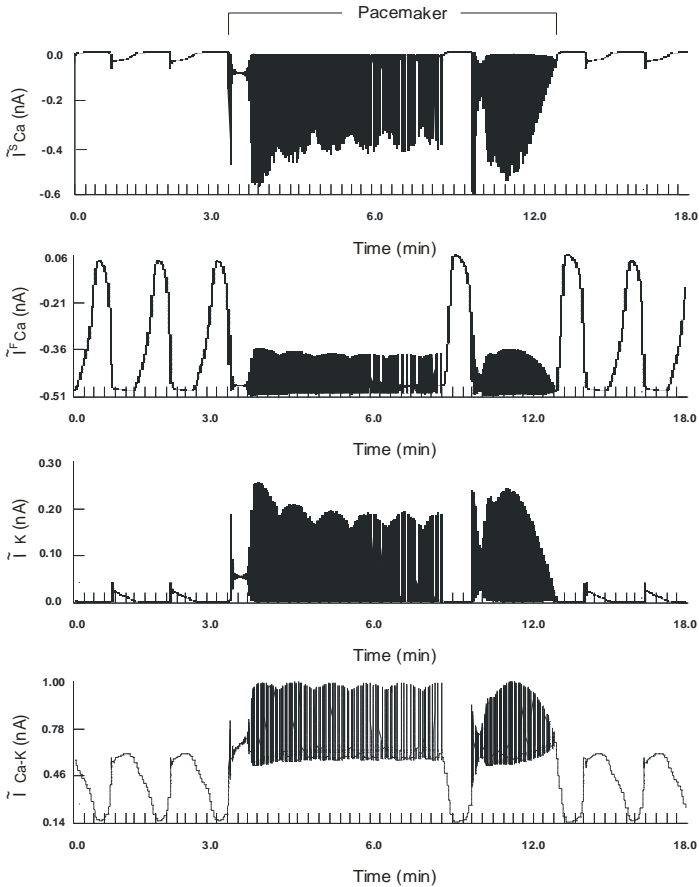


Figure 1: (Continued).

development of active force, 16.6 mN/cm. Upon the termination of electrical discharges the myofiber returns to its unexcited state.

3.2 Changes in Ca_0^{2+}

A gradual increase in the extracellular calcium leads to depolarization of the membrane. Concentrations of Ca_0^{2+} 3-5 times normal causes the up-shift of the resting potential to $V^r = -34$ mV and -31 mV, respectively. This is associated with the exponential rise in free cytosolic calcium to $0.72 \mu\text{M}$. The myometrium undergoes tonic contraction, $T^a = 23.75$ mN/cm.

A concurrent electrical stimulation of the myofiber evokes ion currents, $\tilde{I}_{Ca}^s = 1.3$; $\tilde{I}_{Ca}^f = 0.61$; $\tilde{I}_{K1} = 0.62$, $\tilde{I}_{Ca-K} = 1.63$, $\tilde{I}_{Cl} = 1.89$ (nA), and a transient production of a burst of high frequency, $\nu = 6$ Hz, action potentials of amplitude 53 mV. The T-Ca²⁺ current provides the main influx of intracellular calcium during which a maximum of 0.62 μ M is recorded. The fasciculus generates the active force, $T^a = 20.7$ mN/cm. The reversal of Ca₀²⁺ to its physiological level brings the myofiber to its original electromechanical activity.

Slow wave oscillations cease in a calcium free environment. The fasciculus becomes hyperpolarized at the constant level, $V = -50$ mV. The concentration of intracellular calcium decreases to 0.1 μ M and is insufficient to sustain mechanical contractions. The myofiber remains relaxed.

3.3 Changes in K₀⁺

A two-fold increase in the concentration of extracellular potassium depolarizes the membrane, $V^r = -30$ mV, and abolishes slow waves. The ion currents display a constant dynamics: $\tilde{I}_{Ca}^s = 0.04$; $\tilde{I}_{Ca}^f = 0.48$; $\tilde{I}_{K1} = 0.42$; $\tilde{I}_{Ca-K} = 0.51$ (nA). L- and T-Ca²⁺ currents contribute equally to the rise in [Ca²⁺] to 0.5 μ M and the contraction of the myometrium, $T^a = 15$ mN/cm.

The following four-fold increase in K₀⁺ further depolarizes the membrane, $V^r = -20$ mV. The intensity of the K⁺ current increases to 0.52 nA with a concomitant attenuation of the respective currents: $\tilde{I}_{Ca}^s = 0.032$; $\tilde{I}_{Ca}^f = 0.39$ and $\tilde{I}_{Ca-K} = 0.14$ (nA). There is an exponential decline in [Ca²⁺] to 0.44 μ M and in the intensity of force, $T^a = 13.6$ mN/cm.

A superimposed electrical excitation leads to a burst of high amplitude, $V = 30$ mV, and frequency, $\nu = 7.3$ Hz, action potentials. The intracellular calcium content rises to 0.52 μ M, and the fasciculus produces the active force of 16.8 mN/cm.

A simultaneous elevation in K₀⁺ and Ca₀²⁺ stabilizes the membrane potential at -18 mV. The intracellular [Ca²⁺] = 0.65 μ M triggers a strong contraction of the myofiber, max $T^a = 21.8$ mN/cm.

A gradual reduction of [K₀⁺] hyperpolarizes the fasciculus, $V^r = -70$ and -88 (mV). The slow wave amplitude and frequency increase to 40 mV, $\nu = 0.032$ Hz and 58 mV, $\nu = 0.037$ Hz. Concurrent multiple discharges of a pacemaker evoke the production of spikes of an average amplitude of 60 mV at a frequency of ~ 6 Hz. There is a weakening of the calcium influx, max [Ca²⁺] = 0.25 and



0.18 (μM), and tension, $T^a = 4.5$ and 2.2 (mN/cm). Interestingly, the electrical stimulation further reduces the strength of contraction, $T^a = 1.1$ (mN/cm). The duration of contractions also decreases.

4 Conclusion

The knowledge of electromechanical behaviour of the myometrium is crucial for the integration of motor functions into a biologically plausible biomechanical model of the pregnant uterus. However, because of the paucity of experimental data it is impossible to provide a comprehensive quantitative analysis of the validity, accuracy and applicability of the above results. Qualitative comparison to *in vivo* and *in vitro* recordings of electromechanical activity of the pregnant human myometrial tissue demonstrates a satisfactory correlation with the numerical results.

References

- [1] Vauge, C., Carbonne, B., Papiernik, E. and Ferré, F. (2000). A mathematical model of uterine dynamics and its application to human parturition. *Acta Biotheoretica*, 48, pp. 95-105, 2000
- [2] Bursztyn, L., Eytan, O., Jaffa, A.J. & Elad, D. Mathematical model of excitation-contraction in a uterine smooth muscle cell. *American Journal of Physiology, Cell Physiology* 292, pp. C1816-C1829, 2007
- [3] Young, R. & Hession, R. Three-dimensional structure of the smooth muscle in the term-pregnant human uterus. *Obstetrics & Gynecology*, 93(1), pp. 94-99, 1999
- [4] Garfield R. E. & Maner, W. L. Physiology of electrical activity of uterine contractions. *Seminars on Cell Developmental Biology*, 18(3) pp. 289-295, 2007



Inverse dynamic model of the pupil muscle plant in the simulation of response to sound, stimuli and hippus

E. Suaste Gómez & H. Reyes Cruz

Centro de Investigación y de Estudios Avanzados del Instituto Politécnico Nacional/Depto. Ingeniería eléctrica Sección Bioelectrónica, México

Abstract

The model developed by Usui and Hirata was used to simulate the pupil response to a light stimulus based on autonomic nervous activity, such as sympathetic and parasympathetic activity. This model was recreated in SIMULINK finding that it did not consider the limitations of the pupil in frequency which Stark was reported. The pupil acts as a lowpass filter with a cut-off frequency of 1.5 Hz approximately. These conditions are generated by the unidirectional rate sensitivities. Then, considering this fact, the original model by placing the output of the lowpass filter of -20 dB/decade was modified, which there certain changes are regarding the response of the model by filtering high frequencies, and a delay by the filter.

To obtain the pupil dynamic response induced by sound stimulation, the hippus and flickering of practice mode was using conventional (NTSC) and high speed videoculography thus, to determine sympathetic and parasympathetic activity, in order to recreate such behaviour the Hirata-Usui model was used with a few modification.

Keywords: pupil dynamic, Hirata-Usui's model, autonomic nervous.

1 Introduction

For several years the eye has been an organ of great interest to study, given that it can communicate with the environment by getting information of all kinds, from the fact finding food, to travel without suffering from accidents, getting away from everything that may affect, to name a few. Hence the importance of this is to carry out our daily chores.



The autonomic nervous system (ANS) controls some functions of the eye such as pupil diameter. The pupillary dynamics is used as a non-invasive tool in the study of the ANS [1, 2].

Hence, the interest of using the Hirata-Usui's model, where the first part recreates the model, then we make changes that we consider relevant to the model and finally observed the ability of the model to recreate the dynamic of the pupil to the sound stimulus, hippus and blinking.

In the present chapter uses the reflection of fight/flight [1, 2] or also known as fight/flight response as a means to activate the ANS and obtain the activity of it through the pupillary area. For that purpose, sound stimuli are sent to the person during the study, which would cause thereby activating startle fight/flight response by the ANS.

On the other hand, there is the phenomenon of hippus [3], where the pupil moves even if they receive a stimulus of light, a phenomenon that way considering the innervations by the ANS in the pupil, can be attributed to fact that there is an unbalance by the sympathetic and parasympathetic system.

A response was analyzed but was behaving as the pupil to a flicker, which are thrown over the controls and processes of the pupil to light, however can provide information on pupillary dynamics and activity of ANS.

Finally, seen such processes simulated by a Hirata-Usui model in which you can use the sympathetic and parasympathetic activity to obtain thereby the dynamics of the pupil to react when each of the stimuli described above.

2 Hirata-Usui model

The model was designed considering the innervations of ANS in muscles that governing the pupil diameter, the sphincter and dilator and based on the physiological experimental results describing the behaviour of these muscles in terms of its viscoelasticity and tension generated. Elasticity, viscosity and tension of muscle were described by the following equations:

Elasticity:

$$P_p = \begin{cases} a(x - l_0)^4 + b(x - l_0)^2, & x \geq l_0 \\ 0, & x < l_0 \end{cases} \quad (1)$$

where a and b are constants, and l_0 is the muscle length at the rest.

Viscosity:

$$P_v = \begin{cases} D_+ \frac{dx}{dt}, & \frac{dx}{dt} \geq 0 \\ D_- \frac{dx}{dt}, & \frac{dx}{dt} < 0 \end{cases} \quad (2)$$

where D_+ and D_- are viscous coefficients at the phase of stretch and release, respectively.

Tension:

$$P_a = g(t)p_a(x) \quad (3)$$

$$p_a(x) = \begin{cases} P_0 - c(x - L_0)^2, & P_0 \geq c(x - L_0)^2 \\ 0, & P_0 < c(x - L_0)^2 \end{cases} \quad (4)$$



$$g(t) = g_{stat} + \hat{g}(t) \tag{5}$$

$$g_{stat} = \gamma E_{stat} \tag{6}$$

$$\frac{d^2 \hat{g}(t)}{dt^2} + (2\alpha + \beta) \frac{d\hat{g}(t)}{dt} + \alpha(\alpha + \beta)\hat{g}(t) = \beta \hat{E}(t - t_D) \tag{7}$$

where c and γ are constants. L_0 is the muscle length at which the maximum active tension P_0 is produced α and β are the time constants of the off and on-slope of the isometric twitch response, respectively $g(t)$ and $p_a(x)$ are inputs dependent and muscle length dependent terms of active tension, respectively g_{stat} is a DC part of $g(t)$, while $\hat{g}(t)$ represents a AC part t_D is the delay time of response [4, 5].

To obtain the full model was necessary to combine the action of the dilator and sphincter according to the structure of the pupil. Hirata and Usui simplified the two dimensional plant structures into the one dimensional push-pull structure as it showed in Figure 1.

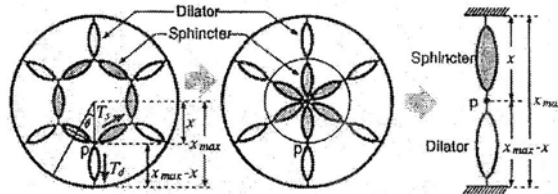


Figure 1: Mechanical model used by Hirata and Usui.

Finally, the model is a differential equations system with 13 equations that simulate the behaviour of the pupil depending on the sympathetic and parasympathetic activity, which has been used to simulate the behaviour to a light stimulus, in our case was used to simulate the pupil response to sound stimulation, the hippus and flicker.

3 Fight/flight response

Anxiety is a response to danger or threat. Scientifically, the short-term anxiety response is called fight/flight. This is because, all effects are designed to fight, or avoid danger. Therefore, the first purpose of anxiety is to protect the human body [1, 6].

The response of fight/flight generates immediate changes in the body that allow the man a better and quicker response to danger. These changes are mediated by activation of the sympathetic nervous system and these effects are [1, 6]:

1. Pupils dilate, to increase the visual field.
2. Heart rate and force of contraction is increased and blood pressure also increases their values to carry nutrients and energy to the muscles preparing them for flight.



3. Blood vessels in the skin and viscera constrict.
4. The remainder of the blood vessels dilate. This causes a faster blood flow of blood to the dilated blood vessels in skeletal muscle, heart and lungs, organs involved in combating the danger.
5. Rapid breathing and deeper and bronchioles dilate to allow more rapid movement of air into and out of the lungs.
6. The contractions of blood sugar increases as the liver glycogen are converted to glucose for energy.
7. The core of the adrenal glands is stimulated to produce adrenaline and noradrenaline, hormones that enhance and prolong sympathetic effects.
8. The processes are not essential to meet stressful situations are inhibited. For example, the muscular movements of the digestive tract and secretions are slower or even come to a halt.

4 Development

For comprise the different pupil responses mentioned (flicker, hippus and sound stimuli), were performed an experimental tests on patients while on its right eye was recording by a high speed camera (DALSA) brand. Infrared and a super-bright white LED were used to illuminate the eye-recorded. Infrared LEDs were employed to find a greater contrast between the pupil and the iris in the images taken from high speed camera to improve digital processing. The white LED current was controlled to supply a constant luminance of 1000 cd/m^2 to prevent the pupil reach the maximum contraction or expansion.

To obtain hippus and sound stimuli pupil responses, the test starting after the patient had been looking the camera for 1 min, then during 10 seconds of capture in which patient was informed that he should not blink. In random manner, sound stimulus is sent to him. The stimulus was a mixture of two different types of music or pure tones. Sound stimulus triggers the fight/flight response and thereby activates the autonomic nervous system [1] which is observed as changes in the pupil diameter. After 10 s, the patient was informed that can do a flick if he wants, in that moment begin the part of the test to record flicker response. This process avoid the patient were forced to flick that could disturb results. Recorded images were processed in Vision Builder 3.5 to obtain corresponding pupilograms. Relationship adjusts between the pixels and distances were done before each test to ensure that images distances corresponded to real proportions. Afterwards, pupillary area was framing and filtering to smooth the pupil. Changes in brightness and contrast were also made to highlight the pupil. Finally a thresholding process to detect the pupil had been taken place to calculate pupillary area. This method is shown in Figure 2.

Experimental result from previous test lead up to the model developed in SIMULINK of Matlab as shown on Figure 3 [5].



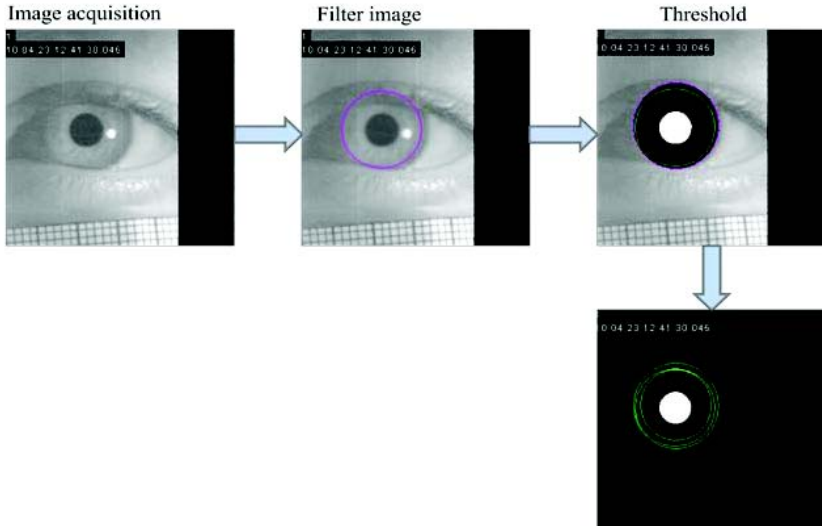


Figure 2: Steps for image processing.

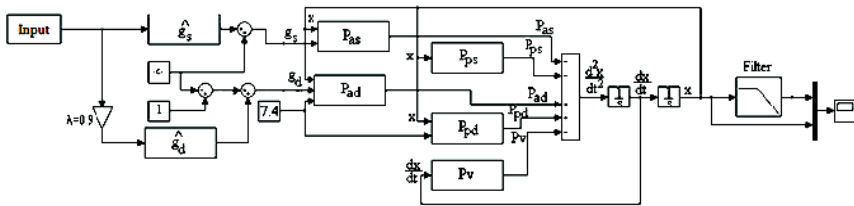


Figure 3: Development of Hirata's model in SIMULINK.

5 Results

The pupillary response that was observed in sound stimuli test was a reduction followed by a dilation of the pupil area which can be seen in Figure 4.

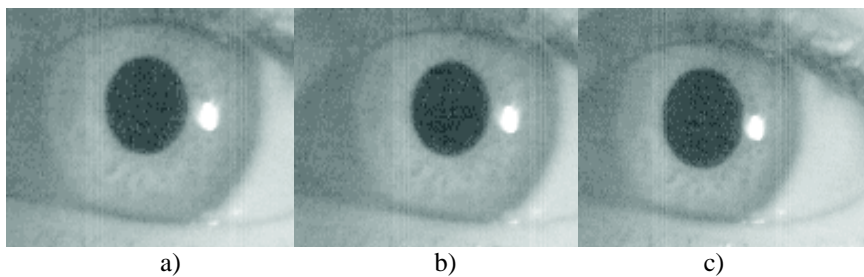


Figure 4: Images of the pupil response. a) Before of the sound stimuli b) when send the sound stimuli c) After of the sound stimuli.

The complete response is shown in Figure 5. From Figure 5, high level pulse corresponds to the activation of the stimulus, low state corresponds to the stage where the person listens to quiet music, the edge where the pulse changes its state corresponds to the part in which person listening to loud music and filtered in this case 600 Hz, resonant frequency of the membrane charge to convert sound into electrical impulses for registration and processing in the nervous system, from that point as there is observed a decrease in area pupil, followed by a further increase in the same.

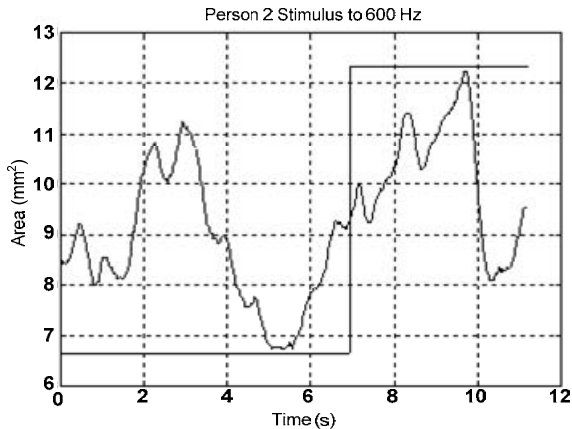


Figure 5: Example of pupil dynamics for acoustic stimulation.

On the other side can also observe the presence of hippus by the absence of one steady pupillary area. Otherwise, we had not been expected pupil response in the time period where the subject listen to classical music, but the pupil response in the subject to it were very similar when he listening to loud music. In the case of pure tones similar behaviour was observed where the stimulus before and after hippus note tone, a contraction followed by expansion.

In the case of hippus there is a particular behaviour cause for the same person there are different answers as shown in Figure 6 where being the same person without a change in the pupillary dynamics.

Referring to flicker was observed behaviour similar to that displayed in the sound stimuli, i.e. a contraction shortly before and after the blink here is a dilation of the pupil.

Once developed the model of Hirata-Usui, a filter was added to the exit of the purpose of simulating the frequency limitations of the eye, considering a cut-off frequency of 1.5 Hz [7, 8]. Since the filter implemented in the model simulation was continued to the previous answers which resulted in the graphs shown in Figure 7.

In Figure 7a) noted as the model is able to recreate the pupillary response to sound stimulation as can be seen in the first instance the contraction and dilation after her.

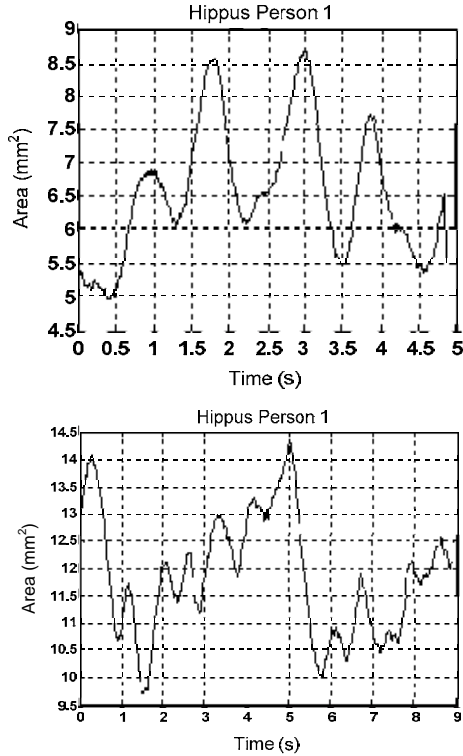


Figure 6: Hippus of the same person and under the same light illumination intensity.

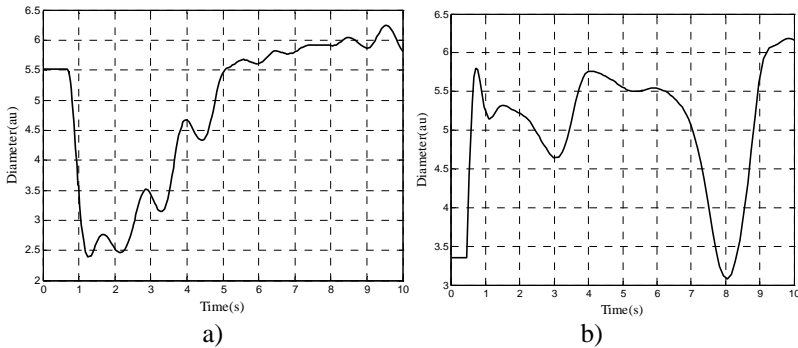


Figure 7: Simulation of: a) the pupillary response to a sound stimulus and a flicker noise b) hippus.

In the case of hippus, to get a random process that results in a random response were used different input to determine the ability of the model. The input was a sine wave with amplitude of 1 V and frequency of 0.5 Hz which

obviously not contain the random part sought. Other entries were random numbers considering a mean 0 and variance 1 and the other entire was white noise, both generated by the software Matlab. These last two options will provide a better result to generate the random process.

6 Conclusions

There is a response from the pupil to sound stimuli which can see initially as a contraction. The first instance activates the parasympathetic system, however after this, there is a noticeable expansion of greater magnitude by activating the sympathetic system. In some cases the contraction is not noticeable, but in all cases the dilation is noted that for all sound stimuli will activate the parasympathetic system. The response observed during blinking is similar to the response of sound stimuli.

The hippus shows us all the time the pupil is moving because they never achieved complete stability by the sympathetic and parasympathetic system.

Hirata and Usui's model is able to simulate the eye's response to stimuli above, the adjustment itself to keep the simulation within the frequency range of the human eye.

References

- [1] G. J. Tortora & S. R. Grabowski; *Anatomy and physiology principles*, Oxford, Mexico, 1998.
- [2] Arthur C. Guyton, John E. Hall; *Medical physiology tractate*, McGraw Hill, Mexico, 2002.
- [3] Clynes M., The non-linear biological dynamics of unidirectional rate sensitivity illustrated by analog computer analysis, pupillary reflex to light and sound, and heart rate behavior, *Annals New York Academy of Sciences*, Vol. 98, pp. 806–845, 1962.
- [4] Hirata Y. & Usui S., Nonlinear dynamical model for human papillary muscle plant, *IEICE J77-DII*, pp. 170-180, 1994.
- [5] Usui S. and Hirata Y., Estimation of autonomic nervous activity using the inverse dynamic model of the pupil muscle plant, *Annals of Biomedical Engineering*, vol. 23, pp. 375-387, 1995.
- [6] Villamar L. & Suaste E., High velocity videoculography to determination of the pupil dynamics *Tenth Symposium on Medical Physics-2008*, edited by G.H. Corral and L. M. Montaña, AIP Conf. Proc. 1032, Melville, New York, pp. 276-279, 2008.
- [7] Stark L., *Neurological controls systems studies in bioengineering*, University of California Berkeley, Plenum press, New York, 1968.
- [8] Clynes M., Unidirectional rate sensitivity: a biocybernetic law of reflex and humorai, systems as physiologic channels of control and communication, *Annals New York Academy of Sciences*, vol. 92, pp. 946–969, 1961.



Section 12
Orthopaedics and
bone mechanics

This page intentionally left blank

Identification of landmarks on lower limb joint from CT images for kinematics studies: a totally semi-automatic procedure

M. Giorgi¹, B. Innocenti², L. Labey², A. Audenino¹ & C. Bignardi¹

¹*Department of Mechanics, Politecnico di Torino, Italy*

²*European Centre for Knee Research, Smith & Nephew, Belgium*

Abstract

The identification of an accurate, reliable and patient specific coordinate system for a bone is fundamental to analyzing the kinematics of a human joint. The accuracy in the localization of anatomical landmarks of joint surfaces is extremely important because even a small variation in their positions could induce a high variation in the definition of anatomical axes and further on the kinematics output. The aim of this study was to develop and validate a semi-automatic, accurate, and reproducible routine able to identify the position of anatomical landmarks on joint surfaces. This routine, starting from a CT of a femoral bone, used as input, is able to identify semi-automatically the femoral head and the medial and lateral distal femoral condyles. Moreover, it allows the identification of the following anatomical landmarks: the Femoral Hip Center (FHC), the Femoral Medial Epicondyle (FME) and the Femoral Lateral Epicondyle (FLE). From these points a standard coordinate system of the femur is univocally determined according to previous literature. Compared to other commercial processes, extensively used in this field, one peculiarity of this routine is that it is not necessary to generate a 3D model of the joint in order to define the anatomical landmarks. Usually, to generate a 3D lower limb model, with the commercial process, 4 to 5 hours are needed, with this approach we can significantly reduce this time. To validate the routine we analyzed ten different CTs of lower limbs. Two different tests were performed. The first test was performed to verify and check the output geometry of the model; the second test was aimed at estimating the repeatability and reproducibility of the procedure. For such a task five different operators identified for each model the three anatomical landmarks, three times each. The Intra-Class Correlation coefficient



(ICC) values (intra and inter) obtained for the landmarks were always higher than 0.996. Comparing the results obtained with this routine with the results obtained using largely used commercial software we found a significant reduction of the error as regards the evaluation of landmarks in terms of inter and intra-observer variability. For example, in the worst condition, on the identification of the femoral lateral condyle point (FLE), the same operator found an average and maximum distance between the real point and the landmark found of respectively 3.5 and 8.8 mm with the use of the commercial software and of respectively 0.8 and 0.9 mm with the use of our routine.

Keywords: knee joint, landmarks, CT images.

1 Introduction

An anatomical landmark is a biologically-meaningful point in an organism. Usually experts define anatomical points to ensure their correspondences within the same species. They provide the link between the CT scan data and surgically relevant reference that can be found by visualization or palpation during the operation. Anatomical landmarks are also important to define anatomical axes. Advances in medical imaging technology have made it possible to routinely acquire high-resolution, 3D images of human anatomy and function using a variety of imaging modalities. The ability to inspect structural relationships in three dimensions and the ever-improving quality of the images have largely increased the number of clinical applications in various medical disciplines, such as neurology, cardiology, surgery, and radiotherapy, that benefit from 3D image information to support critical medical decisions [1]. The use of 3D image processing and visualization techniques allows direct inspection of the scene in three dimensions and facilitates extracting quantitative information. The identification of an accurate, reliable and patient specific coordinate system for a bone [2] and the realization of 3D femoral bone models are fundamental, together with the tibia and patella models, to perform kinematics studies necessary to understand the functioning of an arthroprosthesis.

According to a literature work [3], the aim of this study was to develop a semi-automatic, accurate, reliable and reproducible routine able to generate 3D models and to identify the position of anatomical landmarks on joint surfaces.

2 Materials and methods

Ten unpaired fresh frozen amputated lower limbs were analyzed using a helical CT scan. The specimens were obtained from Caucasian cadavers aged between 78 and 87 years old when they deceased. The images were obtained at 120 kV and 450 mA, with a slice thickness of 1.25 mm and a pitch of 0.5 mm/rev.

Starting from the CT of femoral bones, used as input, a semi-automatic routine able to identify the position of anatomical landmarks on joint surfaces was developed. The routine was implemented using MATLAB (MathWorks – Natick, Massachusetts, USA) [4] and is divided into four main blocks:



1. Image enhancement through a semi-automatic procedure based on thresholding technique;
2. generation of nodes, surfaces, volumes constituting the 3D model through a fully automated procedure;
3. viewing and saving the model through a fully automated procedure;
4. identification of anatomical landmarks.

The first block is based on the threshold technique [5, 6] and it allows us to prepare all the images for the next step. As is known, the threshold technique is useful to convert images in B/W because, given that the values of the pixels that make up the CT images in grayscale are all between 0 and 1 where 0 corresponds to white and 1 corresponds to black, with this technique we can choose a threshold value that establishes which pixels become white and which will become black. If we set a threshold value equal to 0.6 it means that all pixels with values above 0.6 will become 1 so black. In this block the inputs are the original-CT images and, using the threshold technique, we obtain as output the same images converted in B/W and cleaned of all the parts that we do not need for our aim, fig. 1.

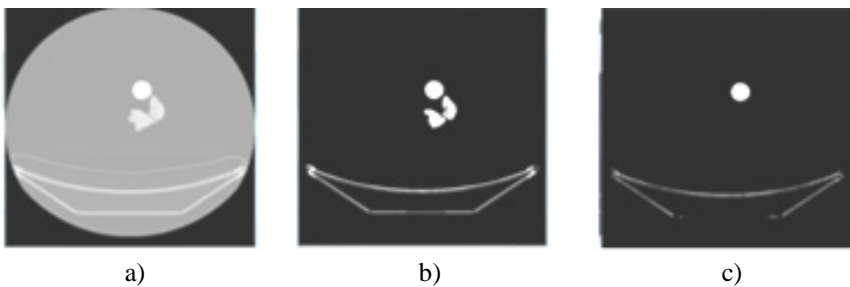


Figure 1: a) original CT, b) 0.72 threshold value, c) 0.76 threshold value.

The second block generates a volumetric mesh creating the nodes, surfaces and volumes constituting the 3D model of the bone section under consideration. This procedure is fully automated and is based on a tetrahedral method for the mesh generation [7]. This block takes as input the images prepared on the block before and provides as output all the nodes, elements, and faces constituting the model.

The third block has been implemented to view and save the 3D model; this routine gives the user, two different kinds of visualization; the Mesh Plot and the Point Cloud Plot, illustrated in figure 2. The Mesh Plot function is used to obtain a quick view of the model surface realized to check if there are some anomalies in the model's geometry. The Point Cloud Plot function is used to visualize all the points that constitute the model and for that is a computationally heavy view.

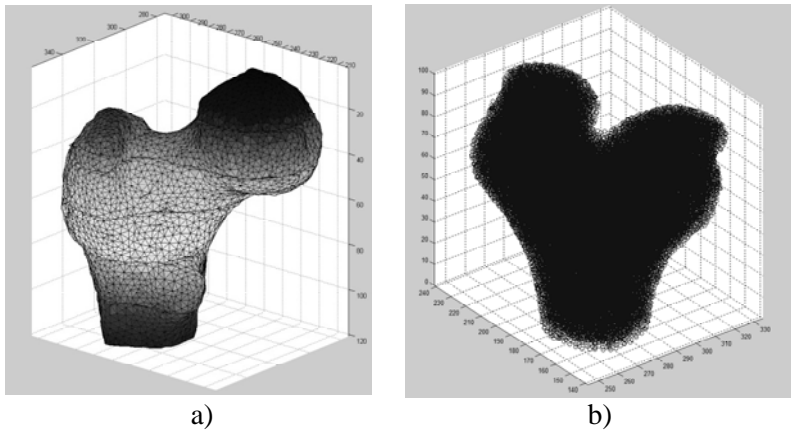


Figure 2: a) Mesh plot, b) point cloud plot.

The anatomical landmarks of the femur identified by the semi-automatic routine are:

- Femoral Hip Center (FHC), defined as the center of best-fit sphere to the head of the femur (fig. 3).
- Femoral Medial Epicondyle (FME), defined as the most anterior and distal osseous prominence over the medial aspect of the medial femoral condyle (fig. 4) [8].
- Femoral Lateral Epicondyle (FLE), defined as the most anterior and distal osseous prominence over the lateral aspect of the lateral femoral condyle (fig. 5) [9].

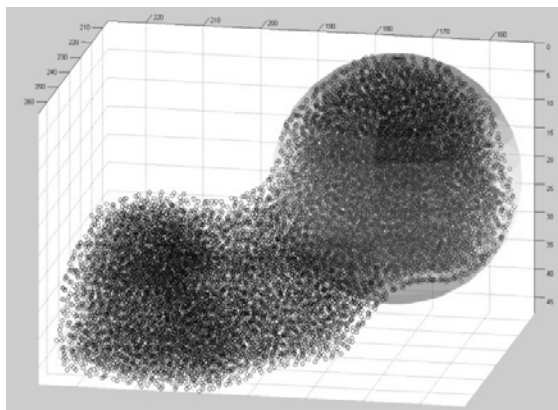


Figure 3: Example of best-fit sphere to the head of the femur.

We chose these anatomical landmarks because, according to literature, from these points a standard coordinate system of the femur is univocally determinate [3].

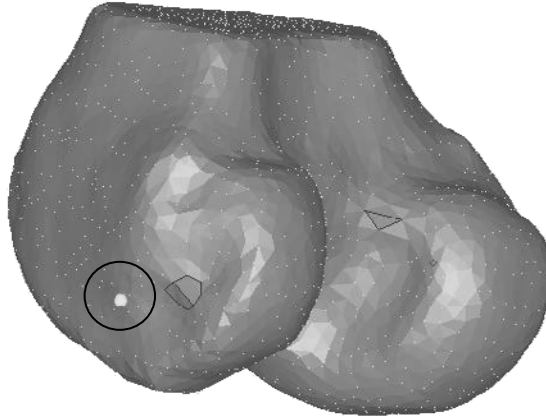


Figure 4: Example of FME found with our routine.

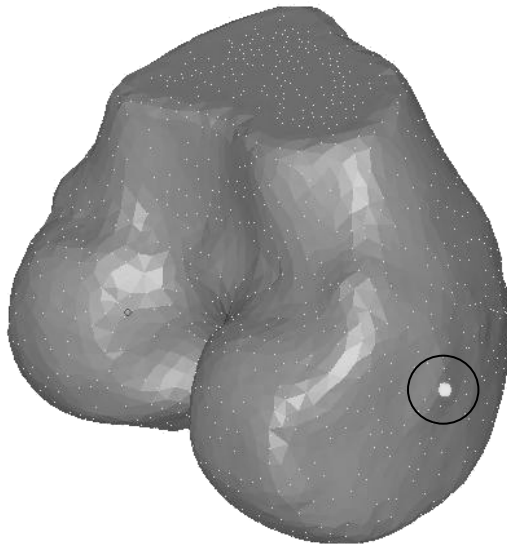


Figure 5: Example of FLE found with our routine.

To validate the routine developed, we decided to perform two different types of tests. The first test was performed to verify if the shape of the 3D models obtained corresponds with those of reference obtained using a spread commercial software (Mimics 11.02 and its MedCAD module (Materialise, Haasrode, Belgium)). For this test we generated with our routine 5 different 3D models, 2 complete femur bones and 3 partial femurs. This test consisted exclusively of a visual comparison between the models, sufficient to check for any anomalies in the geometry of the models (fig. 6).

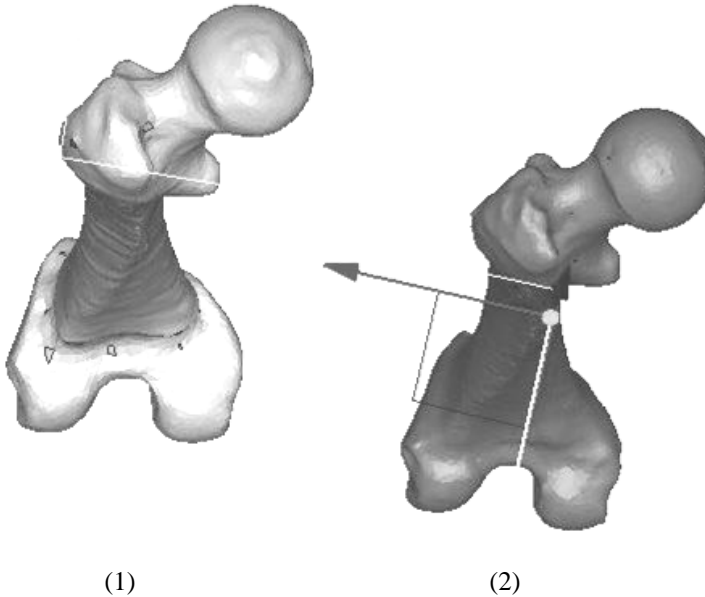


Figure 6: Comparison between the model obtained with our routine (1) and the one obtained with the spread commercial software of comparison (2).

The second test consisted of the generation of other 6 different 3D models of the femur on which 5 different users (only one expert in the localization of the anatomical landmarks) identified, for each model, the 3 anatomical landmarks 3 times each. We have obtained by each operator a set of 9 coordinates for each lower limb. Analyzing 6 lower limbs, we got a set of 54 coordinates for operator, being 5 the number of operators we got in total a set of 270 coordinates.

All these sets of coordinates have been used to estimate the intra-class correlation coefficient (ICC) and the inter-observer variability as the distance between the reference position of a landmark, obtained from the commercial software, to the observer position of the landmark [10]. The ICC describes how strongly units in the same group resemble each other. One prominent application is the assessment of consistency or reproducibility of quantitative measurements made by different observers measuring the same quantity. By definition, the ICC is evaluated according to the following formulation:

$$ICC = \frac{\sigma_b^2}{\sigma^2}$$

where the total variance of measurements by different observers is σ^2 on different subjects, and the variance between subjects is σ_b^2 . ICC values range from 0 to 1, indicating better agreement as the value approaches 1. An ICC value higher than 0.75 should indicate excellent agreement.

3 Results

As shown in table 1, the ICC values for all defined landmarks fall in a range between 0.996 and 0.999, showing a good agreement between the observers and an excellent reliability for all the landmarks.

Table 1: ICC-Intra observer values and ICC-class values.

Landmarks	ICC-IntraObserverValues	ICC-ClassValues
Femoral Hip Center (FHC)	0.9964	0.9961
Femoral Medial Epicondyle (FME)	0.9999	0.9996
Femoral Lateral Epicondyle (FLE)	0.9999	0.9996

The inter observer variability for each landmark is shown in figures 7, 8, and 9 and the results are compared with the other obtained using the commercial software. The observed mean values and maximum values are displayed separately.

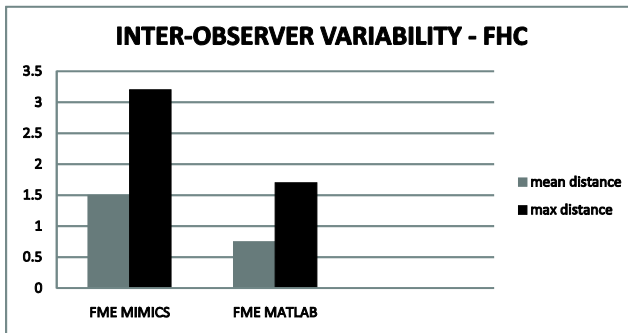


Figure 7: Comparison of the FHC inter-observer variability between the commercial software and our routine, shown as mean value and maximum value [mm].

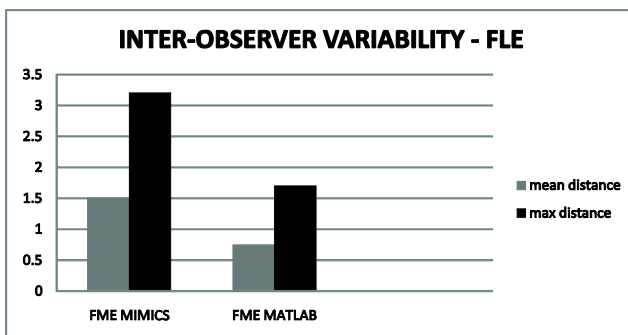


Figure 8: Comparison of the FLE inter-observer variability between the commercial software and our routine, shown as mean value and maximum value [mm].

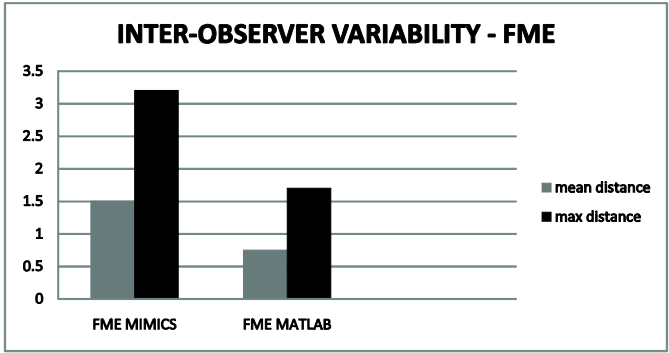


Figure 9: Comparison of the FME inter-observer variability between the commercial process and our routine, shown as mean value and maximum value [mm].

The average of the inter-observer variability obtained using our routine is 0.4 mm (range: 0.19 mm–0.6 mm) and we can see, comparing this result with the one obtained using the commercial software, where the average is 1.9 (range: 0.3 mm–3.5 mm), that the mean value is greatly improved moving from 1.9 mm to 0.4 mm.

Maximum inter-observer variability is also improved moving from values between 0.8 mm to 8.6 mm for the commercial software to values between 0.38 mm to 1.8 mm for our routine.

Tables 2, 3 and 4, show the average and the standard deviation of the distance from observed position to the reference position that each operator (Op) found for each landmark on all femur models.

Table 2: Average distance and standard deviation of the central femoral head.

FEMORAL HIP CENTER – AVERAGE DISTANCE (mm)						
Average distance	Femur1	Femur2	Femur3	Femur4	Femur5	Femur6
Op.1	290.6	338.9	443.2	349.7	463	285.2
Op.2	289,9	337,9	443,5	349,3	462,3	285
Op.3	290	338	443,4	349,5	462,8	285,1
Op.4	290,2	337,6	443,6	349,7	462,5	285,2
Op.5	290,	337,6	443,5	349,3	462,8	285,2
CENTRAL FEMORAL HEAD – STANDARD DEVIATION						
Standard deviation	Femur1	Femur2	Femur3	Femur4	Femur5	Femur6
Op.1	0	0	0	0	0	0
Op.2	0	0,04	0	0,3	0,1	0,04
Op.3	0,1	0,1	0,1	0,3	0,1	0,07
Op.4	0,1	0	0	0	0	0,07
Op.5	0	0	0	0	0	0

Table 3: Average distance and standard deviation of the condylar lateral point.

CONDYLAR LATERAL POINT – AVERAGE DISTANCE (mm)						
Average distance	Femur1	Femur2	Femur3	Femur4	Femur5	Femur6
Op.1	559,9	598,8	643,9	560,6	674	558,9
Op.2	560,5	598,8	642,4	559,8	673,4	558,9
Op.3	560,5	598,8	643,9	560,9	673	559,7
Op.4	557,6	600,4	643,9	560,9	673	559,7
Op.5	559,9	600,1	643,2	559,4	671,8	557
CONDYLAR LATERAL POINT – STANDARD DEVIATION						
Standard deviation	Femur1	Femur2	Femur3	Femur4	Femur5	Femur6
Op.1	0,5	0,4	0	0,4	0,2	0,2
Op.2	0	0,4	0	0	0,1	0,2
Op.3	0	0,4	0	0,4	0,5	0,01
Op.4	0,5	0,4	0	0,4	0,5	0,01
Op.5	0	0,4	2,3	0,2	0	0

Table 4: Average distance and standard deviation of the condylar medial point.

CONDYLAR MEDIAL POINT – AVERAGE DISTANCE (mm)						
Average distance	Femur1	Femur2	Femur3	Femur4	Femur5	Femur6
Op.1	520,9	604,9	688,8	595,5	631,9	523,8
Op.2	521,7	604,9	687,8	594,2	632,3	523,8
Op.3	519,6	604,9	688,8	594,5	631,5	523,6
Op.4	522,8	603,7	688,4	595,3	631,5	525,1
Op.5	523,4	604,2	688	594,3	632,1	529,6
CONDYLAR MEDIAL POINT – STANDARD DEVIATION						
Standard deviation	Femur1	Femur2	Femur3	Femur4	Femur5	Femur6
Op.1	2,1	0	0	0	0,5	0,4
Op.2	1,7	0	0,2	0,6	0,3	0,4
Op.3	0	0	0	0,1	0,2	0
Op.4	1	0,2	0,3	0,5	0,5	0,9
Op.5	0	0,7	0,3	0,2	0,5	0

4 Conclusions

The aim of this study was to develop a semi-automatic, accurate, and reproducible routine able to generate 3D models and able to identify the position of anatomical landmarks on joint surfaces starting from a CT of a femoral bone.

From the results obtained, it is possible to see that there was a clear improvement in reproducibility and repeatability anatomical landmarks identification compared with the ones obtained with commercial software. The average of the inter-observer variability obtained using our routine is 0.4 mm (range: 0.19 mm–0.6 mm) and we can see, comparing this result with the one obtained using the commercial software, where the average is 1.9 (range: 0.3 mm–3.5 mm), that the mean value is greatly improved moving from 1.9 mm to 0.4 mm.



We can say that, using this developed and validated routine we are able to improve the quality of this landmarks identification.

For the moment this routine is able to work only with CT images, that is why we are already thinking to improve it for the MRI images in order to make our routine more complete and useful.

References

- [1] Duncan, J.C. & Ayache, N., Medical image analysis: progress over two decades and the challenges ahead. *Journal IEEE Transactions on Pattern Analysis and Machine Intelligence*, **22(1)**, pp. 85-106, 2000.
- [2] Schafer R.C., *Clinical Biomechanics – Musculoskeletal Actions and Reaction*, Williams & Wilkins: Baltimore, pp.711-717, 1991.
- [3] Victor J., Van Doninck D., Labey L., Innocenti B., Parizel P.M. & Bellemans J., How precise can bony landmarks be determined on CT scan of the knee. *Knee*, **16(5)**, pp. 358-365, 2009.
- [4] <http://www.mathworks.com/matlabcentral/>
- [5] Wong K.P., Medical image segmentation: methods and applications in functional imaging (Chapter 3). *Handbook of Biomedical Image Analysis, Volume II: Segmentation Models Part B*, ed.J.S. Suri, D.L. Wilson and S. Laxminarayan. SpringerLink, pp. 11-182, 2005.
- [6] Dougherty G., *Digital Image Processing for Medical Applications*, Cambridge University Press, 2009.
- [7] <http://iso2mesh.sourceforge.net/cgi-bin/index.cgi>
- [8] Pérez-Pérez A., Alesan A. & Roca L., Measurement error: inter- and intraobserver variability. an empiric study. *International Journal of Anthropology*, **5(2)**, pp. 129-135, 1990.
- [9] LaPrade R.F., Ly T.V., Wentorf F.A. & Engebretsen L., The posterolateral attachments of the knee: a qualitative and quantitative morphologic analysis of the fibular collateral ligament, popliteus tendon, popliteofibular ligament, and lateral gastrocnemius tendon. *The American Journal of Sports Medicine*, **31**, pp.854-860, 2003.
- [10] Bland J.M. & Altman D.G., Measurement error. *BMJ*, **313**, pp. 744-753, 1996.



The effect of time on the results of children's spine examinations

M. Takács¹, E. Rudner¹ & R. M. Kiss²

¹*Department of Orthopaedics MÁV Hospital, Szolnok, Hungary*

²*Department of Structures,*

Budapest University of Technology and Economics, Hungary

Abstract

With the ultrasound based motion analyzing system it is possible to measure the shape of the spine not only of adults but of children too. Ultrasound based spine measurements play an important role in diagnosing spine deformities in children (bad posture, flat back, scoliosis), as well as after diagnosis, during conservative follow-up. Previous research has already justified the accuracy and reliability of the ultrasound-based analysis method. However, the question of whether the short length of time between the two tests had an effect on the results was not examined and answered by previous research. The aim of our study was to clarify whether the shape of the spine changes significantly during the 15 minute-long examination of healthy children and children with various spine deformities. We measured children aged 8 to 11, of whom 115 were healthy (52 boys, 63 girls, average age: 8.7 ± 1.2 years, average weight: 35.8 ± 9.7 kg, average height: 138.8 ± 9.05 cm), 56 had bad posture (21 boys, 35 girls, average age: 8.4 ± 1.26 years, average weight: 30.6 ± 7.67 kg, average height: 137.0 ± 9.18 cm), 6 had flat backs (3 boys, 3 girls, average age: 8.3 ± 1.21 years, average weight: 31.2 ± 6.43 kg, average height: 138.2 ± 7.88 cm) and 20 had scoliosis (10 boys, 10 girls, average age: 9.3 ± 1.13 years, average weight: 32.9 ± 4.95 kg, average height: 134.4 ± 6.76 cm). At first we described the shape of the spine in a straight posture using the Zebris ultrasound motion analysis system, then we repeated the procedure after 15 minutes. When we compared the results it turned out that the differences were significantly smaller than the standard deviations (0.1-2.7 at kyphosis, 0.3-7.4 at lordosis, 0.1-1.1 at sagittal inclination, and finally 0.1-1.0 at frontal inclination). The correlation was strong at kyphosis and lordosis (0.77-0.98), however, it was low at frontal and sagittal inclination (0.18-



0.54). So the time lapse (15 minutes) between the measurements did not affect the results at lordosis and khyphosis. At inclination, however, it is essential to pay extra attention to the postures.

Keywords: bad posture, spine, spine curvature, schoolchildren, ultrasound-based system, Zebris, posture.

1 Introduction

Medical literature describes children's low back pain and back pain as multi-factorial problems and it is also states that further research is needed to reveal their medical background. The influencing factors are complex and in many cases their effects on each other are not clarified. Out of these effects we have to emphasize the body mass index, the mobility and flexibility of muscles and joints, muscular strength, low endurance and asymmetric development of trunk flexors and extensors and the effects of the disturbance of muscle balance [1]. Also sports, furniture in schools, heavy school backpacks, psychological factors and smoking – although in different ways – play an important role in children's spine development [2, 3,]. In most cases, children's back pain experiences are mild and do not affect their daily life [1, 4, 5]. Literary data prove that child and puberty back pain significantly increases the probability of puberty and adulthood back pain and other structural spine problems [1, 6, 7]. Besides prevention, it is necessary to lay emphasis on the screening test and follow-up of childhood spine deformities because many times they are symptomless. When they are discovered late the efficiency of the cure decreases and the probability of different spine problems during adulthood increases. The main cause of spine problems without structural deformities in adulthood is simple bad posture in childhood and puberty. One of the causes of simple bad posture is that in children between the ages of 6 to 10 the muscular development required often lags behind the quick height increase. Diagnosis at an early stage followed by appropriate correction is the first step towards prevention. It can be stated that the survey of children's postures and conditions is essential for the prevention of structural and non-structural spine deformities. The application of screening tests makes it possible to establish an exact diagnosis and to start a conservative therapy at the earliest moment. Beside the well-known diagnostic methods, those measurements are also necessary to be used which can be used in short intervals and allow continuous control of the effects of treatment. In order to measure the state of the children it is necessary to use devices that do not burden their organism with X-ray radiation and produce reliable results [8, 9]. The examination method, just like the causes of the clinical picture, has to be complex. Traditional physical orthopaedic examination, definition of the spine's shape in different postures and the measurement of muscle activity by skin-surface EMG during motion are parts of the whole examination method [8, 10, 11]. In our research we lay emphasis on the examination of the shape of the spine. The simplest way to define the shape of the spine is to make a full X-ray image in a standing and natural position. From the photographs, lumbar lordosis, thoracal kyphosis and the scoliosis of the spine curvature can be defined. On the



images the position of vertebrae can also be identified [12]. The major drawback of this test is that the X-ray load is high so it is proposed to be repeated only annually in spine deformities, while with posture abnormalities it is not suggested for follow-up. Ultrasound based systems are used in a wide range at adults, but we may find some examples in children's tests too [1, 12, 13]. The accuracy and reliability of the examination method can be controlled by comparing it to the results of other measuring devices (e.g. X-ray images) by test-retest examination, but the effect of test time is also important [1, 13–15]. In children, the effect of time on measurement results is unambiguous, particularly in children with weak musculature (e.g. bad posture). In adults it can be neglected because adults' musculature and ability to concentrate enable them to keep the required position (habitual straight position) for a longer time. When the test is performed by Zebris ultrasound-based measurement it is necessary to specify the reference points of comparison, and then to define the shape of the spine. These tests take 10–12 minutes. The aim of the study was to clarify whether the time of the examination influences the results of measurements in different childhood spine deformities. 8 to 11 year old healthy, bad postured, flat backed (dorsum planum) children and children with scoliosis participated in the study. We defined the shape of the spine in straight position by the Zebris ultrasound-based motion analysis system; then, 15 minutes later, we repeated the measurements. The tests were performed by the same examiners on both occasions.

2 Material and method

2.1 Subjects

The subjects of our research were children from two primary schools in Szolnok. One class was chosen from each grade from the first to the fourth grade. The classes were music and art specific. We did not choose sports classes. Parents received the necessary information both orally and in a written form before they filled in their consent. At the end, 195 children were measured, including 84 boys and 111 girls. Based on the results of the previous orthopaedic tests, the children were divided into four groups.

The first group contained 115 healthy children, including 52 boys and 63 girls, with an average age of 8.7 ± 1.2 years, an average weight of 35.8 ± 9.7 kg and an average height of 138.8 ± 9.05 cm. 56 children with bad posture were put into the second group (21 boys, 35 girls) where the average age was 8.4 ± 1.26 years, the average weight 30.6 ± 7.67 kg and the average height 137.0 ± 9.18 cm. 6 children had flat back (3 boys, 3 girls, average age: 8.3 ± 1.21 years, average weight: 31.2 ± 6.43 kg, average height: 138.2 ± 7.88 cm) while the last 20 had scoliosis (10 boys, 10 girls, average age: 9.3 ± 1.13 years, average weight: 32.9 ± 4.95 kg, average height: 134.4 ± 6.76 cm).



2.2 Measurement method

The measurements took place at the Biomechanical Laboratory of MÁV Hospital in Szolnok using a Zebris CMS-HS ultrasound based motion analysing system (Zebris, Isny, Germany). The system and its software, WinSpine (version number: CMS-HS10 2.2, Zebris, Isny Germany) are capable of defining the shape of the spine in different postures. The head containing three ultrasound transmitters was placed behind the person examined and a triplet with three receivers was fixed on the properly palpable bone of the pelvis. Its role was to correct the motions of the pelvis during the measurement. The shape of the spine was determined by a pointer containing two microphones (Figure 1.). The system measured the propagation time of ultrasound, wherefrom the distance between the transmitter and the receiver was calculated. The positions in space (the space coordinates) of the three transmitters of the ultrasound head were known; from them, with the method of triangulation, the software calculated the space coordinates that determined the shape of the spine [8].

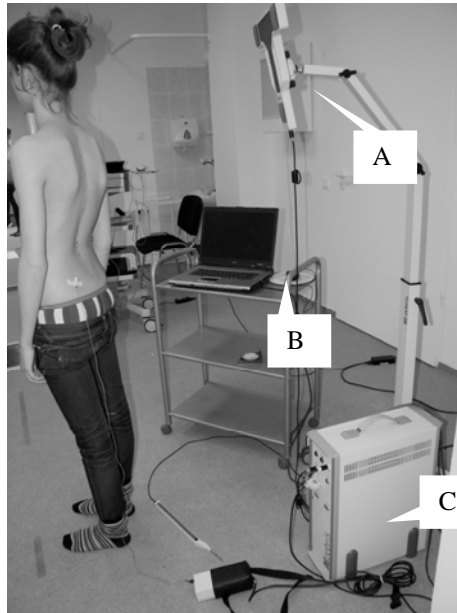


Figure 1: Measurement arrangement. Head (A) is placed behind the person examined. The triplet (B) is on the pelvis. With the pointer (C) the shape of the spine can be determined.

Measurement process (Figure 2.)

1. Positioning the child with his/her back to the measuring head.
2. The child is standing in a naturally straight position, then we call his/her attention to the correct posture, which is to let the shoulders down, press the shoulder blades back, and near to each other. The head, the pelvis, and

- the straight line which goes through the shoulders, the knees and the ankles are fitted onto an imaginary axis crossing the body centre line.
3. Designation of the global coordinate system.
 4. Designation of the anatomical points necessary to define the shape of the spine: right and left shoulder, right and left angle of scapula, right and left spina iliaca posterior superior, point of Th.12-L1
 5. Determining the shape of the spine in straight position three times.
 6. The child stands in this position for 15 minutes.
 7. After 15 minutes we determine the shape of the spine again in straight position.

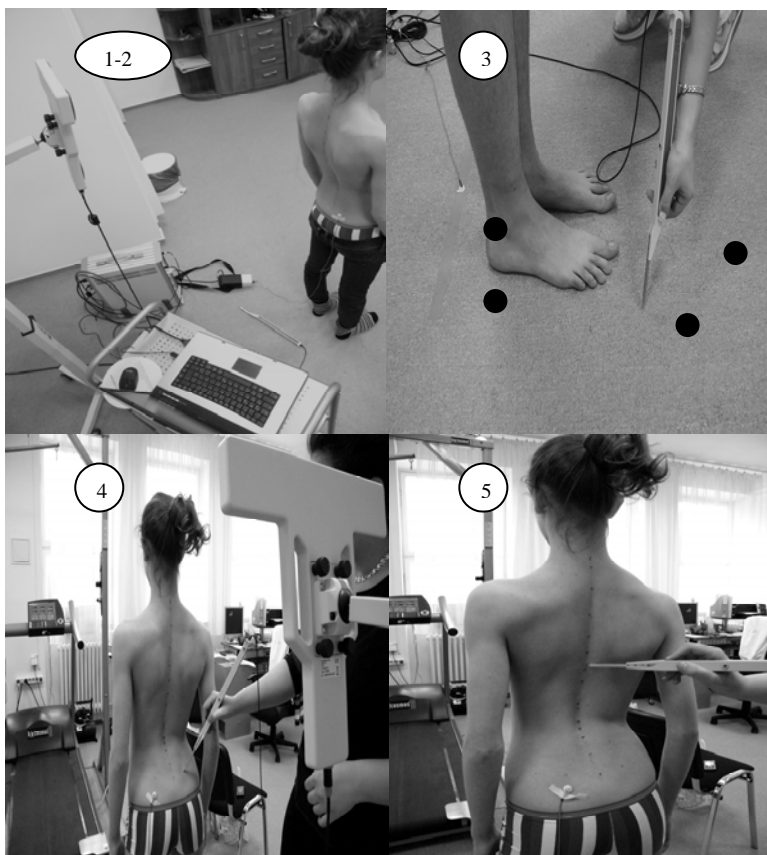


Figure 2: Measurement process.

With both measurements the software (WinSpine) calculates from the measurement results the angle the vertebrae form with each other, the degree of thoracal kyphosis, lumbar lordosis, scoliosis, and frontal and sagittal inclination. For the brief test-retest examination we do not use the data on vertebrae; we only

define the degree of thoracal kyphosis, lumbar lordosis, scoliosis, and frontal and sagittal inclination.

2.3 Statistical analysis

We measured the effect of duration by comparing the results of the test to the results of the retest made shortly after the test. For the analysis we determined the means of the groups at both measurements, the real and the absolute scales of the differences between the two measurements, and we also made a one-sample t-test. The iteration reliability examination was supplemented by the determination of the steepness of the regression line of the two measurement results and by the determination of the Pearson correlation coefficient [16].

Table 1: Mean±standard deviation of spine curvatures (groups: healthy, bad postured, with scoliosis and with dorsum planum) at test and re-test. For calculating differences we subtracted the retest values from the test values.

	healthy				bad posture			
	kyphosis	lordosis	sagittal inclination	frontal inclination	kyphosis	lordosis	sagittal inclination	frontal inclination
test	41.9±7.1	32.5±11.2	2.5±1.8	1.2±0.9	42.5±7.9	30.4±13.2	3.1±2.1	1.5±1.2
re-test	41.9±8.1	32.3±11.8	2.6±2.0	1.3±1.1	42.8±7.4	29.7±14.2	3.0±2.6	1.7±1.3
real difference	0.1±5.3	0.3±7.7	-0.1±1.9	0.0±1.1	-0.4±4.8	0.9±8.2	0.1±2.3	-0.2±0.9
absolute difference	3.7±3.7	4.8±6.1	1.4±1.4	0.8±0.7	3.8±2.9	5.8±5.9	1.6±1.7	0.7±0.6
	dorsum planum				scoliosis			
	kyphosis	lordosis	sagittal inclination	frontal inclination	kyphosis	lordosis	sagittal inclination	frontal inclination
test	35.8±6.6	16.0±10.7	3.4±2.6	1.2±1.0	37.1±6.9	30.7±11.2	3.4±2.0	1.3±1.1
re-test	38.5±7.2	23.4±14.1	2.3±2.3	1.1±0.8	38.6±6.3	31.1±13.4	2.5±1.9	1.5±1.0
real difference	-2.7±1.5	-7.4±5.6	1.1±1.1	0.1±1.1	-1.5±4.4	-0.4±6.5	0.9±1.1	-0.2±1.2
absolute difference	2.7±1.5	7.4±5.6	1.2±1.0	0.8±0.7	3.4±3.0	5.1±3.9	1.1±0.9	1.0±0.6

3 Results

Table 1 shows the mean and standard deviation figures calculated from the measurement results of the test and the retest performed 15 minutes later. The real and absolute scale of the error can be seen. The results indicate that the mean values of the errors are smaller than the standard deviations of the measurement



results. The biggest real and absolute errors were yielded at the lordosis values of children with dorsum planum (7.4 ± 5.6 degrees).

With each group we defined the significance of differences between measurement results (p) (Table 2.) and we can say that no significant differences were found. The next step of statistical analysis was to calculate the correlation coefficient (r) and the steepness of the straight line fitted on the data (m) (Table 2.).

Table 2: Correlation coefficient between the test and retest values (r), the regression line (m) and the significance values between the groups (p).

	healthy				bad posture			
	kyphosis	lordosis	sagittal inclination	frontal inclination	kyphosis	lordosis	sagittal inclination	frontal inclination
r	0.77	0.78	0.48	0.46	0.84	0.82	0.54	0.73
m	0.88	0.82	0.51	0.54	0.76	0.88	0.69	0.80
p	0.462865	0.450093	0.358221	0.373164	0.400377	0.361592	0.440134	0.260105
	dorsum planum				scoliosis			
	kyphosis	lordosis	sagittal inclination	frontal inclination	kyphosis	lordosis	sagittal inclination	frontal inclination
r	0.98	0.93	0.90	0.18	0.78	0.88	0.84	0.36
m	1.07	1.23	0.80	0.14	0.71	1.05	0.80	0.33
p	0.257076	0.16553	0.226076	0.437279	0.242599	0.456956	0.084477	0.280707

The results indicate that the lordosis and kyphosis values show a good accord among the groups, because the correlation coefficient is high (range: 0.98–0.77), which is also proved by the steepness of the regression line values close to one (range: 0.82–1.23).

The correlation between results at sagittal and frontal inclination is only average (healthy, bad postured) or weak at frontal inclination (flat back, scoliosis) (0.18–0.36). These data are also verified by the steepness because its values are far from one (0.14–0.33).

4 Discussion

Previous studies examined the reliability of the measurement method, which means that the tests were repeated after a longer interval (1–3 weeks) [13]. The novelty of our examination was that we examined the effect of the time span of the measurement. The question of the research was whether the results of the test correlate with the results of the measurement 15 minutes later. Results indicate that in terms of the degree of kyphosis and lordosis the correlation between the two results is good, which is confirmed by the steepness value of the regression line which is close to one. These results are similar to those derived from the examination of the reliability of the measurement repeated after a long time (1–3 weeks), when adults were examined, but contradict Geldhof's statements,



who examined the children again one week later and got low correlation coefficients. The cause of the contradiction could be that Geldhof and his colleagues measured the natural posture and did not call the children's attention to correct their posture. The reason for the medium or low correlation between the two values determining the position of the median can be that the position of the median and the centre of gravity changes continuously, which is proved by stability tests based on the examination of the position of the centre of gravity. It is known that in children the movement of the weight centre is much bigger than in adults and, on the other hand, the decline of attention is first shown by inclination.

5 Conclusion

The ultrasound-based motion analyzing system is commonly used for determining the shape of the spine in adults, but it is rarely mentioned in medical literature in connection with children's spine examinations. The advantage of the system is that there is no X-ray radiation; it is quick and gives graphic and numerical information about the temporary status of the spine. For daily use it is very important that the positions examined must be standardized and the time of the examination must not influence the results. The statistical analysis of the measurement results of the test-retest indicates that at straight position, when the degree of kyphosis and lordosis is calculated, the time span of the measurement does not influence measurement results. As regards the measurement of inclination, the correct positioning of the posture examined must be checked before each and every measurement.

Acknowledgements

This work is connected to the scientific program of the "Development of quality-oriented and harmonized R+D+I strategy and functional model at BME" project. This project is supported partly by the New Hungary Development Plan (Project ID: TÁMOP-4.2.1/B-09/1/KMR-2010-0002). This work was supported by the Hungarian Scientific Fund T075018.

References

- [1] Geldhof E., Cardon G., Bourdeaudhuij I. D., & Clercq. D. D., Back posture education in elementary schoolchildren: a 2-year follow-up study. *Eur Spine J.* **16**, pp.841-850, 2007.
- [2] Cardon G., & Balagué F., Low back pain prevention's effects in schoolchildren. What is evidence? *Eur Spine J.* **13**, pp. 663-679, 2004.
- [3] Kratenová J., Zejglicová K., Maly M., & Filipová V., Prevalence and risk factors of poor posture in school children in the Czech Republic. *Journal of School Health.* **77**(3), pp.131-137, 2007



- [4] Jones M.A., Stratton G., Reilly T., & Unnithan V.B., Biological risk indicators for recurrent non-specific low back pain in adolescent. *Br J Sports Med* **39**, pp.137-140, 2005.
- [5] Jones M.A., Stratton G., Reilly T., & Unnithan V.B., A school-based survey of recurrent non-specific low back pain prevalence and consequences in children. *Health Educ Res* **19**, pp.284-289, 2004.
- [6] Salminen J.J., Erkintalo M., Laine M., & Pentti J., Low back Pain in the young a prospective 3 year follow-up-study of subjects without low-back-pain. *Spine* **20**, pp.2101-2107, 1995.
- [7] Brattberg G. Do pain problems in young school children persist into early adulthood? A 13-year follow-up. *Eur J Pain* **8**, pp.187-199, 2004
- [8] Zsidai A., & Kocsis L., Ultrasound-based spinal column examination systems. *Facta Universitatis Physical Education and Sport* **1**(8), pp.1-12, 2001.
- [9] Post R.B., & Leferink V.J.M., Spinal Mobility: sagittal range of motion measured with the Spinal Mouse, a new non-invasive device. *Arch Orthop Trauma Surg* **124**, pp.187-192, 2004
- [10] Viola S., Kocsis L., Szőke Gy., Körmendi Z., & Zsidai A., Kinesiological examinations and cutaneous EMG with integrated 3D UH system in adolescent idiopathic scoliosis (type:King1-13) *Orv. Hetilap* **147**, pp.2367-75, 2006.
- [11] Zsidai A. & Kocsis L., Ultrasound measuring diagnostic and muscle activity measuring system for spinal analysis, *Technology and Health Care* **14**, pp.243-250, 2006.
- [12] Asamoah V, Melleriwicz H, Venus J, & Klöckner C., Measuring the surface of the back. Value in diagnosis of spinal diseases. **29**(6), pp.480-489 2000.
- [13] Geldhof, E., Cardon, G., Bourdeaudhuij I. D., Danneels L., Coorevits P., Vanderstraeten G., & Clarcq D.D., Effects of back posture education on elementary schoolchildren's back function. *Eur Spine J*, **16**, pp.829-839, 2007.
- [14] Malmström E.M., Karlberg M., Melander A., & Magnusson M., Zebris Versus Myrin: A Comparative Study between a Three-Dimensional Ultrasound Movement Analysis and an Inclinator/Compass Method; *Spine* **28**, pp.E 433-E440, 2003
- [15] Mannion A. F., Knecht K., Balaban G., Dvorak J., & Grob D, A new skin-surface device for measuring the curvature and global and segmental range of motion of the spine: reliability of measurements and comparison with data review from the literature. *Eur Spine J*. **13**, pp.122-136, 2004.
- [16] Bland MJ., & Altman D.G., Statistical methods for assessing agreement between two methods of clinical measurement. *The Lancet*, **1**, pp.307-310, 1986.



This page intentionally left blank

Section 13
Data acquisition
and analysis

This page intentionally left blank

Association rule derivation for side effects of medical supplies and its application

H. Shiroyama, Y. Zuo & E. Kita

Graduate School of Information Science, Nagoya University, Japan

Abstract

In drug discovery, it is very important to predict the side effect of the drug accurately. The prediction algorithm of the drug side effect is presented in this study. This algorithm is based on the concept of the structure-activity relationship. Firstly, the drug side effects are gathered from the registration of medical products by using text mining. Next, the chemical structure information of the drug is obtained from the PubChem data base. Then, the association rules between the chemical structure and the side effects are defined. The associate rules are applied to the prediction of the side effect of 10 chemical products.

Keywords: drug, side effect, association rule, PubChem, text mining.

1 Introduction

Several drugs (medicines) have been developed every year. While new drugs are very useful for improving illness and injuries, they sometimes have terrible side effects. Therefore, it is very important for the prediction of the drug side effects in the drug discovery.

A new drug discovery is a very time-consuming process. The drug discovery is mainly composed of four steps; basic study, non-medical study, medical study and approval and production. In the basic study, the potential chemical products are developed. In non-medical study, the effect of the products is confirmed in animal experiment and so on. In medical study, the effect of the products is provided for patients and health persons. Since the side effects of the potential products are confirmed in non-medical and medical studies, the drug discovery needs a long time and enormous cost.

Therefore, some researchers have studied the prediction algorithm of the drug side effect before non-medical and medical studies. Ensein et al. used



multi-regression analysis and discriminant analysis for predicting the side effect [1–3]. Moriguchi et al. have developed adaptive least square (ALS) method and Fuzzy ALS method for huge toxicity data discovery [4–6]. Gilles Klopman has developed the system named as “MULTICASE” which is based on the concept of the quantitative structure activity relationship (QSAR) [7, 8].

In this study, the association rules are used for predicting the drug side effect. This algorithm is based on the concept of structure-activity relationship (SAR). Known drug side effects are gathered from the registration of medical products by using the text mining. The chemical structures of drugs are obtained from the PubChem data base. The association rules between the chemical structures and the side effects are defined. The activity of the side effects is evaluated from the association rules. In the numerical example, the present algorithm is applied for predicting six side effects of 10 chemical products.

The remaining part of this paper is organized as follows. The association rule algorithm is shown in section 2. The present algorithm is explained in section 3. In section 4, the algorithm is applied for predicting side effects of 10 chemical products. The conclusions are summarized again in section 5.

2 Association rule

2.1 Definition of association rule

Association rule learning is a popular and well researched method for discovering interesting relations between variables in large databases. It is introduced for discovering regularities between products in large scale transaction data recorded by point-of-sale (POS) systems in supermarkets.

Let $I = \{i_1, i_2, \dots, i_n\}$ be a set of n binary attributes called items. Let $D = \{t_1, t_2, \dots, t_m\}$ be a set of transactions called the database. Each transaction in D has a unique transaction ID and contains a subset of the items in I . A rule is defined as an implication of the form $X \Rightarrow Y$ where $X, Y \subseteq I$ and $X \cap Y = \emptyset$. The itemsets X and Y are called as antecedent and consequent of the rule, respectively.

The support $supp(X)$ of the association rule $X \rightarrow Y$ is defined as the proportion of transactions in the data set which contain the itemsets X and Y .

$$Support = \frac{\sigma(X \cup Y)}{M} \quad (1)$$

where $\sigma(X \cup Y)$ denotes the total number of transactions which contain the itemset X and Y and M the total number of the transactions.

The confidence of the rule is defined as the portion of the transactions containing the itemsets X and Y and the transactions containing the itemset X alone.

$$Confidence = \frac{\sigma(X \cup Y)}{\sigma(X)} = \frac{Support(X \rightarrow Y)}{Support(X)} \quad (2)$$

The association rule is usually described as follows.

$$Antecedent \rightarrow Consequent (Support = \alpha, Confidence = \beta)$$



2.2 A priori algorithm

Total number of the association rules increases exponentially according to the increase of the transactions and itemsets. It is very time-consuming to calculate the support and the confidence. For this purpose, A priori algorithm was used in this study [9] since it can calculate the support and the confidence in the real-time.

3 Side effect evaluation

3.1 Structure-activity relationship

The present algorithm is based on the concept of Structure-Activity Relationship (SAR).

Structure activity relationship (SAR) is the relationship between the chemical or three-dimensional structure of a molecule and its biological activity. The analysis of SAR enables the determination of the chemical groups responsible for evoking a target biological effect in the organism. This allows modification of the effect or the potency of a bioactive compound (typically a drug) by changing its chemical structure.

This method was refined to build mathematical relationships between the chemical structure and the biological activity, known as quantitative structure-activity relationships (QSAR).

3.2 Side effect information

The drug side effect information is gathered from the registration of medical products by using the text mining. In Japan, the drug effect information of 17,000 drugs is distributed as HTML data by Japan Pharmaceutical Information Center (JPIC). The use of the text mining technique extracts the drug side effect from the HTML data of the registration of medical products.

In this study, we will focus on the side effect for liver, kidney and blood and therefore, gather the information on Aspartate aminotransferase (AST) increase, Alanine aminotransferase (ALT) increase, Blood Urea Nitrogen (BUN) increase, Creatinine (CRE) increase, Red Blood Cell (RBC) decrease, and White Blood Cell (WBC) decrease.

3.3 Chemical structure information

The drug chemical structures are obtained from PubChem database [10] as the description of the simplified molecular input line entry specification (SMILES).

PubChem is a database of chemical molecules and their activities against biological assays. The system is maintained by the National Center for Biotechnology Information (NCBI).



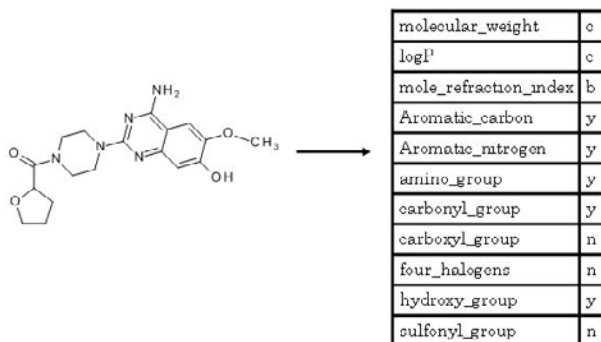


Figure 1: Information of chemical structural formula.

The original SMILES specification was developed in the late 1980s [11]. It has since been modified and extended by others, most notably by Daylight Chemical Information Systems Inc.

We focus on the hydrophobic property (ClogP) and the molar refraction (CMR) of the drug chemical structure. Since the hydrophobic property (ClogP) is one of important indexes for the bioactivity and the bioaccumulation of the drugs, it is the essential factor for QSAR. The molar refraction (CMR) is strongly related to the volume of the molecules and to London dispersive forces that has important effect in drug-receptor interaction.

Once the SMILES information of the drug is obtained through PubChem database, the hydrophobic property (ClogP) and the molar refraction (CMR) of the drug is evaluated through the Bio-Loom [12].

3.4 Algorithm

The association rules are defined as follows.

1. The side effects of known drugs are gathered from the registration of medical products by using the text mining.
2. The drug chemical structures are obtained from PubChem database.
3. The association rules are defined from the information of the side effect and chemical structures.
4. The numbers of the antecedent and the consequent of the rules are counted.

The association rules are used for predicting the drug side effect as follows.

1. The itemset of the drug chemical structures is given.
2. The rules conforming the itemset are gathered.
3. The activity evaluation parameter P of the rule set is evaluated.

$$P = \frac{\sum_i^N N2_i}{\sum_i^N N1_i} \quad (3)$$

where $N1_i$ and $N2_i$ denote total number of items in the antecedent and the consequent of the rules, respectively. N the total number of the rules conforming the itemset.

4. It is shown that the side effect with the parameter $P > P_s$ is active. The threshold P_s is specified as $P_s = 0.6$ in the following numerical examples.

Table 1: Association rule.

ID	rule	Ant.	Con.
1	Aromatic_carbon = y carbonyl_group = y → AST=y	33	29
2	Aromatic_carbon = y carbonyl_group = y hydroxy_group = y → AST=y	33	29
3	mole_refraction_index = c carbonyl_group = n hydroxy_group = y → AST=y	38	31
4	molecular_weight = c carbonyl_group = y hydroxy_group = y → AST=y	39	31
5	Aromatic_nitrogen = y carbonyl_group = n → AST=y	40	31
6	Aromatic_carbon = y Aromatic_nitrogen = y carbonyl_group = y → AST=y	40	31
7	molecular_weight = b carboxyl_group = y → AST=y	30	23
8	molecular_weight = b carbonyl_group = n hydroxy_group = y → AST=y	30	23
9	logP=a Aromatic_carbon = y carbonyl_group = n → AST=y	37	28
10	mole_refraction_index = c carbonyl_group = y → AST=y	56	42



A simple example is shown in Fig. 1 and Table 1. As shown in Fig. 1, the chemical structures are obtained from the drug information through the PubChem. The association rules conforming the itemset are listed (Table 1). The association rules with ID = 1, 2, 4 and 6 conform the chemical structure of the unknown drug.

Table 2: Prediction result of drug ID = 1 to 5.

ID	Side effect	Confidence	Prediction	Actual
1	AST increase	0.654952803	active	active
	ALT increase	0.659446587	active	active
	BUN increase	0.549799017	inactive	active
	CRE increase	0.550037249	inactive	active
	RBC decrease	0.565320665	inactive	inactive
	WBC decrease	0.608465608	active	active
2	AST increase	0.591299678	inactive	active
	ALT increase	0.589204945	inactive	active
	BUN increase	0.55704698	inactive	inactive
	CRE increase	0.522154648	inactive	inactive
	RBC decrease	0.583883752	inactive	inactive
	WBC decrease	0.569427527	inactive	active
3	AST increase	0.648256421	active	active
	ALT increase	0.640763463	active	active
	BUN increase	0.55152027	inactive	inactive
	CRE increase	0.541868255	inactive	inactive
	RBC decrease	0.556363636	inactive	inactive
	WBC decrease	0.58747698	inactive	active
4	AST increase	0.624987293	active	active
	ALT increase	0.619428779	active	active
	BUN increase	0.524590164	inactive	active
	CRE increase	0.527687296	inactive	inactive
	RBC decrease	0.566509115	inactive	inactive
	WBC decrease	0.588581024	inactive	inactive
5	AST increase	0.649959724	active	inactive
	ALT increase	0.648337029	active	inactive
	BUN increase	0.55469217	inactive	inactive
	CRE increase	0.541937581	inactive	inactive
	RBC decrease	0.577151335	inactive	inactive
	WBC decrease	0.587978142	inactive	inactive

Therefore, the activity evaluation parameter P is calculated as follows.

$$P = \frac{29 + 29 + 31 + 31}{33 + 33 + 39 + 40} = 0.82 \quad (4)$$

Table 3: Prediction result of drug ID = 6 to 10.

ID	Side effect	Confidence	Prediction	Actual
6	AST increase	0.624987293	active	active
	ALT increase	0.652334657	active	active
	BUN increase	0.547340425	inactive	active
	CRE increase	0.551418981	inactive	active
	RBC decrease	0.565320665	inactive	active
	WBC decrease	0.608465608	active	active
7	AST increase	0.612885386	active	inactive
	ALT increase	0.619428779	active	inactive
	BUN increase	0.524590164	inactive	active
	CRE increase	0.527687296	inactive	inactive
	RBC decrease	0.566509115	inactive	inactive
	WBC decrease	0.588581024	inactive	inactive
8	AST increase	0.630815473	active	active
	ALT increase	0.632175861	active	active
	BUN increase	0.607453416	active	active
	CRE increase	0.553736875	inactive	inactive
	RBC decrease	0.558091286	inactive	inactive
	WBC decrease	0.577898551	inactive	active
9	AST increase	0.645465612	active	active
	ALT increase	0.646773705	active	active
	BUN increase	0.550055006	inactive	active
	CRE increase	0.547775947	inactive	active
	RBC decrease	0.564935065	inactive	inactive
	WBC decrease	0.613981763	active	active
10	AST increase	0.605838524	active	active
	ALT increase	0.605319041	active	active
	BUN increase	0.519916143	inactive	inactive
	CRE increase	0.532163743	inactive	inactive
	RBC decrease	0.561151079	inactive	inactive
	WBC decrease	0.6	active	active



4 Numerical example

The side effects of ten chemical products are predicted by the present algorithm; AST increase, ALT increase, BUN increase, CRE increase, RBC decrease, and WBC decrease. The products are numbered as ID = 1, 2, . . . , and 10, respectively.

When the confidence of the side effect is greater than 0.6, it is concluded that the side effect is active.

The results are shown in Tables 2 and 3. For example, the product ID = 1 is Levofloxacin. In Levofloxacin, five side effects except for RBC decrease are active. Table 2 shows that the present algorithm can predict four out of six side effects accurately. Totally, the prediction accuracy is 66.7%.

5 Conclusion

In the drug discovery, it is very important to predict the side effect of the drug accurately. The prediction algorithm of the drug side effect was described in this paper. The use of text mining gathers the drug side effects from the registration of medical products and then, the chemical structure information of drug is obtained from the PubChem data base. Then, the association rules between the chemical structure and the side effect of the drug are defined.

In numerical example, the present algorithm was applied for predicting six side effects of ten drugs. The results show that the prediction accuracy of the algorithm is 66.7% totally. In this study, the side effects are gathered from the registration of medical products. Since the activity of the side effects depends on the gender, the age, and so on, the registration of medical products does not have enough information. Therefore, we are planning to update the association rule for improving the prediction accuracy.

References

- [1] K. Enslein and P. N. Craig. A toxicity estimation model. *Journal of Environmental Pathology and Toxicology*, 2:115–121, 1978.
- [2] K. Enslein and P. N. Craig. Carcinogenesis: A predictive structure-activity model. *Journal of Toxicology and Environmental Health*, 10:521–530, 1982.
- [3] K. Enslein, T. R. Lander, M. E. Tomb, and W. G. Landis. A structure-activity model. *Teratogenesis, Carcinogenesis, and Mutagenesis*, 9:503–513, 1983.
- [4] I. Moriguchi, S. Hirono, Q. Liu, Y. Matsushita, and T. Nakagawa. Fuzzy adaptive least squares and its use in quantitative structure-activity relationships. *Chemical and Pharmaceutical Bulletin*, 38:3373–3379, 1990.
- [5] I. Moriguchi, S. Hirono, Y. Matsushita, Q. Liu, and I. Nakagome. Fuzzy adaptive least squares applied to structure-activity and structure-toxicity correlations. *Chemical and Pharma-ceutical Bulletin*, 40:930–934, 1992.
- [6] I. Moriguchi, S. Hirono, Q. Liu, and I. Nakagome. Fuzzy adaptive least squares and its application to structure-activity studies. *Quantitative Structure-Activity Relationships*, 11:325–331, 1992.



- [7] Gilles Klopman. Chemical reactivity and the concept of charge- and frontier-controlled reactions. *Journal of the American Chemical Society*, 90(2):223–234, 1968.
- [8] H. S. Rosenkratz and G. Klopman. A structural analysis of the genotoxic and carcinogenic potentials of cyclosporin a. *Muta-genesis*, 7(2):115–118, 1992.
- [9] R. Agrawal and R. Srikant. Fast algorithms for mining association rules in large databases. In *Proceedings of the 20th International Conference on Very Large Data Bases*, pages 487–499, 1994.
- [10] Pubchem. <http://pubchem.ncbi.nlm.nih.gov/>.
- [11] Smiles. <http://www.daylight.com/dayhtml/doc/theory/theory.smiles.html>.
- [12] Bio-loom. <http://www.biobyte.com/bb/prod/bioloom.html>.



This page intentionally left blank

Estimation of biophysical and functional properties of artery walls from pulse wave measured by photoplethysmography

M. Huotari, K. Määttä & J. Kostamovaara
*Department of Electrical and Information Engineering,
Electronics Laboratory, University of Oulu, Finland*

Abstract

Arterial pulse wave analysis in time and frequency domain was carried out to find out biophysical and functional properties of artery walls measured with a photoplethysmographic (PPG) device. Because peripheral arterial disease (PAD) is a fatal problem all over the world, an easy diagnosis method would be needed. It could probably be diagnosed by PPG which is a non-invasive optical technique for detecting the arterial pulse waves. We present a study to characterize and quantify the arterial pulse wave components based on the use of logarithmic normal function (LNF). The measurements were carried out parallel from the index finger and toe tip with healthy subjects. In addition, a second derivative of the PPG signal (SNPPG) was also analyzed. The tests were applied to arterial pulse waves from 11 subjects between 5 and 69 years. The results show good correlation of pulse wave changes as a function of age.

Keywords: arterial stiffness, photoplethysmography, pulse wave analysis, percussion, tidal, dicrotic, pre-ejection wave component.

1 Introduction

Arterial stiffness has been estimated with many different analysis and procedures. One of them is the contour analysis of pulse waves. It has been proposed as a non-invasive means in assessing arterial stiffness in atherosclerosis. Accurate determination of the conventional parameters is usually precluded by changed waveforms in the aged and atherosclerotic objects. In this paper we introduce a new photoplethysmographic (PPG) way to estimate arterial elasticity or stiffness value. It has good reproducibility and it can also correlate



with common atherosclerosis risk factors. According to our measurement subjects with higher age have very different values as PPG indexes.

Among the many methods used for pulse wave analysis, stiffness index (SI) and reflection index (RI) have been reported to be the two reliable indices for determining stiffness of large arteries. These indices do not take account of complete structure of the pulse wave [1]. They are based on the time interval between the blood pressure systolic and diastolic peaks and ratio of their heights. However, these parameters may be distorted by the other wave components which also belong to the complicated pulse wave structure. SI and RI can be difficult to determine in the ill-defined waveforms of elder people, for example.

The light energy absorption of blood within the visible and infrared regions is partly caused by the oxidized and reduced hemoglobin. The PPG measures the blood flux in human vessels with means of red and infrared light absorption. The absorption of light varies with the oxygen concentration and amount of blood in vessels but also with the vessel wall movement. Our PPG device is based on phase sensitive detection electronics which has proved to be a good solution for the measurement of small changes in the absorption and transmission of light signals simultaneously at two different wavelengths, 660 and 940 nm. The PPG waveforms or simply pulse waves can be rapidly acquired with a PIN photodiode which measures the transmission of red and infra-red LED light simultaneously through the forefinger and the second toe. The waveforms have different characteristics for the young and elderly persons. Our suggestion is to decompose the measured waveform into four or five primary components to improve the accuracy of the analysis, and then to use a parameter calculated from the mutual time. Positions of the individual components characterize the arterial stiffness. In the wave analysis, the first wave is called a percussion wave, the second is a tidal, the third is a dicrotic, and the fourth and fifth are pre-ejection waves.

The PPG measurements may provide a cheap, simple and accurate method of diagnosing arterial and vascular diseases. Moreover, further development of the theoretical model that correlates the waveform of the detected finger and toe tip waves caused by heartbeat oscillations and the hemodynamic parameters could improve the accuracy of the method and potentially lead to a better quantification of the measured parameters used for arterial stiffness.

2 Materials and methodology

When part of the forefinger's and the second toe's nail is illuminated, it is possible to obtain a PPG waveform. PPG technique has not been fully validated except that it measures many hemodynamic parameters, which are not yet exactly known. To obtain a minimum noise PPG, we chose the phase sensitive detection principle based on the transmission probe. In practice, all human subjects were recorded in the supine position with a total measurement time of 300 s PPG probes placed on the left index finger and on the second toe. The infrared LED light has a peak wavelength of 940 nm. To eliminate motion artifact, the subjects were encouraged to keep their fingers and toes relaxed. The



data were collected over the bandwidth of 200 Hz and the integration, derivation, and spectrum calculation done with a digital signal analyzer. The raw data (ECG, phonocardiography (PCG), PPG1, PPG2) and calculated data files were transferred to a PC for later analysis. Baseline restoration was performed in sequential 10 to 12 pulse waves selected for decomposition analysis.

One potential technique for waveform decomposition is Levenberg-Marquardt optimization algorithm (LMO) with non-linear fitting. Preliminary trial of the LMO technique was performed on a PPG data recorded from the elderly and young subjects. With the young subjects, e.g., radial wave is easy for analysis purposes, whereas with the elderly, it is very difficult to analyze completely. When studying wave reflections, it is possible to decompose the measured PPG waveform into the percussion wave and the four reflected components, e.g., the tidal, the dicrotic, and the peripheral reflection waves for necessary index calculation. For the accurate determination of the time of arrival of the reflected waves we realized a trial and error procedure. This analysis can be done in the time domain. This technique has its pros and cons, but the final fitting result based on the residual error and prediction band gave good results.

3 Results and discussion

Figure 1 presents the actual measurement results from a male subject with the age of 25 years. It should be noted that the PPGs are downward because of the absorption. Figure 2 shows the PPG1 waveform separately and Figure 3 its second derivative.

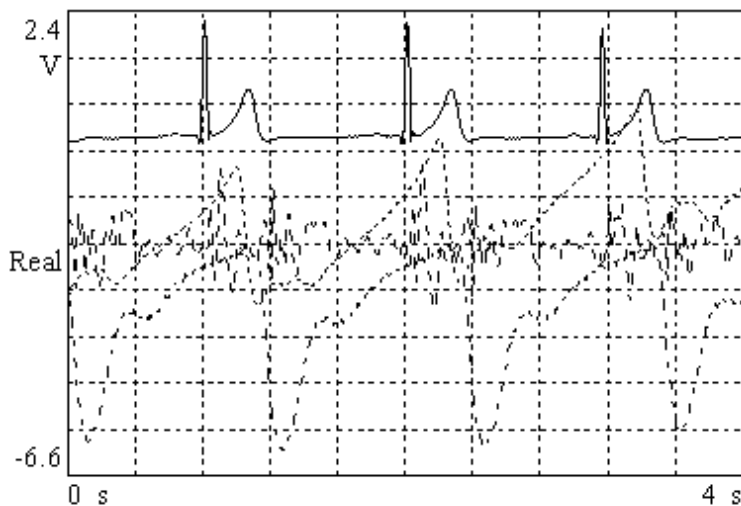


Figure 1: Part of the actual measurement results (4 s): ECG (line), PCG (dash), PPG1 (finger, dots), and PPG2 (toe, dash dots) with a male subject, aged 25 years.

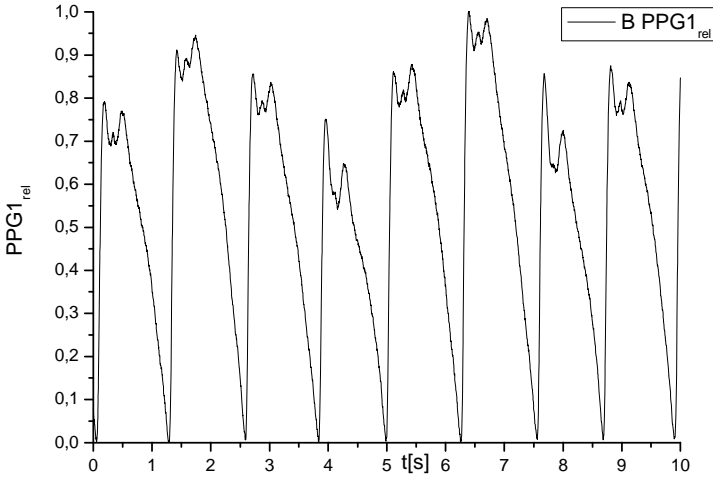


Figure 2: PPG1 during 10s (8 pulse waves of finger) after baseline correction in Figure 1 it is original PPG1 (finger, dots).

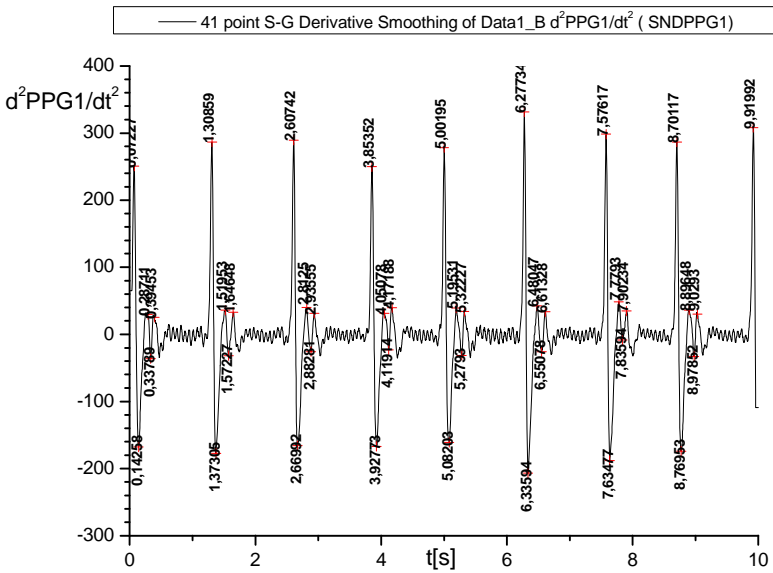


Figure 3: The second derivative of the measured PPG1 during 10s.

From the second derivative of the photoplethysmogram the amplitudes of the all five peaks (A, B, C, D, and E) are easily determined.

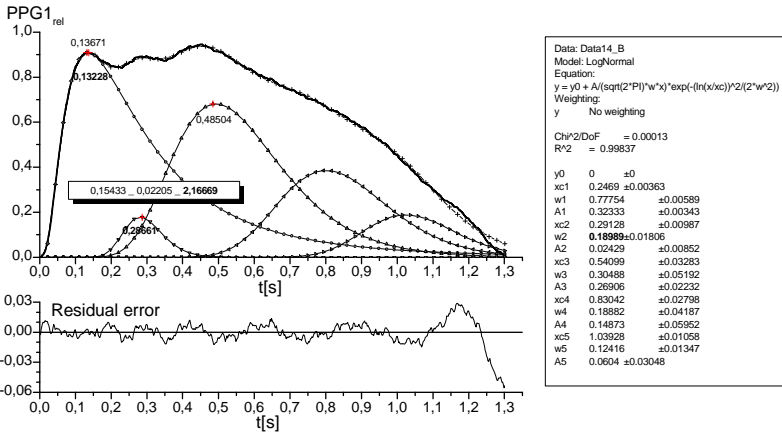


Figure 4: The decomposed PPG1 of Figure 3. It is seen that the tidal component peak time position divided by the percussion component peak time position is 2.1666.

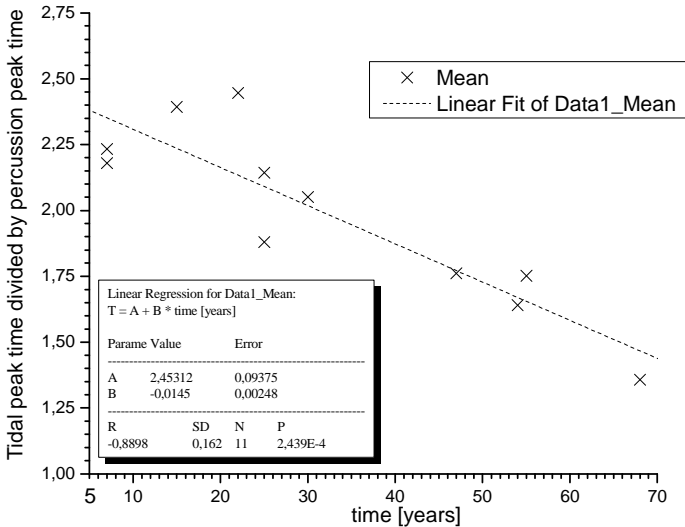


Figure 5: The dependence of the suggested parameter as a function of the age of the subjects under study. It is shown the correlation coefficient is over 0.8 for this small group of healthy persons whose ages are between 7 and 68 years.



Figure 4 depicts the decomposed photoplethysmogram pulse. In this specific pulse the time position of the tidal wave peak with respect to time zero is about two times as large than with the percussion peak time. We suggest that this parameter could probably be related to arterial elasticity and could correlate with the severity of atherosclerosis. Elastic characteristic becomes from the capability of arterial walls being distended or stretched under blood pressure pulse. This makes it an important biophysical property. The dependence of this parameter on age is depicted in Figure 5.

Figure 6 depicts the integrals of ECG, PPG1 and PPG2, respectively. They all have the similar trends, however the ECG integral contains higher frequencies than the PPG integrals.

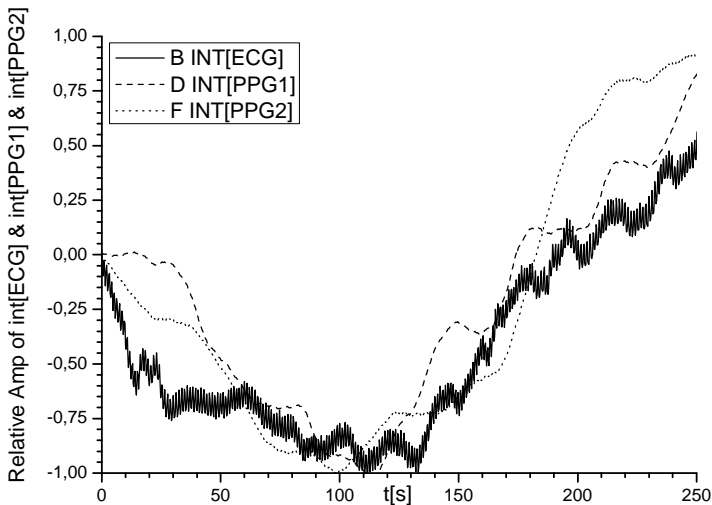


Figure 6: The integrated ECG, PPG1, and PPG2 signals.

The integrals of PPGs are the true DC signal part in PPG measurements. They are generated by autonomic neural system [2]. Each pulse wave is the AC signal part of PPG responsible of e.g. arterial elasticity. An advantage of the PPG measurement and its pulse wave analysis is that the PPG pulse waves can be obtained easily without electrodes, thus making this device useful for epidemiological applications. In this study we are especially interested in the genesis of tidal pulse wave component which is generated after the opening of the aortic valve. The pulse propagates through the aorta storing elastic energy in the aortic wall which is causing the tidal wave phenomena. After the closing the aortic valve the elastic energy of the aorta is recoiled as the tidal component recorded clearly as a part of the PPG waveform in the finger tip. However, the toe tip PPG (=PPG2) contains only traces of the tidal wave component in the second derivative PPG.

4 Conclusion

PPG is a noninvasive method to study peripheral arterial responses, such as pulse waveforms, autonomic fluctuations, and peristaltic of intestine. Simultaneous recording of the ECG and PCG (phonocardiogram) were done in this study for the better interpretation of the PPG pulse wave results. The application of a PPG device with five logarithmic normal functions for the finger PPG waveform analysis gave good accuracy in this small subjects group. In a selected diseased subject group, it could be possible to estimate arterial conditions, e.g. arterial stiffness compared with healthy cohorts. Because the pulse wave characteristics in peripheral pulse depend on the propagation conditions in the arteries, we applied pulse wave decomposition with the hope of a low-cost and noninvasive monitoring system to recognize hidden arterial diseases. PPG could have potential in the so called preventive monitoring of elderly people's health and home care conditions.

Acknowledgement

The present study has been carried out with the support to MH from the Finnish Cultural Foundation.

References

- [1] S. C. Millasseau et al. (2006) Contour analysis of the photoplethysmographic pulse measured at the finger *Journal of Hypertension*, Vol 24 No 8.
- [2] S. M. Yacin et al. (2010) On Non-Invasive Measurement of Gastric Motility from Finger Photoplethysmographic Signal. *Annals of Biomedical Engineering*, Vol. 38, No. 12, pp. 3744–3755.



This page intentionally left blank

Statistical parameter estimation and signal classification in cardiovascular diagnosis

S. Bernhard¹, K. Al Zoukra¹ & C. Schütte¹

¹*Fachbereich Mathematik, Freie Universität Berlin, Germany*

Abstract

Medical technology has seen impressive success in the past decades, generating novel clinical data at an unexpected rate. Even though numerous physiological models have been developed, their clinical application is limited. The major reason for this lies in the difficulty of finding and interpreting the model parameters, because most problems are ill-posed and do not have unique solutions. On the one hand the reason for this lies in the information deficit of the data, which is the result of finite measurement precision and contamination by artifacts and noise and on the other hand on data mining procedures that cannot sufficiently treat the statistical nature of the data. Within this work we introduce a population based parameter estimation method that is able to reveal structural parameters that can be used for patient-specific modeling. In contrast to traditional approaches this method produces a distribution of physiologically interpretable models defined by patient-specific parameters and model states. On the basis of these models we identify disease specific classes that correspond to clinical diagnoses, which enable a probabilistic assessment of human health condition on the basis of a broad patient population. In an ongoing work this technique is used to identify arterial stenosis and aneurisms from anomalous patterns in parameter space. We think that the information-based approach will provide a useful link between mathematical models and clinical diagnoses and that it will become a constituent in medicine in near future.

Keywords: statistical cardiovascular system model, cardiovascular system identification, multi-channel measurement, state-space model, parameter estimation, Bayesian signal classification, patient-specific diagnosis.



1 Introduction

Due to the high morbidity and mortality arising with cardiovascular disorders, an efficient and highly specific diagnosis is of paramount importance for the patient. There exist a variety of different diagnostic approaches that consider several factors and symptoms leading to a diagnosis by an exclusion principle. However, the symptoms are not always well-defined and differ from patient to patient, in other words - not every patient has distinct symptoms that allow a clear disease specific assignment. This demands for a high degree of expertise from the physician and sometimes makes the diagnosis tedious and even misleading diagnoses are the result. Therefore, the attempt of using physiological models combined with knowledge and experience of experts collected in databases to support the diagnosis process by computational methods seems a reasonable approach. The solution to a non-trivial classification task like this is valuable to improve diagnosis.

Typically traditional signal processing techniques are used to extract therapeutically relevant information like for e.g. the heart rate, oxygen saturation and the cardiac output from clinical data. Even though the information content within the data has grown continuously, the number of reliable procedures for feature extraction had not.

On the one hand the difficulty of information extraction of richer data sets into improved therapies lies in the deterministic view immanent in current mathematical models of physiological processes [1]. On the other hand there is a lack of sufficient therapeutic strategies that can handle improved diagnostic information. The former problem is a result of limited statistical data integration into the model, the latter problem is dependent on the time required to transfer the results into novel therapeutic strategies.

According to studies regarding the needs of clinical applications [2-4], we combine physical and physiological aspects of pathological conditions in the cardiovascular system with patient-specific simulations that are based on non-invasively accessible data [1].

Within this study we use two basic approaches to describe the cardiovascular system dynamics on a statistical basis: (i) measurement-based parameter estimation and (ii) model-based prediction and classification methods.

In the first approach, the desired parameters are estimated from physiological measurements using statistical inference techniques. In the current experimental setup the data is either obtained by a series of non-invasive multi-channel measurements from a specific sub-population of patients (e.g. healthy/diseased) or generated by invasive measurements from a fluid-dynamical cardiovascular simulator that models normal and pathological flow conditions. This is a very expensive approach, since it requires a distinct subset of specific patients or the construction of a fluid-dynamical system that can be used to simulate realistic conditions in the vasculature. Furthermore the measurements have to be acquired according to a standard operating procedure (SOP) and analyzed in a predefined statistically setting.



In contrast to this, the second model-based approach is inexpensive and easier to perform, since the system dynamics is obtained by computational methods. However, the model-based approach has some limitations in representing the actual physical state of a real system, since the underlying processes are complex and the number of model parameters is large. Moreover, the choice of parameters in most physiological models is crucial for interpretation and prediction. Even though the sensitivity analysis approach allows to determine specific system features and to identify the critical parameters to which the system is most sensitive, parameter determination is difficult. Not to mention that the interpretation of estimated parameters can only occur on a statistical basis that is based on a broad patient population.

Within this work we combine two approaches, statistical inference methods that are suitable to determine model parameters and states observed in a broad patient population, and Bayesian classification to extract hidden information like for e.g. classes of diseased cardiovascular states that describe the health condition of specific subgroups. This combined approach leads to a novel statistical interpretation of cardiovascular system that optimally uses information of specific sub-populations for diagnostic purposes. The technique provides the potential to develop highly individualized therapeutic strategies – a benefit for the patient.

2 Statistical model of the cardiovascular system

In contrast to traditional cardiovascular system models we are interested in models that include an important feature: randomness. Randomness is characterized by a non-deterministic behavior that can be described by probability theory and the concept of random variables. Randomized processes are described by either time discrete or continuous functions (e.g. probability density functions and distribution functions). For most real world examples state space models are sufficient to describe the underlying dynamics. Having constructed such a model, the time discrete behavior of the system can be simulated and desired measures can be evaluated.

2.1 Complexity reduction

Within the model building process the complexity of the cardiovascular system is a critical problem that requires a tradeoff between accuracy of representing the true dynamic behavior and the ability to solve the model equations in reasonable amount of time.

There exist a variety of approaches to model and solve complex systems. Within this work we follow a very pragmatic decomposition/aggregation approach described in [1]. Here the complexity problem is treated by the construction of sub-models (channels) through the definition of specific interface conditions. The basic idea is to decompose the complex structure of the vasculature into a set of simpler sub-models being solved separately. The solutions are then combined to obtain an aggregate solution for the actual model.



Of particular interest are simple lumped-parameter models (also known as zero dimensional or Windkessel models) that describe the transport of blood distribution within the vasculature [5]. These models were developed to provide answers to important questions in cardiovascular physiology that have absconded intuitive understanding [1]. However until now only very basic parameters can be estimated for individual patients, not to mention that there is no reasonable chance for a population-based interpretation.

In the following example we build a sub-model for a structure of the carotis bifurcation given in [6] and derive the corresponding state-space model.

2.2 Windkessel model for cardiovascular fluid flow

Dynamical systems are generally described by ordinary differential equations (ODEs) in canonical form. It has been shown, that lumped parameter models are reasonable approximations to describe the fluid flow in most elements of the cardiovascular system. Following [5, 7, 8] each segment of the arterial system can be modeled by a 3-element Windkessel electrical circuit analogue (see Figure 1).

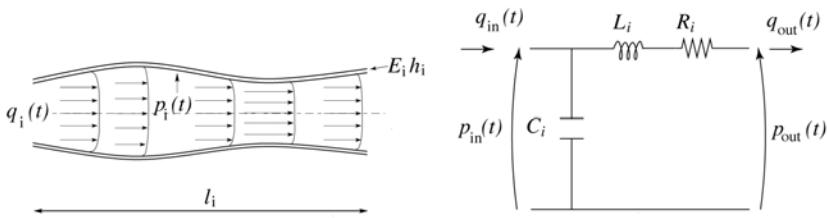


Figure 1: Arterial vessel segment (left) and corresponding three-element Windkessel electric analogue (right).

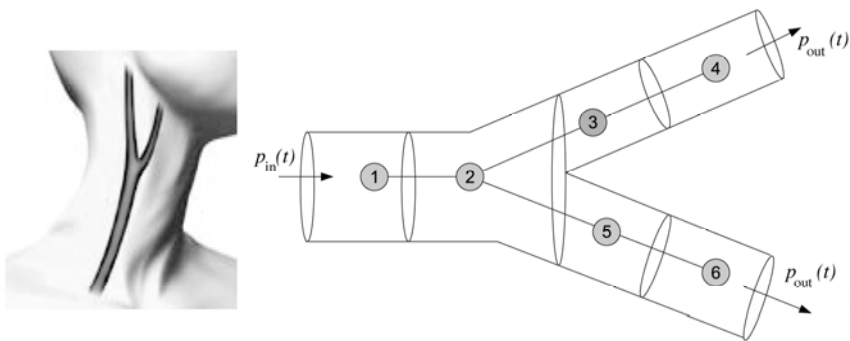


Figure 2: Human carotis bifurcation and the corresponding simplified network structure for $N_s=6$.

In the example model discussed here, every arterial segment $i = 1, \dots, N_s$ is represented by a electrical circuit consisting of a resistance and inductance in

series and a capacitor in parallel. The analogy relates electric current and voltage to arterial blood flow q and pressure p , respectively. The electrical resistances R_i correspond to the viscos flow resistance, the inductances L_i account for the blood inertia forces and the arterial compliances, i.e. the elasticity of the vessel walls, are described by electrical capacitors C_i . The peripheral resistances Z_j for the number of terminating ends N_t of the network account for the viscous flow resistance and compliance in the microcirculation. Within the example of the carotis bifurcation shown in fig. 2, the number of segments is chosen to be $N_s = 6$ and the number of terminals is $N_t = 2$.

In this fundamental form the cardiovascular system dynamics can be represented by a set of $n = 2N_s$ coupled ordinary differential equations of first order that depend on the unknown dynamical parameters λ .

$$\begin{aligned} \dot{x} &= f(t, x, \lambda) & x \in R^n & \quad t \in [T_0, T_0 + T] & (1) \\ x(T_0) &= x_0 \end{aligned}$$

The solution can be given analytically in terms of exponential functions and sine waves, if the right-hand side function f is linear in x . Generally the initial values are also unknown parameters, so that the vector of unknown parameters θ is:

$$\theta = (\lambda, x_0) \in R^{\lambda+n} \tag{2}$$

In analogy to Kirchoff's current and voltage law we obtain a system of n coupled ordinary differential equations for the pressure and flow:

$$\begin{aligned} \dot{q}_1 &= \frac{p_{in} - R_1 q_1 - p_1}{L_1} & \dot{q}_4 &= \frac{p_3 - R_4 q_4 - p_4}{L_4} \\ \dot{p}_1 &= \frac{q_1 - q_2}{C_1} & \dot{p}_4 &= \frac{q_4 - (p_4 - p_{out})/Z_1}{C_4} \\ \dot{q}_2 &= \frac{p_1 - R_2 q_2 - p_2}{L_2} & \dot{q}_5 &= \frac{p_2 - R_5 q_5 - p_5}{L_5} \\ \dot{p}_2 &= \frac{q_2 - q_3 - q_5}{C_2} & \dot{p}_5 &= \frac{q_5 - q_6}{C_5} \\ \dot{q}_3 &= \frac{p_2 - R_3 q_3 - p_3}{L_3} & \dot{q}_6 &= \frac{p_5 - R_6 q_6 - p_6}{L_6} \\ \dot{p}_3 &= \frac{q_3 - q_4}{C_3} & \dot{p}_6 &= \frac{q_6 - (p_6 - p_{out})/Z_2}{C_6} \end{aligned} \tag{3}$$

According to [7], the parameters of the electric analogue circuit are determined from the structural and physiological parameters. Assuming Hagen-Poiseuille flow the electrical parameters become:

$$R_i = \frac{8\nu l_i}{\pi r_i^4}, \quad L_i = \frac{\rho l_i}{\pi r_i^2}, \quad C_i = \frac{2\pi r_i^2 l_i}{E_i h_i} \tag{4}$$



Here every vessel segment i is specified by its length l_i , its radius r_i , the wall thickness h_i and the Youngs modulus E_i . The blood is characterized by the density and viscosity of $\rho = 1050 \text{ kg/m}^3$ and $\nu = 4 * 10^{-4} \text{ Pa s}$, respectively.

Having defined the parameters $\lambda = (R_i, C_i, L_i, Z_j), \forall i, j$ and the pressure at the inlet $p_{in}(t)$ and outlet p_{out} , the system can be numerically solved for the nodal pressures p_i and flows q_i .

2.3 State space model

The state space representation is a useful notation to describe the dynamics in arterial networks. Besides the explicit description of the measurement process, statistical processes, like the measurement noise, can be described in a very simple and efficient way. In state space form the dynamical system is written in terms of input and observation vectors and the state space variables. It is expressed as a first order differential state equation and the observation equation:

$$\dot{x}_t = \mathbf{A}x_{t-1} + \mathbf{B}u_t + w_t \tag{5 a}$$

$$y_t = \mathbf{C}x_t + \mathbf{D}u_t + v_t \tag{5 b}$$

Here x_t is the vector of state space variables, u_t the input vector and y_t the observation vector. The dynamics of the system is described by the state dynamics matrix $\mathbf{A} \in \mathbf{M} (n \times n)$. The input matrix $\mathbf{B} \in \mathbf{M} (n \times i)$ specifies the time dependency of the in- and outflow as boundary values, the observation matrix $\mathbf{C} \in \mathbf{M} (m \times n)$ defines the observation locations, with the number of observations, m , and the input to observation matrix $\mathbf{D} \in \mathbf{M} (m \times i)$ quantifies the influence of the input vectors to the observation vectors (see fig. 3). In the current setting we use synthetic data as measurement data, so we neglect the noise matrix w_t and v_t in the state and observation equation respectively. The noise terms can be included with minimal effort if real data is available.

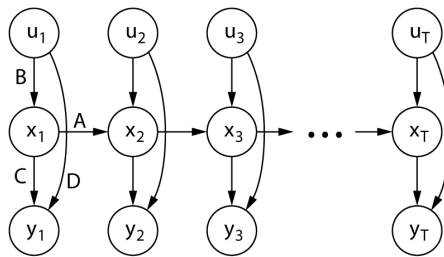


Figure 3: Time discrete state space system with matrix relations between the state, input and observation vectors.

The state equation (5 a) relates the state vector x at a time t to the unknown parameters θ , while the observation equation (5 b) relates the state vector to the measured data y . The state vector x_t contains the flow and pressure functions at

all network locations, whereas the observation vector y_t contains the flow and pressure at selected nodes i , to which measurement time series are available.

We assume that the input pressure p_{in} is a given function of time and that the output pressure p_{out} is known. In the hemodynamic system output pressure corresponds to the mean venous pressure, which is almost constant and has mean values of about 15 mmHg. For these two inputs $a = 2$, the input vector is:

$$u(t) := \begin{pmatrix} p_{in}(t) \\ p_{out}(t) \end{pmatrix} \quad u \in R^a. \tag{6}$$

For m available observations like for e.g. p_i and q_i at nodes 3 and 5 in the network, the observation vector is

$$y(t) := \begin{pmatrix} q_3(t) \\ p_3(t) \\ q_5(t) \\ p_5(t) \end{pmatrix} \quad y \in R^m. \tag{7}$$

Defining the state vector $x := (q_1, p_1, q_2, p_2, q_3, p_3, q_4, p_4, q_5, p_5, q_6, p_6)^T$ leads to a states space system for the carotis bifurcation described in the previous section that is denoted by

$$A = \begin{pmatrix} -\frac{R_1}{L_1} & -\frac{1}{L_1} & 0 & 0 & 0 & 0 & 0 & 0 & 0 & 0 & 0 & 0 & 0 \\ \frac{1}{C_1} & 0 & -\frac{1}{C_1} & 0 & 0 & 0 & 0 & 0 & 0 & 0 & 0 & 0 & 0 \\ 0 & \frac{1}{L_2} & -\frac{R_2}{L_2} & -\frac{1}{L_2} & 0 & 0 & 0 & 0 & 0 & 0 & 0 & 0 & 0 \\ 0 & 0 & \frac{1}{C_2} & 0 & -\frac{1}{C_2} & 0 & 0 & 0 & -\frac{1}{C_2} & 0 & 0 & 0 & 0 \\ 0 & 0 & 0 & \frac{1}{L_3} & -\frac{R_3}{L_3} & -\frac{1}{L_3} & 0 & 0 & 0 & 0 & 0 & 0 & 0 \\ 0 & 0 & 0 & 0 & \frac{1}{C_3} & 0 & -\frac{1}{C_3} & 0 & 0 & 0 & 0 & 0 & 0 \\ 0 & 0 & 0 & 0 & 0 & \frac{1}{L_4} & -\frac{R_4}{L_4} & -\frac{1}{L_4} & 0 & 0 & 0 & 0 & 0 \\ 0 & 0 & 0 & 0 & 0 & 0 & \frac{1}{C_4} & -\frac{1}{Z_1 C_4} & 0 & 0 & 0 & 0 & 0 \\ 0 & 0 & 0 & \frac{1}{L_5} & 0 & 0 & 0 & 0 & -\frac{R_5}{L_5} & -\frac{1}{L_5} & 0 & 0 & 0 \\ 0 & 0 & 0 & 0 & 0 & 0 & 0 & 0 & \frac{1}{C_5} & 0 & -\frac{1}{C_5} & 0 & 0 \\ 0 & 0 & 0 & 0 & 0 & 0 & 0 & 0 & 0 & \frac{1}{L_6} & -\frac{R_6}{L_6} & -\frac{1}{L_6} & 0 \\ 0 & 0 & 0 & 0 & 0 & 0 & 0 & 0 & 0 & 0 & \frac{1}{C_6} & -\frac{1}{Z_2 C_6} & -\frac{1}{C_6} \end{pmatrix},$$

$$B = \begin{pmatrix} \frac{1}{L_1} & 0 \\ 0 & 0 \\ 0 & 0 \\ 0 & 0 \\ 0 & 0 \\ 0 & 0 \\ 0 & 0 \\ 0 & \frac{1}{Z_1 C_4} \\ 0 & 0 \\ 0 & 0 \\ 0 & 0 \\ 0 & \frac{1}{Z_2 C_6} \end{pmatrix},$$

$$C = \begin{pmatrix} 0 & 0 & 0 & 0 & 1 & 0 & 0 & 0 & 0 & 0 & 0 & 0 & 0 \\ 0 & 0 & 0 & 0 & 0 & 1 & 0 & 0 & 0 & 0 & 0 & 0 & 0 \\ 0 & 0 & 0 & 0 & 0 & 0 & 0 & 0 & 1 & 0 & 0 & 0 & 0 \\ 0 & 0 & 0 & 0 & 0 & 0 & 0 & 0 & 0 & 1 & 0 & 0 & 0 \end{pmatrix},$$

and

$$D = \begin{pmatrix} 0 & 0 \\ 0 & 0 \end{pmatrix}.$$

The time discrete state space equations, the parameters θ , and the input vector u_t describe the time evolution of the system in form of the state space variables x_t . In practical applications most of the system parameters are unknown. Furthermore the vector of state variables of the cardiovascular system cannot be measured directly. In the following we propose a parameter estimation method based on the measurements defined in the observation vector y_t . Due to the fact that the measurements are incomplete ($m \neq N_s$) the inverse problem is ill-posed.

3 Parameter estimation in the cardiovascular system

There are several methods to estimate unknown system parameters from time discrete measurements. We assume that we have measured the observation vector $y_i(t)$ for discrete times, $t = 0, \dots, T$, by a multi-channel measurement at locations i in the vascular network. The aim is to estimate the parameters and hidden signals from the measurements, in other words, we seek a solution to the hemodynamic inverse problem that was proposed to have infinite number of solutions [9].

A well-established approach to determine the parameters is the maximum likelihood estimator. It is defined as the vector that minimizes the measurement likelihood L , given θ :

$$\hat{\theta} = \arg \max_{\theta} L(y|\theta). \quad (8)$$

In other words, without assumptions about the parameter to estimate, one chooses the value that makes the output most likely. This maximization problem can be solved even if the data is high dimensional, incomplete and noisy [10]. Due to the fact that the ODE model is not based on a probability model we may assume that the data is normally distributed around the deterministic solution, so that the likelihood is defined in terms of a least square distance. Then the distance function of squared residuals between the measured data and the model trajectory is equivalent to the maximum-likelihood problem. In other words, minimizing the distance function

$$\Xi(d, y) = \sum_{i=1}^m \sum_{k=1}^K (d_i(t_k) - y_i(t_k, \theta))^2, \quad (9)$$

where d_i are data points for the locations i , and $y_i(t_k, \theta)$ is the solution of the dynamical system at times t_1, \dots, t_K is equivalent to maximizing the likelihood function

$$L(d|\theta) = \prod_{i=1}^m \prod_{k=1}^K \frac{e^{-(1/2)(d_i(t_k) - y_i(t_k, \theta))^T \Sigma^{-1} (d_i(t_k) - y_i(t_k, \theta))}}{(2\pi)^{m/2} |\Sigma|^{1/2}}, \quad (10)$$

where the scalar matrix Σ is a diagonal matrix with equal diagonal entries [11]. The maximization of the measurement likelihood may be obtained by two different approaches: application of (i) the expectation maximization (EM) algorithm or (ii) approximate Bayesian computation (ABC) techniques.

In (i) the likelihood function is maximized by the EM algorithm, which iteratively increases the likelihood function. This maximum typically is the global one, if some good initial estimate $\theta(0)$ is available. The initial estimate can be gained from a classical parameter estimation procedure (see section 3.1).

In (ii) the likelihood function is maximized by finding a sufficient approximation $\mathbb{P}(\theta|y^*)$ to the posterior probability distribution $\mathbb{P}(\theta|d)$ in Bayes' formula

$$\mathbb{P}(\theta|d) = \frac{\mathbb{P}[d|\theta]\mathbb{P}[\theta]}{\sum_w \mathbb{P}[d|\theta]\mathbb{P}[\theta]} \quad (11)$$

The ABC algorithm is sample based, i.e. it generates simulation data $y^*(\theta^*)$ for parameter vectors θ^* drawn from the prior probability distribution $\mathbb{P}[\theta]$. The parameters θ^* are accepted if a distance measure $\delta(d, y^*) \leq \varepsilon$ is sufficiently small, then $\mathbb{P}(\theta|d) \cong \mathbb{P}(\theta|y^*)$ and the measurement likelihood consequently is $\mathbb{P}[d|\theta] \cong \mathbb{P}[y^*|\theta]$.

3.1 Solution of the optimization problem

To obtain realistic initial parameters we formulate an optimization problem that includes additional knowledge about the parameters as equality or inequality constraints. In the cardiovascular system all parameters are non-negative and smaller than a parameter specific upper bound, i.e. $\theta_l \leq \theta \leq \theta_h$. Additionally we decompose the optimization problem into s optimization sub-problems for θ_s , and apply the transfer function relations between the interfaces of the sub-models as constraints.

Within this nonlinear optimization problem we seek the vector of parameters θ_s for each sub-model such that:

$$\begin{aligned} &\text{Minimize} && \Xi(d_s, y_s) && (12) \\ &\text{subject to:} && \theta_l \leq \theta_s \leq \theta_h \end{aligned}$$

Due to the nonlinearity iterative algorithms must be used to find a solution. For efficient optimization, at least first derivatives with respect to the parameters (sensitivities) should be provided. According to the large number of variables we decided to use two constraint optimization algorithms: (i) a weighted variant of Levenberg-Marquardt nonlinear least squares algorithm using parameter sensitivities to control the step size (SENSOP) [12] and (ii) a non-linear steepest-descent algorithm (NLSO). The details of the optimization results are discussed in our previous work [1].



4 Bayesian classification as concept in cardiovascular diagnosis

Bayesian signal classification is concerned with two tasks: Firstly the identification of specific sub-populations on the basis of training data sets containing observations whose sub-population is known a priori and secondly the determination of the affiliations of observations where the identity of the sub-population is unknown. The use of Bayesian classifiers in cardiovascular diagnoses is discussed in [1] in more detail. Basically the classifier learns the signal distribution of instances of specific diseases in a sub-population to determine the classification probability of unknown data sets.

In order to outline the classification problem, we start with the assumption that we have a sequence of measurements d_1, \dots, d_M for M different patients that in some appropriate sense form a sampling of a specific patient population. Classification now means to find out which of the M patients belong to certain classes $\mathcal{C}_1, \dots, \mathcal{C}_W$. We further define the class of healthy patients by \mathcal{C}_0 , and the classes of patients that have specific diseases by \mathcal{C}_w , in the following referred to as class w . The classification probability of a patient b in class w is thus the conditional probability of being in class w given the sequence of observed signals, $\mathbb{P}(b \in \mathcal{C}_w | d_{1:M})$. Using Bayes' formula, this probability can be computed from

$$\mathbb{P}(b \in \mathcal{C}_w | d_{1:M}) = \frac{\mathbb{P}[d_{1:M} | b \in \mathcal{C}_w] \mathbb{P}[b \in \mathcal{C}_w]}{\sum_W \mathbb{P}[d_{1:M} | b \in \mathcal{C}_w] \mathbb{P}[b \in \mathcal{C}_w]} \quad (13)$$

Here $\mathbb{P}(b \in \mathcal{C}_w)$ denotes the prior probability of patients of class w and $\mathbb{P}[d_{1:M} | b \in \mathcal{C}_w]$ denotes the probability of measuring the signal from a patient of class w . While the former probability is a classical prior, the latter probability has to be estimated algorithmically from the sequence of observations $d_{1:M}$. Thus the classification algorithm must perform two different estimations simultaneously:

1. Density estimation: Estimate the probability $\mathbb{P}[d_{1:M} | b \in \mathcal{C}_w]$ that a certain signal is observed from a patient of class w .
2. Classification: Find the hidden information whether the signal of a patient, d_b , belongs to class w .

The combination of these two tasks in the sense of a joint likelihood optimization again leads to the EM algorithm. In other words, in every step of the EM iteration the density is estimated before the classification probabilities are evaluated. The iteration again converges if we choose appropriate initial values and results in the optimal densities and classifications based on the available observation. Consequently, the accuracy of the results increases when data is reintegrated.

The aim of the above classification algorithm is to classify measured data into classes with common properties – i.e. with a relation to specific diseases. These classes are then used to classify unknown data measured at patients with unknown diagnosis by means of fuzzy probabilities. As obvious from the above description the Bayesian classification method comprises two steps:



Firstly, in the learning phase, the measurement data and known relationships to cardiovascular diseases (training data) are used to train the priors and densities needed in the EM algorithm. The probability distributions over these training datasets are learned from examples verified by the gold standard (valid diagnosis), thus allowing the generation of new relationships that describe disease specific classes. The gold standard relationships can include any properties of time series related or unrelated to a particular disease. In general, these gold standards are formed by data obtained for a sub-population of patients with known diagnosis.

Secondly, in the prediction phase, the classification probabilities are predicted by the classification algorithm based on newly acquired signals (testing data) without available diagnosis. The prediction is generally based on a network indicating how likely the observation of measurements fits to a specific class. If one considers this network as a connection matrix, it is just a collection of fuzzy like measures, each representing a probability of functional relationship between the measurement and the class. According to the classification probabilities the procedure provides a diagnostic hint about the existence of afore characterized diseases. In other words, the algorithm sets up a series of hypothesis, that are based on the prior information of a sub-population obtained in clinical observations, to classify the health condition of the patient.

The algorithmic classification procedure is as follows:

1. Use training data $d_{1:M}^{\dagger}$ to determine optimal parameters θ , priors and density estimation via the EM or ABC algorithm.
2. Classify testing data $d_{1:M}^{\ddagger}$ via (fuzzy) classification probabilities $\mathbb{P}^M(d_{1:M}^{\ddagger})$.
3. Integrate testing data into training data set and re-optimize parameters.

In order to realize this approach for cardiovascular diseases we will have to train the algorithm on a significantly large population of patients, which is the next challenge we will have to face. Then the statistical classification becomes a method that allows us to identify cardiovascular diseases in an early state that are followed by therapeutic intervention convenient for individual patients. In contrast to other methods that determine a set of selected parameters with pretended relevance for diagnosis, the classification method automatically selects and quantifies all relevant parameters to prove a series of proposed diseases in the fashion of differential diagnosis.

5 Conclusion and outlook

Within this work we have outlined the solution of the constraint hemodynamic inverse problem. The proposed statistical inference approach provides various advantages including quantitative parameter estimates, determination of confidence intervals and error estimates given incomplete and noisy measurement data. Further more the classification algorithm quantifies all disease specific model parameters in terms of classes in the fashion of differential diagnosis. These techniques are proposed to be the basis in patient



specific diagnoses, because they provide a statistical framework for the description of the cardiovascular system allowing improved therapeutic interventions for individual patients.

Although the interdisciplinary challenges involved in the ongoing project are daunting, it is important to recognize the potential gains for cardiovascular diagnosis. However, up to now the progress has been inhibited by the lack of a broad data basis of non-invasive hemodynamic measurements, advanced inverse modeling tools and databases for large-scale data integration and classification. Nevertheless we are sure that the new modeling techniques will find several applications in cardiovascular medicine. The progress will depend on the level of support from funding and industry and the interest of clinicians. There are signs suggesting strong interest from all areas.

References

- [1] Bernhard, S., Al Zoukra, A. and Schütte, C., From non-invasive hemodynamic measurements towards patient-specific cardiovascular diagnosis (Chapter) to appear in: *Quality Assurance in Healthcare Service Delivery, Nursing and Personalized Medicine: Technologies and Processes*, ed. A. Lazakidou & A. Daskalaki. IGI-Global, 2011.
- [2] Capova, K., Blazek, V., Cap, I., & Buckuliakova, L., Physiological Fluid Systems Modelling For Non-Invasive Investigation. *Advances in Electrical and Electronical Engineering*, pp. 38-42, 2002.
- [3] Xiao, X., Ozawa, E. T., Huang, Y. & Kamm, R. D., Model-Based Assessment of Cardiovascular Health from Noninvasive Measurements. *Annals of Biomedical Engineering*, **30**, pp. 612-623, 2002.
- [4] Wessel, N., Voss, A., Malberg, H., Ziehmman, Ch., Voss, H. U., Schirdewan, A., Meyerfeldt, U., & Kurths, J., Nonlinear analysis of complex phenomena in cardiological data. *Herzschrittmachertherapie und Elektrophysiologie*, **11(3)**, pp. 159-173, 2000.
- [5] Olufsen, M. S., & Nadim, A., On Deriving Lumped Models for Blood Flow and Pressure in the Systemic Arteries. *Math. Biosc. & Eng.*, **1(1)**, pp. 61-80, 2004.
- [6] Neil, W., Parametric geometry exploration of the human carotid artery bifurcation, *Journal of Biomechanics* **40**, pp. 2484-2491, 2007.
- [7] Alastruey, J., Parker, K. H., Peiró, J., & Sherwin, S. J., Lumped Parameter Models for 1-D Blood Flow Simulations: Effect on Pulse Waves and Parameter Estimation. *Communications in Computational Physics*, **4(2)**, pp. 317-336, 2008.
- [8] Quateroni, A., Ragni, S., & Veneziani, A., Coupling between lumped and distributed models for blood flow problems. *Computational Visual Sciences*, **4(2)**, pp. 111-124, 2001.
- [9] Quick, C. M., Young, W. L., & Noordergraaf, A., Infinite number of solutions to the hemodynamic inverse problem. *American Journal of Physiology - Heart and Circulatory Physiology*, **280(4)**, pp. 1472-1479, 2001.



- [10] Hartley, H. O., Maximum likelihood estimation from incomplete data. *Biometrics*, **14**, pp. 174-194, 1958.
- [11] Toni, T., Welch, D., Strelkowa, N., Ipsen, A., & Stumpf, M.P.H., Approximate Bayesian computation scheme for parameter inference and model selection in dynamical systems. *J. R. Soc. Interface*, **6**, pp. 187-202, 2009.
- [12] Chan I.S., Goldstein A.A., & Bassingthwaighte J.B., SENSOP: A derivative-free solver for non-linear least squares with sensitivity scaling. *Ann Biomed Eng.*, **21**, pp. 621-631, 1993.



This page intentionally left blank

MRI: a tool for measuring turbulent intensities in flow systems

O. Adegbite¹, L. Kadem² & B. Newling¹

¹*Department of Physics, University of New Brunswick, Fredericton, Canada*

²*Laboratory of Cardiovascular Fluid dynamics, Department of Mechanical and Industrial Engineering, Concordia University, Montreal, Canada*

Abstract

Understanding the fluid-structure interaction and fluid dynamics downstream of an obstruction is crucial in the design and fabrication of devices that find application in both medicine and industry. It is known that the fluid flow patterns downstream of an obstruction may be very complex and are three dimensional, including the formation of vortices, recirculating flow, flow separation and the onset of turbulence. The development of any such pattern of flow might be detrimental to the optimal performance of the flow system. In this work we have used the magnetic resonance imaging (MRI) technique to investigate flow dynamics downstream of an artificial heart valve. MRI is a naturally three-dimensional, non-invasive technique that finds application in clinical, biomedical research and materials research. It has the capability to visualize the internal structure of materials and also to quantify mass transport properties. In this *in vitro* study, we have measured the turbulent diffusivity and velocity downstream of the valve in two configurations (fully opened and partially opened). Our particular implementation of the MRI measurement (known as SPRITE imaging) is unusually robust to fast turbulent flows and has been demonstrated effective at Reynolds numbers on the order 10^5 , much higher than possible with most conventional, clinical MRI techniques. The results showed a low turbulent diffusivity downstream of the fully opened valve configuration, while the turbulent diffusivity is higher downstream of the partially opened valve coupled with a high-velocity fluid jet and recirculating flow. There are distinct



differences between the downstream velocity profiles of the two configurations, which have diagnostic implications.

Keywords: mechanical heart valve, aorta, spiral-SPRITE, turbulent flow, turbulence, velocity, gradient, MRI.

1 Introduction

Magnetic Resonance imaging (MRI) was developed more than three decades ago. It is a well established method in medicine for the imaging of brain, spinal cord, bone and other organs in the body. MRI has several unique advantages. It is both non-invasive and non destructive, which makes it a preferred choice for the investigation of physiological problems and for clinical diagnosis. MRI has further been extended to study the flow dynamics of fluid that are of interest to clinicians and non-clinicians alike. Several studies have demonstrated the use of MRI for measuring fluid velocities and visualizing flow dynamic without disrupting the target [2]. Flow is a natural phenomenon, which can exist in different forms. It can be laminar in which case the flow is orderly and steady, or it can be turbulent, characterized by a complex flow pattern. Turbulent flow is described as irregular eddying motion in which velocity and pressure perturbations occur about their mean values. These perturbations can be irregular, random and even chaotic, in both time and space. This type of turbulent flow is advantageous in mixing. In cardiovascular system however, it may cause physiological complications. In engineering facilities, it is responsible for; among other things, erosion. This complex pattern of fluid flow is often related to the interaction of fluid with the structure through which it flows or interaction of the structure with the fluid in which it is immersed. Some other physical phenomena associated with such interaction are vortex formation, flow separation, flow recirculation, etc.

Understanding the dynamics of this flow and fluid structure interaction plays a crucial role in design and fabrication of devices that are prone to these physical phenomena. An example of such is the prosthetic heart valve. This valve is widely used to replace the diseased heart valves. The most popular and frequently implanted among this family of valves is the mechanical heart valve because of its durability. However, it suffers a major drawback due to its vulnerability to blood coagulation resulting in valve related complications such as haemolysis, platelet activation and thromboembolic events [3]. This shortcoming has been attributed to the complex flow pattern and turbulent flow that characterizes the flow downstream of this artificial heart valve [4]. The first prosthetic heart valve implant of this valve was preformed in 1960, and ever since, attention has been drawn to the study of flow dynamics past such valves and to the investigation of related physiological complications. Among the methods used to study are pulse Doppler ultrasound, laser Doppler anemometry, hot wire-film anemometry, and numerical methods such as computational fluid dynamics [CFD] [3, 5]. Recently, particle image velocimetry (PIV) [6] and particle tracking velocimetry [7] were used in *in vitro* studies of flow dynamics downstream of prosthetic valves. These optical techniques are known for their



high speed, measurement of instantaneous velocities. They have been used to provide information about the spatial and temporal dependence of fluid velocities under a wide range of conditions including laminar flow and turbulence. However, optical techniques are generally ineffective with opaque materials, and are often invasive. Even with some of the ultrasound-based velocimetry techniques that overcome the problem of optical opacity, there remain technical difficulties in resolving fluid within structures, which prevent access to the volume of interest [8]. MRI circumvents these problems; since it is capable of probing internal structure in any radiofrequency (RF) transparent material.

Magnetic Resonance technique performed well in quantifying the properties of steady laminar flow or flow in which the motion of the individual fluid elements were well defined. However, characterization of turbulent flows is more complex. One major problem associated with turbulent flow when using magnetic resonance is signal loss. This occurs because of the additional phase variation that is generated by the presence of turbulent fluctuation of the velocities resulting in a loss of coherence and subsequently signals attenuation. To address this challenge, methods have been developed [9, 10] which are capable of resolving the velocity of fast moving fluid with Reynolds number up to 10000. A Reynolds number is a dimensionless quantity which indicates whether the flow of fluid is steady (laminar) or steady on average but with small unsteady changes (turbulent). Single Point Ramped Imaging with T_1 Enhancement (SPRITE) [11] with motion encoding [1] is capable of resolving turbulent flow with Reynolds numbers of up to 10^5 without signal loss. SPRITE with motion encoding is particularly well suited to characterizing highly turbulent fluid flow (in a wind tunnel style experiment) and fluid with short lived MR signals.

The SPRITE imaging sequence is a pure phase encoding method with no signal loss over a wide range of fluid velocities. This is achieved by the acquisition of a single k-space point (see theory below) at a fixed time interval after radio frequency excitation, in the presence of a constant magnetic field gradient, which is then ramped to a new value before acquisition of the next k-space point. A bipolar gradient is superimposed on the ramped gradient, which introduces sensitivity to spin motion. This approach avoids problems arising from susceptibility variations and field inhomogeneities [11]. This technique is employed in this work to investigate the complex flow pattern downstream resulting from the interaction of the bi-leaflets of a mechanical heart valve with the flowing fluid, with the aim (i) of determining velocity distribution profile downstream, (ii) visualizing the turbulent flow and (iii) estimating eddy diffusivity without signal loss or cancellation.

2 Theory

Magnetic Resonance Imaging relies on the fundamental properties of molecular nuclei, which interact with an externally applied static magnetic field, to obtain spatially resolved information about the structure or dynamical properties of the



material of interest. The magnetic moment of the nucleus arises because it has spin and hence spin angular momentum. When hydrogen nuclei experience a static magnetic field, the spins re-orient nearly parallel and anti-parallel (lower and higher energies respectively) to the magnetic field and undergo a rotation about the magnetic field called precession with a frequency that depends on the static magnetic field strength.

In Magnetic Resonance, an oscillating radio-frequency (RF) pulse with a frequency equal to the precessing frequency is applied perpendicular to the static field. The absorbed energy induces transitions between the parallel and anti-parallel states. The return to thermal equilibrium is referred to as relaxation. Immediately following the RF pulse, the MR signal known as the *free-induction decay* (FID), is acquired. The signals persist as long as the precessing nuclei remain coherent, or precess “in phase,” and induce an emf in the detector coil. Over time increasing incoherence results in the decay of the signal. In MRI, a magnetic field gradient is applied across the sample, leading to a spatially variant distribution of resonant frequencies. A two dimensional Fourier transform reconstructs the image in the spatial domain. The reconstructed image can be based on the magnitude of the signal (*i.e.* magnitude image) or the phase of the signal (*i.e.* phase image).

Most conventional MRI methods acquire many data points in the presence of a constant magnetic field gradient, an approach referred to as frequency encoding. In contrast, the SPRITE method, is a purely phase encode technique that acquires a single data point at a constant time interval, $t = t_p$ (encoding time) after the RF pulse, and at a specific gradient value \vec{G} , which is incremented after each excitation. The phase encoded signal arising from a single point acquired in the presence of a magnetic field gradient, say $\vec{G} = G_x \hat{x}$ is given by

$$S(k_x) = \int \rho(x) \exp(-i2\pi k_x x) dx \quad (1)$$

where

$$k_x = \frac{1}{2\pi} \gamma G_x t_p \quad (2)$$

γ is the gyromagnetic ratio for hydrogen nuclei, G_x is the phase encoding magnetic field gradient, t_p is the encoding time and ρ is the nuclear spin density. If the spins are in motion along this direction, they will develop a phase offset $\Delta\phi$ that is proportional to the magnitude and duration of the gradient field given by:

$$\Delta\phi = \gamma \int G_x x(t) dt \quad (3)$$

Expanding the equation with Taylor series expansion, we have

$$x(t) = x_o + vt + \frac{1}{2} at^2 \dots\dots\dots \quad (4)$$

Substituting equation (4) into (3)

$$\Delta\phi = \gamma \int G_x (x_o + vt + \frac{1}{2} at^2 \dots\dots\dots) dt \quad (5)$$

where x_0 is the initial position encoded by the zeroth gradient moment with respect to time. Velocity (v) is encoded by the first gradient moment and acceleration (a) by the second. The power of SPRITE lies in the short encoding times possible, much less than the signal lifetimes of most materials, permitting the acquisition of density weighted images. This characteristic of SPRITE also makes it possible to image fast and turbulent fluid flow. In our implementation, the phase encode gradient is ramped through 2564 points, as shown in figure 1(inset). This phase encoding gradient is bipolar, switching from $G_x - g$ to $G_x + g$ during the time constant t_p , allowing for controlled separation of the first and second gradient moments in equation (5) through the use of different values of the motion sensitising gradient g .

Typically, 8 values of g were used to acquire 8 images of a $64 \times 64 \times 8$, 3-dimensional array. Z is the flow direction. The set of images, when analysed (with a custom IDL program called jAIMS designed by the Centre for the analysis of flowing fluids) give maps of the mean velocity and turbulent diffusivity.

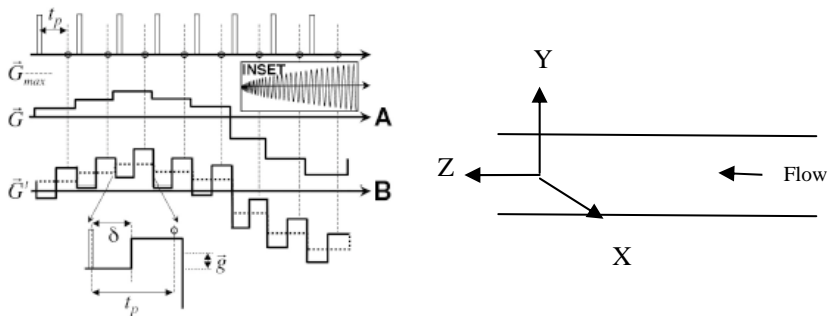


Figure 1: Shows the first few values of the magnetic field gradient for the spiral trajectory acquisition (complete trajectory in inset).

3 Experiment

The experimental setup for this study consists of a 1.2m long glass tube with an internal diameter of 3.2cm. The glass tube is long enough to allow the flow to be fully developed before the fluid reaches the probe. Fitted in the middle [test section] of the glass tube in an upright position was the prosthetic aortic valve in a fully opened configuration. The working fluid is water doped with gadolinium III chloride hexahydrate for fast relaxation and the longitudinal relaxation time (T_1) is 30ms.

The encoding time (t_p) is 1ms and a repetition time (TR = the time interval between RF pulses) is 3.2ms. This model was placed in a re-circulating loop that was driven by a pump with a variable voltage control (0–100V), placed approximately 3m away from the magnet. The water volumetric flow rate was

13.1L/min. Spiral SPRITE was implemented on a 2.4T 32-cm i.d horizontal bore superconducting magnet. [Nolarac Cryogenic Inc. Martinez, CA]. A water cooled 7.5cm i.d gradient set driven by Techron [Elkhart, IN]8710 amplifier that generates a maximum of 50 G/cm was used for all experiments. The probe was a homebuilt 32-rung birdcage coil driven by a 2kW AMT (Brea, CA) 3445 RF amplifier. A Tecmag (Houston, TX, USA), Apollo console was employed. Image acquisitions were performed with the motion encoding gradient along the z-direction, i.e. parallel to the bore of the magnet and the principal direction of flow.

Two set of data images were acquired; one with flow and the other without. The set of images, were analysed by jAIMS program to give the maps of the mean velocity and turbulent diffusivities.

4 Result and discussion

All of the results presented were for flow of Reynolds number of approximately

10000, which was calculated from $Re = \frac{\rho VD}{\mu}$, for which ρ is density

(1000kg/m³), V is fluid velocity (m/s), D = inside upstream glass tube diameter and μ = viscosity (0.001kg/m-s). The 3D velocity map acquired using SPRITE with motion encoding was of two configurations: (i) fully opened leaflets or (ii) one partially opened leaflet with the other fully opened. Figure 2 shows the three orifices of the prosthetic heart valve in the fully open position. Figure 3(a), is the velocity map showing the flow pattern upstream and downstream in the fully opened configuration. The blank region in-between upstream and downstream is the location of the artificial valve. The prosthetic valve appeared blank because the valve is not transparent to the RF pulse because it is made up of pyrolytic carbon. Hence, the valve cannot be “seen” through and the content inside it cannot be visualized. However, of interest to us the flow pattern downstream of

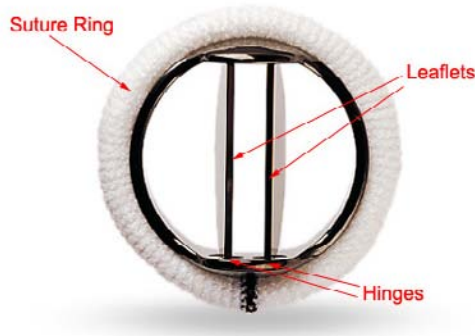


Figure 2: Depicts the prosthetic heart valve in the laboratory in a fully opened position [12].

this valve. The map showed a 2D ZX section through a 3D (12cmx5cmx4cm) map of the z-component velocity. The 12cm is from left to right but top to bottom is 5cm, so that the tube appears stretched in this direction. The nominal spatial resolution were $\delta z=1.875\text{mm}$, $\delta x=0.781\text{mm}$ and $\delta y=5\text{mm}$. The actual spatial resolution is usually less because of blurring. The edges of the map are the region outside the homogenous field of the magnet. The velocity map showed the three regions of jet velocity of value $>0.35\text{m/s}$ through the three orifices. The flow through the central core region disappeared quickly as the distance extends farther away from the valve. The flow through the other two lateral orifices appears turbulent, which gradually reduced downstream as shown in figure 4(a). The unequal intensities of the velocities jet seen in figure 3(a) were due to the variation in the opening angle of the leaflet. The leaflets were opened at an angle of 10° relative to each other, which might be due to the hinge mechanism [13]. This angular variation introduced unequal resistance to the flow dynamics, which in turn results in the difference in turbulent intensities through the three orifices. Figure 3(b) shows the velocity map of the other configuration of the valve (one completely opened leaflet and half closed leaflet). To achieve this configuration, a strand of thread was tied vertically along the middle of this leaflet (restriction), which held it in position as the water flows past it; a situation that mimics stenosis (narrowing). The map revealed a high velocity jet immediately downstream, which is more turbulent at both lateral orifices, with complete disappearance of the flow through the central core region as shown in figure 3(b). The jet through the open orifice extends a distance greater than 2 Diameter downstream while the flow through other orifice was directed against the glass wall. In-between, was the region of some recirculation flow, which appeared behind the restricted section of the leaflet. This region is distinct as far as 2 diameters from the valve but shows a much smaller fluid speed than the principal flow. Some fluid speeds were zero velocities and some were of negative values as seen in figure [5].

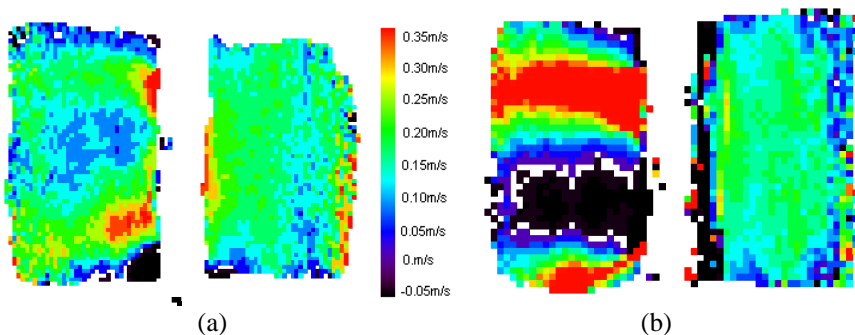


Figure 3: (a) Velocity map for the fully opened configuration, and (b) is the map for the one leaflet fully and other half closed, the white pixels indicate that the signal level fell below the noise level outside the tube.

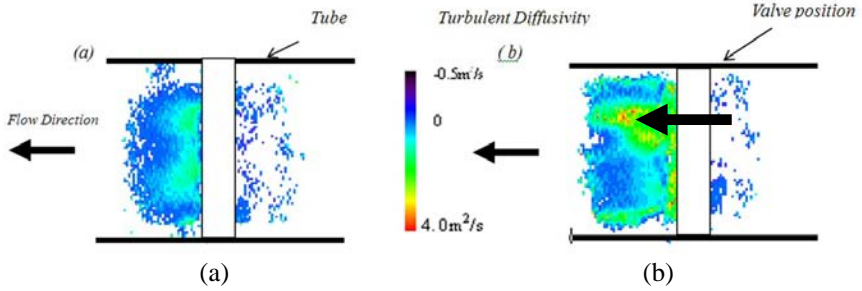


Figure 4: (a) and (b) show turbulent diffusivity maps of downstream of the heart valve when fully open (a), configuration I) and partially open (b), configuration II).

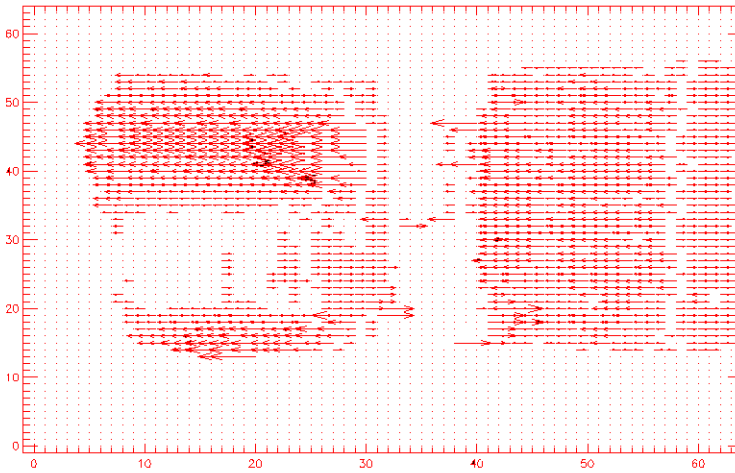


Figure 5: Showing the velocity field vector for the configuration II.

The negative velocities oppose the flow direction, some of which appeared upstream of the valve. Fluid behaviours such as this recirculation have a direct effect on cardiac function and are clinically referred to as valvular regurgitation [14].

Figure 6(a) and (b) show the velocity distribution profile for both configurations at 0.2 tube diameters downstream (notice the differing vertical scales). The jet velocities for configuration II climb up to more than 1m/s in the half closed leaflet and a little below 1m/s in the other fully opened leaflet. This is consistent with the conservation of mass principle that requires the fluid velocity to increase as it flows through the smaller cross-sectional area of the restriction. At the same time the pressure (since the fluid is incompressible) downstream is

reduced compared to the open configuration. Immediately downstream, the flow through the central orifice completely vanished and at the two lateral orifices. Fundamentally, the relationship between the flow through a stenosed valve and its pressure difference, pressure recovery downstream and energy loss in such a flow system has been estimated [15]. We conjecture that the pressure recovery region for this configuration extended beyond that of configuration I, in conjunction with the propagation further downstream of the turbulence. In contrast, figure 4(a) showed the configuration wherein the bi-leaflets were fully opened and the jet velocities were through all the three orifices at 0.36m/s, though the velocity through the central orifice vanishes quickly. The velocity profile at the three orifices of the valve at 0.2D were consistent with the profile obtained in [4], and the diffusivities reduced at some distance $>2D$ downstream. In contrast to ultrasound measurements of centreline velocity, the profiles showed the velocity distribution across the tube. Figure 4(a) and (b) above also showed the on-set and development of the turbulent diffusivities in both configurations. In configuration II, where the restriction existed, the regions of high velocities showed correspondingly higher turbulent diffusivities. The diffusivities at the half-opened bi-leaflet spread out to the wall of the tube. At the opened leaflet, the fluid jet carries turbulent velocity fluctuations further downstream than in configuration I.

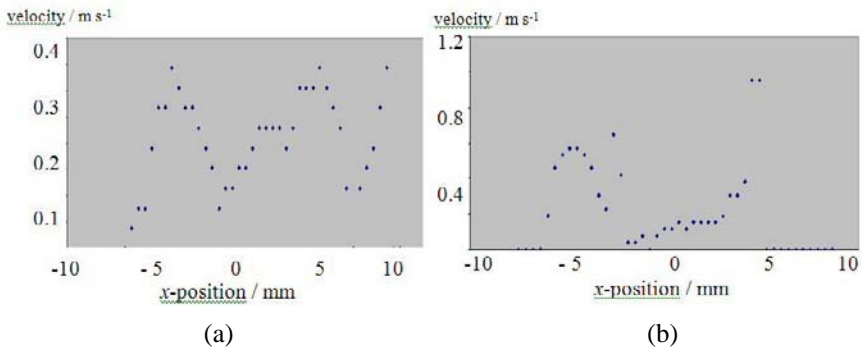


Figure 6: (a) showing the velocity distribution profile for configuration I and (b) for configuration II.

The region of lower counter flow velocities which is in-between the high turbulent diffusivities that resulted from jet velocities is bounded by regions of high shear [5]. This recirculation phenomenon has been known to have a physiological impact. For instance, it has been shown to initiate red blood cells damage or platelet activation in blood flow due to blood cells residence time in this region [12], and also, a stethoscope placed on the chest of a subject that has this flow pattern results in an audible murmuring sound, which is due to the turbulent pressure fluctuation downstream of the stenosis, and consequently results in the vibration of the aortic wall that is transmitted through the chest. In

figure 4(a) the diffusivities of turbulent flow is very mild and disappear downstream.

5 Conclusion

In this study, the flow dynamics through a mechanical heart valve in two configurations of the bi-leaflets has been investigated using a specialised magnetic resonance imaging technique. The effect of the inclination of the leaflet is to create a significant velocity gradient across the flow field. The turbulent diffusivities are much higher in the second configuration, which appear to have great diagnostic implications. The MRI technique is rather naturally capable in three spatial and velocity dimensions and the efficient extension of these MRI techniques measurements with all three velocity components is underway.

References

- [1] Newling B, Poirier C. C., Zhi Y, Rioux J. A., Coristine A. J, Roach D and Balcom B. J. Velocity Imaging of Highly Turbulent Gas Flow. *Phys. Rev. Lett.* (93), 2004
- [2] Bonn D, Rodts S, Groenink M, Rafai S, Shahidzacteh-Bonn N. and Cossot P. Some Applications of Magnetic Resonance Imaging in Fluid Mechanics: Complex Flows and Complex Fluids. *Annu. Rev. Fluid Mech.* (40) pp 209–233, 2008
- [3] Hasenkam J. M, Westphal D, Nygaard H, Reul H, Giersiepen M, and Stadkilde-Jorgensen H. In vitro stress measurements in the vicinity of six mechanical aortic valves using Hot-film anemometry in steady flow. *J. Biomechanics* Vol. 21 No.3 pp 235–247, 1988
- [4] Ge L, Leo H, Sotiropoulos F. and Yoganathan A. P. Flow in a mechanical Bileaflet Heart Valve at Laminar and Near-Peak Systole flow Rates: CFD simulations and Experiments. *J. Biomech. Engng* 127 (5), 782–797, 2005
- [5] Yokoyama Y, Medart D, Hormes M, Schmitz C, Hamilton K, Kwant P B, Takatani S, Schmitz-Rode T and Steinseifer U. CFD simulation of a novel bileaflet mechanical heart valve prosthesis: an estimation of the Venturi passage formed by the leaflets. *Int J Artif Organs.* 29(12):1132–9, 2006
- [6] Lim W. L, Chew Y. T., Chew T. C and Low H. T. Pulsatile flow studies of a porcine bioprosthetic aortic valve in vitro; PIV measurements and shear-induced blood damage. *J. Biomech.* 34 (11);1417–1421, 2001
- [7] Balducci A, Grigioni M., Querzoli G., Romano G. P, Daniele C., D’Avenio G., and Barbaro V. Investigation of the flow field downstream of an artificial heart valve by means of PIV and PTV. *Experiments in fluids.* (36) pp 204–213, 2004
- [8] Song – I Han, Kimberly L. Pierce, and Pines. NMR Velocity Mapping of Gas Flow around Solid Objects. *Phy. Rev. E* (74) pp 0613023–5, 2006
- [9] Rodriguez A. O. Study of Turbulent flow using Half-Fourier Echo-planar imaging. *Brazilian Journal of Physics* V(36) (1) pp 1–3, 2006



- [10] Guilfoyle D.N, Gibbs P, Ordidge R. J. and Mansfield P. Real-Time Flow Measurement using echo-planar imaging. *Magnetic Resonance in Medicine* (18) pp 1–8, 1991
- [11] Balcom B. J, MacGregor R. P, Beyea S. D, Green D. P, Armstrong R. L, and Bremmer T. W.. Single-Point Ramped Imaging with T1 Enhancement (SPRITE), *J. Magn. Reson. A* (123) pp 131–134, 1996
- [12] Govindaraj V, Udaykumar H.S. and Chandran K. B. Two Dimensional simulations of flow and platelet dynamics in the hinge region of a mechanical heart valve. *J Biomech Eng.* 131(3), 031002, 2009
- [13] Detullio M. D, Cristallo K, Balaras E. and Verzicco R. Direct numerical simulation of the pulsatile flow through an aortic bi-leaflet mechanical heart valve. *J Fluid mech.* V(622) pp 259–290, 2009
- [14] Chatzimavroudis G. P. Blood flow measurement with magnetics resonance phase velocity mapping. *Measurement* (37) pp 201–212, 2005
- [15] Clark C. Energy losses in flow through stenosed valves. *J. Biomechanics.* (12) pp 737–746, 1979



This page intentionally left blank

Author Index

- | | | | |
|------------------------|-----|-----------------------|----------|
| Abrahart R. J..... | 79 | Fitzgerald R. | 47 |
| Adegbite O..... | 471 | Focardi S..... | 183 |
| Akay E. M..... | 383 | Fried J. | 59 |
| Akay G..... | 383 | Gagliano A..... | 105 |
| Akhmadeev N..... | 397 | Galesi A..... | 105 |
| Al Zoukra K..... | 457 | Garrido M. J..... | 209 |
| Araujo M..... | 209 | Gastaldi L. | 361 |
| Audenino A..... | 417 | Ghorbani M. | 33 |
| Averbach M. | 323 | Giorgi M. | 417 |
| Bake M. A..... | 221 | Gospavic R. | 197 |
| Benov L. | 171 | Haque M. N. | 197 |
| Berglind R..... | 291 | Huotari M. | 449 |
| Bernhard S. | 457 | Hurbánková M..... | 135 |
| Bertolatti D. | 11 | Innocenti B. | 417 |
| Biagini T..... | 183 | Johnson J. | 91 |
| Bianchi E. G. | 69 | Kadem L. | 471 |
| Bignardi C..... | 417 | Kiss R. M..... | 373, 427 |
| Bokhari M. A. | 383 | Kita E..... | 439 |
| Bonotto D. M..... | 279 | Kostamovaara J..... | 449 |
| Bozkurt O. | 115 | Kováčiková Z. | 135 |
| Bui A..... | 347 | Kovalchuk L. A. | 267 |
| Caramella M. | 361 | Kulshreshtha S..... | 33 |
| Carvalho F. P. | 3 | Labey L..... | 417 |
| Černá S. | 135 | Lauzon H. L..... | 197 |
| Chen H..... | 21 | Leroi F. | 197 |
| Chutakositkanon C..... | 323 | Levy M. | 91 |
| Cirule J..... | 221 | Liffman K. | 347 |
| Corsi I. | 183 | Liljedahl B. E..... | 291 |
| de Oliveira E. G. | 279 | Lu D..... | 47 |
| Della Torre C..... | 183 | Määttä K. | 449 |
| Dimanico U..... | 361 | Macpherson A. K..... | 323 |
| Draine Y. | 91 | Macpherson P. A. | 323 |
| Eglite M..... | 221 | Majorošová M. | 135 |
| Eyles J..... | 59 | Malta M. | 3 |
| Fanany D..... | 147 | | |
| Firozarea A. | 33 | | |

Manasseh R.....	347	Sabino R.	127
Martinson E I.....	221	Schütte C.	457
Martinson Z.....	221	Seile A.	221
Matisane L.	221	Shen R.	115
Miftahof R.	397	Shimano K.	309
Monti M.....	183	Shiroyama H.....	439
Mullins B.....	11	Shittu W. J.	79
Munir S.....	21	Shoucri R. M.	333
		Sjöström J.	291
Nakagawa Y.	309	Smith G.....	241
Nathanail C. P.....	79	Sprudza D.	221
Neti S.	323	Stockwell W. R.....	47
Newling B.....	471	Suaste Gómez E.....	407
Nocera F.	105	Sueiro R. A.	209
		Sumrall W.....	91
Okumus Z.	383	Šutalo I. D.....	347
Oliveira J. M.	3	Suuberg E. M.....	115
Oushy N.....	255		
Oyabu T.....	161	Takács M.	427
		Tarkhanov A. A.	267
Pangallo D.	135	Tarkhanova A. E.....	267
Pastorelli S.....	361	Tchounwou P. B.	47
Patania F.	105	Thomas M.....	171
Pennell K. G.	115		
Piecková E.	135	Vanadzins I.	221
Popov V.	197	Veríssimo C.	127
		Viegas C.	127
Qvarfort U.....	291	Viegas S.....	233
Reddy R. S.....	47	Williams Q. L.	47
Reste J.....	221	Wilson S. L.....	255
Reyes Cruz H.....	407	Winder C.	241
Ropkins K.....	21		
Rosado L.....	127	Yao Y.....	115
Rudner E.....	427	Yildirim O. S.	383
Rumchev K.....	11		
		Zuo Y.....	439

This page intentionally left blank



WITPRESS ...for scientists by scientists

Biological Monitoring

Theory and Applications

Edited by: M.E. CONTI, University of Rome 'La Sapienza', Italy

Provides the reader with a basic understanding of the use of bioindicators both in assessing environmental quality and as a means of support in environmental impact assessment (EIA) procedures. The book primarily deals with the applicability of these studies with regard to research results concerning the basal quality of ecosystems and from an industrial perspective, where evaluations prior to the construction of major projects (often industrial plants) are extremely important.

Environmental pollution and related human health concerns have now reached critical levels in many areas of the world. International programs for researching, monitoring and preventing the causes of these phenomena are ongoing in many countries.

There is an imperative call for reliable and cost-effective information on the basal pollution levels both for areas already involved in intense industrial activities, and for sites with industrial development potential.

Biomonitoring methods can be used as unfailing tools for the control of contaminated areas, as well as in environmental prevention studies. Human biomonitoring is now widely recognised as a tool for human exposure assessment, providing suitable and useful indications of the 'internal dose' of chemical agents.

Bioindicators, biomonitors, and biomarkers are all well-known terms among environmental scientists, although their meanings are sometimes misrepresented. Therefore, a better and full comprehension of the role of biological monitoring, and its procedures for evaluating polluting impacts on environment and health, is needed. This book gives an overview of the state of the art of relevant aspects of biological monitoring for the evaluation of ecosystem quality and human health.

Series: The Sustainable World, Vol 17

ISBN: 978-1-84564-002-6 eISBN: 978-1-84564-302-7

Published 2008 / 256pp / £84.00

WIT Press is a major publisher of engineering research. The company prides itself on producing books by leading researchers and scientists at the cutting edge of their specialities, thus enabling readers to remain at the forefront of scientific developments. Our list presently includes monographs, edited volumes, books on disk, and software in areas such as: Acoustics, Advanced Computing, Architecture and Structures, Biomedicine, Boundary Elements, Earthquake Engineering, Environmental Engineering, Fluid Mechanics, Fracture Mechanics, Heat Transfer, Marine and Offshore Engineering and Transport Engineering.



WITPRESS ...for scientists by scientists

Environmental Toxicology III

Edited by: V. POPOV and C.A. BREBBIA, Wessex Institute of Technology, UK

This book contains the proceedings of the Third International Conference in a series that addresses the need for the exchange of scientific information among experts on issues related to environmental toxicology, toxicity assessment and hazardous waste management. With large numbers of new chemicals entering the market every year, it has become necessary to assess their effects on ecosystems as well as minimise their impact on the environment.

Environmental Toxicology is one of the most interdisciplinary sciences, developed through the collaborative work of biologists, microbiologists, chemists, engineers, environmentalists, ecologists and other scientists. Assessment of the environmental effects of chemicals is complicated as it depends on the organisms tested and involves not only the toxicity of individual chemicals, but also their interactive effects (including synergistic ones), and genotoxicity, mutagenicity and immunotoxicity testing. Hazardous waste management is closely related to environmental toxicology and there is a growing need for techniques and practices that will minimise the effects of chemicals on the environment and for corresponding principles to be applied by policy planners and decision-makers.

The Third International Conference on Environmental Toxicology brings together a wide range of people working within the many disciplines associated with environmental toxicology and hazardous waste management, and includes the following topics: Environmental Health Risk; Ecosystem Health; Biodegradation, Bioremediation and Biomonitoring; and New Trends in Environmental Toxicology.

WIT Transactions on Ecology and the Environment, Vol 132

ISBN: 978-1-84564-438-3 eISBN: 978-1-84564-439-0

Published 2010 / 208pp / £79.00

WITPress

**Ashurst Lodge, Ashurst, Southampton,
SO40 7AA, UK.**

Tel: 44 (0) 238 029 3223

Fax: 44 (0) 238 029 2853

E-Mail: witpress@witpress.com





WITPRESS ...for scientists by scientists

Environment and Health

Protecting our Common Future

K. DUNCAN, University of Toronto, Canada

Environmental degradation and illness and disease prevent millions of people in many countries from surviving and achieving their potential. This book serves as a comprehensive guide to key environmental and health issues confronting the planet, enumerates approaches and techniques to address these issues, and provides real-world examples of good corporate citizenship.

Specifically the book addresses a range of issues that will be invaluable to many specialists such as organization leaders who want to improve the environment and health of their colleagues at home and globally, practitioners in corporate social responsibility, managers involved in environmental, health and safety issues and finally business students who work to enhance the well-being of their colleagues and the health of the planet and humanity.

ISBN: 978-1-84564-130-6 eISBN: 978-1-84564-307-2

Published 2008 / 192pp / £63.00

Disaster Management and Human Health Risk II

Reducing Risk, Improving Outcomes

Edited by: C.A. BREBBIA, Wessex Institute of Technology, UK, A.J. KASSAB, University of Central Florida, USA, and E. DIVO, Daytona State College, USA

The increase in the number of large-scale natural disasters in recent years has been alarming. Major floods, hurricanes, earthquakes and many others have affected millions of people, with great destruction of property and loss of life, while forest fires, pipeline failures, and bombings have had equally devastating effects over a smaller scale. It is clear that future threats stem both from human failures and from terrorism, as well as from less predictable natural phenomena.

The increased threats make the convening of the Second International Conference on Disaster Management and Human Health Risk important for the sharing of knowledge among experts on public health, security, and disaster management. This book contains their contributions to the conference. Topics covered will include: Emergency Preparedness; Risk Mitigation; Natural Disasters; Man-made Disasters; Learning from Disasters; Disaster Analysis, Monitoring and Mitigation; Global Risks and Health; Pandemic and Biological Threats; Surveillance and Early Warning Systems; Public Health Preparedness; Socio-economic Issues; Service Sustainability.

WIT Transactions on the Built Environment, Vol 119

ISBN: 978-1-84564-536-6 eISBN: 978-1-84564-537-3

Published 2011 / 336pp / £145.00



WITPRESS ...for scientists by scientists

Human Respiration

Anatomy and Physiology, Mathematical Modeling, Numerical Simulation and Applications

Edited by: V. KULISH, Nanyang Technological University, Singapore

"The collection is quite valuable as it represents a rich set of observations, insights, and results useful to many readers based on the various applications."

AMERICAN JOURNAL OF HUMAN BIOLOGY

Books on human respiration are usually written either by physicians or engineers. The product of close collaboration between both, this volume presents the latest developments and major challenges in the area of biomedical engineering concerned with studies of the human respiratory system.

The contributors cover the anatomy and physiology of human respiration, some of the newest macro and microscopic models of the respiratory system, numerical simulation and computer visualisation of gas transport phenomena, and applications of these models to medical diagnostics, treatment and safety.

Series: Advances in Bioengineering, Vol 3

ISBN: 1-85312-944-5

eISBN: 978-1-84564-228-0

Published 2006 / 240pp / £95.00

Wall-Fluid Interactions in Physiological Flows

Edited by: M.W. COLLINS, London South Bank University, UK, G. PONTRELLI, C.N.R., Istituto per le Applicazioni del Calcolo, Italy and M.A. ATHERTON, London South Bank University, UK

All fluid flow problems in the human body involve interaction with the vessel wall. This volume presents a number of studies where primarily mathematical modelling has been applied to a variety of medical wall-fluid interaction problems. The medical applications discussed are highly varied, while some key clinical areas are also addressed. Unusually, a number of important medical challenges involving fluid flow are considered in combination with the relevant solid mechanics. For the researcher this book offers new scope for developing and demonstrating a mastery of the scientific principles involved.

Partial Contents: Numerical Simulation of Arterial Pulse Propagation Using One-Dimensional Models; Modelling the Reopening of Liquid-Lined Lung Airways; A Finite-Volume Model of the Guldner 'Frogger' – A Training Device for Skeletal Muscle in Cardiac Assist Use Both in Training Mode and Coupled to a Ventricular Assist Device; Geometric Constraints in the Feto-Placental Circulation – Umbilical Cord Coiling and Ductus Venosus Dilatation; Numerical Modelling of Blood Flow in a Stented Artery.

Series: Advances in Computational Bioengineering, Vol 6

ISBN: 1-85312-899-6

Published 2004 / 204pp / £85.00